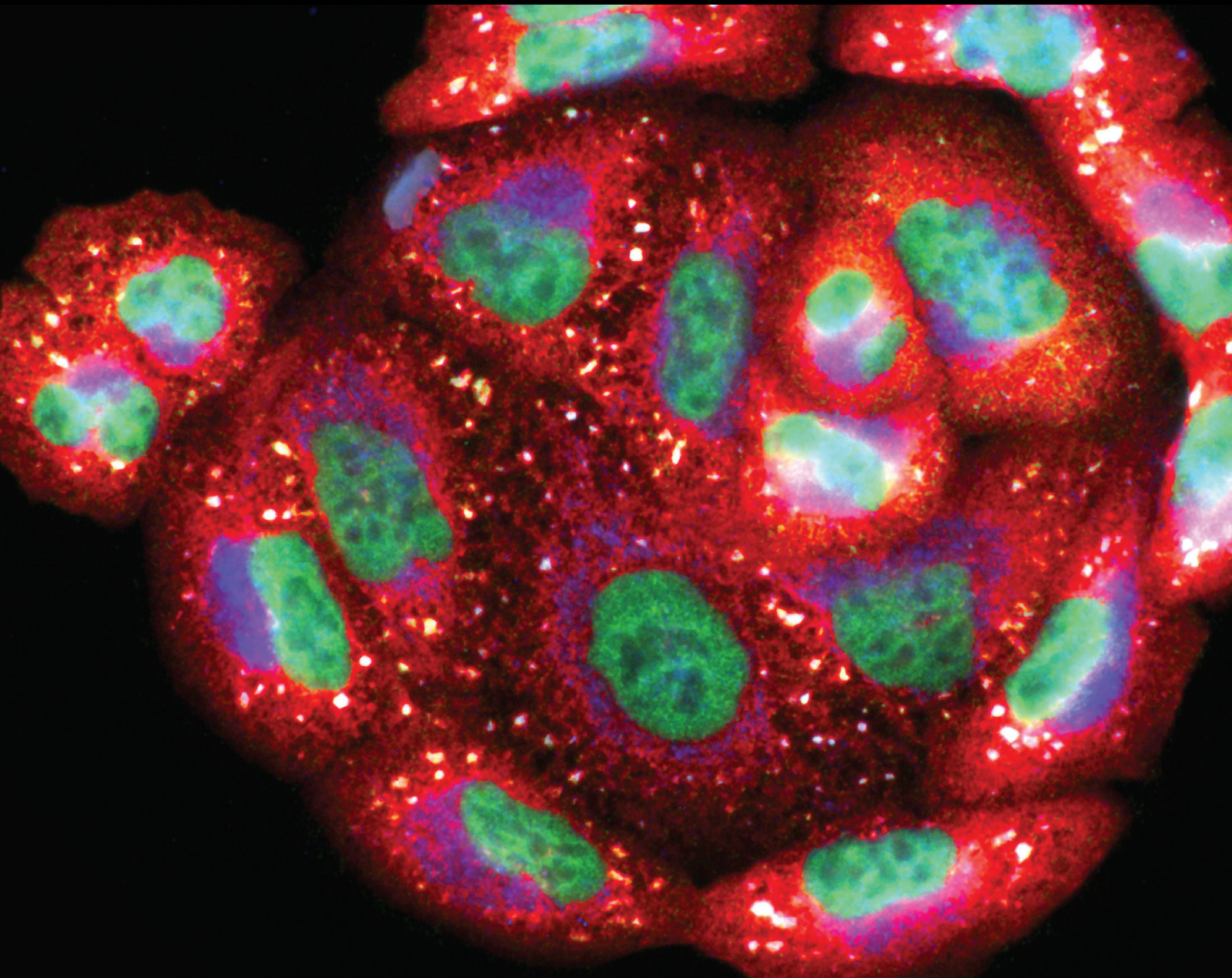


# Using Reactive Oxygen and Nitrogen Species in Cancer Treatment

Lead Guest Editor: Nagendra K. Kaushik

Guest Editors: Kai Masur, Vittorio Colombo, and Rizwan Wahab





---

# **Using Reactive Oxygen and Nitrogen Species in Cancer Treatment**

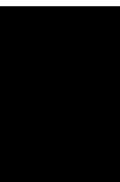
Oxidative Medicine and Cellular Longevity

---

## **Using Reactive Oxygen and Nitrogen Species in Cancer Treatment**

Lead Guest Editor: Nagendra K. Kaushik

Guest Editors: Kai Masur, Vittorio Colombo, and  
Rizwan Wahab



---

Copyright © 2020 Hindawi Limited. All rights reserved.

This is a special issue published in "Oxidative Medicine and Cellular Longevity" All articles are open access articles distributed under the Creative Commons Attribution License, which permits unrestricted use, distribution, and reproduction in any medium, provided the original work is properly cited.

# Chief Editor

Jeannette Vasquez-Vivar, USA

## Associate Editors

Amjad Islam Aqib, Pakistan  
Angel Catalá , Argentina  
Cinzia Domenicotti , Italy  
Janusz Gebicki , Australia  
Aldrin V. Gomes , USA  
Vladimir Jakovljevic , Serbia  
Thomas Kietzmann , Finland  
Juan C. Mayo , Spain  
Ryuichi Morishita , Japan  
Claudia Penna , Italy  
Sachchida Nand Rai , India  
Paola Rizzo , Italy  
Mithun Sinha , USA  
Daniele Vergara , Italy  
Victor M. Victor , Spain

## Academic Editors

Ammar AL-Farga , Saudi Arabia  
Mohd Adnan , Saudi Arabia  
Ivanov Alexander , Russia  
Fabio Altieri , Italy  
Daniel Dias Rufino Arcanjo , Brazil  
Peter Backx, Canada  
Amira Badr , Egypt  
Damian Bailey, United Kingdom  
Rengasamy Balakrishnan , Republic of Korea  
Jiaolin Bao, China  
Ji C. Bihl , USA  
Hareram Birla, India  
Abdelhakim Bouyahya, Morocco  
Ralf Braun , Austria  
Laura Bravo , Spain  
Matt Brody , USA  
Amadou Camara , USA  
Marcio Carochio , Portugal  
Peter Celec , Slovakia  
Giselle Cerchiaro , Brazil  
Arpita Chatterjee , USA  
Shao-Yu Chen , USA  
Yujie Chen, China  
Deepak Chhangani , USA  
Ferdinando Chiaradonna , Italy

Zhao Zhong Chong, USA  
Fabio Ciccarone, Italy  
Alin Ciobica , Romania  
Ana Cipak Gasparovic , Croatia  
Giuseppe Cirillo , Italy  
Maria R. Ciriolo , Italy  
Massimo Collino , Italy  
Manuela Corte-Real , Portugal  
Manuela Curcio, Italy  
Domenico D'Arca , Italy  
Francesca Danesi , Italy  
Claudio De Lucia , USA  
Damião De Sousa , Brazil  
Enrico Desideri, Italy  
Francesca Diomede , Italy  
Raul Dominguez-Perles, Spain  
Joël R. Drevet , France  
Grégory Durand , France  
Alessandra Durazzo , Italy  
Javier Egea , Spain  
Pablo A. Evelson , Argentina  
Mohd Farhan, USA  
Ioannis G. Fatouros , Greece  
Gianna Ferretti , Italy  
Swaran J. S. Flora , India  
Maurizio Forte , Italy  
Teresa I. Fortoul, Mexico  
Anna Fracassi , USA  
Rodrigo Franco , USA  
Juan Gambini , Spain  
Gerardo García-Rivas , Mexico  
Husam Ghanim, USA  
Jayeeta Ghose , USA  
Rajeshwary Ghosh , USA  
Lucia Gimeno-Mallench, Spain  
Anna M. Giudetti , Italy  
Daniela Giustarini , Italy  
José Rodrigo Godoy, USA  
Saeid Golbidi , Canada  
Guohua Gong , China  
Tilman Grune, Germany  
Solomon Habtemariam , United Kingdom  
Eva-Maria Hanschmann , Germany  
Md Saquib Hasnain , India  
Md Hassan , India

Tim Hofer , Norway  
John D. Horowitz, Australia  
Silvana Hrelia , Italy  
Dragan Hrnčić, Serbia  
Zebo Huang , China  
Zhao Huang , China  
Tariq Hussain , Pakistan  
Stephan Immenschuh , Germany  
Norsharina Ismail, Malaysia  
Franco J. L. , Brazil  
Sedat Kacar , USA  
Andleeb Khan , Saudi Arabia  
Kum Kum Khanna, Australia  
Neelam Khaper , Canada  
Ramoji Kosuru , USA  
Demetrios Kouretas , Greece  
Andrey V. Kozlov , Austria  
Chan-Yen Kuo, Taiwan  
Gaocai Li , China  
Guoping Li , USA  
Jin-Long Li , China  
Qiangqiang Li , China  
Xin-Feng Li , China  
Jialiang Liang , China  
Adam Lightfoot, United Kingdom  
Christopher Horst Lillig , Germany  
Paloma B. Liton , USA  
Ana Lloret , Spain  
Lorenzo Loffredo , Italy  
Camilo López-Alarcón , Chile  
Daniel Lopez-Malo , Spain  
Massimo Lucarini , Italy  
Hai-Chun Ma, China  
Nageswara Madamanchi , USA  
Kenneth Maiese , USA  
Marco Malaguti , Italy  
Steven McAnulty, USA  
Antonio Desmond McCarthy , Argentina  
Sonia Medina-Escudero , Spain  
Pedro Mena , Italy  
V́ctor M. Mendoza-Núñez , Mexico  
Lidija Milkovic , Croatia  
Alexandra Miller, USA  
Sara Missaglia , Italy

Premysl Mladenka , Czech Republic  
Sandra Moreno , Italy  
Trevor A. Mori , Australia  
Fabiana Morroni , Italy  
Ange Mouithys-Mickalad, Belgium  
Iordanis Mourouzis , Greece  
Ryoji Nagai , Japan  
Amit Kumar Nayak , India  
Abderrahim Nemmar , United Arab Emirates  
Xing Niu , China  
Cristina Nocella, Italy  
Susana Novella , Spain  
Hassan Obied , Australia  
Pál Pacher, USA  
Pasquale Pagliaro , Italy  
Dilipkumar Pal , India  
Valentina Pallottini , Italy  
Swapnil Pandey , USA  
Mayur Parmar , USA  
Vassilis Paschalis , Greece  
Keshav Raj Paudel, Australia  
Ilaria Peluso , Italy  
Tiziana Persichini , Italy  
Shazib Pervaiz , Singapore  
Abdul Rehman Phull, Republic of Korea  
Vincent Pialoux , France  
Alessandro Poggi , Italy  
Zsolt Radak , Hungary  
Dario C. Ramirez , Argentina  
Erika Ramos-Tovar , Mexico  
Sid D. Ray , USA  
Muneeb Rehman , Saudi Arabia  
Hamid Reza Rezvani , France  
Alessandra Ricelli, Italy  
Francisco J. Romero , Spain  
Joan Roselló-Catafau, Spain  
Subhadeep Roy , India  
Josep V. Rubert , The Netherlands  
Sumbal Saba , Brazil  
Kunihiro Sakuma, Japan  
Gabriele Saretzki , United Kingdom  
Luciano Saso , Italy  
Nadja Schroder , Brazil





Anwen Shao , China  
Iman Sherif, Egypt  
Salah A Sheweita, Saudi Arabia  
Xiaolei Shi, China  
Manjari Singh, India  
Giulia Sita , Italy  
Ramachandran Srinivasan , India  
Adrian Sturza , Romania  
Kuo-hui Su , United Kingdom  
Eisa Tahmasbpour Marzouni , Iran  
Hailiang Tang, China  
Carla Tatone , Italy  
Shane Thomas , Australia  
Carlo Gabriele Tocchetti , Italy  
Angela Trovato Salinaro, Italy  
Rosa Tundis , Italy  
Kai Wang , China  
Min-qi Wang , China  
Natalie Ward , Australia  
Grzegorz Wegrzyn, Poland  
Philip Wenzel , Germany  
Guangzhen Wu , China  
Jianbo Xiao , Spain  
Qiongming Xu , China  
Liang-Jun Yan , USA  
Guillermo Zalba , Spain  
Jia Zhang , China  
Junmin Zhang , China  
Junli Zhao , USA  
Chen-he Zhou , China  
Yong Zhou , China  
Mario Zoratti , Italy

## Contents





### **Corrigendum to “IMCA Induces Ferroptosis Mediated by SLC7A11 through the AMPK/mTOR Pathway in Colorectal Cancer”**

Lei Zhang , Wen Liu, Fangyan Liu, Qun Wang , Mengjiao Song, Qi Yu, Kun Tang, Tieshan Teng , Dongdong Wu, Xijing Wang, Wuqi Han, and Yanzhang Li   
Corrigendum (2 pages), Article ID 6901472, Volume 2020 (2020)






### **ZNRD1 and Its Antisense Long Noncoding RNA ZNRD1-AS1 Are Oppositely Regulated by Cold Atmospheric Plasma in Breast Cancer Cells**

Hyeon Woo Kim , Dawoon Jeong, Juyeon Ham, Heejoo Kim, Hwee Won Ji , Eun Ha Choi , and Sun Jung Kim   
Research Article (9 pages), Article ID 9490567, Volume 2020 (2020)



### **IMCA Induces Ferroptosis Mediated by SLC7A11 through the AMPK/mTOR Pathway in Colorectal Cancer**

Lei Zhang , Wen Liu, Fangyan Liu, Qun Wang , Mengjiao Song, Qi Yu, Kun Tang, Tieshan Teng , Dongdong Wu, Xijing Wang, Wuqi Han, and Yanzhang Li   
Research Article (14 pages), Article ID 1675613, Volume 2020 (2020)



### **Fasting Induces Hepatocellular Carcinoma Cell Apoptosis by Inhibiting SET8 Expression**

Jie Qi, Xiangyuan Chen , Qichao Wu, Jing Wang, Hao Zhang , Anrong Mao , Minmin Zhu , and Changhong Miao   
Research Article (19 pages), Article ID 3985089, Volume 2020 (2020)




### **Chidamide Inhibits Glioma Cells by Increasing Oxidative Stress via the miRNA-338-5p Regulation of Hedgehog Signaling**

Haixia Zhou, Liang Han, Han Wang, Jun Wei, Zhigang Guo , and Zhaohui Li   
Research Article (17 pages), Article ID 7126976, Volume 2020 (2020)






### **Chemopreventive Effects of Propolis in the MNU-Induced Rat Mammary Tumor Model**

A. F. Gal, L. Stan, F. Tăbăran, D. Rugină , A. F. Cătoi , and S. Andrei  
Research Article (13 pages), Article ID 4014838, Volume 2020 (2020)

### **Anticancer Activity of Liquid Treated with Microwave Plasma-Generated Gas through Macrophage Activation**







Chae Bok Lee, Il Hwan Seo, Myoung-Won Chae, Jae Woo Park, Eun Ha Choi , Han Sup Uhm , and Ku Youn Baik   
Research Article (13 pages), Article ID 2946820, Volume 2020 (2020)

### **Hydroethanolic Extract of *Solanum paniculatum* L. Fruits Modulates ROS and Cytokine in Human Cell Lines**

Ana Paula C. R. Ferraz , Alessandra Sussulini, Jéssica L. Garcia, Mariane R. Costa, Fabiane V. Francisqueti-Ferron , Artur J. T. Ferron, Carol Cristina V. de A. Silva, José Eduardo Corrente , Vanessa M. Manfio, Vickeline Namba, Giuseppina P. P. Lima, Bismarque S. Pereira, Denise Fecchio, Igor O. Minatel, Klinsmann C. dos Santos , and Camila R. Corrêa   
Research Article (10 pages), Article ID 7240216, Volume 2020 (2020)



**The Phenoxyphenol Compound 4-HPPP Selectively Induces Antiproliferation Effects and Apoptosis in Human Lung Cancer Cells through Aneuployploidization and ATR DNA Repair Signaling**

Wangta Liu , Chang-Yi Wu, Mei-Jei Lu, Yung-Jen Chuang , Eing-Mei Tsai , Steve Leu, I-Ling Lin, Chih-Jan Ko , Chien-Chih Chiu , and Wen-Tsan Chang 





Research Article (14 pages), Article ID 5167292, Volume 2020 (2020)

**Artichoke Polyphenols Sensitize Human Breast Cancer Cells to Chemotherapeutic Drugs via a ROS-Mediated Downregulation of Flap Endonuclease 1**

Anna Maria Mileo , Donato Di Venere , Stefania Mardente, and Stefania Miccadei 

Research Article (11 pages), Article ID 7965435, Volume 2020 (2020)

**Antitumoral and Immunomodulatory Effect of *Mahonia aquifolium* Extracts**

Andra Diana Andreicuț, Eva Fischer-Fodor , Alina Elena Pârvu , Adrian Bogdan Țigu, Mihai Cenariu , Marcel Pârvu, Florinela Adriana Cătoi , and Alexandru Irimie

Research Article (13 pages), Article ID 6439021, Volume 2019 (2019)

**Spotlight on ROS and  $\beta$ 3-Adrenoreceptors Fighting in Cancer Cells**

Maura Calvani , Angela Subbiani , Marina Vignoli , and Claudio Favre 




Review Article (15 pages), Article ID 6346529, Volume 2019 (2019)

**Mechanisms of Anthracycline-Enhanced Reactive Oxygen Metabolism in Tumor Cells**

James H. Doroshov 




Research Article (14 pages), Article ID 9474823, Volume 2019 (2019)

**Corn Silk (*Zea mays L.*) Induced Apoptosis in Human Breast Cancer (MCF-7) Cells via the ROS-Mediated Mitochondrial Pathway**

Mai M. Al-Oqail, Ebtesam S. Al-Sheddi, Nida N. Farshori , Shaza M. Al-Massarani , Eman A. Al-Turki, Javed Ahmad, Abdulaziz A. Al-Khedhairi, and Maqsood A. Siddiqui 



Research Article (9 pages), Article ID 9789241, Volume 2019 (2019)

**Elevated H2AX Phosphorylation Observed with kINPen Plasma Treatment Is Not Caused by ROS-Mediated DNA Damage but Is the Consequence of Apoptosis**

Sander Bekeschus , Clarissa S. Schütz, Felix Nießner, Kristian Wende , Klaus-Dieter Weltmann, Nadine Gelbrich, Thomas von Woedtke, Anke Schmidt, and Matthias B. Stope 






Research Article (15 pages), Article ID 8535163, Volume 2019 (2019)

**Targeting Reactive Oxygen Species in Cancer via Chinese Herbal Medicine**

Qiaohong Qian, Wanqing Chen, Yajuan Cao, Qi Cao, Yajing Cui, Yan Li , and Jianchun Wu 

Review Article (23 pages), Article ID 9240426, Volume 2019 (2019)

**Plasma Medicine: Applications of Cold Atmospheric Pressure Plasma in Dermatology**



Thoralf Bernhardt , Marie Luise Semmler , Mirijam Schäfer , Sander Bekeschus , Steffen Emmert, and Lars Boeckmann 

Review Article (10 pages), Article ID 3873928, Volume 2019 (2019)

## Contents



---

### **Antiproliferative and Antitumour Effect of Nongenotoxic Silver Nanoparticles on Melanoma Models**

Lucía M. Valenzuela-Salas, Nayeli G. Girón-Vázquez, Juan C. García-Ramos, Olivia Torres-Bugarín, Claudia Gómez, Alexey Pestryakov, Luis J. Villarreal-Gómez , Yanis Toledano-Magaña , and Nina Bogdanchikova


Research Article (12 pages), Article ID 4528241, Volume 2019 (2019)

### **DpdtbA-Induced Growth Inhibition in Human Esophageal Cancer Cells Involved Inactivation of the p53/EGFR/AKT Pathway**

Zhuo Wang, Cuiping Li, Yongli Li, Xingshuang Guo, Zhaoyu Yan, Fulian Gao , and Changzheng Li 

Research Article (14 pages), Article ID 5414670, Volume 2019 (2019)

### **p53-Mediated PI3K/AKT/mTOR Pathway Played a Role in Ptox<sup>Dpt</sup>-Induced EMT Inhibition in Liver Cancer Cell Lines**

Yongli Li, Tingting Wang, Yanjie Sun, Tengfei Huang, Cuiping Li, Yun Fu, Yichun Li, and Changzheng Li 

Research Article (15 pages), Article ID 2531493, Volume 2019 (2019)

## Corrigendum

# Corrigendum to “IMCA Induces Ferroptosis Mediated by SLC7A11 through the AMPK/mTOR Pathway in Colorectal Cancer”

Lei Zhang <sup>1</sup>, Wen Liu,<sup>1</sup> Fangyan Liu,<sup>1</sup> Qun Wang <sup>1</sup>, Mengjiao Song,<sup>1</sup> Qi Yu,<sup>1</sup> Kun Tang,<sup>1</sup> Tieshan Teng <sup>1</sup>, Dongdong Wu,<sup>1</sup> Xijing Wang,<sup>2</sup> Wuqi Han,<sup>3</sup> and Yanzhang Li <sup>1</sup>

<sup>1</sup>*Institute of Biomedical Informatics, Bioinformatics Center, Laboratory for Nanomedicine, School of Basic Medical Sciences, Henan University, Kaifeng 475004, China*

<sup>2</sup>*Department of Dermatology, Second People's Hospital of Zhengzhou, Zhengzhou 450006, China*

<sup>3</sup>*Kaifeng Food and Drug Inspection Institute, Kaifeng 475004, China*

Correspondence should be addressed to Qun Wang; wangqun011@163.com

Received 1 October 2020; Accepted 1 October 2020; Published 27 October 2020

Copyright © 2020 Lei Zhang et al. This is an open access article distributed under the Creative Commons Attribution License, which permits unrestricted use, distribution, and reproduction in any medium, provided the original work is properly cited.

In the article titled “IMCA Induces Ferroptosis Mediated by SLC7A11 through the AMPK/mTOR Pathway in Colorectal Cancer” [1], the authors have identified that the panels in Figure 2(h) were incorrectly duplicated due to an error in manuscript preparation. The corrected image is provided below.

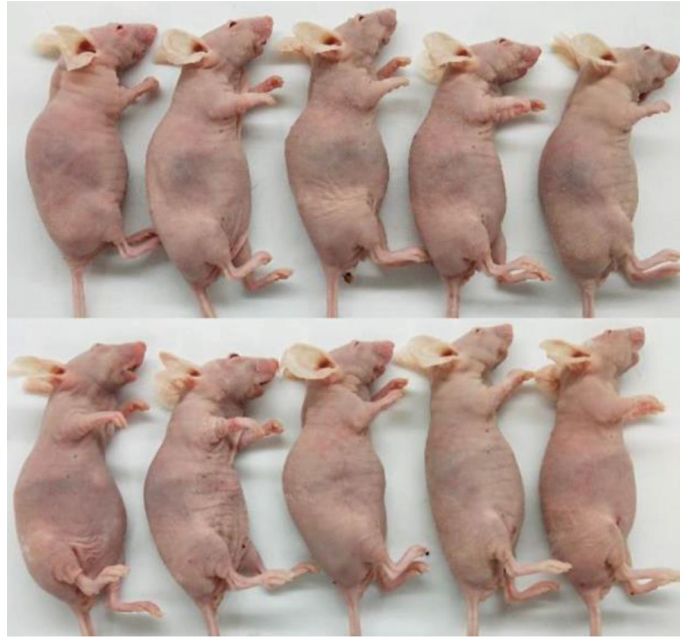


FIGURE 2h

## References

- [1] L. Zhang, W. Liu, F. Liu et al., "IMCA induces ferroptosis mediated by SLC7A11 through the AMPK/mTOR pathway in colorectal cancer," *Oxidative Medicine and Cellular Longevity*, vol. 2020, Article ID 1675613, 14 pages, 2020.

## Research Article

# ZNRD1 and Its Antisense Long Noncoding RNA ZNRD1-AS1 Are Oppositely Regulated by Cold Atmospheric Plasma in Breast Cancer Cells

Hyeon Woo Kim <sup>1</sup>, Dawoon Jeong,<sup>1</sup> Juyeon Ham,<sup>1</sup> Heejoo Kim,<sup>1</sup> Hwee Won Ji <sup>1</sup>,  
Eun Ha Choi <sup>2</sup> and Sun Jung Kim <sup>1</sup>

<sup>1</sup>Department of Life Science, Dongguk University-Seoul, Goyang 10326, Republic of Korea

<sup>2</sup>Plasma Bioscience Research Center, Kwangwoon University, Seoul 01897, Republic of Korea

Correspondence should be addressed to Sun Jung Kim; [sunjungk@dongguk.edu](mailto:sunjungk@dongguk.edu)

Received 21 August 2019; Revised 20 December 2019; Accepted 22 April 2020; Published 6 May 2020

Academic Editor: Elena Azzini

Copyright © 2020 Hyeon Woo Kim et al. This is an open access article distributed under the Creative Commons Attribution License, which permits unrestricted use, distribution, and reproduction in any medium, provided the original work is properly cited.

Cold atmospheric plasma (CAP) has been recognized as a potential alternative or supplementary cancer treatment tool, which is attributed by its selective antiproliferation effect on cancer cells over normal cells. Standardization of the CAP treatment in terms of biological outputs such as cell growth inhibition and gene expression change is essential for its clinical application. This study aims at identifying genes that show consistent expression profiles at a specific CAP condition, which could be used to monitor whether CAP is an appropriate treatment to biological targets. To do this, genes showing differential expression by two different CAP treatment conditions were screened in the MCF-7 breast cancer cells. As a result, ZNRD1 was identified as a potential marker with being consistently upregulated by 600 s but downregulated by the 10 × 30 s CAP treatment scheme. Expression of ZNRD1 was increased in breast cancer tissues compared to normal tissues, judged by cancer tissue database analysis, and supported by the antiproliferation after siRNA-induced downregulation in MCF-7. Interestingly, the antisense long noncoding RNA (lncRNA) of ZNRD1, ZNRD1-AS1, was regulated to the opposite direction of ZNRD1 by CAP. The siRNA-based qPCR analysis indicates that ZNRD1 downregulates ZNRD1-AS1, but not *vice versa*. ZNRD1-AS1 was shown to increase a few cis-genes such as HLA-A, HCG9, and PPP1R11 that were also regulated by CAP. Altogether, this study identified a pair of gene and its antisense lncRNA of which expression is precisely controlled by CAP in a dose-dependent manner. These genes could help elucidate the molecular mechanism how CAP regulates lncRNAs in cancer cells.

## 1. Introduction

Cold atmospheric plasma (CAP) is a specific type of plasma produced at low atmospheric temperature. CAP consists of charged particles, free radicals, neutral atoms, ultraviolet (UV) photons, and reactive oxygen and nitrogen species [1, 2]. When CAP is applied to biological materials ranging from cultured cells to xenografted tumor tissues, it successfully induces cell death [3–5]. Above all, CAP has the advantage of preferentially damaging cancer cells over normal cells. This is attributed to the higher ROS level in cancer cells than in normal cells [6]. CAP increases the ROS level in both cell types, but the resulting ROS level in cancer cells is past the

threshold of cellular survival, leading to cell death, while still below the threshold in normal cells [7, 8]. This characteristic of CAP has been utilized in various cancer cell types for cancer treatment in vitro cultures cells and in vivo animal models [9–11].

In the course of using CAP as a medical treatment option, one of the pivotal considerations is to standardize the whole process from the plasma-generating apparatus through the composition of medium to the response of target cells. The plasma sources are relatively well established for standardization [12, 13]. Currently, two types of devices have been developed: DBD and jet type [14]. In both types, the treatment conditions can be represented using V and Hz with time set

for the required duration. Park et al. applied 0.46 kV and 12.89 kHz for 600 s, which caused MCF-7 breast cancer cell apoptosis of up to 13.5% [3]. In another study, plasma treatment of 20 kV and 500 Hz for 120 s induced Jurkat leukemia cancer cell apoptosis of up to 26.6% [15]. The response of cells to plasma is also affected by the composition of media added to the cultured cells [16–18]. The need for standardization of media is more essential in the case of using CAP indirectly, via plasma-treated medium (PTM). In this case, the concentration of specific chemicals dissolved in the media is determined. Hattori et al. used PTM to treat Capan-2 pancreatic cancer cells, inducing 47% cancer cells apoptosis [19].

The top priority of standardization is the outcome of cellular and/or molecular change induced by CAP. The efficacy of CAP can be expressed with the percentage of cells that are induced to death. However, standardization is not easy, because the death rate is vulnerable depending on the origin of cultured cells and culture conditions [20, 21]. As the molecular change, including RNA and protein expression, is the eventual response by CAP, searching for marker genes that show expression change in proportion to the CAP energy will contribute to establishing the standardization of CAP treatment. To date, various genes have been identified as having expression affected by plasma. Among them, DNA damage- and apoptotic pathway-related genes such as  $\gamma$ -H2AX [22] and caspases [10, 23] have been frequently identified. In spite of the large number of affected genes, few studies have shown the association between the gene expression level and the CAP treatment condition, which is an essential requisite to establish marker genes.

In this study, we identified ZNRD1 and its antisense long noncoding RNA (lncRNA) ZNRD1-AS1, the expression of which was increased or decreased in two different CAP treatment conditions. In addition, the regulatory relationship of the two genes was elucidated through inhibition study of each gene. These genes, to the best of our knowledge, are the first pair of a coding gene and antisense lncRNA to show opposite expression by different CAP energies.

## 2. Materials and Methods

**2.1. Cell Culture and CAP Treatment.** Human breast cancer cell lines MCF-7 and T-47D and a normal cell line, MCF-10A, were purchased from the American Type Culture Collection (ATCC). Cancer cell lines were cultured in RPMI1640 (Gibco, Grand Island, NY, USA) supplemented with 10% fetal bovine serum and 2% penicillin and streptomycin. MCF-10A was cultured in MEGM (Lonza, Basel, Switzerland) supplemented with the MEGM SingleQuot Kit and 100 ng/mL cholera toxin. All cells were incubated in a humidified cell incubator with 5% CO<sub>2</sub> at 37°C. The mesh-dielectric barrier discharge- (DBD-) type CAP device was developed at the Plasma Bioscience Research Center of Kwangwoon University (Seoul, Korea) (Figure S1) [24]. The effect of CAP on the production of reactive oxygen or nitrogen species was examined in our previous study [25]. The voltage, current, and frequency of the CAP were 0.38 kV, 12.6 mA, and 12.9 kHz, respectively (Table S1).

CAP was generated with 1 L/min argon gas and exposed 10 times for 30 s every hour or in single treatment for 600 s to the cells at a 4 mm distance from the surface of the medium.

**2.2. Cell Transfection.** siRNAs for ZNRD1 and ZNRD1-AS1 were synthesized by Bioneer (Daejeon, Korea) and Qiagen (Redwood City, CA, USA), respectively. A control siRNA (siNC) was synthesized by Bioneer. Cells were seeded in 60 mm plates and transfected at a final concentration of 20 or 40 nM using Lipofectamine RNAi MAX (Invitrogen, Carlsbad, CA, USA) in serum-free Opti-MEM I Medium (Gibco) according to the manufacturer's protocol. RNA extraction and functional assay were performed 24 h after transfection. The sequence of siRNAs is shown in Table S2.

**2.3. Colony Formation Assay.** For colony formation assay,  $5 \times 10^3$  cells were seeded in 60 mm plates with 2 mL medium. CAP treatment was performed 24 h after transfection and the cells were maintained for 14 days. The colonies were gently washed with PBS, fixed with methanol/acetic acid (7:1), and then stained with 0.2% crystal violet (Sigma-Aldrich, St. Louis, MO, USA). The relative colony area was analyzed using the ImageJ software [26].

**2.4. Cell Proliferation Assay.** The cells were seeded in a 96-well plate at a density of  $2 \times 10^3$  cells/well and transfected with siRNAs. CAP treatment was performed 24 h after transfection, and the cell growth rate was monitored at 0, 24, 48, 96, and 144 h. At each time point, 10  $\mu$ L of CCK-8 solution (Dojindo, Kumamoto, Japan) was added to each well, and the absorbance was measured after 1 h using a microplate reader at 450 nm.

**2.5. Quantitative Real-Time RT-PCR (qPCR).** Total RNA was isolated using the AllPrep DNA/RNA/miRNA Universal Kit (Qiagen) with a 50  $\mu$ L elution volume according to the manufacturer's protocol. cDNA was synthesized from 2  $\mu$ g of RNA using the ReverTra Ace qPCR RT Master Mix with gDNA remover (Toyobo, Osaka, Japan). qPCR was performed using a KAPA SYBR Fast qPCR Kit (Kapa Biosystems, Woburn, MA, USA) on the ABI 7300 instrument (Applied Biosystems, Foster City, CA, USA). GAPDH was used for normalization and calculated using the  $2^{-\Delta\Delta Ct}$  method. Primer sequences used for qPCR are listed in Table S2.

**2.6. Methylation-Specific Polymerase Chain Reaction (MSP).** Chromosomal DNA was extracted using the AllPrep DNA/RNA/miRNA Universal Kit (Qiagen) with a 50  $\mu$ L elution volume. Bisulfite conversion was conducted using 1  $\mu$ g of DNA with an EZ DNA methylation Kit (Zymo Research, Irvine, CA, USA) on the ABI 7300 instrument (Applied Biosystems). A methylation index ( $\beta$ ) was calculated for each sample using the following formula: methylation index =  $1/[1 + 2^{-(CTu-CTme)}] \times 100\%$ . CTu is the average cycle threshold (CT) obtained from PCR analysis using the unmethylated primer pair, and CTme is average CT obtained using the methylated primer pair. Primer sequences used for MSP are listed in Table S2.

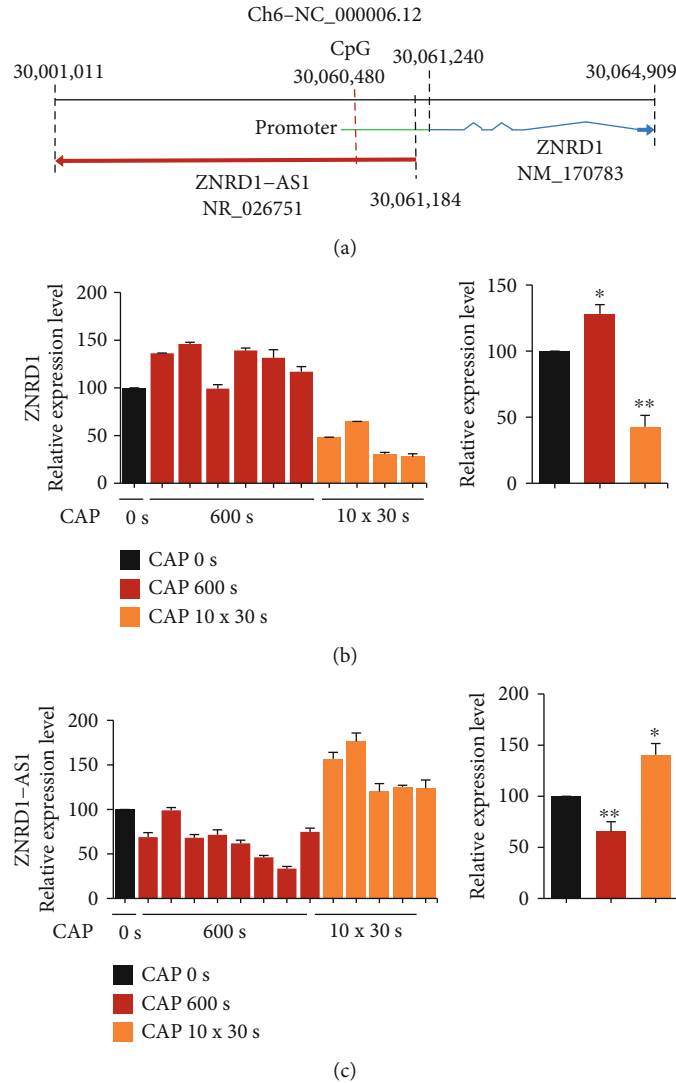


FIGURE 1: Induction of opposite expression of ZNRD1 and ZNRD1-AS1 under different CAP conditions. (a) Schematic structure of ZNRD1 and ZNRD1-AS1 on chromosome. ZNRD1 is indicated by the blue line, with its promoter in green. ZNRD1-AS1 is indicated by the red line. The arrowheads are the transcription direction of each gene. The location of the CpG hypermethylated by CAP is indicated with a red vertical dotted line. (b, c) Expression of ZNRD1 and ZNRD1-AS1 was examined by qPCR after treatment of MCF-7 cells with CAP at the indicated doses. The CAP treatment was performed multiple times, with each time in triple culture dishes. The overall average is indicated on the right with mean  $\pm$  SE. \* $P < 0.05$ , \*\* $P < 0.01$ .

**2.7. Statistical Analysis.** The methylation data for the CpG at the ZNRD1 promoter in breast cancer patients was retrieved from the TCGA Wanderer database (<http://www.maplab.imppc.org/wanderer>). The expression data for ZNRD1 and ZNRD1-AS1 was retrieved from the GEPIA database (<http://gepia.cancer-pku.cn>). All experimental results were independently performed at least three times and analyzed by the two-sided Student's *t*-test. Differences were considered statistically significant when the *P* value was lower than 0.05.

### 3. Results

**3.1. ZNRD1 and ZNRD1-AS1 Are Oppositely Regulated by CAP.** In our previous genome-wide methylation analysis, a specific CpG site near the ZNRD1 promoter (-760 from the

transcription start site) was identified to be hypermethylated ( $\Delta\beta = 0.198$ , fold change = 2.152) by CAP in the MCF-7 breast cancer cells [3]. This study was performed to elucidate the mechanism by which CAP regulates the methylation level of CpG and ZNRD1 expression. At first, the CpG was mapped on the chromosome, found to be located 760 bases upstream of the transcription start site of ZNRD1 (Figure 1(a)). Notably, an antisense lncRNA, ZNRD1-AS1, is encoded from the other strand of ZNRD1 with sharing the CpG at its transcript-coding region. ZNRD1 is a zinc ribbon domain-containing protein and is downregulated in a few cancers including esophageal cancer [27] and gastric cancer [28]. ZNRD1-AS1 is the antisense lncRNA of ZNRD1 and is located in the upstream region of the ZNRD1 [29]. Little is known about the function of the lncRNA in the development of cancer, and none is available in breast cancer.

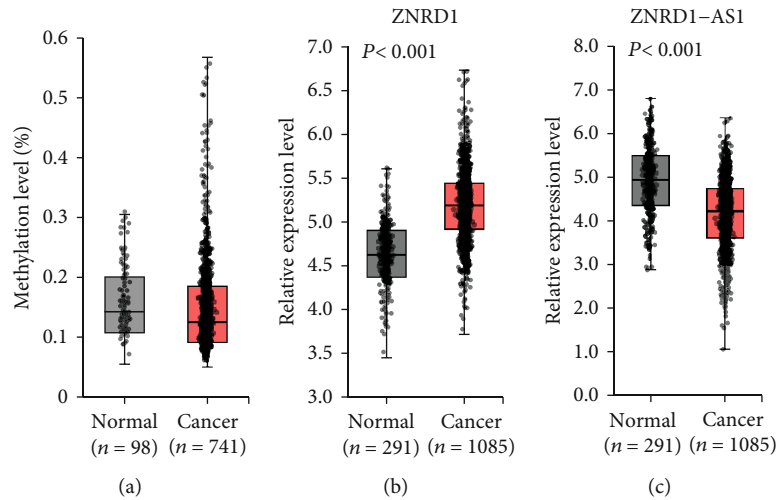


FIGURE 2: DNA methylation and expression profile of ZNRD1 and ZNRD1-AS1 in breast cancer. (a) The methylation level of the specific CpG (CpG ID; cg02078039) at ZNRD1 promoter in breast cancer tissues, which was hypermethylated by CAP in MCF-7, was examined using the data retrieved from the TCGA Wanderer database. No significant difference was found between the normal and cancer tissues. Expression of ZNRD1 (b) and ZNRD1-AS1 (c) was analyzed for tissues in the database GEPIA. Upregulation of ZNRD1 and downregulation of ZNRD1-AS1 were observed in breast cancer tissues. *n*: sample number.

The expression of ZNRD1 after CAP treatment was examined by qPCR. The MCF-7 cells were independently treated six times by CAP. Results showed that ZNRD1 was upregulated by CAP of 600 s, being confirmed in five of six independent experiments (Figure 1(b)). A different CAP energy of 30 s for 10 times with an hour interval was also applied to the cell. Surprisingly, expression of ZNRD1 was rather decreased in the case of the  $10 \times 30$  s treatment, confirmed by four independent experiments (Figure 1(b)). ZNRD1-AS1 also showed an opposite regulation under the two CAP treatment schemes, but surprisingly showing the opposite expression pattern to that of ZNRD1 (Figure 1(c)). The treatment of argon gas only did not induce any significant change of gene expression (Figure S2).

To see any association between the methylation of the CpG and expression of the two genes, the methylation level of the CpG was examined after treatment of MCF-7 with CAP. Results showed that both 600 s and  $10 \times 30$  s CAP induced hypermethylation, although the increased methylation levels were different, with 96.2% increase in 600 s and 38.4% increase in  $10 \times 30$  s (Figure S3). This result indicates that the CpG site does not affect the expression of ZNRD1 and ZNRD1-AS1, although its methylation level is influenced by CAP.

**3.2. ZNRD1 Induces Downregulation of ZNRD1-AS1 with Being Upregulated in Breast Cancer.** The CpG methylation and expression of ZNRD1 and ZNRD1-AS1 were analyzed from the data of normal and cancer tissues, of which information was retrieved at the TCGA Wanderer database and GEPIA database. The methylation level of the CpG did not show a significant difference between the normal breast tissues ( $n = 98$ ) and cancer tissues ( $n = 741$ ) (Figure 2(a)). The expression of ZNRD1 was upregulated in the cancer tissues ( $n = 1,085$ ) compared to the normal tissues ( $n = 291$ ) ( $P < 0.001$ ) (Figure 2(b)). Meanwhile, expression of ZNRD1-AS1 was downregulated in the cancer tissues compared to

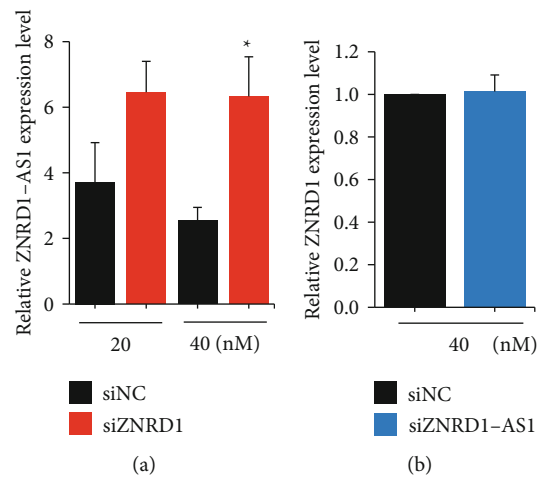


FIGURE 3: ZNRD1 downregulates ZNRD1-AS1 in the MCF-7 cells. Downregulation of ZNRD1 or ZNRD1-AS1 was induced in the MCF-7 cells using siRNA, and their expression was examined by qPCR. (a) Expression of ZNRD1-AS1 after transient transfection of siRNA for ZNRD1 (siZNRD1). (b) Expression of ZNRD1 after transient transfection of siRNA for ZNRD1-AS1 (siZNRD1-AS1). All of the experiments were performed in triplicate, and the values are presented as the mean  $\pm$  SE. \* $P < 0.05$ .

the normal tissues (Figure 2(c)). These results are in parallel with those of the CAP-treated MCF-7 cells, i.e., opposite regulation of the two genes by CAP, but no association with CpG methylation.

To examine whether the opposite expression of ZNRD1 and ZNRD1-AS1 by CAP is due to the regulation by each other, expression of each gene was examined after inhibiting expression of the other using siRNA (Figure S4). A siRNA targeting ZNRD1 induced upregulation of ZNRD1-AS1; however, siRNA targeting ZNRD1-AS1 did not affect the expression of ZNRD1 (Figure 3). This result implies that



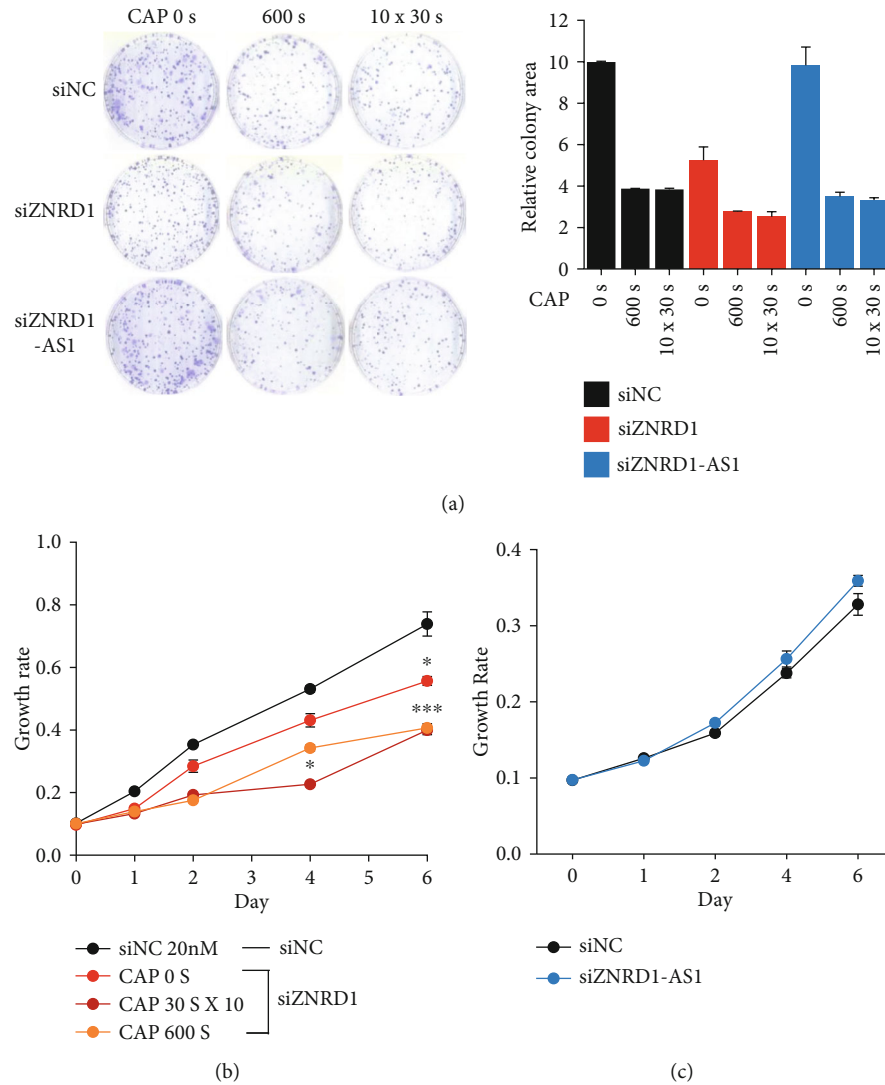


FIGURE 4: ZNRD1 but not ZNRD1-AS1 stimulates proliferation of MCF-7. (a) Either ZNRD1 or ZNRD1-AS1 was downregulated in MCF-7 using siRNA, and cell survival was examined by colony formation assay. Three independent experiments were performed, and representative images are shown. The effect of the siRNA-driven downregulation of ZNRD1 (b) or ZNRD1-AS1 (c) on cell proliferation was examined by CCK-8 assays. The experiments were performed independently at least three times, and the values are presented as the mean  $\pm$  SE. siNC: control siRNA; siZNRD1: siRNA for ZNRD1; siZNRD1-AS1: siRNA for ZNRD1-AS1. \* $P < 0.05$ , \*\*\* $P < 0.001$ .

ZNRD1 is upregulated and downregulated by CAP of 600 s and 10  $\times$  30 s, respectively, and the altered expression accompanies the down- and upregulation of ZNRD1-AS1.

**3.3. ZNRD1 Stimulates Proliferation of MCF-7 Breast Cancer Cells.** Although ZNRD1 and ZNRD1-AS1 were revealed to contribute the development of cancer in a few cancer types, their role in breast cancer remains obscure. To address their contribution to the proliferation of breast cancer cells, each gene was downregulated in MCF-7 using siRNA and cell proliferation was monitored by colony formation assay and a dye-based growth rate assay. As a result, when ZNRD1 was suppressed, less colony formation was observed with being further inhibited by combined CAP treatment (Figure 4(a)). The dye-based growth rate assay also showed the similar inhibition pattern (Figure 4(b)). However, when ZNRD1-AS1 was suppressed, no significant

change of cell proliferation was found in either the colony formation assay or dye-based growth rate assay (Figure 4(a) and 4(c)).

Many lncRNAs have been known to regulate nearby genes in the so-called cis-mode. To identify any cis-genes regulated by ZNRD1-AS1, expressions of five cis-genes were examined by qPCR after suppressing ZNRD1-AS1 using siRNA (Figure 5(a)). As a result, four genes were upregulated while one gene was slightly downregulated (Figure 5(b)). Notably, expression of the cis-genes was reversed when ZNRD1 was suppressed by siRNA, supporting our observation that ZNRD1-AS1 is downregulated by ZNRD1 (Figure 5(c)). Furthermore, CAP treatment for 600 s and 10  $\times$  30 s induced upregulation and downregulation of the four genes, respectively, which showed upregulation when siRNA for ZNRD1-AS1 was treated, although only HCG9 showed statistical significance (Figure 5(d)).

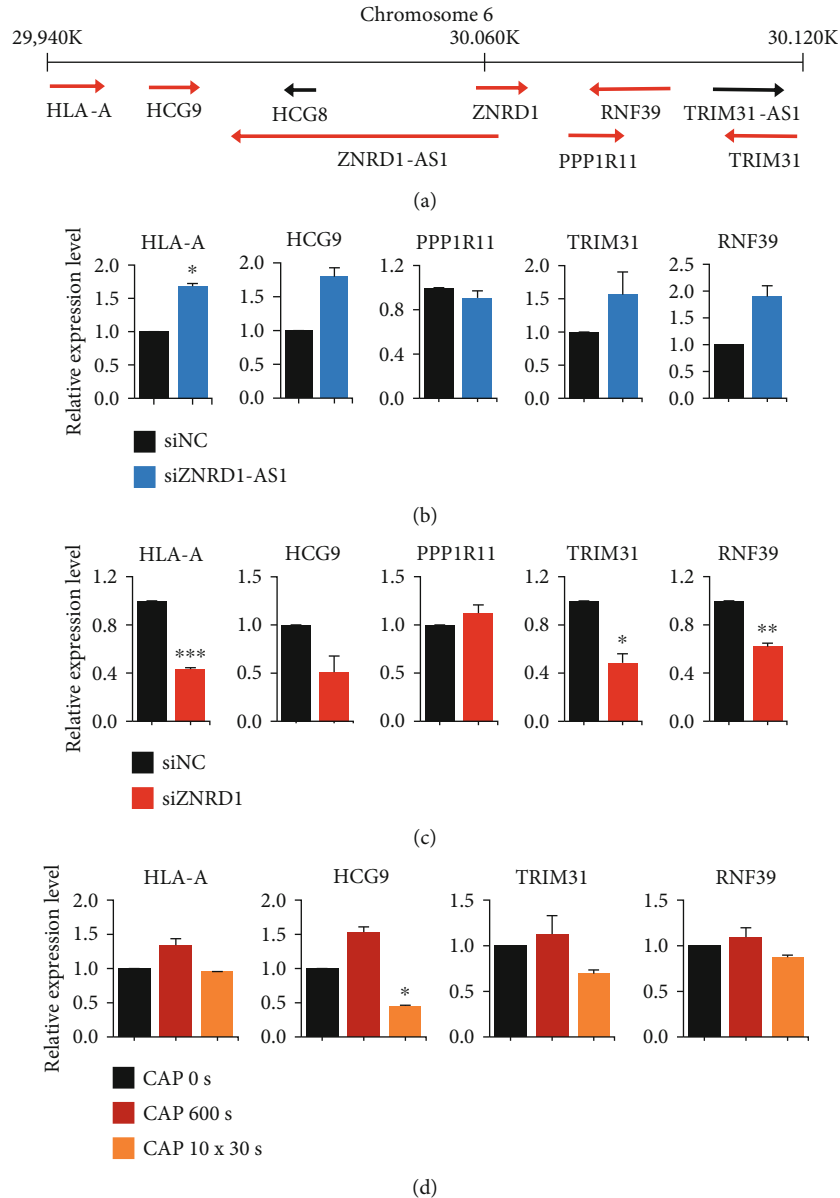


FIGURE 5: The effect of siRNA for ZNRD1-AS1 and CAP on the regulation of cis-genes. (a) A schematic map of the relative position of ZNRD1-AS1 and its nearby cis-genes. The numbers on the horizontal line are the nucleotides of a subfragment on chromosome 6. The arrows indicate the expression direction. The MCF-7 cells were treated with a siRNA for ZNRD1-AS1 (b) or a siRNA for ZNRD1 (c), and the expression levels of the cis-genes were examined using qPCR. (d) The MCF-7 cells were treated with CAP and the expression of the cis-genes was examined using qPCR. All of the experiments were performed independently at least three times, and the values are presented as the mean  $\pm$  SE. \* $P < 0.05$ , \*\* $P < 0.01$ , \*\*\* $P < 0.001$ .

#### 4. Discussion

This study was performed to identify genes that show consistent expression change under independent CAP treatments and thereby to be able to monitor whether CAP is an appropriate treatment to biological targets. Two different CAP treatment conditions induced the opposite expression for ZNRD1 and ZNRD1-AS1. However, the specific CpG at the ZNRD1 promoter (Figure 1) was hypermethylated by the two different CAP treatment conditions in MCF-7 cells. Furthermore, no significant difference of methylation level

between normal and cancer tissues in breast was found (Figure 2). These facts imply that the specific CpG is not responsible for the regulation of ZNRD1 and ZNRD1-AS1. Other CpG(s) or regulatory mechanism than the epigenetic way may be responsible for the regulation of the genes.

Considering the fact that ZNRD1 is oncogenic in breast cancer, the CAP treatment condition of  $10 \times 30$  s is recommended to inhibit the MCF-7 cancer cell growth, because CAP in that condition, rather than 600 s, suppressed ZNRD1. In accordance, a few cis-genes of ZNRD1-AS1, HLA-A, HCG9, TRIM31, and RNF39 were upregulated at 600 s,

but downregulated at the  $10 \times 30$  s CAP treatment. Among the four genes, HLA-A and TRIM31 are known for their association with cancer, but their contribution to cancer development is not the same. Downregulation of HLA-A expression has been known to contribute to a poor prognosis in cancer patients, suggesting its tumor-suppressive activity [30]. TRIM31 is an oncogene promoting proliferation, invasion, and migration of glioma cells through Akt and NF- $\kappa$ B pathways [31, 32]. More accumulation of data is needed to comprehensively understand the contribution of the cis-genes of ZNRD1-AS1 to the tumor development.

A limitation remains for the CAP treatment scheme because the cell growth inhibition appeared at the both CAP conditions. Therefore, it is speculated that just alteration of ZNRD1 and ZNRD1-AS1 is not sufficient to induce cancer cell death. Setting up CAP conditions that include one inhibiting cancer cell growth and another stimulating cell growth would be helpful to establish more reliable marker genes. This seems possible, as low dose of CAP stimulated cancer cell growth in a few cancers, even though CAP induced cancer cell death in the majority of previous studies [33]. Low doses of CAP activated fibroblast proliferation in wound tissue of mouse model, but over doses suppressed wound healing by causing cell death [33]. Another limitation of this work is in the lack of genome-wide expression analysis for the different CAP treatments. ZNRD1 and ZNRD1-AS1 were just selected from a genome-wide methylation array dataset. To further screen marker genes, extensive analysis through a genome-wide approach after treatment of CAP at diverse CAP conditions is required.

For the standardization of CAP, CAP condition, chemical composition of cell culture, media, and cellular responses are key factors, but standardizing these alone is still insufficient. For example, the distance from the outlet of CAP device to the surface of culture media should be also considered. In addition, different cancer cell types represent their unique molecular response. In our previous study, even two cell lines originated from breast tissue, MCF-7 and MDA-MB-231, showed a genome-wide difference of DNA methylation by the same CAP treatment condition [3]. In addition, MCF-10A cells showed the similar expression profile for ZNRD1 and ZNRD1-AS1 by CAP, but T-47D showed the opposite expression at the two CAP conditions in the current study (Figure S5). Nonetheless, the expression profile that ZNRD1-AS1 is downregulated when ZNRD1 is upregulated, and vice versa, has not changed even in T-47D. The standardization becomes further complicated when even a single cell line shows various responses depending with the genetic and physiological status, such as number of subcultures. Therefore, a comprehensive approach is essential for the development of reliable marker genes. Another finding of this study is to have established the regulatory relationship between ZNRD1 and ZNRD1-AS1. A few studies dealt with the expression association between the two genes in cancer, all presenting their opposite expression profile [29, 34]. However, no regulatory pathway has been identified. Our current study indicates that ZNRD1 downregulates ZNRD1-AS1 with no feedback regulation.

## 5. Conclusions

ZNRD1 and its antisense lncRNA ZNRD1-AS1 were revealed to be regulated in opposite ways depending on the CAP treatment conditions. The specific condition of  $10 \times 30$  s was found to suppress the ZNRD1 expression, while the 600 s scheme induced upregulation. A regulatory pathway that CAP regulates ZNRD1, which in turn downregulates ZNRD1-AS1, is suggested. In addition, a few cis-genes of ZNRD1-AS1 were found to be regulated by the lncRNA and CAP. The two genes could contribute to precisely establishing the relationship between the CAP treatment condition and target gene expression.

## Data Availability

All generated and analyzed data used to support the findings of this study are included within the article.

## Conflicts of Interest

The authors declare no conflict of interest.

## Acknowledgments

This work was supported by the Leading Foreign Research Institute Recruitment Program (NRF-2016K1A4A3914113) and the Basic Science Research Program (NRF-2016R1D1A1B01009235) of the National Research Foundation of Korea, funded by the Ministry of Education, Science, and Technology.

## Supplementary Materials

Table S1: specification and electrical characterization of the 90 mm mesh DBD plasma device. Table S2: sequences of primers for qPCR and siRNAs employed in this study. Figure S1: CAP source used in this study. Schematic diagram (a) and voltage-current waveform (b) of the 90 mm mesh DBD plasma device are shown. (c) pH change of culture media after CAP treatment. Figure S2: treatment of argon gas only does not affect the expression of ZNRD1 and ZNRD1-AS1. The MCF-7 cells were treated with only argon gas in the two CAP conditions (600 s and  $10 \times 30$  s), and the expression of ZNRD1 (a) and ZNRD1-AS1 (b) was examined by qPCR. All the experiments were performed in triplicate and the values are presented as the mean  $\pm$  SE. Figure S3: hypermethylation of the CpG at ZNRD1 promoter by CAP treatment to the MCF-7 cells. The effect of CAP on the methylation status of the CpG at the promoter of ZNRD1, which was identified to be hypermethylated from the microarray analysis, was examined by the methylation-specific PCR. All the experiments were performed in triplicate and the values are presented as the mean  $\pm$  SE. \* $P < 0.05$ . Figure S4: optimization of siRNA concentration for the transfection into MCF-7 cells. MCF-7 cells are transiently transfected with a siRNA to induce downregulation of ZNRD1 (a) and ZNRD1-AS1 (b). Downregulation of each gene was judged by qPCR. All the experiments were performed in triplicate and the values are presented as the mean  $\pm$  SE. \*\* $P < 0.01$ , \*\*\* $P < 0.001$ .

Figure S5: effect of CAP on the expression of ZNRD1 and ZNRD1-AS1 in the T-47D and MCF-10A cells. Expression of ZNRD1 (a) and ZNRD1-AS1 (b) was examined in T-47D and MCF-10A cell line by qPCR after CAP treatment of the cells. All the experiments were performed in triplicate and the values are presented as the mean  $\pm$  SE. \* $P < 0.05$ , \*\* $P < 0.01$ , \*\*\* $P < 0.001$ . (Supplementary Materials)

## References

- [1] T. Adachi, H. Tanaka, S. Nonomura, H. Hara, S. Kondo, and M. Hori, "Plasma-activated medium induces A549 cell injury via a spiral apoptotic cascade involving the mitochondrial-nuclear network," *Free Radical Biology & Medicine*, vol. 79, pp. 28–44, 2015.
- [2] M. Keidar, R. Walk, A. Shashurin et al., "Cold plasma selectivity and the possibility of a paradigm shift in cancer therapy," *British Journal of Cancer*, vol. 105, no. 9, pp. 1295–1301, 2011.
- [3] S. B. Park, B. Kim, H. Bae et al., "Differential epigenetic effects of atmospheric cold plasma on MCF-7 and MDA-MB-231 breast cancer cells," *PLoS One*, vol. 10, no. 6, article e0129931, 2015.
- [4] F. Utsumi, H. Kajiyama, K. Nakamura et al., "Effect of indirect nonequilibrium atmospheric pressure plasma on anti-proliferative activity against chronic chemo-resistant ovarian cancer cells in vitro and in vivo," *PLoS One*, vol. 8, no. 12, article e81576, 2013.
- [5] H. Tanaka, M. Mizuno, K. Ishikawa et al., "Plasma-activated medium selectively kills glioblastoma brain tumor cells by down-regulating a survival signaling molecule, AKT kinase," *Plasma Medicine*, vol. 1, no. 3-4, pp. 265–277, 2011.
- [6] J. Liu and Z. Wang, "Increased oxidative stress as a selective anticancer therapy," *Oxidative Medicine and Cellular Longevity*, vol. 2015, Article ID 294303, 12 pages, 2015.
- [7] S. J. Kim and T. H. Chung, "Cold atmospheric plasma jet-generated RONS and their selective effects on normal and carcinoma cells," *Scientific Reports*, vol. 6, no. 1, article 20332, 2016.
- [8] S. Mitra, L. N. Nguyen, M. Akter, G. Park, E. H. Choi, and N. K. Kaushik, "Impact of ROS generated by chemical, physical, and plasma techniques on cancer attenuation," *Cancers*, vol. 11, no. 7, article 1030, 2019.
- [9] J. Körtzner, V. Boxhammer, A. Schäfer et al., "Restoration of sensitivity in chemo-resistant glioma cells by cold atmospheric plasma," *PLoS One*, vol. 8, no. 5, article e64498, 2013.
- [10] S. Arndt, E. Wacker, Y. F. Li et al., "Cold atmospheric plasma, a new strategy to induce senescence in melanoma cells," *Experimental Dermatology*, vol. 22, no. 4, pp. 284–289, 2013.
- [11] L. I. Partecke, K. Evert, J. Haugk et al., "Tissue tolerable plasma (TTP) induces apoptosis in pancreatic cancer cells in vitro and in vivo," *BMC Cancer*, vol. 12, no. 1, p. 473, 2012.
- [12] P. Attri, Y. H. Kim, D. H. Park et al., "Generation mechanism of hydroxyl radical species and its lifetime prediction during the plasma-initiated ultraviolet (UV) photolysis," *Scientific Reports*, vol. 5, no. 1, article 9332, 2015.
- [13] N. K. Kaushik, N. Kaushik, N. N. Linh et al., "Plasma and nanomaterials: fabrication and biomedical applications," *Nanomaterials*, vol. 9, no. 1, p. 98, 2019.
- [14] J. Napp, G. Daeschlein, M. Napp et al., "On the history of plasma treatment and comparison of microbiostatic efficacy of a historical high-frequency plasma device with two modern devices," *GMS Hygiene and Infection Control*, vol. 10, article Doc08, 2015.
- [15] E. Turrini, R. Laurita, A. Stancampiano et al., "Cold atmospheric plasma induces apoptosis and oxidative stress pathway regulation in T-lymphoblastoid leukemia cells," *Oxidative Medicine and Cellular Longevity*, vol. 2017, Article ID 4271065, 13 pages, 2017.
- [16] J. Tornin, M. Mateu-Sanz, A. Rodríguez, C. Labay, R. Rodríguez, and C. Canal, "Pyruvate plays a main role in the antitumoral selectivity of cold atmospheric plasma in osteosarcoma," *Scientific Reports*, vol. 9, no. 1, article 10681, 2019.
- [17] H. Mokhtari, L. Farahmand, K. Yaserian, N. Jalili, and K. Majidzadeh-A, "The antiproliferative effects of cold atmospheric plasma-activated media on different cancer cell lines, the implication of ozone as a possible underlying mechanism," *Journal of Cellular Physiology*, vol. 234, no. 5, pp. 6778–6782, 2019.
- [18] P. Attri, J. H. Park, A. Ali, and E. H. Choi, "How does plasma activated media treatment differ from direct cold plasma treatment?," *Anti-Cancer Agents in Medicinal Chemistry*, vol. 18, no. 6, pp. 805–814, 2018.
- [19] N. Hattori, S. Yamada, K. Torii et al., "Effectiveness of plasma treatment on pancreatic cancer cells," *International Journal of Oncology*, vol. 47, no. 5, pp. 1655–1662, 2015.
- [20] M. Dezest, L. Chavatte, M. Bourdens et al., "Mechanistic insights into the impact of cold atmospheric pressure plasma on human epithelial cell lines," *Scientific Reports*, vol. 7, no. 1, article 41163, 2017.
- [21] D. Yan, J. H. Sherman, and M. Keidar, "Cold atmospheric plasma, a novel promising anti-cancer treatment modality," *Oncotarget*, vol. 8, no. 9, pp. 15977–15995, 2017.
- [22] G. J. Kim, W. Kim, K. T. Kim, and J. K. Lee, "DNA damage and mitochondria dysfunction in cell apoptosis induced by non-thermal air plasma," *Applied Physics Letters*, vol. 96, no. 2, article 021502, 2010.
- [23] A. Schmidt, S. Bekeschus, H. Jablonowski, A. Barton, K. D. Weltmann, and K. Wende, "Role of ambient gas composition on cold physical plasma-elicited cell signaling in keratinocytes," *Biophysical Journal*, vol. 112, no. 11, pp. 2397–2407, 2017.
- [24] N. Kaushik, N. Kumar, C. H. Kim, N. K. Kaushik, and E. H. Choi, "Dielectric barrier discharge plasma efficiently delivers an apoptotic response in human monocytic lymphoma," *Plasma Processes and Polymers*, vol. 11, no. 12, pp. 1175–1187, 2014.
- [25] S. Lee, H. Lee, D. Jeong et al., "Cold atmospheric plasma restores tamoxifen sensitivity in resistant MCF-7 breast cancer cell," *Free Radical Biology and Medicine*, vol. 110, pp. 280–290, 2017.
- [26] C. Guzmán, M. Bagga, A. Kaur, J. Westermarck, and D. Abankwa, "ColonyArea: an ImageJ plugin to automatically quantify colony formation in clonogenic assays," *PLoS One*, vol. 9, no. 3, article e92444, 2014.
- [27] Y. Zhao, L. Hong, R. Wang, and D. Fan, "Expression and prognostic value of ZNRD1 in esophageal squamous cell carcinoma," *Digestive Diseases and Sciences*, vol. 54, no. 3, pp. 586–592, 2009.
- [28] L. Hong, Y. Han, R. Shi et al., "ZNRD1 gene suppresses cell proliferation through cell cycle arrest in G1 phase," *Cancer Biology & Therapy*, vol. 4, no. 1, pp. 67–71, 2014.

- [29] L. Guo, J. Wen, J. Han et al., “Expression quantitative trait loci in long non-coding RNA ZNRD1-AS1 influence cervical cancer development,” *American Journal of Cancer Research*, vol. 5, no. 7, pp. 2301–2307, 2015.
- [30] K. Mimura, K. Shiraishi, A. Mueller et al., “The MAPK pathway is a predominant regulator of HLA-A expression in esophageal and gastric cancer,” *The Journal of Immunology*, vol. 191, no. 12, pp. 6261–6272, 2013.
- [31] L. Zhou, Z. Z. Deng, H. Y. Li et al., “TRIM31 promotes glioma proliferation and invasion through activating NF-kappaB pathway,” *OncoTargets and Therapy*, vol. 12, pp. 2289–2297, 2019.
- [32] P. Guo, X. Ma, W. Zhao et al., “TRIM31 is upregulated in hepatocellular carcinoma and promotes disease progression by inducing ubiquitination of TSC1-TSC2 complex,” *Oncogene*, vol. 37, no. 4, pp. 478–488, 2018.
- [33] G. M. Xu, X. M. Shi, J. F. Cai et al., “Dual effects of atmospheric pressure plasma jet on skin wound healing of mice,” *Wound Repair and Regeneration*, vol. 23, no. 6, pp. 878–884, 2015.
- [34] D. Li, L. Song, Z. Wen et al., “Strong evidence for LncRNA ZNRD1-AS1, and its functional Cis- eQTL locus contributing more to the susceptibility of lung cancer,” *Oncotarget*, vol. 7, no. 24, pp. 35813–35817, 2016.

## Research Article

# IMCA Induces Ferroptosis Mediated by SLC7A11 through the AMPK/mTOR Pathway in Colorectal Cancer

Lei Zhang <sup>1</sup>, Wen Liu,<sup>1</sup> Fangyan Liu,<sup>1</sup> Qun Wang <sup>1</sup>, Mengjiao Song,<sup>1</sup> Qi Yu,<sup>1</sup> Kun Tang,<sup>1</sup> Tieshan Teng <sup>1</sup>, Dongdong Wu,<sup>1</sup> Xijing Wang,<sup>2</sup> Wuqi Han,<sup>3</sup> and Yanzhang Li <sup>1</sup>

<sup>1</sup>Cell Signal Transduction Laboratory, Bioinformatics Center, Laboratory for Nanomedicine, Henan International Joint Laboratory for Nuclear Protein Regulation, School of Basic Medical Sciences, Henan University, Kaifeng 475004, China

<sup>2</sup>Department of Dermatology, Second People's Hospital of Zhengzhou, Zhengzhou 450006, China

<sup>3</sup>Kaifeng Food and Drug Inspection Institute, Kaifeng 475004, China

Correspondence should be addressed to Qun Wang; wangqun011@163.com and Yanzhang Li; yanzhang206@163.com

Received 27 July 2019; Revised 1 December 2019; Accepted 28 January 2020; Published 4 April 2020

Academic Editor: Carlo Gabriele Tocchetti

Copyright © 2020 Lei Zhang et al. This is an open access article distributed under the Creative Commons Attribution License, which permits unrestricted use, distribution, and reproduction in any medium, provided the original work is properly cited.

Ferroptosis, implicated in several diseases, is a new form of programmed and nonapoptotic cell death triggered by iron-dependent lipid peroxidation after inactivation of the cystine/glutamate antiporter system  $x_c^-$ , which is composed of solute carrier family 7 membrane 11 (SLC7A11) and solute carrier family 3 membrane 2 (SLC3A2). Therefore, inducing ferroptosis through inhibiting the cystine/glutamate antiporter system  $x_c^-$  may be an effective way to treat cancer. In previous screening tests, we found that the benzopyran derivative 2-imino-6-methoxy-2H-chromene-3-carbothioamide (IMCA) significantly inhibited the viability of colorectal cancer cells. However, the impact of IMCA on ferroptosis remains unknown. Hence, this study investigated the effect of IMCA on ferroptosis and elucidated the underlying molecular mechanism. Results showed that IMCA significantly inhibited the cell viability of colorectal cancer cells *in vitro* and inhibited tumor growth with negligible organ toxicity *in vivo*. Further studies showed that IMCA significantly induced the ferroptosis of colorectal cancer cells. Mechanistically, IMCA downregulated the expression of SLC7A11 and decreased the contents of cysteine and glutathione, which resulted in reactive oxygen species accumulation and ferroptosis. Furthermore, overexpression of SLC7A11 significantly attenuated the ferroptosis caused by IMCA. In addition, IMCA regulated the activity of the AMPK/mTOR/p70S6k signaling pathway, which is related to the activity of SLC7A11 and ferroptosis. Collectively, our research provided experimental evidences on the activity and mechanism of ferroptosis induced by IMCA and revealed that IMCA might be a promising therapeutic drug for colorectal cancer.

## 1. Introduction

Colorectal cancer (CRC) is a common malignant tumor and an important health problem worldwide. According to the cancer statistics worldwide for 36 cancers in 185 countries in 2018, both sexes combined, colorectal cancer is the third diagnosed cancer (10.2% of the total cases) globally and the second leading cause (10.2% of total cancer deaths) of cancer-related deaths worldwide [1, 2]. Conventional treatment options for cancer include chemotherapy, radiation, and surgery [3]. In addition, new treatment methods, such as biotargeted therapy, immunotherapy, and precise treatment, have been gradually applied for CRC treatment [4,

5]. In order to improve the therapeutic effect, chemotherapy, radiation, and surgery are often used in combination. However, conventional treatments are often associated with serious side effects and toxicity, thus significantly affecting patients' quality of life. In addition, cancer cells have also been found to be able to develop resistance toward chemotherapy and radiotherapy over time. Therefore, it is still an important task for researchers to find new drugs with high efficiency and low side effects for CRC.

The mainly regulated cell deaths are apoptosis, necroptosis, autophagy, ferroptosis, and pyroptosis, which are believed to be critical for development, homeostasis, disease occurrence, and treatment, such as malignant tumors [6–8].

Identified as a new mode of programmed cell death in 2012, ferroptosis is a unique iron-reliant and reactive oxygen species- (ROS-) dependent form of nonautophagic and nonapoptotic programmed cell death [6, 9]. Mitochondrial morphological change is characterized by decreased or vanished mitochondria cristae, a ruptured outer mitochondrial membrane, and a condensed mitochondrial membrane in ferroptotic cells [7, 9]. The small molecule erastin induces ferroptosis through inhibiting the import of cystine, which is decomposed into two molecules of cysteine (Cys), resulting in glutathione (GSH) exhaustion and inactivation of the phospholipid peroxidase glutathione peroxidase 4 (GPX4) [8, 10]. GPX4 reduces the toxic lipid hydroperoxides (L-OOH) to the nontoxic lipid alcohols (L-OH) by oxidizing GSH to glutathione disulfide (GSSG) [8, 11]. Cystine, one of the raw materials for the synthesis of the major antioxidant GSH, is transported to the intracellular space through transporting glutamate to the extracellular space by a heterodimeric cystine/glutamate antiporter system  $xc^-$ , which is mainly composed of a twelve-pass transmembrane catalytic subunit solute carrier family 7 member 11 (SLC7A11) and a single-pass transmembrane anchoring protein solute carrier family 3 member 2 (SLC3A2) [7, 12]. Pharmacological inhibition of the system  $xc^-$ -reliant antioxidant defense system leads to ROS accumulation and ferroptosis, such as erastin, sulfasalazine, and sorafenib [7].

2-Imino-6-methoxy-2H-chromene-3-carbothioamide (IMCA) is a benzopyran derivative, with a wide variety of biological activities for the treatment of cancer, type 2 diabetes, inflammation, skin diseases, Alzheimer's disease (AD), the polycystic kidney disease, and viral and bacterial infections [13]. We report for the first time that IMCA inhibits the viability of medullary thyroid cancer through inducing apoptosis [14]. In the course of studying the anti-CRC effect of IMCA, we found for the first time that IMCA leads to the death of CRC cells.

In the current study, two types of CRC cell lines and xenograft model were utilized to evaluate the anti-CRC effects and the mechanism of IMCA. The effects of IMCA on the biological phenotype of CRC cells were examined, and the underlying molecular mechanisms of IMCA-induced ferroptosis were elucidated. Mechanistically, we found that IMCA downregulated the expression of SLC7A11 and decreased the contents of Cys and glutathione, which resulted in ROS accumulation and ferroptosis. Furthermore, overexpression of SLC7A11 significantly attenuated ferroptosis caused by IMCA through downregulating the expression of SLC7A11. In addition, IMCA regulated the activity of the AMPK/mTOR/p70S6k signaling pathway, which is related to the activity of SLC7A11 and ferroptosis. For the first time, we found a novel small-molecule compound against CRC and demonstrated that IMCA induced ferroptosis mediated by SLC7A11 through the AMPK/mTOR pathway in CRC.

## 2. Materials and Methods

**2.1. Cell Lines and Cell Culture.** Human CRC cell lines DLD-1 and HCT-116 were purchased from a typical cell culture

collection committee of the Chinese Academy of Sciences Library (Shanghai, China). These cells were grown in Roswell Park Memorial Institute 1640 (Gibco, 11875119) medium containing 10% heat-inactivated fetal bovine serum (Gibco, 16000-044), 100 U/mL penicillin and 100  $\mu$ g/mL streptomycin (Solarbio, P1400), and 5% CO<sub>2</sub> at 37°C. The solvent dimethyl sulfoxide (DMSO) used in the experiments was less than 0.1%.

**2.2. Chemicals and Reagents.** IMCA was purchased from Tao Su Biochemical Technology Co. Ltd. (AE-848/32005043, Shanghai, China). GPX4, glutathione synthetase (GSS), and SLC7A11 antibodies were purchased from Proteintech Co. Ltd. (Wuhan, China). PCR primers were designed and synthesized by Sangon Biotech Co. Ltd. (Shanghai, China). The SYBR green PCR Master Mix was purchased from Thermo Scientific (Waltham, MA, USA). MTT cell proliferation and cytotoxicity detection kit, ROS detection kit, GSH detection kit, GSSG detection kit, and Cys detection kit were purchased from Solarbio Co. Ltd. (Beijing, China).

**2.3. Cell Viability Assay.** IMCA cytotoxicity was detected with the MTT cell proliferation and cytotoxicity detection kit in accordance with the manufacturer's instructions. In brief, DLD-1 and HCT-116 cells were seeded into 96-well cell culture plates with  $5 \times 10^3$  cells per well and cultured continuously for 12 h. Different intervention reagents were added to the cultural plates and cultured continuously for 48 h. A 10  $\mu$ L MTT solution (10 mg/mL in PBS) was added to the cultural plates and cultured continuously for 4 h. Then, 100  $\mu$ L of DMSO was added to the cultural plates and the absorbance of the samples was measured using a multifunctional enzyme marker (Varioskan Flash, Thermo Scientific) at the wave length of 570 nm.

**2.4. ROS Analysis.** ROS was detected with the ROS detection kit in accordance with the manufacturer's instructions. Briefly, DLD-1 and HCT-116 cells were seeded into 6-well cell culture plates with  $2 \times 10^5$  cells per well and cultured continuously for 12 h. Different intervention reagents were added to the cultural plates and cultured continuously for 48 h.

**2.4.1. Detection with Multifunctional Enzyme Marker.** Cells were harvested and washed once with PBS. The harvested cells were suspended in DCFH-DA, diluted 1000 times in serum-free medium, and incubated for 20 min. Subsequently, the cells were washed three times with serum-free medium and were then detected with a multifunctional enzyme marker (Varioskan Flash, Thermo Scientific) at the excitation wavelength of 488 nm and emission wavelength of 525 nm.

**2.4.2. Detection by Confocal Microscopy.** As previously described [15], the cells were washed once with PBS, incubated in DCFH-DA, and diluted 1000 times in serum-free medium for 20 min. Then, the cells were washed three times with serum-free medium and detected via confocal microscopy (A1R+Storm, Nikon).

TABLE 1: The PCR primers.

CHAC1 reverse	5'-CCTGATGTCCACATGAGCACTCC-3'
CHAC1 forward	5'-ACCTTGAATACTTGCTGCGTCTGG-3'
PTGS2 reverse	5'-CCTGCTTGTCTGGAACAACACTGCTC-3'
PTGS2 forward	5'-TGGTCTGGTGCCTGGTCTGATG-3'
GPX4 reverse	5'-GCAGCCGTTCTTGTCGATGAGG-3'
GPX4 forward	5'-CCGCTGTGGAAGTGATGAAGATC-3'
GSS reverse	5'-AGCCTTCGGTCTTGGTCCAGAG-3'
GSS forward	5'-CCAGCGTGCCATAGAGAATGAGC-3'
SLC7A11 forward	5'-GGCTCCATGAACGGTGGTGTG-3'
SLC7A11 reverse	5'-GCTGGTAGAGGAGTGTGCTTGC-3'
$\beta$ -Actin forward	5'-CATGTACGTTGCTATCCAGGC-3'
$\beta$ -Actin reverse	5'-CTCCTTAATGTCACGCACGAT-3'

**2.5. Cys Analysis.** Cys was detected with the Cys detection kit according to the manufacturer's instructions. Briefly, DLD-1 and HCT-116 cells were seeded into 6-well cell culture plates with  $2 \times 10^5$  cells per well and cultured continuously for 12 h. Different intervention reagents were added to the cultural plates and cultured continuously for 48 h. The cells were crushed by ultrasound and centrifuged at 8000 g for 10 min. Then, 100  $\mu$ L of the supernatant, 500  $\mu$ L of reagent I, and 500  $\mu$ L of reagent II were mixed and detected with a multifunctional enzyme marker (Varioskan Flash, Thermo Scientific) at the wavelength of 600 nm.

**2.6. GSH Analysis.** GSH was detected with the GSH detection kit in accordance with the manufacturer's instructions. Briefly, DLD-1 and HCT-116 cells were seeded into 6-well cell culture plates with  $2 \times 10^5$  cells per well and cultured continuously for 12 h. Different intervention reagents were added to the cultural plates and cultured continuously for 48 h. Cells were harvested and washed twice with PBS. The cells were resuspended in reagent I and frozen and thawed three times with liquid nitrogen. A 20  $\mu$ L supernatant from the cell suspension centrifuged at 8000 rpm was mixed with 140  $\mu$ L of reagent II and 40  $\mu$ L of reagent III and detected with a multifunctional enzyme marker (Varioskan Flash, Thermo Scientific) at the wavelength of 412 nm.

**2.7. qRT-PCR Assay.** As previously described [16], total RNA was extracted using Trizol reagent in accordance with the manufacturer's instructions. mRNA was reversed transcribed into cDNA with the PrimeScript RT reagent kit (Takara, DRR047A) in a 20  $\mu$ L reaction system. qPCR analysis was conducted with on an ABI 7500 Fast Real-Time PCR System (Applied Biosystems, Waltham, MA, USA). The PCR primers are listed in Table 1.

**2.8. Western Blot Analysis.** As previously described [17], protein expression was determined by Western blot in accordance with standard protocols. Briefly, cells were harvested

and lysed in RIPA buffer with a protease inhibitor. Cell lysates were quantitated with a Bradford reagent, separated with a denatured sodium dodecyl sulfate 4%-20% polyacrylamide gel electrophoresis (SDS-PAGE), and transferred onto a polyvinylidene fluoride (PVDF) membrane through wet electroblotting. The PVDF membrane was blocked with dried skimmed milk and incubated with primary antibodies specific for GPX4, GSS, and SLC7A11. A HRP-conjugated secondary antibody was incubated at room temperature for 2 h, and the blot analysis was visualized with a chemiluminescence analyzer (Amersham Biosciences, Boston, MA, USA).

**2.9. Overexpression of SLC7A11.** The recombinant overexpression plasmid of SLC7A11 was constructed by Hanbio Technical Co., Ltd. (Shanghai, China). The overexpression plasmid of SLC7A11 was transfected into DLD-1 and HCT-116 cells by Lipofectamine 3000 and P3000 to produce SLC7A11-overexpressing transient cell lines. After 48 h of transfection, the cells were collected and transfection efficiency was determined using Western blot.

**2.10. In Vivo Experiments.** As previously described [18], the animal experiments involved in this project have been approved by the Medical and Scientific Research Ethics Committee of Henan University School of Basic Medical Sciences. Five-week-old female BALB/c nude mice were purchased from Beijing Weitong Lihua Experimental Animal Technical Co., Ltd. (Beijing, China).  $10^5$  DLD-1 cells suspended in normal saline were injected subcutaneously into nude mice. The volume of tumors was calculated using the following formula:  $L$  (the long diameter)  $\times W$  (the short diameter)  $\times W \times 1/2$ . The mice were randomly assigned to the treatment and control groups until the tumor size reached approximately 100 mm<sup>3</sup>. The mice in the treatment group were injected with 0.174 mg/mL IMCA (100  $\mu$ L), and those in the control group were injected with an equal volume of normal saline. The nude mice were euthanized, and samples were obtained from their tumor, heart, hepar, kidney, and blood after 33 days of IMCA treatment. The serum was separated, and alanine aminotransferase and urea nitrogen were determined using the animal specific automatic biochemical analyzer (Catalyst Dx, IDEXX, Maine, USA) to evaluate the effects of IMCA on liver and kidney functions. Blood was obtained, and the number of blood cells was determined by an animal hematology analyzer (BC-5000 vet, Mindray, Shenzhen, China) to evaluate the effect of IMCA on blood routine. Organ index was calculated by dividing organ mass by body weight and multiplying by 100% to evaluate the effect of IMCA on organs.

**2.11. Transmission Electron Microscopy.** DLD-1 and HCT-116 cells were seeded into 6-well cell culture plates with  $2 \times 10^5$  cells per well and cultured continuously for 12 h. Different intervention reagents were added to the cultural plates and cultured continuously for 48 h. Cells were harvested and fixed in 2% glutaraldehyde. Samples were treated and detected in the electron microscopy room of Xi'an Jiaotong University.



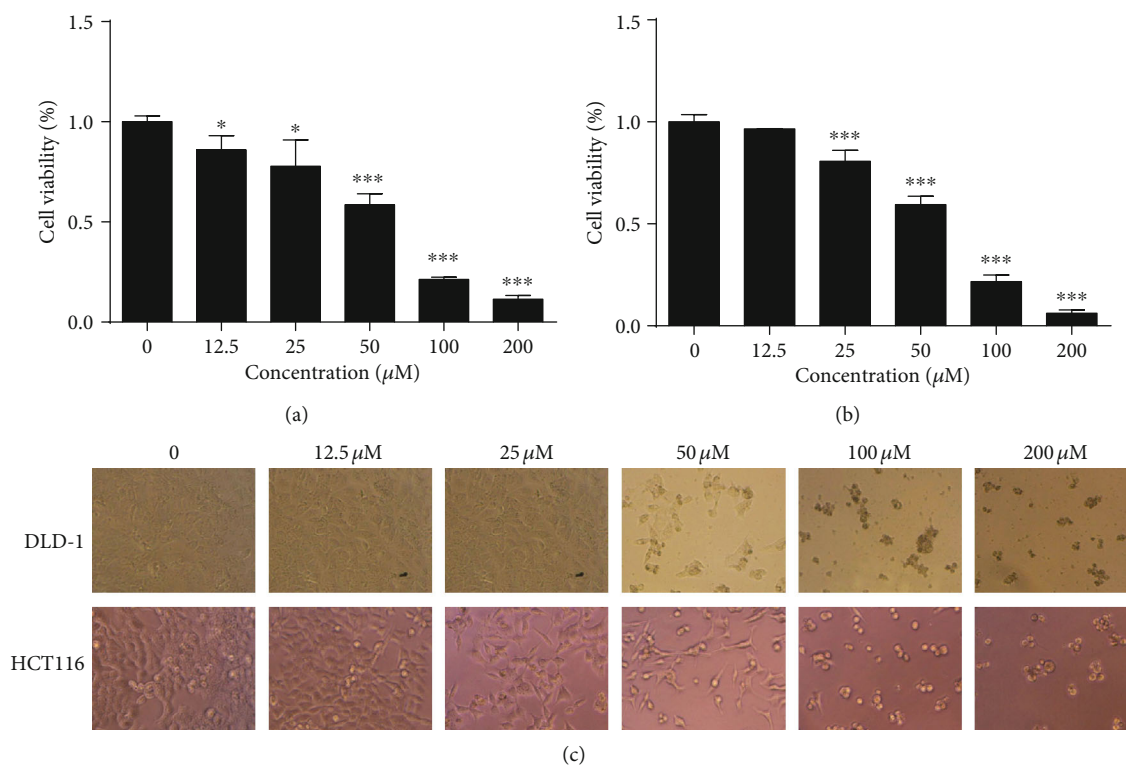


FIGURE 1: IMCA reduced the viability of CRC cell lines. Human CRC cell lines DLD-1 and HCT-116 were treated with different concentrations of IMCA (12.5–200  $\mu\text{M}$ ) for 48 h. The cell viability was determined by the MTT assay kit at 48 h. Results showed that IMCA significantly reduced the viability of DLD-1 (a) and HCT116 (b) in a dose-dependent manner *in vitro*. The values of viability were expressed as mean  $\pm$  standard deviation. (c) The cell morphology treated with different concentrations of IMCA (12.5–200  $\mu\text{M}$ ) for 48 h was photographed under an inverted microscope. \* $p < 0.05$ ; \*\*\* $p < 0.001$ .

**2.12. Statistical Analysis.** All statistical analyses were completed by SPSS16.0. The statistical difference between the treatment and control groups of IMCA was analyzed by Student's *t*-test.

### 3. Results

**3.1. IMCA Reduced the Viability of CRC Cell Lines.** The cell viability of human CRC cell lines DLD-1 and HCT116 treated with different concentrations of IMCA for 48 h was determined using the MTT method to confirm the inhibition efficiency of IMCA on the proliferation of CRC cell lines. The viability of the two CRC cell lines significantly reduced in a dose-dependent manner compared with that of the control cells (Figures 1(a) and 1(b)). The IC<sub>50</sub> values of IMCA for DLD-1 and HCT116 cells were 50.2  $\mu\text{M}$  and 44.5  $\mu\text{M}$ , respectively. The cell morphology was photographed with an inverted microscope (Figure 1(c)). Compared with the control group cells, the CRC cells treated with IMCA for 48 h were characterized by shattered, metamorphous, and multi-directional cell morphology. The above results showed that IMCA significantly reduced the viability of CRC cell *in vitro*.

**3.2. IMCA Inhibited the Growth of Xenograft In Vivo.** Since we observed a significantly inhibitory effect of IMCA on CRC cell viability, we next dissected the antitumor effects of

IMCA using the BALB/c nude mouse xenografts bearing DLD-1 cells *in vivo*. As shown in Figures 2(a) and 2(b), the tumor volume and weight in the IMCA-treated group mice dramatically reduced and the inhibition rate reached 76.4% compared with those in the saline negative control group. We monitored the body weight of nude mice every three days during the treatment period to determine the impact of IMCA on the health of the mice. The nude mice did not significantly lose weight during the entire treatment period compared with the control group (Figure 2(c)). For health measurements, we also measured liver and kidney function index, organ index, and blood routine, including alanine aminotransferase (ALT), blood urea nitrogen (BUN), heart index, liver index, kidney index, red blood cells (RBC), white blood cells (WBC), lymphocytes (Lym), and monocytes (Mon) (Figures 2(d)–2(g)). The results showed that no significant health figure changes were observed. To further assess the toxicity of IMCA on healthy animals, nontumor-bearing nude mice were injected with equal doses of IMCA and normal saline through the tail vein, and the body weight of nude mice was monitored every three days during the treatment period. Results showed that IMCA did not significantly affect the weight gain of nude mice, compared with the normal saline groups (Figures 2(h) and 2(i)). There were no significant changes in liver, kidney, heart, and spleen indices, compared with the normal saline groups (Figure 2(j)).

Collectively, the above data indicate that IMCA significantly inhibits tumor growth with negligible organ toxicity *in vivo*.

**3.3. IMCA Induced ROS-Mediated Ferroptosis of CRC Cell Lines.** Ferroptosis is a unique iron-reliant and nonapoptotic form of programmed cell death, which is characterized by ROS accumulation induced by lipid peroxidation and ineffective GPX4 [19, 20]. In order to determine the cause that cell viability was inhibited by IMCA, human CRC cell lines DLD-1 and HCT-116 were treated with different concentrations of IMCA (12.5–200  $\mu\text{M}$ ) with or without iron chelator DFO, ferroptosis inhibitor Ferrostatin-1, or apoptosis inhibitor z-Vad-FMK for 48 h. Results showed that both DFO and Ferrostatin-1 rescued the cell viability induced by IMCA, while z-Vad-FMK failed to rescue the cell viability induced by IMCA (Figures 3(a)–3(f)). To further establish the impact of IMCA on ferroptosis, we next sought to determine the ROS accumulation induced by IMCA using a confocal microscope and a multifunctional microplate reader. Results showed that IMCA significantly induced ROS accumulation at a concentration of 50  $\mu\text{M}$  for 48 h in DLD-1 and HCT116 cells (Figures 3(g)–3(i)). The morphological changes of ferroptosis were mainly characterized by membrane thickening, mites disappearing, and rupture of the mitochondria [6]. To establish the impact of IMCA on mitochondrial morphology, we next examined the mitochondrial morphology of the cells treated with IMCA under a transmission electron microscope. Results showed that IMCA significantly induced the disappearance of mitochondrial crista at a concentration of 50  $\mu\text{M}$  in DLD-1 cells (Figures 3(l)–3(m)). Gene expression markers associated with cells undergoing ferroptosis include increases in CHAC1 and PTGS2 mRNA expression [21–23]. IMCA significantly induced the mRNA expression of CHAC1 and PTGS2 at a concentration of 50  $\mu\text{M}$  in DLD-1 and HCT116 cells (Figures 3(j)–3(k)). Collectively, these data suggest that IMCA induces CRC cell ferroptosis *in vitro*.

**3.4. IMCA Inhibited the Expression of SLC7A11 In Vitro.** Ferroptosis is characterized by the accumulation of ROS, which is scavenged by GPX4 through conversion of reduced GSH into the oxidized form GSSG [24–26]. Therefore, the expression of GPX4 and the GSH level were explored and we found that IMCA significantly reduced GSH levels with negligible impact on the expression of GPX4 in DLD-1 and HCT116 cells (Figures 4(a) and 4(b); Fig. S1). GSH is synthesized from glutamate, Cys, and glycine by the ATP-dependent catalysis of glutathione synthetase (GSS) [27]. The rate of GSH synthesis is primarily limited by the Cys content [28]. The expression of GSS and the Cys level were determined to elucidate the mechanism of GSH reduction triggered by IMCA. Results showed that IMCA significantly reduced Cys levels with negligible impact on the expression of GSS in DLD-1 and HCT116 cells with negligible changes in the expression of GSS (Figures 4(c)–4(h)). The heterodimeric cystine/glutamate antiporter system  $\text{xc}^-$  transports Cys into the intracellular space to synthesize GSH, which inhibited ferroptosis. SLC7A11 is the catalytic subunit of system  $\text{xc}^-$  [29]. The expression of SLC7A11 was determined to dissect the mecha-

nism by which IMCA triggers Cys reduction. Results showed that IMCA significantly reduced the expression of SLC7A11 in DLD-1 and HCT116 cells (Figures 4(i)–4(m)). Collectively, these data suggest that IMCA induces CRC cell ROS accumulation and ferroptosis by downregulating SLC7A11 expression, inhibiting Cys transport and reducing GSH synthesis *in vitro*.

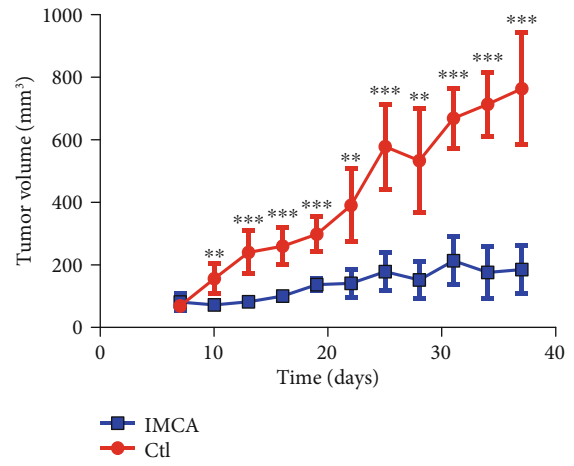
**3.5. Overexpression of SLC7A11 Rescues IMCA-Induced Ferroptosis of CRC Cells In Vitro.** SLC7A11 plays an important role in regulating ROS-mediated ferroptosis. Knocking down the expression of SLC7A11 results in elevated levels of endogenous ROS levels. Overexpression of SLC7A11 results in a cancer stem cell phenotype that contributes to severe chemoresistance [30, 31]. SLC7A11-overexpressing DLD-1 and HCT116 CRC cells were generated. Cys, GSH, ROS, and cell viability were detected, and results showed that the overexpression of SLC7A11 significantly rescued the IMCA-induced reduction of Cys, GSH, and cell viability and increased the ROS levels in SLC7A11-overexpressing DLD-1 and HCT116 CRC cells (Figures 5(a) and 5(b)). Collectively, these data suggest that SLC7A11 inhibits the ferroptosis induced by IMCA.

**3.6. IMCA Inhibits mTOR/P70S6K Activity through Phosphorylating AMPK.** AMPK phosphorylation at Thr172 blocks the activity of SLC7A11, which inhibits the activity of system  $\text{xc}^-$  to transport cystine into cells and eventually leads to ferroptosis [12, 32]. As expected, the present studies showed that IMCA promoted the phosphorylation of AMPK in DLD-1 and HCT116 cells (Figures 6(a) and 6(b)). AMPK activation inhibits mTOR activity, which counteracts the elevated expression of SLC7A11 induced by APR246 and the protective cellular responses, and eventually results in cell death [33–35]. Furthermore, our results showed that the phosphorylation of mTOR and the downstream target protein P70S6K had been significantly decreased by 50  $\mu\text{M}$  IMCA treatment in DLD-1 and HCT116 cells.

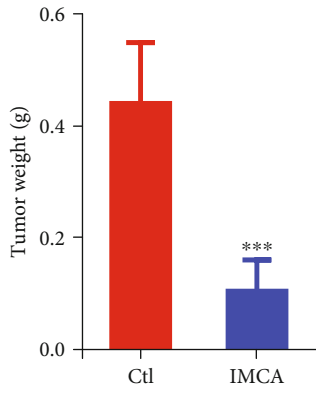
## 4. Discussion

Chemotherapy is increasingly used in CRC as a complementary treatment strategy for CRC after surgery [36, 37]. In consideration of the high morbidity and mortality of CRC [2], new therapeutic drugs with high efficiency and low side effects for CRC must be developed. The present study showed that IMCA significantly inhibited the viability of human CRC cell lines DLD-1 and HCT116 (Figure 1). Further *in vivo* experiments showed that IMCA significantly inhibited the growth of xenograft and did not significantly affect the main organ index and blood biochemical parameters, such as aspartate transaminase (AST) and urea nitrogen (BUN). *In vitro* and *in vivo* results revealed that IMCA may be an effective drug candidate for CRC.

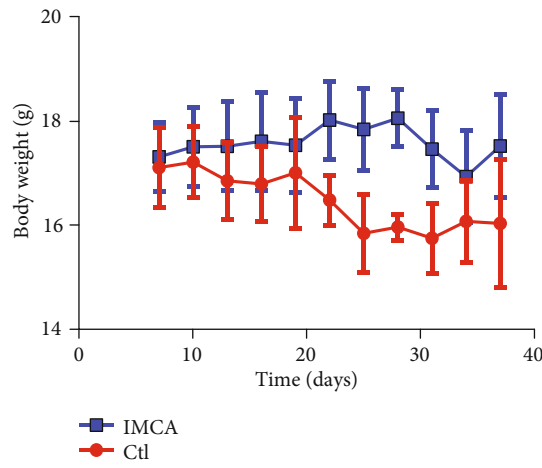
IMCA is a benzopyran derivative, provided with a wide variety of biological activities, including regulating cell death by ferroptosis execution [38]. For example, benzopyran derivative vitamin E hydroquinone is an endogenous regulator of ferroptosis [38]. Further transcript profile



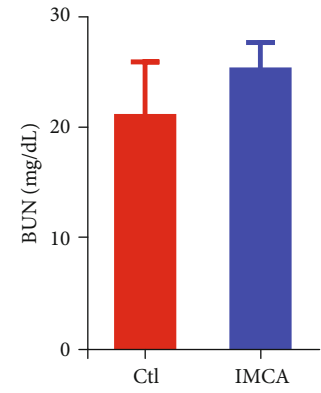
(a)



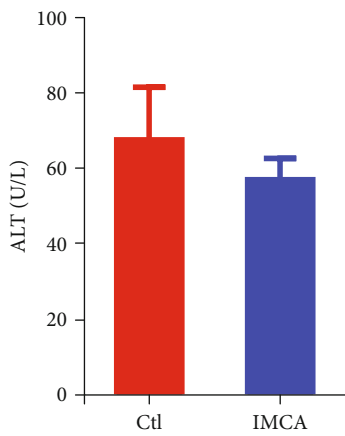
(b)



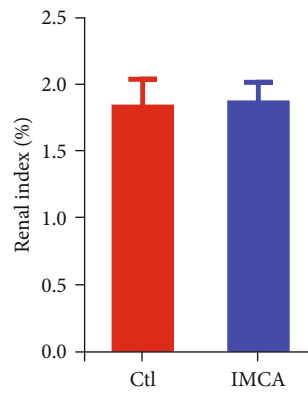
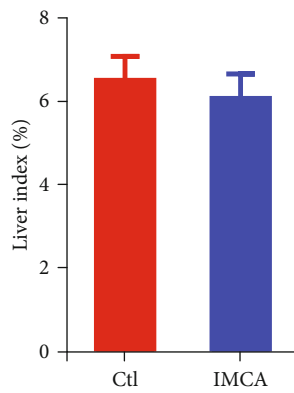
(c)



(d)



(e)



(f)

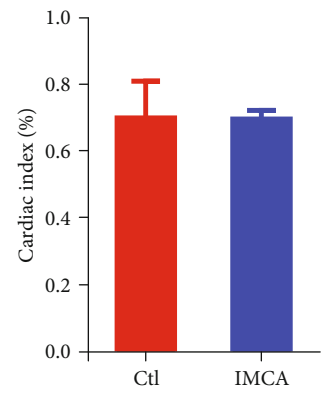


FIGURE 2: Continued.

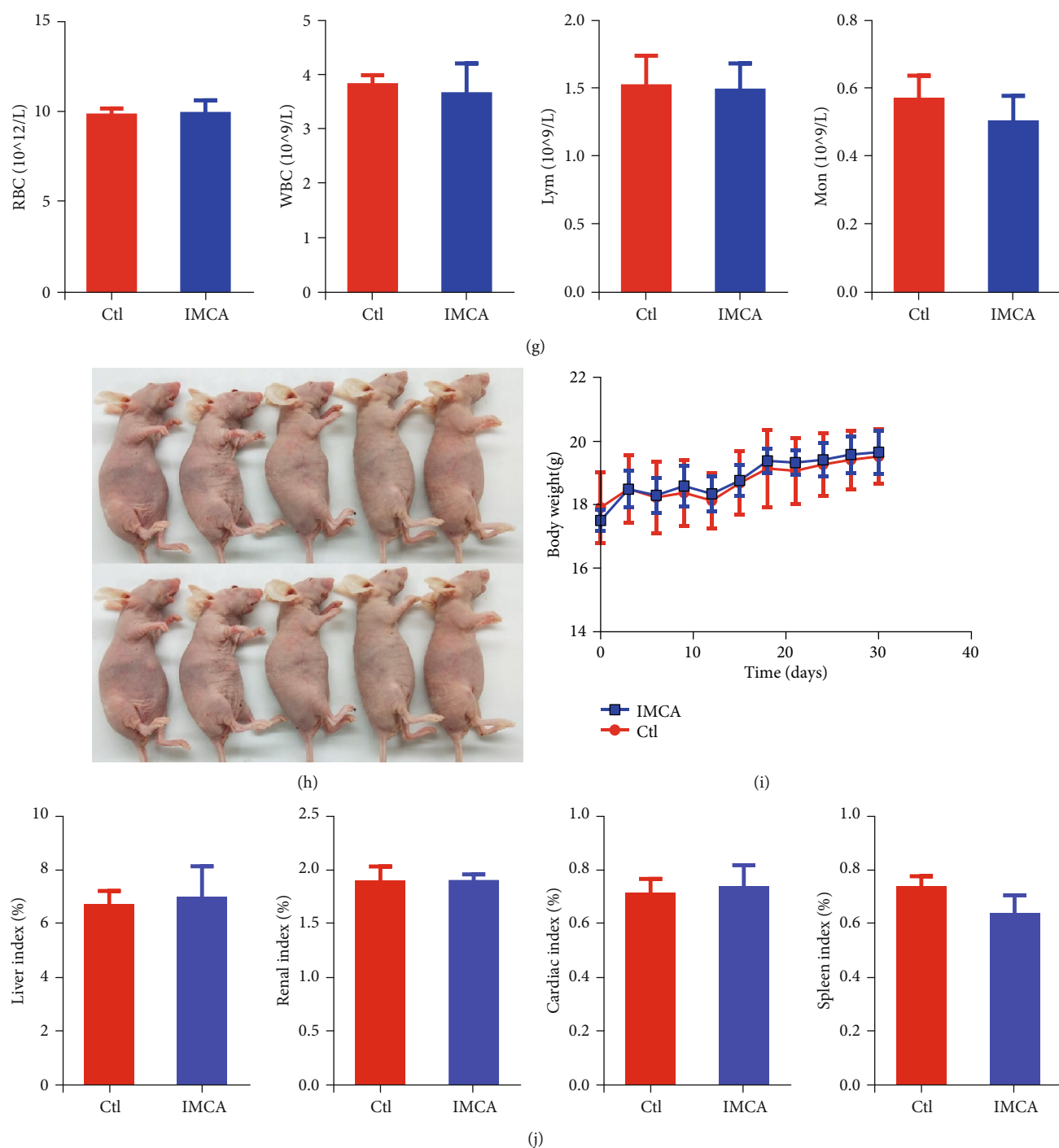
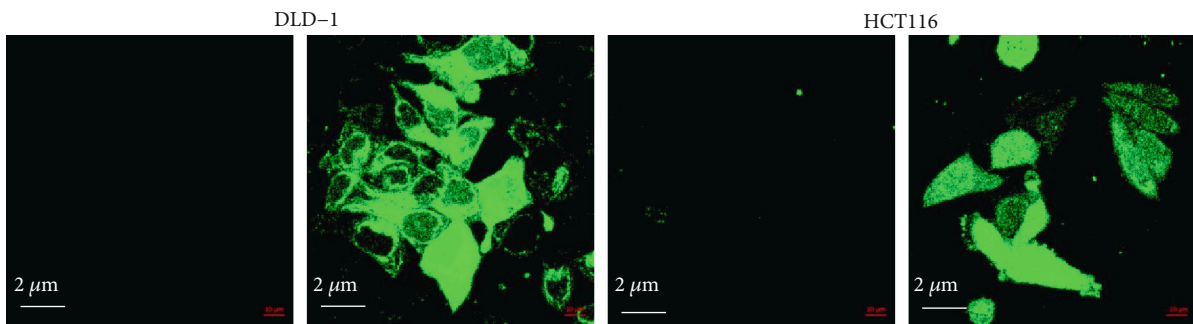
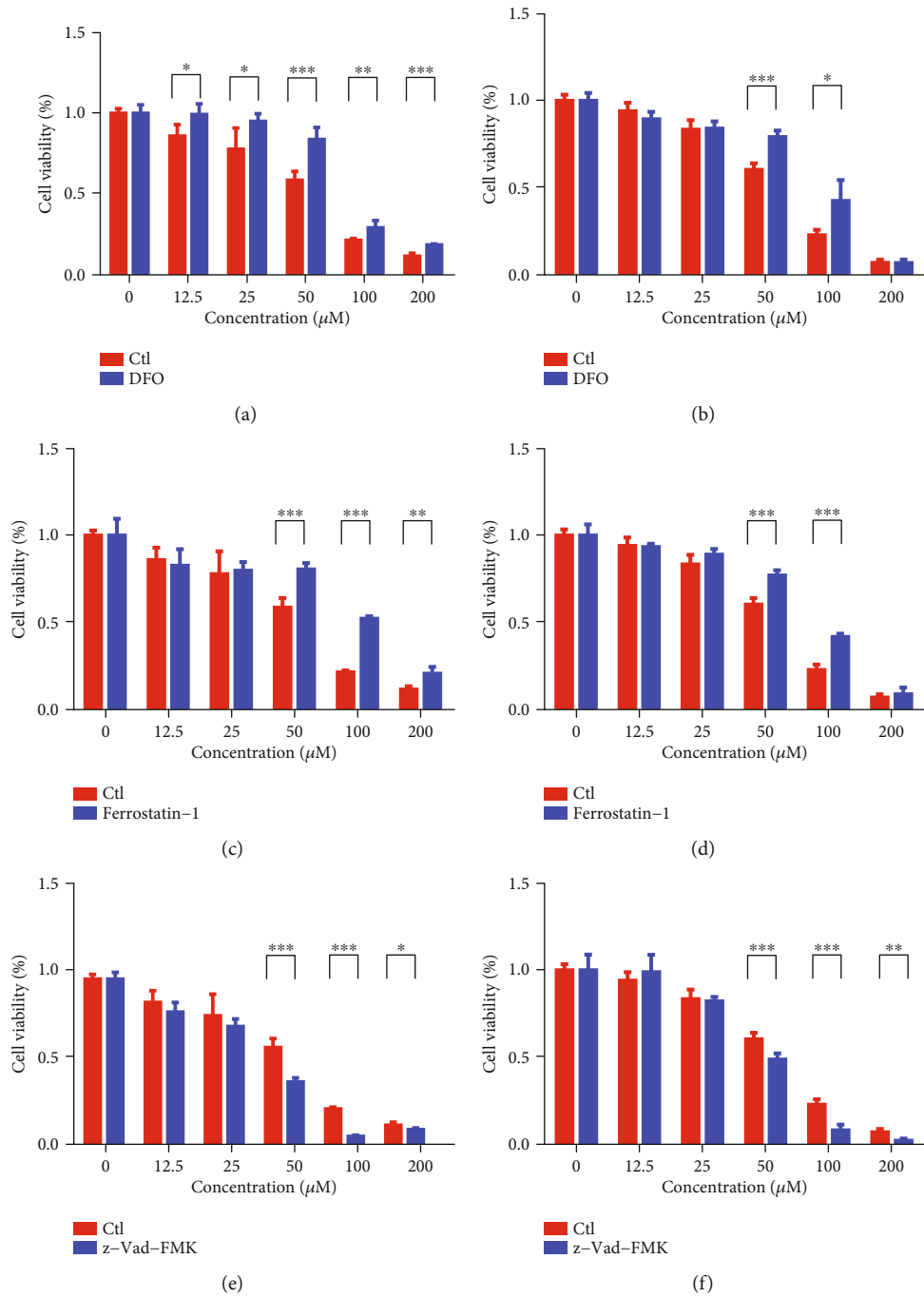


FIGURE 2: IMCA inhibited the growth of xenograft *in vivo*. (a) Representative photographs of tumor-bearing nude mice and tumor volume changes of mice in the experimental period. (b) Tumor weight was determined and compared between the IMCA treatment and control groups. (c) Body weight changes of mice in the experimental period. BUN (d) and ALT (e) were determined and compared between the IMCA treatment and control groups. (f) Liver, renal, and cardiac indices were determined and compared between IMCA treatment groups and controls. (g) RBC, WBC, Lym, and Mon contents were determined and compared between IMCA treatment and control groups. (h) Representative photographs of nontumor-bearing nude mice. (i) Body weight changes of nontumor-bearing nude mice in the experimental period. (j) Liver, renal, cardiac, and spleen indices were determined and compared between the IMCA treatment and control groups. \*\* $p < 0.01$ ; \*\*\* $p < 0.001$ .

analysis showed that IMCA-regulated CRC cell death was associated with ferroptosis-related gene expression. Ferroptosis is a new form of nonautophagic and nonapoptotic

programmed cell death characterized by the accumulation of lethal ROS and decreased or vanished mitochondria cristae [6, 10, 39]. Our results were consistent with the



(g)

FIGURE 3: Continued.

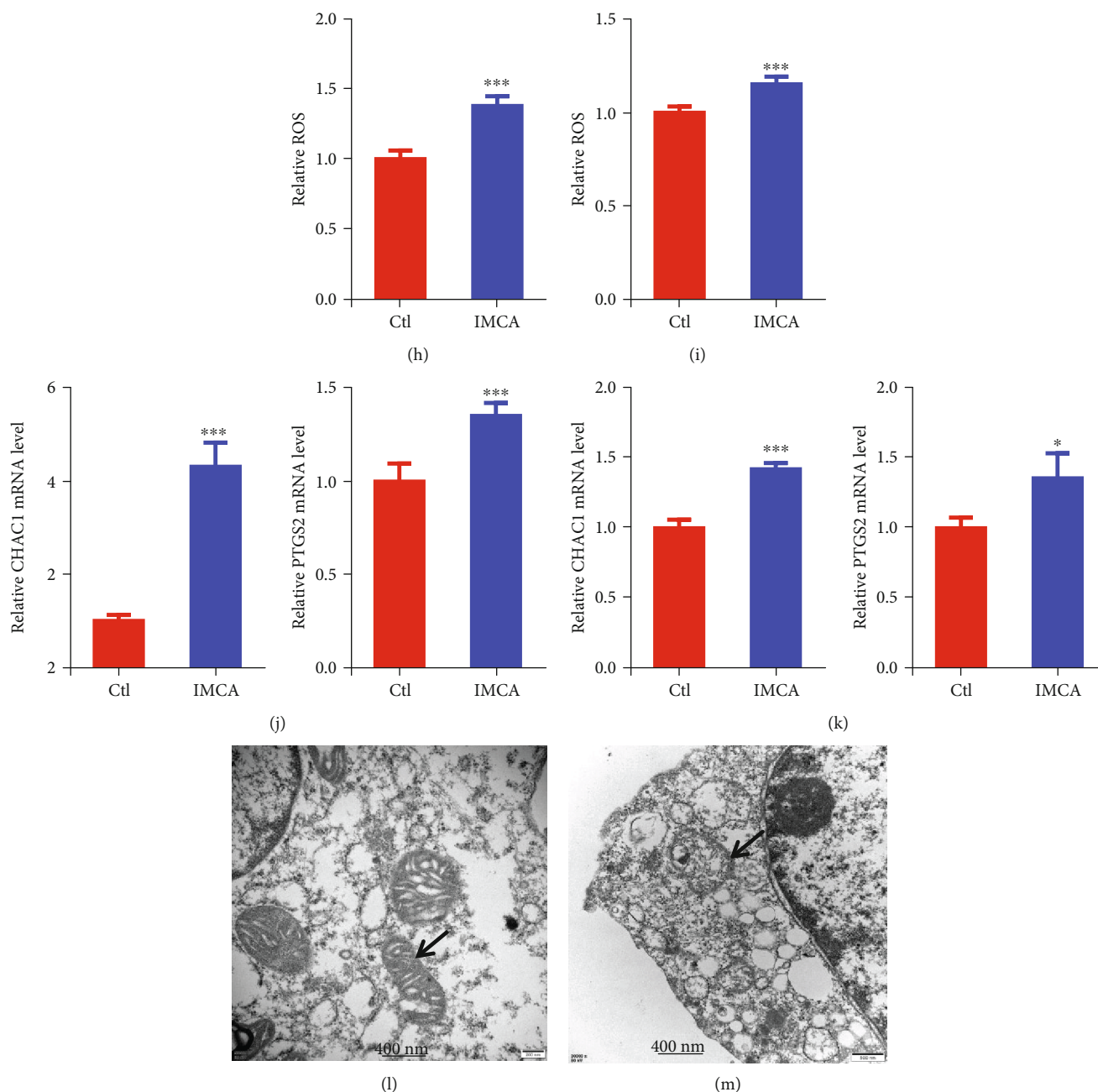


**FIGURE 3:** IMCA induced the ROS-mediated ferroptosis of CRC cell lines *in vitro*. Human CRC cell lines DLD-1 and HCT-116 were treated with different concentrations of IMCA (12.5–200  $\mu\text{M}$ ) with or without DFO, Ferrostatin-1, and z-Vad-FMK for 48 h. The cell viability was determined by the MTT assay kit at 48 h. Results showed that iron chelator DFO (0.2  $\mu\text{M}$ ) rescued the cell viability inhibited by IMCA in DLD-1 (a) and HCT116 (b) cell lines. The cell viability was also rescued by ferroptosis inhibitor Ferrostatin-1 (2  $\mu\text{M}$ ) in DLD-1 (c) and HCT116 (d) cell lines. The results also showed that apoptosis inhibitor z-Vad-FMK (3  $\mu\text{M}$ ) did not rescue the cell viability inhibited by IMCA in DLD-1 (e) and HCT116 (f) cell lines. (g) Confocal laser scanning microscope images of ROS generation were obtained and compared between the IMCA treatment and control groups in DLD-1 and HCT116 cells. Relative ROS accumulation was determined with a multifunctional enzyme marker in DLD-1 (h) and HCT116 (i) cells. Relative mRNA expression of ferroptosis markers CHAC1 and PTGS2 was determined and compared between the IMCA treatment and control groups in DLD-1 (j) and HCT116 (k) cells. Transmission electron microscopy images of mitochondrial morphology were obtained and compared between the IMCA treatment groups (m) and control groups (l) in DLD-1 cells. The black tip points to mitochondria. \* $p < 0.05$ ; \*\* $p < 0.01$ ; \*\*\* $p < 0.001$ .

characteristics of ferroptosis, which showed that IMCA at 50  $\mu\text{M}$  significantly promoted the ROS accumulation and induced the disappearance of mitochondria in DLD-1 and

HCT116 cells. Increased mRNA expression of CHAC1 and PTGS2 is considered a marker of ferroptosis cell death [8, 40]. Consistent with the characteristics of ferroptosis,

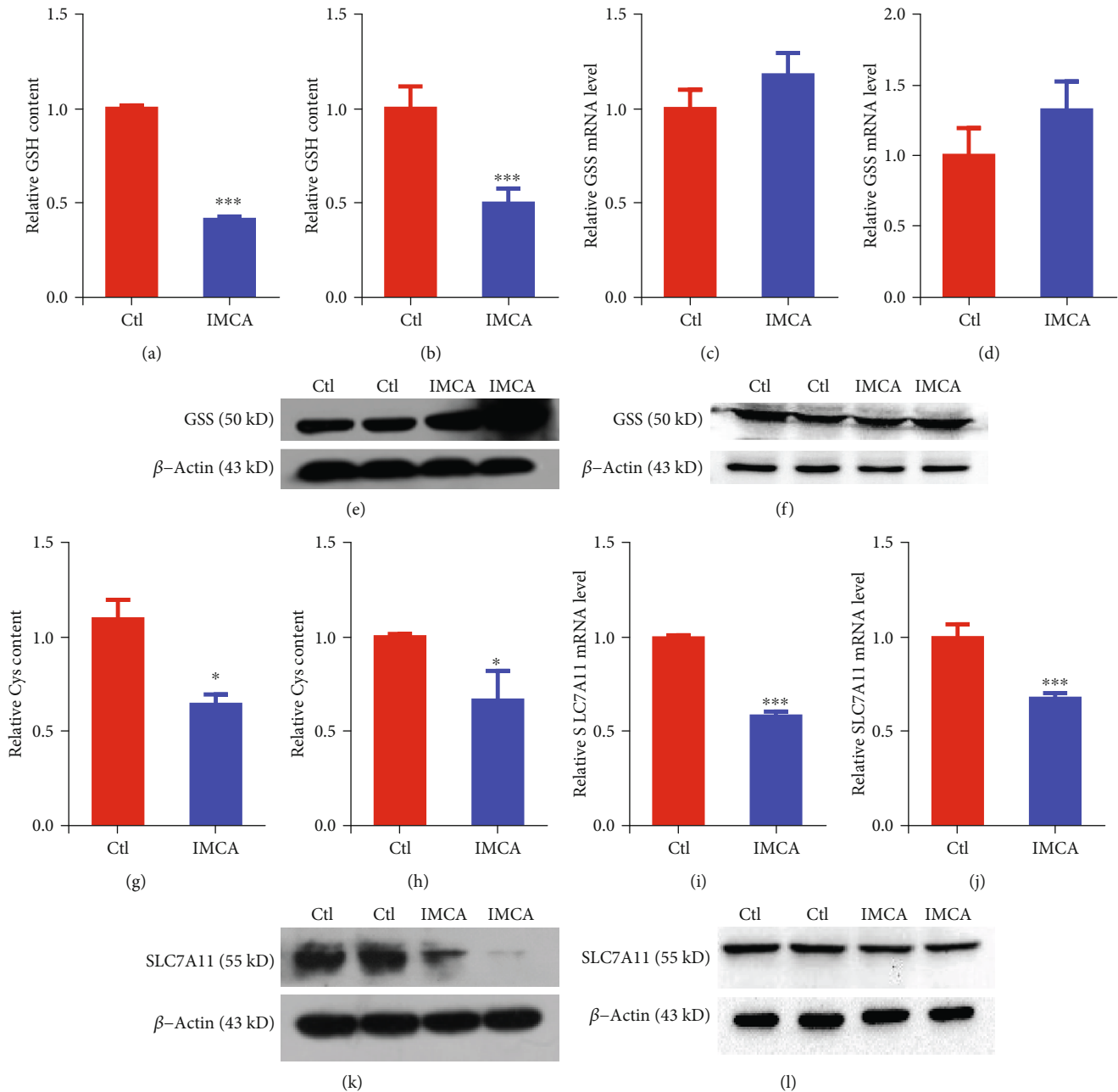


FIGURE 4: IMCA inhibited the expression of SLC7A11. The relative GSH contents were determined and compared between the IMCA treatment and control groups in DLD-1 (a) and HCT116 (b) cells. Relative mRNA expression of GSS was determined and compared between the IMCA treatment and control groups in DLD-1 (c) and HCT116 (d) cells. Relative protein expression of GSS was determined and compared between the IMCA treatment and control groups in DLD-1 (e) and HCT116 (f) cells. The relative Cys contents were determined and compared between the IMCA treatment and control groups in DLD-1 (g) and HCT116 (h) cells. Relative mRNA expression of SLC7A11 was determined and compared between the IMCA treatment and control groups in DLD-1 (i) and HCT116 (j) cells. Relative protein expression of SLC7A11 was determined and compared between the IMCA treatment and control groups in DLD-1 (k) and HCT116 (l) cells. \* $p < 0.05$ ; \*\* $p < 0.01$ ; \*\*\* $p < 0.001$ .

our results showed that IMCA at  $50 \mu\text{M}$  significantly promoted the mRNA expression of CHAC1 and PTGS2 in DLD-1 and HCT116 cells. Overall, our results provided evidence that IMCA causes cell death through ferroptosis.

GSH is a momentous intracellular antioxidant that acts as a reducing substrate of GPX4 to mitigate the accumula-

tion of ROS and protect cells from oxidative damage [7, 41]. Results showed that IMCA at  $50 \mu\text{M}$  significantly reduced the content of GSH in DLD-1 and HCT116 cells. One of the committed substrates used to synthesize GSH catalyzed by GSS is Cys, which has limited intracellular content owing to neurotoxicity [42–44]. Cys should be

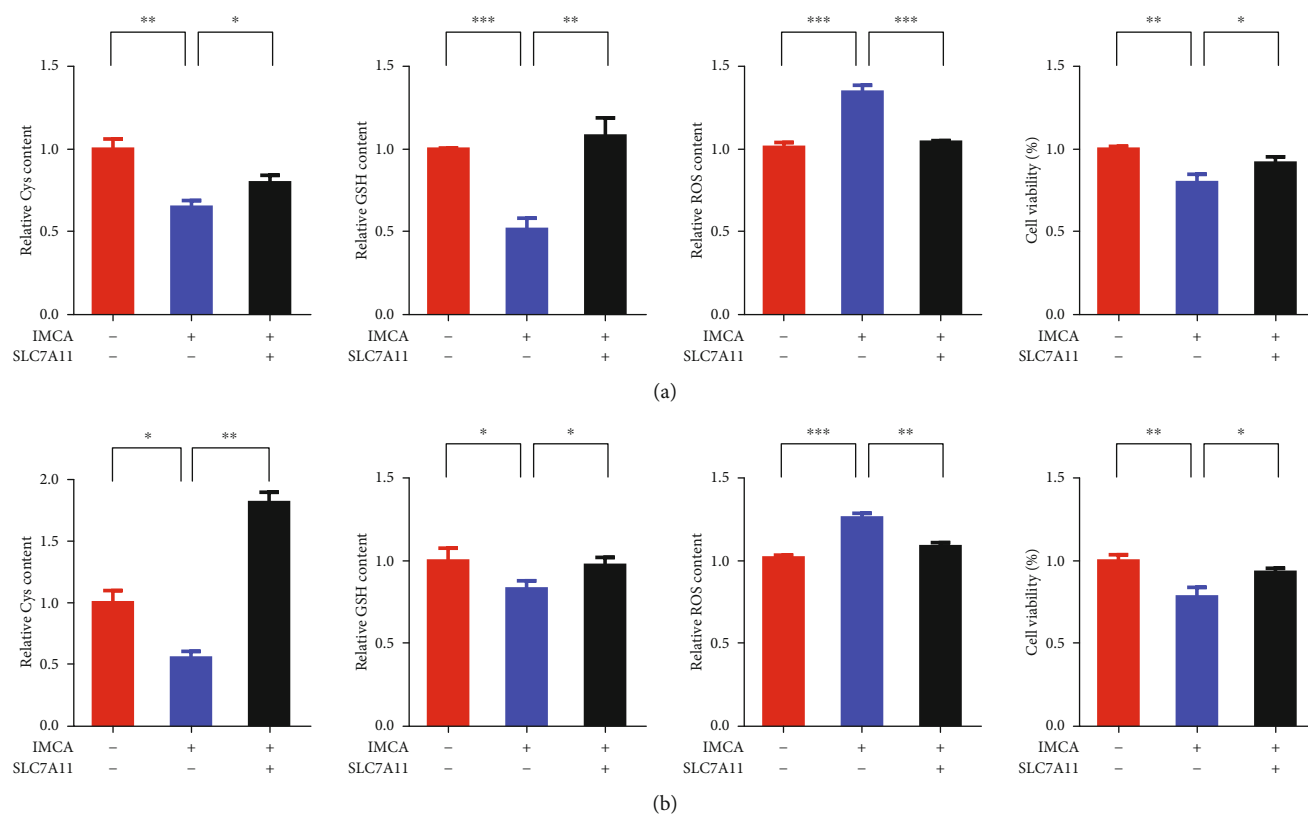


FIGURE 5: The overexpression of SLC7A11 rescues IMCA-induced CRC cell ferroptosis *in vitro*. Overexpression of SLC7A11 restored the decrease of Cys and glutathione content, the increase of ROS, and the decrease of cell viability induced by IMCA in DLD-1 (a) and HCT116 (b) cells.

supplemented extracellularly to ensure that sufficient GSH is synthesized to protect cells from oxidative damage. Cys is derived from the decomposition of cystine, which is imported into the cells through the cystine/glutamate antiporter system  $xc^-$  [45, 46]. Inhibition of system  $xc^-$  significantly depletes the intracellular Cys, retards GSH synthesis, and eventually results in ferroptosis [47]. Erastin [6], sulfasalazine [48], sorafenib [6], Artesunate [49], Lanperisone [50], and Piperazine erastin [10] are the most investigated inhibitors targeting system  $xc^-$  and inducing ferroptosis. In the present study, IMCA did not significantly downregulate GSS expression but depleted the intracellular Cys. These results revealed that IMCA depleted the intracellular Cys and GSH and induced ferroptosis. We overexpressed SLC7A11 in DLD-1 and HCT116 cell lines to determine the role of SLC7A11 in ferroptosis induced by IMCA. We next determined the effect of SLC7A11 overexpression on cell Cys, GSH, and ROS amounts and cell viability regulated by IMCA in DLD-1 and HCT116 cells. As a result, overexpression of SLC7A11 recovered the Cys and GSH depleted by IMCA and inhibited the ROS levels enhanced by IMCA. Ultimately, overexpression of SLC7A11 restored the viability of DLD-1 and HCT116 cells inhibited by IMCA at  $50 \mu\text{M}$ . Taken together, our results provide a novel mechanism that IMCA induces cell death by ferroptosis through downregulating the expression of SLC7A11.

As a central energy metabolic switch, AMP-activated protein kinase (AMPK) exerts a paramount effect in cellular physiology and the pathological development of chronic diseases including cancer [51]. The activity of SLC7A11 is inhibited by AMPK phosphorylation through phosphorylating BECN1, which plays distinct roles in regulating cell ferroptosis [12, 32]. In addition, the activity of SLC7A11 is inhibited by the mTORC pharmacological inhibitor rapamycin, which counteracts the elevated expression of SLC7A11 induced by APR246 and the protective cellular responses, leading to cell death [34]. Consistent with these two mechanisms, DHA induces the lethal ROS accumulation and ferroptosis of leukemia cells through the AMPK/mTOR pathway [25]. The present study showed that IMCA at  $50 \mu\text{M}$  induced AMPK phosphorylation activation, mTOR dephosphorylation inhibition, and ultimately lethal ROS accumulation and ferroptosis in DLD-1 and HCT116 cells. Therefore, the SLC7A11 downregulation and ferroptosis induced by IMCA are related to the AMPK/mTOR pathway.

This study discovered a novel small-molecule compound (IMCA) for CRC treatment *in vitro* and *in vivo*, and elucidated that IMCA induces ferroptosis by downregulating SLC7A11 expression through the AMPK/mTOR pathway. These results provided a new therapeutic potential compound for CRC and new insights to induce ferroptosis.



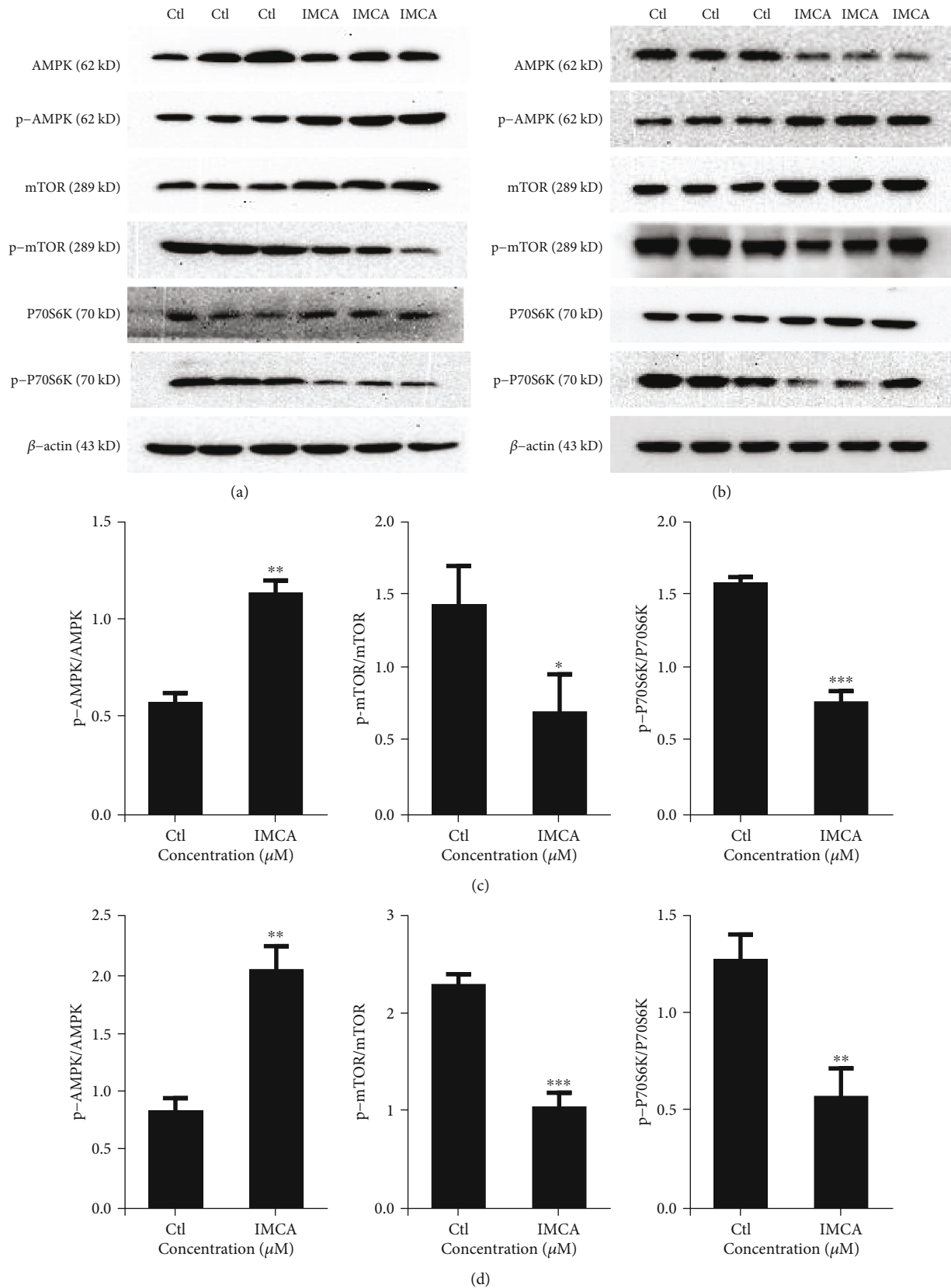


FIGURE 6: IMCA inhibited the mTOR/P70S6K activity through phosphorylating AMPK. DLD-1 (a) and HCT116 (b) cells were treated with 50  $\mu$ M IMCA for 48 h, and the protein expression was assessed by Western blot. The intensities of the p-AMPK, p-mTOR, and p-P70S6K bands were quantified by densitometry analyses and normalized by the amount of AMPK, mTOR, and P70S6K in DLD-1 (c) and HCT116 (d) cells, respectively ( $n = 3$ ). \* $p < 0.05$ , \*\* $p < 0.01$ , and \*\*\* $p < 0.001$  compared with the control group.

## Data Availability

All the data can be obtained from the corresponding authors.

## Disclosure

None of the contents of this manuscript has been previously published or is under consideration elsewhere.

## Conflicts of Interest

The authors declare no conflict of interest.

## Authors' Contributions

L.Z., Q.W., and Y.L. participated in the conception and design of the study. L.Z. wrote most of the manuscript. W.L. and F. L. assisted with the cell culture and animal experiments. M.S., Q.Y., K.T., and T.T. assisted with all other experiments. D.W., X.J., and W.H. assisted with the statistical design and data analysis. Q.W. and Y.L. revised the manuscript. All the authors read and approved the final version of the manuscript prior to submission.

## Acknowledgments

This work is supported by the National Natural Science Foundation of China (Nos. 81803573, 81870591, and 81872023), China Postdoctoral Science Foundation (No. 2018M640672), and Key R&D and Promotion Projects in Henan Province (Nos. 202102310155 and 192102310156).

## Supplementary Materials

Figure S1: IMCA did not significantly upregulate GPX4 expression. DLD-1 (a) and HCT116 (b) cells were treated with 50  $\mu$ M IMCA for 48 h, and the protein expression was assessed by Western blot. Figure S2: schematic illustration of IMCA for colorectal cancer therapy through inducing ferroptosis mediated by SLC7A11. The small molecule IMCA induces ferroptosis through downregulating the expression of SLC7A11, inhibiting the import of cystine, which resulted in glutathione (GSH) exhaustion. The downregulated expression of SLC7A11 is related to the phosphorylation of AMPK and dephosphorylation mediated by IMCA. (*Supplementary Materials*)

## References

- [1] K. El Kinany, M. M. S. Deoula, Z. Hatime et al., "Consumption of modern and traditional Moroccan dairy products and colorectal cancer risk: a large case control study," *European Journal of Nutrition*, vol. 59, no. 3, pp. 953–963, 2019.
- [2] F. Bray, J. Ferlay, I. Soerjomataram, R. L. Siegel, L. A. Torre, and A. Jemal, "Global cancer statistics 2018: GLOBOCAN estimates of incidence and mortality worldwide for 36 cancers in 185 countries," *CA: a Cancer Journal for Clinicians*, vol. 68, no. 6, pp. 394–424, 2018.
- [3] K. E. Wong, S. C. Ngai, K. G. Chan, L. H. Lee, B. H. Goh, and L. H. Chuah, "Curcumin nanoformulations for colorectal cancer: a review," *Frontiers in Pharmacology*, vol. 10, p. 152, 2019.
- [4] M. M. Yallapu, M. Jaggi, and S. C. Chauhan, "Curcumin nanomedicine: a road to cancer therapeutics," *Current Pharmaceutical Design*, vol. 19, no. 11, pp. 1994–2010, 2013.
- [5] J. Sandhu, V. Lavingia, and M. Fakhri, "Systemic treatment for metastatic colorectal cancer in the era of precision medicine," *Journal of Surgical Oncology*, vol. 119, no. 5, pp. 564–582, 2019.
- [6] S. J. Dixon, K. M. Lemberg, M. R. Lamprecht et al., "Ferroptosis: an iron-dependent form of nonapoptotic cell death," *Cell*, vol. 149, no. 5, pp. 1060–1072, 2012.
- [7] Y. Xie, W. Hou, X. Song et al., "Ferroptosis: process and function," *Cell Death and Differentiation*, vol. 23, no. 3, pp. 369–379, 2016.
- [8] B. R. Stockwell, J. P. Friedmann Angeli, H. Bayir et al., "Ferroptosis: a regulated cell death nexus linking metabolism, redox biology, and disease," *Cell*, vol. 171, no. 2, pp. 273–285, 2017.
- [9] Y. Mou, J. Wang, J. Wu et al., "Ferroptosis, a new form of cell death: opportunities and challenges in cancer," *Journal of Hematology & Oncology*, vol. 12, no. 1, p. 34, 2019.
- [10] W. S. Yang, R. SriRamaratnam, M. E. Welsch et al., "Regulation of ferroptotic cancer cell death by GPX4," *Cell*, vol. 156, no. 1–2, pp. 317–331, 2014.
- [11] F. Ursini, M. Maiorino, M. Valente, L. Ferri, and C. Gregolin, "Purification from pig liver of a protein which protects liposomes and biomembranes from peroxidative degradation and exhibits glutathione peroxidase activity on phosphatidylcholine hydroperoxides," *Biochimica et Biophysica Acta*, vol. 710, no. 2, pp. 197–211, 1982.
- [12] X. Song, S. Zhu, P. Chen et al., "AMPK-Mediated BECN1 Phosphorylation Promotes Ferroptosis by Directly Blocking System Xc<sup>-</sup> Activity," *Current Biology*, vol. 28, no. 15, pp. 2388–2399.e5, 2018.
- [13] C. Xiu, Z. Hua, B. S. Xiao, W. J. Tang, H. P. Zhou, and X. H. Liu, "Novel benzopyran derivatives and their therapeutic applications: a patent review (2009–2016)," *Expert Opinion on Therapeutic Patents*, vol. 27, no. 9, pp. 1031–1045, 2017.
- [14] L. Zhang, W. Liu, Q. Wang et al., "New drug candidate targeting the 4A1 orphan nuclear receptor for medullary thyroid cancer therapy," *Molecules*, vol. 23, no. 3, p. 565, 2018.
- [15] M. Chen, K. Li, H. Li, C. P. Song, and Y. Miao, "The Glutathione Peroxidase Gene Family in *Gossypium hirsutum*: Genome-Wide Identification, Classification, Gene Expression and Functional Analysis," *Scientific Reports*, vol. 7, no. 1, article 44743, 2017.
- [16] L. Q. Chai, J. H. Meng, J. Gao, Y. H. Xu, and X. W. Wang, "Identification of a crustacean  $\beta$ -1,3-glucanase related protein as a pattern recognition protein in antibacterial response," *Fish & Shellfish Immunology*, vol. 80, pp. 155–164, 2018.
- [17] X. S. Cheng, M. S. Li, J. du et al., "Neuronal apoptosis in the developing cerebellum," *Anatomia, Histologia, Embryologia*, vol. 40, no. 1, pp. 21–27, 2011.
- [18] H.-B. Yu, D.-Y. Li, H.-F. Zhang et al., "Resveratrol inhibits invasion and metastasis of hepatocellular carcinoma cells," *Journal of Animal and Veterinary Advances*, vol. 9, no. 24, pp. 3117–3124, 2010.
- [19] H. Imai, M. Matsuoka, T. Kumagai, T. Sakamoto, and T. Koumura, "Lipid peroxidation-dependent cell death regulated by GPX4 and ferroptosis," *Current Topics in Microbiology and Immunology*, vol. 403, pp. 143–170, 2017.
- [20] W. S. Yang and B. R. Stockwell, "Ferroptosis: death by lipid peroxidation," *Trends in Cell Biology*, vol. 26, no. 3, pp. 165–176, 2016.

- [21] M. S. Chen, S. F. Wang, C. Y. Hsu et al., "CHAC1 degradation of glutathione enhances cystine-starvation-induced necroptosis and ferroptosis in human triple negative breast cancer cells via the GCN2-eIF2 $\alpha$ -ATF4 pathway," *Oncotarget*, vol. 8, no. 70, pp. 114588–114602, 2017.
- [22] S. J. Dixon, D. N. Patel, M. Welsch et al., "Pharmacological inhibition of cystine-glutamate exchange induces endoplasmic reticulum stress and ferroptosis," *eLife*, vol. 3, article e02523, 2014.
- [23] Z. Zhang, Z. Yao, L. Wang et al., "Activation of ferritinophagy is required for the RNA-binding protein ELAVL1/HuR to regulate ferroptosis in hepatic stellate cells," *Autophagy*, vol. 14, no. 12, pp. 2083–2103, 2018.
- [24] G. O. Latunde-Dada, "Ferroptosis: role of lipid peroxidation, iron and ferritinophagy," *Biochimica et Biophysica Acta (BBA) - General Subjects*, vol. 1861, no. 8, pp. 1893–1900, 2017.
- [25] J. Du, T. Wang, Y. Li et al., "DHA inhibits proliferation and induces ferroptosis of leukemia cells through autophagy dependent degradation of ferritin," *Free Radical Biology and Medicine*, vol. 131, pp. 356–369, 2019.
- [26] Y. Song, Y. Miao, and C. P. Song, "Behind the scenes: the roles of reactive oxygen species in guard cells," *The New Phytologist*, vol. 201, no. 4, pp. 1121–1140, 2014.
- [27] S. C. Lu, "Glutathione synthesis," *Biochimica et Biophysica Acta*, vol. 1830, no. 5, pp. 3143–3153, 2013.
- [28] W. J. Chung, S. A. Lyons, G. M. Nelson et al., "Inhibition of cystine uptake disrupts the growth of primary brain tumors," *The Journal of Neuroscience*, vol. 25, no. 31, pp. 7101–7110, 2005.
- [29] Y. Zhang, P. Koppula, and B. Gan, "Regulation of H2A ubiquitination and SLC7A11 expression by BAP1 and PRC1," *Cell Cycle*, vol. 18, no. 8, pp. 773–783, 2019.
- [30] M. D. Polewski, R. F. Reveron-Thornton, G. A. Cherryholmes, G. K. Marinov, and K. S. Aboody, "SLC7A11 overexpression in glioblastoma is associated with increased cancer stem cell-like properties," *Stem Cells and Development*, vol. 26, no. 17, pp. 1236–1246, 2017.
- [31] P. Koppula, Y. Zhang, J. Shi, W. Li, and B. Gan, "The glutamate/cystine antiporter SLC7A11/xCT enhances cancer cell dependency on glucose by exporting glutamate," *The Journal of Biological Chemistry*, vol. 292, no. 34, pp. 14240–14249, 2017.
- [32] R. Kang, S. Zhu, H. J. Zeh, D. J. Klionsky, and D. Tang, "BECN1 is a new driver of ferroptosis," *Autophagy*, vol. 14, no. 12, pp. 2173–2175, 2018.
- [33] Y. Su, T. Wang, N. Wu et al., "Alpha-ketoglutarate extends Drosophila lifespan by inhibiting mTOR and activating AMPK," *Aging*, vol. 11, no. 12, pp. 4183–4197, 2019.
- [34] D. Ali, D. K. Mohammad, H. Mujahed et al., "Anti-leukaemic effects induced by APR-246 are dependent on induction of oxidative stress and the NFE2L2/HMOX1 axis that can be targeted by PI3K and mTOR inhibitors in acute myeloid leukaemia cells," *British Journal of Haematology*, vol. 174, no. 1, pp. 117–126, 2016.
- [35] X. Zheng, Y. Li, R. Zhao et al., "xCT deficiency induces autophagy via endoplasmic reticulum stress activated p38-mitogen-activated protein kinase and mTOR in sut melanocytes," *European Journal of Cell Biology*, vol. 95, no. 6–7, pp. 175–181, 2016.
- [36] K. Mody and T. Bekaii-Saab, "Clinical trials and progress in metastatic colon cancer," *Surgical Oncology Clinics of North America*, vol. 27, no. 2, pp. 349–365, 2018.
- [37] C. Wu, "Systemic therapy for colon cancer," *Surgical Oncology Clinics of North America*, vol. 27, no. 2, pp. 235–242, 2018.
- [38] A. Hinman, C. R. Holst, J. C. Latham et al., "Vitamin E hydroquinone is an endogenous regulator of ferroptosis via redox control of 15-lipoxygenase," *PLoS One*, vol. 13, no. 8, article e0201369, 2018.
- [39] M. Liu, B. Liu, Q. Liu, K. du, Z. Wang, and N. He, "Nanomaterial-induced ferroptosis for cancer specific therapy," *Coordination Chemistry Reviews*, vol. 382, pp. 160–180, 2019.
- [40] Q. Li, X. Han, X. Lan et al., "Inhibition of neuronal ferroptosis protects hemorrhagic brain," *JCI Insight*, vol. 2, no. 7, article e90777, 2017.
- [41] J. P. F. Angeli, R. Shah, D. A. Pratt, and M. Conrad, "Ferroptosis inhibition: mechanisms and opportunities," *Trends in Pharmacological Sciences*, vol. 38, no. 5, pp. 489–498, 2017.
- [42] F. E. Ö. Bayram, H. Sipahi, E. T. Acar, R. K. Ulugöl, K. Buran, and H. Akgün, "The cysteine releasing pattern of some antioxidant thiazolidine-4-carboxylic acids," *European Journal of Medicinal Chemistry*, vol. 114, pp. 337–344, 2016.
- [43] O. W. Griffith and A. Meister, "Glutathione: interorgan translocation, turnover, and metabolism," *Proceedings of the National Academy of Sciences*, vol. 76, no. 11, pp. 5606–5610, 1979.
- [44] M. Puka-Sundvall, P. Eriksson, M. Nilsson, M. Sandberg, and A. Lehmann, "Neurotoxicity of cysteine: interaction with glutamate," *Brain Research*, vol. 705, no. 1–2, pp. 65–70, 1995.
- [45] X. Ji, J. Qian, S. M. J. Rahman et al., "xCT (SLC7A11)-mediated metabolic reprogramming promotes non-small cell lung cancer progression," *Oncogene*, vol. 37, no. 36, pp. 5007–5019, 2018.
- [46] A. Y. Shih and T. H. Murphy, "xCT cystine transporter expression in HEK293 cells: pharmacology and localization," *Biochemical and Biophysical Research Communications*, vol. 282, no. 5, pp. 1132–1137, 2001.
- [47] R. Brigelius-Flohe and M. Maiorino, "Glutathione peroxidases," *Biochimica et Biophysica Acta*, vol. 1830, no. 5, pp. 3289–3303, 2013.
- [48] W. S. Yang and B. R. Stockwell, "Synthetic lethal screening identifies compounds activating iron-dependent, nonapoptotic cell death in oncogenic-RAS-harboring cancer cells," *Chemistry & Biology*, vol. 15, no. 3, pp. 234–245, 2008.
- [49] N. Eling, L. Reuter, J. Hazin, A. Hamacher-Brady, and N. R. Brady, "Identification of artesunate as a specific activator of ferroptosis in pancreatic cancer cells," *Oncoscience*, vol. 2, pp. 517–532, 2015.
- [50] A. T. Shaw, M. M. Winslow, M. Magendantz et al., "Selective killing of K-ras mutant cancer cells by small molecule inducers of oxidative stress," *Proceedings of the National Academy of Sciences*, vol. 108, no. 21, pp. 8773–8778, 2011.
- [51] X. Jiang, H.-Y. Tan, S. Teng, Y.-T. Chan, D. Wang, and N. Wang, "The role of AMP-activated protein kinase as a potential target of treatment of hepatocellular carcinoma," *Cancers*, vol. 11, no. 5, p. 647, 2019.

## Research Article

# Fasting Induces Hepatocellular Carcinoma Cell Apoptosis by Inhibiting SET8 Expression

Jie Qi,<sup>1</sup> Xiangyuan Chen ,<sup>1</sup> Qichao Wu,<sup>1</sup> Jing Wang,<sup>1</sup> Hao Zhang ,<sup>1</sup> Anrong Mao ,<sup>2</sup> Minmin Zhu ,<sup>1</sup> and Changhong Miao <sup>1</sup>

<sup>1</sup>Department of Anaesthesiology, Fudan University Shanghai Cancer Center, Department of Oncology, Shanghai Medical College, Fudan University, Shanghai, China

<sup>2</sup>Department of Hepatic Surgery, Fudan University Shanghai Cancer Center, Department of Oncology, Shanghai Medical College, Fudan University, Shanghai, China

Correspondence should be addressed to Anrong Mao; 13020143060@163.com, Minmin Zhu; zhu\_mm@126.com, and Changhong Miao; miao\_chh@126.com

Received 10 November 2019; Accepted 26 December 2019; Published 21 March 2020

Guest Editor: Rizwan Wahab

Copyright © 2020 Jie Qi et al. This is an open access article distributed under the Creative Commons Attribution License, which permits unrestricted use, distribution, and reproduction in any medium, provided the original work is properly cited.

**Background.** Hepatocellular carcinoma (HCC) is a life-threatening cancer, and the Kelch-like ECH-associated protein 1 (Keap1)/NF-E2-related factor 2 (Nrf2)/antioxidant response element (ARE) signalling pathway plays a crucial role in apoptosis resistance in cancer cells. Fasting is reported to mediate tumour growth reduction and apoptosis. SET8 is involved in cancer proliferation, invasiveness, and migration. However, whether SET8 participates in fasting-mediated apoptosis in HCC remains unclear. **Methods.** We used immunohistochemical staining to analyse the expression of SET8, Keap1, and Nrf2 in HCC tissues. Cell viability, apoptosis, and cellular reactive oxygen species (ROS) were assessed, and Western blot and qPCR analyses were used to examine the expression of Keap1/Nrf2 in HCC cells under fasting, SET8 overexpression, and PGC1 $\alpha$  overexpression conditions. Mass spectrometry, coimmunoprecipitation, and confocal microscopy were used to determine whether PGC1 $\alpha$  interacts with SET8. **In vivo** experiments were performed to verify the conclusions from the *in vitro* experiments. **Results.** Our data indicate that SET8 expression is associated with poor survival in HCC patients. Both *in vitro* and *in vivo* results demonstrated that fasting decreased cell viability and downregulated expression of SET8, Nrf2, and downstream effectors of Nrf2, while it upregulated Keap1 expression, mediated ROS accumulation, and induced HCC cell apoptosis. These results were similar to what is observed in SET8-deficient cells. Furthermore, SET8 was found to interact with PGC1 $\alpha$ , and both PGC1 $\alpha$  and H4K20me1, a downstream target of SET8, were found to be enriched at the Keap1 promoter region. These two factors were further determined to attenuate Keap1 promoter activity. **Conclusions.** The results of our study demonstrate that fasting induces HCC apoptosis by inhibiting SET8 expression and that SET8 interacts with PGC1 $\alpha$  to activate the Nrf2/ARE signalling pathway by inhibiting Keap1 expression.

## 1. Introduction

The incidence rate of hepatocellular carcinoma ranks sixth among cancers and third for cancer-related mortality worldwide [1]. Resisting apoptosis and sustaining cell growth are recognized as two hallmark features of hepatocellular carcinoma and other cancers [2]. Apoptosis resistance is a major factor responsible for the failure of traditional cancer treatment [3]. Therefore, apoptosis in cancer cells has emerged

as a promising target for cancer therapies in hepatocellular carcinoma patients [4].

Fasting, also named dietary restriction or caloric restriction, is a decrease in ad libitum balanced caloric intake by 30% to 60% without causing malnutrition [5]. Cancer is characterized by metabolic dysregulation with increased glucose consumption via upregulation of glycolysis (Warburg effect) and downregulation of oxidative phosphorylation [6]. Fasting is reported to be associated with increased longevity

and can provide protection against cancer, cardiovascular disease, diabetes, and cognitive dysfunction [7–10]. Moreover, fasting can reduce tumour growth and induce tumour cell apoptosis [11, 12].

NF-E2-related factor 2 (Nrf2) is a regulator of many genes encoding antioxidant and detoxification enzymes that prevent reactive oxygen species (ROS) accumulation [13]. The stability and accumulation of Nrf2 are modulated by Kelch-like ECH-associated protein 1 (Keap1) [14]. The Keap1/Nrf2/antioxidant response element (ARE) signalling pathway plays a critical role in cellular redox homeostasis. Nrf2 is activated in various types of tumours [15]. Moreover, Nrf2 is abundantly expressed in hepatocellular carcinoma (HCC) cells and is associated with poor HCC prognosis [16].

SET8, also known as SETD8, KMT5A, or PR-Set7, is the only enzyme that generates histone H4 monomethylation on lysine 20 (H4K20me1) in multicellular organisms [17]. SET8 is functional in multiple cellular pathways, such as DNA replication, chromosome compaction, cell cycle progression, transcriptional modulation, genomic instability, and cellular metabolism [17–20]. Moreover, SET8 is involved in cancer proliferation, invasiveness, and migration and is thus associated with a poor survival rate in cancer patients [21, 22]. Some reports show that high methyltransferase activity of SET8 is associated with a high recurrence rate and poor overall survival rate in patients with liver cancer [23]. Consistently, a reduction in SET8 methyltransferase activity increases cellular ROS accumulation [24] and results in massive apoptosis in the epithelium [25]. The role of SET8 in fasting-induced apoptosis in HCC is still not well known. In this study, we investigated the mechanism by which fasting induces HCC cell apoptosis.

## 2. Material and Methods

**2.1. Clinical Samples.** Tumour specimens and paired adjacent liver specimens were randomly collected during surgical resections performed in select patients with HCC at Fudan University Shanghai Cancer Center. The study included a total of 40 participants, each of whom provided informed consent. All the procedures performed in this study were approved by the Ethics Committee of Fudan University.

**2.2. Analysis of The Cancer Genome Atlas (TCGA) RNASeqV2 Data.** TCGA assembly program was used to download hepatocellular carcinoma RNASeqV2 data and clinical data. Cox regression analyses were used to calculate the prognosis in 365 liver cancer patients divided into either the low gene expression group or the high gene expression group of SET8. The overall survival rates of the high and low gene expression groups were compared using Kaplan-Meier analysis and the log-rank test.

**2.3. Cell Culture and Reagents.** MHCC-97H (RRID: CVCL\_4972) and HCC-LM3 (RRID: CVCL\_6832) cells, which are HCCs, were purchased from the Institute of Biochemistry and Cell Biology, Chinese Academy of Sciences, Shanghai, China. All cell lines were cultured in DMEM containing 1% penicillin-streptomycin and 10% foetal bovine serum at

37°C in a humidified 5% carbon dioxide incubator that was mycoplasma-free.

For starvation experiments, cells were washed with PBS to remove the complete medium and further cultured in DMEM with low glucose (1 mM) and 1% foetal bovine serum, as previously described [26].

**2.4. Cell Proliferation Assay.** The cell counting kit-8 (CCK8) assay (CCK8; Dojindo Molecular Technologies, Inc., Japan) was performed according to the manufacturer's instructions. Cells were plated in 96-well plates at a density of  $5 \times 10^3$  cells/well. After 24 h, some of the cells were transferred to a fasting concentration (1 mM). Then, 10  $\mu$ l of CCK8 solution was added to each well, and the cells were incubated with the solution for 2 h. Optical density (OD) values were measured at 450 nm using a microplate reader to indicate the relative cell viability.

**2.5. Intracellular ROS Detection.** Intracellular ROS were measured using a Reactive Oxygen Species Assay Kit (Beyotime Biotechnology) according to the manufacturer's instructions. DCFH-DA (5  $\mu$ M) was added to the cells, and they were incubated at 37°C for 30 min in the dark. Cells were then washed with serum-free medium three times and analysed for ROS production by flow cytometry.

**2.6. Apoptosis Assay.** Apoptosis was measured by fluorescence-activated cell sorting (FACS) analysis (Cytomics FC 500 MPL; Beckman Coulter, Fullerton, USA) using double staining with Annexin V-FITC and propidium iodide (PI; BD Biosciences, San Jose, USA). Briefly, after different treatments, cells were harvested and incubated with PI and Annexin V-FITC for 30 min at 37°C in the dark and then analysed by flow cytometry.

**2.7. Immunohistochemistry.** Biological specimens were collected as mentioned above. The wax was removed from the tissue slices by washes with PBS, and then, the slices were fixed in 95% alcohol for 30 min and incubated with 3% H<sub>2</sub>O<sub>2</sub> for 10 min at room temperature to remove endogenous peroxidase activity. Goat serum was added for 10 min at room temperature to block nonspecific staining. Primary SET8 (Abcam, Cambridge, UK), Nrf2 (ProteinTech, 16396-1-AP), and Keap1 (ProteinTech, 10503-2-AP) antibodies were diluted 1:200 in the blocking solution and incubated with sections at 37°C for 2 h. Secondary antibody and biotinylated horseradish peroxidase were sequentially added at room temperature for 10 min. Diaminoaniline (DAB) (ZSGB-BIO, China) was added, and samples were counterstained with haematoxylin. Finally, the slides were gradually dehydrated with a graded ethanol series and sealed with neutral glue. Images were acquired with a vertical microscope (Olympus BX53).

**2.8. Western Blot Analysis.** Whole-cell extracts were prepared using cell lysis buffer (Cell Signaling Technology, Danvers, MA). Protein samples were boiled for 5 min in sample loading buffer and were separated by 8–10% SDS-PAGE and transferred to PVDF membranes. Membranes were blocked with 5% skim milk for 1 h and then incubated with primary

antibodies overnight at 4°C. The primary antibodies used were as follows: monoclonal antibodies against  $\beta$ -actin (ProteinTech, 66009-1-Ig, 1/5000), SET8 (ProteinTech, 14063-1-AP, 1/1000), H4K20me1 (Abcam, Cambridge, UK), Keap1 (ProteinTech, 10503-2-AP, 1/1000), Nrf2 (ProteinTech, 16396-1-AP, 1/1000), Heme oxygenase-1 (HO1) (ProteinTech, 10701-1-AP, 1/1000), Glutamate cysteine ligase subunit catalysis (GCLC) (ProteinTech, 12601-1-AP, 1/1000), Glutamate cysteine ligase modifier subunit (GCLM) (ProteinTech, 14241-1-AP, 1/1000), Malic enzyme 1 (ME1) (ProteinTech, 16619-1-AP, 1/1000), Thioredoxin reductase 1 (TXNRD1) (ProteinTech, 11117-1-AP, 1/1000), and Peroxisome proliferator-activated receptor  $\gamma$  coactivator 1 $\alpha$  (PGC1 $\alpha$ ) (ProteinTech, 66369-1-Ig, 1/1000). After washing the membranes, an HRP-conjugated secondary antibody was then added for 1 h at room temperature, and the membranes were further washed 5 times with TBS-T. Subsequently, the signal was detected by an ECL system. The density of the protein bands was analysed by Scan-gel-it software. Protein expression was normalized to  $\beta$ -actin.

**2.9. Quantitative Polymerase Chain Reaction (qPCR).** Total RNA was isolated from cells by Trizol® reagent (Tiangen Biotech, Beijing, China). cDNA was synthesized using a Hifair® II 1st Strand cDNA Synthesis SuperMix for qPCR (gDNA digester plus) (Yeasen, Shanghai). Quantitative real-time PCR (qPCR) was performed with a Hieff UNICON® qPCR TaqMan Probe Master Mix (Yeasen, Shanghai) to analyse the gene expression of  $\beta$ -actin, SET8, Keap1, Nrf2, PGC1 $\alpha$ , ME1, TXNRD1, GCLC, HO1, and GCLM with a QuantStudio 7 Flex Real-Time PCR System (Applied Biosystems, Life Technologies, Waltham, USA). The qPCR primers used in this study can be found in Table 1.

**2.10. Immunofluorescence (IF).** Cells were grown on coverslips. After treatment, cells were washed with PBS and fixed in 4% paraformaldehyde for 15 min. After washing 3 times with PBS for 5 min, cells were permeabilized with 0.3% Triton X-100 for 5 min and blocked for 1 h with 1% bovine serum albumin at room temperature. Cells were then incubated with primary anti-SET8 (ProteinTech, 14063-1-AP, 1/200) and anti-PGC1 $\alpha$  (ProteinTech, 66369-1-Ig, 1/200) antibodies overnight at 4°C. The next day, following washing with PBS, cells were incubated with fluorescent secondary antibodies. After washing 3 times with PBS, cell nuclei were stained with 4,6-diaminophenylindole (DAPI). Images were taken using a confocal fluorescence microscope (Leica).

**2.11. Coimmunoprecipitation (Co-IP).** Whole cell protein lysates were extracted with a cell lysis buffer with PMSF (Beyotime Biotechnology, Shanghai). For endogenous IP, lysates were incubated with corresponding primary antibodies and 50  $\mu$ l of protein A/G Dynabeads (Thermo Fisher, USA) at 4°C overnight. Then, 10  $\mu$ l of input, IgG negative control, and the IP were subjected to Western blotting.

**2.12. Mass Spectrometry.** Cells were transfected with a SET8 plasmid, and protein lysate was extracted 48 h after transfection. The endogenous IP was performed as described above. Silver staining was performed using a fast silver staining kit

(Beyotime Biotechnology, Shanghai) according to the manufacturer's instructions. Mass spectrometric analysis of stained gel strips was performed using high-performance liquid chromatography (1260 Series, Agilent Technologies) and mass spectrometry (Agilent 6460, Agilent Technologies).

**2.13. Chromatin Immunoprecipitation (ChIP).** ChIP assays were carried out with a Simple ChIP Plus Sonication Chromatin IP Kit (Cell Signaling Technology, MA) according to the manufacturer's instructions. Briefly, cells ( $1 \times 10^7$ ) were fixed with 1% formaldehyde for 10 min at room temperature to cross-link DNA and proteins. Glycine was then added to stop the cross-linking reaction. Chromatin was sheared using a Microson Ultrasonic Cell Disruptor XL (Misonix) with 16 cycles of sonication (15 s each, 2 min rest, amplitude = 10, power = 15 W). Ten microliters of sonicate was collected from each sample as input, and the remaining sample was incubated with anti-PGC1 $\alpha$  (Abcam, USA) or anti-H4K20me1 (Abcam, USA) antibodies or an IgG negative control at 4°C overnight. Immunoprecipitants were bound to protein G magnetic beads, and the DNA-protein cross-linking was reversed by incubating at 65°C for 2 h. Then, the DNA was purified, and enriched DNA sequences were analysed by qPCR. Keap1 oligonucleotide sequences for PCR primers were as follows: forward 5'-TGACAAACTG AGCCTCCTAGC-3' and reverse 5'-GCATCAAAGAGTG ATGCTGAATG-3'.

**2.14. Dual-Luciferase Assay.** A Promega Dual-Luciferase Assay Kit (Madison, WI, United States) was used to assess the impact of SET8 and PGC1 $\alpha$  on Keap1 promoter activity. The Keap1 promoter was amplified from genomic DNA of HCC-LM3 cells and ligated into a pGL3-Basic vector to generate a pGL3-Keap1 construct. pGL3-Keap1 was transfected with a Renilla luciferase vector into HCC-LM3 cells, and the impact of SET8 and PGC1 $\alpha$  on Keap1 promoter activity was assessed using a dual-luciferase assay kit.

**2.15. siRNA Treatments.** MHCC-97H and HCC-LM3 cells were transfected with siRNA against PGC1 $\alpha$  using Lipofectamine 3000 (Invitrogen, USA) according to the manufacturer's instructions. The PGC1 $\alpha$  siRNA sequences (Biotend, Shanghai) were sense, 5'-GCUCCAAGACUCUAGAAdTdT-3', and anti-sense, 5'-UUGUCUAGAGUCUUGGAGCdTdT-3'; for siRNA #2, the sequences were sense, 5'-GGCA GUAGAUCUCUCAAAdTdT-3', and anti-sense, 5'-UUG AAGAGGAUCUACUGCCdTdT-3'.

**2.16. SET8 Lentivirus Containing Short Hairpin RNAs (shRNAs) and Mutant Treatments.** SET8 shRNAs (Genechem, Shanghai) and mutant SET8<sup>R295G</sup> plasmid were transfected into HCC cells. The shRNA sequences were as follows: shRNA-1, 5'-CAACAGAATCGCAAActTA-3'; shRNA-2, 5'-CAACAGAATCGCAAActTA-3'.

**2.17. Fasting in Mice.** All animal studies and procedures adhered to the recommendations of the Medicine and Public Health Animal Care and Use Committee of Shanghai Medical College at Fudan University. Wild-type BALB/c

TABLE 1: Primer sequences.

Genes	Sequences	
	Forward (5'-3')	Reverse (5'-3')
<i>β-Actin</i>	ATGCCCTGAGGCTCTTTCCAGCC	CCAGGATGGAGCCACCGATCCACA
<i>SET8</i>	AGCTCCAGGAAGAGCAAAGCCGAG	GGCGTCGGTGATCTCGATGAGGT
<i>Keap1</i>	CACCACAACAGTGTGGAGAGGTA	TACAGTTGTGCAGGACGCAGACG
<i>Nrf2</i>	CCAATTCAGCCAGCCAGCACAT	GGTGACTGAGCCTGATTAGTAGC
<i>PGC1α</i>	CGGAAATCATATCCAACCAG	TGAGGACCGCTAGCAAGTTTG
<i>ME1</i>	CCTCACTACTGCTGAGGTTATAGC	CGGTTCCAGGATAAACTGTGGCTG
<i>TXNRD1</i>	GCAATCCAGGCAGGAAGATTGCT	CTCTTGACGGAATCGTCCATTCC
<i>GCLC</i>	GTGGTACTGCTACCAGAGTG	AGCTCCGTGCTGTTCTGGGCCTT
<i>HO1</i>	AGCGGGCCAGCAACAAAAGTGCAA	CAGCATGCCTGCATTACATGGC
<i>GCLM</i>	ATCTTGCCTCCTGCTGTGTGATGC	CAATGACCGAATACCGCAGTAGCC

mice (female, 6 weeks, 20–25 g) were purchased from Shanghai Sippr-BK Laboratory Animal Co. Ltd. Mice were divided into four groups based on the interventions ( $N = 6$  per group): group 1: mice injected with MHCC-97H control cells; group 2: mice injected with shSET8 knockdown MHCC-97H cells; group 3: mice injected with MHCC-97H cells and fasted; group 4: mice injected with SET8-overexpressing MHCC-97H cells and fasted. Mice in all groups were injected subcutaneously in the right flank with  $100 \mu\text{l}$  of cells in PBS at a density of  $2 \times 10^6$  cells/ml. Animals were divided into 4 groups at 5–7 days after inoculation of tumour cells. Group 1 and group 2 mice were maintained under standard conditions throughout the study. Group 3 mice, which were injected with MHCC-97H cells, and group 4 mice, which were injected with SET8-overexpressing MHCC-97H cells, were subjected to alternating days of fasting and days of ad libitum diet (on nonfasting days). Animals were given free access to water every day [26]. Mice were individually housed in clean new cages to avoid cannibalism or cofeeding. Tumour size, body weight, and general behaviour were monitored every 4 days. The tumour size was calculated using callipers, and the tumour volume was calculated as follows: tumour volume ( $\text{mm}^3$ ) = (length  $\times$  width  $\times$  width)  $\times \pi/6$ , where expression length and width are in millimetres. Tumours were harvested and weighed for WB and qPCR analysis.

**2.18. Statistical Analysis.** The results are presented as the mean  $\pm$  SD (standard deviation). Two-tailed unpaired  $t$ -tests or one-way ANOVA with GraphPad Prism Version 6 (GraphPad Software, San Diego, CA) was performed to compare the groups.  $P < 0.05$  was considered significant.

### 3. Results

**3.1. SET8 Is Upregulated and Associated with a Poor Prognosis in Hepatocellular Carcinoma.** First, we analysed the expression of SET8, Keap1, and Nrf2 by immunohistochemical staining in tumour tissues and adjacent nontumour tissues from hepatocellular carcinoma patients who underwent a surgical resection. We found that both Nrf2 and SET8 were highly expressed in HCC tissues in comparison

to paracarcinoma tissues, and the staining was mainly restricted to the nucleus. In contrast, Keap1 was more highly expressed in paracarcinoma tissues than in HCC tissues and was mainly present in the cytoplasm (Figure 1(a)). Similar results were found by analysing protein expression by Western blot, which showed that SET8 and Nrf2 expression was higher in HCC tissues than in adjacent nontumour tissues, while Keap1 expression was higher in adjacent tissues (Figure 1(b)). Next, we assessed the overall survival rates of HCC patients using TCGA dataset of HCC. Patients were divided into two groups on the basis of SET8 expression. We found that higher SET8 expression was positively associated with a poorer overall survival rate in patients with HCC (Figure 1(c)).

**3.2. Effects of Fasting on Cell Viability, Apoptosis, and Expression of Components of the SET8 and Keap1/Nrf2/ARE Signalling Pathways.** MHCC-97H and HCC-LM3 cells were cultured in fasting medium or complete DMEM (control). Compared to the control group, fasting reduced cell viability (Figure 2(a)) and induced apoptosis (Figure 2(b)) in MHCC-97H and HCC-LM3 cells. Moreover, compared with the control group, fasting increased ROS accumulation in HCC (Figure 2(c)). Previous studies have reported that the Keap1/Nrf2/ARE signalling pathway plays a critical role in cellular redox homeostasis. We analysed the expression of the Keap1/Nrf2/ARE signalling pathway components in MHCC-97H and HCC-LM3 cells by qPCR or Western blotting. The results showed that fasting increased the expression of Keap1 but decreased the expression of Nrf2, ME1, TXNRD1, HO1, GCLM, and GCLC at the protein (Figure 2(d)) and mRNA (Figure 2(e)) levels. Furthermore, the mRNA and protein expression of SET8 and its substrate H4K20me1 was decreased under fasting conditions (Figures 2(f) and 2(g)).

To determine the role of Keap1 in response to fasting, we constructed a Keap1 knockdown model by treating HCC cells with Keap1 siRNA under fasting treatments. Keap1 knockdown improved fasting-mediated loss of cell viability and increased apoptosis in HCC cells (Supplementary Figures S1A and B). Furthermore, knockdown of Keap1 counteracted fasting-mediated ROS accumulation in HCC

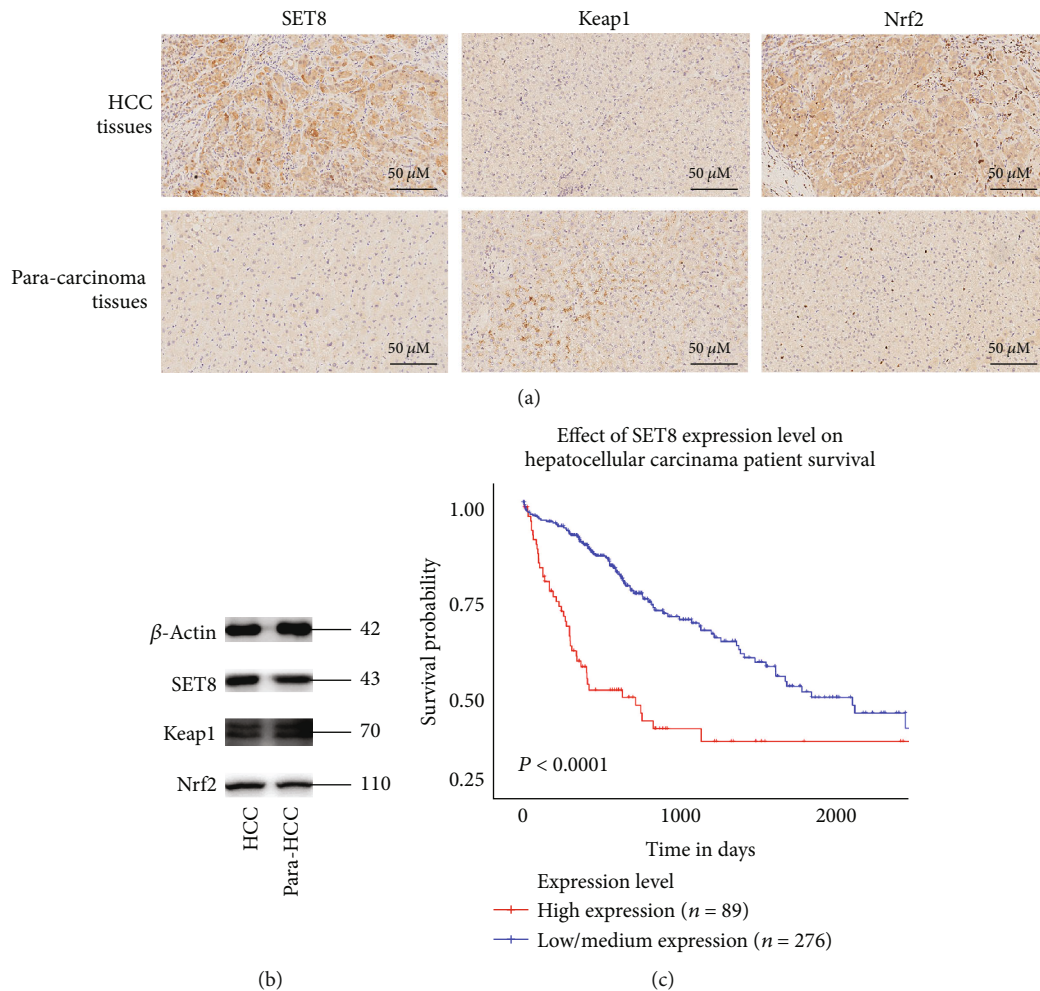


FIGURE 1: SET8 is upregulated in HCC and is positively associated with a poor prognosis. (a) Immunohistochemical analysis of SET8, Keap1, and Nrf2 expression in HCC tissues and paracarcinoma normal liver tissue specimens from patients with HCC. Nuclei (blue) were stained by haematoxylin. (b) Western blot analysis of SET8, Keap1, and Nrf2 expression in HCC specimens and adjacent paracarcinoma normal liver tissue specimens from patients with HCC. (c) Kaplan-Meier OS survival curve for patients with high or low SET8 expression in TCGA dataset of HCC; \* $P < 0.05$ .

cells (Supplementary Figure S1C). Moreover, the additional knockdown of Keap1 led to an increase in the expression of Nrf2/ARE signalling pathway components in fasting-treated HCC cells (Supplementary Figures S1D and E). These data indicated that fasting mediated HCC apoptosis, ROS accumulation, and inhibition of the Nrf2/ARE signalling pathway via upregulation of Keap1 expression.

**3.3. Role of SET8 in HCC Cell Viability, Apoptosis, ROS Accumulation, and the Expression of Keap1/Nrf2/ARE Signalling Pathway Components in response to Fasting.** To understand the role of SET8 in fasting-mediated decreases in cell viability and increases in apoptosis, SET8 was overexpressed or silenced in MHCC-97H and HCC-LM3 cells. We found that overexpression of SET8 reversed fasting-mediated loss of cell viability (Figure 3(a)) and increased apoptosis (Figure 3(b)). Moreover, knockdown of SET8 resulted in decreased cell viability (Supplementary Figure S2A) and increased apoptosis (Supplementary Figure S2B) in HCC

cells, which was similar to the effects observed with fasting. Furthermore, overexpression of SET8 counteracted fasting-mediated ROS accumulation (Figure 3(c)). Similarly, SET8 knockdown augmented ROS accumulation in HCC cells, which was similar to the effect observed with fasting (Supplementary Figure S2C). We then analysed the effect of SET8 on the expression of the Keap1/Nrf2/ARE signalling pathway by qPCR or Western blotting. SET8 overexpression under fasting conditions in HCC cells decreased Keap1 expression, while it increased the expression of Nrf2/ARE signalling pathway components at the protein (Figure 3(d)) and mRNA (Figure 3(e)) levels. Moreover, SET8 knockdown increased the expression of Keap1 and decreased the expression of the Nrf2/ARE signalling pathway in HCC cells, which was similar to the effect observed with fasting (Supplementary Figures S2D and E). These data indicated that fasting induced HCC apoptosis and inhibition of the Keap1/Nrf2/ARE signalling pathway via a decrease in SET8 expression.



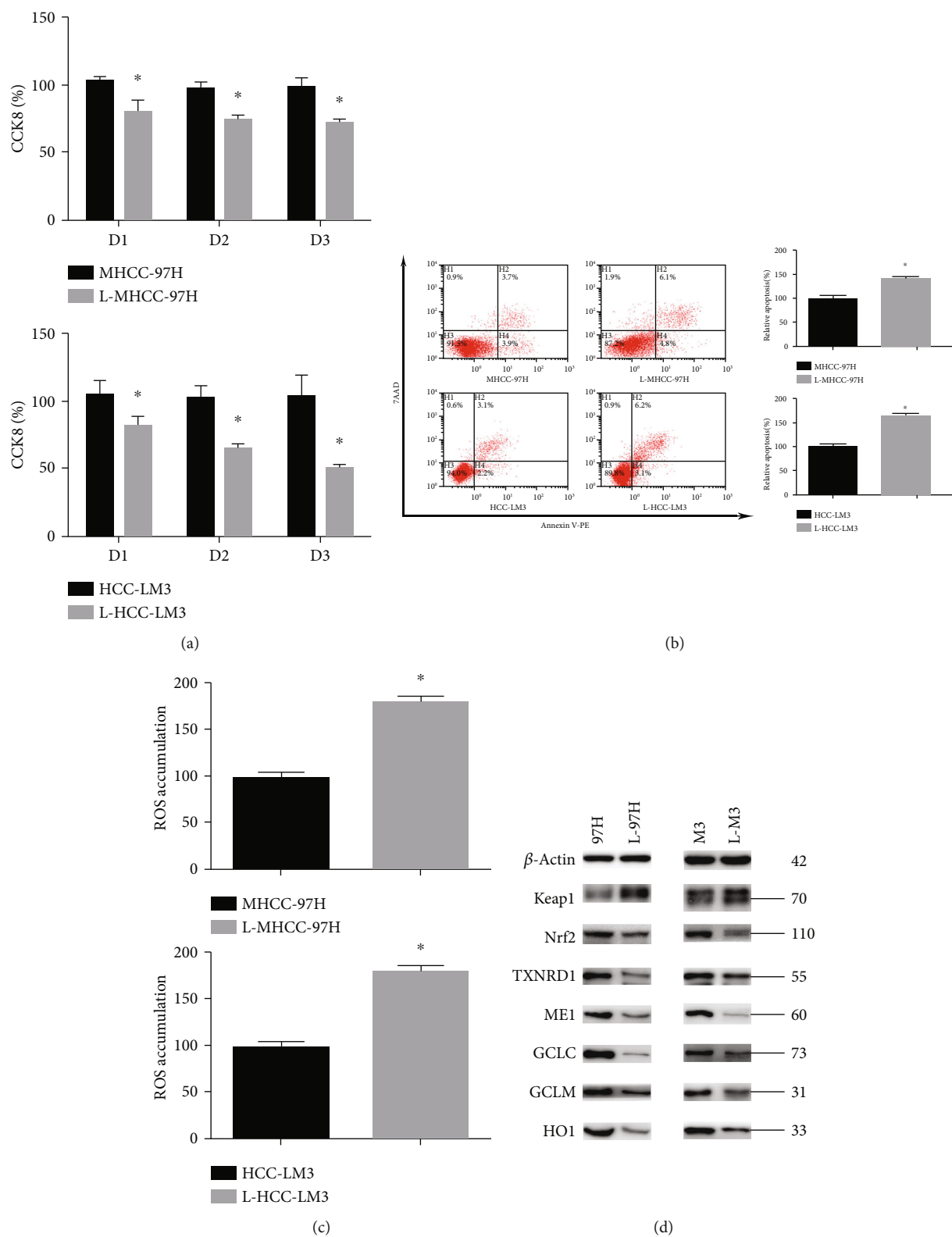


FIGURE 2: Continued.

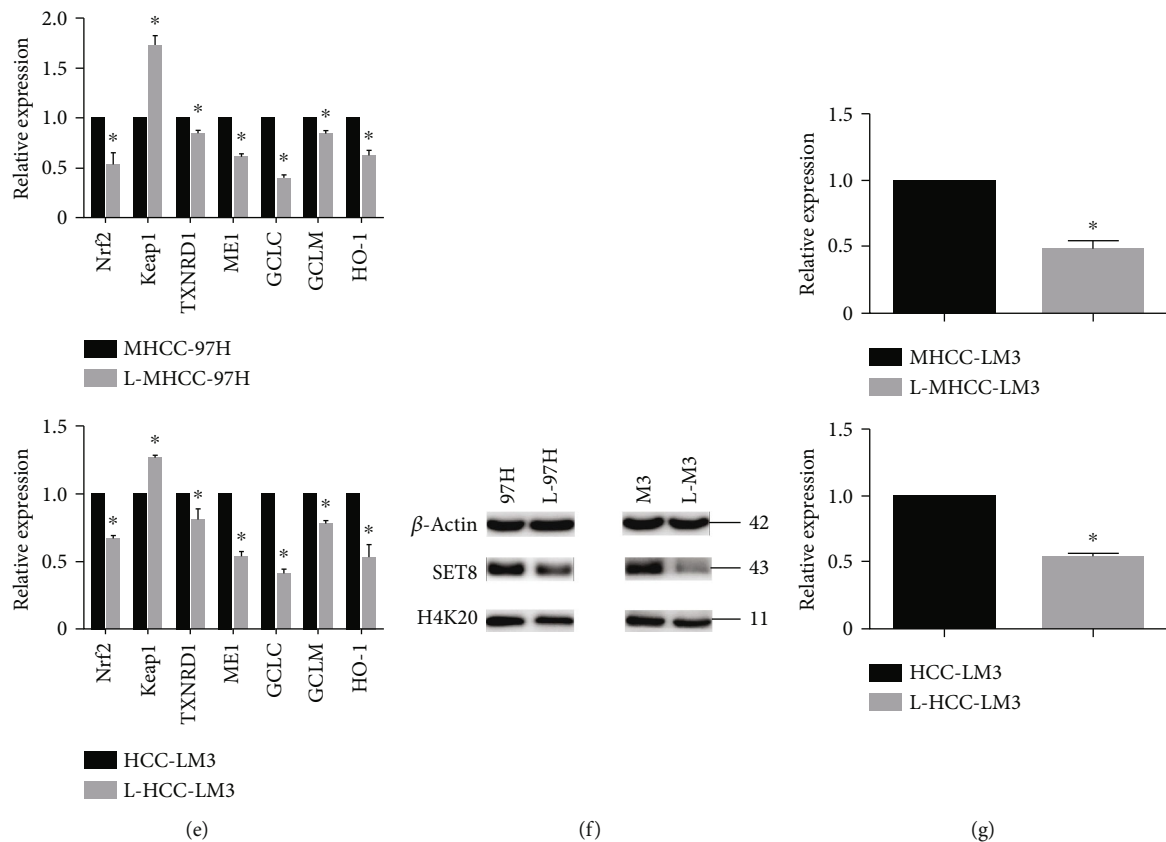


FIGURE 2: Effects of fasting on cell viability, apoptosis, ROS level, and expression of Keap1/Nrf2/ARE signalling pathway components and SET8. (a) Proliferation of MHCC-97H and HCC-LM3 cells in normal or fasting conditions for 24 h, as measured by CCK8. (b) Flow cytometry was used to detect apoptotic MHCC-97H and HCC-LM3 cells cultured in normal or fasting medium for 24 h. (c) The level of ROS was detected by flow cytometry in MHCC-97H and HCC-LM3 cells cultured in normal or fasting medium for 24 h. (d) Western blot analysis of the Keap1/Nrf2/ARE signalling pathway in MHCC-97H and HCC-LM3 cells cultured in normal or fasting conditions for 24 h. (e) The mRNA expression of the Keap1/Nrf2/ARE signalling pathway components in HCC cells grown in normal or fasting medium for 24 h was examined by qPCR. (f) Western blot analysis of SET8 and H4K20me1 in HCC cells cultured in normal or fasting medium for 24 h. (g) The mRNA expression of SET8 was examined by qPCR in cells grown in normal or fasting medium for 24 h. Data are shown as the mean  $\pm$  SD of five independent experiments. \* $P < 0.05$  vs. the control group.

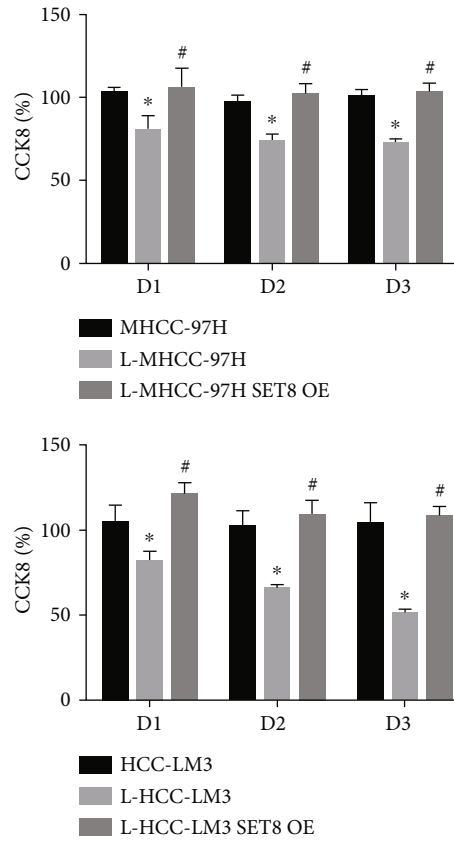
Next, to identify whether Keap1 is targeted by SET8, we examined the genome-wide distribution of H4K20me1, a downstream target of SET8, in HCC-LM3 cells by ChIP assay. H4K20me1 was found to enrich at the Keap1 promoter region (Figure 3(f)). Luciferase reporter assays indicated that SET8 knockdown enhanced Keap1 promoter activity (Figure 3(g)).

Then, we demonstrated the role of Keap1 in SET8 knockdown HCC cells. Keap1 was silenced in MHCC-97H and HCC-LM3 cells by Keap1 siRNA. Knockdown of Keap1 by siRNA reversed SET8 knockdown-mediated loss of cell viability (Supplementary Figure S3A) and increased apoptosis (Supplementary Figure S3B) in HCC cells. Moreover, Keap1 knockdown weakened ROS accumulation in SET8-silenced HCC cells (Supplementary Figure S3C). Furthermore, the additional knockdown of Keap1 led to an increase in the expression of Nrf2/ARE signalling pathway components in SET8-silenced MHCC-97H and HCC-LM3 cells (Supplementary Figures S3D and E). These data indicated that SET8 positively regulated Nrf2/ARE signalling

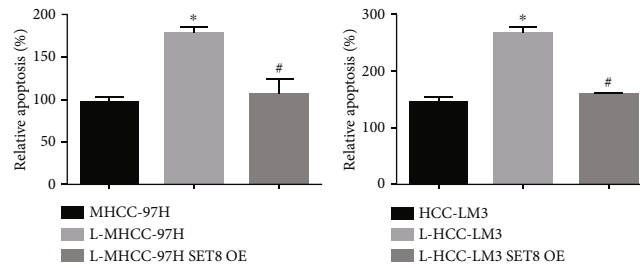
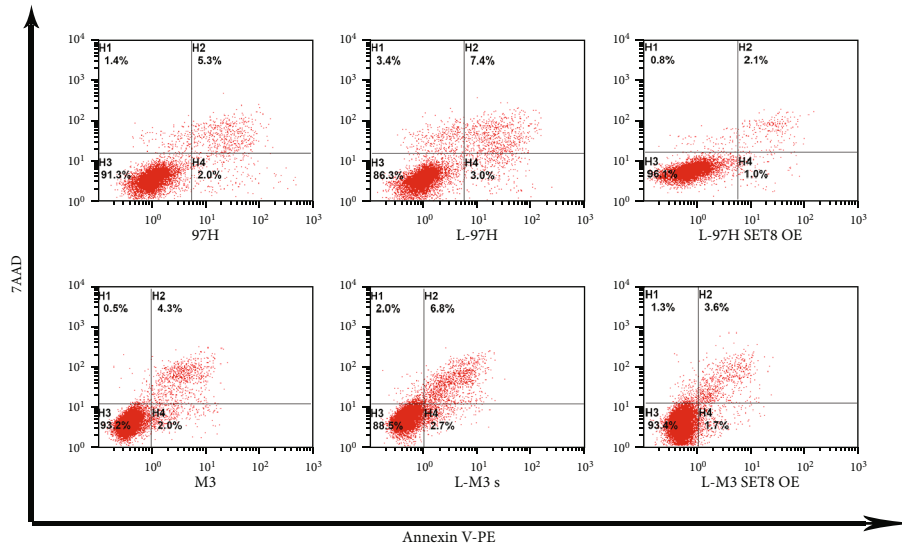
pathway expression and HCC malignant potential by inhibiting Keap1 expression.

**3.4. SET8 Interacts with PGC1 $\alpha$ .** Purified SET8 complexes were resolved by SDS-PAGE followed by silver staining. The differential protein bands were isolated and analysed by mass spectrometry. Among several other proteins, we found that PGC1 $\alpha$  probably interacts with SET8 (Figure 4(a)). Furthermore, we verified that SET8 coprecipitated with PGC1 $\alpha$  in MHCC-97H and HCC-LM3 cells (Figure 4(b)). Finally, we demonstrated by confocal microscopy that SET8 and PGC1 $\alpha$  colocalized with each other (Figure 4(c)).

**3.5. Role of PGC1 $\alpha$  in HCC Cell Viability, Apoptosis, ROS Accumulation, and Expression of Keap1/Nrf2/ARE Signalling Pathway Components in response to Fasting.** PGC1 $\alpha$  was overexpressed or silenced in MHCC-97H and HCC-LM3 cells. We found that overexpression of PGC1 $\alpha$  reversed fasting-mediated decreases in cell viability (Figure 5(a)) and increases in apoptosis (Figure 5(b)). Moreover, knockdown

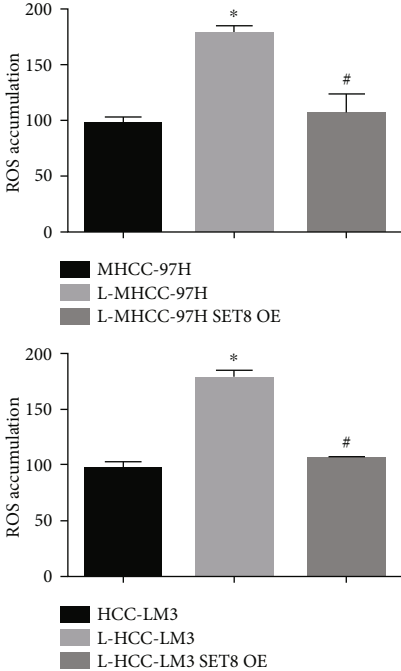


(a)

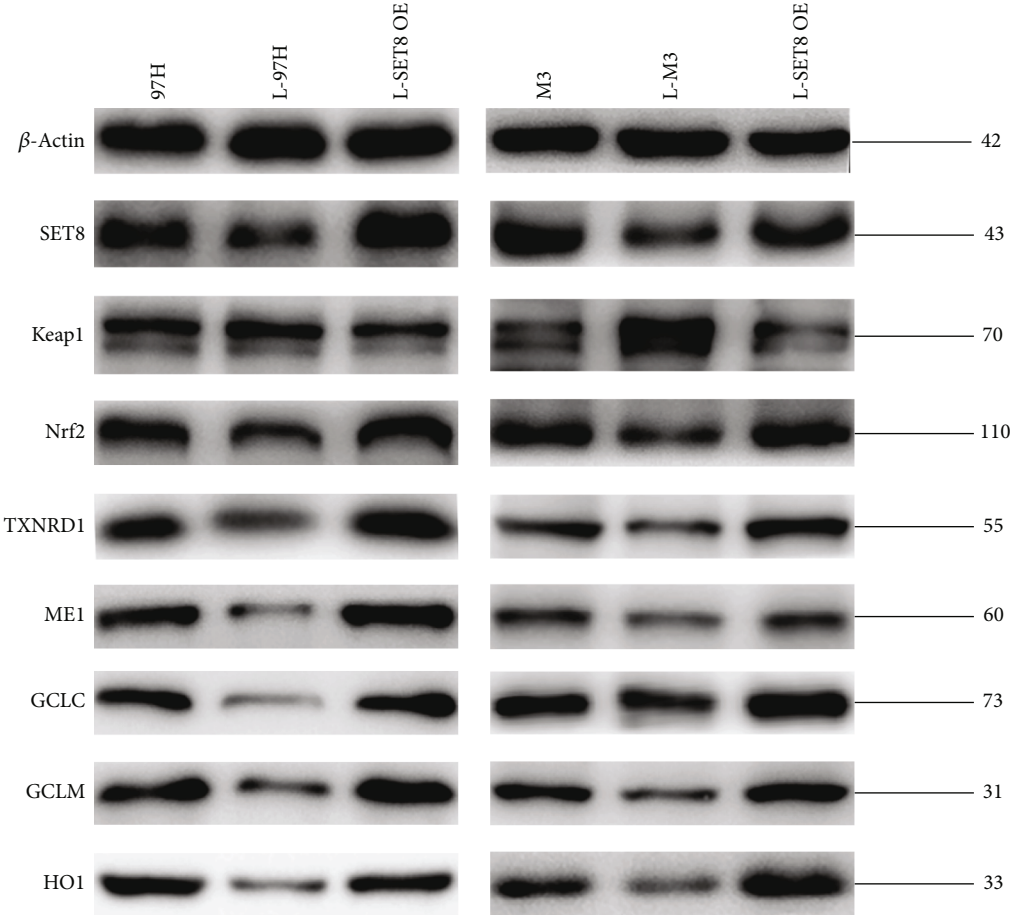


(b)

FIGURE 3: Continued.



(c)



(d)

FIGURE 3: Continued.

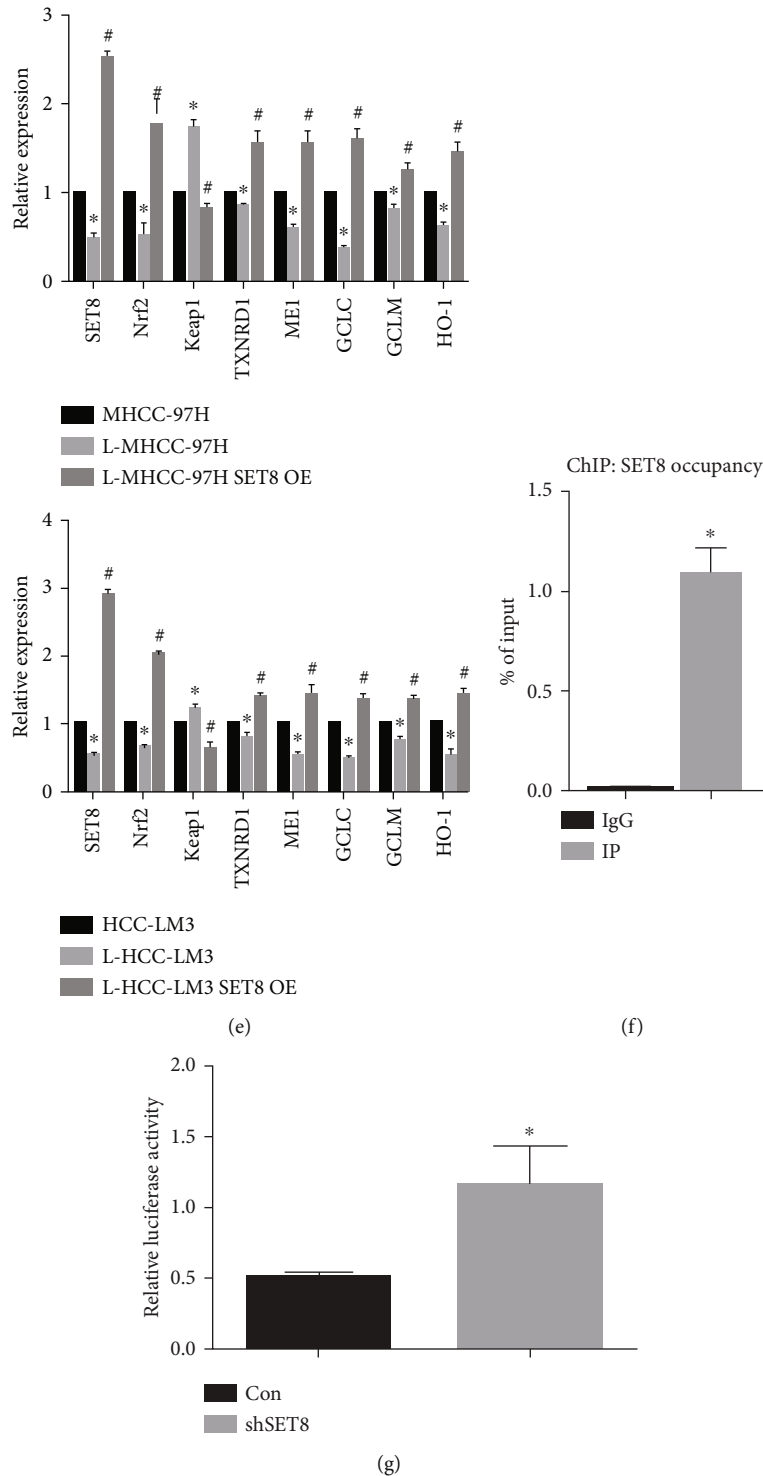


FIGURE 3: Role of SET8 in HCC cell viability and apoptosis in response to fasting. (a) Proliferation of MHCC-97H and HCC-LM3 cells under fasting conditions for 24 h or fasting in combination with overexpressed SET8. (b) Flow cytometry was used to detect the number of apoptotic MHCC-97H and HCC-LM3 cells under fasting conditions for 24 h or fasting in combination with overexpressed SET8. (c) The level of reactive oxygen species in MHCC-97H and HCC-LM3 cells under fasting conditions for 24 h or fasting in combination with overexpressed SET8. (d) Western blot analysis of SET8 and Keap1/Nrf2/ARE signalling pathway components in MHCC-97H and HCC-LM3 cells under fasting conditions for 24 h or fasting in combination with overexpressed SET8. (e) qPCR analysis of SET8 and Keap1/Nrf2/ARE signalling pathway components in MHCC-97H and HCC-LM3 cells under fasting conditions for 24 h or fasting in combination with overexpressed SET8. (f) ChIP assay of H4K20me1 presence at the promoter region of Keap1. Normal IgG was used as a control. (g) SET8 knockdown increased Keap1 luciferase activity in HCC-LM3 cells. Data are shown as the mean  $\pm$  SD of five independent experiments. \* $P < 0.05$  vs. the control group. # $P < 0.05$  vs. the fasting group.

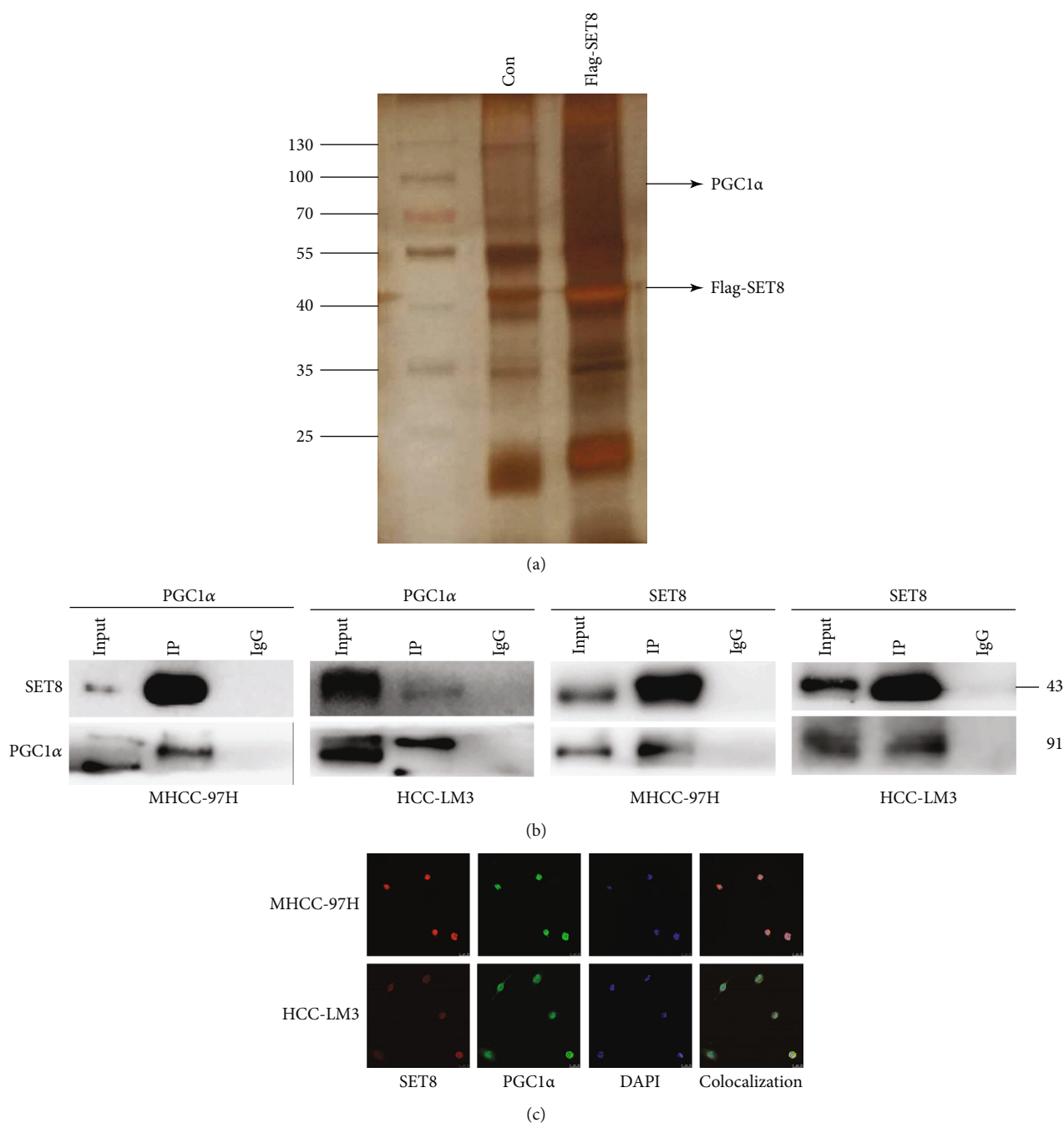
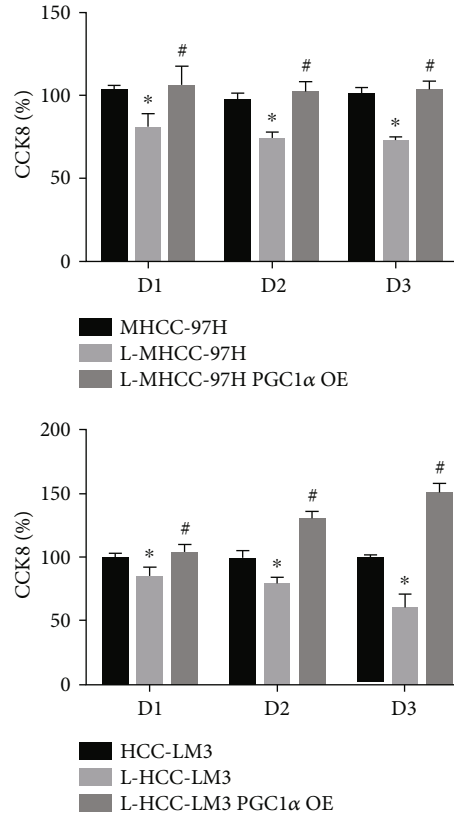


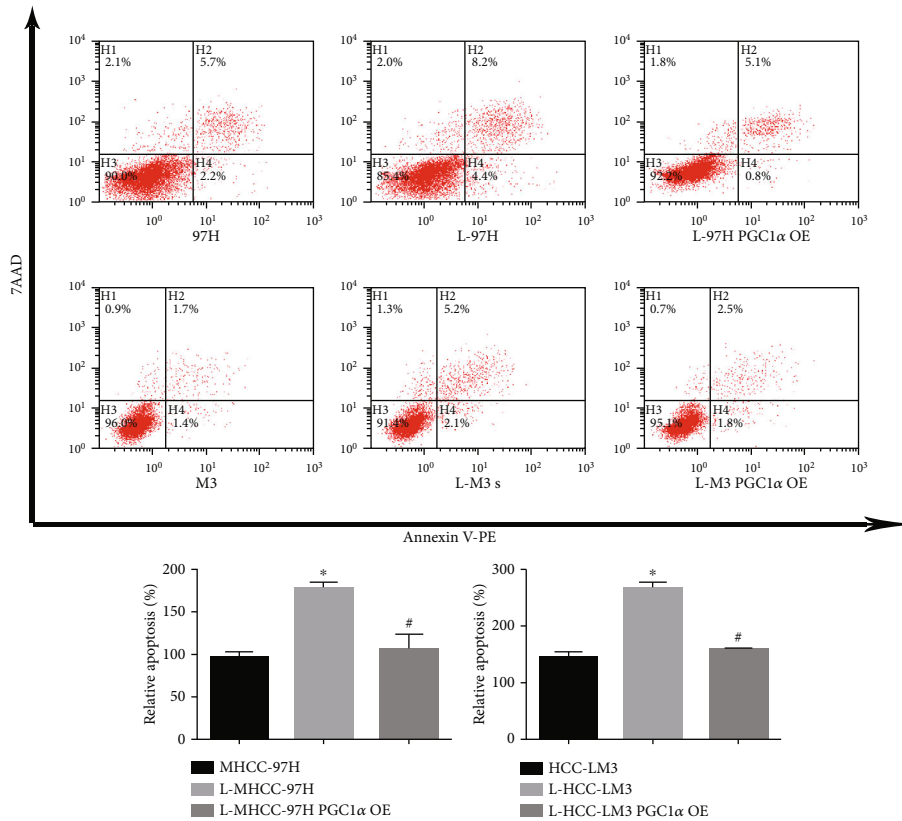
FIGURE 4: SET8 interacts with PGC1. (a) Mass spectrometry was used to analyse protein bands in the purified SET8 complex. (b) Interaction between SET8 and PGC1 $\alpha$  in HCC cells was measured by immunoprecipitation. (c) Colocalization of SET8 and PGC1 $\alpha$  in HCC cells as detected by confocal microscopy.

of PGC1 $\alpha$  resulted in decreased cell viability (Supplementary Figure S4A) and increased apoptosis (Supplementary Figure S4B) in MHCC-97H and HCC-LM3 cells, which was similar to the effect observed in fasting cells. Furthermore, overexpression of PGC1 $\alpha$  counteracted fasting-mediated ROS accumulation in HCC (Figure 5(c)). Similarly, PGC1 $\alpha$  knockdown augmented ROS accumulation in HCC cells (Supplementary Figure S4C), which was similar to the effect observed in fasting cells. We then analysed the effect of

PGC1 $\alpha$  on Keap1/Nrf2/ARE signalling pathway expression by qPCR or Western blotting. PGC1 $\alpha$  overexpression led to a decrease in Keap1 expression and an increase in Nrf2/ARE signalling pathway expression under fasting conditions (Figures 5(d) and 5(e)). Moreover, PGC1 $\alpha$  knockdown increased the expression of Keap1 while decreasing the expression of Nrf2/ARE signalling pathway components in HCC cells (Supplementary Figures S4D and E), which was similar to the effects observed in fasting cells.



(a)



(b)

FIGURE 5: Continued.

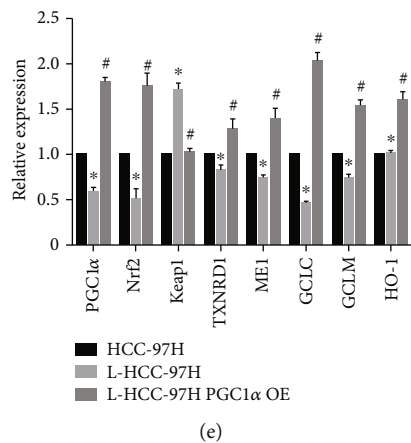
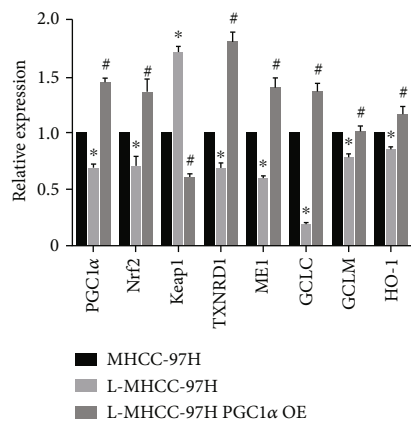
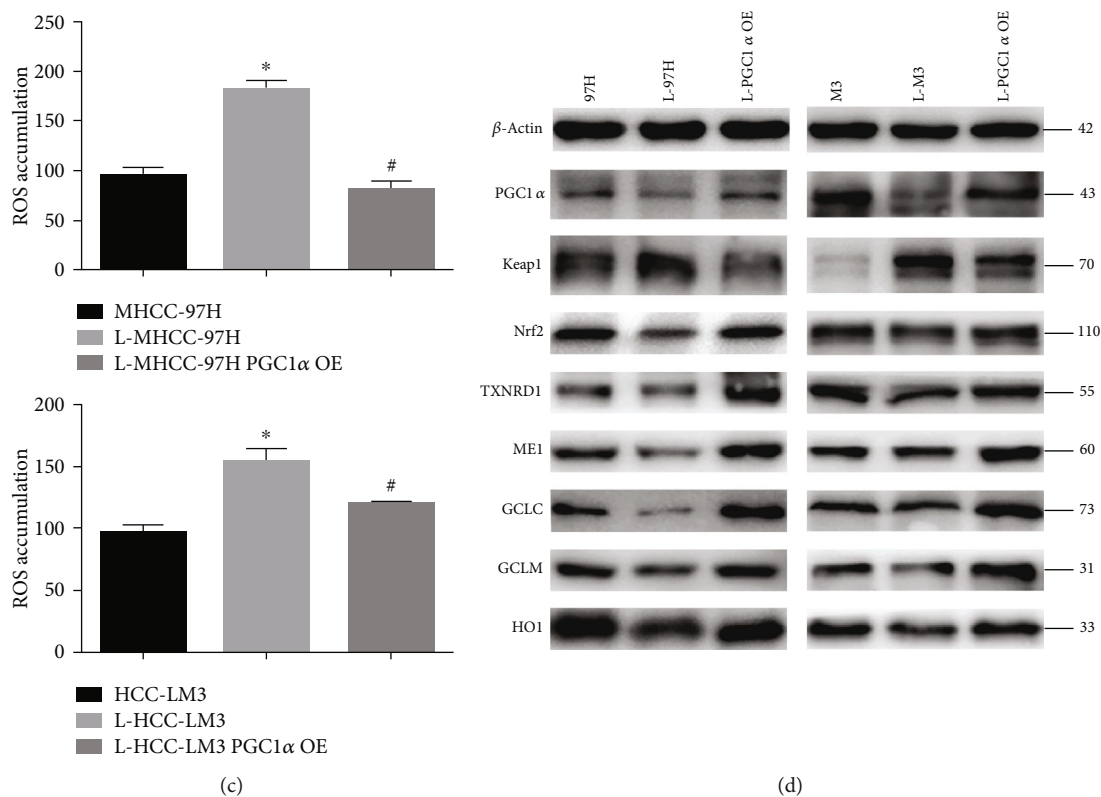


FIGURE 5: Continued.



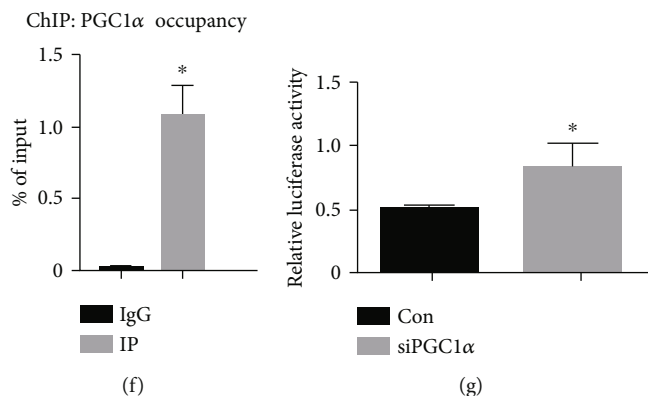


FIGURE 5: Role of PGC1 $\alpha$  in HCC cell viability and apoptosis in response to fasting. (a) Proliferation of MHCC-97H and HCC-LM3 cells under fasting conditions for 24 h or fasting in combination with overexpressed PGC1 $\alpha$ . (b) Flow cytometry was used to detect the number of apoptotic MHCC-97H and HCC-LM3 cells under fasting conditions for 24 h or fasting in combination with overexpressed PGC1 $\alpha$ . (c) The level of reactive oxygen species in MHCC-97H and HCC-LM3 cells under fasting conditions for 24 h or fasting in combination with overexpressed PGC1 $\alpha$ . (d) Western blot analysis of PGC1 $\alpha$  and Keap1/Nrf2/ARE signalling pathway components in MHCC-97H and HCC-LM3 cells under fasting conditions for 24 h or fasting in combination with overexpressed PGC1 $\alpha$ . (e) qPCR analysis of PGC1 $\alpha$  and Keap1/Nrf2/ARE signalling pathway components in MHCC-97H and HCC-LM3 cells under fasting conditions for 24 h or fasting in combination with overexpressed PGC1 $\alpha$ . (f) ChIP assay of PGC1 $\alpha$  presence at the promoter region of Keap1. Normal IgG was used as a control. (g) PGC1 $\alpha$  knockdown increased Keap1 luciferase activity in HCC-LM3 cells. Data are shown as the mean  $\pm$  SD of five independent experiments. \* $P < 0.05$  vs. the control group. # $P < 0.05$  vs. the fasting group.

3.6. *SET8 Interacts with PGC1 $\alpha$  to Positively Regulate Keap1 in HCC In Vitro, and Fasting Inhibits HCC Growth via SET8 Inhibition In Vivo.* Luciferase reporter assays indicated that SET8 not only attenuated Keap1 promoter activity but also strengthened the negative effect of PGC1 $\alpha$  on Keap1 promoter activity (Figure 6(a)). Moreover, mutant SET8<sup>R295G</sup> had no effect on Keap1 promoter activity in HCC cells (Figure 6(a)). Furthermore, Nrf2 expression was upregulated, while Keap1 expression was decreased in HCC cells overexpressing SET8 but not in those expressing mutant SET8<sup>R295G</sup> (Figure 6(b)).

Then, *in vivo* experiments were performed to verify the above conclusion. We found that fasting mice and mice injected with SET8 knockdown HCC cells had repressed tumour growth compared to the control group (Figures 6(c) and 6(d)). Additionally, in these mice, the expression of Nrf2 and its downstream effectors was decreased, while the expression of Keap1 was elevated (Figures 6(e) and 6(f)). We also found that the antitumour effects of fasting could be counteracted by overexpressing SET8 (Figures 6(c)–6(f)).

#### 4. Discussion

Mitochondria are the major cellular organelles that generate intracellular ROS and play a key role in apoptosis [27]. Excessive ROS production results in biomolecule damage and cancer cell apoptosis, and ROS have been widely found to play a crucial role in apoptosis upon cancer treatment [28]. Nrf2 is a member of the basic leucine zipper transcription factor NF-E2 family, which coordinates the induction of antioxidant and phase II detoxifying enzymes [29]. Keap1 is a component of the Cullin 3-based E3 ubiquitin ligase complex that controls the stability and accumulation of Nrf2 [30]. Normally, Nrf2 binds to Keap1 in the cytoplasm and is then degraded

by the proteasome pathway. Once activated, Nrf2 is translocated to the nucleus and binds to ARE to activate downstream phase II cell protective enzymes, including TXNRD1, ME1, GCLC, GCLM, and HO-1. After translation, the Nrf2 protein is rapidly degraded in the cytoplasm by the ubiquitin-proteasome system [30]. The Keap1/Nrf2/ARE signalling pathway is one of the most crucial antioxidant stress pathways in cells, and it plays an important role in redox regulation and oncogenic pathways [31]. Many studies have established that cancer cells survive under stress conditions via Nrf2-mediated oxidation resistance [32]. The mechanism by which Nrf2 promotes cancer cell formation and progression includes inhibition of apoptosis, induction of detoxification enzymes, and expression of antioxidative stress genes [33]. The activation of cell protective factors downstream of Nrf2 is conducive to the survival of cancer cells and resistance of cancer cells to chemotherapy [34]. It has been reported that Nrf2 is involved in the expression of antiapoptotic proteins, promotes chemotherapy tolerance of liver cancer, and is associated with the expression of Bcl-xl, an antiapoptotic gene [35]. In addition, it has been observed that ME1 expression is positively correlated with larger tumour size, higher grade, poorer survival, and chemotherapy resistance in breast cancer patients [36]. In the present study, knockdown of Keap1 under fasting conditions resulted in enhanced cell viability, the inhibition of apoptosis and ROS accumulation, and increased expression of Nrf2/ARE signalling pathway components (Supplementary Figures S1A–C). These data indicate that fasting mediated HCC apoptosis and Nrf2/ARE signalling pathway inhibition by upregulating Keap1 expression (Figures 2(a)–2(c)).

SET8 is the only enzyme that generates histone H4 monomethylation on lysine 20 (H4K20me1) in multicellular

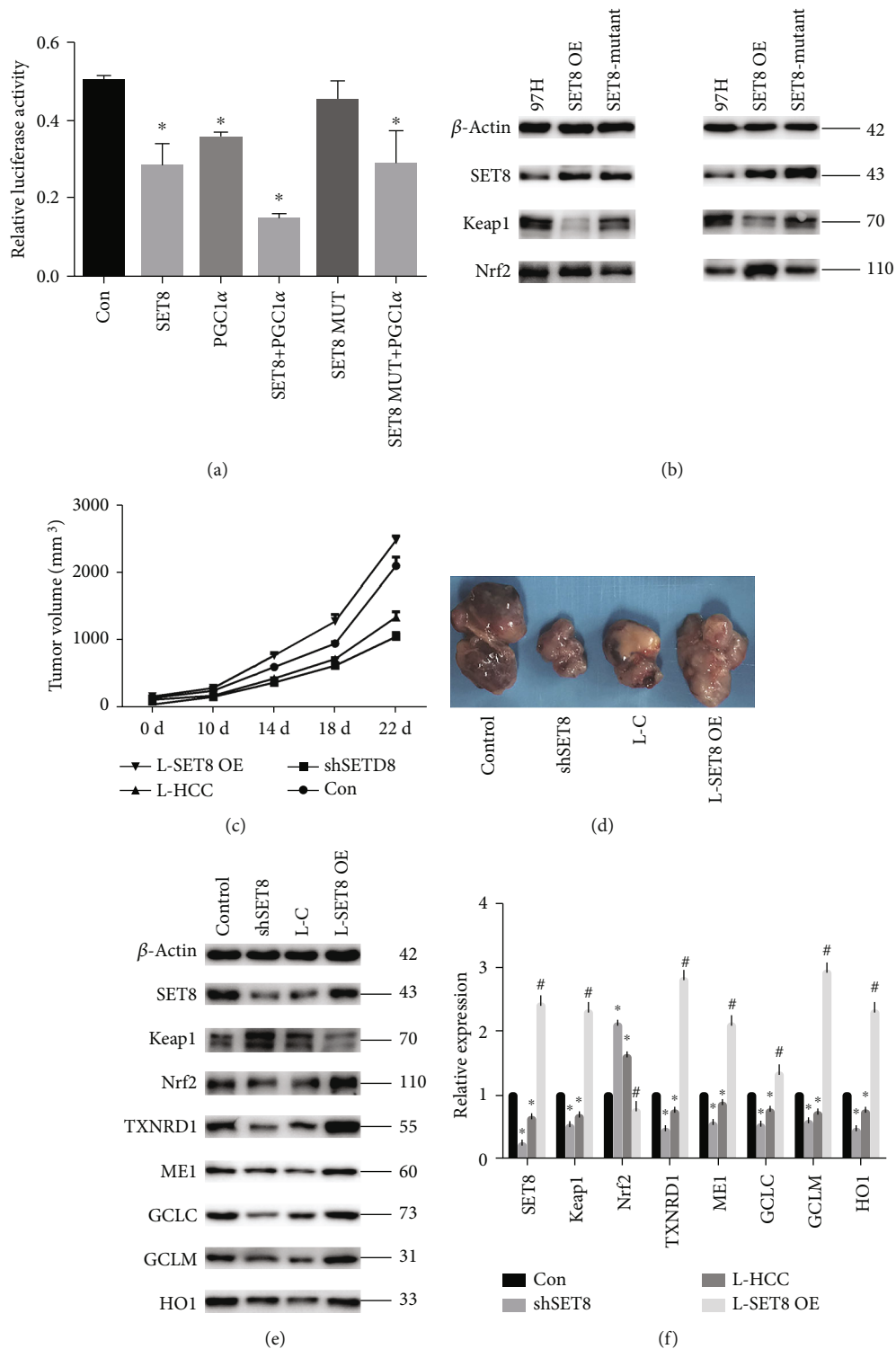


FIGURE 6: SET8 interacts with PGC1α to regulate Keap1 in HCC cells *in vitro*, and fasting inhibits HCC growth via SET8 inhibition *in vivo*. (a) The effects of SET8, PGC1α, and mutant SET8 on Keap1 luciferase activity in HCC-LM3 cells. (b) Western blotting was used to detect the SET8, Keap1, and Nrf2 proteins in MHCC-97 and HCC-LM3 cells overexpressing wild-type or mutant SET8. (c, d) Tumour growth following subcutaneous injection in the right flanks of Balb/c nude mice with 97H control cells, 97H-shSET8 cells, or 97H-SET8 overexpression cells (*n* = 6). (e) Western blotting was used to detect proteins SET8 and Keap1/Nrf2/ARE signalling pathway components in mice. (f) The mRNA expression of SET8 and Keap1/Nrf2/ARE signalling pathway components was examined by qPCR *in vivo*. Data are shown as the mean ± SD of five independent experiments. \**P* < 0.05 vs. the control group. #*P* < 0.05 vs. the fasting group.

organisms [17]. SET8 plays a key role in the epigenetic regulation of genes in many cellular processes [37]. Higher expression of SET8 in tumours is associated with high recurrence and low overall survival [23]. These observations indicate that SET8 may be a potential therapeutic target for tumour therapy. There is also evidence that SET8 may function as a barrier to mitochondrial oxidative phosphorylation activity [38]. SET8 was found to induce NQO1, a reductase that inhibits inflammation and apoptosis in cells [39]. Our previous study indicated that SET8 aggravated glycolytic metabolism and thus induced HCC progression [40]. Therefore, downregulation of SET8 expression could attenuate the malignant potential of cancer cells. In the present study, we found that SET8 was expressed at higher levels in HCC tissues than it was in paracarcinoma tissues (Figures 1(a) and 1(b)). To investigate the possible role of SET8 in the Keap1/Nrf2/ARE system in HCC, we transfected HCC cells to cause either knockdown or overexpression of SET8. We found that knockdown of SET8 downregulated the expression of Nrf2 and its downstream effectors and upregulated Keap1 expression (Supplementary Figures S2D and E). Moreover, the additional knockdown of Keap1 led to an increase in the expression of Nrf2/ARE signalling pathway components in SET8-silenced HCC cells (Supplementary Figures S3D and E). Furthermore, the ChIP assay in this study revealed that H4K20me1 is enriched in the Keap1 promoter region (Figure 3(f)). Luciferase reporter assays indicated that SET8 knockdown enhanced Keap1 promoter activity (Figure 3(g)), while SET8 overexpression attenuated Keap1 promoter activity (Figure 6(a)). These findings suggest that SET8 negatively modulates Keap1 expression and thus participates in fasting-mediated HCC cell apoptosis.

PGC1 $\alpha$  is a transcriptional coactivator of several transcription factors and nuclear receptors that regulate mitochondrial biogenesis and mitochondrial function [41]. PGC1 $\alpha$  is important for rapid cell adaptation to energy-demanding environments because it regulates oxidative phosphorylation, Krebs cycle enzymes, fatty acid oxidation, antioxidant components, and ROS levels [42]. Thus, PGC1 $\alpha$  is expressed especially in metabolically active tissues such as the liver, kidneys, and brain [43]. The role of PGC1 $\alpha$  in carcinogenesis has not been clear. Most experts believe early in carcinogenesis, PGC1 $\alpha$  may be downregulated, while in the later stages of tumour progression, PGC1 $\alpha$  is often upregulated [44]. A study in mice showed that PGC1 $\alpha$  regulates mitochondrial function and promotes tumour growth [45]. PGC1 $\alpha$  is highly upregulated and facilitates cancer metastasis in lung cancer [46]. To investigate whether PGC1 $\alpha$  affects the Keap1/Nrf2/ARE system in HCC, we transfected HCC cells to either knock down or overexpress PGC1 $\alpha$ . Our data demonstrated that knockdown of PGC1 $\alpha$  enhanced apoptosis, mediated ROS accumulation, and inhibited the Nrf2/ARE signalling pathway via upregulation of Keap1 expression. Moreover, PGC1 $\alpha$  overexpression attenuated fasting-mediated apoptosis and increased the tumour antioxidant capacity (Figures 5(b) and 5(c), Figure S4B and C). Furthermore, ChIP assay results indicated that PGC1 $\alpha$  was enriched at the Keap1 promoter region (Figure 5(f)). Luciferase reporter assays further indicated that PGC1 $\alpha$

knockdown enhanced Keap1 promoter activity (Figure 5(g)). These data indicate that PGC1 $\alpha$  negatively modulates Keap1 expression, thus participating in fasting-mediated Nrf2/ARE signalling pathway inhibition and HCC cell apoptosis. Furthermore, we found that PGC1 $\alpha$  interacted with SET8 by mass spectrometry analysis (Figure 4(a)). Co-IP and immunofluorescence analysis validated the interaction between and colocalization of PGC1 $\alpha$  and SET8 (Figures 4(b) and 4(c)). In addition, luciferase reporter assays indicated that SET8 not only attenuated Keap1 promoter activity but also strengthened the negative effect of PGC1 $\alpha$  on Keap1 promoter activity (Figure 6(a)). These results suggest that SET8 binds to PGC1 $\alpha$  to attenuate the activity of the promoter of Keap1, which leads to high expression of Nrf2 and a high level of oxidation resistance in HCC cells.

In previous studies, fasting was shown to reduce mammary carcinogenesis and decrease cancer cell proliferation [47, 48]. Another report in 4T1 breast cancer cells showed that the antitumour effect of fasting was mediated by increased oxidative stress and apoptosis [49]. Additionally, caloric restriction is reported to decrease proliferation, increase apoptosis, and decrease the metastatic burden in triple-negative breast cancers [50]. Other studies have observed that a fasting-mimicking diet downregulated the expression of HO-1 [48, 51]. The ketogenic diet is a type of fasting diet, and it can exacerbate metabolic oxidative stress in tumour cells [52]. In this study, we found that fasting increased apoptosis and ROS accumulation and inhibited the Nrf2/ARE signalling system via upregulation of Keap1 expression in HCC (Figures 2(a)–2(e)).

It is well known that fasting is the most physiological means of inducing autophagy [53]. Moreover, a previous study indicated that the inhibitory effect of fasting on tumour growth depends on autophagy [48]. Whether fasting-mediated autophagy was also regulated by SET8 deserves further research.

## 5. Conclusions

In summary, the present study demonstrated that fasting increased apoptosis and ROS accumulation and downregulated Nrf2/ARE signalling pathway expression via upregulation of Keap1 expression in HCC cells. Moreover, fasting inhibited SET8 and PGC1 $\alpha$  expression in HCC. Furthermore, SET8 interacted with PGC1 $\alpha$  to negatively regulate Keap1 expression, which participated in fasting-induced HCC apoptosis.

## Data Availability

The data that support the findings of this study are available from the corresponding authors upon reasonable request.

## Conflicts of Interest

The authors certify that there is no conflict of interest with any financial organization regarding the material discussed in the manuscript.

## Authors' Contributions

Jie Qi, Xiangyuan Chen, Qichao Wu, Jing Wang, and Hao Zhang contributed equally to this work.

## Acknowledgments

This work was supported by the National Science Foundation of China (Nos. 81871590, 81873948, and 81901999), the Natural Science Foundation of Shanghai (18ZR1407400), the Shanghai Municipal Commission of Health and Family Planning, the Key Developing Disciplines (2015ZB0104), the Program of Shanghai Subject Chief Scientist (16XD1400900), the Shanghai Shengkang Hospital Development Center Clinical Science and Technology Innovation Project (SHDC12018105), and the National Key R&D Program of China (No. 2018YFC2001900-04).

## Supplementary Materials

Supplementary Figure S1: (A) proliferation of MHCC-97H and HCC-LM3 cells under fasting conditions for 24 h or fasting in combination with Keap1 knockdown, (B) flow cytometry was used to detect the number of apoptotic MHCC-97H and HCC-LM3 cells under fasting conditions for 24 h or fasting in combination with Keap1 knockdown, (C) the level of reactive oxygen species in MHCC-97H and HCC-LM3 cells under fasting conditions for 24 h or fasting in combination with Keap1 knockdown, (D) Western blot analysis of SET8 and Keap1/Nrf2/ARE signalling pathway components in MHCC-97H and HCC-LM3 cells under fasting conditions for 24 h or fasting in combination with Keap1 knockdown, (E) qPCR analysis of SET8 and Keap1/Nrf2/ARE signalling pathway components in MHCC97H and HCC-LM3 cells under fasting conditions for 24 h or fasting in combination with Keap1 knockdown. Data are shown as the mean  $\pm$  SD of five independent experiments. \* $P < 0.05$  vs. the control group. # $P < 0.05$  vs. the fasting group. Supplementary Figure S2: (A) proliferation of MHCC-97H and HCC-LM3 cells following SET8 knockdown, (B) flow cytometry was used to detect the number of apoptotic MHCC-97H and HCC-LM3 cells following SET8 knockdown, (C) the level of reactive oxygen species in MHCC-97H and HCC-LM3 cells following SET8 knockdown, (D) Western blot analysis of SET8 and Keap1/Nrf2/ARE signalling pathway components in MHCC-97H and HCC-LM3 cells following SET8 knockdown, (E) qPCR analysis of SET8 and Keap1/Nrf2/ARE signalling pathway components in MHCC-97H and HCC-LM3 cells following SET8 knockdown. Data are shown as the mean  $\pm$  SD of five independent experiments. \* $P < 0.05$  vs. the control group. Supplementary Figure S3: (A) proliferation of MHCC-97H and HCC-LM3 cells following SET8 knockdown alone or in combination with Keap1 knockdown, (B) flow cytometry was used to detect the number of apoptotic MHCC-97H and HCC-LM3 cells following SET8 knockdown alone or in combination with Keap1 knockdown, (C) the level of reactive oxygen species in MHCC97H and HCC-LM3 cells following SET8 knockdown alone or in combination with Keap1 knockdown,

(D) Western blot analysis of SET8 and Keap1/Nrf2/ARE signalling pathway components in MHCC-97H and HCC-LM3 cells following SET8 knockdown alone or in combination with Keap1 knockdown, (E) qPCR analysis of SET8 and Keap1/Nrf2/ARE signalling pathway components in MHCC-97H and HCC-LM3 cells following SET8 knockdown alone or in combination with Keap1 knockdown. Data are shown as the mean  $\pm$  SD of five independent experiments. \* $P < 0.05$  vs. the control group. # $P < 0.05$  vs. the SET8 knockdown group. Supplementary Figure S4: (A) proliferation of MHCC-97H and HCC-LM3 cells following PGC1 $\alpha$  knockdown, (B) flow cytometry was used to detect the number of apoptotic MHCC-97H and HCC-LM3 cells following PGC1 $\alpha$  knockdown, (C) the level of reactive oxygen species in MHCC-97H and HCC-LM3 cells following PGC1 $\alpha$  knockdown, (D) Western blot analysis of PGC1 $\alpha$  and Keap1/Nrf2/ARE signalling pathway components in MHCC-97H and HCC-LM3 cells following PGC1 $\alpha$  knockdown, (E) qPCR analysis of PGC1 $\alpha$  and Keap1/Nrf2/ARE signalling pathway components in MHCC97H and HCC-LM3 cells following PGC1 $\alpha$  knockdown. Data are shown as the mean  $\pm$  SD of three independent experiments. \* $P < 0.05$  vs. the control group. (*Supplementary Materials*)

## References

- [1] P. Bertuccio, F. Turati, G. Carioli et al., "Global trends and predictions in hepatocellular carcinoma mortality," *Journal of Hepatology*, vol. 67, no. 2, pp. 302–309, 2017.
- [2] D. Hanahan and R. A. Weinberg, "The hallmarks of cancer," *Cell*, vol. 100, no. 1, pp. 57–70, 2000.
- [3] L. L. Fan, G. P. Sun, W. Wei et al., "Melatonin and doxorubicin synergistically induce cell apoptosis in human hepatoma cell lines," *World Journal of Gastroenterology*, vol. 16, no. 12, pp. 1473–1481, 2010.
- [4] J. Martin-Renedo, J. L. Mauriz, F. Jorquera, O. Ruiz-Andres, P. Gonzalez, and J. Gonzalez-Gallego, "Melatonin induces cell cycle arrest and apoptosis in hepatocarcinoma HepG2 cell line," *Journal of Pineal Research*, vol. 45, no. 4, pp. 532–540, 2008.
- [5] R. J. Ortiz-Bautista, C. A. Aguilar-Salinas, and A. Monroy-Guzman, "Caloric restriction: about its positive metabolic effects and cellular impact," *Cirugia y Cirujanos*, vol. 81, no. 5, pp. 459–464, 2013.
- [6] O. Warburg, "On the origin of cancer cells," *Science*, vol. 123, no. 3191, pp. 309–314, 1956.
- [7] L. Fontana, L. Partridge, and V. D. Longo, "Extending healthy life span—from yeast to humans," *Science*, vol. 328, no. 5976, pp. 321–326, 2010.
- [8] F. Madeo, D. Carmona-Gutierrez, S. J. Hofer, and G. Kroemer, "Caloric restriction mimetics against age-associated disease: targets, mechanisms, and therapeutic potential," *Cell Metabolism*, vol. 29, no. 3, pp. 592–610, 2019.
- [9] S. Golbidi, A. Daiber, B. Korac, H. Li, M. F. Essop, and I. Laher, "Health benefits of fasting and caloric restriction," *Current Diabetes Reports*, vol. 17, no. 12, p. 123, 2017.
- [10] H. Yaribeygi, S. L. Atkin, M. Ramezani, and A. Sahebkar, "A review of the molecular pathways mediating the improvement in diabetes mellitus following caloric restriction," *Journal of Cellular Physiology*, vol. 234, no. 6, pp. 8436–8442, 2019.

- [11] H. J. Thompson, Z. Zhu, and W. Jiang, "Identification of the apoptosis activation cascade induced in mammary carcinomas by energy restriction," *Cancer Research*, vol. 64, no. 4, pp. 1541–1545, 2004.
- [12] M. S. De Lorenzo, E. Baljinnyam, D. E. Vatner, P. Abarzua, S. F. Vatner, and A. B. Rabson, "Caloric restriction reduces growth of mammary tumors and metastases," *Carcinogenesis*, vol. 32, no. 9, pp. 1381–1387, 2011.
- [13] K. M. Holmstrom, R. V. Kostov, and A. T. Dinkova-Kostova, "The multifaceted role of Nrf2 in mitochondrial function," *Current Opinion in Toxicology*, vol. 1, pp. 80–91, 2016.
- [14] A. Kobayashi, M. I. Kang, H. Okawa et al., "Oxidative stress sensor Keap1 functions as an adaptor for Cul3-based E3 ligase to regulate proteasomal degradation of Nrf2," *Molecular and Cellular Biology*, vol. 24, no. 16, pp. 7130–7139, 2004.
- [15] K. Itoh, N. Wakabayashi, Y. Katoh et al., "Keap1 represses nuclear activation of antioxidant responsive elements by Nrf2 through binding to the amino-terminal Neh2 domain," *Genes & Development*, vol. 13, no. 1, pp. 76–86, 1999.
- [16] M. Zhang, C. Zhang, L. Zhang et al., "Nrf2 is a potential prognostic marker and promotes proliferation and invasion in human hepatocellular carcinoma," *BMC Cancer*, vol. 15, no. 1, 2015.
- [17] S. Jorgensen, G. Schotta, and C. S. Sorensen, "Histone H4 lysine 20 methylation: key player in epigenetic regulation of genomic integrity," *Nucleic Acids Research*, vol. 41, no. 5, pp. 2797–2806, 2013.
- [18] M. Shoaib, D. Walter, P. J. Gillespie et al., "Histone H4K20 methylation mediated chromatin compaction threshold ensures genome integrity by limiting DNA replication licensing," *Nature Communications*, vol. 9, no. 1, p. 3704, 2018.
- [19] F. Yang, L. Sun, Q. Li et al., "SET8 promotes epithelial-mesenchymal transition and confers TWIST dual transcriptional activities," *The EMBO Journal*, vol. 31, no. 1, pp. 110–123, 2012.
- [20] H. Oda, I. Okamoto, N. Murphy et al., "Monomethylation of histone H4-lysine 20 is involved in chromosome structure and stability and is essential for mouse development," *Molecular and Cellular Biology*, vol. 29, no. 8, pp. 2278–2295, 2009.
- [21] T. Liao, Y. J. Wang, J. Q. Hu et al., "Histone methyltransferase KMT5A gene modulates oncogenesis and lipid metabolism of papillary thyroid cancer in vitro," *Oncology Reports*, vol. 39, no. 5, pp. 2185–2192, 2018.
- [22] F. Guo, B. C. Parker Kerrigan, D. Yang et al., "Post-transcriptional regulatory network of epithelial-to-mesenchymal and mesenchymal-to-epithelial transitions," *Journal of Hematology & Oncology*, vol. 7, no. 1, article 19, 2014.
- [23] Z. Lin, H. Jia, L. Hong et al., "Prognostic impact of SET domain-containing protein 8 and protein arginine methyltransferase 5 in patients with hepatocellular carcinoma following curative resection," *Oncology Letters*, vol. 16, no. 3, pp. 3665–3673, 2018.
- [24] X. Chen, Q. Wu, H. Jiang et al., "SET8 is involved in the regulation of hyperglycemic memory in human umbilical endothelial cells," *Acta Biochimica et Biophysica Sinica*, vol. 50, no. 7, pp. 635–642, 2018.
- [25] T. Cui, B. He, S. Kong et al., "PR-Set7 deficiency limits uterine epithelial population growth hampering postnatal gland formation in mice," *Cell Death and Differentiation*, vol. 24, no. 12, pp. 2013–2021, 2017.
- [26] G. Bianchi, R. Martella, S. Ravera et al., "Fasting induces anti-Warburg effect that increases respiration but reduces ATP-synthesis to promote apoptosis in colon cancer models," *Oncotarget*, vol. 6, no. 14, pp. 11806–11819, 2015.
- [27] H. Vakifahmetoglu-Norberg, A. T. Ouchida, and E. Norberg, "The role of mitochondria in metabolism and cell death," *Biochemical and Biophysical Research Communications*, vol. 482, no. 3, pp. 426–431, 2017.
- [28] M. Wojcik, M. Krawczyk, P. Wojcik, K. Cypryk, and L. A. Wozniak, "Molecular mechanisms underlying curcumin-mediated therapeutic effects in type 2 diabetes and cancer," *Oxidative Medicine and Cellular Longevity*, vol. 2018, Article ID 9698258, 14 pages, 2018.
- [29] A. Bresciani, A. Missineo, M. Gallo et al., "Nuclear factor (erythroid-derived 2)-like 2 (NRF2) drug discovery: biochemical toolbox to develop NRF2 activators by reversible binding of Kelch-like ECH-associated protein 1 (KEAP1)," *Archives of Biochemistry and Biophysics*, vol. 631, pp. 31–41, 2017.
- [30] H. K. Bryan, A. Olayanju, C. E. Goldring, and B. K. Park, "The Nrf2 cell defence pathway: Keap1-dependent and -independent mechanisms of regulation," *Biochemical Pharmacology*, vol. 85, no. 6, pp. 705–717, 2013.
- [31] T. Nguyen, P. Nioi, and C. B. Pickett, "The Nrf2-antioxidant response element signaling pathway and its activation by oxidative stress," *The Journal of Biological Chemistry*, vol. 284, no. 20, pp. 13291–13295, 2009.
- [32] M. K. Kwak and T. W. Kensler, "Targeting NRF2 signaling for cancer chemoprevention," *Toxicology and Applied Pharmacology*, vol. 244, no. 1, pp. 66–76, 2010.
- [33] K. Taguchi, H. Motohashi, and M. Yamamoto, "Molecular mechanisms of the Keap1-Nrf2 pathway in stress response and cancer evolution," *Genes to Cells*, vol. 16, no. 2, pp. 123–140, 2011.
- [34] F. Jeddi, N. Soozangar, M. R. Sadeghi, M. H. Somi, and N. Samadi, "Contradictory roles of Nrf2/Keap1 signaling pathway in cancer prevention/promotion and chemoresistance," *DNA Repair*, vol. 54, pp. 13–21, 2017.
- [35] S. K. Niture and A. K. Jaiswal, "Nrf2-induced antiapoptotic Bcl-xL protein enhances cell survival and drug resistance," *Free Radical Biology and Medicine*, vol. 57, pp. 119–131, 2013.
- [36] R. Liao, G. Ren, H. Liu et al., "ME1 promotes basal-like breast cancer progression and associates with poor prognosis," *Scientific Reports*, vol. 8, no. 1, p. 16743, 2018.
- [37] J. F. Couture, E. Collazo, J. S. Brunzelle, and R. C. Trievel, "Structural and functional analysis of SET8, a histone H4 Lys-20 methyltransferase," *Genes & Development*, vol. 19, no. 12, pp. 1455–1465, 2005.
- [38] H. Tanaka, S. I. Takebayashi, A. Sakamoto et al., "The SETD8/PR-Set7 methyltransferase functions as a barrier to prevent senescence-associated metabolic remodeling," *Cell Reports*, vol. 18, no. 9, pp. 2148–2161, 2017.
- [39] V. Singh, P. Prakhar, R. S. Rajmani, K. Mahadiq, S. M. Borbora, and K. N. Balaji, "Histone methyltransferase SET8 epigenetically reprograms host immune responses to assist mycobacterial survival," *The Journal of Infectious Diseases*, vol. 216, no. 4, pp. 477–488, 2017.
- [40] X. Chen, X. Ding, Q. Wu, J. Qi, M. Zhu, and C. Miao, "Monomethyltransferase SET8 facilitates hepatocellular carcinoma growth by enhancing aerobic glycolysis," *Cell Death & Disease*, vol. 10, no. 4, p. 312, 2019.

- [41] P. Puigserver, Z. Wu, C. W. Park, R. Graves, M. Wright, and B. M. Spiegelman, "A cold-inducible coactivator of nuclear receptors linked to adaptive thermogenesis," *Cell*, vol. 92, no. 6, pp. 829–839, 1998.
- [42] J. St-Pierre, J. Lin, S. Krauss et al., "Bioenergetic analysis of peroxisome proliferator-activated receptor gamma coactivators 1 $\alpha$  and 1 $\beta$  (PGC-1 $\alpha$  and PGC-1 $\beta$ ) in muscle cells," *Journal of Biological Chemistry*, vol. 278, no. 29, pp. 26597–26603, 2003.
- [43] J. A. Villena, "New insights into PGC-1 coactivators: redefining their role in the regulation of mitochondrial function and beyond," *The FEBS Journal*, vol. 282, no. 4, pp. 647–672, 2015.
- [44] F. Mastropasqua, G. Girolimetti, and M. Shoshan, "PGC1 $\alpha$ : friend or foe in cancer?," *Genes*, vol. 9, no. 1, p. 48, 2018.
- [45] K. Bhalla, B. J. Hwang, R. E. Dewi et al., "PGC1 $\alpha$  promotes tumor growth by inducing gene expression programs supporting lipogenesis," *Cancer Research*, vol. 71, no. 21, pp. 6888–6898, 2011.
- [46] J. D. Li, Q. C. Feng, Y. Qi, G. Cui, and S. Zhao, "PPARGC1A is upregulated and facilitates lung cancer metastasis," *Experimental Cell Research*, vol. 359, no. 2, pp. 356–360, 2017.
- [47] H. J. Thompson, J. N. McGinley, N. S. Spoelstra, W. Jiang, Z. Zhu, and P. Wolfe, "Effect of dietary energy restriction on vascular density during mammary carcinogenesis," *Cancer Research*, vol. 64, no. 16, pp. 5643–5650, 2004.
- [48] F. Pietrocola, J. Pol, E. Vacchelli et al., "Caloric restriction mimetics enhance anticancer immunosurveillance," *Cancer Cell*, vol. 30, no. 1, pp. 147–160, 2016.
- [49] C. Lee, L. Raffaghello, S. Brandhorst et al., "Fasting cycles retard growth of tumors and sensitize a range of cancer cell types to chemotherapy," *Science Translational Medicine*, vol. 4, no. 124, article 124ra27, 2012.
- [50] B. A. Simone, T. Dan, A. Palagani et al., "Caloric restriction coupled with radiation decreases metastatic burden in triple negative breast cancer," *Cell Cycle*, vol. 15, no. 17, pp. 2265–2274, 2016.
- [51] S. Di Biase, C. Lee, S. Brandhorst et al., "Fasting-mimicking diet reduces HO-1 to promote T cell-mediated tumor cytotoxicity," *Cancer Cell*, vol. 30, no. 1, pp. 136–146, 2016.
- [52] A. F. Branco, A. Ferreira, R. F. Simões et al., "Ketogenic diets: from cancer to mitochondrial diseases and beyond," *European Journal of Clinical Investigation*, vol. 46, no. 3, pp. 285–298, 2016.
- [53] N. Mizushima, A. Yamamoto, M. Matsui, T. Yoshimori, and Y. Ohsumi, "In vivo analysis of autophagy in response to nutrient starvation using transgenic mice expressing a fluorescent autophagosome marker," *Molecular Biology of the Cell*, vol. 15, no. 3, pp. 1101–1111, 2004.

## Research Article

# Chidamide Inhibits Glioma Cells by Increasing Oxidative Stress via the miRNA-338-5p Regulation of Hedgehog Signaling

Haixia Zhou,<sup>1</sup> Liang Han,<sup>2</sup> Han Wang,<sup>3</sup> Jun Wei,<sup>4</sup> Zhigang Guo ,<sup>5</sup> and Zhaohui Li <sup>5</sup>

<sup>1</sup>VIP Unit, China-Japan Union Hospital of Jilin University, Changchun 130033, China

<sup>2</sup>Department of Pathology, China-Japan Union Hospital of Jilin University, Changchun 130033, China

<sup>3</sup>Department of Clinical Laboratory, Chinese Medicine University Affiliated Hospital, Changchun 130021, China

<sup>4</sup>Surgery Institute, China-Japan Union Hospital of Jilin University, Changchun 130033, China

<sup>5</sup>Department of Neurosurgery, China-Japan Union Hospital of Jilin University, Changchun 130033, China

Correspondence should be addressed to Zhigang Guo; [guozhigangjlu@126.com](mailto:guozhigangjlu@126.com) and Zhaohui Li; [lizhaohuijlu@163.com](mailto:lizhaohuijlu@163.com)

Received 8 August 2019; Revised 28 October 2019; Accepted 5 November 2019; Published 11 March 2020

Guest Editor: Nagendra K. Kaushik

Copyright © 2020 Haixia Zhou et al. This is an open access article distributed under the Creative Commons Attribution License, which permits unrestricted use, distribution, and reproduction in any medium, provided the original work is properly cited.

**Objective.** Chidamide has a broad spectrum of antitumor activity but its function on glioma remains unknown. The increase of reactive oxygen species (ROS) and reactive nitrogen species (RNS) may control glioma risk by promoting its apoptosis and necrosis. Hedgehog pathway is crucial to glioma cell proliferation and controls ROS production. We aimed to explore the effects of chidamide on the levels of miR-338-5p (glioma cell inhibitor), which may regulate Hedgehog signaling, resulting in the changes of RNS. **Materials and Methods.** Migration and invasion activities of glioma cells were measured by using the Transwell chamber assay. The expression levels of Sonic Hedgehog (Shh), Indian Hedgehog (Ihh), Desert Hedgehog (Dhh), miR-338-5p, and related molecules were detected by using real-time PCR (RT-PCR) and or Western Blot in U87 and HS683 glioma cells. The effects of chidamide on these molecules were measured by using the miR-338-5p inhibitor or mimics in U87 and HS683 glioma cell lines. ROS and RNS were measured by DCF DA and DAF-FM DA fluorescence. Biomarkers of oxidative stress were measured by using a corresponding kit. Apoptosis and necrosis rates were measured by using flow cytometry. **Results.** Chidamide inhibited the growth rate, migration, and invasion of human malignant glioma cells and increased the level of miR-338-5p. miR-338-5p inhibitor or mimics increased or inhibited the growth rate of U87 and HS683 glioma cells. Chidamide inhibited the levels of Shh, Ihh, migration protein E-cadherin, and invading protein MMP-2. The increase in the level of Shh and Ihh led to the reduction in the ROS and RNS levels. miR-338-5p inhibitor or mimics also showed a promoting or inhibitory function for the levels of Shh and Ihh. Furthermore, miR-338-5p mimics and inhibitor inhibited or promoted the migration and invasion of the glioma cells ( $P < 0.05$ ). Evaluated levels of miR-338-5p increased oxidative stress level and apoptosis and necrosis rate by regulating the levels of biomarkers of oxidative stress ( $P < 0.05$ ). **Conclusion.** Chidamide inhibits glioma cells by increasing oxidative stress via the miRNA-338-5p regulation of Hedgehog signaling. Chidamide may be a potential drug in the prevention of glioma development.

## 1. Introduction

Gliomas are glial brain tumors derived from astrocytic, oligodendroglial, and ependymal cells. Malignant glioma accounts for 14,000 deaths annually and more than 20,000 new cases are found each year [1]. The specific pathogenesis of glioma remains unclear. Exploring drugs [2] and therapeutic targets [3, 4], improving survival [5], and reducing mortality is a hotspot in glioma research [6].

Histone deacetylase (HDAC) is often found to be upregulated in human malignancy. HDAC1 [7, 8], HDAC2 [9, 10], and HDAC3 [9, 11] have been reported to play an important role in the growth of glioma cells or the tumorigenesis of glioma. Thus, the inhibitor of HDAC may be beneficial in the prevention of glioma. Chidamide is a HDAC inhibitor which can inhibit HDAC1, HDAC2, HDAC3, and HDAC10 [12, 13] and can also inhibit the growth of cancer cells such as lung cancer [14] and pancreatic cancer cells [15] and

promote their apoptosis [16]. Thus, chidamide may be a potential drug for controlling glioma cell proliferation. However, its effects on glioma growth and related molecular mechanisms remain unknown.

Numerous growth factors play a regulatory role in glioma formation, and Hedgehog (Hh) gene-encoded protein or Hedgehog (*Hh*) gene function in glioma development has received much attention [17]. The Hedgehog signaling pathway is essential for glioma-initiating cell proliferation and maybe the pathogenesis of glioma [18]. Hedgehog signaling reduces apoptosis in cancer cells by controlling oxidative stress [19], and oxidative stress may control glioma development via the upregulation of apoptosis. There are at least three Hh genes in vertebrates, namely, Sonic Hedgehog (Shh), Indian Hedgehog (Ihh), and Desert Hedgehog (Dhh) [20]. The N-terminal structure of the Ihh protein is 93%, identical to Shh, and both have similar activities and receptor and signal transduction pathways.

Whether chidamide affects Hedgehog signalling is not well understood. MicroRNAs (miR) are potential molecules for affecting cancer cell behavior [21]. MicroRNA-34a can promote apoptosis in glioma cells by enhancing the levels of reactive oxygen species (ROS) production and NOX2 expression [22]. The coding gene for the miR-338-5p subtype of miR-338 is located in the 8th intron of the gene encoding the apoptosis-associated tyrosine kinase. miR-338-5p may be a potential inhibitor in the prevention of glioma risk [23]. ROS and reactive nitrogen species (RNS) are associated with the changes of the redox system in a glioma angiogenic microenvironment [24]. Chidamide may affect miR-338-5p, which regulates Hedgehog signaling, resulting in the changes of ROS and RNS. ROS and RNS may promote the apoptosis of glioma and control its progression.

## 2. Materials and Methods

**2.1. Cell Culture.** U87 and HS683 cells are the most representative glioma cell lines [25, 26] and are very sensitive to chidamide; therefore, they have been chosen in the present work. U87 and HS683 glioma cell lines were purchased from Cell Bank (Shanghai, China). The cells were cultured in DMEM medium containing 10% fetal bovine serum in a 5% CO<sub>2</sub>, 37°C incubator, and grown to 80% confluency. The cells were digested by using 1 mL of 0.25% trypsin and 0.2% EDTA and passed to a new dish for further culture. The cell lines used in this experiment were with the best activity in culture for 4 passages.

**2.2. Cell Transfection.** Transfection reaction was carried out when the cells were grown to 80% confluency in a six-well plate. The miR-338-5p mimic and the miR-338-5p inhibitor were designed and synthesized by Guangzhou Ruibo Biotechnology Co., Ltd. (Guangzhou, China). The sequence for the negative mimic control was 5'-UCACAA CCUCCUAGAAAGAGUAGA-3', the sequence for the has-miR-338-5p mimic was 5'-AACAAUAUCCUGGUC UGAGUG-3', and the sequence for the miR-338-5p inhibitor was 5'-AACAAUAUCCUGGUCUGAGUG-3' [27].

Experiments were performed using the RNAiMAX Transfection Reagent from Thermo Fisher Scientific (MA, USA). The procedure of the cell transfection experiment was as follows: 100 nM miR-338-5p mimic, miR-338-5p inhibitor, and control were prepared using 250  $\mu$ L of DMEM medium. 4  $\mu$ L of RNAiMAX was added to 250  $\mu$ L of DMEM medium, gently mixed, and allowed to stand at room temperature for 5 min. The mixture was sequentially added to the corresponding six wells. In each well of the plate, 1.5 mL of medium was added. After 6 hours of transfection, the solution in each well was replaced with 2 mL of medium and continued to culture for 24 h. All cells were assigned into the following groups: control group (CG, wild type without chidamide treatment), chidamide group (CHG, treated with 10  $\mu$ M chidamide for 24 h), miR-338-5p mimic group (MG), miR-338-5p inhibitor group (IG), chidamide-treated miR-338-5p mimic group (CHMG), and chidamide-treated miR-338-5p inhibitor group (CHIG). After transfection, luciferase activity was measured using the Dual Luciferase Reporter Assay System (Promega Corporation, Madison, MA, USA). Firefly luciferase activity was normalized against miR-338-5p activity.

**2.3. Measurement of HDAC Activity.** A HDAC assay kit was purchased from BioVision, Inc. (Milpitas, CA, USA). HDAC activity was detected by an optical density method according to the kit instructions, and 6 wells were used in each group. HDAC activity was detected by hypoxia and reoxygenation, and the results were presented as the ratio of a positive control in the kit. The IC<sub>50</sub> value was calculated according to time- and dose-response curves by using the SPSS probit model analysis (SPSS v20.0; SPSS, Inc., Chicago, IL, USA).

**2.4. DNA Synthesis Assay of Tritiated Thymidine (<sup>3</sup>H-TdR) in Glioma Cells.** Glioma cell lines U87 and HS683 were inoculated in 96-well plates at a density of 5  $\times$  10<sup>3</sup>. A <sup>3</sup>H-TdR kit was purchased from China Isotope & Radiation Corporation (Beijing, China). Logarithmic cells were digested into single cells with 0.25% trypsin+0.02% EDTA-2Na. The DMEM medium containing 10% FBS was adjusted to a cell concentration of 5  $\times$  10<sup>3</sup>/mL. 100  $\mu$ L of cell suspension was added to each well and cultured in a 37°C, 5% CO<sub>2</sub>, and saturated humidity incubator for 24 h until the cells were attached, and then cultured in DMEM containing 4% FBS. After 24 h, the plates were removed and chidamide was added at different concentrations (0-14  $\mu$ M chidamide). Each group was given 5 replicate wells and cultured for 24 h. The plate was taken out and 100  $\mu$ L of <sup>3</sup>H-TdR was added to each well to a final concentration of 3.7  $\times$  10<sup>7</sup> Bq/mL. The cells were continually cultured for 24 h, the liquid was discarded, and the cells were washed 3 times with PBS, and then 2 mL of pre-cooled 10% TCA was added and treated for 10 min. 0.5 mL of 0.3 M NaOH was added to each well, treated at 60°C for 30 min, and then allowed to cool to room temperature. The lysate was collected, transferred to a scintillation vial, and 5 mL of scintillation fluid was added, and the radioactivity count (r/min) of each bottle was measured in a FJ-2107PFJ-2107P liquid scintillator (Xi'an, China). A long half-life of chidamide ranging between 16.8-18.3 h and 24 h may be a



TABLE 1: The primers used in the present study.

Gene	Forward primer (5'-3')	Reverse primer (5'-3')
miR-338-5p	GGGAACAATATCCTGGTGC	GTGCAGGGTCCGAGGT
Shh	AGCTGGAGAAGTTTAGGGTG	CAAGCCAGGGCAGAGGTAG
Ihh	CCGCAATAAGTATGGACTGC	TTGGCTGCGGCCGAGTGCT
Dhh	AGGAGCGGGTGAACGCTTTG	GCGCCAGCAACCCATACTTG
E-cadherin	CCTCGACACCCGATTCAAAG	CCACTGTATTTCAGCGTGAC
MMP-2	TGCACTGATACCGGCCGCAG	AACTTGCAGGGCTGTCCCTC
GAPDH	GTCTCCTCTGACTTCAA	ACCACCCTGTTGCTGTA

Note: Shh—Sonic Hedgehog; Ihh—Indian Hedgehog; Dhh—Desert Hedgehog; MMP-2—matrix metalloproteinase-2.

better period for evaluating its function [28]. Thus, 24 h was chosen in the subsequent experiment.

**2.5. Cell Migration Ability Analysis.** The malignant glioma cell lines U87 and HS683 were cultured in a 6-well Transwell plate. When the cell confluency was close to 100%, a 20  $\mu$ L tip was used to scratch each well in a 6-well plate in one direction, and followed by PBS wash. Net floating cells were treated with a solvent group containing 0.1% DMSO (control group) and 10  $\mu$ M chidamide for 24 h. Microscopy photographed the width of the scratched area at 0 and 24 h. Quantitative assessment was performed to measure the effect of chidamide on glioma cell migration. Relative migration distance was calculated as follows: the 0 h and 24 h invaded distances were recorded as  $D_0$  and  $D_{24}$ . Relative migration distance rate =  $(D_0 - D_{24})/D_0 \times 100\%$ .

**2.6. Cell Invasion Ability Analysis.** Matrigel was thawed in a refrigerator at 4°C overnight. Matrigel and serum-free DMEM were placed in each cell at a ratio of 1 : 8 in 60  $\mu$ L/cell. After incubation in a 37°C incubator for 3 h, culture medium was removed using a pipette, washed twice with PBS solution, and 1 mL of trypsin was used to treat the cells for 3 min at 37°C. 3 mL of serum-free DMEM medium was placed into a petri dish, and the cells were prepared as a uniform suspension using a pipette. 200  $\mu$ L each of U87 and HS683 were divided into each sterile cell of a 24-cell Transwell plate. U87 and HS683 were incubated for 24 h in the incubator. A culture solution was poured, and the small chambers were wiped with a cotton swab. After washing the cells with a PBS solution for 2 times, crystal violet staining solution was added to each chamber. After 15 min staining, the solution was poured and washed with PBS solution for 2 times. Five fields were chosen to take photos, and the average distances of cells in each field of view to pass through the matrix were calculated.

**2.7. Real-Time qPCR.** Total RNA was extracted from the cells using the Trizol Reagent and its concentration and quality was measured using NanoDrop 2000. The total RNA was reversely transcribed into cDNA using the SuperScript III Reverse Transcriptase (Invitrogen). The primers (Shh, Ihh, Dhh, E-cadherin, MMP-2, and GAPDH) for reverse transcription and qPCR of miR-338-5p and U6 (Table 1) were synthesized by Guangzhou Ruibo Biotechnology Co., Ltd. (Guangzhou, China). Invitrogen's Platinum SYBR Green

qPCR SuperMix-UDG kit was used in this reaction. The specificity of SYBR Green qPCR was validated using melt curve analysis. qPCR was performed using the following: reagent used was 10  $\mu$ L of Platinum® SYBR® Green qPCR (Invitrogen), 1  $\mu$ L of forward primer, 1  $\mu$ L of reverse primer, 2  $\mu$ L of cDNA template, and 6  $\mu$ L RNase free ddH<sub>2</sub>O. U6 and GAPDH were used as controls. Real-time PCR reaction conditions were set as follows: Roche LighterCycler 480 denaturation was set to 95°C for 30 seconds and cycle amplification conditions were set to 95°C for 5 seconds and 60°C for 30 seconds for a total of 40 cycles. The  $2^{-\Delta\Delta C_T}$  method was used to calculate the relative expression level of miR-338-5p, Shh, Ihh, Dhh, E-cadherin, and MMP-2 in glioma cells.

**2.8. Western Blot.** Acetyl-histone H3 (Lys14) (D4B9) Rabbit mAb, anti-HDAC1 (cat. no. 5356), anti-HDAC2 (cat. no. 2540), and anti-HDAC3 (cat. no. 3949) antibodies were purchased from Cell Signaling Technology, Inc. (Danvers, MA, USA). Anti-Sonic Hedgehog antibody (ab53281), anti-India Hedgehog antibody (ab52919), anti-Desert Hedgehog antibody (ab97287), anti-E-Cadherin antibody (ab15148), anti-MPP-2 antibody (ab97292), anti-GAPDH antibody (ab37168), and HRP Goat Anti-Rabbit (IgG) secondary antibody (ab205718) were purchased from Abcam (Chicago, IL, USA). Malignant glioma lines U87 and HS683 were adhered to a 6-well plate and treated with 10  $\mu$ M of chidamide for 24 h. The medium in each well was discarded and washed with ice-cold PBS. The cells were mixed with 100  $\mu$ L of RIPA lysate with 100 mM PMSF and 5 mM DTT for a total of 200  $\mu$ L per well. The lysate in each tube was vortexed on a vortex shaker for 5 min. The protein in the EP tube was centrifuged at 12,000  $\times g$  for 15 min at 4°C. Proteins were separated by using SDS-PAGE and then transferred to a PVDF membrane. The PVDF membrane was blocked using 5% skim milk and washed 3 times with TBST solution for 5 min/time. The membrane was placed in the matched primary antibody at 1 : 2000 to 1 : 5000 dilution and incubated in a horizontal shaker at 4°C. The secondary antibody at 1 : 5000 dilution was incubated with the abovementioned washed membrane at room temperature for 1 h. ECL chemiluminescence reagents A and B were mixed at a ratio of 1 : 1 and were carefully dripped onto the PVDF membrane. The recorded gel image was taken up by an ECL chemiluminescence. Western Blots were quantified using GAPDH as internal standard control, and relative expression levels were calculated via the comparison with the quantitative value.

**2.9. Biomarkers of Oxidative Stress.** The levels of reduced glutathione (GSH), superoxide dismutase (SOD), catalase (CAT), and malondialdehyde (MDA) were measured by using a Glutathione Assay Kit (ab156681), a SOD Assay Kit (ab65354), a Catalase Assay Kit (ab118184), and a Malondialdehyde Assay Kit (ab238537). All assays were performed on a Beckman Coulter UniCel Dx C 800 automatic biochemistry analyzer (Brea, CA, USA).

**2.10. Oxidative Stress Measurement.** The oxidative stress was evaluated by ROS and RNS, which was measured by DCF DA and or DAF-FM DA fluorescence. In brief, glioma cells ( $1 \times 10^6$ ) were incubated with DCF DA with DAF-FM DA and incubated for 15 min at 37°C avoiding light. The cells were washed twice with fresh medium and finally resuspended in PBS buffer (20 mM, pH 7.0). The fluorescence was measured using a Synergy H1 Hybrid Multimode Microplate Reader (BioTek Instruments, Vermont, USA).

**2.11. Flow Cytometry Detection of Cell Apoptosis, Necrosis, and Cycle.** Glioma cells were reprecipitated (4°C) in 10 mM PBS and adjusted to  $1 \times 10^5$ /mL, then 100  $\mu$ L of Annexin V-FITC was added and placed into a flow test tube. Five  $\mu$ L of Annexin V-FITC and 15  $\mu$ L of propidium iodide were added and mixed by avoiding light. The samples were measured by using flow cytometry (Beckman Coulter FC500 Flow Cytometer, IL, USA). The apoptosis and necrosis rates were calculated by using flow FlowJo 7.5 (TreeStar Inc., Ashland, USA). For the assay of cell cycle, the cells were washed with icy PBS after the treatment with different concentrations of chidamide for 48 h. Icy 75% ethanol was used to fix cells. Subsequently, the cells were treated with PI/RNase solution for a quarter after being washed with PBS and detected by using flow cytometry instrument.

**2.12. Statistical Analysis.** Experimental data results were analyzed using GraphPad Prism 5 software. The results of all analyses were expressed as mean  $\pm$  SD, and a one-tailed, paired sample *t*-test or one-way ANOVA with post hoc Tukey's test was used to compare variables between two groups.  $P < 0.05$  was considered statistically significant.

### 3. Results

**3.1. Chidamide Inhibited Cell Growth of U87 and HS683 Cells.** A long half-life of chidamide ranging between 16.8–18.3 h and 24 h may be a better period for evaluating its function. [28] Thus, the 24 h culture was chosen in the experiment. U87 and HS683 cells were treated with different concentrations of chidamide (0–14  $\mu$ M) for 24 h, and the proliferation inhibition of chidamide on U87 and HS683 cell lines was detected by a  $^3$ H-TdR assay. The results showed that chidamide inhibited the relative cell activity of U87 (Figure 1(a)) and HS683 (Figure 1(b)) cells in a time-dependent and dose-dependent way when the concentration was more than 8  $\mu$ M for a 24-hour culture in all glioma cells ( $P < 0.05$ ). The  $IC_{50}$  values at 24 h were different from each other in U87 and HS683 cells; the  $IC_{50}$  value in U87 cells was  $11.09 \pm 1.58 \mu$ M, whereas the  $IC_{50}$  value for HS683 cells was  $12.16 \pm 2.51 \mu$ M. 10  $\mu$ M of chidamide was

chosen so that inhibition caused by high-concentration toxicity may be avoided.

**3.2. Chidamide Inhibited the Growth Rate of U87 and HS683 Glioma Cells via miR-338-5p.** Chidamide and the miR-338-5p inhibitor inhibited the growth rate of U87 (Figure 1(c)) and HS683 cells (Figure 1(d)). However, chidamide could not inhibit the growth rates of two kinds of cells when the miR-338-5p inhibitor was used and the statistical difference for the growth was insignificant between the IG and CHIG groups ( $P > 0.05$ ). The miR-338-5p mimic promoted the growth of U87 (Figure 1(c)) and HS683 cells (Figure 1(d)). Further chidamide treatment still could inhibit the growth of two kinds of cells, and the statistical difference for the growth was significant between the MG and CHMG groups ( $P < 0.05$ ). The results suggested that chidamide inhibited the growth rate of U87 and HS683 glioma cells via miR-338-5p.

**3.3. Chidamide Inhibited HDAC Activity of U87 and HS683 Cells.** The HDAC activities of U87 (Figure 2(a)) and HS683 (Figure 2(b)) cells were reduced with the increase in the concentration of chidamide ( $P < 0.05$ ). Chidamide inhibited the HDAC activities of U87 and HS683 cells in a time-dependent and dose-dependent way. Western Blot analysis showed that chidamide inhibited the expression of HDAC1, HDAC2, and HDAC3 in a dose-dependent manner in U87 and HS683 cells. Additionally, the acetylation of H3 histones was significantly increased following exposure to chidamide U87 and HS683 cells. These results demonstrated that chidamide decreased the expression of HDACs and increased the acetylation levels of histone.

**3.4. Chidamide Blocked Glioma Cells at  $G_0/G_1$  Phase due to Cell Necrosis and Apoptosis.** Figures 3(a)–3(b) showed that the number of chidamide-blocked U87 glioma cells was increased at the  $G_0/G_1$  phase with the increase in the concentration of chidamide. In similar cases, Figures 3(e)–3(f) showed that the number of chidamide-blocked HS683 glioma cells was increased at the  $G_0/G_1$  phase with the increase in the concentration of chidamide. The number of blocked HS683 glioma cells after being treated with 4 and 8  $\mu$ M chidamide was significantly higher than those being treated with 0  $\mu$ M chidamide (Figure 3(g),  $P < 0.05$ ). The number of blocked U87 glioma cells after being treated with 8  $\mu$ M chidamide was significantly higher than those being treated with 0 and 4  $\mu$ M chidamide (Figure 3(h),  $P < 0.05$ ). The number of blocked HS683 glioma cells after being treated with 8  $\mu$ M chidamide was significantly higher than those being treated with 0 and 4  $\mu$ M chidamide (Figure 3(i),  $P < 0.05$ ). Figures 3(j)–3(l) showed that the proportion of U87 glioma cells with apoptosis and necrosis was increased with the increase in the concentration of chidamide. In similar cases, Figures 3(m)–3(o) showed that the proportion of HS683 glioma cells with apoptosis and necrosis was increased with the increase in the concentration of chidamide. The proportion of U87 glioma cells with apoptosis and necrosis after being treated with 8  $\mu$ M chidamide was significantly higher than those being treated with 0 and 4  $\mu$ M chidamide (Figure 3(p),  $P < 0.05$ ). The

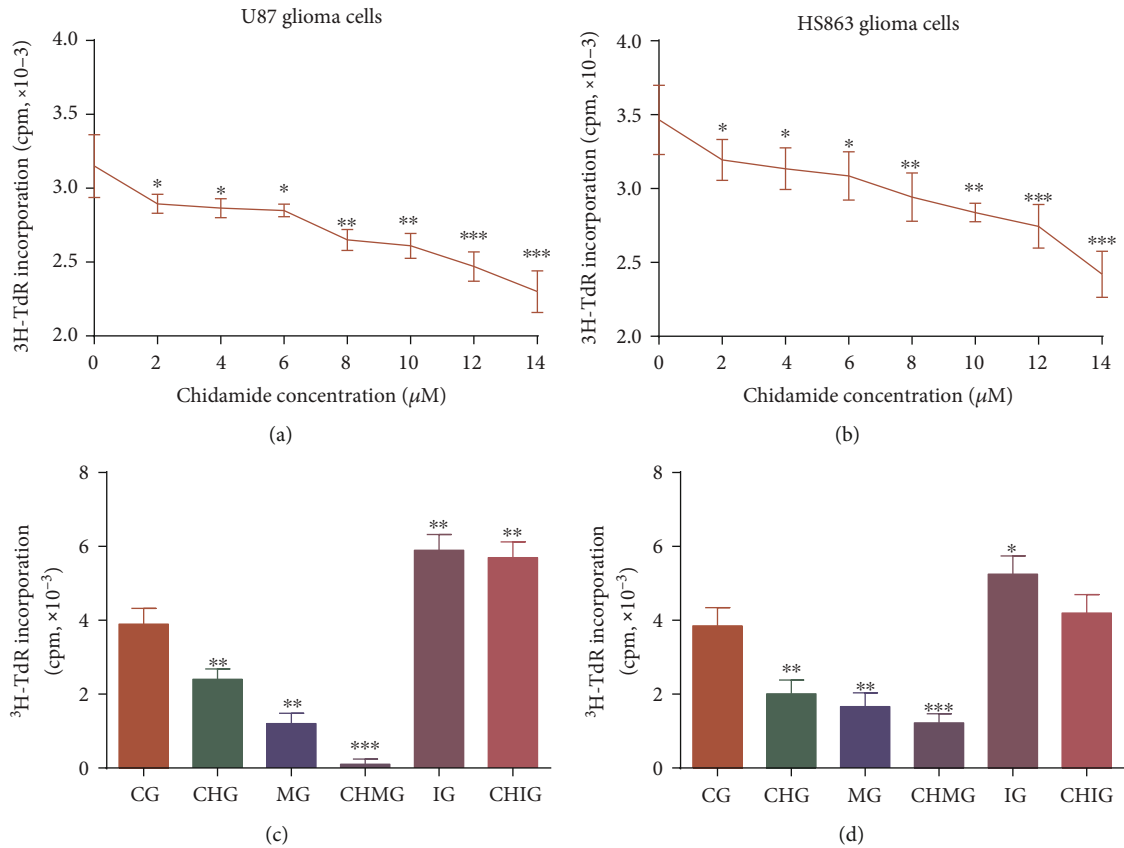


FIGURE 1: <sup>3</sup>H-TdR incorporation analysis of the growth rate of U87 and HS683 glioma cells. (a) The effects of chidamide on the growth rate of U87 glioma cells. (b) The effects of chidamide on the growth rate of HS683 glioma cells. (c) The growth rate of U87 glioma cells among different groups. (d) The growth rate of HS683 glioma cells among different groups. CG: control group; CHG: chidamide group; MG: miR-338-5p mimic group; IG: miR-338-5p inhibitor group; CHMG: chidamide-treated miR-338-5p mimic group; CHIG: chidamide-treated miR-338-5p inhibitor group. *N* = 5 for each group and \**P* < 0.05, \*\**P* < 0.01, and \*\*\**P* < 0.001 vs. the CG group.

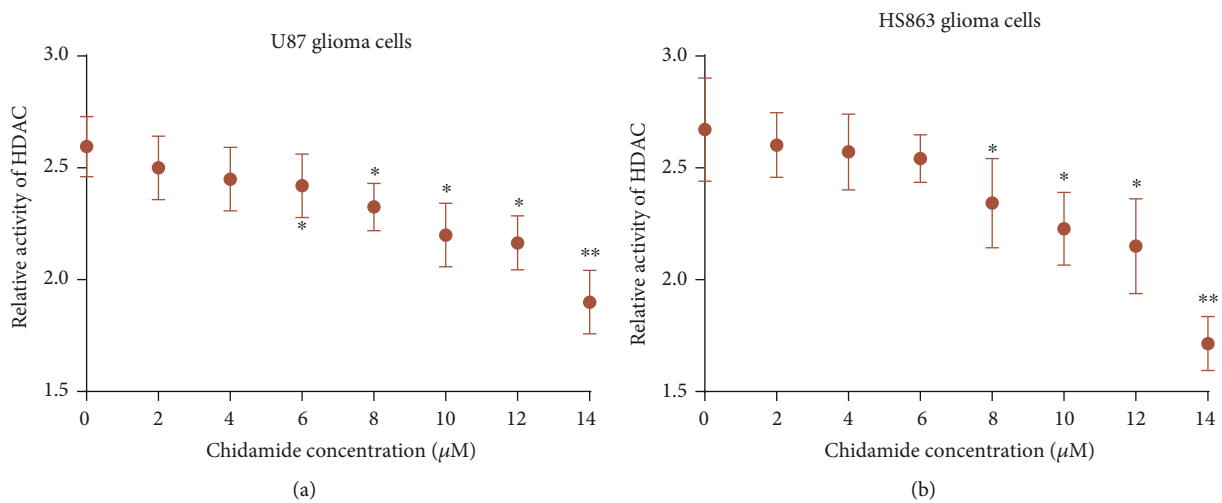


FIGURE 2: The effects of chidamide on the activity of HDAC in U87 and HS683 glioma cells. (a) Relative activity of HDAC in U87 glioma cells. (b) Relative activity of HDAC in HS683 glioma cells.

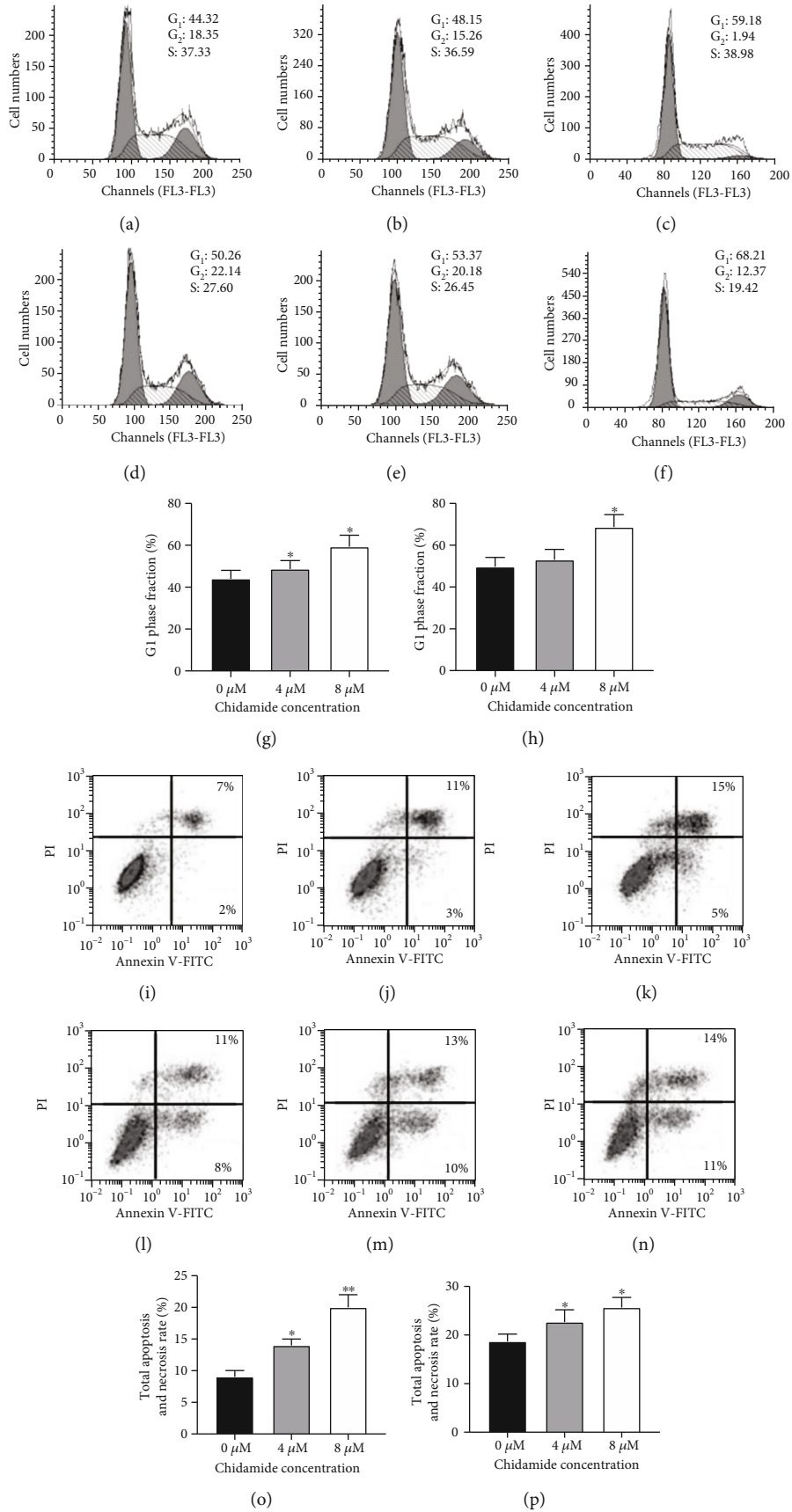


FIGURE 3: Continued.

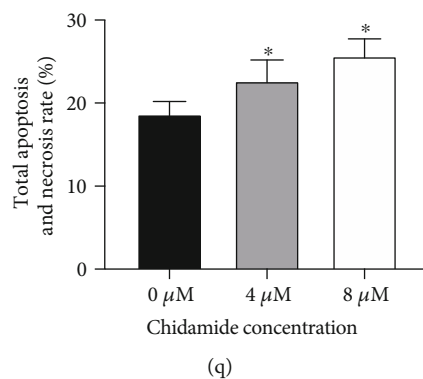


FIGURE 3: Flow cytometry analysis of the cell cycle, necrosis, and apoptosis. (a) The proportions of the U87 cells blocked at the  $G_0/G_1$  phase after being treated with  $0 \mu\text{M}$  chidamide. (b) The proportions of the U87 cells blocked at the  $G_0/G_1$  phase after being treated with  $4 \mu\text{M}$  chidamide. (c) The proportions of the U87 cells blocked at the  $G_0/G_1$  phase after being treated with  $8 \mu\text{M}$  chidamide. (d) The proportions of the HS683 cells blocked at the  $G_0/G_1$  phase after being treated with  $0 \mu\text{M}$  chidamide. (e) The proportions of the HS683 cells blocked at the  $G_0/G_1$  phase after being treated with  $4 \mu\text{M}$  chidamide. (f) The proportions of the HS683 cells blocked at the  $G_0/G_1$  phase after being treated with  $8 \mu\text{M}$  chidamide. (g) Phase fraction in HS683 cells after being treated with different concentrations of chidamide. (h)  $G_1$  phase fraction in U87 cells after being treated with different concentrations of chidamide. (i)  $G_1$  phase fraction in HS683 cells after being treated with different concentrations of chidamide. (j) The proportions of the U87 cells with apoptosis and necrosis after being treated with  $0 \mu\text{M}$  chidamide. (k) The proportions of the U87 cells with apoptosis and necrosis after being treated with  $4 \mu\text{M}$  chidamide. (l) The proportions of the U87 cells with apoptosis and necrosis after being treated with  $8 \mu\text{M}$  chidamide. (m) The proportions of the HS683 cells with apoptosis and necrosis after being treated with  $0 \mu\text{M}$  chidamide. (n) The proportions of the HS683 cells with apoptosis and necrosis after being treated with  $4 \mu\text{M}$  chidamide. (o) The proportions of the HS683 cells with apoptosis and necrosis after being treated with  $8 \mu\text{M}$  chidamide. (p) The total apoptosis and necrosis rates in U87 cells after being treated with different concentrations of chidamide. (q) The total apoptosis and necrosis rates in HS683 cells after being treated with different concentrations of chidamide. All data are expressed as mean  $\pm$  SD ( $N = 6$ ) and \* $P < 0.05$  and \*\* $P < 0.01$  vs. the  $0 \mu\text{M}$  chidamide group.

total apoptosis and necrosis rates of HS683 glioma cells after being treated with  $8 \mu\text{M}$  chidamide were significantly higher than those being treated with  $0$  and  $4 \mu\text{M}$  chidamide (Figure 3(q),  $P < 0.05$ ). The results suggest that chidamide blocks glioma cells at the  $G_0/G_1$  phase probably through cell necrosis and apoptosis.

**3.5. Chidamide Increased Relative Level of miR-338-5p.** U87 and HS683 cells were treated with different concentrations of chidamide ( $0$ – $14 \mu\text{M}$ ) for 24 h, and the related levels of miR-338-5p in U87 and HS683 cell lines were detected by real-time qPCR. The results showed that chidamide increased the relative level of miR-338-5p in U87 (Figure 4(a)) and HS683 (Figure 4(b)) cells in a time-dependent and dose-dependent way ( $P < 0.05$ ).

miR-338-5p plays an important role in promoting solid tumors. Therefore, we investigated whether chidamide inhibited glioma cells via miR-338-5p. We detected the level of miR-338-5p in human malignant glioma cell lines U87 and HS683 by real-time PCR. The results showed that the relative level of miR-338-5p increased in the mimic group and the chidamide-treated group in U87 (Figure 4(c)) and HS683 (Figure 4(d)) cells and decreased in the inhibitor group ( $P < 0.05$ ). Further chidamide treatment still reduced the growth rate of the cells after the miR-338-5p mimic was used, and the statistical difference for miR-338-5p was significant between the MG and CHMG groups ( $P < 0.05$ ). Chidamide may inhibit glioma cells via miR-338-5p.

**3.6. Chidamide Inhibited the Activity of Glioma Cells via miR-338-5p.** To investigate the effect of chidamide on the migration of human malignant glioma cell lines U87 and HS683, the cells were treated with  $10 \mu\text{M}$  of chidamide for 24 h. The scratch test showed the migration of the two cells before and after treatment. Chidamide inhibited the invasion of glioma cells U87 (Figure 5(a)) and HS683 (Figure 5(b)) ( $P < 0.05$ ). Furthermore, the miR-338-5p mimic inhibited the invasion ability, whereas the inhibitor promoted the invasion ability ( $P < 0.05$ ). Further chidamide treatment still reduced the invaded cells after the miR-338-5p mimic was used, and the statistical difference for the invaded cells was significant between the MG and CHMG groups ( $P < 0.05$ ). The results suggested that chidamide inhibited the migration ability of malignant glioma cells via miR-338-5p.

To investigate the effect of chidamide on the relative migration distance of human malignant glioma cell lines U87 and HS683, the cells were treated with  $10 \mu\text{M}$  of chidamide for 24 h. Chidamide inhibited the relative migration distance of human malignant glioma cells U87 (Figure 6(a)) and HS683 (Figure 6(b)) ( $P < 0.05$ ). Furthermore, the miR-338-5p mimic inhibited the relative migration distance of glioma cells, whereas the inhibitor of miR-338-5p increased the relative migration distance of glioma cells. Further chidamide treatment still reduced the invading ability of the cells after the miR-338-5p mimic was used, and the statistical difference for the migration ability was significant between the MG and CHMG groups ( $P < 0.05$ ). The results suggested that chidamide inhibited the invading ability of malignant glioma cells via miR-338-5p.

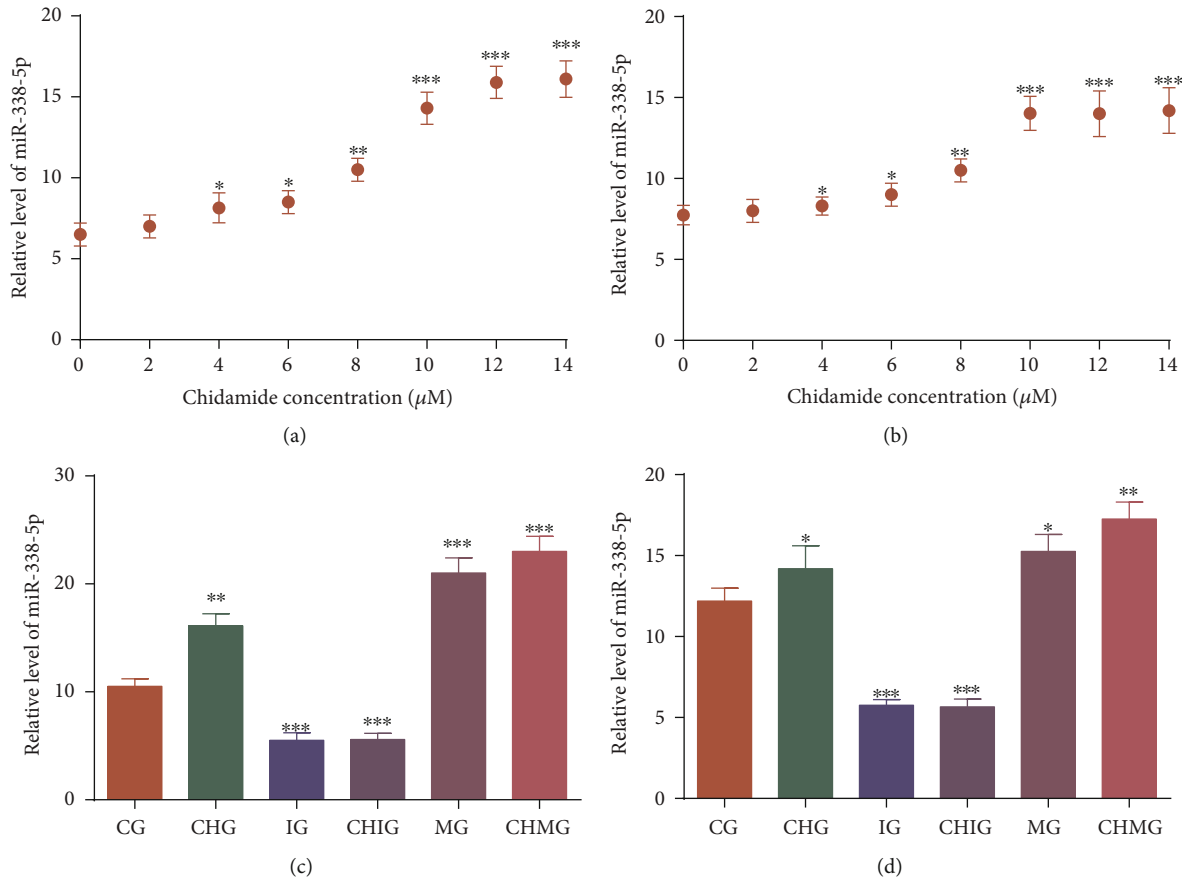


FIGURE 4: Relative mRNA levels of miR-338-5p. (a) The effects of chidamide on the level of miR-338-5p in U87 cells. (b) The effects of chidamide on the level of miR-338-5p in HS683 cells. (c) Relative mRNA levels of miR-338-5p in U87 glioma cells. (d) Relative mRNA levels of miR-338-5p in HS683 glioma cells. CG: control group; CHG: chidamide group; MG: miR-338-5p mimic group; IG: miR-338-5p inhibitor group; CHMG: chidamide-treated miR-338-5p mimic group; CHIG: chidamide-treated miR-338-5p inhibitor group.  $N = 5$  for each group and \* $P < 0.05$ , \*\* $P < 0.01$ , and \*\*\* $P < 0.001$  vs. the CG group.

### 3.7. Chidamide Reduced Relative mRNA Levels of Hedgehog Signaling, Migration, and Invading Proteins via miR-338-5p.

Real-time qPCR analysis showed that chidamide treatment reduced relative mRNA levels of Shh, Ihh, migration marker E-cadherin, and invading marker MMP-2 in U87 (Figure 7(a),  $P < 0.05$ ). Comparatively, chidamide treatment reduced relative mRNA levels of Shh, Ihh, Dhh, E-cadherin, and MMP-2 in HS683 glioma cells (Figure 7(b),  $P < 0.05$ ). In similar cases, miR-338-5p mimics and inhibitor reduced or increased the relative mRNA levels of these molecules. However, chidamide could not inhibit these molecules anymore when the miR-338-5p inhibitor was used and the statistical difference for these molecules was insignificant between the IG and CHIG groups ( $P < 0.05$ ). Further chidamide treatment still reduced the levels of these molecules after miR-338-5p mimic was used, and the statistical difference for the levels of these molecules was significant between the MG and CHMG groups ( $P < 0.05$ ). The result suggested that chidamide reduced the relative mRNA levels of Hedgehog signaling, migration, and invading proteins via miR-338-5p.

### 3.8. Chidamide Reduced Relative Protein Levels of Hedgehog Signaling, Migration, and Invading Proteins via miR-338-5p.

Western Blot analysis showed that chidamide treatment reduced the relative protein levels of Shh, Ihh, migration marker E-cadherin, and invading marker MMP-2 in U87 (Figure 8(a),  $P < 0.05$ ). Comparatively, chidamide treatment reduced relative protein levels of Shh, Ihh, Dhh, E-cadherin, and MMP-2 in HS683 (Figure 8(b),  $P < 0.05$ ). In similar cases, miR-338-5p mimics and inhibitor reduced or increased the relative protein levels of these molecules. Further chidamide treatment still reduced the levels of these molecules after miR-338-5p mimic was used, and the statistical difference for the levels of these molecules was significant between the MG and CHMG groups ( $P < 0.05$ ). The result suggested that chidamide reduced the relative protein levels of Hedgehog signaling, migration, and invading proteins via miR-338-5p.

### 3.9. miR-338-5p Increased Oxidative Stress of Glioma Cells.

The serum levels of MDA were significantly increased, while the levels of GSH, CAT, and SOD were significantly reduced in the CHMG and MG groups and the reverse results were found in the IG group in both cells (Table 2,  $P < 0.05$ ). Thus, miR-338-5p mimics or inhibitor increased or reduced the biomarker levels of oxidative stress in both glioma cells.

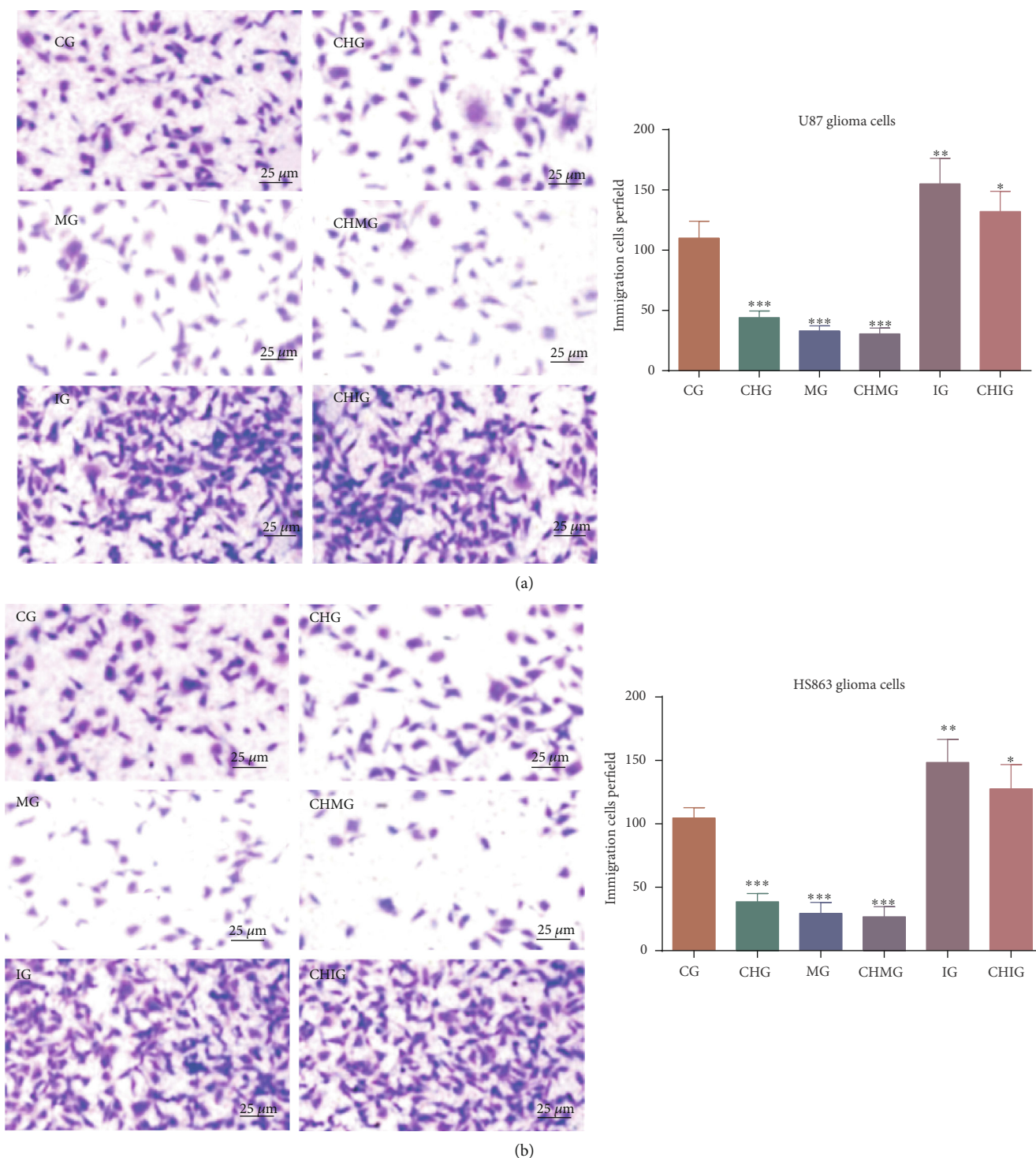


FIGURE 5: The effects of miR-338-5p on the function of chidamide (10  $\mu$ M) for controlling cell invasion per field. CG: control group; CHG: chidamide group; MG: miR-338-5p mimic group; IG: miR-338-5p inhibitor group; CHMG: chidamide-treated miR-338-5p mimic group; CHIG: chidamide-treated miR-338-5p inhibitor group. (a) The invasion of U88 glioma cells. (b) The invasion of HS683 cells. Values are mean  $\pm$  SD ( $N = 5$ ) and \* $P < 0.05$ , \*\* $P < 0.01$ , and \*\*\* $P < 0.001$  vs. the CG group.

miR-338-5p mimics or inhibitor increased or reduced the oxidative stress of glioma cells in U87 by increasing or reducing the levels of ROS and RNS (Figures 9(a) and 9(b),  $P < 0.05$ ). Comparatively, miR-338-5p mimics or inhibitor also increased or reduced the oxidative stress of

glioma cells in HS683 by increasing or reducing the levels of ROS and RNS (Figures 9(c) and 9(d),  $P < 0.05$ ). Further chidamide treatment increased the levels of oxidative stress by increasing the level of miR-338-5p. The result suggested that chidamide prevents glioma by increasing the level of

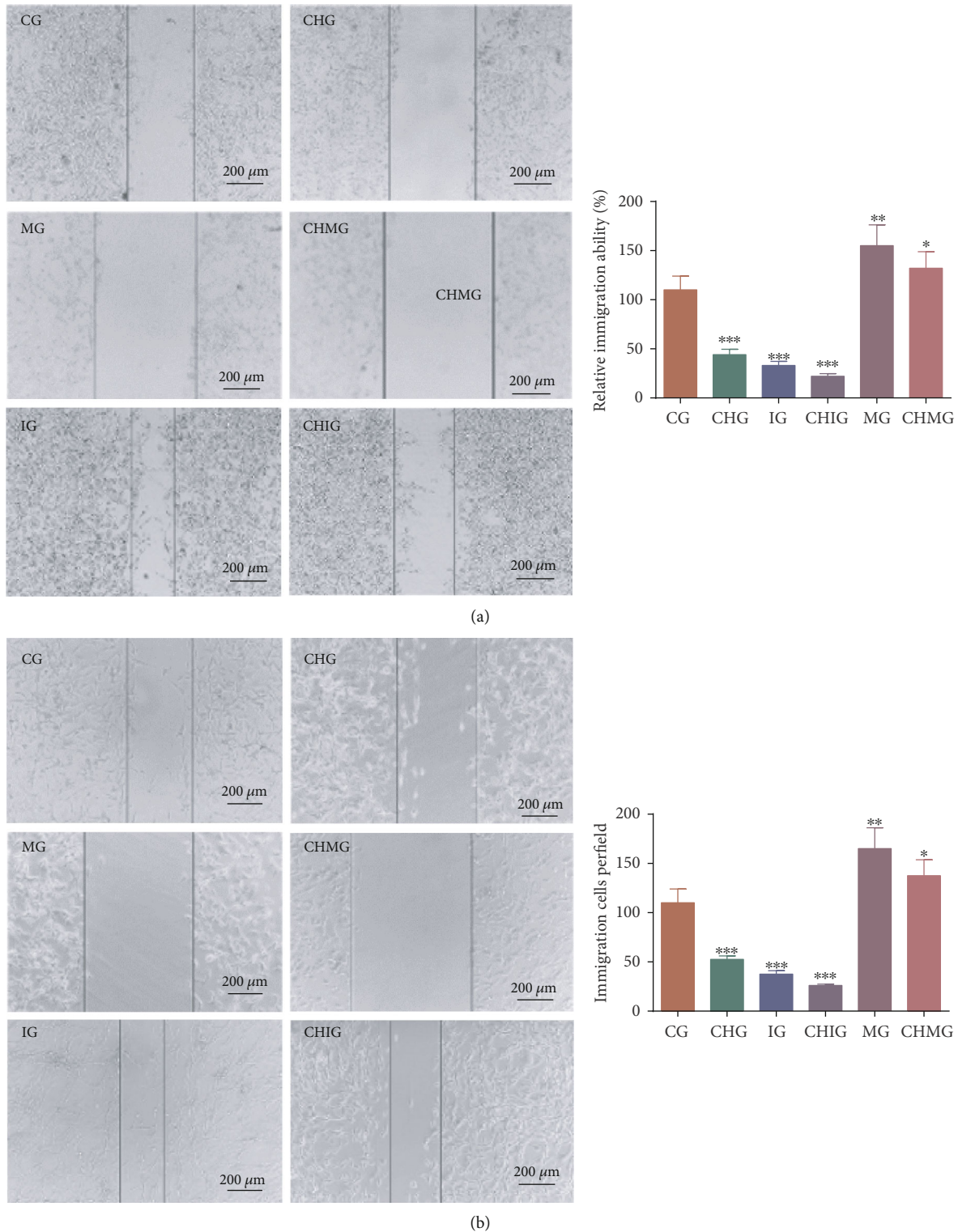


FIGURE 6: The effects of miR-338-5p on the function of chidamide ( $10 \mu\text{M}$ ) for controlling cell immigration. CG: control group; CHG: chidamide group; MG: miR-338-5p mimic group; IG: miR-338-5p inhibitor group; CHMG: chidamide-treated miR-338-5p mimic group; CHIG: chidamide-treated miR-338-5p inhibitor group. (a) The migration of U87 glioma cells. (b) The migration of HS683 glioma cells. Values are mean  $\pm$  SD ( $N = 5$ ) and \* $P < 0.05$ , \*\* $P < 0.01$ , and \*\*\* $P < 0.001$  vs. the CG group.

miR-338-5p, which inactivates Hedgehog signaling, resulting in the increase of oxidative stress and inhibition of glioma growth.

**3.10. Oxidative Stress Increased Apoptosis and Necrosis of Glioma Cells.** Flow cytometry analysis showed that the apoptosis and necrosis rates were highest in the CHMG group



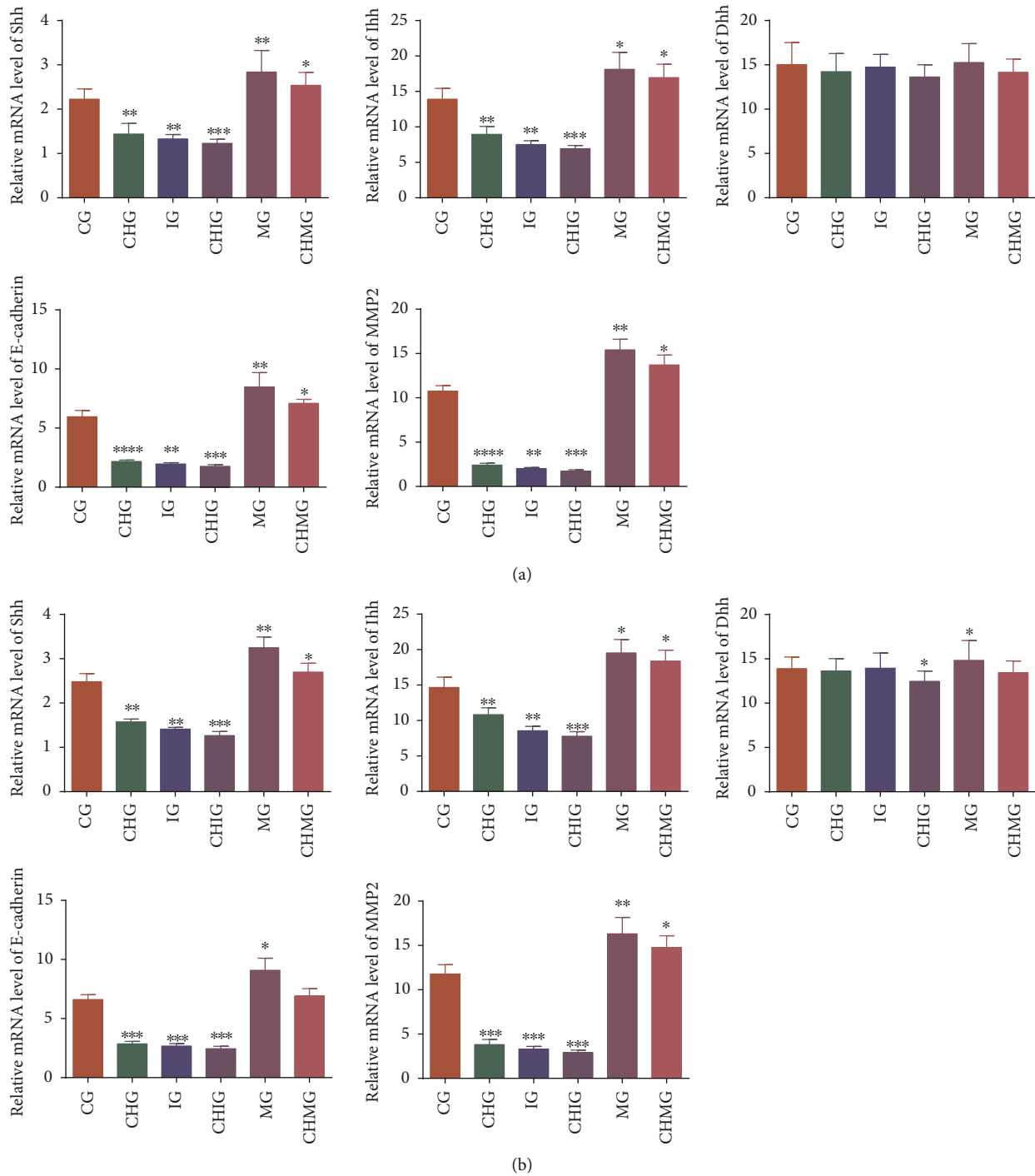


FIGURE 7: Real-time qPCR analysis of the effects of chidamide (10  $\mu$ M) on relative mRNA Hedgehog signaling and migration proteins. (a) U87 glioma cells. (b) HS683 glioma cells. CG: control group; CHG: chidamide group; MG: miR-338-5p mimic group; IG: miR-338-5p inhibitor group; CHMG: chidamide-treated miR-338-5p mimic group; CHIG: chidamide-treated miR-338-5p inhibitor group; Shh: Sonic Hedgehog; Ihh: Indian Hedgehog; Dhh: Desert Hedgehog; MMP-2: matrix metalloproteinase-2.  $N = 5$  for each group and \* $P < 0.05$ , \*\* $P < 0.01$ , and \*\*\* $P < 0.001$  vs. the CG group.

(Figure 10(a)) with highest level of oxidative stress (Figures 9(a) and 9(b)) and lowest in the IG group (Figure 10(a)) with the lowest oxidative stress in U87 cells (Figures 9(a) and 9(b)). In similar cases, the apoptosis and necrosis rates were highest

in the CHMG group (Figure 10(b)) with highest level of oxidative stress (Figures 9(c) and 9(d)) and lowest in IG group (Figure 10(b)) with the lowest oxidative stress in HS683 cells (Figures 9(c) and 9(d)).

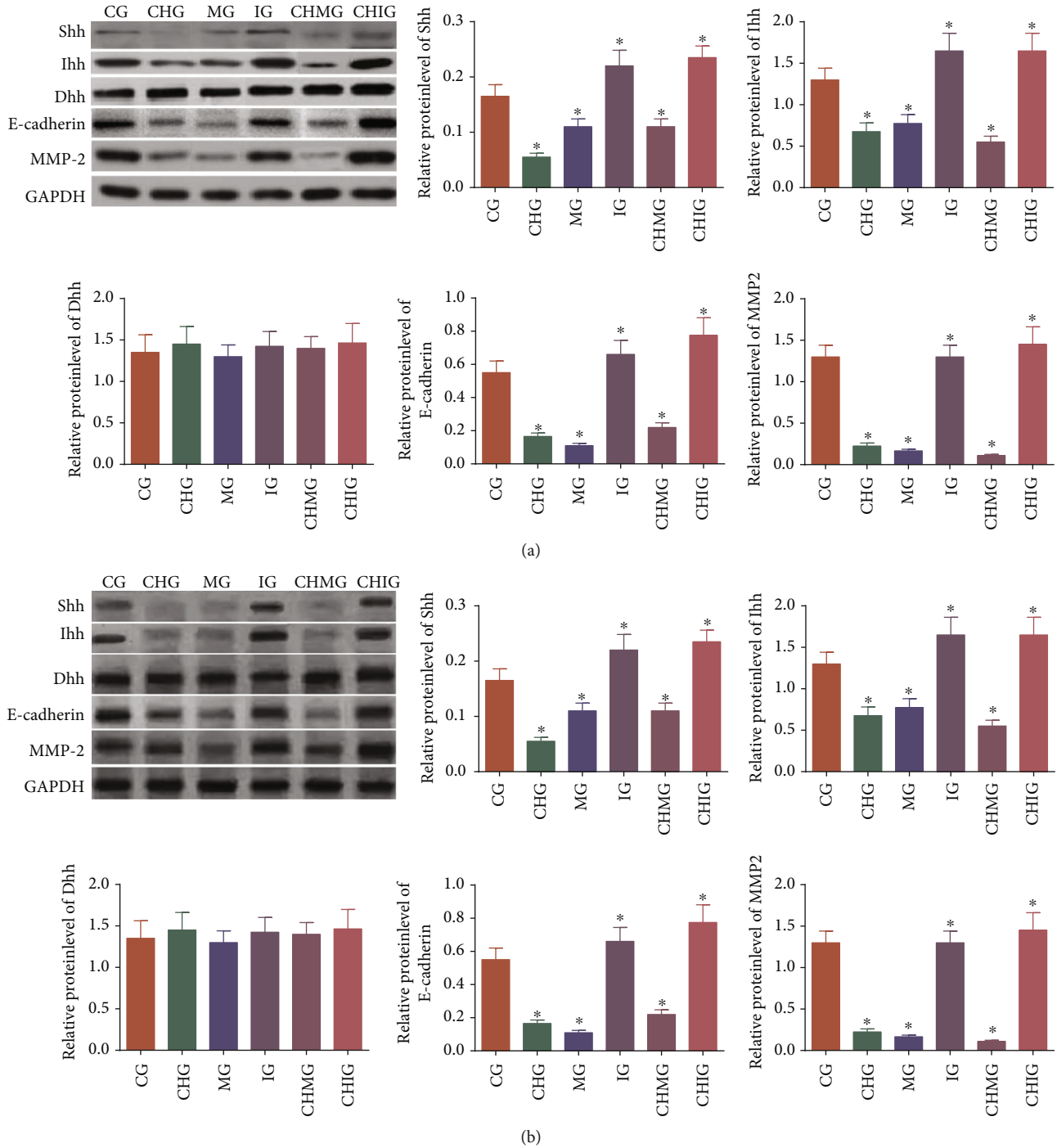


FIGURE 8: Western Blot analysis of the effects of chidamide (10  $\mu$ M) on the relative protein level of the Hedgehog signaling and migration protein. (a) U87 glioma cells. (b) HS683 glioma cells. CG: control group; CHG: chidamide group; MG: miR-338-5p mimic group; IG: miR-338-5p inhibitor group; CHMG: chidamide-treated miR-338-5p mimic group; CHIG: chidamide-treated miR-338-5p inhibitor group; Shh: Sonic Hedgehog; Ihh: Indian Hedgehog; Dhh: Desert Hedgehog; MMP-2: matrix metalloproteinase-2.  $N = 5$  for each group and \* $P < 0.05$ , \*\* $P < 0.01$ , and \*\*\* $P < 0.001$  vs. the CG group.

#### 4. Discussion

As an epigenetic modification regulator, chidamide regulates gene expression mainly by increasing the acetylation of histone lysine residues. An MTT assay showed that chidamide inhibited the proliferation of U87 and HS683 cells in a

time-dependent manner and dose-dependent way (Figure 1). The present results suggest that chidamide blocks glioma cells at the  $G_0/G_1$  phase probably through cell necrosis and apoptosis. The results were consistent with previous reports that the HDAC inhibitor induced cellular necrosis [29] and chidamide promoted cellular apoptosis

TABLE 2: The levels of oxidative stress biomarkers.

Parameters	CG	CHG	MG	CHMG	IG	CHIG
U87						
GSH (mg/L)	11.9 ± 1.5	10.1 ± 1.7*	8.5 ± 0.9**	7.8 ± 0.9**	15.6 ± 2.0***	14.3 ± 2.2**
CAT (mg/L)	16.4 ± 3.1	14.8 ± 5.4*	7.2 ± 2.7***	6.8 ± 1.4***	17.5 ± 3.2	16.1 ± 3.4
MDA (mmol/L)	4.9 ± 1.3	7.8 ± 2.2**	8.4 ± 2.4**	8.5 ± 1.3**	3.7 ± 1.2**	3.9 ± 2.0*
SOD (U/L)	371.4 ± 62.3	221.5 ± 60.7**	202.3 ± 80.5***	200.8 ± 34.3***	491.2 ± 69.6**	470.5 ± 60.1**
HS683						
GSH (mg/L)	14.1 ± 2.3	11.5 ± 1.9**	7.5 ± 1.4***	7.9 ± 1.2***	16.3 ± 2.0*	16.0 ± 2.5*
CAT (mg/L)	15.8 ± 3.4	12.0 ± 3.8*	7.9 ± 3.7***	6.8 ± 1.0***	18.8 ± 3.6*	18.0 ± 3.1*
MDA (mmol/L)	4.2 ± 1.4	8.6 ± 2.5**	11.7 ± 2.1***	10.6 ± 2.3***	3.5 ± 1.1**	3.2 ± 1.3**
SOD (U/L)	345.5 ± 59.1	303.7 ± 63.4*	281.3 ± 49.6**	257.9 ± 36.8**	396.1 ± 69.3*	390.2 ± 60.7*

Note: CG—control group; CHG—chidamide group; MG—miR-338-5p mimic group; IG—miR-338-5p inhibitor group; CHMG—chidamide-treated miR-338-5p mimic group; CHIG—chidamide-treated miR-338-5p inhibitor group.  $N = 5$  for each group and \* $P < 0.05$ , \*\* $P < 0.01$ , and \*\*\* $P < 0.001$  vs. the CG group.

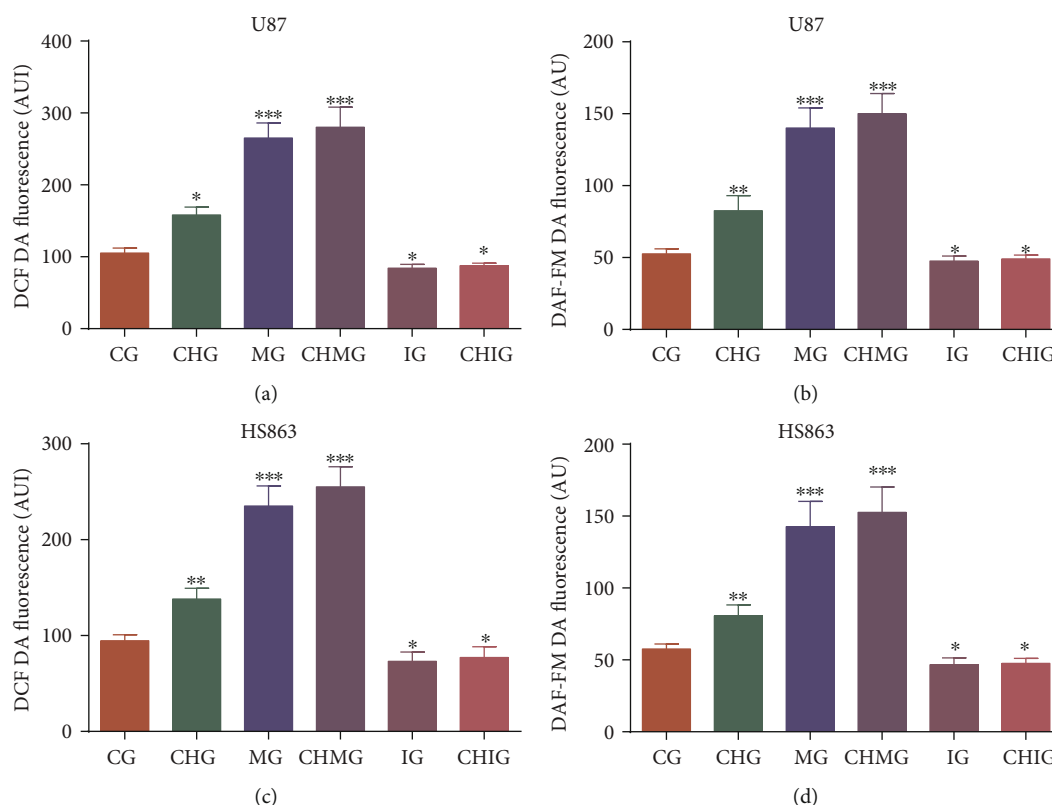


FIGURE 9: The oxidative levels among different groups. Glioma cells were labeled with (a) DCF DA and/or DAF-FM DA, and intracellular fluorescence was measured using a plate reader to estimate ROS and RNS. (a) ROS levels in U87 glioma cells. (b) RNS levels in U87 glioma cells. (c) ROS levels in HS683 glioma cells. (d) RNS levels in HS683 cells. CG: control group; CHG: chidamide group; MG: miR-338-5p mimic group; IG: miR-338-5p inhibitor group; CHMG: chidamide-treated miR-338-5p mimic group; CHIG: chidamide-treated miR-338-5p inhibitor group.  $N = 5$  for each group and \* $P < 0.05$ , \*\* $P < 0.01$ , and \*\*\* $P < 0.001$  vs. the CG group.

[30]. On the other hand, HDAC inhibitors have been reported to increase the expression of tumor necrosis factor-related apoptosis-inducing ligand (TRAIL) receptors and result in apoptosis [31, 32].

miRNAs play an important role in gliomagenesis as dominant predictors of outcome and determinants for the resistance to radio- and chemotherapy [33]. miR-338-5p is one

of the members of the miR-338 family whose brain-specific microRNA precursors are found in humans [34]. Evaluated levels of miR-338-5p have been reported to prevent cell proliferation, migration, and invasion and promote cell apoptosis in glioblastoma cells [23]. Thus, the effects of miR-338-5p on glioma cells were explored in the present work. Chidamide treatment often increased the relative level of miR-

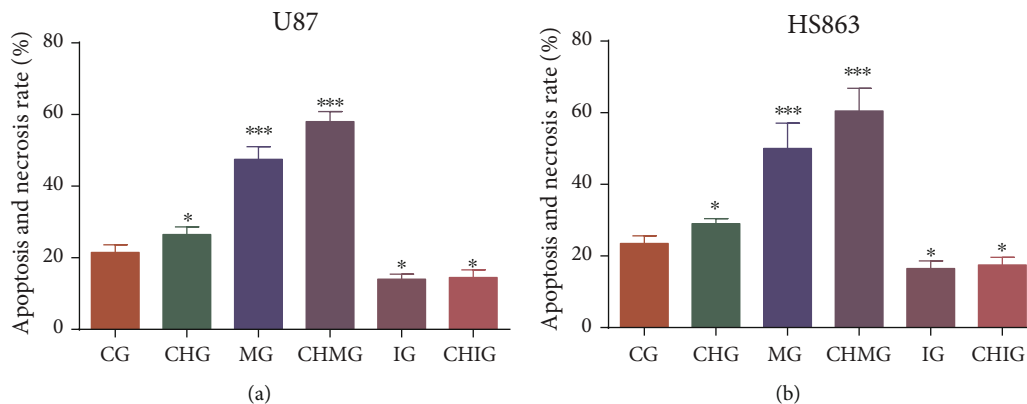


FIGURE 10: Flow cytometry detection of apoptosis rate. (a) Apoptosis rate in U87 glioma cells. (b) Apoptosis rate in HS683 glioma cells.  $N = 5$  for each group and  $*P < 0.05$ ,  $**P < 0.01$ , and  $***P < 0.001$  vs. the CG group.

338-5p (Figures 4(a) and 4(b)). Thus, chidamide may inhibit glioma cells via miR-338-5p since chidamide could not show the inhibitory function when miR-338-5p was inhibited. Chidamide has a direct inhibitory effect on tumor cells. The Hedgehog signaling pathway is highly activated not only in solid tumors such as gastrointestinal tumors [35, 36], lung cancer [37, 38], and breast cancer [39, 40] but also in leukemia [41, 42], lymphoma [43, 44], myeloma [45, 46], and brain tumor [47, 48]. According to a previous report, the inhibition of Hedgehog signaling also inhibited the growth of glioma cells [17]. The development of tumors involves the involvement of the Hedgehog pathway, and the formation of resistance to chemotherapeutic drugs is also involved in the Hedgehog pathway [49, 50]. Studies on the Hedgehog pathway and hematological malignancies have found that when the pathway is overexpressed, cells can show strong resistance to drug therapy [51, 52], so the inhibition of Hedgehog signaling can be improved to increase drug sensitivity and antitumor effects.

In this study, qPCR and Western Blot were used to determine the related molecules in the Hedgehog pathway and glioma cell migration and invasion. Chidamide inhibited the levels of Shh and Ihh and N-Cadherin and MMP-2 in U87 and HS683 glioma cells. Hedgehog signaling pathways play an important role in the growth of glioma cells [17]. We mainly studied the effects of chidamide on the proliferation and growth of glioma cells. The strong migration and invasion of tumor cells are the main processes associated with glioma [53, 54]. We investigated the effects of chidamide on the migration and invasion of malignant glioma cells by a scratch test and cell invasion assay. Chidamide had an inhibitory effect on the migration and invasion of glioma cells. Subsequently, we used real-time qPCR and Western Blot to examine the effect of chidamide on the expression of related proteins during the migration and invasion of malignant glioma cells. It was found that chidamide can significantly reduce E-cadherin and MMP-2. A study found that the cell adhesion factor E-cadherin and the invading protein MMP-2 could be reduced by chidamide in two kinds of glioma cells (Figures 7–8). The inhibition of the cell adhesion factor E-cadherin [55, 56] and the invading protein MMP-2 is a potential way to control tumor cell migration and invasion [57, 58].

It has been found that the abnormal activation of the Hedgehog signaling pathway is involved in the occurrence, invasion, and metastasis of malignant tumors. The significance of the Hedgehog signaling pathway was proved in the invasion and metastasis of malignant tumors by affecting cadherin [59]. miR-338-5p has been reported to be a potential biomarker of cancers [60]. Hedgehog signaling is a well-known pathway for the pathogenesis of cancers [61]. NCBI Blast showed that SHH signaling genes had the two target sequences (P1, 5'-AAGGCCCCAGCTCTACCCCTG-3' and P2, 5'-ATACCCGAGGTCCCAGAGCCAGA-3') of miR-338-5p. Thus, we considered the relationship between miR-338-5p and Hedgehog signaling. The present work showed that miR-338-5p promoted Hedgehog signaling, and its function was contrary with miR-338-3p, which downregulated Hedgehog signaling [62]. miR-338-5p upregulated E-cadherin expression in glioma [63]. MiR-338-5p has been found to promote glioma cell invasion by affecting MMP-2 [64].

The results suggested that chidamide controlled Hedgehog signaling and inhibited glioma cell migration and invasion via miR-338-5p. The increase of reactive oxygen species (ROS) and reactive nitrogen species (RNS) may control glioma risk by promoting its apoptosis. The Hedgehog pathway is crucial to glioma cell proliferation and controls reactive species production. The present findings demonstrated that chidamide treatment increased the levels of miR-338-5p (glioma cell inhibitor), which inhibited the activity of Hedgehog signaling, while Hedgehog signaling can inhibit oxidative stress by reducing the levels of ROS and RNS and preventing the apoptosis induced by oxidative stress. Thus, chidamide prevents glioma risk by increasing oxidative stress via miR-338-5p regulation of Hedgehog signaling.

There was some limitation in the present work. The present work was limited by the absence of in vivo testing. Moreover, primary human glioblastoma can be obtained from patient tumors and this could have approximated an actual situation but was not performed in the present paper. The glioma-associated oncogene homolog 1 (GLI1) of a zinc finger transcription factor regulates the Hedgehog signaling and was not analyzed in the present work. Further work is highly needed to be performed to address these important issues in the future.

## 5. Conclusions

Chidamide has a significant inhibitory effect on the proliferation of U87 and HS683 glioma cells via miR-338-5p. Proliferation inhibition has a time-dose dual dependence. Chidamide is involved in cell proliferation inhibition in U87 and HS683 glioma cells and is involved in the Hedgehog signaling pathway. Chidamide can inhibit the tumorigenic ability of malignant glioma cells in vitro and has long-term inhibitory effects on proliferation and growth. Chidamide inhibits the migration and invasion of glioma cells by inhibiting the expression of the stromal cell marker E-cadherin and the matrix metalloproteinase MMP-2, which is closely related to invasion. More importantly, chidamide treatment increased the levels of miR-338-5p, which reduced the activity of Hedgehog signaling, while Hedgehog signaling inhibited oxidative stress by reducing the levels of ROS and RNS and preventing the apoptosis induced by oxidative stress. Thus, chidamide prevents glioma risk by increasing oxidative stress via miR-338-5p regulation of Hedgehog signaling. Further work is highly demanded to confirm the relationship between the Hedgehog pathway and oxidative stress.

## Data Availability

The necessary data are included within the article. All data are available from the corresponding authors on reasonable request.

## Conflicts of Interest

The authors declare that there are no other nonfinancial competing interests.

## Authors' Contributions

HZ, LH, HW, and JW designed and performed the present experiments and analyzed all data. ZG and ZL analyzed all data and wrote the paper. All authors gave their final approval for the submission of the present paper.

## Acknowledgments

The project was supported by the Youth Technology Backbone Training Program of the Health Department of Jilin Province (2018Q025).

## References

- [1] M. Jensen, *Chimeric Immunoreceptor Useful in Treating Human Gliomas*, 2009, Google Patents.
- [2] F. Costa Nunes, L. B. Silva, E. Winter et al., "Tacrine derivatives stimulate human glioma SF295 cell death and alter important proteins related to disease development: an old drug for new targets," *Biochimica et Biophysica Acta (BBA) - General Subjects*, vol. 1862, no. 7, pp. 1527–1536, 2018.
- [3] C. Hoeman, C. Shen, and O. J. Becher, "CDK4/6 and PDGFRA signaling as therapeutic targets in diffuse intrinsic pontine glioma," *Frontiers in Oncology*, vol. 8, 2018.
- [4] L. Zang, S. M. Kondengaden, F. Che, L. Wang, and X. Heng, "Potential epigenetic-based therapeutic targets for glioma," *Frontiers in Molecular Neuroscience*, vol. 11, 2018.
- [5] S. Watanabe, Y. Kuwabara, S. Suehiro et al., "Valproic acid reduces hair loss and improves survival in patients receiving temozolomide-based radiation therapy for high-grade glioma," *European Journal of Clinical Pharmacology*, vol. 73, no. 3, pp. 357–363, 2017.
- [6] R. Maxwell, A. S. Luksik, T. Garzon-Muvdi et al., "Population-based study determining predictors of cancer-specific mortality and survival in pediatric high-grade brainstem glioma," *World Neurosurgery*, vol. 119, pp. e1006–e1015, 2018.
- [7] Y. Song, Y. Jiang, D. Tao et al., "NFAT2-HDAC1 signaling contributes to the malignant phenotype of glioblastoma," *Neuro-Oncology*, 2019.
- [8] X. Q. Wang, H. M. Bai, S. T. Li et al., "Knockdown of HDAC1 expression suppresses invasion and induces apoptosis in glioma cells," *Oncotarget*, vol. 8, no. 29, pp. 48027–48040, 2017.
- [9] Y. Leng, J. Wang, Z. Wang et al., "Valproic acid and other HDAC inhibitors upregulate FGF21 gene expression and promote process elongation in glia by inhibiting HDAC2 and 3," *The International Journal of Neuropsychopharmacology*, vol. 19, no. 8, 2016.
- [10] H. Zhang, B. Zhao, C. Huang, X. M. Meng, E. B. Bian, and J. Li, "Melittin restores PTEN expression by down-regulating HDAC2 in human hepatocellular carcinoma HepG2 cells," *PLoS ONE*, vol. 9, no. 5, p. e95520, 2014.
- [11] S. Zhong, Y. Fan, B. Wu et al., "HDAC3 expression correlates with the prognosis and grade of patients with glioma: a diversification analysis based on transcriptome and clinical evidence," *World Neurosurgery*, vol. 119, pp. e145–e158, 2018.
- [12] Z.-Q. Ning, Z.-B. Li, M. J. Newman et al., "Chidamide (CS055/HBI-8000): a new histone deacetylase inhibitor of the benzamide class with antitumor activity and the ability to enhance immune cell-mediated tumor cell cytotoxicity," *Cancer Chemotherapy and Pharmacology*, vol. 69, no. 4, pp. 901–909, 2012.
- [13] D.-S. Pan, Q. J. Yang, X. Fu et al., "Discovery of an orally active subtype-selective HDAC inhibitor, chidamide, as an epigenetic modulator for cancer treatment," *Medicinal Chemistry Communications*, vol. 5, no. 12, pp. 1789–1796, 2014.
- [14] S. Luo, K. Ma, H. Zhu et al., "Molecular, biological characterization and drug sensitivity of chidamide-resistant non-small cell lung cancer cells," *Oncology Letters*, vol. 14, no. 6, pp. 6869–6875, 2017.
- [15] M. He, Z. Qiao, Y. Wang et al., "Chidamide inhibits aerobic metabolism to induce pancreatic cancer cell growth arrest by promoting Mcl-1 degradation," *PLOS One*, vol. 11, no. 11, 2016.
- [16] J. Mao, S. Li, H. Zhao et al., "Effects of chidamide and its combination with decitabine on proliferation and apoptosis of leukemia cell lines," *American Journal of Translational Research*, vol. 10, no. 8, pp. 2567–2578, 2018.
- [17] L. Xu, H. Liu, Z. Yan, Z. Sun, S. Luo, and Q. Lu, "Inhibition of the Hedgehog signaling pathway suppresses cell proliferation by regulating the Gli2/miR-124/AURKA axis in human glioma cells," *International Journal of Oncology*, vol. 50, no. 5, pp. 1868–1878, 2017.
- [18] T. Takezaki, T. Hide, H. Takanaga, H. Nakamura, J. I. Kuratsu, and T. Kondo, "Essential role of the Hedgehog signaling

- pathway in human glioma-initiating cells,” *Cancer Science*, vol. 102, no. 7, pp. 1306–1312, 2011.
- [19] K.-Y. Chen, C.-H. Chiu, and L.-C. Wang, “Anti-apoptotic effects of Sonic hedgehog signalling through oxidative stress reduction in astrocytes co-cultured with excretory-secretory products of larval *Angiostrongylus cantonensis*,” *Scientific Reports*, vol. 7, 2017.
- [20] C. Adolphe, M. Narang, T. Ellis, C. Wicking, P. Kaur, and B. Wainwright, “An in vivo comparative study of sonic, desert and Indian hedgehog reveals that hedgehog pathway activity regulates epidermal stem cell homeostasis,” *Development*, vol. 131, no. 20, pp. 5009–5019, 2004.
- [21] J. Godlewski, M. O. Nowicki, A. Bronisz et al., “Targeting of the Bmi-1 oncogene/stem cell renewal factor by microRNA-128 inhibits glioma proliferation and self-renewal,” *Cancer Research*, vol. 68, no. 22, pp. 9125–9130, 2008.
- [22] S.-Z. Li, Y.-Y. Hu, J. Zhao et al., “MicroRNA-34a induces apoptosis in the human glioma cell line, A172, through enhanced ROS production and NOX2 expression,” *Biochemical and biophysical research communications*, vol. 444, no. 1, pp. 6–12, 2014.
- [23] D. Lei, F. Zhang, D. Yao, N. Xiong, X. Jiang, and H. Zhao, “MiR-338-5p suppresses proliferation, migration, invasion, and promote apoptosis of glioblastoma cells by directly targeting EFEMP1,” *Biomedicine & Pharmacotherapy*, vol. 89, pp. 957–965, 2017.
- [24] M. Wierzbicki, E. Sawosz, B. Strojny, S. Jaworski, M. Grodzik, and A. Chwalibog, “NF- $\kappa$ B-related decrease of glioma angiogenic potential by graphite nanoparticles and graphene oxide nanoplatelets,” *Scientific Reports*, vol. 8, no. 1, p. 14733, 2018.
- [25] Y. Jiang, J. Miao, D. Wang et al., “MAP30 promotes apoptosis of U251 and U87 cells by suppressing the LGR5 and Wnt/ $\beta$ -catenin signaling pathway, and enhancing Smac expression,” *Oncology Letters*, vol. 15, no. 4, pp. 5833–5840, 2018.
- [26] Y. X. Jiang, Y. Ma, and Y. Cheng, “Transcriptome and co-expression network analysis of the human glioma cell line Hs683 exposed to candoxin,” *Journal of International Medical Research*, vol. 40, no. 3, pp. 887–898, 2012.
- [27] X. L. Ma, F. Shang, W. Ni, J. Zhu, B. Luo, and Y. Q. Zhang, “MicroRNA-338-5p plays a tumor suppressor role in glioma through inhibition of the MAPK-signaling pathway by binding to FOXD1,” *Journal of Cancer Research and Clinical Oncology*, vol. 144, no. 12, pp. 2351–2366, 2018.
- [28] M. Dong, Z. Q. Ning, P. Y. Xing et al., “Phase I study of chidamide (CS055/HBI-8000), a new histone deacetylase inhibitor, in patients with advanced solid tumors and lymphomas,” *Cancer Chemotherapy and Pharmacology*, vol. 69, no. 6, pp. 1413–1422, 2012.
- [29] J. Zhang and Q. Zhong, “Histone deacetylase inhibitors and cell death,” *Cellular and Molecular Life Sciences*, vol. 71, no. 20, pp. 3885–3901, 2014.
- [30] L. Liu, B. Chen, S. Qin et al., “A novel histone deacetylase inhibitor chidamide induces apoptosis of human colon cancer cells,” *Biochemical and Biophysical Research Communications*, vol. 392, no. 2, pp. 190–195, 2010.
- [31] Y. Li, K. Chen, Y. Zhou et al., “A new strategy to target acute myeloid leukemia stem and progenitor cells using chidamide, a histone deacetylase inhibitor,” *Current Cancer Drug Targets*, vol. 15, no. 6, pp. 493–503, 2015.
- [32] P. Maiso, X. Carvajal-Vergara, E. M. Ocio et al., “The histone deacetylase inhibitor LBH589 is a potent antimyeloma agent that overcomes drug resistance,” *Cancer Research*, vol. 66, no. 11, pp. 5781–5789, 2006.
- [33] M. Henriksen, K. B. Johnsen, H. H. Andersen, L. Pilgaard, and M. Duroux, “MicroRNA expression signatures determine prognosis and survival in glioblastoma multiforme—a systematic overview,” *Molecular Neurobiology*, vol. 50, no. 3, pp. 896–913, 2014.
- [34] A. Aschrafi, A. D. Schwechter, M. G. Mameza, O. Natera-Naranjo, A. E. Gioio, and B. B. Kaplan, “MicroRNA-338 regulates local cytochrome c oxidase IV mRNA levels and oxidative phosphorylation in the axons of sympathetic neurons,” *The Journal of Neuroscience*, vol. 28, no. 47, pp. 12581–12590, 2008.
- [35] J. L. Merchant and M. Saqui-Salces, “Inhibition of Hedgehog signaling in the gastrointestinal tract: targeting the cancer microenvironment,” *Cancer Treatment Reviews*, vol. 40, no. 1, pp. 12–21, 2014.
- [36] M. Saqui-Salces and J. L. Merchant, “Hedgehog signaling and gastrointestinal cancer,” *Biochimica et Biophysica Acta (BBA) - Molecular Cell Research*, vol. 1803, no. 7, pp. 786–795, 2010.
- [37] W. Jian, Y. Bai, X. Li, J. Kang, Y. Lei, and Y. Xue, “Phosphatidylethanolamine-binding protein 4 promotes the epithelial-to-mesenchymal transition in non-small cell lung cancer cells by activating the sonic hedgehog signaling pathway,” *Journal of Cellular Biochemistry*, vol. 120, no. 4, pp. 5386–5395, 2019.
- [38] X. Liu, J. Liu, X. Zhang, Y. Tong, and X. Gan, “MiR-520b promotes the progression of non-small cell lung cancer through activating Hedgehog pathway,” *Journal of Cellular and Molecular Medicine*, vol. 23, no. 1, pp. 205–215, 2019.
- [39] X. Liu, T. Zhao, X. Bai et al., “LOC101930370/MiR-1471 axis modulates the Hedgehog signaling pathway in breast cancer,” *Cellular Physiology and Biochemistry*, vol. 48, no. 3, pp. 1139–1150, 2018.
- [40] X. Xu, J. Ye, C. Huang, Y. Yan, and J. Li, “M2 macrophage-derived IL6 mediates resistance of breast cancer cells to hedgehog inhibition,” *Toxicology and Applied Pharmacology*, vol. 364, pp. 77–82, 2018.
- [41] M. A. Burns, Z. W. Liao, N. Yamagata et al., “Hedgehog pathway mutations drive oncogenic transformation in high-risk T-cell acute lymphoblastic leukemia,” *Leukemia*, vol. 32, no. 10, pp. 2126–2137, 2018.
- [42] A. Pession, A. Lonetti, S. Bertuccio, F. Locatelli, and R. Masetti, “Targeting Hedgehog pathway in pediatric acute myeloid leukemia: challenges and opportunities,” *Expert Opinion on Therapeutic Targets*, vol. 23, no. 2, pp. 87–91, 2018.
- [43] P. Liu and L. Chen, “Inhibition of sonic hedgehog signaling blocks cell migration and growth but induces apoptosis via suppression of FOXQ1 in natural killer/T-cell lymphoma,” *Leukemia Research*, vol. 64, pp. 1–9, 2018.
- [44] X. Xin, Y. Ding, Y. Yang et al., “Protease nexin-1 prevents growth of human B cell lymphoma via inhibition of sonic hedgehog signaling,” *Blood Cancer Journal*, vol. 8, no. 2, p. 24, 2018.
- [45] N. Jin, X. Zhu, F. Cheng, and L. Zhang, “Disulfiram/copper targets stem cell-like ALDH(+) population of multiple myeloma by inhibition of ALDH1A1 and Hedgehog pathway,” *Journal of Cellular Biochemistry*, vol. 119, no. 8, pp. 6882–6893, 2018.
- [46] B. Tang, A. Xu, J. Xu et al., “MicroRNA-324-5p regulates stemness, pathogenesis and sensitivity to bortezomib in multiple myeloma cells by targeting hedgehog signaling,” *International Journal of Cancer*, vol. 142, no. 1, pp. 109–120, 2018.

- [47] S. Natarajan, Y. Li, E. E. Miller et al., "Notch1-induced brain tumor models the sonic hedgehog subgroup of human medulloblastoma," *Cancer Research*, vol. 73, no. 17, pp. 5381–5390, 2013.
- [48] G. W. Robinson, B. A. Orr, G. Wu et al., "Vismodegib exerts targeted efficacy against recurrent sonic hedgehog-subgroup medulloblastoma: results from phase II pediatric brain tumor consortium studies PBTC-025B and PBTC-032," *Journal of Clinical Oncology*, vol. 33, no. 24, pp. 2646–2654, 2015.
- [49] E. Giroux Leprieur, T. Vieira, M. Antoine et al., "Sonic Hedgehog Pathway Activation Is Associated With Resistance to Platinum- Based Chemotherapy in Advanced Non-Small-Cell Lung Carcinoma," *Clinical Lung Cancer*, vol. 17, no. 4, pp. 301–308, 2016.
- [50] C. Yoon, D. J. Park, B. Schmidt et al., "CD44 expression denotes a subpopulation of gastric cancer cells in which Hedgehog signaling promotes chemotherapy resistance," *Clinical Cancer Research*, vol. 20, no. 15, pp. 3974–3988, 2014.
- [51] T. Usui, M. Sakurai, K. Umata et al., "Hedgehog signals mediate anti-cancer drug resistance in three-dimensional primary colorectal cancer organoid culture," *International Journal of Molecular Sciences*, vol. 19, no. 4, p. 1098, 2018.
- [52] R. J. Whitson, A. Lee, N. M. Urman et al., "Noncanonical hedgehog pathway activation through SRF-MKL1 promotes drug resistance in basal cell carcinomas," *Nature Medicine*, vol. 24, no. 3, pp. 271–281, 2018.
- [53] H. X. Liang, L. B. Sun, and N. J. Liu, "Neferine inhibits proliferation, migration and invasion of U251 glioma cells by down-regulation of miR-10b," *Biomedicine & Pharmacotherapy*, vol. 109, pp. 1032–1040, 2019.
- [54] Y. Wang, Q. Yang, Y. Cheng, M. Gao, L. Kuang, and C. Wang, "Myosin heavy chain 10 (MYH10) gene silencing reduces cell migration and invasion in the glioma cell lines U251, T98G, and SHG44 by inhibiting the Wnt/ $\beta$ -Catenin pathway," *Medical Science Monitor*, vol. 24, pp. 9110–9119, 2018.
- [55] M. Ozarowski, P. L. Mikolajczak, A. Piasecka et al., "Effect of *Salvia miltiorrhiza* root extract on brain acetylcholinesterase and butyrylcholinesterase activities, their mRNA levels and memory evaluation in rats," *Physiology & Behavior*, vol. 173, pp. 223–230, 2017.
- [56] P. Zhao, S. Guo, Z. Tu et al., "Grhl 3 induces human epithelial tumor cell migration and invasion via downregulation of E-cadherin," *Acta Biochimica et Biophysica Sinica*, vol. 48, no. 3, pp. 266–274, 2016.
- [57] J. Pei, I. H. Park, H. H. Ryu et al., "Sublethal dose of irradiation enhances invasion of malignant glioma cells through p53-MMP 2 pathway in U87MG mouse brain tumor model," *Radiation Oncology*, vol. 10, p. 164, 2015.
- [58] L. Yang, X. Song, J. Zhu et al., "Tumor suppressor microRNA-34a inhibits cell migration and invasion by targeting MMP-2/MMP-9/FNDC3B in esophageal squamous cell carcinoma," *International Journal of Oncology*, vol. 51, no. 1, pp. 378–388, 2017.
- [59] H. W. Chun and R. Hong, "Significance of the hedgehog pathway-associated proteins Gli-1 and Gli-2 and the epithelial-mesenchymal transition-associated proteins Twist and E-cadherin in hepatocellular carcinoma," *Oncology Letters*, vol. 12, no. 3, pp. 1753–1762, 2016.
- [60] E. Bilegsaikhan, H. N. Liu, X. Z. Shen, and T. T. Liu, "Circulating miR-338-5p is a potential diagnostic biomarker in colorectal cancer," *Journal of Digestive Diseases*, vol. 19, no. 7, pp. 404–410, 2018.
- [61] A. Salaritabar, I. Berindan-Neagoe, B. Darvish et al., "Targeting Hedgehog signaling pathway: paving the road for cancer therapy," *Pharmacological Research*, vol. 141, pp. 466–480, 2019.
- [62] N. Huang, Z. Wu, L. Lin et al., "MiR-338-3p inhibits epithelial-mesenchymal transition in gastric cancer cells by targeting ZEB2 and MACC1/Met/Akt signaling," *Oncotarget*, vol. 6, no. 17, pp. 15222–15234, 2015.
- [63] D. Z. Liu, H. Zhao, Q. G. Zou, and Q. J. Ma, "MiR-338 suppresses cell proliferation and invasion by targeting CTBP2 in glioma," *Cancer Biomarkers*, vol. 20, no. 3, pp. 289–297, 2017.
- [64] Y. Li, Y. Huang, Z. Qi, T. Sun, and Y. Zhou, "MiR-338-5p promotes glioma cell invasion by regulating TSHZ3 and MMP2," *Cellular and Molecular Neurobiology*, vol. 38, no. 3, pp. 669–677, 2018.

## Research Article

# Chemopreventive Effects of Propolis in the MNU-Induced Rat Mammary Tumor Model

A. F. Gal,<sup>1</sup> L. Stan,<sup>2</sup> F. Tăbăran,<sup>1</sup> D. Rugină <sup>1</sup>, A. F. Cătoi <sup>3</sup> and S. Andrei<sup>1</sup>

<sup>1</sup>Faculty of Veterinary Medicine, University of Agricultural Sciences and Veterinary Medicine Cluj-Napoca, 3-5 Mănăştur Street, 400372 Cluj-Napoca, Romania

<sup>2</sup>Faculty of Food Science and Technology, University of Agricultural Sciences and Veterinary Medicine Cluj-Napoca, 3-5 Mănăştur Street, 400372 Cluj-Napoca, Romania

<sup>3</sup>Faculty of Medicine, "Iuliu Hațieganu" University of Medicine and Pharmacy, 8 Victor Babes Street, 400000 Cluj-Napoca, Romania

Correspondence should be addressed to D. Rugină; [dumitrita.rugina@usamvcluj.ro](mailto:dumitrita.rugina@usamvcluj.ro)

Received 28 October 2019; Revised 27 December 2019; Accepted 10 February 2020; Published 27 February 2020

Guest Editor: Nagendra K. Kaushik

Copyright © 2020 A. F. Gal et al. This is an open access article distributed under the Creative Commons Attribution License, which permits unrestricted use, distribution, and reproduction in any medium, provided the original work is properly cited.

Currently, one of the central problems in cancer management is the relapse of disease following conventional treatments, yet few therapeutic agents targeting resistance and tolerance exist. Propolis is known as a healing agent since ancient times. Therefore, over time, its curative properties have kept the interest of scientists, thus leading permanently to investigations of its other possible undiscovered effects. In this context, current experiments were performed to establish the chemopreventive potential of propolis extract (PE) (1.05 mg/kg BW/day) in N-methyl-N-nitrosourea- (MNU-) induced rat mammary tumors. MNU-inoculated/PE-treated rats had tumors of different physical attributes compared with control rats MNU-inoculated. The number of developed tumors (mean 49% versus 100%), incidence (mean 49% versus 100%), multiplicity (1.8 versus 3.7 ( $p < 0.001$ )), tumor volume (mean 10 cm<sup>3</sup> versus 16 cm<sup>3</sup> ( $p < 0.001$ )), and weight of the tumor mass (mean 7.42 g versus 9.00 g ( $p < 0.05$ )) were noted. The numbers of grade I tumors recorded for MNU-inoculated rats were 24 (Group 1) and 7 (Group 2) for MNU-induced/PE-treated rats. In the serum of rats MNU-inoculated/PE-treated were found higher levels of antioxidative enzymes (SOD, CAT, and GPx) than in MNU-induced. Taken together, these data indicate that propolis could be a chemopreventive agent against MNU-induced mammary carcinogenesis.

## 1. Introduction

The human breast cancer and the canine mammary cancer are the most frequently detected malignancies in women and female dogs worldwide, in which, regardless of an intensive cancer control effort, it remains one of the main leading causes of cancer deaths [1, 2]. Nowadays, a lot of efforts are made in order to find new complementary and alternative therapies for different cancer types, because of their highly resistance or tolerance to the conventional treatment. The curative properties of the bee glue called propolis have kept the interest of scientists worldwide, leading permanently to investigations of its other undiscovered possible effects. Till now, propolis received the scientific attention due to its proved antioxidant [3–6], anti-inflammatory [7, 8], and anti-tumor [3, 9–11] properties. Propolis is generally composed of

50% to 60% resins and vegetable balsam, 30% to 40% bee wax, 5% to 10% essential and aromatic oils, 5% pollen grains, and 5% other substances as micronutrients or small amounts of vitamins B1, B2, B6, C, and E [12]. In these 5% of other substances, more than 300 bioactive molecules are present, between them being phenolic acids, flavonoids, diterpenoids, and triterpenoids [13]. The European propolis contains predominantly phenolic compounds, including several flavonoids [14]. The chemical composition of propolis could be influenced by the geographical region and bee species which collect the raw material and produces it. Consequently, biological properties of propolis from different geographical regions could exert particular biological properties.

The literature data contain *in vitro* studies about many propolis samples resulted from various geographic locations, which have been investigated for their antitumoral activities



[7, 10, 15–17]. For instance, propolis originally from Chile proved to have an antiproliferative capacity on KB (human mouth epidermoid carcinoma cells), respective on Caco-2 (colon adenocarcinoma cells) and DU-145 (androgen-insensitive prostate cancer cells) human tumor cell lines [10]. There are several studies done on mammary tumor cells, in which a major compound found in propolis such as caffeic acid phenethyl ester inhibited MCF-7 (hormone receptor positive, HR+) and MDA-231 (a model of triple-negative breast cancer) tumor growth, both *in vitro* and *in vivo* without affecting the normal mammary cells [18]. The same compound was able to decrease the malignancy potential in breast cancer stem cells, by inhibition of self-renewal, progenitor formation, clonal growth in soft agar, and concurrent significant decrease in CD44 content [19]. A recent paper sustains that caffeic acid phenethyl ester is rather most efficient than caffeic acid, inducing cell cycle arrest in S phase and triggering apoptosis in the triple-negative human Caucasian breast adenocarcinoma line cells (MDA-MB-231) [20]. In a similar report, caffeic acid phenethyl ester inhibited breast cancer MDA-MB-231 cells proliferation, activating apoptosis and autophagy, and inhibiting TLR4 signaling pathway [21]. The antiproliferative and proapoptotic activity of Lebanese propolis was demonstrated on breast adenocarcinoma MDA-MB-231 cells, Jurkat leukemic T-cells and glioblastoma U251 cells [16]. Therefore, more papers sustain that the apoptosis is the mechanism involved in the death of tumor cells as human lung adenocarcinoma epithelial (A549), human cervical adenocarcinoma (HeLa), and human breast adenocarcinoma (MCF-7) treated with propolis [22–24].

In literature, several *in vivo* studies assessing the properties of propolis in carcinogenesis were reported, but particularly the clinical trials are scarce. Usually, in experimental studies of breast cancer, the main animal species used are rats or mice, due to the high similarity between human and rodent's mammary, thus being possible to foresee the development process of mammary carcinogenesis in both species [25]. The common carcinogenic agent used in rodents to induce breast cancer development is N-methyl-N-nitrosourea (MNU) [26]. The most malignant lesions induced were carcinomas of the cribriform and papillary types [27].

In this context, this study came to prove that propolis could be a chemopreventive agent against MNU-induced mammary carcinogenesis. To achieve this goal, one propolis sample collected from Transylvania region of Romania was examined for its chemopreventive potential of a long-term day-to-day administration of propolis in MNU-induced rat mammary tumors. Consequently, the data resulted contributes to a better understanding of the geographical region influence to the composition and biological properties of propolis related to those reported in other studies from other parts of the world.

## 2. Materials and Methods

**2.1. Animals.** Thirty-days-old juvenile female Sprague-Dawley rats acquired from the Cantacuzino Institute,

Romania, were utilized. The rats were acclimated to laboratory environments in advance of the study, being kept under standard conditions (22–23°C, humidity 60%, light-dark cycle 12 h). All experiments were conducted in agreement with the European Union regulation on animal testing and performed according to the practices of the Romanian Board of Animal Research, having permission of Committee of Animal Ethics of the University of Agricultural Sciences and Veterinary Medicine of Cluj-Napoca (UASVMCN), Romania (UASVM Bio-Ethical Committee Agreement Form no. 9753/22.06.2016).

**2.2. Preparation of Propolis Extract (PE).** Propolis was collected from the Corund area, Transylvania, Romania (46° 28' 13" N 25° 11' 8" E). Briefly, preparation of propolis extract (PE) used in this experiment was done accordingly: 1 g propolis was left to macerate overnight in 30 mL of 95% ethanol at room temperature and under continuous agitation. Then, the extract obtained was filtered and the residue was extracted again under the same conditions. Finally, both extracts were mixed up to a final volume of 100 mL adjusted with ethanol. PE was analyzed for (a) total flavones and flavonols content by a method based on aluminum chloride complex formation (equation of calibration curve for methanolic galangin (4–30 µg/mL)  $Y = 2.04832 \times X - 0.00233$ ;  $r^2 = 0.99935$ ), (b) total flavanone and dihydroflavonol content through the colorimetric method with dinitrophenylhydrazine (equation of calibration curve of methanolic pinocembrin (0.2–2.0 mg/mL)  $Y = 0.11034 \times X - 0.00416$ ;  $r^2 = 0.99910$ ), and (c) total phenolics by the Folin-Ciocalteu method (equation of calibration curve  $Y = 0.00709 \times X - 0.00109$ ;  $r^2 = 0.99932$  of methanolic mixture pinocembrin and galangin at a 2:1 ratio (w/w) in the concentration range of 25–300 µg/mL) according to methods previously published [28, 29].

**2.3. Experimental Design.** MNU was utilized to induce mammary tumors (Sigma-Aldrich Chemical Co., St. Louis, USA). MNU was dissolved in standard saline solution, being utilized immediately after preparation. The experimental model of induced carcinogenesis was previously used in our laboratory [30]. The female rats were divided in four groups (10 rats per group) and treated as follows: (a) Group 1, inoculated with a single dose of 55 mg MNU/kg body weight (BW) intraperitoneally (i.p.) and received regular rat food (provided by Cantacuzino Institute, Bucharest, Romania); (b) Group 2, inoculated with a single dose of 55 mg MNU/kg BW i.p. and received regular rat food supplemented with PE in a dose of 1.05 mg/kg BW/day (i.e., 15 droplets of PE/kg BW/day, which were applied on the pelleted diet to avoid the daily handling stress of the rat individuals in this group); (c) Group 3, inoculated with a single dose of saline solution i.p. and received regular rat food supplemented with PE in a dose of 1.05 mg PE/kg BW/day (i.e., 15 droplets of PE/kg BW/day, which were applied on the pelleted diet to avoid the daily handling stress of the rat individuals in this group); (d) Group 4, inoculated with a single dose of saline solution i.p. and received regular rat food. In our experimental model,

the daily dose of PE supplemented in the diet of rats was 1.05 mg/kg BW/day.

PE administration was introduced in the diet at the age of 33 days (i.e., 4 days before MNU administration) in order to ensure a proper body condition before the inoculation of the carcinogenic agent. Rats from Groups 2 and 3 were housed alone to ensure the ingestion of the whole daily dose of PE. Rats from Groups 1 and 4 were kept in groups of 10 individuals. The experiment (including the daily administration of PE for the Groups 2 and 3) were then continued for 290 days (9½ months). Food ingestion and the general body condition were appreciated weekly throughout the experiment. Rats were examined once a week to evaluate the possible existence and location of mammary tumors.

Due to welfare grounds and destabilizing body condition induced by the tumor progression in some individuals, the experiment was stopped at 290 days from MNU-inoculation (or after 294 days of daily intake of PE). At the end of the study, animals from all four groups were humanly exsanguinated after deep narcosis with halothane. The following details were recorded in all groups: the number of developed tumors, incidence, multiplicity, size of the tumor mass, and weight of the tumor mass. The size of each tumor was assessed using a micrometer caliper.

**2.4. Necropsy and Histopathology.** A complete necropsy survey was performed on the biological material used in the study. Concerning the gross examination of the tumors detected throughout the body, the following details were recorded: the mass location, dimension, weight, consistency, and the status of regional lymph nodes (e.g., hypertrophy, mobility). Additionally, for each rat from the Groups 1 and 2 the subsequent parameters of the detected mammary tumors were calculated: (a) the percentage of the mammary tumor mass (MTm) relative to the final body weight (FBW) of the rat, by using the formula:  $MTm(g) \times 100 / FBW(g) = MTm(\%)$ ; (b) the volume of each tumor was calculated using the formula suggested by Woditschka et al. (2008):  $0.5 \times \text{tumor length} \times \text{tumor width} \times \text{tumor height}$  [31]; (c) mammary tumors multiplicity (MTM) for the Groups 1 and 2 (i.e., average mammary tumor number/rat in each of the two groups).

Furthermore, necropsy included a gross and histological examination of the internal organs. In all animals, several tissue samples were harvested from a number of organs (e.g., stomach, intestine, pancreas, liver, lung, spleen, kidney, lymph nodes, and central nervous system) for further histological inspection. Harvested samples were fixed in 10% buffered formalin, embedded later in paraffin blocks, and eventually, the tissue sections (5 µm in thickness) were stained by hematoxylin and eosin procedure. The mammary tumors were categorized according to their histological type and as benign or malignant [32]. In the case of malignant mammary tumors, a grading system was utilized [33].

**2.5. Assays of Serum Components and Enzymes.** Serum analysis of various liver marker enzymes such as total protein, albumin, globulin, alkaline phosphatase (ALP), alanine aminotransferase (ALT), amylase (AMY), calcium (Ca),

phosphorus (Pa), sodium (Na), potassium (K), blood urea nitrogen (BUN), total bilirubin (TBIL), creatinine (CRE), and glucose (GLU) were estimated by using VetScan® Comprehensive Diagnostic Profile reagent rotor used with the VetScan Chemistry Analyzer (Diamond Diagnostics, Holliston, MA, USA).

## 2.6. Assays of Antioxidant Profile

**2.6.1. Total Protein Extract.** Samples of hepatic tissue were twice washed with saline solution. Then each sample of hepatic tissue was homogenized using an ultraturax and the total proteins were extracted with potassium phosphate buffer (50 mM, pH 7.35) [34]. Samples were analyzed by determining the total proteins concentration, the activity of antioxidant enzymes (SOD, CAT, GPx), the lipid peroxidation level, and the amount of oxidized proteins produced in the liver of MNU- and/or PE-exposed rats as previously was assessed in our laboratory [35].

**2.6.2. Superoxide Dismutase Assay.** Superoxide dismutase (SOD) assay kit (Cayman Chemical Company, Michigan, USA) is based on the conversion of a tetrazolium salt to formazan by superoxide radicals generated in xanthine/xanthinoxidase system. The current method measures the activities of all three SOD types. One unit of enzyme is defined as the amount of enzyme needed to exhibit 50% dismutation of the superoxide radical. Absorbances were monitored at 450 nm by HT BioTek Synergy (BioTek Instruments, USA) microplate plate reader.

**2.6.3. Catalase Assay.** Catalase (CAT) assay kit (Cayman Chemical Company, Michigan, USA) is based on the reaction of the enzyme with methanol in the presence of H<sub>2</sub>O<sub>2</sub>. The formaldehyde produced is measured colorimetrically with 4-amino-3-hydrazino-5-mercapto-1,2,4-triazole (Purpald) as the chromogen. A standard curve of bovine liver catalase was used for the determination of enzyme activity. One unit is defined as the amount of enzyme that will cause the formation of 1 nmol of formaldehyde per minute at 25°C. Absorbances were recorded at 540 nm wavelength by using microplate plate reader HT BioTek Synergy (BioTek Instruments, USA).

**2.6.4. Glutathione Peroxidase Assay.** Glutathione peroxidase activity (GPx) Ransel kit (Randox Laboratories Ltd., London, UK) is based on the oxidation reaction of glutathione (GSH), using cumene hydroperoxide as a substrate. In the presence of glutathione reductase (GR) and NADPH+H<sup>+</sup>, glutathione disulfide (GSSG) is reduced to sulfhydryl form glutathione (GSH). This mechanism is possible due to the oxidation process of NADPH into NADP<sup>+</sup>. The decrease in absorbance was measured at 340 nm wavelength by using microplate plate reader HT BioTek Synergy (BioTek Instruments, USA).

**2.6.5. Determination of Lipids Peroxidation Level.** The most common indicator of peroxidation is the chemical compound malondialdehyde (MDA), being the final degradation product resulted in lipids peroxidation. The assay is based on the interaction between the resulted MDA and thiobarbituric

acid (TBA). The MDA-TBA adduct formed by the reaction between the resulted MDA and thiobarbituric acid (TBA) under high temperature (90–100°C) and acidic conditions was measured colorimetrically at 540 nm, by using microplate plate reader HT BioTek Synergy (BioTek Instruments, USA). The protocol assay TBARS kit was followed as the producer (Cayman Chemical Company, Michigan, USA) indicated.

**2.6.6. Determination of Protein Degree Oxidation.** The most significant two compounds resulted from the oxidation process of proteins are glutamic semialdehyde and amino adipic semialdehyde. The method recommended by the assay kit (Cayman Chemical Company, Michigan, USA) is based on the reaction between aldehydes and 2,4 dinitrophenylhydrazine (DNPH). Products resulted from protein oxidation processes reacted with DNPH and formed a colorful compound, which was quantified spectrophotometrically. The quantity of DNPH that reacted with the products obtained due to the oxidation process was expressed as g protein per g tissue.

### 3. Results

**3.1. Characterization of Propolis Extract (PE).** The presence of phenolic compounds in PE was verified by the Folin-Ciocalteu reaction and total phenolic content was  $46.27 \pm 1.18$ . Moreover, the PE was subjected to the spectrophotometric analysis for total flavones and flavonols content assessment by using the method based on aluminum chloride complex formation and the value obtained was  $7.90 \pm 0.32\%$ . Using the colorimetric method with dinitrophenylhydrazine, the total flavanone and dihydroflavonol content of PE was  $3.85 \pm 0.61\%$ .

**3.2. Chemopreventive Effects of Propolis on Mammary Tumor Development.** The tumor development occurred only in subjects of Groups 1 and 2, i.e., MNU-exposed rats. In Group 1, all animals developed tumors (Figures 1(a) and 1(b)), in contrast to rats of Group 2 where only 7 out of 10 presented tumors (Figures 1(c) and 1(d)). It was observed in Group 1 a variation of 1 to 9 tumors/rat; meanwhile in Group 2, 0 up to 5 tumors/rat occurred (Tables 1 and 2).

Microscopically, mammary tumors were classified as benign or malignant (in situ or invasive) mammary carcinomas. In the case of malignant mammary lesions, in Group 1 were identified 64.86% of grade I (Figure 1(e)), 18.91% of grade II, and 2.7% of grade III mammary carcinomas (Figures 1(f) and 1(g)), the rest of 13.51% being benign mammary lesions. In the case of Group 2, the abundance of identified mammary carcinomas of grade I was 38.88%, of grade II was 33.33%, and 16.66% of grade III (Figure 1(h)), while 11.11% were benign mammary lesions (Figure 1(i)). Histologically, mammary tumor types detected did not present structural differences in subjects from Group 1 versus Group 2.

The total number of tumors recorded in the Group 1 was 41 (i.e., 37 mammary and 4 non-mammary tumors), whereas subjects of Group 2 developed 20 tumors (i.e., 18 mammary and 2 non-mammary tumors). Therefore, the mammary

tumors induction ratio was 90.24% in Group 1, respective to 90% in Group 2. Regarding the mammary tumors multiplicity, a significant variation occurred between both groups as follows:  $3.7 \pm 2.75$  mammary tumors/rat in Group 1 and  $1.8 \pm 1.39$  mammary tumors/rat in Group 2 ( $p < 0.001$ ) (Table 3). Moreover, in Table 3 can be seen the difference in the average of mammary tumors volume ( $16.68 \pm 33.32$  in Group 1 vs  $10.76 \pm 17.17$  in Group 2;  $p > 0.05$ ) and average MTM (%) relative to FBW ( $9.00 \pm 10.86$  in Group 1 vs  $7.42 \pm 11.43$  in Group 2;  $p > 0.05$ ).

**3.3. Blood Biochemical Profile in All Experimental Groups.** Blood biochemical parameters of rats inoculated with normal saline solution were taken as reference values. In general, inoculation of MNU (Group 1) caused a slight decrement of total blood proteins, associated with a significant decrease of albumins and a very significant increase of globulins. Concerning the activity of sanguine enzymes, ALT was slightly increased, but ALP and AMY were non-significantly decreased in MNU-inoculated rats comparing with control (Group 4) (Table 4). The rats MNU-treated had levels of TBIL, BUN, and CRE decreased in contrast to rats of control Group 4. The concentration of GLU in blood of MNU-inoculated rats assessed was highly significant than that of rats from the control group. On the other hand, levels of microminerals were non-statistically changed after the MNU-inoculation.

The administration of PE into the diet of MNU-inoculated rats did not change total proteins concentration but slightly increased albumins and significantly decreased globulins. The activity of ALT enzyme decreased and AMY increased, but non-statistically relevant, in MNU-inoculated/PE-treated rats comparing with MNU-inoculated ones (Group 1). Hematological values of BUN, GLU (statistic relevant,  $p < 0.0001$ ) for MNU-inoculated/PE-treated rats were lower than of MNU-inoculated rats, but increased levels of TBIL and CRE were recorded. Microminerals profile was not statistically significant modified by the PE administration in the diet of MNU-inoculated rats. Overall, varying strengths of PE in the diet of MNU-inoculated rats showed a potentiating effect on albumins, AMY, TBIL, and CRE while a lowering effect on globulins, ALT, BUN, and GLU compared with that of MNU-treated rats. PE from the diet of MNU-inoculated rats seems able to restore these values close to the physiological normal ones.

**3.4. The Effects of MNU and Propolis on the Antioxidative Status.** Inoculation of the MNU carcinogenic agent produced a significant drop of antioxidant enzymes (SOD, CAT, GPx) in rats, in contrast to control (Figure 2). The PE administration in the diet of rats determined substantial increases of all three antioxidant enzymes levels. Moreover PE induced a significant decrease of the oxidized proteins, increased previously by the MNU-inoculation (Figure 2). The PE presence in the diet of MNU-inoculated rats did not induce significant changes in levels of malondialdehyde (MDA) (Figure 2). The oxidized proteins level in MNU-inoculated rats increased in contrast to rats of the group considered control. It seems that after the PE administration in the diet of MNU-inoculated

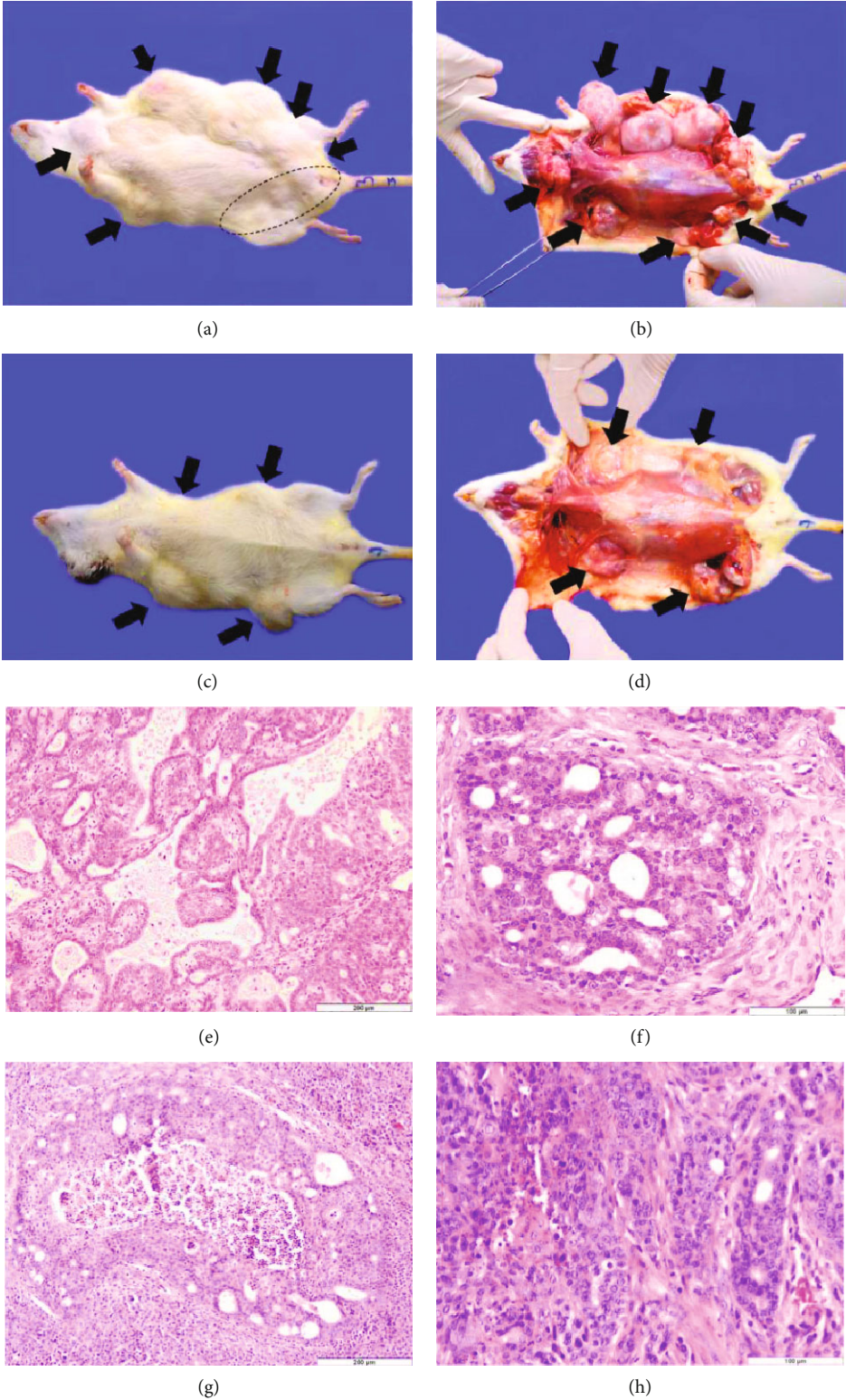
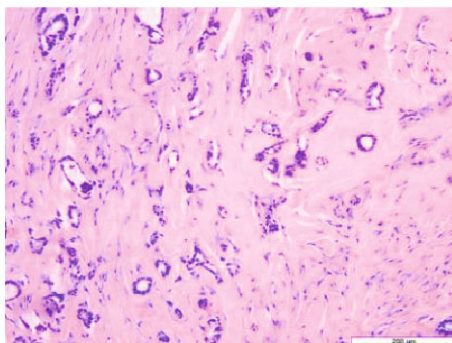


FIGURE 1: Continued.



(i)

FIGURE 1: (a) MNU-induced mammary tumors visible as subcutaneous masses of different sizes (arrows and selected area); Rat no. 3, Group 1. (b) Gross features of MNU-induced mammary tumors following skinning (arrows); Rat no. 3, Group 1. (c) and (d) are comparative features regarding the location and gross features of the MNU-induced mammary tumors (arrows) in Group 2 individuals (Rat no. 7). (e) Invasive tubular carcinoma, grade 1, represented by tubular and tubulopapillary structures; HE stain (Group 1, Rat 1, 5<sup>th</sup> left mammary gland). (f) Ductal *in situ* cribriform carcinoma, grade 2, made of a solid proliferation with formation of secondary lumina; HE stain (Group 1, Rat 3, 1<sup>st</sup> right mammary gland). (g) Ductal *in situ* comedo-carcinoma, grade 2, which appears as distended ductal structures with a multilayered epithelium surrounding a necrotized area; HE stain (Group 1, 2<sup>nd</sup> left mammary gland). (h) Invasive tubular carcinoma, grade 3, composed of tubular structures with increased nuclear size and prominent nucleoli; HE stain (Group 2, Rat 4, 2<sup>nd</sup> left mammary gland). (i) Fibroadenoma composed of ductal structures surrounded by fibrous tissue; HE stain (Group 2, Rat 9, 4<sup>th</sup> right mammary gland).

rats, the level of oxidized proteins is decreased, but data obtained are not statistically relevant (Figure 2).

#### 4. Discussion

Breast cancer is the leading cause of cancer-related deaths among women worldwide. Literature studies sustain that the breast cancer, a heterogeneous tumor, has a varying response to treatments. Despite the improved efficacy offered by modern treatments, their toxicity and often unpleasant side-effects remain a major source of concern for patients and clinicians. New approaches to improve tolerance of the cancer chemotherapy are urgently needed and the present topic focuses on this issue. Over the time, the biological properties of propolis collected from different areas of the world to exert antiproliferative and cytotoxic potential toward tumor cells were evaluated and observed [10, 13, 16, 20, 36]. A recent study sustains that the biological activity of propolis is positively influenced by the presence of flavonoids and phenolic acids in it [29]. Therefore for this study, a propolis sample collected from Transylvania, rich in phenolic acids  $46.27 \pm 1.18\%$ , containing flavones/flavonols ( $7.90 \pm 0.32\%$ ) and flavanone  $3.85 \pm 0.61\%$  was selected. The biochemical characterization reported here for the Transylvanian propolis is in accordance with that reported in literature for a typical poplar propolis [37].

Our study highlights some data regarding the propolis usage as a potential chemopreventive agent.

Sprague-Dawley rat model was selected to be the animal model for the current study, because it bears histological features of mammary tumors closely to that of human and canine mammary tumors. As an agent to induce mammary adenocarcinomas in female rats, the N-methyl-N-nitrosourea (MNU) agent was used to be inoculated intra peritoneal to healthy rats, because the mammary tumors induced by it seem to be more aggressive and their occur-

rence higher [38, 39]. Moreover, MNU-induced rat mammary tumors possess some similar features of human breast cancer, such as the growth addiction on ovarian hormones [40] and presence of lymphocytic infiltrates in the reactive stroma [38]. In our study, the mammary tumors induction ratio by MNU was around 90% in both Groups 1 and 2. Histological analysis of mammary tumor sections classified tumors as benign or malignant (*in situ* or invasive) mammary carcinomas. No histomorphological differences were related to the chemoprevention using propolis.

Results of our study demonstrate that a diet containing PE is able to slow down the progression of breast tumors development with lower multiplicity, weight, and size compared with control. 30% of rats from Group 2, MNU-induced/PE-treated, were found to have no tumor at the end of the study. Moreover, the number of grade I tumors recorded for MNU-inoculated rats was 24 and decreased to 7 tumors after the PE administration in the diet of rats MNU-inoculated. Our findings are consistent with another previous *in vivo* study investigated by Ahmed and colleagues that another bee product as honey may modulate tumor latency, incidence, multiplicity, and progression [41].

It has been demonstrated that tumors can be eliminated or diminished by chronic administration of low doses of chemotherapeutic drugs [42]. It is quite possible that propolis treatment behaves similarly, because doses used in the current study are about 1 mg/body weight/day. As a well-known natural product, being widely consumed by humans, propolis seems to be associated with a high rate of allergic reactions rather than toxicity. It was demonstrated that no toxicity effect was observed for a propolis dose of 1400 mg/body weight/day administered to each mouse in a study with 90 animals.

Regarding the sanguine biochemical profile, the administration of MNU-inoculation in Group 1 of rats triggered a negligible reduction of total blood proteins, a decrease of

TABLE 1: Mammary tumor occurrence in Group 1: histological features, tumors location, and size; non-mammary tumors detected.

Rat no.	Mammary tumor type	Group 1 (MNU)		Other tumor types
		Mammary tumor size (cm)	MTM(%) <sup>1</sup> relative to FBW <sup>2</sup>	
1	Invasive tubular carcinoma, G-1 (M <sub>1</sub> right)	1.3/1.3	17.39	—
	Carcinosarcoma, G-1 (M <sub>4</sub> right)	3.5/2.6		
	Invasive tubular carcinoma, G-1 (M <sub>2</sub> left)	1.3/2.1		
	Invasive tubular carcinoma, G-1 (M <sub>5</sub> left)	6.8/3.5		
2	Invasive cribriform carcinoma, G-1 (M <sub>1</sub> right)	1.4/1	10.78	Interstitial renal tumor (1.3/1 cm)
	Ductal <i>in situ</i> cribriform carcinoma, G-1 (M <sub>2</sub> right)	1.7/1.2		
	Invasive tubular carcinoma, G-2 (M <sub>3</sub> right)	6.0/3.5		
	Invasive tubular carcinoma, G-1 (M <sub>5</sub> right)	1.7/1.2		
	Ductal <i>in situ</i> cribriform carcinoma, G-2 (M <sub>2</sub> left)	2.4/2.2		
	Invasive tubular carcinoma, G-1 (M <sub>3</sub> left)	2.1/2.0		
3	Invasive tubular carcinoma, G-1 (M <sub>5</sub> left)	1.3/0.9	29.27	—
	Ductal <i>in situ</i> cribriform carcinoma, G-1 (M <sub>1</sub> right)	3/2.5		
	Invasive tubular carcinoma, G-1 (M <sub>3</sub> right)	3.5/3		
	Ductal <i>in situ</i> solid carcinoma, G-1 (M <sub>4</sub> right)	2.5/2.2		
	Invasive tubular carcinoma, G-1 (M <sub>5</sub> right)	1.3/1.2		
	Invasive tubular carcinoma, G-1 (M <sub>1</sub> left)	2.5/2		
	Fibroadenoma (M <sub>2</sub> left)	5/4.5		
	Ductal <i>in situ</i> papillary carcinoma, G-1 (M <sub>3</sub> left)	6.5/5.1		
	Invasive tubular carcinoma, G-1 (M <sub>4</sub> left)	6.2/5.6		
4	Ductal <i>in situ</i> papillary carcinoma, G-1 (M <sub>5</sub> left)	4/3.5	23.87	Malignant lymphoma (diffuse in both mammary chains)
	Ductal <i>in situ</i> solid carcinoma, G-3 (M <sub>2</sub> right)	0.8/0.5		
	Ductal <i>in situ</i> cribriform carcinoma, G-1 (M <sub>5</sub> right)	7.9/6.5		
	Ductal <i>in situ</i> comedo-carcinoma, G-2 (M <sub>2</sub> left)	3/2.7		
5	Ductal <i>in situ</i> papillary carcinoma, G-1 (M <sub>4</sub> left)	5.4/3.2	0.25	—
	Fibroadenoma (M <sub>4</sub> right)	1.7/1.4		
6	Ductal <i>in situ</i> cribriform carcinoma, G-2 (M <sub>1</sub> right)	0.8/0.6	4.76	—
	Invasive tubular carcinoma, G-2 (M <sub>3</sub> left)	4.2/3.7		
7	Invasive tubular carcinoma, G-1 (M <sub>1</sub> right)	1.2/0.5	0.97	—
	Adenoma (M <sub>2</sub> right)	1.1/1		
	Adenoma (M <sub>2</sub> left)	1.0/0.7		
	Invasive papillary carcinoma, G-1 (M <sub>3</sub> left)	0.9/0.9		
8	Invasive tubular carcinoma, G-1 (M <sub>4</sub> left)	0.9/0.6	1.82	—
	Invasive tubular carcinoma, G-2 (M <sub>2</sub> right)	1.3/1.2		
	Invasive tubular carcinoma, G-1 (M <sub>2</sub> left)	2.8/2.3		

TABLE 1: Continued.

Rat no.	Mammary tumor type	Group 1 (MNU)		Other tumor types
		Mammary tumor size (cm)	MTM(%) <sup>1</sup> relative to FBW <sup>2</sup>	
9	—	—	—	Liposarcoma in the omentum (1.7/1.2 cm) Ovarian fibrosarcoma (1.5/1.2 cm)
10	Invasive tubular carcinoma, G-2 (M <sub>3</sub> right)	1.2/1.2	0.95	—
	Fibroadenoma (M <sub>1</sub> left)	1.4/1.2		
	Ductal <i>in situ</i> cribriform carcinoma, G-1 (M <sub>5</sub> left)	1.2/1		

<sup>1</sup>MTm: mammary tumor mass; <sup>2</sup>FBW: final body weight; MNU: N-methyl-N-nitrosourea; M<sub>1-5</sub>: mammary gland number and its side (i.e., right, left); G: histological grade.

TABLE 2: Chemopreventive effects of propolis on mammary tumor occurrence in Group 2: histological features, tumors location, and size; non-mammary tumors detected.

Rat no.	Mammary tumor type	Group 2 (MNU+PE)		Other tumor types
		Mammary tumor size (cm)	MTM(%) <sup>1</sup> relative to FBW <sup>2</sup>	
1	Invasive cribriform carcinoma, G-1 (M <sub>1</sub> left)	1.5/1.5	22	—
	Invasive cribriform carcinoma, G-3 (M <sub>2</sub> left)	4.5/3		
	Invasive cribriform carcinoma, G-2 (M <sub>5</sub> left)	7.5/4.4		
2	Invasive tubular carcinoma, G-2 (M <sub>4</sub> left)	3.5/2.4	32.8	Rhabdomyosarcoma (diaphragm)
	Invasive tubular carcinoma, G-2 (M <sub>5</sub> left)	4.5/2.2		
	Invasive tubular carcinoma, G-1 (M <sub>1</sub> right)	1.5/0.8		
3	Invasive tubular carcinoma, G-2 (M <sub>1</sub> right)	2.5/2.8	1.33	
	Invasive papillary carcinoma, G-2 (M <sub>1</sub> left)	1.1/0.6		
4	Invasive tubular carcinoma, G-3 (M <sub>1</sub> left)	1/0.7	5.78	—
	Invasive tubular carcinoma, G-3 (M <sub>2</sub> left)	5.5/3.2		
5	—	—	—	—
6	—	—	—	—
7	Invasive tubular carcinoma, G-1 (M <sub>2</sub> right)	3.5/3.2	11.56	Squamous carcinoma (facial skin)
	Invasive tubular carcinoma, G-2 (M <sub>4</sub> right)	5/3.5		
	Invasive tubular carcinoma, G-1 (M <sub>2</sub> left)	3.5/1.5		
	Invasive tubular carcinoma, G-1 (M <sub>4</sub> left)	5.2/2.5		
8	Ductal <i>in situ</i> cribriform carcinoma, G-1 (M <sub>4</sub> right)	1.1/0.6	0.55	
	Invasive tubular carcinoma, G-1 (M <sub>2</sub> left)	1.8/1.3		
9	Fibroadenoma (M <sub>4</sub> right)	1.2/1.1	0.22	—
	Fibroadenoma (M <sub>1</sub> left)	1.1/1		
10	—	—	—	—

<sup>1</sup>MTm: mammary tumor mass; <sup>2</sup>FBW: final body weight; MNU: N-methyl-N-nitrosourea; PE: propolis; M<sub>1-5</sub>: mammary gland number and its side (i.e., right, left); G: histological grade.

albumins concentration, and an increase of globulins. Hypoalbuminemia observed in MNU-exposed group can be a consequence of the injurious effects of the MNU carcinogen on the hepatic polyribosomes and protein-soluble factors, and the result of alkylation and carboxylation of RNA and proteins [43]. However, the negligible reduction of total blood proteins can be a consequence of proteolysis. The hydrolytic

degradation of proteins can be done directly, by protein oxidation, or indirectly by their increased susceptibility to proteolytic enzymes [44].

In the current study, the MNU-exposed group triggered a major increase in blood glucose, but its effect on blood minerals was insignificant. The insignificant activity of sanguine enzymes (i.e., ALP, ALT, and AMY) was observed

TABLE 3: Comparative data concerning mammary and non-mammary tumors developed in rats of Groups 1 and 2.

Experimental group	Multiplicity <sup>1</sup>	Average MTM(%) <sup>2</sup> relative to FBW <sup>3</sup>	Average mammary tumors volume <sup>4</sup>	Total number of mammary tumors/group	Non-mammary tumors/group
Group 1	3.7 ± 2.75	9.00 ± 10.86	16.68 ± 33.32	37	4
Group 2	1.8 ± 1.39 <sup>ns</sup>	7.42 ± 11.43 <sup>ns</sup>	10.76 ± 17.17 <sup>ns</sup>	18	2

<sup>1</sup>Multiplicity (i.e., average mammary tumor number/rat); <sup>2</sup>MTM: mammary tumor mass; <sup>3</sup>FBW: final body weight; <sup>4</sup>Mammary tumor volume calculated using the formula suggested by Woditschka et al., 2008. In order to determine significant differences between mean values, Student's *t* test was used (GraphPad Prism version 6.07).

TABLE 4: Modulatory influences of MNU and propolis on blood biochemical parameters.

Blood parameter	Experimental group			
	Group 1 MNU	Group 2 MNU/PE	Group 3 PE	Group 4 Control
Blood proteins				
Total proteins (g/dL)	7.08 ± 0.77 <sup>ns</sup>	7.05 ± 1.34 <sup>ns</sup>	7.37 ± 0.17 <sup>ns</sup>	7.66 ± 0.44
Albumins (g/dL)	4.98 ± 1.07*	5.45 ± 1.31 <sup>ns</sup>	5.35 ± 0.29 <sup>ns</sup>	6.06 ± 0.24
Globulins (g/dL)	2.08±0.43**	1.70 ± 0.22 <sup>#</sup>	2.15±0.26***	1.60 ± 0.21
The activity of blood enzymes				
ALP (U/L)	147.71 ± 72.24 <sup>ns</sup>	147.71 ± 72.24 <sup>ns</sup>	130.00 ± 3.16 <sup>ns</sup>	151.66 ± 53.09
ALT (U/L)	117.14 ± 85.40 <sup>ns</sup>	80.66 ± 35.53 <sup>ns</sup>	70.50 ± 1.50 <sup>ns</sup>	98.33 ± 31.04
AMY (U/L)	527.28 ± 96.89 <sup>ns</sup>	628.16 ± 112.82 <sup>ns</sup>	615.75 ± 166.09 <sup>ns</sup>	592.66 ± 29.10
Blood biochemical parameters				
TBIL (mg/dL)	0.21 ± 0.09*	0.22 ± 0.04 <sup>ns</sup>	0.33 ± 0.04 <sup>ns</sup>	0.30 ± 0.08
BUN (mg/dL)	16.00 ± 2.00 <sup>ns</sup>	14.83 ± 2.60 <sup>ns</sup>	12.75±1.08***	17.66 ± 1.24
CRE (mg/dL)	0.18±0.09**	0.20 ± 0.05 <sup>ns</sup>	0.22 ± 0.08*	0.30 ± 0.06
GLU (mg/dL)	158.25±5.26***	97.33 ± 26.78 <sup>###</sup>	48.83 ± 16.72 <sup>ns</sup>	61.00 ± 13.20
Blood microminerals				
Ca (mg/dL)	11.77 ± 1.09 <sup>ns</sup>	11.11 ± 2.26 <sup>ns</sup>	11.37 ± 0.28 <sup>ns</sup>	11.53 ± 0.23
Pa (mg/dL)	6.48 ± 1.86 <sup>ns</sup>	5.71 ± 1.54 <sup>ns</sup>	5.10 ± 0.15 <sup>ns</sup>	5.30 ± 0.28
Na (mmol/L)	144.14±1.24**	142.60 ± 1.85 <sup>ns</sup>	142.25 ± 1.47 <sup>ns</sup>	142.00 ± 1.41
K (mmol/L)	8.50 ± 0.49 <sup>ns</sup>	8.00 ± 1.4 <sup>ns</sup>	7.70 ± 0.78 <sup>ns</sup>	7.60 ± 0.21 <sup>ns</sup>

Values are mean ± SD. Each group contains ten animals. Comparisons were made on the basis of the one-way ANOVA followed by Dunnett's test (GraphPad Prism version 6.07). Group 1 (MNU-inoculated rats) and Group 3 (PE-treated rats) were compared with the normal control group (Group 4) (ns: nonsignificant, \**p* < 0.05, \*\**p* < 0.01, \*\*\**p* < 0.0001), respective Group 1 MNU-inoculated with Group 2 (MNU-inoculated/PE-treated) (MNU) (ns: nonsignificant, <sup>#</sup>*p* < 0.05, <sup>##</sup>*p* < 0.01, <sup>###</sup>*p* < 0.0001).

in rats MNU-inoculated comparing with those recorded for control group.

PE included in the diet of MNU-inoculated rats seems able to restore these values close to the physiological normal ones. Overall, varying strengths of PE in the diet of MNU-inoculated rats showed a tendency to restore the concentration of albumins and globulins, and to normalize the biochemical blood parameters TBIL, CRE, and GLU values and the activity of ALT enzyme. There is evidence that propolis is able to normalize ALT activity by different doses of propolis in female albino rats of Sprague–Dawley strain [45]. Propolis administered to rats, previously aluminum chloride-treated, normalized the increased transaminases and lactate dehydrogenase (LDH) activity [46].

The enzymatic antioxidant system is composed of superoxide dismutase (SOD), catalase (CAT), and glutathione

peroxidase (GPx), which scavenges the reactive oxygen species and lipid peroxidation. It is known that tumor cells exhibit heterogeneity in the levels of oxidative stress and for this reason could have various levels of antioxidant enzymes. Several reports have cited decreased activities of SOD and catalase in various carcinogenic conditions [47–49]. SOD is able to disrupt the potent oxidizing radicals such as superoxide radicals, which are highly diffusible and thus being able to pass through cell membranes causing injuries far apart the tumor site [50]. The superoxide radicals are converted by SOD to hydrogen peroxide and oxygen. CAT is able to catalyse the breakdown of hydrogen peroxide produced by tumor cells. Another equally important antioxidant enzyme involved in the preventing intracellular damage caused by hydrogen peroxide is GPx. In tumor cells, low activities of GPx were reported, maybe due to the altered antioxidant



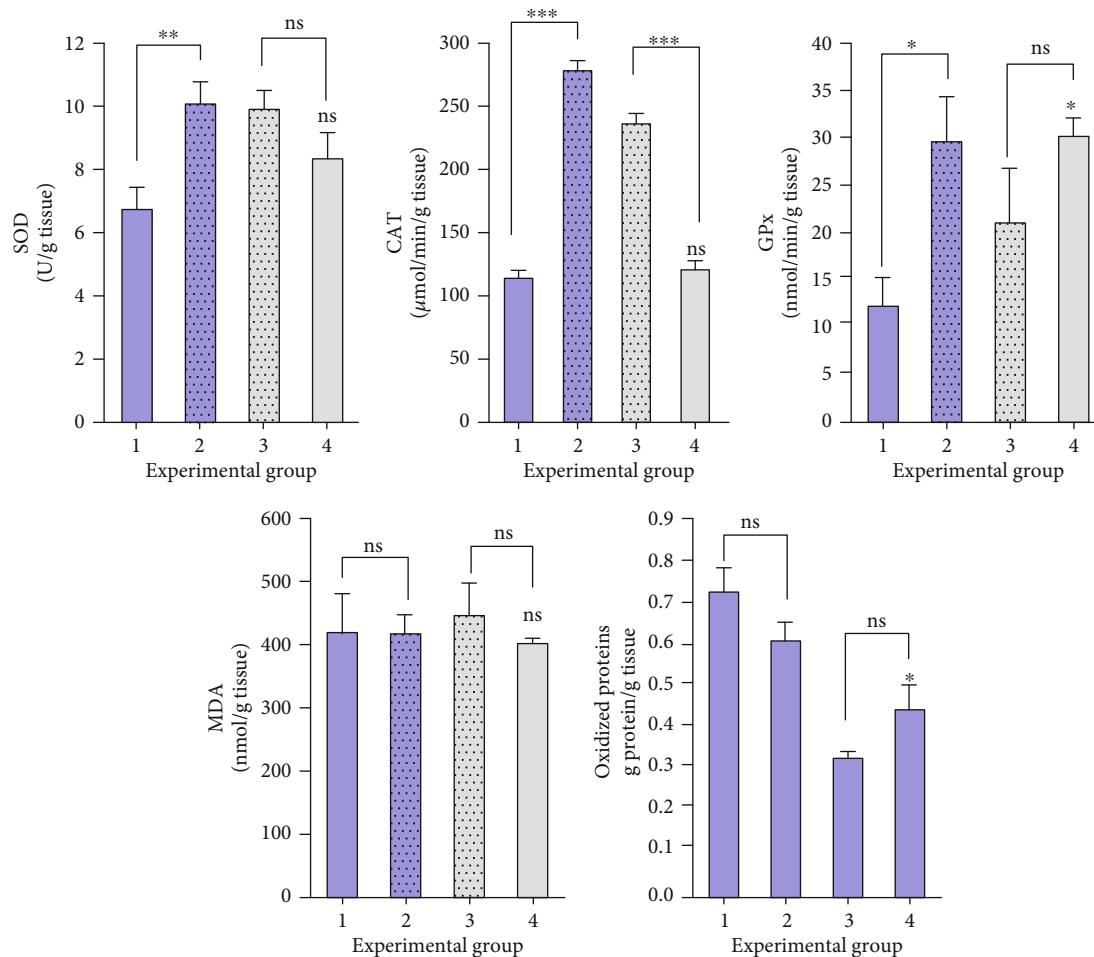


FIGURE 2: Effect of MNU-inoculation and propolis diet administration on hepatic antioxidative markers in rats. Statistically, all groups were compared with Group 1 (MNU-inoculated), respective to Group 4 control (normal saline inoculation and normal rat food) ( $p < 0.05$ ,  $**p < 0.01$ ,  $***p < 0.0001$ ). Comparisons for the antioxidant profile were made on the basis of the one-way ANOVA followed by Bonferroni's test (GraphPad Prism version 6.07).

defense system caused by enormous production of free radicals in DMBA-induced carcinogenesis [47].

In the present study, the activity of antioxidant enzymes determined from the liver of exposed rats to MNU carcinogen agent was decreased significantly from a statistical point of view if comparing with control rats, exposed only to normal saline solution. The PE administration in the diet of rats previously MNU-inoculated determined an increment of the antioxidative enzymes (SOD, CAT, GPx) analyzed. A similar effect was reported for propolis and paclitaxel treatment, which increased the activities of enzymatic antioxidants SOD, CAT, and GPx in rats-treated compared with breast cancer-bearing animals treated with either paclitaxel or propolis alone [51].

Malondialdehyde (MDA) is an indicator of lipid peroxidation, which was found to be increased in various cancers, including breast cancer. In the lipid peroxidation process, the polyunsaturated fatty acids (PUFA) in cell membranes are oxidized by reactive oxygen species, resulting metabolites such as MDA, 4-hydroxynoneal (4-HNF) and acrolein. These metabolites bind to proteins and induce functional

changes, then cause enzyme inhibition and receptor changes and consequently cell injury [52]. In our study, no significant modification in MDA level was recorded for MNU-inoculated rats or MNU-inoculated/PE-treated rats as compared with control group. In a recent study, da Silvera et al. (2016) observed that the ethanolic extract of yellow propolis induced a decrease in the production of malondialdehyde and nitric oxide in 3-months-old Wistar rats, without affecting levels of superoxide dismutase and catalase antioxidative enzymes [53].

Protein carbonyl levels are the most frequently used biomarker of protein oxidation, because increased levels may be associated with breast cancer risk [54]. Carbonyl groups are formed during the oxidation of protein side chains, mainly on proline, arginine, lysine, and threonine residues [55].

In our study, the oxidized proteins level in MNU-inoculated rats increased. It seems that the PE administration in the diet of MNU-inoculated rats could decrease the level of oxidized proteins, but our data are not statistically relevant. Literature data come to support our evidence and attest that propolis supplementation leads to a reduction in protein

oxidation, together with a lowering effect on the level of glucose and cholesterol [56].

The biological effects exhibited by Transylvanian propolis could be related to an overall effect of the phenolic compounds present in the extract. For instance, CAPE (caffeic acid phenethyl ester) is known to be one of the major biologically active principles in propolis with chemoprevention and antitumor properties [18]. CAPE is able to inhibit the nuclear factor kappa B (NF- $\kappa$ B) and to induce apoptosis in breast cancer cells [57]. In tumor cells, transformation via NF- $\kappa$ B results also elevated ROS levels, accompanied with downregulation of cellular antioxidant enzyme systems [58]. Inhibition of antioxidant enzymes is considered a therapeutic approach in the induction of ROS production in tumor cells. Recently, it was proved that propolis can upregulate the intracellular ROS, decrease mitochondrial membrane potential, and induce apoptosis in MCF-7 and MDA-MB-231 cells [11].

## 5. Conclusions

Taken together, these data indicate that propolis could be a chemopreventive agent against MNU-induced mammary carcinogenesis. However, before declaring propolis a chemopreventive agent against human breast cancer, further investigations are needed for a complete identification and characterization of specific bioactive molecules with biological properties and for finding its proper mechanism of action at mammary gland level.

## Data Availability

The data used to support the findings of this study are available from the corresponding author Rugina D. upon request (email: dumitrita.rugina@usamvcluj.ro).

## Disclosure

The founding sponsors had no role in the design of the study; in the collection, analyses, or interpretation of data; in the writing of the manuscript; and in the decision to publish the results.

## Conflicts of Interest

The authors declare that they have no conflict of interest.

## Authors' Contributions

Conceptualization of the study was done by Gal A.F.; methodology, necropsy, and histopathology analysis were realized by Gal A.F., Tăbăran F., and Cătoi A.F.; Stan L. characterized the propolis extract; Rugină D. assessed the antioxidant assays; writing—original draft preparation—was done by Rugină D. and Gal A.F.; writing—review and editing—was done by Rugină D. and Gal A.F.; supervision, Cătoi A.F. and Andrei S. Authorship was limited to those who have contributed substantially to the work reported.

## Acknowledgments

We kindly thank Cantacuzino Institute, Romania, for the female Sprague–Dawley rats utilized in the experiments performed for this manuscript. This research was funded by the Ministry of Research and Innovation through Development of the National Research and Development System Program, grant number 37PFE/06.11.2018.

## Supplementary Materials

Propolis reduced the number of grade I tumors in MNU-induced/propolis-treated rats. 4 propolis increased the levels of antioxidative enzymes (SOD, CAT, and GPx) and restored blood 5 parameters values close to the physiological normal ones. (*Supplementary Materials*)

## References

- [1] J. Ferlay, I. Soerjomataram, R. Dikshit et al., "Cancer incidence and mortality worldwide: sources, methods and major patterns in GLOBOCAN 2012," *International Journal of Cancer*, vol. 136, no. 5, pp. E359–E386, 2015.
- [2] M. H. Goldschmidt, L. Peña, and V. Zappulli, "Tumors of the mammary gland," in *Tumors in Domestic Animals*, D. J. Meuten, Ed., pp. 723–765, John Wiley & Sons, Inc., 2016.
- [3] F. R. G. Silva, T. M. S. Matias, L. I. O. Souza et al., "Phytochemical screening and in vitro antibacterial, antifungal, antioxidant and antitumor activities of the red propolis Alagoas," *Brazilian Journal of Biology*, vol. 79, no. 3, pp. 452–459, 2019.
- [4] D. M. Kasote, M. V. Pawar, S. S. Gundu et al., "Chemical profiling, antioxidant, and antimicrobial activities of Indian stingless bees propolis samples," *Journal of Apicultural Research*, vol. 58, no. 4, pp. 617–625, 2019.
- [5] N. S. S. Guimarães, J. C. Mello, J. S. Paiva et al., "*Baccharis dracunculifolia*, the main source of green propolis, exhibits potent antioxidant activity and prevents oxidative mitochondrial damage," *Food and Chemical Toxicology*, vol. 50, no. 3–4, pp. 1091–1097, 2012.
- [6] J. F. Campos, U. P. dos Santos, L. F. B. Macorini et al., "Antimicrobial, antioxidant and cytotoxic activities of propolis from *Melipona orbignyi* (Hymenoptera, Apidae)," *Food and Chemical Toxicology*, vol. 65, pp. 374–380, 2014.
- [7] R. Zeitoun, F. Najjar, B. Wehbi et al., "Chemical composition, antioxidant and anti-inflammatory activity evaluation of the Lebanese propolis extract," *Current Pharmaceutical Biotechnology*, vol. 20, no. 1, pp. 84–96, 2019.
- [8] C. M. Batista, A. V. F. Alves, L. A. Queiroz et al., "The photoprotective and anti-inflammatory activity of red propolis extract in rats," *Journal of Photochemistry and Photobiology B: Biology*, vol. 180, pp. 198–207, 2018.
- [9] Y. Akao, H. Maruyama, K. Matsumoto et al., "Cell growth inhibitory effect of cinnamic acid derivatives from propolis on human tumor cell lines," *Biological & Pharmaceutical Bulletin*, vol. 26, no. 7, pp. 1057–1059, 2003.
- [10] A. Russo, V. Cardile, F. Sanchez, N. Troncoso, A. Vanella, and J. A. Garbarino, "Chilean propolis: antioxidant activity and antiproliferative action in human tumor cell lines," *Life Sciences*, vol. 76, no. 5, pp. 545–558, 2004.
- [11] H. Xuan, Z. Li, H. Yan et al., "Antitumor Activity of Chinese Propolis in Human Breast Cancer MCF-7 and

- MDA- MB-231 Cells,” *Evidence-based Complementary and Alternative Medicine*, vol. 2014, Article ID 280120, 11 pages, 2014.
- [12] Y. K. Park, S. M. Alencar, and C. L. Aguiar, “Botanical origin and chemical composition of Brazilian propolis,” *Journal of Agricultural and Food Chemistry*, vol. 50, no. 9, pp. 2502–2506, 2002.
- [13] Y. A. Elnakady, A. I. Rushdi, R. Franke et al., “Characteristics, chemical compositions and biological activities of propolis from Al-Bahah, Saudi Arabia,” *Scientific Reports*, vol. 7, no. 1, article 41453, 2017.
- [14] G. A. Burdock, “Review of the biological properties and toxicity of bee propolis (propolis),” *Food and Chemical Toxicology*, vol. 36, no. 4, pp. 347–363, 1998.
- [15] T. Kamiya, H. Nishihara, H. Hara, and T. Adachi, “Ethanol extract of Brazilian red propolis induces apoptosis in human breast cancer MCF-7 cells through endoplasmic reticulum stress,” *Journal of Agricultural and Food Chemistry*, vol. 60, no. 44, pp. 11065–11070, 2012.
- [16] H. Noureddine, R. Hage-Sleiman, B. Wehbi et al., “Chemical characterization and cytotoxic activity evaluation of Lebanese propolis,” *Biomedicine & Pharmacotherapy*, vol. 95, pp. 298–307, 2017.
- [17] F. Yang, H. Jin, J. Pi et al., “Anti-tumor activity evaluation of novel chrysin-organogermanium(IV) complex in MCF-7 cells,” *Bioorganic & Medicinal Chemistry Letters*, vol. 23, no. 20, pp. 5544–5551, 2013.
- [18] J. Wu, C. Omene, J. Karkoszka et al., “Caffeic acid phenethyl ester (CAPE), derived from a honeybee product propolis, exhibits a diversity of anti-tumor effects in pre-clinical models of human breast cancer,” *Cancer Letters*, vol. 308, no. 1, pp. 43–53, 2011.
- [19] C. O. Omene, J. Wu, and K. Frenkel, “Caffeic acid phenethyl ester (CAPE) derived from propolis, a honeybee product, inhibits growth of breast cancer stem cells,” *Investigational New Drugs*, vol. 30, no. 4, pp. 1279–1288, 2012.
- [20] A. Kabała-Dzik, A. Rzepecka-Stojko, R. Kubina et al., “Comparison of two components of propolis: caffeic acid (CA) and caffeic acid phenethyl ester (CAPE) induce apoptosis and cell cycle arrest of breast cancer cells MDA-MB-231,” *Molecules*, vol. 22, no. 9, article 1554, 2017.
- [21] H. Chang, Y. Wang, X. Yin, X. Liu, and H. Xuan, “Ethanol extract of propolis and its constituent caffeic acid phenethyl ester inhibit breast cancer cells proliferation in inflammatory microenvironment by inhibiting TLR4 signal pathway and inducing apoptosis and autophagy,” *BMC Complementary and Alternative Medicine*, vol. 17, no. 1, p. 471, 2017.
- [22] S. Khacha-Ananda, K. Tragoolpua, P. Chantawannakul, and Y. Tragoolpua, “Propolis extracts from the northern region of Thailand suppress cancer cell growth through induction of apoptosis pathways,” *Investigational New Drugs*, vol. 34, no. 6, pp. 707–722, 2016.
- [23] N. Taira, B. C. Q. Nguyen, P. T. Be Tu, and S. Tawata, “Effect of Okinawa propolis on PAK1 activity, *Caenorhabditis elegans* longevity, melanogenesis, and growth of cancer cells,” *Journal of Agricultural and Food Chemistry*, vol. 64, no. 27, pp. 5484–5489, 2016.
- [24] M. Tartik, E. Darendelioglu, G. Aykutoglu, and G. Baydas, “Turkish propolis suppresses MCF-7 cell death induced by homocysteine,” *Biomedicine & Pharmacotherapy*, vol. 82, pp. 704–712, 2016.
- [25] R. D. Cardiff and S. R. Wellings, “The comparative pathology of human and mouse mammary glands,” *Journal of Mammary Gland Biology and Neoplasia*, vol. 4, no. 1, pp. 105–122, 1999.
- [26] E. Y. Ko, S. H. Lee, H. H. Kim et al., “Evaluation of tumor angiogenesis with a second-generation US contrast medium in a rat breast tumor model,” *Korean Journal of Radiology*, vol. 9, no. 3, pp. 243–249, 2008.
- [27] I. Malicka, K. Siewierska, B. Pula et al., “The effect of physical training on the N-methyl-N-nitrosourea-induced mammary carcinogenesis of Sprague-Dawley rats,” *Experimental Biology and Medicine*, vol. 240, no. 11, pp. 1408–1415, 2015.
- [28] M. Popova, B. Trusheva, and V. Bankova, “Content of biologically active compounds in Bulgarian propolis: a basis for its standardization,” *Bulgarian Chemical Communications*, vol. 49, pp. 115–120, 2017.
- [29] V. Bankova, D. Bertelli, R. Borba et al., “Standard methods for *Apis mellifera* propolis research,” *Journal of Apicultural Research*, vol. 58, no. 2, pp. 1–49, 2019.
- [30] A. F. Gal, S. Andrei, C. Cernea, M. Taulescu, and C. Catoi, “Effects of astaxanthin supplementation on chemically induced tumorigenesis in Wistar rats,” *Acta Veterinaria Scandinavica*, vol. 54, no. 1, p. 50, 2012.
- [31] S. Woditschka, J. D. Haag, B. Mau, R. A. Lubet, and M. N. Gould, “Chemopreventive effects of celecoxib are limited to hormonally responsive mammary carcinomas in the neu-induced retroviral rat model,” *Breast Cancer Res*, vol. 10, no. 1, article R18, 2008.
- [32] J. Russo and I. H. Russo, “Atlas and histologic classification of tumors of the rat mammary gland,” *Journal of Mammary Gland Biology and Neoplasia*, vol. 5, no. 2, pp. 187–200, 2000.
- [33] M. Goldschmidt, L. Pena, R. Rasotto, and V. Zappulli, “Classification and grading of canine mammary tumors,” *Veterinary Pathology*, vol. 48, no. 1, pp. 117–131, 2011.
- [34] S. Andrei, S. Matei, D. Rugina, L. Bogdan, and C. Stefanut, “Interrelationships between the content of oxidative markers, antioxidative status, and somatic cell count in cow’s milk,” *Czech Journal of Animal Science*, vol. 61, no. 9, pp. 407–413, 2016.
- [35] D. Rugina, Z. Diaconeasa, C. Coman, A. Bunea, C. Socaciu, and A. Pinte, “Chokeberry anthocyanin extract as pancreatic  $\beta$ -cell protectors in two models of induced oxidative stress,” *Oxidative Medicine and Cellular Longevity*, vol. 2015, Article ID 429075, 10 pages, 2015.
- [36] B. A. S. Machado, R. P. D. Silva, G. . A. Barreto et al., “Chemical composition and biological activity of extracts obtained by supercritical extraction and ethanolic extraction of brown, green and red propolis derived from different geographic regions in Brazil,” *PLoS One*, vol. 11, no. 1, article e0145954, 2016.
- [37] V. Bankova, “Chemical diversity of propolis and the problem of standardization,” *Journal of Ethnopharmacology*, vol. 100, no. 1-2, pp. 114–117, 2005.
- [38] B. Pula, I. Malicka, K. Pawlowska et al., “Immunohistochemical characterization of N-methyl-N-nitrosourea-induced mammary tumours of Sprague-Dawley rats,” *In Vivo*, vol. 27, no. 6, pp. 793–801, 2013.
- [39] H. J. Thompson and M. Singh, “Rat models of premalignant breast disease,” *Journal of Mammary Gland Biology and Neoplasia*, vol. 5, no. 4, pp. 409–420, 2000.
- [40] T. Yuri, Y. C. Lai, K. Yoshizawa, and A. Tsubura, “Human chorionic gonadotropin inhibits N-methyl-N-nitrosourea-

- induced mammary carcinoma growth in female Lewis rats," *In Vivo*, vol. 26, no. 3, pp. 361–367, 2012.
- [41] S. Ahmed and N. H. Othman, "The anti-cancer effects of Tualang honey in modulating breast carcinogenesis: an experimental animal study," *BMC Complementary and Alternative Medicine*, vol. 17, no. 1, p. 208, 2017.
- [42] V. R. Rozados, A. M. Sanchez, S. I. Gervasoni, H. H. Berra, P. Matar, and O. Graciela Scharovsky, "Metronomic therapy with cyclophosphamide induces rat lymphoma and sarcoma regression, and is devoid of toxicity," *Annals of Oncology*, vol. 15, no. 10, pp. 1543–1550, 2004.
- [43] M. O. T. Badr, A. N. F. Neamat-Allah, A. A. M. Abdallah et al., "Biochemical and antioxidant effect of doxorubicin hydrochloride and propolis on N-methyl-N-nitrosourea (MNU) induced adenocarcinoma in rats," *Bulletin of University of Agricultural Sciences and Veterinary Medicine Cluj-Napoca. Veterinary Medicine*, vol. 72, no. 2, 2015.
- [44] S. Andrei, A. Gal, A. Pinteau, I. Bedecian, A. Arion, and A. I. Baba, "Influence of astaxanthin administration on hepatic oxidative stress markers in rats injected with methyl nitrosourea," *Bulletin of University of Agricultural Sciences and Veterinary Medicine Cluj-Napoca. Veterinary Medicine*, vol. 65, no. 1, pp. 160–164, 2008.
- [45] M. Bhadauria, S. K. Nirala, and S. Shukla, "Multiple treatment of propolis extract ameliorates carbon tetrachloride induced liver injury in rats," *Food and Chemical Toxicology*, vol. 46, no. 8, pp. 2703–2712, 2008.
- [46] A. S. Newairy, A. F. Salama, H. M. Hussien, and M. I. Yousef, "Propolis alleviates aluminium-induced lipid peroxidation and biochemical parameters in male rats," *Food and Chemical Toxicology*, vol. 47, no. 6, pp. 1093–1098, 2009.
- [47] F. B. Daniel and N. J. Joyce, "DNA adduct formation by 7,12-dimethylbenz[a]anthracene and its noncarcinogenic 2-fluoro analogue in female Sprague-Dawley rats," *Journal of the National Cancer Institute*, vol. 70, no. 1, pp. 111–118, 1983.
- [48] K. Selvendiran, J. P. Singh, K. B. Krishnan, and D. Sakthisekaran, "Cytoprotective effect of piperine against benzo[a]pyrene induced lung cancer with reference to lipid peroxidation and antioxidant system in Swiss albino mice," *Fitoterapia*, vol. 74, no. 1-2, pp. 109–115, 2003.
- [49] C. Thirunavukkarasu and D. Sakthisekaran, "Effect of selenium on N-nitrosodiethylamine-induced multistage hepatocarcinogenesis with reference to lipid peroxidation and enzymic antioxidants," *Cell Biochemistry and Function*, vol. 19, no. 1, pp. 27–35, 2001.
- [50] L. W. Oberley and G. R. Buettner, "Role of superoxide dismutase in cancer: a review," *Cancer Research*, vol. 39, no. 4, pp. 1141–1149, 1979.
- [51] R. Padmavathi, P. Senthilnathan, D. Chodon, and D. Sakthisekaran, "Therapeutic effect of paclitaxel and propolis on lipid peroxidation and antioxidant system in 7,12 dimethyl benz(a)anthracene-induced breast cancer in female Sprague Dawley rats," *Life Sciences*, vol. 78, no. 24, pp. 2820–2825, 2006.
- [52] A. Gonenc, D. Tokgoz, S. Aslan, and M. Torun, "Oxidative stress in relation to lipid profiles in different stages of breast cancer," *Indian Journal of Biochemistry & Biophysics*, vol. 42, no. 3, pp. 190–194, 2005.
- [53] C. C. S. de Menezes da Silveira, L. M. P. Fernandes, M. L. Silva et al., "Neurobehavioral and antioxidant effects of ethanolic extract of yellow propolis," *Oxidative Medicine and Cellular Longevity*, vol. 2016, Article ID 2906953, 14 pages, 2016.
- [54] P. Rossner Jr., M. B. Terry, M. D. Gammon et al., "Plasma protein carbonyl levels and breast cancer risk," *Journal of Cellular and Molecular Medicine*, vol. 11, no. 5, pp. 1138–1148, 2007.
- [55] I. Dalle-Donne, R. Rossi, D. Giustarini, A. Milzani, and R. Colombo, "Protein carbonyl groups as biomarkers of oxidative stress," *Clinica Chimica Acta*, vol. 329, no. 1-2, pp. 23–38, 2003.
- [56] C. Lisbona, J. Diaz-Castro, M. J. Alferez, I. M. Guisado, R. Guisado, and I. Lopez-Aliaga, "Positive influence of a natural product as propolis on antioxidant status and lipid peroxidation in senescent rats," *Journal of Physiology and Biochemistry*, vol. 69, no. 4, pp. 919–925, 2013.
- [57] M. Watabe, K. Hishikawa, A. Takayanagi, N. Shimizu, and T. Nakaki, "Caffeic acid phenethyl ester induces apoptosis by inhibition of NF $\kappa$ B and activation of Fas in human breast cancer MCF-7 cells," *The Journal of Biological Chemistry*, vol. 279, no. 7, pp. 6017–6026, 2004.
- [58] V. Aggarwal, H. S. Tuli, A. Varol et al., "Role of reactive oxygen species in cancer progression: molecular mechanisms and recent advancements," *Biomolecules*, vol. 9, no. 11, p. 735, 2019.

## Research Article

# Anticancer Activity of Liquid Treated with Microwave Plasma-Generated Gas through Macrophage Activation

Chae Bok Lee,<sup>1,2</sup> Il Hwan Seo,<sup>3</sup> Myoung-Won Chae,<sup>4</sup> Jae Woo Park,<sup>3</sup> Eun Ha Choi ,<sup>3,4</sup> Han Sup Uhm ,<sup>5</sup> and Ku Youn Baik <sup>3</sup>

<sup>1</sup>Department of Medical Science, Chungnam National University, Daejeon 35015, Republic of Korea

<sup>2</sup>Department of Microbiology, College of Medicine, Chungnam National University, Daejeon 35015, Republic of Korea

<sup>3</sup>Department of Electrical and Biological Physics, Kwangwoon University, Seoul 01897, Republic of Korea

<sup>4</sup>Plasma Bioscience Research Center, Kwangwoon University, Seoul 01897, Republic of Korea

<sup>5</sup>New Industry Convergence Technology R&D Center, Ajou University, Suwon 16499, Republic of Korea

Correspondence should be addressed to Han Sup Uhm; [hsuhm1970@gmail.com](mailto:hsuhm1970@gmail.com) and Ku Youn Baik; [kybaik@kw.ac.kr](mailto:kybaik@kw.ac.kr)

Received 16 August 2019; Accepted 11 October 2019; Published 31 January 2020

Guest Editor: Vittorio Colombo

Copyright © 2020 Chae Bok Lee et al. This is an open access article distributed under the Creative Commons Attribution License, which permits unrestricted use, distribution, and reproduction in any medium, provided the original work is properly cited.

Reactive nitrogen species (RNS), including nitric oxide (NO<sup>•</sup>) has been known as one of the key regulatory molecules in the immune system. In this study, we generated RNS-containing water treated with microwave plasma-generated gas in which the major component was nitric oxide (PGNO), and the effect on the macrophage polarization was investigated. The RNS-containing water was diluted in complete cell culture media (PGNO-solution) into the concentration that did not induce cell death in RAW 264.7 murine macrophages. PGNO-solution upregulates M1-type macrophage activation and downregulates the characteristics of M2-type macrophage at the transcriptional level. In addition, the PGNO-solution-treated M2-like macrophages had higher potential in killing melanoma cells. The anticancer potential was also investigated in a syngeneic mouse model. Our results show that PGNO-solution has the potential to convert the fate of macrophages, suggesting PGNO-solution treatment as a supportive method for controlling the function of macrophages under the tumor microenvironment.

## 1. Introduction

Recently, plasma-activated water (PAW) or media (PAM) has been introduced as an effective solution in killing various kinds of cancer cells, including ovarian cancer, cervical cancer, pancreatic cancer and glioblastoma [1–6]. PAW or PAM has several merits comparing to the direct plasma treatment. PAM does not have any possibility of electrical hazards, it can be stored at low temperature for a certain period, and it can be injected into any part of the body. Many researchers have tried to understand the working mechanisms of PAM in its tumoricidal activity. Since PAM contains relatively long-lived reactive species compared to direct plasma treatment, hydrogen peroxide and nitric oxide ions were identified as the main players in PAM reactivity [7–16]. The actions of reactive oxygen species (ROS) and reactive nitrogen species (RNS) are distinguished

in biological systems [17]. In general, ROS induces oxidative stress which can generally activate redox responses in cells; meanwhile, RNS induces nitrosylation or nitrosation which initiates different cellular signaling pathways that are known to be related to cell differentiation or the wound-healing process [18–20]. In this study, we generated PAW that mainly contained RNS and applied them to innate immune cell macrophages, to study their polarized differentiation especially when they interact with cancer cells.

One of the important factors in anticancer treatment is the microenvironment of cancer tissues. It is well known that cancer cells create microenvironments that support their growth and suppress antitumor immune activities. It is typically characterized by low oxygen, low pH, high lactate, high RNS, etc., which results in differentiated responses of cellular components [21]. Monocytes, one of the most prominent components, are recruited in tumor tissues and are polarized

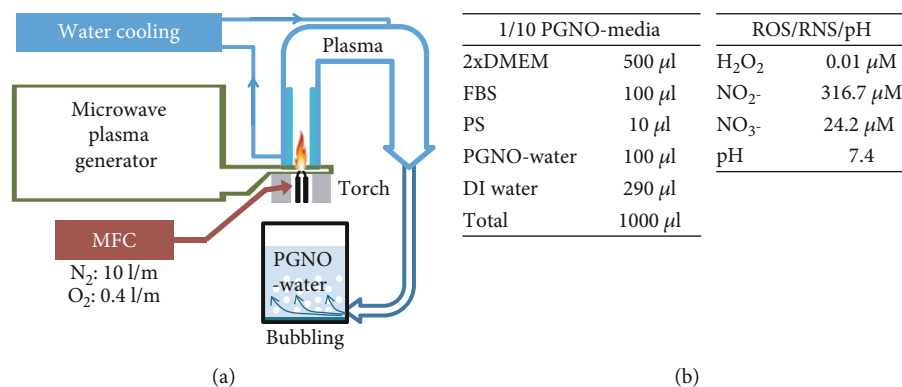


FIGURE 1: (a) Schematics of the microwave plasma generator and reactor to generate PGNO-water. (b) Composition of 1/10 PGNO-media and its characteristics; concentrations of NO<sub>x</sub> and H<sub>2</sub>O<sub>2</sub>, and pH.

to tumor-supporting macrophages, instead of the well-known inflammatory M1 polarized one [22–24]. They are called tumor-associated macrophages (TAMs), which are classified to alternative polarization that is simply called M2 polarization. Since TAMs are known to promote all aspects of tumor initiation, growth, and development and affect the antitumor efficacy of chemotherapy and radiotherapy, converting TAMs to M1 macrophages is a very important issue in cancer therapy.

Though the complex process of programming TAMs has not yet been elucidated, it has been known that immune responses in tumor tissues are tailored by RNS as well as by cytokines, chemokines, or metabolites [25–27]. RNS have shown both immune-suppressive and immune-activate effects in the tumor region in various conditions [27–29]. RNS are mainly synthesized by inducible nitric oxide synthase (iNOS) in response to external stimuli. M1 macrophages express high amounts of iNOS to induce cancer apoptosis; however, the expression of iNOS in TAM was suppressed in tumor microenvironment to maintain low concentration of NO<sup>•</sup> that is related to angiogenesis or metastasis [25–29]. The expression of iNOS is closely related to the polarization of macrophages, and therefore, the expression of iNOS in macrophage is used as a marker for their anticancer activity [24, 30].

In this study, we generated RNS-containing water treated with microwave plasma-generated gas in which the major component was nitric oxide (PGNO) and investigated its effects on the anticancer effect of macrophages *in vitro* and *in vivo* [31–33]. Pure water was treated with PGNO and the water was diluted in complete media (PGNO-media) for cell study. The proliferation, polarization, and anticancer function of macrophages were examined. Among various kinds of cancer, we chose melanoma, a type of skin cancer, due to the ease of approach as well as its malignancy [34]. It was reported that melanoma also regulates the microenvironment, to let macrophages promote angiogenesis and tumor growth [35]. Murine cell lines Raw 264.7 macrophage and B16F10 melanoma were used for *in vitro* study, and C57BL/6 normal mice were used for *in vivo* study. C57BL/6 has normal immune functions, and the syngeneic models were made by subcutaneously injecting B16F10

cells. To mimic TAM, Raw 264.7 macrophage cells were pretreated with interleukin-4 (IL-4) [36, 37]. The effects of RNS-containing PAW on tumor immunity were discussed.

## 2. Materials and Methods

**2.1. PGNO-Generating Microwave Plasma.** Figure 1(a) shows a schematic of PGNO-generating microwave plasma. The microwave plasma device consists of power supply, magnetron, waveguide components (WR-340 for 2.45 GHz), and a microwave plasma torch. The microwave radiation from the magnetron passes through the circulator, through the power meter, through the tuner, which tunes the impedance of the plasma, and through the torch. Nitrogen gas enters the discharge tube in the form of a swirling gas through a feeder, which leads to a vortex flow in the discharge tube. The gas flow rate was controlled by mass flow controller, which keeps the flow rate of N<sub>2</sub> gas 10.0 L per min and O<sub>2</sub> gas 0.4 L per min. The detailed design and function of the microwave plasma torch system are reported in previous reports [31, 32]. The torch is initiated by an igniter, and 400 W electric power is applied. The heated gas from the torch flame is cooled to room temperature with passing through a water cooling tube, and then, the cooled gas is injected into 1 L deionized (DI) water for 50 min. To reduce the reactions of the cooled gas with dissolved O<sub>2</sub> in water, DI water is purged with pure N<sub>2</sub> gas for 1 h, before the plasma ignition. NO radicals generated from the microwave plasma device are dissolved in DI water, and it is diluted with cell culture media (PGNO-media), as shown in Figure 1(b).

**2.2. Measurement of pH, NO<sub>x</sub>, and H<sub>2</sub>O<sub>2</sub> in PGNO-Media.** The concentration of H<sub>2</sub>O<sub>2</sub> was determined with Amplex red reagents (A22188, Thermo Fisher Scientific), and the concentrations of NO<sub>2</sub><sup>-</sup> and NO<sub>3</sub><sup>-</sup> were measured with a nitric oxide colorimetric assay kit (K262-200, BioVision), following the manufacturer's protocols. All the measurements were made within 5 min from PGNO-media generation and were repeated at least three times. The fluorescence intensity and color changes were measured by a plate reader (Synergy HT, BioTek). The pH was measured by a pH meter (Eutech Instruments, Singapore).

**2.3. Cell Culture and Viability Assays.** Raw 264.7 and B16F10 mouse cell lines were purchased from the Korean cell line bank. Cells were cultured in complete DMEM (LM001-05, Welgene) containing 10% fetal bovine serum (FBS; Biowest) and 1% of antibiotics (LS203-01, Welgene). Cells were maintained in 5% CO<sub>2</sub> and humidified air at 37°C. To measure the influence of the PGNO-media on cell viability, cells were plated in 96-well plates (SPL30096, SPL or 3610, Corning Inc.), with a density of  $5 \times 10^3$  per well. Cell viability was measured using the CellTiter 96 Aqueous one solution cell proliferation assay solution (G3582, Promega) and CellTiter-Glo luminescent cell viability assay solution (G7572, Promega) at 1, 2, and 3 days elapsed from PGNO-media treatment. The absorbance at 490 nm and luminescence were measured by a plate reader (Synergy HT, BioTek). Cell morphology was observed by inverted microscopy (Eclipse Ti-U, Nikon).

**2.4. Flow Cytometry.** For intracellular NO<sup>-</sup> measurement, DAF-FM DA (D23844, Thermo Fisher Scientific) was used. Raw 264.7 cells were seeded in a 6-well plate with a density of  $4 \times 10^5$  per well. Cells were incubated with 20 ng/mL IL-4 (recombinant mouse IL-4, R&D Systems) for 24 h, and the media was replaced with PGNO-media. After 24 h incubation with PGNO-media, cells were stained with 10 μM DAF-FM DA in DPBS (LB001-02, Welgene) for 20 min at 37°C. After washing 2 times with DPBS, cells were incubated in media for an extra 20 min. Then, cells were detached, and the fluorescent signal per cell was analyzed by a flow cytometer (BD Verse, BD Biosciences). LPS (L4391, Sigma) was used with a concentration of 10 ng/mL, SNAP (S-Nitroso-N-Acetyl-D,L-Penicillamine; Sigmal) was used with a concentration of 50 μM, and cPTIO (2-(4-carboxyphenyl)-4,5-dihydro-4,4,5,5-tetramethyl-1H-imidazolyl-1-oxy-3-oxide, monopotassium salt; Cayman) was used with a concentration of 50 μM.

For staining with antibodies, anti-iNOS-PE (12-5920-80, eBioscience), anti-CD163-PE (bs-2527R-PE, Bioss), and anti-CD86-FITC (bs-1035R-FITC, Bioss) were used. Cells were fixed in 4% paraformaldehyde at 4°C for 10 min. After washing two times with DPBS, cells were permeabilized in 0.05% triton X-100 at RT for 15 minutes. After washing two times with DPBS, cells were blocked with 1% BSA 4°C for 1 hr. Then, they were stained with antibodies (1:200) at 4°C for 1 hr. After washing three times with DBPS, fluorescence was analyzed by flow cytometry (BD Verse, BD Biosciences).

For apoptosis analysis, Annexin V-FITC apoptosis detection kit (BD 556547, BD Biosciences) was used. After 24 h incubation with PGNO-media, cells were washed with cold DPBS, resuspended in 1x binding buffer, and then stained with Annexin V-FITC and propidium iodide (PI). After washing with 1x binding buffer, cells were analyzed by flow cytometry (BD Verse, BD Biosciences).

For staining of peritoneal macrophages, Alexa Fluor 594 anti-mouse/human CD11b antibody (101254, BioLegend) and anti-mouse iNOS-PE (12-5920-80, eBioscience) were used. Peritoneal macrophages were harvested from mouse peritoneal and treated with 1 mL RBC lysis buffer at 4°C for

5 min for two times. Cells were fixed in 4% paraformaldehyde at 4°C for 10 min. After washing two times with DPBS, cells were permeabilized in 0.05% triton X-100 at RT for 15 minutes. After washing two times with DPBS, cells were blocked with 1% BSA 4°C for 1 hr. Then, they were stained with CD11b antibody (1:200) at 4°C for 1 hr. After washing three times, they were stained with iNOS antibody (1:200) at 4°C for 1 hr. After washing three times with DBPS, fluorescence was analyzed by flow cytometry (BD Verse, BD Biosciences).

**2.5. Measurement of a Transcription Level (qPCR).** Raw 264.7 cells were seeded in a 6-well plate with a density of  $4 \times 10^5$  per well. Cells were incubated with 20 ng/mL mouse IL-4 from 24 h before PGNO-media stimulus. After 24 h incubation in PGNO-media, cells were harvested and total RNAs were extracted using the RNeasy Mini Kit (Qiagen). The total RNAs were converted to cDNAs using reverse transcriptase and random primers (ReverTra Ace qPCR Master Mix, Toyobo), according to the manufacturer's protocol. The same amount of extracted total RNA taken from each sample was used in cDNA synthesis. The synthesized cDNAs were used in real-time PCR (CFX96TM Real-Time System, Bio-Rad). SYBR was used to quantify the amount of dsDNA. The relative amount of mRNA expression was normalized by that of GAPDH and expressed as a fold change to control. The relative gene expression was evaluated by the comparative cycle-threshold method. The experiments were repeated at least three times. The primer sequences are as follows: NOS2 (F: 5'-GTGGTGACAAGCACAT TTGG, R: 5'-AAGGCCAAACACAGCATACC), ARG-1 (F: 5'CGCCTTTCTCAAAAGGACAG, R: 5'GACATC AACAAAGGCCAGGT), IL-6 (F: 5'AGTTGCCTTCT TGGGACTGA, R: 5'TCCACGATTTCCCAGAGAAC), TNF-α (F: 5'TGTTGCCTCCTCTTTTGTCT, R: 5'TGGT CACCAAATCAGCGTTA), IL-10 (F: 5'CATGGGCTTG GGAAGAGAA, R: 5'AACTGGCCACAGTTTTCAGG), CCL17 (F: 5'ACATAAAACGGCCTGTGACC, R: 5'TTTG TGTTGCGCTGTAGTGC), MMP9 (F: 5'AGGTGGACC ATGAGGTGAAC, R: 5'CGGTTGAAGCAAAGAAGGA G), EGF (F: GAACAAGAGGACTGGCCAAA, R: 5'ATGG ATGGACCACAACCAGT), VEGFA (F: 5'CCAGGAGGA CCTTGTGTGAT, R: 5'GGGAAGGGAAGATGAGGAAG), and GAPDH (F: 5'AGAACATCATCCCTGCATCC, R: 5' ACACATTGGGGGTAGGAACA).

**2.6. Western Blot Analysis.** Cells were washed with DPBS, lysed with RIPA lysis buffer (GenDepot, Barker, TX) containing 1% of 100x protease inhibitor cocktail (GenDepot, Barker, TX), and incubated for 30 min on ice. Lysates were centrifuged at 19,000 g for 30 min at 4°C, and the supernatant was mixed with 25% of 4x denaturing buffer (100 mM Tris-HCl, pH 6.8, 4% SDS, and 20% glycerol with bromophenol blue) and heated for 5 min. The proteins were separated through 10% SDS-PAGE gels and were transferred to a nitrocellulose membrane by Mini Trans-Blot Cell (Bio-Rad, CA). The membrane was blocked in 5% BSA in TBS containing

0.1% Tween 20 (TBS-T) for 1 h and incubated overnight with the intended antibodies in and 3% BSA. Excess primary antibodies were then removed by washing with TBS-T for 3 times. The membrane was then incubated with HRP-conjugated secondary antibodies (0.1  $\mu\text{g}/\text{mL}$ , anti-rabbit) for 1 h. After three washes with TBS-T, bands were visualized by western blot and exposed to X-ray film, or by ChemiDoc Imaging Systems (Bio-Rad). The original film images were supported in Figs. S1 and S2 (the supporting information).

**2.7. Coculture of B16F10 and Raw 264.7 Cells.** For in-direct coculture of Raw 264.7 with cancer cells, an insert made of polycarbonate with pores of 0.4  $\mu\text{m}$  in diameter was used in a 24-well plate (37024, SPL). Raw 264.7 cells were cultured on insert membrane with a density of  $1 \times 10^4$  per well, and B16F10 were cultured in the lower 24-well plate with a density of  $2.5 \times 10^4$  per well, separately. When cells were fully adhered, cells faced each other with 500  $\mu\text{L}$  and 700  $\mu\text{L}$  media for insert and well plate, respectively. Some of Raw 264.7 cells were pretreated with 20 ng/mL IL-4 from 24 h before 1/10 PGNO-media stimuli, where PGNO-water was diluted 1/10 with complete media.

**2.8. Subcutaneous Administration of PAW in the Mice.** Twelve C57BL/6 mice were purchased from OrientBio in Korea. The animals were fed with sterile and commercial mouse diet and were provided with water *ad libitum*. Animal experiments were approved by the Institutional Research and Ethics Committee at Kwangwoon University (permission number: KWU-PBRC1701004). All the animal experiments were performed in accordance with relevant guidelines and regulations. B16F10 in the concentration of  $1 \times 10^5$  cells/mL was injected subcutaneously at the right side of the back of mice [38]. Seven days later, mouse hair was shaved for observation. Then, 1 mL of 1/10 PGNO-media or 1x DPBS was administered subcutaneously near the position where the cancer cells were injected every day for the following 12 days. The body weights were measured every day (Fig. S3, the supporting information). After 12 days' treatment, mice were euthanized by  $\text{CO}_2$  gas, and the tumor tissues were harvested. The width, length, and height of tumor tissues were measured, and the tissue volumes were calculated with multiplication of those values. Lastly, peritoneal macrophages were harvested with DPBS lush three times. Total 6 mL ice-cold DPBS was poured in the peritoneal cavity and retracted by a syringe. The harvested solution was centrifuged, and the precipitated cells were analyzed for further analysis.

**2.9. Statistical Analysis.** Statistical significance was determined using unpaired Student's *t*-test (two-tail, equal SD). It is considered statistically significant when  $p < 0.01$  and  $p < 0.05$  (\*,  $p < 0.05$ ; †,  $p < 0.01$ ). Means and standard errors were calculated and plotted in the graphs. Analysis was completed using Microsoft Excel.

### 3. Results

**3.1. Properties of PGNO-Media.** Figure 1(a) shows a schematic of the microwave plasma torch that was designed to generate  $\text{NO}^\cdot$  radicals when  $\text{N}_2$  and  $\text{O}_2$  mixture gas was fed

into the discharge area. According to the previous reports, we flowed 10 L/min  $\text{N}_2$  gas and 0.4 L/min  $\text{O}_2$  gas through the discharge area, and the plasma was cooled during passing through water-cooling tubes [32]. Finally,  $\text{NO}^\cdot$  containing gas from the microwave plasma passed through 1 L of deionized (DI) water for 50 min, which was previously purged with  $\text{N}_2$  gas for 1 h to expel the dissolved oxygen molecules. The concentration of  $\text{NO}^\cdot$  in this water was measured as 117  $\mu\text{M}$  by an electrochemical method, and it was called PGNO-water [33]. In order to estimate the biological effects of PAW, we diluted PAW in cell culture media as shown in Figure 1(b) and measured the long-lived reactive species,  $\text{H}_2\text{O}_2$  and  $\text{NO}_x^-$  within 30 min from generation. The concentration of total  $\text{NO}_x^-$  was measured to be about 340  $\mu\text{M}$  in 1/10 diluted solution. Most of them were in the form of  $\text{NO}_2^-$ , while about 5% were  $\text{NO}_3^-$ . The concentration of  $\text{H}_2\text{O}_2$  was very low and was almost nondetectable. The pH of PGNO-water was initially 2.8, but the value became 7.4 in buffered PGNO-media. Figure 1(b) summarizes in table form the characteristics of 1/10 PGNO-media made for cell studies.

**3.2. Macrophage Cell Viability after Stimulation with PGNO-Media.** The cytotoxic effects of PGNO-media on Raw 264.7 macrophages were evaluated by measuring the mitochondrial activity and the intracellular ATP amount. Figures 2(a) and 2(b) show each measurement for 3 days that was expressed relative to the control of each day. Both values were enhanced in highly diluted PGNO-media, while both were reduced in slightly diluted PGNO-media. These data support that the dilution more than 20 times was not toxic at all and even enhanced cellular viability. The cytotoxicity of PGNO-media was again confirmed with Annexin V and PI (propidium iodide) staining after 24 hours of incubation in PGNO-media. Figure 2(c) shows the flow cytometry data whose *x*-axis is the fluorescence intensity of Annexin-V and *y*-axis is the fluorescence intensity of PI. Most cells were plotted in the lower left region, which supports that PGNO-media diluted more than 10 times did not induce apoptosis in macrophages. Interestingly, the ratio of necrotic and apoptotic cells rather decreased in PGNO-media as shown in the averaged bar graphs of four repetitive experiments. It seems that the PGNO-media diluted more than 10 times did not induce apoptosis, though it reduced metabolic activity slightly. In the following studies, we used the same dilution factors to examine the effects of PGNO-media on the physiology of macrophages.

**3.3. Morphological Changes of Macrophages in PGNO-Media.** PGNO-media induced morphological changes and size variations in macrophages. Figure 3(a) shows the phase-contrasted bright field images of Raw 264.7 cells that were incubated in PGNO-media for 24 h. Some round macrophages became somewhat fibroblastic when stimulated with PGNO-media. The morphological changes were confirmed statistically using flow cytometry. Figure 3(b) shows the plots of forward scattering (FSC) and side scattering (SSC) light intensity of cells in each group. It is clear that the ratio of red spots increased, where the mean values of FSC and SSC



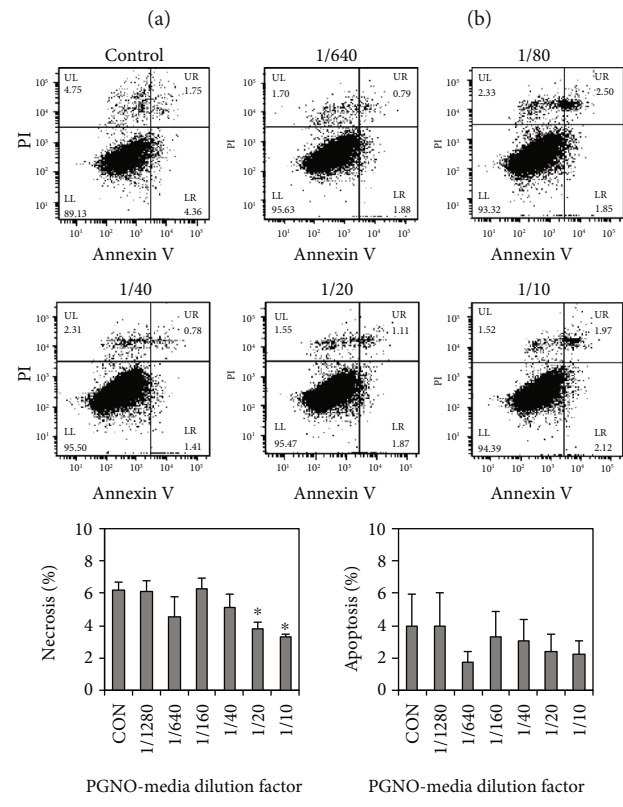
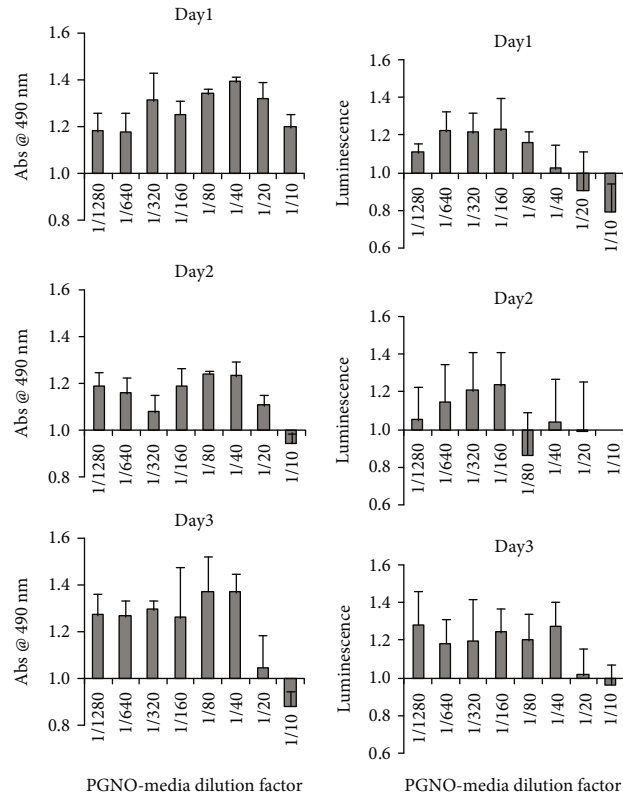


FIGURE 2: Viability assays of Raw 264.7 macrophages after PGNO-media treatment in various dilution ratios: (a, b) Measurements of MTS and intracellular ATP amount, respectively, at days 1, 2, and 3 elapsed from PGNO-media treatment ( $n = 3$ ). (c) Flow cytometric measurement of Annexin V and PI staining at day 1 elapsed from PGNO-media treatment, and bar graphs of the averaged values for four repetitive experiments. \* $p < 0.05$ .

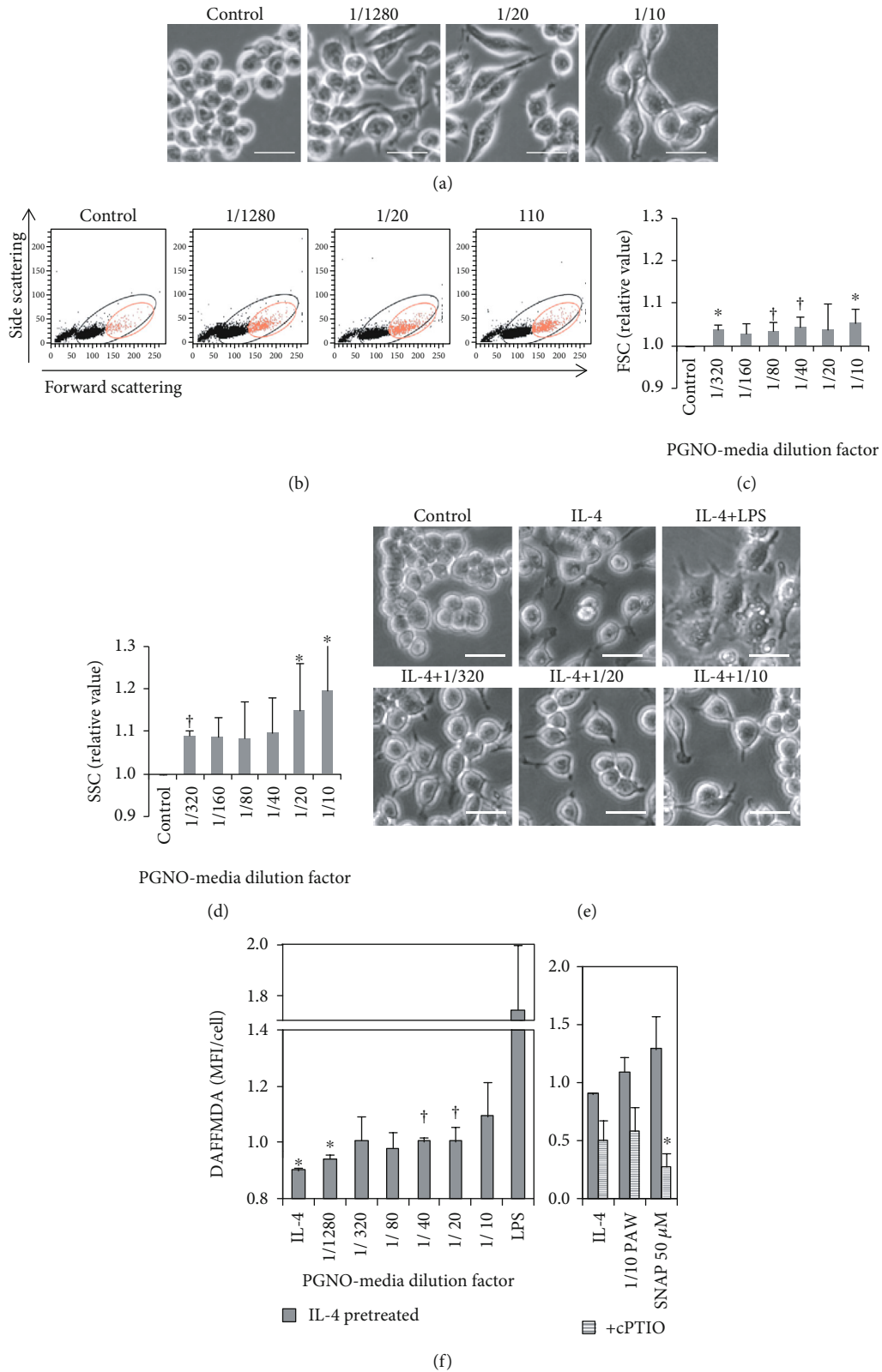


FIGURE 3: Activation of Raw 264.7 at 24h elapsed from PGNO-media treatment in various dilution ratios: (a) phase contrast bright field images showing morphological changes. Scale bars are 20  $\mu\text{m}$ . (b) Flow cytometry plot of forward scattering (FSC) and side scattering (SSC) showing morphological changes ( $n = 6$ ). (c, d) Mean values of FSC and SSC ratios, respectively. (e) Phase contrast bright field images of IL-4-pretreated cells for 24 h. Cells were then incubated in LPS and PGNO-media dilutions for 24 h. (f) MFI of DAFFMDA-stained cells that were treated the same as (e) ( $n = 3$ ). IL-4-pretreated macrophages were incubated in PGNO-media or 50  $\mu\text{M}$  SNAP with or without cPTIO for 24 h. \* $p < 0.05$ ; † $p < 0.01$ .

were higher. The increase of FSC value implies the increase of cell size, and the increase of SSC implies the increase of surface roughness or internal granularity. The data are plotted as bar graphs in Figures 3(c) and 3(d), which show that the mean values of FSC and SSC of macrophages increased together with the dilution factor. These data imply that PGNO-media induced morphological changes and size variation of macrophages. In order to mimic TAM, cells were pretreated with IL-4 for 24 h, and the medium was changed to PGNO-media, LPS (lipopolysaccharides), or cell culture media. Figure 3(e) shows the phase contrast bright field images of IL-4-pretreated cells. Compared to small and round control cells, IL-4-treated cells became more flattened and elongated. PGNO-media-treated cells did not induce more morphological changes as LPS that made cells be severely deformed.

**3.4. Increase of the Intracellular NO<sup>•</sup> inside the Macrophage in PGNO-Media.** The intracellular NO<sup>•</sup> has been intensively studied as a main indicator and as an important factor for macrophage activation [20]. Intracellular NO<sup>•</sup> was stained with DAF-FDA, and the fluorescence intensity per cell was measured by flow cytometry after 24 h of incubation with PGNO-media. In order to check an intracellular NO<sup>•</sup> increase in polarized macrophages like TAM, Raw 264.7 cells were preincubated with IL-4 for 24 h. Figure 3(f) shows the mean fluorescence intensities (MFI) per cell, which were expressed as relative values to control. The first bar value is significantly lower than control, which represents the significant reduction of the intracellular NO when macrophages were incubated with IL-4. However, it is clear that PGNO-media enhanced the amount of intracellular NO<sup>•</sup> in IL-4-treated M2-like macrophages. The change of intracellular NO<sup>•</sup> could be related to the iNOS expression, which is a regulatory molecule in macrophage polarization. These changes in intracellular NO<sup>•</sup>, as well as cell morphology, suggest possible regulatory effects of our PGNO-media on macrophage activations. In order to confirm whether the enhanced values were intracellular NO<sup>•</sup>, we used well-known NO<sup>•</sup> scavenger (cPTIO) and the well-known NO<sup>•</sup> donor (SNAP). The intracellular NO<sup>•</sup> level increased with the addition of SNAP as with PGNO-media, and the levels decreased with the addition of cPTIO into similar levels to control.

**3.5. Action of PGNO-Media on Repolarization of M2-Like Macrophage.** In order to examine the effect of PGNO-media on the polarization of M2-like macrophages, we analyzed the expression levels of M1- or M2-related proteins in mRNA levels in IL-4-pretreated macrophages after 24 h of incubation in PGNO-media. The mRNA expression of M1-polarization-related proteins, such as iNOS and IL-6, increased according to PGNO-media dilution factor, but the increase of TNF- $\alpha$  was not significant (Figure 4(a)). On the other hand, the mRNA expression of M2-polarization-related proteins, such as ARG1, IL-10, TGF- $\beta$ , CCL17, EGF, and MMP9, was mostly reduced significantly (Figure 4(b)). The expression of iNOS was further examined at a protein level. Figure 4(c) shows the upregulation of iNOS

in IL-4-pretreated macrophages at a translational level. The expression of M1 or M2 marker proteins was analyzed by using flow cytometry (Figure 4(d)). Graphs show the upregulation of iNOS and Cd86 (markers for M1 polarization) and slight downregulation of Cd163 (a marker for M2 polarization). These results imply that PGNO-media may be able to limit M2-related gene transcription and elicit M1 macrophage polarization [22].

**3.6. The Anticancer Effects of PGNO-Media Stimulated Macrophages In Vitro.** In order to test the anticancer effects of PGNO-media-activated macrophages, macrophages were cocultured in an indirect contact with B16F10 mouse melanoma cells as shown in Figure 5(a). B16F10 cells were cocultured with IL-4-pretreated or nontreated macrophages in a 0.4  $\mu$ m pore-sized transwell system. The cytotoxic immune actions of macrophages were analyzed by measuring intracellular ATP of melanoma cells after 24 h of cocultures (Figure 5(b)). The values were expressed relatively to monocultured control cells. The coculture of cancer with macrophage reduced the ATP values of cancer cells significantly in all cases. When PGNO-media was added, the reduction became more significant, especially when macrophages were pretreated with IL-4. It was confirmed by PI dye penetration assay that shows dead cell ratios as shown in Figure 5(c). The ratios of dead cells increased with addition of PGNO-media, especially when macrophages were pretreated with IL-4. This coculture study suggests that PGNO-media enhance the cytotoxicity of macrophages through activating secretion of cytokines.

**3.7. The Anticancer Effects of PGNO-Media Stimulated Macrophages In Vivo.** The anticancer effects of PGNO-media were examined with a melanoma syngeneic model in mice. Figure 6(a) shows a simple scheme of the animal experiment. Mice administered with DPBS were used as sham controls, and there were no dead mice during experiments for 19 days. Figure 6(b) shows the 6 mice of the sham group and the 6 mice of the experimental group after daily administration of DPBS or PGNO-media near the melanoma for 12 days, respectively. Arrows in each picture indicate the positions of tumor. It is clearly evident that the sizes of tumors were significantly smaller with PGNO-media, in comparison with DPBS treatment. Figure 6(c) shows the tumor tissues extracted from mice in the order shown in Figure 6(b). The width, length, and height of tumor tissues were measured, and Figure 6(d) summarizes the volumes in the table. The average value was smaller more than two times. When the biggest one in the DPBS group was removed, the difference was still more than two times. This shows the tendency of retarded growth of tumor by PGNO-media. Though we could not measure the exact growth rate of tumor from the beginning, photos taken at days 7, 10, and 11 that showed the growth rates of tumors as well as their sizes were quite different in two groups (Fig. S3 supporting information).

In order to evaluate the effect of PGNO-media on macrophage activation during tumor growth *in vivo*, we harvested tumor tissues and analyzed their expression of

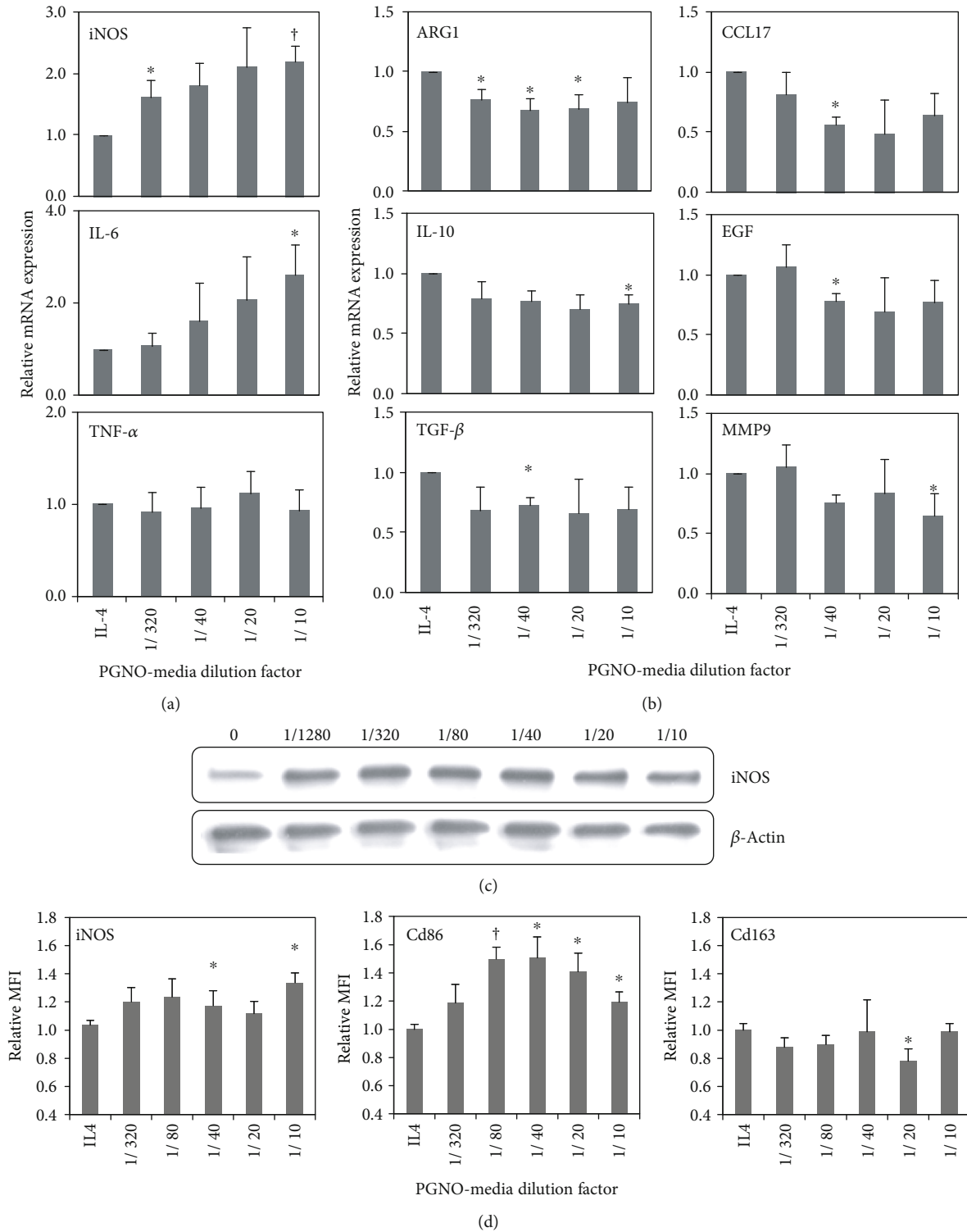


FIGURE 4: Depolarization of IL-4-pretreated Raw 264.7 macrophages at 24 h elapsed from PGNO-media treatment in various dilution ratios: (a, b) transcriptional level changes of macrophage M1 polarization-related genes, (a) including iNOS, IL6, and TNF- $\alpha$ , and (b) M2 polarization-related genes, including ARG, IL10, TGF- $\beta$ , CCL17, EGF, and MMP9. (c) Protein level changes of iNOS. All tests were repeated three times. (\* $p < 0.05$ ; † $p < 0.01$ ). (d) Flow cytometry analysis of iNOS, CD86, and CD163 proteins.

iNOS and Arg1. Due to the small sizes of some tissues, we used 6 samples from the PBS-treated group and 4 samples from the PGNO-media-treated group. Figure 7(a) shows the western blot images, while Figure 7(b) shows the

quantitative intensity values relative to actin protein. The protein expression levels were not significantly different from each other. Additionally, the peritoneal macrophages were harvested after sacrifice and stained with CD11b and

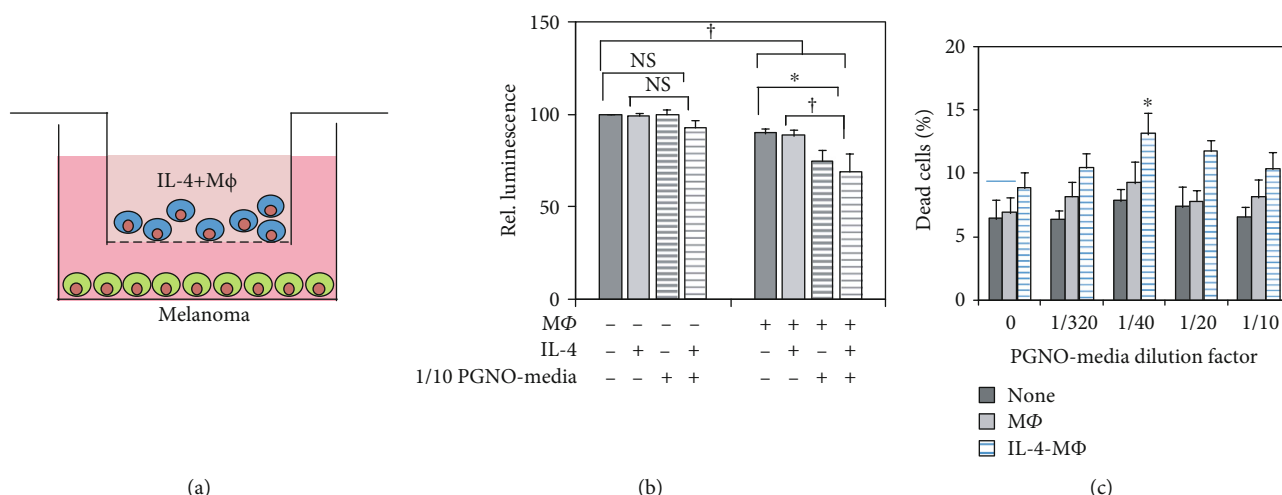


FIGURE 5: The anticancer effects of PGNO-media stimulated macrophages *in vitro*. (a) Illustrations showing indirect coculture of Raw 264.7 macrophages with B16F10 melanoma cancer cells. (b) Measurement of intracellular ATP of B16F10 cells with and without PGNO-media with coculture. 20 ng/mL IL-4 was pretreated to macrophage before 24 h of PGNO-media. (c) Flow cytometric measurement of PI-stained B16F10 cells at day 1 elapsed from coculture ( $*p < 0.05$ ). All the experiments were repeated three times.  $*p < 0.05$ ;  $†p < 0.01$ .

iNOS antibodies. Figure 7(c) shows the 2D plot of CD11b and iNOS stained peritoneal macrophages, where the CD11b-positive cells were gated with red squares. Figure 7(d) shows the increased fluorescence of iNOS of CD11b+ cells from PGNO-media-administered mice. This data implies that when PGNO-media was injected during tumor growth, the peritoneal macrophages expressed more iNOS proteins.

#### 4. Discussions

First of all, we successfully generated PGNO-media that contained RNS exclusively. Colorimetric analysis showed that our PGNO-media mainly contained RNS and did not contain ROS such as  $H_2O_2$ . Since our whole PGNO-generating system was isolated from atmospheric environment, PGNO-media components were solely controlled by inlet gases,  $N_2$  and  $O_2$  in this study. Hot reactive species were generated by focused microwave, but the primary species were cooled down through a cooling system to make more stable chemical species such as NO and  $NO_2$ . Therefore, the chemical species that purged into DI water did not contain free electrons to generate OH $\cdot$  or O/H atoms which possibly resulted in the generation of ROS. The expected chemical reactions were suggested in a previous report [31]. In addition, we guess those RNS have long lifetime, because PGNO-water was generated after purging water of dissolved oxygen elimination. The lifetime of NO $\cdot$  in aqueous solution is about several min and decreases with an increase of the environmental  $O_2$  concentration [39–41]. The half-life time of NO in our PGNO-water was electrochemically measured for about 6 h, and NO was not completely perished after 16 h from PGNO generation [33]. To confirm the species measured by an electrochemical method in our PGNO-water, we tried other modalities such as EPR with MGC (N-(dithiocarbamoyl)-N-methyl-D-glucamine, sodium salt, Dojindo Molecular Technologies, Inc.) and spectroscopic

analysis with hemoglobin molecules following a previous report [42]. We found radical forms in EPR measurement and hemoglobin oxidations in spectroscopy (data are not included here). However, the signals were different from a control experiment with well-known NO donor SNAP. Though the molecular form is not exactly understood yet, we can assume those reactive nitrogen radicals as well as  $NO_x^-$  may react with biomolecules in the media to induce cascade processes in biological systems.

The effects of RNS on biological systems are known to depend on their concentrations [43, 44]. NO in low concentration can activate cell function initiating cGMP signaling pathways, but in high concentration, it can induce cell death, releasing cytochrome C from mitochondria [43, 44]. In a previous report, it was shown that NO radicals in PAW also increased cell growth in low concentration and became fungicidal in high concentration [45]. In the case of PGNO-media, we found that dilution in the range of 1/1280 to 1/20 is nontoxic and activates metabolic activity of macrophages. Even dilution of 1/10 did not induce apoptosis, though it reduced metabolic activity slightly. Figures 2 and 3 show that the potential of PGNO-media for macrophage activation can be enhanced when it was less diluted. Based on the *in vitro* data, we used 1/10 PGNO-media in coculture or animal studies, in order to add the metabolic toxicity on cancer cells, as well as to induce proinflammatory responses from M2-polarized macrophages. However, in a coculture study, we found that 1/10 PGNO-media did not reduce the metabolic activity of B16F10 cells at all. This implies that the sensitivity to PGNO-media is different according to cell type. Based on this cell study, we can hypothesize that the reduction of tumor size in mouse experiments was attributed to the modulation of immune systems rather than to the direct cytotoxicity of PGNO-media on melanoma cells. The results of western blot of tumor tissues and the flow cytometry analysis of peritoneal macrophages support that 1/10 PGNO-media can modulate whole body immune activities

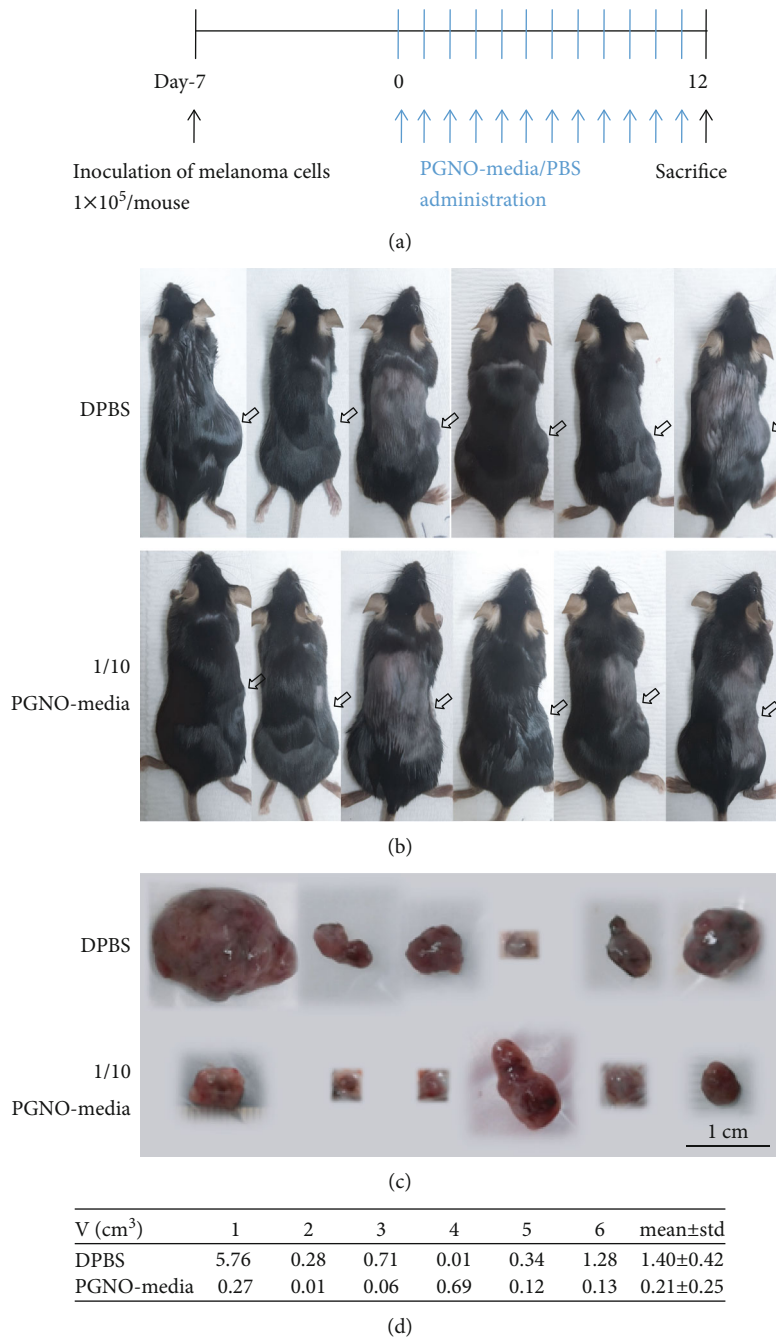


FIGURE 6: The anticancer effects of PGNO-media *in vivo*. (a) Simple scheme of animal experiment. (b) Pictures of 12 mice with melanoma syngeneic mice after 11 days of daily administration of DPBS or PGNO-media. Arrows mark the positions of tumor. (c) Pictures of tumor tissue from each mice at day 12. (d) A table showing the volume of tumor tissue from each mice and the average and standard deviation for the two groups.

[46]. We speculate that RNS inside PGNO-media played roles in modulating the macrophage polarization.

Over decades, there have been many trials to inhibit the function of TAM and to convert them into M1-polarized cells [25]. Injecting NO donor NOC-18 or M1 activated macrophage to form a high concentration of NO/RNS in tumor tissues of a mouse renal cell carcinoma model, which could weaken tumor growth, but could not degenerate tumor [47, 48]. Macrophages separated from a malignant mesothelioma patient were M1 activated *in vitro* and transferred back

to the host. Though a high level of  $\text{TNF-}\alpha$  was produced in tumors and the tumor size was reduced, the injected macrophages were returned back to the M2-like mode in tumors by secreting anti-inflammatory cytokines and lipid mediators in the tumoral microenvironment [49–51]. Thus, maintaining the M1 activation of macrophages in tumor tissues was indicated as a solution.

Our experimental data support that PGNO-media stimulation can restrain the function of TAM-like macrophages and convert their function to M1-like macrophages. IL-4 is

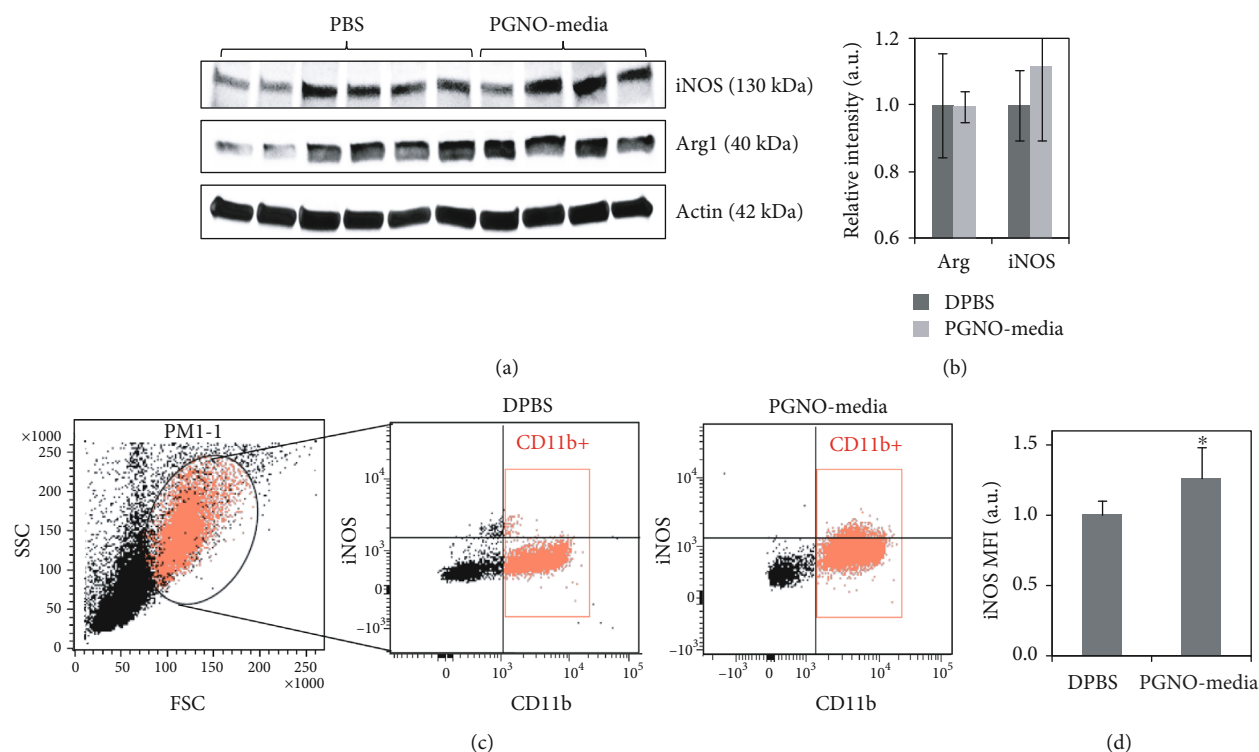


FIGURE 7: (a) The expression of iNOS and Arg1 protein in each tumor tissue. (b) The relative quantification of proteins to actin protein. (c) Flow cytometry data of cells harvested from mice peritoneal and immunostained with antibodies to iNOS and CD11b. Red boxed mark the CD11b+ cells. (d) The MFI of iNOS of the CD11b+ cells. \* $p < 0.05$ .

known to induce polarization of M2 by inducing downstream pathways such as a phosphorylation of STAT6 and an expression of IRF4 [35, 36]. Treatment of PGNO-media to IL-4-induced M2-like macrophages resulted in upregulation and downregulation of M1- and M2-related genes, respectively. In vivo treatment of PGNO-media also resulted in an inhibition of tumor growth and an upregulation of iNOS expression in peritoneal macrophages. Our study indicates that PGNO-media negatively regulates tumor-mediated manipulation of macrophages. In addition, it should be pointed that the action of PGNO-media on the macrophage activation and anticancer activity was not linearly dose dependent as metabolic activity and intracellular NO level were (Figures 2 and 3). The curves of the Cd86 transcription level (Figure 4(d)) as well as the tumor cytotoxicity level (Figure 5(c)) showed some optimal dose ranges for M2-like macrophage activation. This would give further information on these processes, as it points to a dual mode of action.

Our data proposes a new RNS donor that can maintain the M1-like activation of TAM. Since the PGNO-media is purely composed of RNS, there are no remaining chemicals or unexpected byproducts. Furthermore, there is a possibility that PGNO-media can enhance a whole body immune activity as shown in Figure 7. This can be helpful for the patients who suffer from the low immune activity due to anticancer drug administration. We believe that our experiments provide the possibility of PGNO-media application in anticancer therapy to retard tumor growth as well as activate innate immune activities. However, further studies using primary

macrophages instead of Raw 264.7 cell line derived from leukaemic mice should be performed to confirm the action of PGNO-media in innate immune cells. And also, the tumor-associated macrophages instead of peritoneal macrophages should be investigated to understand the direct effects of PGNO-media on the microenvironment of tumors.

## Data Availability

The data used to support the findings of this study are available from the corresponding author upon request.

## Conflicts of Interest

The authors declare no potential conflicts of interest with respect to the authorship and/or publication of this article.

## Authors' Contributions

Chae Bok Lee and Il Hwan Seo contributed equally to this work.

## Acknowledgments

This research was supported by the Leading Foreign Research Institute Recruitment Program through the National Research Foundation of Korea (NRF) funded by the Korea government (MSIP) (NRF-2016K1A4A3914113) and by the research grant of Kwangwoon University in 2017.

## Supplementary Materials

Figure S1: the original film image of Figure 4(c). In order to reduce the amount of antibodies, we cut the protein-transferred membrane at the position for the target protein size. Each cut membrane was reacted with specific antibodies and then incubated with chemiluminescence solution. They were arranged and fixed on a cassette. The X-ray film was reacted with them for four different times and then developed in a dark condition. (a) The original film image. The red colored rectangles were selected for the data. (b) The cut film image. (c) The band at 130 kDa was used for iNOS, and the band at 42 kDa was used for  $\beta$ -actin. Figure S2: the original film images of Figure 7(a). After staining with antibodies, the film images were acquired using a ChemiDoc machine (Bio-Rad). (a) The images acquired by the ChemiDoc. From left to right, the image is HRP chemiluminescence, colorimetric, and composition, respectively. (b) The red colored rectangles were selected for the data. Figure S3: daily measured weight and photos taken at day 7 and day 10 of experimental mice (a). The photos of mice taken at days 7, 10, and 11. Since we used normal mice with hair, it was difficult to measure tumor without sacrifice. To estimate roughly the tumor size, photos were taken with anesthesia. The sizes of tumor tissues were measured at the end of the experiment after sacrifice, and the data was put in the text. (b) The weight of mice was measured daily. Though we could not measure the size of tumor daily, we measured animal weight. Since it was performed without anesthesia, it had quite big errors. The units are gram (bar graph). (*Supplementary Materials*)

## References






- [1] H. Tanaka, M. Mizuno, K. Ishikawa et al., "Plasma-activated medium selectively kills glioblastoma brain tumor cells by down-regulating a survival signaling molecule, AKT kinase," *Plasma Medicine*, vol. 1, no. 3-4, pp. 265–277, 2011.
- [2] Y. Li, M. Ho Kang, H. Sup Uhm, G. Joon Lee, E. Ha Choi, and I. Han, "Effects of atmospheric-pressure non-thermal biocompatible plasma and plasma activated nitric oxide water on cervical cancer cells," *Scientific Reports*, vol. 7, no. 1, article 45781, 2017.
- [3] F. Utsumi, H. Kajiyama, K. Nakamura et al., "Effect of indirect nonequilibrium atmospheric pressure plasma on anti-proliferative activity against chronic chemo-resistant ovarian cancer cells *in vitro* and *in vivo*," *PLoS One*, vol. 8, no. 12, article e81576, 2013.
- [4] T. Adachi, H. Tanaka, S. Nonomura, H. Hara, S. I. Kondo, and M. Hori, "Plasma-activated medium induces A549 cell injury via a spiral apoptotic cascade involving the mitochondrial-nuclear network," *Free Radical Biology and Medicine*, vol. 79, pp. 28–44, 2015.
- [5] K. Nakamura, Y. Peng, F. Utsumi et al., "Novel intraperitoneal treatment with non-thermal plasma-activated medium inhibits metastatic potential of ovarian cancer cells," *Scientific Reports*, vol. 7, no. 1, article 6085, 2017.
- [6] K. R. Liedtke, S. Bekeschus, A. Kaeding et al., "Non-thermal plasma-treated solution demonstrates antitumor activity against pancreatic cancer cells *in vitro* and *in vivo*," *Scientific Reports*, vol. 7, no. 1, article 8319, 2017.
- [7] K. Wende, P. Williams, J. Dalluge et al., "Identification of the biologically active liquid chemistry induced by a nonthermal atmospheric pressure plasma jet," *Biointerphases*, vol. 10, no. 2, article 029518, 2015.
- [8] F. Judée, C. Fongia, B. Ducommun, M. Yousfi, V. Lobjois, and N. Merbahi, "Short and long time effects of low temperature plasma activated media on 3D multicellular tumor spheroids," *Scientific Reports*, vol. 6, article 21421, 2016.
- [9] R. Matsumoto, K. Shimizu, T. Nagashima et al., "Plasma-activated medium selectively eliminates undifferentiated human induced pluripotent stem cells," *Regenerative Therapy*, vol. 5, pp. 55–63, 2016.
- [10] S. Mohades, M. Laroussi, J. Sears, N. Barekzi, and H. Razavi, "Evaluation of the effects of a plasma activated medium on cancer cells," *Physics of Plasmas*, vol. 22, no. 12, article 122001, 2015.
- [11] D. Yan, H. Cui, W. Zhu et al., "The specific vulnerabilities of cancer cells to the cold atmospheric plasma-stimulated solutions," *Scientific Reports*, vol. 7, no. 1, p. 4479, 2017.
- [12] D. Yan, A. Talbot, N. Nourmohammadi et al., "Principles of using cold atmospheric plasma stimulated media for cancer treatment," *Scientific Reports*, vol. 5, no. 1, article 18339, 2015.
- [13] J. Chauvin, F. Judée, M. Yousfi, P. Vicendo, and N. Merbahi, "Analysis of reactive oxygen and nitrogen species generated in three liquid media by low temperature helium plasma jet," *Scientific Reports*, vol. 7, no. 1, article 4562, 2017.
- [14] P.-M. Girard, A. Arbabian, M. Fleury et al., "Synergistic effect of H<sub>2</sub>O<sub>2</sub> and NO<sub>2</sub> in cell death induced by cold atmospheric He plasma," *Scientific Reports*, vol. 6, no. 1, article 29098, 2016.
- [15] N. Kurake, H. Tanaka, K. Ishikawa et al., "Cell survival of glioblastoma grown in medium containing hydrogen peroxide and/or nitrite, or in plasma-activated medium," *Archives of Biochemistry and Biophysics*, vol. 605, pp. 102–108, 2016.
- [16] G. Bauer, "The synergistic effect between hydrogen peroxide and nitrite, two long-lived molecular species from cold atmospheric plasma, triggers tumor cells to induce their own cell death," *Redox Biology*, vol. 26, article 101291, 2019.
- [17] B. Fubini and A. Hubbard, "Reactive oxygen species (ROS) and reactive nitrogen species (RNS) generation by silica in inflammation and fibrosis," *Free Radical Biology and Medicine*, vol. 34, no. 12, pp. 1507–1516, 2003.
- [18] A. Martínez-Ruiz, I. M. Araújo, A. Izquierdo-Álvarez, P. Hernansanz-Agustín, S. Lamas, and J. M. Serrador, "Specificity in S-nitrosylation: a short-range mechanism for NO signaling?," *Antioxidants & Redox Signaling*, vol. 19, no. 11, pp. 1220–1235, 2013.
- [19] D. D. Thomas, L. A. Ridnour, J. S. Isenberg et al., "The chemical biology of nitric oxide: implications in cellular signaling," *Free Radical Biology and Medicine*, vol. 45, no. 1, pp. 18–31, 2008.
- [20] C. Bogdan, "Nitric oxide and the immune response," *Nature Immunology*, vol. 2, no. 10, pp. 907–916, 2001.
- [21] R. T. Netea-Maier, J. W. A. Smit, and M. G. Netea, "Metabolic changes in tumor cells and tumor-associated macrophages: a mutual relationship," *Cancer Letters*, vol. 413, pp. 102–109, 2018.
- [22] W. J. Lee, S. Tateya, A. M. Cheng et al., "M2 macrophage polarization mediates anti-inflammatory effects of endothelial nitric oxide signaling," *Diabetes*, vol. 64, no. 8, pp. 2836–2846, 2015.



- [23] R. Noy and J. W. Pollard, "Tumor-associated macrophages: from mechanisms to therapy," *Immunity*, vol. 41, no. 1, pp. 49–61, 2014.
- [24] P. Allavena, A. Sica, G. Solinas, C. Porta, and A. Mantovani, "The inflammatory micro-environment in tumor progression: the role of tumor-associated macrophages," *Critical Reviews in Oncology/Hematology*, vol. 66, no. 1, pp. 1–9, 2008.
- [25] M. A. Rahat and B. Hemmerlein, "Macrophage-tumor cell interactions regulate the function of nitric oxide," *Frontiers in Physiology*, vol. 4, 2013.
- [26] D. Fukumura, S. Kashiwagi, and R. K. Jain, "The role of nitric oxide in tumour progression," *Nature Reviews Cancer*, vol. 6, no. 7, pp. 521–534, 2006.
- [27] F. Vannini, K. Kashfi, and N. Nath, "The dual role of iNOS in cancer," *Redox Biology*, vol. 6, pp. 334–343, 2015.
- [28] I. M. Sektioglu, R. Carretero, N. Bender et al., "Macrophage-derived nitric oxide initiates T-cell diapedesis and tumor rejection," *OncoImmunology*, vol. 5, no. 10, article e1204506, 2016.
- [29] F. De Sanctis, S. Sandri, G. Ferrarini et al., "The emerging immunological role of post-translational modifications by reactive nitrogen species in cancer microenvironment," *Frontiers in Immunology*, vol. 5, p. 69, 2014.
- [30] M. J. Davis, T. M. Tsang, Y. Qiu et al., "Macrophage M1/M2 polarization dynamically adapts to changes in cytokine micro-environments in *Cryptococcus neoformans* infection," *mBio*, vol. 4, no. 3, 2013.
- [31] H. S. Uhm, Y. H. Na, C. B. Lee, E. H. Choi, and G. Cho, "Dissociation and excitation coefficients of nitrogen molecules and radical generation in nitrogen plasma," *Current Applied Physics*, vol. 14, pp. S162–S166, 2014.
- [32] Y. H. Na, N. Kumar, M. H. Kang et al., "Production of nitric oxide using a microwave plasma torch and its application to fungal cell differentiation," *Journal of Physics D: Applied Physics*, vol. 48, no. 19, article 195401, 2015.
- [33] M. H. Kang, S. S. Jeon, S. M. Shin et al., "Dynamics of nitric oxide level in liquids treated with microwave plasma-generated gas and their effects on spinach development," *Scientific Reports*, vol. 9, no. 1, p. 1011, 2019.
- [34] M. R. Hussein, "Tumour-associated macrophages and melanoma tumourigenesis: integrating the complexity," *International Journal of Experimental Pathology*, vol. 87, no. 3, pp. 163–176, 2006.
- [35] M. Pieniazek, R. Matkowski, and P. Donizy, "Macrophages in skin melanoma—the key element in melanomagenesis," *Oncology Letters*, vol. 15, no. 4, pp. 5399–5404, 2018.
- [36] Y.-C. Liu, X.-B. Zou, Y.-F. Chai, and Y.-M. Yao, "Macrophage polarization in inflammatory diseases," *International Journal of Biological Sciences*, vol. 10, no. 5, pp. 520–529, 2014.
- [37] T. Lawrence and G. Natoli, "Transcriptional regulation of macrophage polarization: enabling diversity with identity," *Nature Reviews Immunology*, vol. 11, no. 11, pp. 750–761, 2011.
- [38] Y. Ogawa, T. Kawamura, M. Furuhashi, K. Tsukamoto, and S. Shimada, "Improving chemotherapeutic drug penetration in melanoma by imatinib mesylate," *Journal of Dermatological Science*, vol. 51, no. 3, pp. 190–199, 2008.
- [39] D. D. Thomas, X. Liu, S. P. Kantrow, and J. R. Lancaster, "The biological lifetime of nitric oxide: implications for the perivascular dynamics of NO and O<sub>2</sub>," *Proceedings of the National Academy of Sciences of the United States of America*, vol. 98, no. 1, pp. 355–360, 2001.
- [40] J. R. Lancaster Jr., "A tutorial on the diffusibility and reactivity of free nitric oxide," *Nitric Oxide*, vol. 1, no. 1, pp. 18–30, 1997.
- [41] C. V. Suschek and C. Opländer, "The application of cold atmospheric plasma in medicine: the potential role of nitric oxide in plasma-induced effects," *Clinical Plasma Medicine*, vol. 4, no. 1, pp. 1–8, 2016.
- [42] S. H. Ki, S. Sin, J. H. Shin et al., "Hemoglobin as a diagnosing molecule for biological effects of atmospheric-pressure plasma," *Plasma Chemistry and Plasma Processing*, vol. 38, no. 5, pp. 937–952, 2018.
- [43] C. Napoli, G. Paolisso, A. Casamassimi et al., "Effects of nitric oxide on cell proliferation: novel insights," *Journal of the American College of Cardiology*, vol. 62, no. 2, pp. 89–95, 2013.
- [44] A. W. Carpenter and M. H. Schoenfisch, "Nitric oxide release: part II. therapeutic applications," *Chemical Society Reviews*, vol. 41, no. 10, pp. 3742–3752, 2012.
- [45] Y. Tian, J. Guo, D. Wu, K. Wang, J. Zhang, and J. Fang, "The potential regulatory effect of nitric oxide in plasma activated water on cell growth of *Saccharomyces cerevisiae*," *Journal of Applied Physics*, vol. 122, no. 12, article 123302, 2017.
- [46] A. dos Anjos Cassado, M. R. D'Império Lima, and K. R. Bortoluci, "Revisiting mouse peritoneal macrophages: heterogeneity, development, and function," *Frontiers in Immunology*, vol. 6, p. 225, 2015.
- [47] C. Perske, N. Lahat, S. S. Levin, H. Bitterman, B. Hemmerlein, and M. A. Rahat, "Loss of inducible nitric oxide synthase expression in the mouse renal cell carcinoma cell line RENCA is mediated by microRNA miR-146a," *The American Journal of Pathology*, vol. 177, no. 4, pp. 2046–2054, 2010.
- [48] R. Andreesen, B. Hennemann, and S. W. Krause, "Adoptive immunotherapy of cancer using monocyte-derived macrophages: rationale, current status, and perspectives," *Journal of Leukocyte Biology*, vol. 64, no. 4, pp. 419–426, 1998.
- [49] I. Monnet, J.-L. Breau, D. Moro et al., "Intrapleural infusion of activated macrophages and  $\gamma$ -interferon in malignant pleural mesothelioma: a phase II study," *Chest*, vol. 121, no. 6, pp. 1921–1927, 2002.
- [50] T. Kees and M. Egeblad, "Innate immune cells in breast cancer—from villains to heroes?," *Journal of Mammary Gland Biology and Neoplasia*, vol. 16, no. 3, pp. 189–203, 2011.
- [51] M. De Palma and C. E. Lewis, "Macrophage regulation of tumor responses to anticancer therapies," *Cancer Cell*, vol. 23, no. 3, pp. 277–286, 2013.

## Research Article

# Hydroethanolic Extract of *Solanum paniculatum* L. Fruits Modulates ROS and Cytokine in Human Cell Lines

Ana Paula C. R. Ferraz <sup>1</sup>, Alessandra Sussulini,<sup>2</sup> Jéssica L. Garcia,<sup>1</sup> Mariane R. Costa,<sup>1</sup> Fabiane V. Francisqueti-Ferron <sup>1</sup>, Artur J. T. Ferron,<sup>1</sup> Carol Cristina V. de A. Silva,<sup>1</sup> José Eduardo Corrente <sup>1</sup>, Vanessa M. Manfio,<sup>1</sup> Vickeline Namba,<sup>1</sup> Giuseppina P. P. Lima,<sup>3</sup> Bismarque S. Pereira,<sup>1</sup> Denise Fecchio,<sup>1</sup> Igor O. Minatel,<sup>3</sup> Klinsmann C. dos Santos <sup>1</sup>, and Camila R. Corrêa <sup>1</sup>

<sup>1</sup>São Paulo State University (UNESP), Medical School, Botucatu 18618-687, Brazil

<sup>2</sup>University of Campinas (UNICAMP), Institute of Chemistry, Campinas 6154, Brazil

<sup>3</sup>São Paulo State University (UNESP), Institute of Biosciences, Botucatu, 18618-689 São Paulo, Brazil

Correspondence should be addressed to Ana Paula C. R. Ferraz; ferrazapcr@gmail.com

Received 14 August 2019; Revised 20 November 2019; Accepted 7 December 2019; Published 22 January 2020

Guest Editor: Nagendra K. Kaushik

Copyright © 2020 Ana Paula C. R. Ferraz et al. This is an open access article distributed under the Creative Commons Attribution License, which permits unrestricted use, distribution, and reproduction in any medium, provided the original work is properly cited.

*Solanum paniculatum* L. or popularly known as “jurubeba” is an herbal medicinal plant. A few studies have investigated its biological effects; however, research aimed at elucidating the redox balance effects from its fruits has not been reported so far. ROS interplays in various fields of medicine such as chemotherapy. Here, we evaluated antioxidant and inflammatory activities of the hydroethanolic extract of *Solanum Paniculatum* L. (HESPL) fruits in breast cancer cells, as well as its phytochemical profile. The antioxidant profile (carotenoids and phenolic compounds) was obtained by HPLC-DAD-UV and HPLC-APCI-MS. Cancer cell lines and human vein endothelial cells (HUVECs) were cultivated and treated with 1.87-30  $\mu\text{g}/\text{mL}$  of HESPL for 24 hrs. Cytotoxicity, oxidative, and inflammation biomarkers were evaluated. The dose of 30  $\mu\text{g}/\text{mL}$  of the HESPL extract presented cytotoxicity in the MCF-7 cell line. However, for MDA-MB-231, the cytotoxicity was observed in the dose of 1.87  $\text{g}/\text{mL}$ . The 1.87  $\mu\text{g}/\text{mL}$  and 3.75  $\mu\text{g}/\text{mL}$  doses decreased the concentration of IL-6 in MCF-7 cells. In the MDA-MB-231 cells, the HESPL did not decrease the IL-6 concentration; however, in the doses of 15 and 30  $\mu\text{g}/\text{mL}$ , an increase in this parameter was observed. The HESPL increased IL-1 $\beta$  concentration in HUVECs. The ROS level in MCF-7 was elevated only at the 30  $\mu\text{g}/\text{mL}$  dose. Regarding MDA-MB-231, HESPL promoted increased ROS levels at all doses tested. HUVEC showed no increase in ROS under any dose. HESPL treatment may modulate cytotoxicity, ROS, and cytokine levels due to its phytochemical profile, and it has shown an antioxidant or anti-inflammatory effect.

## 1. Introduction

Cancer is a multidimensional and complex onset of diseases with deregulated mechanisms and biochemical signaling, leading to pathology progress in a biological system [1]. Among all cancers, breast cancer is the main cause of worldwide women’s death; therefore, it is a target for research studies involving early diagnosis detection and therapies [2].

ROS, a type of unstable molecules that contain oxygen, which are rapidly transformed into other species can induce

oxidation of free amino acids, residues, and proteins. On the other hand, they can be a target of multiresistant drugs, enhancing cell death [3]. These species play a role in various fields of biology and medicine of cancer on protumorigenic signaling, cell proliferation, and tumorigenesis and transcription factor activation, which in turn can promote cytokines and chemokines such as IL-6 production in inflammation pathways as well as regulating and inducing apoptosis [4]. These reactive species were counteracted or stimulated by substances known as antioxidants, acting on the endogenous

cellular and exogenous environments, or by interactions of low molecular mass antioxidants such as carotenoids and phenolic compounds [5].

Natural products from medicinal and nonconventional plants and functional food intake have also been reported by data, which prevent the onset of several diseases or are used as a treatment for several diseases, providing ethnopharmacological knowledge on nutrition therapeutic formulations containing antioxidants on their phytochemical profile [6]. Several studies show their effectiveness in modulating ROS, inflammation, and chemotherapeutic resistance [7, 8].

*Solanum paniculatum* L. (Roem. and Schult.), Solanaceae family, popularly known as “jurubeba,” “jurupeba,” “jubeba,” or “juna” is an unconventional fruit-vegetable native to Tropical America. Its leaves and roots are widely used in traditional Brazilian medicine as tonic eupeptic agents to treat gastric and liver dysfunctions [9]. Its fruits are consumed by decoctions in culinary preparations and with oil or vinegar on pickled jurubeba [10]. Evidence has reported the presence of many steroidal compounds such as glycoalkaloids and saponins [11] and  $\beta$ -sitosterol [12] used in folk medicine. Endringer and colleagues showed chemoprevention in liver cells via NF- $\kappa$ B inhibitory activity after *Solanum paniculatum* L. treatment [13]. On the other hand, the study of Rios et al. (2017) showed its potential treatment of inflammatory conditions, reducing cell proliferation, IL-4, NO production, and other inflammatory markers; however, no chemical investigation of the antioxidant profile of *Solanum paniculatum* L. fruits as an hydroethanolic formulation and its biological mechanisms in breast cancer has been reported so far. These evaluations provided by HESPL response could be important on ROS and cytokine pathway knowledge. The present study was undertaken to investigate the phytochemical profile of HESPL fruit formulation and its effects on ROS and cytokine production in human breast cancer and endothelial cells.

## 2. Materials and Methods

**2.1. Plant Material.** *Solanum paniculatum* L. (in natura) fruits were collected on December 31, 2017, in the south of Mato Grosso State (Campo Grande region), with the coordinates 20°47'27" S latitude and 54°56'86" S longitude, by Ana Paula Costa Rodrigues Ferraz; these were deposited to the herbarium at the Institute of Biosciences, São Paulo State University (UNESP), Botucatu, SP, Brazil, under the voucher number 33072. Fruiting ratios for jurubeba were established according to Nurit et al. [14] and Forni-Martins et al. [15] through its globulous greenish to yellow appearance releasing from a peduncle; after this, 392 g of fruits was separated according to their appearance, washed in water, and stored at -80°C until the extraction process.

**2.2. Preparation of the HESPL Extract.** Jurubeba fruits were macerated in a cryogenic mill (6775 Freezer/Mill® Cryogenic Grinder), and lyophilized in a lyophilizer (Liotop L108®), obtaining a dry weight of 129 g of the powdered extract. The powdered extract (109 g) was percolated by exhaustion

according to the Brazilian Homeopathic Pharmacopoeia (2011) with a slow rate of 3 mL/min/kg using 70% ethanol. After twenty-four days of percolation, solvents were evaporated in a vacuum rotating evaporator with a horizontal condenser (Marconi MA-122) under low pressure (45°) and the remaining liquid was lyophilized to obtain the HESPL crude extract (24.12 g). The yield of the extract was calculated by

$$x = \left( \frac{\text{final weight (g)}}{\text{dry weight (g)}} \right) \times 100. \quad (1)$$

**2.3. Extraction of Carotenoids and Vitamin E via HPLC-DAD-UV and HPLC-APCI-MS.** The hydroethanolic extract (100 mg) was subjected to basic hydrolysis to separate the liposoluble components using 30% KOH in ethanol and solubilized with ether/hexane (2:1), using the saponification method adapted for plant samples from Qin et al. (1997). For HPLC-DAD-UV analysis, aliquots of 20  $\mu$ L were injected into the Waters Alliance 2695e Separation Module (Waters Corporation, Milford, MA, USA) coupled with the Waters PDA 2998 detector and analytical C<sub>30</sub> column (Thermo Scientific—3  $\mu$ m (4.6  $\times$  150 mm)). The mobile phases were composed of methanol/methyl tert-butyl ether/water: (A) 85/12/3 (v/v/v) and (B) 8/90/2 (v/v/v), with 6 mmol/L of ammonium acetate. The gradient was 2 min at 5% B, 3 min at 10% B, 6 min at 15% B, 10 min at 25% B, 12 min at 40% B, 16 min at 83%B, 20 min at 95% B, 24 min at 95% B, 26 min at 40% B, 30 min at 5% B, and 32 min at 5% B with a flow rate of 1.0 mL/min. Complementary to these data and with the same method for sample extraction (2.5 mg), HPLC-APCI-MS analysis of carotenoids was determined. Aliquots of 10  $\mu$ L were injected into an Agilent 1290 Infinity High-Performance Liquid Chromatography system (Agilent Technologies, United States) adapted by Etzbach et al. for total carotenoids, performed on 40-minute run and at 0.5 mL/min flow rate. The eluent B proportion was modified for 30/60/10 (v/v/v) using the same HPLC-DAD-UV column previously described [16].

**2.3.1. HPLC-APCI-Mass Spectrometry (MS) Instrumentation and Carotenoid Identification.** Mass spectrometry was performed in an AB Sciex Triple Quad™ QTRAP® 5500 Mass Spectrometer equipped with an Atmospheric-Pressure Chemical Ionization (APCI) source on a positive mode for carotenoid analysis. Also, 5 mmol/L of ammonium acetate was added to the mobile phases for improving compound ionization, as well as the column temperature (25°C). The conditions for mass spectrometry were adapted from Etzbach et al. (2018) with the following modifications: entrance potential (EP), 10 V; collision energy (CE), 30 V; collision cell exit potential (CXP), 8 V; time, 50 ms; curtain gas, 10 (API); medium collision gas (CAD); ion spray voltage, 5500 V; temperature, 450°C; and arbitrary units for ion source gas 1 (GS1), 30.0.

A selective reaction monitoring (SRM) experiment was performed to identify the analytes, the first mass transition following two or three mass transitions was used to confirm the compound profile, and these transitions were determined by the literature [16] (see Table 1).

TABLE 1: SRM transitions for total carotenoids.

Compound name	[M+H] <sup>+</sup> ( <i>m/z</i> )	Fragment ion	Declustering potential (V)
Lutein	569.0	476.0	80
		175.0	
		551.0	
		533.0	
Zeaxanthin	569.0	551.1	50
		533.1	
		395.0	
		93.0	
		135.1	
$\beta$ -Cryptoxanthin	553.5	119.0	50
$\beta$ -Cryptoxanthin	553.0	135.0	50
		495.0	
$\alpha$ -Carotene	537.0	461.0	50
		123.0	
		481.0	
		444.1	
		177.2	
$\beta$ -Carotene	537.0	445.4	50
		413.3	
		269.2	

The major carotenoids (see Figure S1 in Supplementary Materials) constituent from HPLC-DAD-UV were focused on these evaluations, and the SRM identification transition selected was 569.00/551.00. The Analyst® 1.5.1 software (AB Sciex®) and MultiQuant™ 3.0.3 software (AB Sciex®) were used for data analysis.

See Figure S1 in Supplementary Materials for comprehensive carotenoid image analysis.

**2.4. Extraction and Identification of Phenolic Compounds via HPLC-DAD-UV.** The HESPL extraction (100 mg) was determined by modifications of the method described by Palafox-Carlos et al. [17]. The extract was dried in N<sub>2</sub>, resuspended in HPLC-grade methanol, and filtered on a 0.22  $\mu$ m Analytical® nylon membrane. Aliquots (20  $\mu$ L) were injected into a UHPLC Thermo Scientific Dionex UltiMate 3000 system (Thermo Fisher Scientific Inc., MA, USA), coupled with a quaternary pump, an Ultimate 3000RS autosampler, and a diode array detector (DAD-3000RS) using a C<sub>18</sub> column, and the flow rate was 0.8 mL/min. The mobile phase was composed of phosphoric acid/water (A) (0.85/99.15, *v/v*) and acetonitrile (C) (100, *v*). The gradient was 2 min at 7% B, 3 min at 9% B, 5 min at 10% B, 7 min at 12% B, 8.5 min at 13% B, 11 min at 15% B, 12.5 min at 20% B, 13 min at 21% B, 14 min at 23% B, 15 min at 25% B, 17 min at 30% B, 19 min at 45% B, 22 min at 65% B, 23 min at 75% B, and 24 min at 30% B. See Figure S2 in Supplementary Materials for comprehensive phenolic compound image analysis.

## 2.5. Antioxidant Capacity

**2.5.1. Radical Sequestration Method (DPPH) and FRAP Assay.** A methanolic solution was prepared for the extraction with 0.100 g of jurubeba for both methods. The DPPH method was performed according to Brand-Williams et al. [18], and the FRAP assay was adapted according to the methodology proposed by Benzie and Strain [19], which is efficient in the determination of antioxidant activity by iron reduction.

**2.6. Cell Culture Experimental Design.** Breast cancer cell lines were MCF-7 (ATCC® HTB22™), luminal, HER2+, and estrogen- and progesterone-positive receptors and MDA-MB-231 (ATCC® HTB26™), basal and with invasive potential. MCF-7 were cultivated in RPMI Medium 1640 supplemented with 10% FBS, 1% NEAA, 1% sodium pyruvate, and 1% antibiotic and MDA-MB-231 were cultivated with 10% FBS and 1% antibiotic (anti-anti). HUVECs (ATCC® CRL-1730) were cultivated in F-12K Medium (Thermo Fisher Scientific® Gibco DMEM/F12 DULBEC) with 10% FBS and 1% antibiotic. All cell lines were maintained in a humidified incubator (5% CO<sub>2</sub> at 37°C). Cells were plated onto 175 cm<sup>2</sup> tissue culture flasks, and treatments proceeded when the cells reached 80% of confluence between passages 6 and 8. A stock solution for HESPL induction (10 mg/mL) was made in DMSO as a vehicle according to recommendations by Jamalzadeh et al. (2016) for an experimental application. Different doses (30, 15, 7.5, 3.75, and 1.87  $\mu$ g/mL) were established by Rios et al. (2017) and were diluted in medium without FBS for further *in vitro* experimental research.

The cell viability was performed by the Trypan Blue assay. After 24 hours of treatment, cells were harvested and submitted to trypsinization, the pellet was resuspended in appropriate concentration of medium, and 10  $\mu$ L was collected and diluted in 10  $\mu$ L of Trypan Blue. The cells were counted on an improved Neubauer Haemocytometer (Weber Scientific International Ltd., UK). Viable and nonviable cells were counted under light microscopy, and the viable cells are considered above 80%.

**2.7. Cytotoxic Activity.** Approximately 1  $\times$  10<sup>6</sup> cells were incubated on six-well plates for 12 hours on RPMI 1640 culture medium with 10% FBS and 24 hrs with 0.1% FBS and maintained at 37°C and an atmosphere of 5% CO<sub>2</sub>. Different doses were applied for 24 hrs aimed at providing a nonlethal dose for further research. Subsequently, cytotoxicity was determined using the rapid colorimetric assay based on the tetrazolium salt MTT (3-(4,5-dimethylthiazol-2-yl)-2,5-diphenyl tetrazolium bromide) (0.5 mg/mL in HBSS) which can measure metabolic living cells and proliferation [20]. The cells were solubilized in DMSO and read at 570 nm using a scanning multiwell spectrophotometer (SpectraMax 190, Molecular Devices).

**2.8. Analysis of ROS Production.** The cells were cultivated onto 75 cm<sup>2</sup> flasks for each dose, and following the treatments, these were collected using trypsin and resuspended on Muse™ Oxidative Stress Assay Buffer (4700-1330, Merck Millipore) with a minimum of 1  $\times$  10<sup>6</sup> cells for each replicate;

these were performed through flow cytometry using Muse® Cell Analyzer (Merck, Darmstadt, Germany) with Muse™ Oxidative Stress Kit (MCH100111, Merck Millipore). The results were shown positively ROS (ROS (+)) which has the cell exhibiting ROS significance.

**2.9. Inflammation Measurement.** IL-6 and IL-1 $\beta$  evaluations were performed in a commercial immunoassay ELISA kit using 100  $\mu$ L of cell supernatant according to the manufacturers' instructions (Linco Research Inc., R&D Systems®, Millipore, and B-Bridge International Inc.) and were determined by absorbance using a microplate reader (SpectraMax 190, Molecular Devices).

### 3. Statistics

Results are expressed as mean  $\pm$  SD. One-way ANOVA followed by the Tukey test was performed by normal distribution in SigmaPlot using Windows 10. Statistical significance was considered when  $p < 0.05$ .

### 4. Results

**4.1. HESPL Extract and Bioactive Compounds.** The results for a phytochemical profile of HESPL in HPLC-DAD-UV presented with four carotenoids (lutein, zeaxanthin,  $\beta$ -cryptoxanthin,  $\beta$ -carotene), one vitamin E ( $\gamma$ -tocopherol), two phenolic compounds (chlorogenic and caffeic acids), and one flavonoid (quercetin) (see Table 2).

The major active compound in HESPL is lutein, identified for the retention time of 17.52 min based on similar [M+H]<sup>+</sup> ( $m/z$ ) (569.0) and fragments (175/135/551) on a sample (Figure 1(a)) compared with the lutein standard (Figure 1(b)).

HESPL has a yield of 22.19%. The FRAP procedure measures the antioxidant capacity through the interaction between the reductants (antioxidants) and Fe<sup>II</sup>-TPTZ creating a blue color showing  $423.32 \pm 1.70 \mu\text{mol}$  of quercetin  $100 \text{ g}^{-1}$  DW (CV = 0.40). Additionally, the DPPH method has an affinity of reducing a free radical by a hydrophilic affinity, and HESPL shows  $89.13 \pm 1.20$  (mg of quercetin  $100 \text{ g}^{-1}$ ) (CV = 1.34) of % DPPH reduction.

**4.2. Cell Viability of the Cell Lines Submitted to Different Doses.** The dose of 30  $\mu\text{g/mL}$  ( $82.29 \pm 19.11$ , CV = 23.22) shows a significant toxicity ( $p < 0.05$ ) when compared with control in MCF-7 cells (see Figure 2). However, for MDA-MB-231, the cytotoxicity was observed in the dose of 1.87  $\mu\text{g/mL}$  ( $97.22 \pm 2.04$ , CV = 2.10). Regarding the HUVEC, the extract did not show cytotoxicity.

**4.3. Concentration of Interleukin in the Cell Lines in Different Doses of HESPL.** In this study, the 1.87  $\mu\text{g/mL}$  ( $0.04 \pm 0.02$ ,  $p < 0.005$ ) and 3.75  $\mu\text{g/mL}$  ( $0.03 \pm 0.00$ ,  $p < 0.005$ ) concentrations decreased with significance in MCF-7 cells (Figure 3(a)). In the MDA-MB-231 cells, the HESPL did not decrease the IL-6 concentration; however, in the doses of 15 and 30  $\mu\text{g/mL}$ , an increase in this parameter was observed ( $130.88 \pm 1.52 / 125.46 \pm 4.88$ ,  $p < 0.005$ ) (Figure 3(b)). The HESPL increased IL-1 $\beta$  concentration in HUVECs (dose of

3.75  $\mu\text{g/mL}$  ( $4.513 \pm 0.280$ ,  $p < 0.05$ ) vs. control ( $2.965 \pm 1.108$ ); Figure 3(c)).

**4.4. The Levels of ROS Were Increased by the Dose of 7.5  $\mu\text{g/mL}$  of HESPL vs. Control.** The higher dose of 7.5  $\mu\text{g/mL}$  of HESPL improves ROS levels (see Figure 4(a)) in MDA-MB-231 ( $15.47 \pm 4.88$ ,  $p < .0001$ ) vs. control ( $2.87 \pm 0.57$ ) and also improved increased levels in all tested doses. HUVECs did not present higher levels of ROS. See Figure 5 for a comprehensive example of cell flux analysis.

### 5. Discussion

Dietary phytochemicals can act as an antioxidant or prooxidant and may participate in the development of new anticancer drugs [21]. Elevated levels of ROS and deregulated redox signaling are common hallmarks of cancer progression and resistance to treatment [22]. ROS production is involved in two faces of the cancer environment: in basal levels, these species are involved in PI3K/Akt-mediated cell survival and proliferation, or when excessive intracellular ROS accumulation occurs, these are involved in the cleavage of caspase-3 and caspase-7 also damaging nucleic acid bases and other compounds [4].

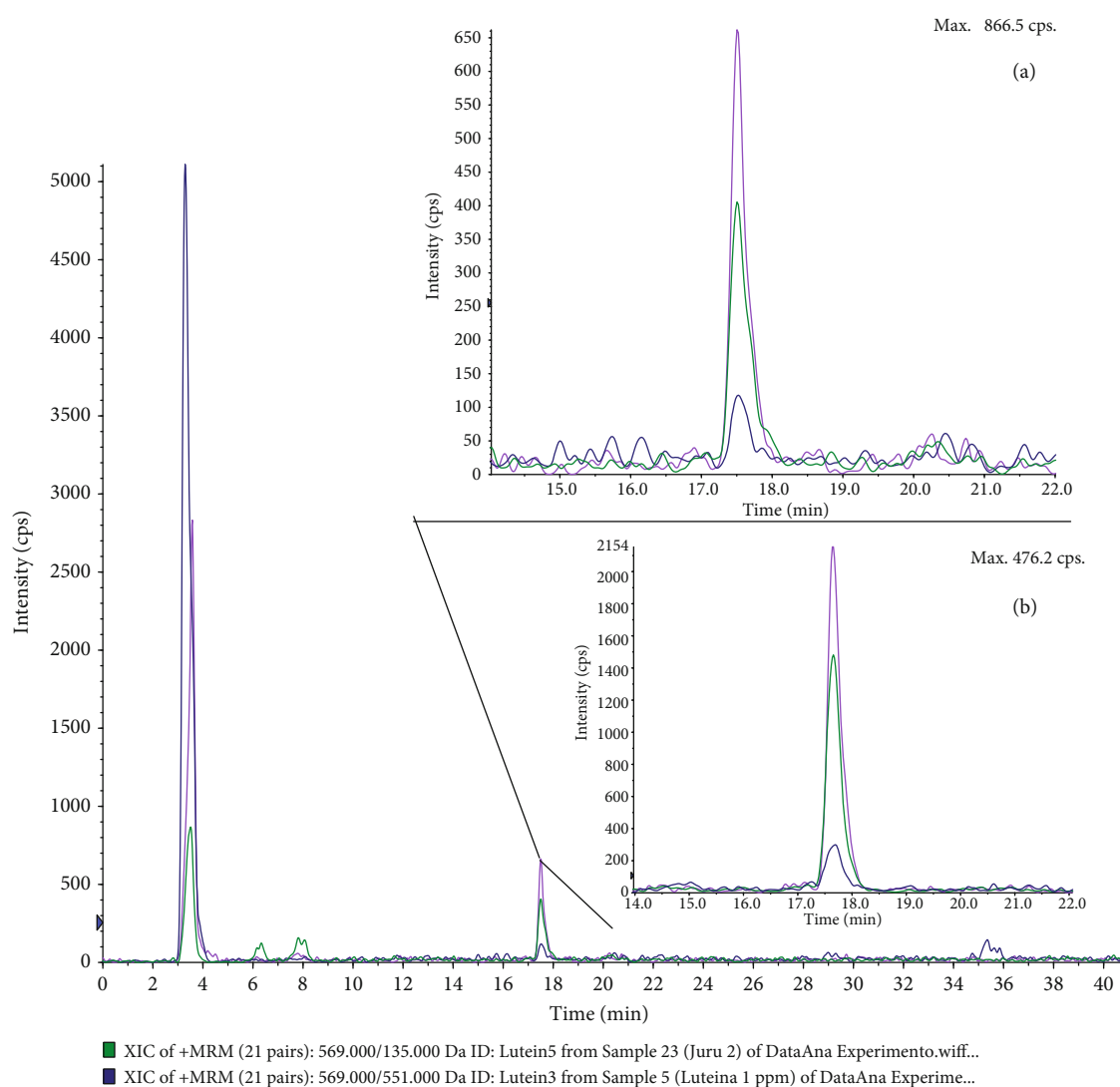
It is known that MDA-MB-231 are malignant cells, and in this study, they could be a great model to investigate the effects of natural products on ROS modulation since this kind of cell is classified with invasive potential [23]. Our dose-response study demonstrated that the dose ranging from 1.87 to 7.5  $\mu\text{g/mL}$  of HESPL enhanced ROS production (Figure 4). These results suggest that the phytochemical profile of plant- and food-based diets may act on the redox balance. Phytochemicals present in plants can act as a prooxidant via the Fenton reaction whose mechanism occurs via iron-dependent ROS production [24]. It can also inhibit NADPH expression and the blockade of the Nrf-2 signaling pathway [25]. This transcription factor was commonly elevated in various types of cancer and consequently as a result of the activation of oncogenes such as K-Ras, B-Raf, and c-Myc which in turn are involved in survival and cell proliferation [21].

The mechanism of action of plant-based diets may possess intervention capacity acting at specific pathways such as reduction of NF- $\kappa$ B DNA-binding activity, TNF- $\alpha$  inhibition, increased caspase-3 and caspase-7, bax/bcl-2 ratio, and fraction with sub-G0/G1 DNA content in apoptosis [26]. Additionally, Sinha et al. demonstrated that phytoconstituents of tea (*Camellia sinensis*) modulate epidermal growth factor receptor, B-cell lymphoma 2 (Bcl-2), and Bcl-2-associated X protein in the breast carcinoma [27].

The phytochemical profile of the jurubeba fruit extract consists of phenolic compounds, vitamin E, and carotenoids. Polyphenols can act via noncovalent interaction with cellular proteins promoting the inhibition of prooxidant enzymes and diminishing DNA damage and lipid peroxidation as well as inhibition of ROS-dependent signal transduction [28]. In our phytochemical profile, caffeic acid is the major phenolic compound, but we also identified chlorogenic acid and

TABLE 2: Phytochemical profile of HESPL determined by HPLC-DAD-UV.

Analyte	RT	Linearity range (ng/ $\mu$ L)	LOD/LOQ (ng/ $\mu$ L)	$r^2$	<i>Solanum paniculatum</i> L. (pg/mL) in 100 mg of extract	SD (%)	CV (%)
Carotenoids							
Lutein	3.449	5-100	1.45/5	0.9988	103.70	2.3049	2.222719
Zeaxanthin	4.133	2.28-36.5	0.80/2.28	0.9972	8.9	0.48608	5.461573
$\beta$ -Cryptoxanthin	9.017	5.30-84.9	0.97/5.30	0.9963	8.8	0.5913	6.719318
$\beta$ -Carotene	15.666	15.6-250	0.89/15.6	0.9821	8.7	1.1533	0.131655
Vitamin E							
$\gamma$ -Tocopherol	5.333	0.075-2.42	1.09/0.075	0.9999	1.6	0.00206	0.12875
Phenols							
Chlorogenic acid	3.517	10-500	1.40/10	0.9956	17.5	0.7415	4.237143
Flavonoids							
Caffeic acid	6.617	10-500	1.30/10	0.9991	23.9	0.9641	4.033891
Quercetin	19.12	10-500	1.33/10	0.9999	2.9	0.1306	4.503448

FIGURE 1: Carotenoid profile of *Solanum paniculatum* L. by HPLC-APCI-MS: (a) lutein compound in the sample; (b) lutein standard.

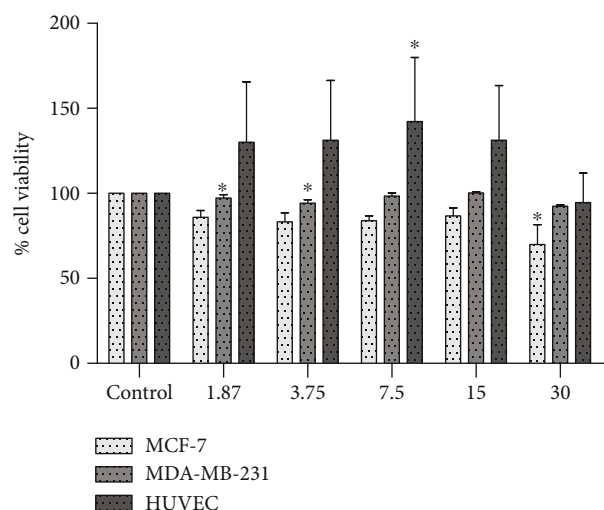


FIGURE 2: % cell viability from MCF-7, MDA-MB-231, and HUVECs. \*Versus control when  $p < 0.05$ . The viability was determined by the MTT assay. The dose of  $30 \mu\text{g/mL}$  presented cytotoxicity.

quercetin. Yu et al. demonstrated that caffeic acid can lead to apoptosis in YD-15 (human mucoepidermoid carcinoma), HSC-4, and HN22 (human oral squamous cell carcinoma). Moreover, the authors have shown the apoptotic effect by cleavages of caspase-3 and poly (ADP-ribose) polymerase and activation of Bax protein [29]. In parallel, Abou-Hashem et al. showed the apoptotic effect of chlorogenic acid via cell cycle arrest at the sub-G<sub>0</sub> phase and DNA fragmentation [30], whereas quercetin can induce apoptosis through proteasome inhibition such as the 20S and 26S proteasome in Jurkat T cells and accumulation of polyubiquitinated proteins [28].

Evidence suggests that dietary carotenoids may help in reducing the risk of breast cancer [31]. Lutein is the major carotenoid identified in our extract. Lutein acts by suppressing inflammation, and it was involved in the inhibition of NF- $\kappa$ B signaling [32]. In summary, benefits of lutein intake consist in eye health and antioxidant and anti-inflammatory activities. It is suggested that lutein mechanisms of action in cancer might be involved in cell growth inhibition by inducing cell cycle arrest and caspase-independent cell death also, activating p53 signaling [33]. Juin et al. showed the apoptotic effect of zeaxanthin through the expression of the BRAF V600E oncogene [34]. Additionally, Gao et al. demonstrated the antiproliferation effect of  $\beta$ -cryptoxanthin by G<sub>0</sub>/G<sub>1</sub> cell cycle arrest and AMPK signal inactivation [35]. The effects of  $\beta$ -carotene on metastasis was evidenced by Kim et al. where it downregulated the expression of CSC markers, MMPs, and HIF-1 $\alpha$  in cancer tissues [36]. Inhibition of the HMG-CoA reductase enzyme and inhibition of the NF- $\kappa$ B pathway are the main antiangiogenic mechanisms found for tocotrienols such as  $\gamma$ -tocopherol [37].

Cytokine levels are naturally enhanced in conditions such as obesity and cancer [38]. A few reports related the reduction of IL-6 to a targeted therapy for cancer [39, 40]. In our study, the HESPL treatment diminished the levels of IL-6 in MCF-7

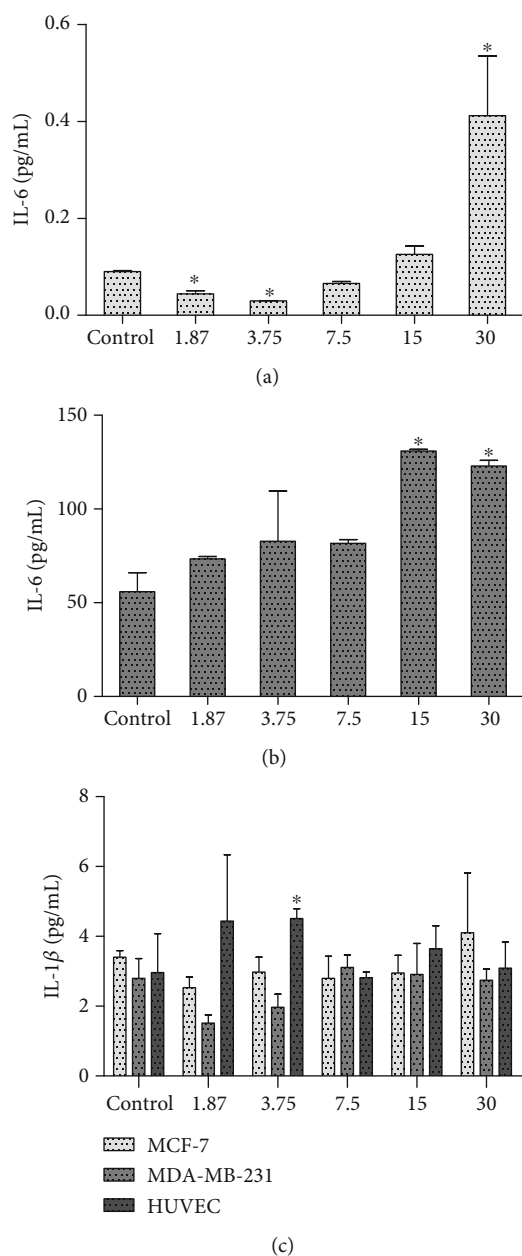


FIGURE 3: Different doses of HESPL effect in interleukin-6: (a) MCF-7 cells, (b) MDA-MB-231 cells, and (c) different doses of HESPL effect in IL-1 $\beta$  in the cell lines. \*Versus control when  $p < 0.05$ . The dose of  $3.75 \mu\text{g/mL}$  diminished significantly compared with other doses. On the other hand, the doses of 15 and  $30 \mu\text{g/mL}$  were increased in MDA-MB-231, and for IL-1 $\beta$ , the dose  $3.75 \mu\text{g/mL}$  was enhanced.

cells (Figures 3(a) and 3(b)), enhancing the importance of this cytokine acting as having multifaceted cellular displayed and physiological functions on biological systems [41]. Primary tumors such as MCF-7 cells may be an important tool on research focusing on chemopreventive actions [42]. The chemopreventive actions can attenuate cell cycle arrest [43] and other various tumor-promoting pathways in cancer [44]. IL-6 seems to be an important cytokine in breast cancer studies [39, 44, 45] acting in several pathways involved in

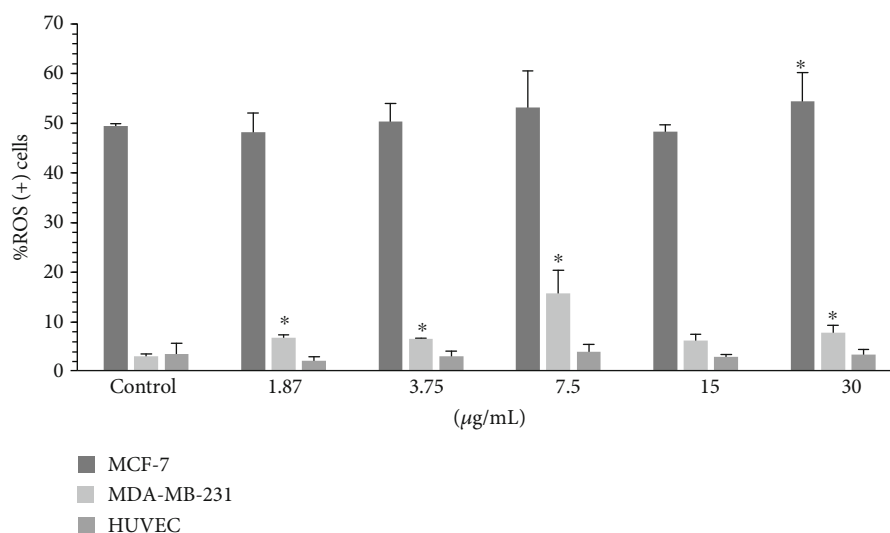


FIGURE 4: ROS parameter from MCF-7, MDA-MB-231, and HUVECs. \*Versus control when  $p < 0.05$ . The ROS was enhanced in all doses tested in invasive cells, and the dose 30 µg/mL was increased in MCF-7 cells.

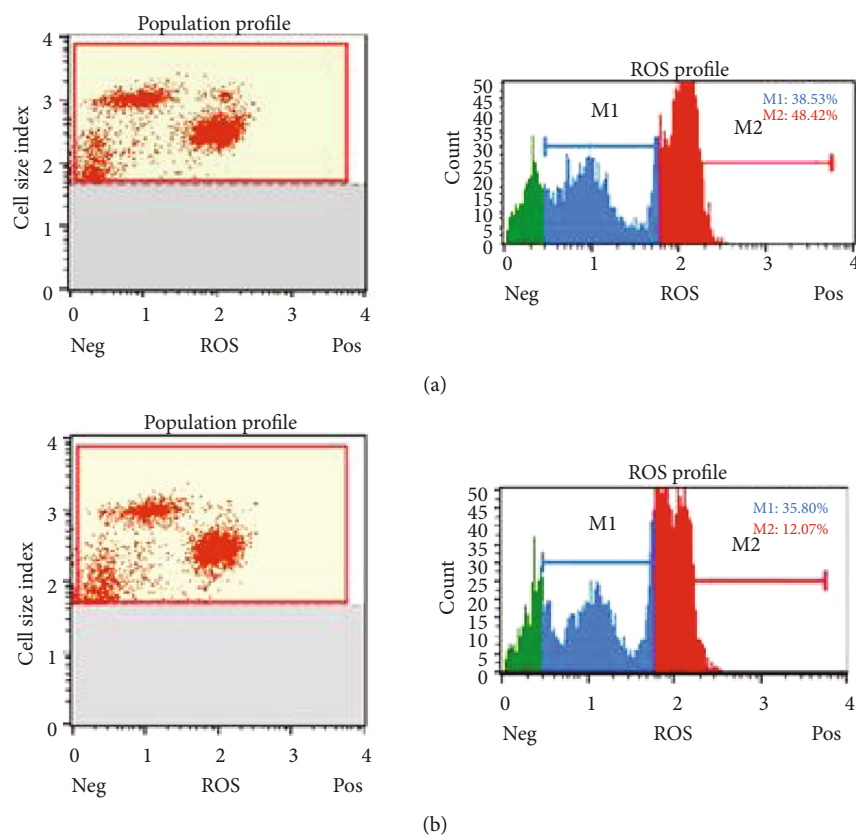


FIGURE 5: Cell flux analysis in MCF-7 cells: (a) 30 µg/mL treatment; (b) control.

cancer progression [46]. Moreover, IL-1 $\beta$ , another important cytokine in the chronic inflammation process, was enhanced in HUVECs after treatment with 3.75 µg/mL HESPL (Figure 3(c)).

The synergic effects of different compounds presented in the HESPL might provide an adjuvant strategy on cancer therapies since multiple phytochemicals may act on various

biological microenvironments. We have shown in this study that phytochemicals presented in the crude extract of jurubeba fruits can act on the oxidative and inflammation balance. A positive control study may be a scientific contribution for our current findings since the isolated phytochemicals contribute to antitumoral mechanisms such as apoptosis. However, its known that individual compounds



have not shown benefits in some clinical trials since bioactivity might be affected or do not react in the same effective way when compared to crude extracts of plant-based foods [26]. Our data suggests a redox/inflammation modulation network of the *Solanum paniculatum* L. fruits, and its potential as a nutraceutical was shown to be enhanced as it successfully modulates ROS and cytokine production as well as inhibiting the growth of cancerous cells.

## 6. Conclusions

The molecular mechanisms of ROS and cytokine play an important role in various cancer models evidenced in both *in vitro* and *in vivo* studies. ROS and cytokine modulation seems to be a promising chemotherapeutic target for treatments. Here, we demonstrated that HEPSL can act by diminishing ROS production and modulate levels of IL-6 and IL-1 $\beta$ . Most importantly, our dose-response studies demonstrated that different concentrations of phytochemicals, acting synergically, might affect the outcomes either positively or negatively, raising the importance of ingestion-response ratio effects of diets. Our findings, even as a basic research model, provide information that can guide future studies aimed at elucidating new therapeutic alternatives for cancer.

## Data Availability

The data used to support the findings of this study are available from the corresponding author upon request.

## Conflicts of Interest

The authors declare that there are no conflicts of interest regarding the publication of this paper.

## Authors' Contributions

All authors participated in the study design, interpretation, analysis, and review of the final version of the manuscript. Ferraz APCR, dos Santos KC, and Correa CR elaborated the experimental design. Ferraz APCR, dos Santos KC, Garcia JL, Namba V, and Pereira BS conducted the experiment. Corrente JE performed the statistical analysis, and Ferraz APCR, dos Santos KC, Garcia JL, Costa MR, Francisqueti-Ferron FV, Ferron AJT, Silva CCVA, Manfio VM, Minatel IO, and Correa CR analyzed the data and revised and wrote the manuscript. Klinsmann C. dos Santos is the joint last author.

## Acknowledgments

The authors thank Dra. Alessandra Sussulini, Dra. Denise Fecchio, Dra. Gisela Ferreira, Dra. Daisy Maria Favero Salvadori, Dra. Giuseppina Pace Pereira Lima, and CIE (Centro de Isótopos Estáveis-IBB UNESP) for providing experimental analysis, financial and equipment support, and plant material. They also thank Danilo, Rogério, Regina, Vickeline, Paulo Cesar, Cibele, and Nadia for their technical support. This work was supported by Conselho Nacional de Desenvolvimento Científico e Tecnológico/CNPQ (Process:

130379/2016-6) and Coordenação de Aperfeiçoamento de Pessoal de Nível Superior (CAPES/DS) for the financial support and scholar stipend.

## Supplementary Materials

Figure S1: molecular structures of carotenoids. Figure S2: molecular structures of phenolic compounds. (*Supplementary Materials*)

## References

- [1] F. Spill, C. Bakal, and M. Mak, "Mechanical and systems biology of cancer," *Computational and Structural Biotechnology Journal*, vol. 16, pp. 237–245, 2018.
- [2] American Cancer Society, *Breast Cancer: Facts & Figures 2017-2018*, American Cancer Society, 2018.
- [3] Q. Cui, J.-Q. Wang, Y. G. Assaraf et al., "Modulating ROS to overcome multidrug resistance in cancer," *Drug Resistance Updates*, vol. 41, pp. 1–25, 2018.
- [4] C. R. Reczek and N. S. Chandel, "The two faces of reactive oxygen species in cancer," *Annual Review of Cancer Biology*, vol. 1, no. 1, pp. 79–98, 2017.
- [5] H. H. H. W. Schmidt, R. Stocker, C. Vollbracht et al., "Antioxidants in translational medicine," *Antioxidants & Redox Signaling*, vol. 23, no. 14, pp. 1130–1143, 2015.
- [6] A. M. de Carvalho, A. A. F. Carioca, R. M. Fisberg, L. Qi, and D. M. Marchioni, "Joint association of fruit, vegetable, and heterocyclic amine intake with DNA damage levels in a general population," *Nutrition*, vol. 32, no. 2, pp. 260–264, 2016.
- [7] T. Zhang, P. Zheng, X. Shen et al., "Curcuminoid WZ26, a TrxR1 inhibitor, effectively inhibits colon cancer cell growth and enhances cisplatin-induced cell death through the induction of ROS," *Free Radical Biology & Medicine*, vol. 141, pp. 93–102, 2019.
- [8] R. Thangam, S. Gokul, M. Sathuvan, V. Suresh, and S. Sivasubramanian, "A novel antioxidant rich compound 2-hydroxy 4-methylbenzaldehyde from *Decalepis arayalpathra* induces apoptosis in breast cancer cells," *Biocatalysis and Agricultural Biotechnology*, vol. 21, article 101339, 2019.
- [9] BRASIL, *Consulta Pública nº 73, de 16 de julho de 2010. D.O.U de 20/07/2010*, Agência Nacional de Vigilância Sanitária, 2010.
- [10] M. B. da Silva, L. F. O. S. Rodrigues, T. C. Rossi, M. C. de Souza Vieira, I. O. Minatel, and G. P. P. Lima, "Effects of boiling and oil or vinegar on pickled jurubeba (*Solanum paniculatum* L.) fruit," *African Journal of Biotechnology*, vol. 15, no. 6, pp. 125–133, 2016.
- [11] G. M. V. Júnior, C. Q. da Rocha, T. de Souza Rodrigues, C. A. Hiruma-Lima, and W. Vilegas, "New steroidal saponins and antiulcer activity from *Solanum paniculatum* L.," *Food Chemistry*, vol. 186, pp. 160–167, 2015.
- [12] R. Rios, H. B. F. Silva, N. V. Q. Carneiro et al., "*Solanum paniculatum* L. decreases levels of inflammatory cytokines by reducing *NFKB*, *TBET* and *GATA3* gene expression *in vitro*," *Journal of Ethnopharmacology*, vol. 209, pp. 32–40, 2017.
- [13] D. C. Endringer, Y. M. Valadares, P. R. V. Campana et al., "Evaluation of Brazilian plants on cancer chemoprevention targets *in vitro*," *Phytotherapy Research*, vol. 24, no. 6, 2009.
- [14] K. Nurit, M. de Fátima Agra, and e. I. J. L. D. Basílio, "Estudo farmacobotânico comparativo entre *Solanum paniculatum* L. e

- Solanum rhytidoandrum* Sendtn. (Solanaceae),” *Revista Brasileira de Biociências*, vol. 5, no. 1, pp. 243–245, 2007.
- [15] E. R. Forni-Martins, M. C. M. Marques, and M. R. Lemes, “Biologia floral e reprodução de *Solanum paniculatum* L. (Solanaceae) no estado de São Paulo, Brasil,” *Revista Brasileira de Botânica*, vol. 21, no. 2, pp. 117–124, 1998.
- [16] L. Etzbach, A. Pfeiffer, F. Weber, and A. Schieber, “Characterization of carotenoid profiles in goldenberry (*Physalis peruviana* L.) fruits at various ripening stages and in different plant tissues by HPLC-DAD-APCI-MS,” *Food Chemistry*, vol. 245, no. August 2017, pp. 508–517, 2018.
- [17] H. Palafox-Carlos, E. M. Yahia, and G. A. González-Aguilar, “Identification and quantification of major phenolic compounds from mango (*Mangifera indica*, cv. Ataulfo) fruit by HPLC-DAD-MS/MS-ESI and their individual contribution to the antioxidant activity during ripening,” *Food Chemistry*, vol. 135, no. 1, pp. 105–111, 2012.
- [18] W. Brand-Williams, M. E. Cuvelier, and C. Berset, “Use of a free radical method to evaluate antioxidant activity,” *LWT - Food Science and Technology*, vol. 28, no. 1, pp. 25–30, 1995.
- [19] I. F. F. Benzie and J. J. Strain, “The ferric reducing ability of plasma (FRAP) as a measure of “antioxidant power”: the FRAP assay,” *Analytical Biochemistry*, vol. 239, no. 1, pp. 70–76, 1996.
- [20] T. Mosmann, “Rapid colorimetric assay for cellular growth and survival: application to proliferation and cytotoxicity assays,” *Journal of Immunological Methods*, vol. 65, no. 1-2, pp. 55–63, 1983.
- [21] W. Fernando, H. P. V. Rupasinghe, and D. W. Hoskin, “Dietary phytochemicals with anti-oxidant and pro-oxidant activities: A double-edged sword in relation to adjuvant chemotherapy and radiotherapy?,” *Cancer Letters*, vol. 452, pp. 168–177, 2019.
- [22] S. Kumari, A. K. Badana, M. M. G. S. G., and R. R. Malla, “Reactive oxygen species: a key constituent in cancer survival,” *Biomarker Insights*, vol. 13, p. 117727191875539, 2018.
- [23] R. M. Neve, K. Chin, J. Fridlyand et al., “A collection of breast cancer cell lines for the study of functionally distinct cancer subtypes,” *Cancer Cell*, vol. 10, no. 6, pp. 515–527, 2006.
- [24] L. M. Bystrom, M. L. Guzman, and S. Rivella, “Iron and reactive oxygen species: friends or foes of cancer cells?,” *Antioxidants and Redox Signaling*, vol. 20, no. 12, pp. 1917–1924, 2014.
- [25] T. Maraldi, “Natural compounds as modulators of NADPH oxidases,” *Oxidative Medicine and Cellular Longevity*, vol. 2013, 10 pages, 2013.
- [26] A. Kapinova, P. Stefanicka, P. Kubatka et al., “Are plant-based functional foods better choice against cancer than single phytochemicals? A critical review of current breast cancer research,” *Biomedicine & Pharmacotherapy*, vol. 96, pp. 1465–1477, 2017.
- [27] D. Sinha, J. Biswas, S. M. Nabavi, and A. Bishayee, “Tea phytochemicals for breast cancer prevention and intervention: from bench to bedside and beyond,” *Seminars in Cancer Biology*, vol. 46, pp. 33–54, 2017.
- [28] A. Golonko, T. Pienkowski, R. Swislocka, R. Lazny, M. Roszko, and W. Lewandowski, “Another look at phenolic compounds in cancer therapy the effect of polyphenols on ubiquitin-proteasome system,” *European Journal of Medicinal Chemistry*, vol. 167, pp. 291–311, 2019.
- [29] H. J. Yu, J. A. Shin, I. H. Yang et al., “Apoptosis induced by caffeic acid phenethyl ester in human oral cancer cell lines: involvement of Puma and Bax activation,” *Archives of Oral Biology*, vol. 84, pp. 94–99, 2017.
- [30] M. M. M. Abou-Hashem, D. M. Abo-elmatty, N. M. Mesbah, and A. M. Abd el-Mawgoud, “Induction of sub-G<sub>0</sub> arrest and apoptosis by seed extract of *Moringa peregrina* (Forssk.) Fiori in cervical and prostate cancer cell lines,” *Journal of Integrative Medicine*, vol. 17, no. 6, pp. 410–422, 2019.
- [31] M. Eggersdorfer and A. Wyss, “Carotenoids in human nutrition and health,” *Archives of Biochemistry and Biophysics*, vol. 652, pp. 18–26, 2018.
- [32] N. Hadad and R. Levy, “The synergistic anti-inflammatory effects of lycopene, lutein,  $\beta$ -carotene, and carnosic acid combinations via redox-based inhibition of NF- $\kappa$ B signaling,” *Free Radical Biology & Medicine*, vol. 53, no. 7, pp. 1381–1391, 2012.
- [33] X. Gong, J. Smith, H. Swanson, and L. Rubin, “Carotenoid lutein selectively inhibits breast cancer cell growth and potentiates the effect of chemotherapeutic agents through ROS-mediated mechanisms,” *Molecules*, vol. 23, no. 4, p. 905, 2018.
- [34] C. Juin, R. G. de Oliveira Junior, A. Fleury et al., “Zeaxanthin from *Porphyridium purpureum* induces apoptosis in human melanoma cells expressing the oncogenic BRAF V600E mutation and sensitizes them to the BRAF inhibitor vemurafenib,” *Brazilian Journal of Pharmacognosy*, vol. 28, no. 4, pp. 457–467, 2018.
- [35] M. Gao, F. Dang, and C. Deng, “ $\beta$ -Cryptoxanthin induced anti-proliferation and apoptosis by G0/G1 arrest and AMPK signal inactivation in gastric cancer,” *European Journal of Pharmacology*, vol. 859, p. 172528, 2019.
- [36] Y. S. Kim, X. Gong, L. P. Rubin, S. W. Choi, and Y. Kim, “ $\beta$ -Carotene 15,15'-oxygenase inhibits cancer cell stemness and metastasis by regulating differentiation-related miRNAs in human neuroblastoma,” *The Journal of Nutritional Biochemistry*, vol. 69, pp. 31–43, 2019.
- [37] A. Abraham, A. J. Kattoor, T. Saldeen, and J. L. Mehta, “Vitamin E and its anticancer effects,” *Critical Reviews in Food Science and Nutrition*, vol. 59, no. 17, pp. 2831–2838, 2019.
- [38] J. Gyamfi, M. Eom, J. S. Koo, and J. Choi, “Multifaceted roles of interleukin-6 in adipocyte-breast cancer cell interaction,” *Translational Oncology*, vol. 11, no. 2, pp. 275–285, 2018.
- [39] Y. Guo, F. Xu, T. Lu, Z. Duan, and Z. Zhang, “Interleukin-6 signaling pathway in targeted therapy for cancer,” *Cancer Treatment Reviews*, vol. 38, no. 7, pp. 904–910, 2012.
- [40] J. Milovanović, N. Todorović-Raković, and M. Radulovic, “Interleukin-6 and interleukin-8 serum levels in prognosis of hormone-dependent breast cancer,” *Cytokine*, vol. 118, pp. 93–98, 2019.
- [41] X. Yao, J. Huang, H. Zhong et al., “Targeting interleukin-6 in inflammatory autoimmune diseases and cancers,” *Pharmacology & Therapeutics*, vol. 141, no. 2, pp. 125–139, 2014.
- [42] G. E. Abd-elrahman, O. Ahmed, E. Abdel-Reheim, and A.-H. Abdel-Hamid, “*Ulva lactuca* polysaccharides prevent Wistar rat breast carcinogenesis through the augmentation of apoptosis, enhancement of antioxidant defense system, and suppression of inflammation,” *Breast Cancer: Targets and Therapy*, vol. Volume 9, pp. 67–83, 2017.
- [43] J. Du, Y. Sun, Y. Y. Lu et al., “Berberine and evodiamine act synergistically against human breast cancer MCF-7 cells by

- inducing cell cycle arrest and apoptosis,” *Anticancer Research*, vol. 37, no. 11, pp. 6141–6151, 2017.
- [44] A. Masjedi, V. Hashemi, M. Hojjat-Farsangi et al., “The significant role of interleukin-6 and its signaling pathway in the immunopathogenesis and treatment of breast cancer,” *Bio-medicine & Pharmacotherapy*, vol. 108, no. July, pp. 1415–1424, 2018.
- [45] H. Knüpfer and R. Preiß, “Significance of interleukin-6 (IL-6) in breast cancer (review),” *Breast Cancer Research and Treatment*, vol. 102, no. 2, pp. 129–135, 2007.
- [46] N. Kumari, B. S. Dwarakanath, A. Das, and A. N. Bhatt, “Role of interleukin-6 in cancer progression and therapeutic resistance,” *Tumor Biology*, vol. 37, no. 9, pp. 11553–11572, 2016.

## Research Article

# The Phenoxyphenol Compound 4-HPPP Selectively Induces Antiproliferation Effects and Apoptosis in Human Lung Cancer Cells through Aneuployploidization and ATR DNA Repair Signaling

Wangta Liu <sup>1,2</sup>, Chang-Yi Wu,<sup>1,3</sup> Mei-Jei Lu,<sup>1</sup> Yung-Jen Chuang <sup>4</sup>, Eing-Mei Tsai <sup>5</sup>, Steve Leu,<sup>1,6</sup> I-Ling Lin,<sup>7</sup> Chih-Jan Ko <sup>8,9</sup>, Chien-Chih Chiu <sup>1,3,5,10,11</sup> and Wen-Tsan Chang <sup>10,12,13</sup>

<sup>1</sup>Department of Biotechnology, Kaohsiung Medical University, Kaohsiung 807, Taiwan

<sup>2</sup>Department of Medical Research, Kaohsiung Medical University Hospital, Kaohsiung 807, Taiwan

<sup>3</sup>Department of Biological Sciences, National Sun Yat-Sen University, Kaohsiung 804, Taiwan

<sup>4</sup>Department of Medical Science & Institute of Bioinformatics and Structural Biology, National Tsing Hua University, Hsinchu 300, Taiwan

<sup>5</sup>Graduate Institute of Medicine, College of Medicine, Kaohsiung Medical University, Kaohsiung 807, Taiwan

<sup>6</sup>Institute for Translational Research in Biomedicine, Kaohsiung Chang Gung Memorial Hospital, Kaohsiung 833, Taiwan

<sup>7</sup>Department of Medical Laboratory Science and Biotechnology, Kaohsiung Medical University, Kaohsiung 807, Taiwan

<sup>8</sup>Department of General Surgery, Changhua Christian Hospital, Changhua 500, Taiwan

<sup>9</sup>School of Medicine, Kaohsiung Medical University, Kaohsiung 807, Taiwan

<sup>10</sup>Center for Cancer Research, Kaohsiung Medical University, Kaohsiung 807, Taiwan

<sup>11</sup>Drug Development and Value Creation Research Center, Kaohsiung Medical University, Kaohsiung 807, Taiwan

<sup>12</sup>Division of General and Digestive Surgery, Department of Surgery, Kaohsiung Medical University Hospital, Kaohsiung 807, Taiwan

<sup>13</sup>Department of Surgery, School of Medicine, College of Medicine, Kaohsiung Medical University, Kaohsiung 807, Taiwan

Correspondence should be addressed to Chih-Jan Ko; 91681@cch.org.tw, Chien-Chih Chiu; cchiu@kmu.edu.tw, and Wen-Tsan Chang; wtchang@kmu.edu.tw

Received 18 February 2019; Revised 4 October 2019; Accepted 10 October 2019; Published 8 January 2020

Guest Editor: Nagendra K. Kaushik

Copyright © 2020 Wangta Liu et al. This is an open access article distributed under the Creative Commons Attribution License, which permits unrestricted use, distribution, and reproduction in any medium, provided the original work is properly cited.

Lung cancer is a leading cause of cancer death worldwide, and non-small-cell lung cancer (NSCLC) accounts for 85% of lung cancer, which is highly metastatic, leading to the poor survival rate of patients. We recently reported that 4-[4-(4-hydroxyphenoxy)phenoxy]phenol (4-HPPP), a phenoxyphenol, exerts antihepatoma effects by inducing apoptosis and autophagy. In this study, we further examined the effect of 4-HPPP and its analogs on NSCLC cells. Colony formation assays showed that 4-HPPP exerts selective cytotoxicity against NSCLC H1299 cells; furthermore, the inhibitory effect of 4-HPPP on the proliferation and migration of NSCLC cells was validated using an *in vivo* zebrafish-based tumor xenograft assay. The flow cytometry-based dichlorofluorescein diacetate (DCF-DA) assays indicated that 4-HPPP caused an increase in reactive oxygen species (ROS) in NSCLC cells, and Western blot assays showed that the major ROS scavenging enzymes superoxide dismutases- (SODs-) 1/2 were upregulated, whereas peroxidase (PRX) was downregulated. Furthermore, 4-HPPP caused both aneuploidization and the accumulation of  $\gamma$ H2AX, a sensor of DNA damage, as well as the activation of double-strand break (DSB) markers, especially Ataxia-telangiectasia-mutated and Rad3-related (ATR) in NSCLC cells. Our present work suggests that the antiproliferative effects of 4-HPPP on lung cancer cells could be due to its phenoxyphenol structure, and 4-HPPP could be a candidate molecule for treating NSCLC by modulating ROS levels and lowering the threshold of polyploidy-specific cell death in the future.

## 1. Introduction

Lung cancer has a high incidence and is the leading cause of cancer-associated deaths in both males and females [1–3]. Non-small-cell lung carcinoma (NSCLC) is the most common type of lung cancer, accounting for 80% to 85% of lung cancer, and it shows a low proliferation rate and metastatic ability. Large-cell lung carcinoma accounts for 10% to 15% of NSCLC and is poorly differentiated [4, 5]. These tumors are large peripheral masses associated with early metastases. Surgery, radiotherapy, and chemotherapy are the main treatments for lung cancer. Although chemotherapy is the most common treatment for NSCLC [2–4, 6], NSCLC usually develops acquired resistance to chemotherapy and is associated with poor prognosis and low survival rates; therefore, continued efforts are still needed to overcome these difficulties [7, 8].

Aneuploidy is frequently observed in advanced cancer cells, and previous studies reported that at least 70% of common solid cancers are aneuploidy [9–11]. Cancer cells with aneuploidy may have enhanced proliferation and the ability to adapt to external stress or may be more chemoresistant [12]. A high rate of chromosomal missegregation has been reported to cause instability of chromosomes and poor prognosis in patients with diffuse large B cell lymphoma [13]. However, hyperaneuploidy beyond a certain level can be lethal or harmful to cancer cells [14, 15]. Therefore, elevating the rates of chromosome instability, such as aneuploidization or polyploidization, thereby inducing vulnerability of cancer cells to mitotic catastrophe [16] or apoptosis [14, 17], may be a promising strategy for treating cancer.

Phenoxyphenol derivatives have been reported to possess the capacity to prevent and treat colon and prostate cancers [18, 19]. Specifically, Parsai et al. reported that 4 phenoxyphenol derivatives exerted antimetastasis and anti-inflammatory activity by possibly binding to the active site of matrix metalloproteinase- (MMP-) 9 and cyclooxygenase (COX) 2 [20]. Additionally, we previously demonstrated that synthetic phenoxyphenol 4-[2356-tetrafluoro-4-(4-hydroxyphenoxy)phenoxy]phenol (TFPP) preconditioned NSCLC to respond to the anticancer agent camptothecin possibly by lowering the threshold for initiating apoptosis [21].

More recently, we identified that the synthetic phenoxyphenol 4-[4-(4-hydroxyphenoxy)phenoxy]phenol (4-HPPP) selectively killed hepatocellular carcinoma (HCC) cells and induced significant accumulation of  $\gamma$ H2AX, a DNA damage sensor [22], through modulating autophagy and inducing apoptosis. However, the effect of 4-HPPP on other cancer cells and its underlying mechanism remain unclear.

Given the potential anti-HCC activity of 4-HPPP, we further tested whether 4-HPPP exerts inhibitory effects on NSCLC using *in vitro* and *in vivo* zebrafish-based xenograft assays. Furthermore, the possible mechanisms by which 4-HPPP induced increased reactive oxygen species (ROS) and modulated the threshold of polyploidy-specific cell death of NSCLC are discussed.

## 2. Materials and Methods

**2.1. Source of Diphenoxy Benzene Compounds.** Four diphenoxy benzene compounds, including 4-HPPP, were purchased from the Enamine Ltd. (<http://www.enamine.net>, Kyivska region, Ukraine) chemical database (REAL Database). Four diphenoxy benzene compounds were freshly dissolved in DMSO at a concentration of 10 mM and stored at  $-20^{\circ}\text{C}$ , and concentrations of 0.5, 1, 5, and  $10\ \mu\text{M}$  were used to treat cells and zebrafish.

**2.2. Cell Lines.** The human NSCLC cell line H1299 was obtained from the American Type Culture Collection (ATCC, Manassas, VA, USA), and the human bronchial epithelium cell line BEAS-2B was kindly provided by Dr. Poling-Kuo (Kaohsiung Medical University, Taiwan). All the tested cells were maintained in Dulbecco's modified Eagle's medium (DMEM)/F-12 (3:2 ratio) and supplemented with 10% fetal bovine serum (FBS), 2 mM glutamine, and antibiotics (100 units/ml penicillin and  $100\ \mu\text{g}/\text{ml}$  streptomycin) at  $37^{\circ}\text{C}$  with a humidified atmosphere of 5%  $\text{CO}_2$ .

**2.3. Reagents.** The following compounds were obtained from Gibco BRL (Gaithersburg, MD, USA): DMEM, FBS, trypan blue, penicillin G, and streptomycin. Dimethyl sulfoxide (DMSO), paraformaldehyde (#P6148), ribonuclease A (RNase A, #R-4642), and propidium iodide (PI) were purchased from Sigma-Aldrich (St. Louis, MO, USA). An annexin V-fluorescein isothiocyanate (FITC) staining kit was purchased from Strong Biotech (#AVK050, Taipei, Taiwan). 4-[3-(4-iodophenyl)-2-(4-nitrophenyl)-2H-5-tetrazolo]-1,3-benzenedisulphonate (WST-1) was purchased from Takara Biomedicals (#MK400, Otsu, Japan). Antibodies against  $\gamma$ H2AX (#sc-101696), phosphorylated Akt (Ser<sup>473</sup>, #sc-7985-R), phospho-ATR (#sc-109912), and phospho-ATM (#sc-47739) proteins were purchased from Santa Cruz Biotechnology (Santa Cruz, CA, USA). Phospho-Akt (Thr<sup>450</sup>, #3188-1) was purchased from Epitomics (Burlingame, CA, USA). Akt1 (#ab32505) was purchased from Abcam (Cambridge, UK). Bcl-2 (#GTX100064), peroxidase (PRX1) (#GTX101705), superoxide dismutase 1 (SOD1) (#GTX100659), SOD2 (#GTX116093), and glyceraldehyde-3-phosphate dehydrogenase (GAPDH) (#GTX627408) were purchased from GeneTex (Irvine, CA, USA). DNA-dependent protein kinase (DNA-PK) (#556456) was purchased from BD Pharmingen™ (San Jose, CA, USA). Horseradish peroxidase- (HRP-) conjugated secondary antibodies (#20102 for goat anti-mouse IgG and #20202 for goat anti-rabbit IgG) were purchased from Leadgene Biomedical Inc., Tainan, Taiwan. Fluorescein isothiocyanate- (FITC-) conjugated secondary antibodies (#GTX26816 for goat anti-mouse IgG and #GTX26798 for goat anti-rabbit IgG) were purchased from GeneTex.

**2.4. Colony Formation Assay.** A total of  $1 \times 10^2$  H1299 cells were seeded onto a 6-well plate and then incubated for 24 h. The cells were treated with four diphenoxy benzene compounds at different concentrations (0, 0.5, 1, 5, and  $10\ \mu\text{M}$ ). After 14 days of incubation, the cell colonies were fixed in glutaraldehyde and stained with crystal violet (1%

w/v; Merck, #1408, Darmstadt, Germany) for 1 h. The diameter of the colonies was determined by Image-Pro Plus software (Media Cybernetics, Maryland, USA).

**2.5. Cell Viability Assay.** Cell viability was assessed by a WST-1 assay as described previously. Briefly,  $1 \times 10^3$  cells/well were seeded on a 96-well plate (tissue culture grade, flat bottom) in a final volume of  $100 \mu\text{l}$ /well culture medium in a humidified atmosphere ( $37^\circ\text{C}$ , 5%  $\text{CO}_2$ ); after 24 h, the cells were treated with different concentrations of Akt-target compounds (0, 0.5, 1, 5, and  $10 \mu\text{M}$ ) and cultured for 48 h. Next,  $10 \mu\text{l}$ /well WST-1 reagent was added to each well, and cells were incubated for 30 minutes in a humidified atmosphere ( $37^\circ\text{C}$ , 5%  $\text{CO}_2$ ). The absorbance of the samples was measured at 450 nm against the background of a blank control using a microplate (ELISA) reader (Multiskan Ascent 354 microplate reader, Thermo Fisher Scientific, Rockford, IL, USA).

**2.6. Cell Cycle Distribution Assay.** A total of  $2 \times 10^5$  cells were seeded on a 12-well plate. After 24 h, different concentrations of Akt-targeting compounds (0, 0.5, 1, 5, and  $10 \mu\text{M}$ ) were treated for 48, 72, and 96 h. The supernatant and cells were collected in a 1.5 ml tube, washed with PBS, fixed with 70% ethanol, and stored at  $-20^\circ\text{C}$  for at least two hours. The ethanol was then removed, and the samples were washed with PBS and treated with Ribonuclease (RNase) A in  $100 \mu\text{l}$  PBS ( $40 \mu\text{g}/\text{ml}$ ) for 30 minutes. The RNase A was removed and washed with PBS, and the samples were treated with  $20 \mu\text{g}/\text{ml}$  PI in PBS. The cells were analyzed by flow cytometry (FACSCalibur, BD Biosciences, San Jose, CA, USA) using FlowJo 7.5.5 software (Tree Star, Inc., San Carlos, CA).

**2.7. Assessment of Apoptosis.** To examine the apoptosis-inducing potential of 4-HPPP in H1299 cells, annexin V/PI double staining was performed to detect the externalization of phosphatidylserine (PS). In brief,  $2 \times 10^5$  cells were seeded onto 12-well plates and treated with or without 4-HPPP for 48 h and 72 h. Subsequently, the cells were harvested and stained with the annexin V/PI kit (Strong Biotech) according to the manufacturer's instructions. Cells were analyzed by flow cytometry (FACSCalibur) using FlowJo v7.5.5 software (Tree Star, Inc.).

**2.8. Intracellular ROS Detection Assay.** The amount of endogenous  $\text{H}_2\text{O}_2$  was detected through an oxidation-sensitive fluorescence dye 2',7'-dichlorofluorescein diacetate (DCF-DA). DCF-DA is able to penetrate the cell membrane. While entering the cell, it is cleaved and oxidized by  $\text{H}_2\text{O}_2$  in cells, forming a DCF product with green fluorescence at wavelengths between 488 and 530 nm [23–26]. Briefly,  $2 \times 10^5$  cells were seeded on a 12-well plate and treated with or without 4-HPPP for 24 h and 48 h. Afterward, cells were treated with different concentrations of 4-HPPP and its analogs (from 0.5 to  $10 \mu\text{M}$ ) for 24 h and 48 h. The supernatants were removed and washed with PBS, followed by the addition of  $0.1 \mu\text{M}$  DCF-DA (2',7'-dichlorofluorescein diacetate) (Sigma-Aldrich, St. Louis, Missouri, USA) to the 12-well plates for 30 minutes at  $37^\circ\text{C}$ . Then, the DCF-DA was

removed, and the cells were washed with PBS. Cells were collected in 1.5 ml tubes and analyzed by flow cytometry (FACSCalibur) using FlowJo v7.5.5.

**2.9. Cytometric Assessment of Protein Phosphorylation.** DNA damage was analyzed in H1299 cells after 4-HPPP treatment by a flow cytometry-based assay to detect the activation of  $\gamma\text{H2AX}$ , phosphor-ATM, phosphor-ATR, and DNA-PK in cells [27]. A total of  $2 \times 10^5$  cells were seeded on a 12-well plate and treated with or without 4-HPPP. After 24 h, cells were treated with the indicated concentrations (0, 0.5, 1, 5, and  $10 \mu\text{M}$ ) of 4-HPPP. Cells were harvested and washed with PBS and fixed with 70% ethanol at  $-20^\circ\text{C}$ . The alcohol was removed, and cells were washed with BSA-T-PBS (1% BSA, 0.5% Triton in PBS), followed by the addition of  $\gamma\text{H2AX}$ , phosphor-ATM, phosphor-ATR, or DNA-PK primary antibodies. The samples were then washed with BSA-T-PBS, and the fluorescent secondary antibody was added. Finally, the samples were washed with BSA-T-PBS and treated with  $20 \mu\text{g}/\text{ml}$  PI in BSA-T-PBS. The cells were analyzed by flow cytometry (FACSCalibur, BD Biosciences, San Jose, CA, USA) using FlowJo 7.5.5 software (Tree Star, Inc.).

**2.10. Western Blot Analysis.** Western blotting assays were conducted as described previously [28]. Briefly, the cells were harvested and lysed. Lysates were centrifuged, and the protein lysate concentrations were determined using a Pierce™ bicinchoninic acid (BCA) protein assay kit (#23225, Thermo Scientific Pierce Protein Research, Rockford, IL, USA). Equal amounts of protein ( $20 \mu\text{g}$ ) were separated by SDS-polyacrylamide gel electrophoresis (SDS-PAGE) and then electrotransferred to a  $0.2 \mu\text{m}$  polyvinylidene difluoride (PVDF) membrane (Pall, FL, USA). The PVDF membrane was blocked with 5% nonfat milk and sequentially incubated with primary and secondary antibodies against specific proteins. The signal intensities were detected using an enhanced chemiluminescence (ECL) detection kit (Amersham, Piscataway, NJ, USA).

**2.11. Cellular Motility Assessment.** The cellular motility was determined using Boyden's transwell assay. Briefly, H1299 cells were seeded on a transwell insert with  $8 \mu\text{m}$  pore polycarbonate filters (Greiner Bio-One, Frickenhausen, Germany), and the lower well contained medium with 10% FBS without or with the indicated concentrations of 4-HPPP for 18 h. Cells on the bottom surface of the filters were paraformaldehyde-fixed and Giemsa-stained; then, all cells were counted under a microscope (Nikon Eclipse TE2000-U, Tokyo, Japan). The experiment was performed in triplicate, and the results of three independent experiments are presented as the mean  $\pm$  SD.

**2.12. Zebrafish Husbandry.** Adult  $Tg(\text{Flil}:GFP)^{y1}$  zebrafish were provided by the Zebrafish International Resource Center (ZIRC), Taiwan Zebrafish Core at National Health Institutes and Tsing Hua University (TZeTH), Hsinchu, Taiwan (<http://icob.sinica.edu.tw/tzcas/fishlineszeth.html>). Zebrafish were maintained in a 14 h light/10 h dark cycle at  $28^\circ\text{C}$ .

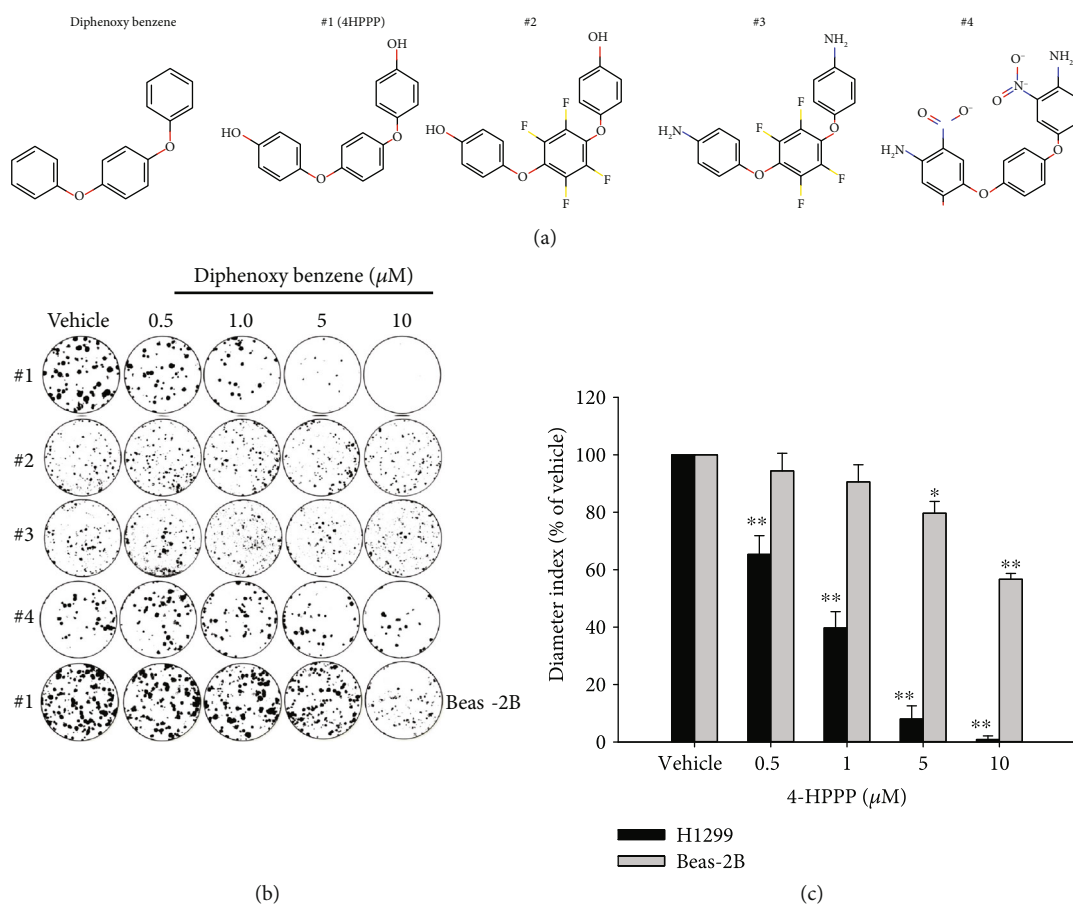


FIGURE 1: The inhibitory effect of compounds on the long-term proliferation of NSCLC cells. NSCLC H1299 cells and BEAS-2B human bronchial epithelial cells were treated with the indicated concentrations (from 0.5 to 10  $\mu\text{M}$ ) of tested compounds for 14 days. Afterward, the cells were paraformaldehyde-fixed and stained with crystal violet. (a) Chemical structures of 4-HPPP and its structural analogs. (b) Representative results of the colony formation of H1299 and BEAS-2B cells following compound treatment. (c) The quantitative results of (b) were statistically analyzed with one-way ANOVA. \* $p < 0.05$ ; \*\* $p < 0.001$ . Vehicle control vs. 4-HPPP treatments. #1: 4-HPPP; #2: 4-[2356-tetrafluoro-4-(4-hydroxyphenoxy)phenoxy]phenol; #3: 4-[4-(4-aminophenoxy)-2356-tetrafluorophenoxy]aniline; #4: 4-[4-(4-amino-3-nitrophenoxy)phenoxy]-2-nitroaniline.

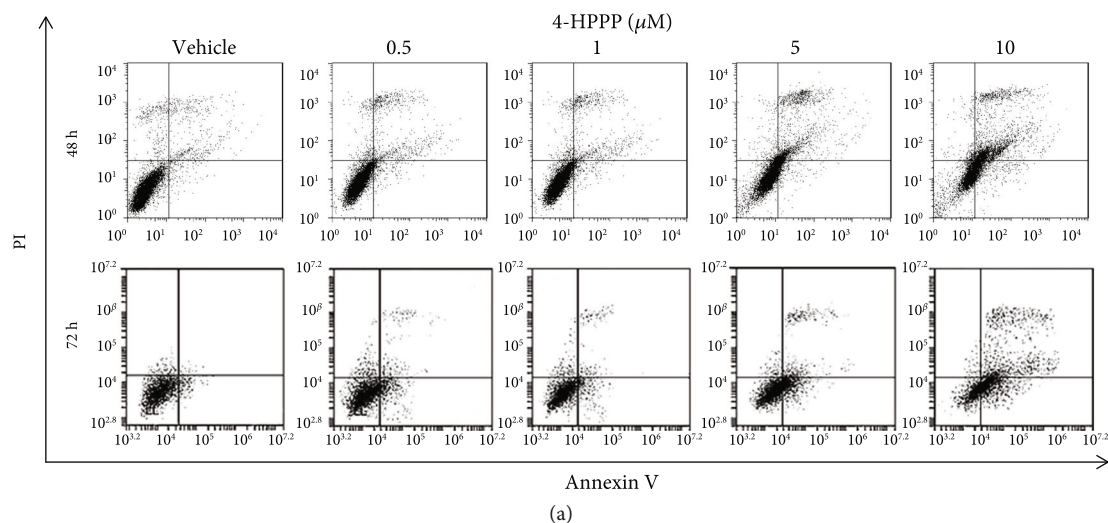
**2.13. Toxicity in Zebrafish.** Before the xenograft assay, the toxicity of 4-HPPP in zebrafish was tested by exposing zebrafish larvae at 2 days postfertilization (dpf) to 4-HPPP for 48 h. As toxicological endpoints, the images of abnormal larvae were recorded and calculated after 24 and 48 h of exposure.

**2.14. Zebrafish Xenograft.** To further validate the antitumor effect of 4-HPPP, we transfected the plasmid pDsRed-Express-C1 (Clontech, Mountain View, CA, USA) into human tumor cells for tracking the xenografted cells by fluorescence microscopy. The zebrafish-based xenograft assay was performed according to our previous study with minor modifications [29]. Briefly, 48 h postfertilization (hpf) zebrafish larvae were anesthetized with 0.01% tricaine and transplanted with approximately 50 lung cancer cells per larva by microinjection. The larvae were incubated in water with 4-HPPP for 24 h and 48 h postinjection. Afterward, images were captured with an inverted fluorescence microscope (Nikon Eclipse TE2000-U, Tokyo, Japan).

**2.15. Statistical Analysis.** Differences between 4-HPPP- and DMSO- (as vehicle control) treated cells were analyzed in at least triplicate experiments. The differences were analyzed by one-way analysis of variance (ANOVA) with  $p < 0.05$  considered significant. For the *in vivo* zebrafish xenograft assay, the metastasis potential was assessed by Fisher's exact test according to the previous study of Tang et al. [30].

### 3. Results

**3.1. 4-HPPP Reduces Colony Formation Capacity in NSCLC.** Because 4-HPPP also belongs to the diphenoxy benzene family, we were interested whether other diphenoxy benzene compounds with different modifications could have cytotoxicity effects similar to those of 4-HPPP against cancer cells; the diphenoxy benzene compounds were obtained from the chemical company Enamine Ltd. (<https://enamine.net/>) and predicted to have Akt-targeting effects according to the bioinformatics approaches of Enamine Ltd. (Figure 1(a)). The results of the WST-1 assay showed that 4-HPPP moderately inhibited cell viability, but not in a dose-dependent



		4-HPPP ( $\mu\text{M}$ )				
		Vehicle	0.5	1	5	10
48 h	Necrosis	3.32 $\pm$ 0.37	2.89 $\pm$ 0.14	2.5 $\pm$ 0.19	3.39 $\pm$ 0.19	2.52 $\pm$ 0.21
	Late apoptosis	6.10 $\pm$ 0.09	8.10 $\pm$ 0.01*	12.23 $\pm$ 0.38**	20.1 $\pm$ 0.1 C*	31.57 $\pm$ 0.29**
	Early apoptosis	1.64 $\pm$ 0.13	3.20 $\pm$ 0.21	3.38 $\pm$ 0.14	8.41 $\pm$ 0.28**	22 $\pm$ 1.04**
	Health	88.93 $\pm$ 1.24	85.8 $\pm$ 0.10*	81.87 $\pm$ 0.38**	68.13 $\pm$ 0.31**	43.9 $\pm$ 1.44**
72 h	Necrosis	6.7 $\pm$ 0.28	6.95 $\pm$ 0.7	6.4 $\pm$ 0.28	4.55 $\pm$ 0.64*	1.55 $\pm$ 0.64**
	Late apoptosis	3.5 $\pm$ 0.42	7.2 $\pm$ 0.14	7.75 $\pm$ 1.2	15.05 $\pm$ 1.48*	28.65 $\pm$ 3.04**
	Early apoptosis	5.9 $\pm$ 0.14	7.55 $\pm$ 0.35	13.8 $\pm$ 0.85*	21.5 $\pm$ 3.39**	41.7 $\pm$ 1.56**
	Health	83.9 $\pm$ 0.42	78.3 $\pm$ 0.14	72.05 $\pm$ 2.33**	58.95 $\pm$ 4.31**	28.1 $\pm$ 3.96**

(b)

FIGURE 2: 4-HPPP induces apoptosis of NSCLC H1299 cells. The apoptosis induced by 4-HPPP was assessed using flow cytometry-based annexin V-PI staining. (a) H1299 cells were treated with 4-HPPP for the indicated time course. (b) The quantitative results of (a).  $p < 0.05$  (vehicle vs. 4-HPPP treatment) was considered statistically significant. \* $p < 0.05$ ; \*\* $p < 0.001$ .

manner (Figure S1). We then examined whether 4-HPPP reduced the clonogenicity of NSCLC cells, and a colony formation assay was conducted (Figure 1(b)). Interestingly, the results showed that 4-HPPP dramatically reduced the clonogenicity capacity of H1299 cells in a dose-dependent manner, suggesting a long-term inhibitory effect of 4-HPPP on the clonogenic capacity of NSCLC cells compared to that of other diphenoxy benzene compounds. Importantly, only a slight reduction in colony formation of 4-HPPP-treated normal lung bronchia BEAS-2B cells was observed (Figures 1(b) and 1(c)) compared with NSCLC cells, showing that the inhibitory effects of 4-HPPP were selective to NSCLC cells rather than normal lung cells.

**3.2. 4-HPPP Induces Apoptosis in NSCLC Cells.** As shown in Figures 2(a) and 2(b), the apoptosis of H1299 cells signifi-

cantly increased at treatment concentrations of 5 and 10  $\mu\text{M}$ . In addition, the Western blot results revealed that after 4-HPPP treatment, both the phosphorylation of pro-survival p-Akt (Ser<sup>473</sup> and Thr<sup>450</sup>) and its downstream protein Bcl-2 were downregulated, whereas there were no significant changes in total Akt protein (Figure 3), suggesting that 4-HPPP regulates the activity of Akt rather than its protein level.

**3.3. 4-HPPP Induces Polyploidy in NSCLC Cell Lines.** To examine whether 4-HPPP induced NSCLC cell cycle disturbances, H1299 cells were treated with different concentrations of 4-HPPP (from 0.5 to 10  $\mu\text{M}$ ) for 48 and 72 h. The cells were then stained with PI to assess cell cycle distribution. The results showed that treatment with higher concentrations (5 and 10  $\mu\text{M}$ ) of 4-HPPP for 48 h significantly



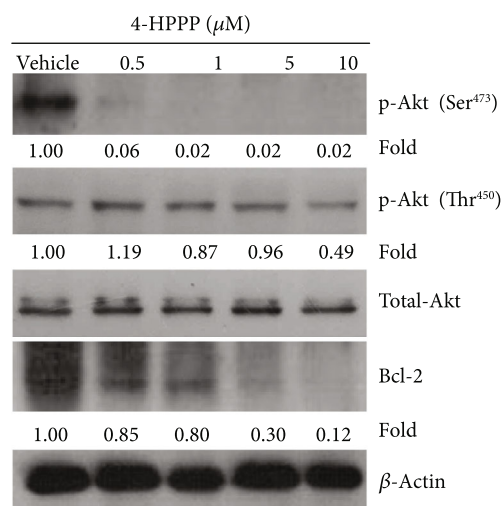


FIGURE 3: The effect of 4-HPPP on Akt phosphorylation changes in NSCLC cells. The phosphorylation changes at serine<sup>473</sup> and threonine<sup>450</sup> of Akt along with the prosurvival factor Bcl-2 were assessed using the Western blotting assay.  $\beta$ -Actin was used as an internal control to ensure equal loading.

increased polyploidy or aneuploidy. After treatment for 72 h, the population of sub-G<sub>1</sub>, a hallmark of apoptosis, dramatically accumulated, suggesting that the induction of apoptosis by 4-HPPP is both dose- and time-dependent (Figures 4(a) and 4(b)).

**3.4. 4-HPPP Induces DNA Damage of H1299.** DNA damage is the major cause of aneuploidy or polyploidy in cancer cells [31, 32]. To determine whether 4-HPPP caused aneuploidy or polyploidy or triggered apoptosis in NSCLC cells, we conducted flow cytometry-based immunostaining and Western blotting to detect changes in the DNA damage sensor  $\gamma$ H2AX (the phosphorylated form of the histone protein H2AX) [33]. The results showed that the fold of  $\gamma$ H2AX-activated cells was increased by increasing the 4-HPPP concentration (Figures 5(a) and 5(b)). Consistently, the level of  $\gamma$ H2AX was increased in a dose-dependent manner at 48 h post-4-HPPP treatment (Figure 5(c)). We also evaluated the distributions of foci of  $\gamma$ H2AX in 4-HPPP-treated H1299 cells using immunofluorescence staining. Significant accumulation of  $\gamma$ H2AX foci was detected in cells treated with 5 and 10  $\mu\text{M}$  4-HPPP (Figure 5(d)), indicating that 4-HPPP induced DNA damage, especially DNA double-strand breaks (DSBs), in H1299 cells.

To study whether markers of DNA damage were activated in 4-HPPP-treated cells, phosphor-ATM, phosphor-ATR, and DNA-PK were detected by flow cytometry. As shown in Figures 6(a) and 6(b), significantly more phosphor-ATR-positive cells were found than both ATM- and DNA-PK-positive cells, which revealed that 4-HPPP causes DNA damage, leading to ATR activation.

**3.5. 4-HPPP Increased Hydrogen Peroxide Production.** To determine whether 4-HPPP induces apoptosis through ROS, we detected intracellular hydrogen peroxide ( $\text{H}_2\text{O}_2$ ), one of the major types of intracellular ROS, using flow

cytometer-based DCF-DA staining. The results showed that 4-HPPP caused a dose-dependent increase in  $\text{H}_2\text{O}_2$  (Figures 7(a) and 7(b)). Furthermore, Western blotting showed that the protein level of SOD2 was increased; in contrast, the peroxidase PRX1 was significantly decreased in a dose-dependent manner following 4-HPPP treatment (Figures 7(c) and 7(d)).

**3.6. 4-HPPP Attenuates the Motility of NSCLC Cells.** Figures 8(a) and 8(b) reveal that the motility of H1299 cells treated with the indicated concentrations of 4-HPPP at 0, 0.5, 1, 5, and 10  $\mu\text{M}$  was  $100 \pm 2.00$ ,  $75.85 \pm 5.99$ ,  $69.48 \pm 4.58$ ,  $43.22 \pm 3.07\%$ , and  $31.48 \pm 6.54\%$  ( $n = 3$ ), respectively, indicating that 4-HPPP attenuates motility, an index of metastasis of cancer in H1299 cells.

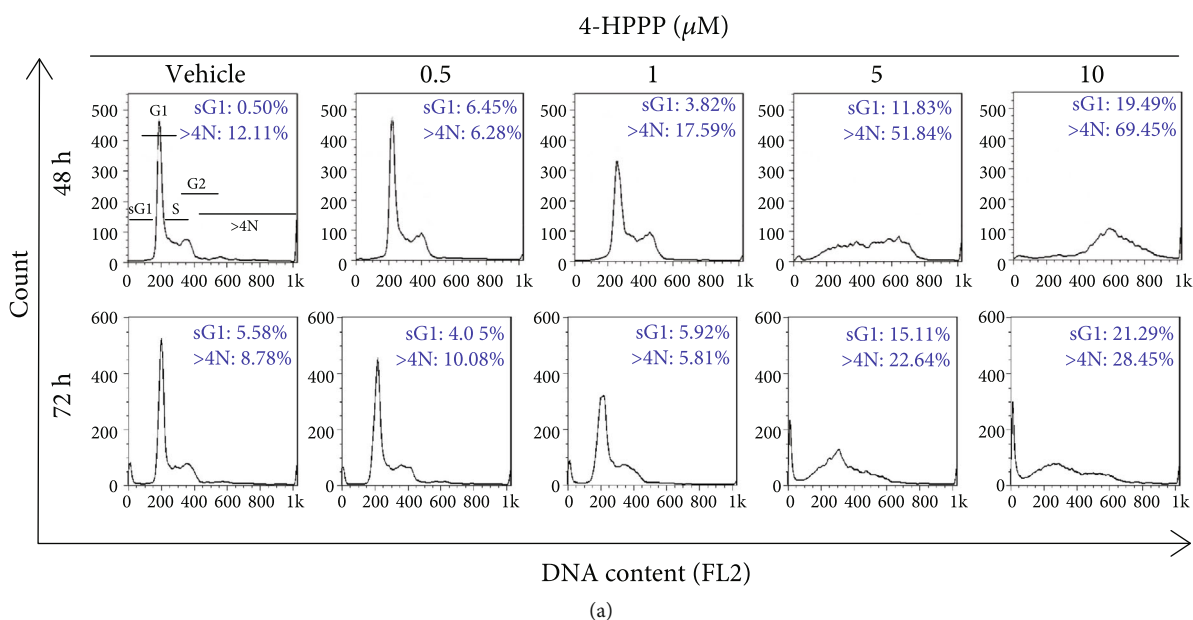
**3.7. 4-HPPP Inhibits H1299 Cell Proliferation and Migration in Zebrafish Xenografts.** Before evaluating the anticancer activity of 4-HPPP, we examined whether 4-HPPP causes side effects in zebrafish. The results showed that the survival rates of zebrafish larvae did not change below 1  $\mu\text{M}$  4-HPPP. However, the survival rate was only 42.2% after treatment with 5  $\mu\text{M}$  4-HPPP for 48 h (Figure 9(a)). The higher concentrations of 5  $\mu\text{M}$  and 10  $\mu\text{M}$  4-HPPP caused slight bending of the body axes and edema in the zebrafish larvae (Figure 9(b)), indicating that a high concentration of 4-HPPP induced moderate side effects in zebrafish.

To further examine the anticancer effect of 4-HPPP *in vivo*, we generated a lung cancer xenograft zebrafish model by microinjection of fluorescent H1299 cells. Red fluorescent reporter H1299 cells were obtained by transfection with the pDsRed-Express-C1 vector (Figure 9(c)). Fluorescent images at 48 h posttreatment revealed a reduction in tumor volume and migration in 4-HPPP-treated xenografted H1299 cells (Figures 9(d) and 9(e)).

## 4. Discussion

It has been reported that most NSCLC cells with mutations and deletions of the tumor suppressor p53 are insensitive to anticancer drugs such as cisplatin [34]. In contrast, Akt signaling has been reported to be frequently overexpressed or dysregulated in NSCLC, resulting in the activation of the PI3K/Akt pathway, which inhibits apoptosis and is correlated with radioresistance [35]. Furthermore, Akt activity increases as cells progress through the G<sub>2</sub>/M phase [36]. Given that both p53 mutation and Akt overexpression are closely correlated with the chemoresistance and prognosis of NSCLC patients, Akt may play a pivotal role in NSCLC pathogenesis and, thus, represents an ideal target for therapeutic intervention.

We previously demonstrated that the synthetic phenoxyphenol 4-[4-(4-hydroxyphenoxy)phenoxy]phenol (4-HPPP) inhibits cellular proliferation and induces apoptosis in hepatocellular carcinoma cells [22]. In this study, we used H1299 cells, which carry null-p53 and constitutively active Akt, as a cell model to further examine the effect of 4-HPPP on NSCLC cells. First, we examined the effects of 4-HPPP and three structurally similar compounds (diphenoxy benzenes)



(a)

		4-HPPP ( $\mu\text{M}$ )				
		Vehicle	0.5	1	5	10
48 h	% phase					
	G0/G1	57.31 $\pm$ 0.09	46.21 $\pm$ 1.3	11.41 $\pm$ 1.35 **	9.49 $\pm$ 0.34 **	2.34 $\pm$ 0.12 **
	S	12.76 $\pm$ 0.09	22.84 $\pm$ 0.37 **	47.57 $\pm$ 1.03 **	12.44 $\pm$ 0.62	3.62 $\pm$ 0.21 **
	G2/M	17.33 $\pm$ 0.04	18.22 $\pm$ 0.24 *	19.61 $\pm$ 0.06 **	14.39 $\pm$ 0.28 **	5.09 $\pm$ 0.33 **
	Sub-G1	0.50 $\pm$ 0.05	6.45 $\pm$ 0.3 **	3.82 $\pm$ 0.06 **	11.83 $\pm$ 0.25 **	19.49 $\pm$ 0.33 **
>4N	12.11 $\pm$ 0.04	6.28 $\pm$ 0.87 **	17.59 $\pm$ 0.53 **	51.84 $\pm$ 0.65 **	69.45 $\pm$ 0.71 **	
72 h	G0/G1	56.51 $\pm$ 0.37	51.8 $\pm$ 0.97 *	54.62 $\pm$ 0.13	16.91 $\pm$ 0.77 **	17.35 $\pm$ 0.54 **
	S	7.86 $\pm$ 0.19	9.46 $\pm$ 0.2 *	10.06 $\pm$ 0.44 *	13.61 $\pm$ 0.11 **	9.75 $\pm$ 0.59 *
	G2/M	21.26 $\pm$ 0.87	24.62 $\pm$ 0.81 *	23.6 $\pm$ 0.53	31.73 $\pm$ 0.68 **	23.17 $\pm$ 0.6
	Sub-G1	5.58 $\pm$ 0.2	4.05 $\pm$ 0.16 *	5.92 $\pm$ 0.34	15.11 $\pm$ 0.07 **	21.29 $\pm$ 0.33 **
	>4N	8.78 $\pm$ 0.28	10.08 $\pm$ 0.39	5.81 $\pm$ 0.06 *	22.64 $\pm$ 0.17 **	28.45 $\pm$ 0.97 **

(b)

FIGURE 4: The effect of 4-HPPP on cell cycle progression. (a) The accumulation of sub-G<sub>1</sub> and aneuploidy (N>4N) in NSCLC cells. H1299 cells were seeded and treated with different concentrations of 4-HPPP for 48 and 72 h. The treated cells were 70% ethanol-fixed and PI-stained and then subjected to a cell cycle distribution analysis by flow cytometry. Changes in cell cycle progression, the sub-G<sub>1</sub> population, and aneuploidy following 4-HPPP treatment. (b) Quantitative analysis of cell cycle progression. \* $p < 0.05$ ; \*\* $p < 0.001$ .

on the viability and clonogenicity of H1299 cells. The results showed that among the tested compounds, 4-HPPP moderately inhibited the viability of NSCLC H1299 cells at 24 h and 48 h (Figure S1(a) and (b)). However, 4-HPPP had the most potential for inhibiting the colony formation of NSCLC cells (Figure 1), suggesting the long-term inhibitory effect of 4-HPPP on NSCLC cell clonogenicity. Importantly, 4-HPPP also preferentially inhibited colony formation in H1299 cells but not in BEAS-2B normal lung cells. The results suggested that the selective inhibitory effect of 4-HPPP may be a promising treatment in the future.

Our previous study showed that 4-HPPP potentially inhibits the phosphorylation of Akt at Ser<sup>473</sup> and Thr<sup>450</sup> in HCC Huh7 cells. Consistently, our results showed that 4-

HPPP inhibited the activation of Akt in NSCLC H1299 cells (Figure 3). These observations confirmed that 4-HPPP could be a specific inhibitor of Akt, which may benefit the development of Akt-targeting drugs for treating cancer in the future.

We further assessed the cell cycle distribution after 4-HPPP treatment. The results revealed that 4-HPPP induced hyperaneuploidization of NSCLC cells in a dose-dependent manner (Figure 4). A recent study proposed that the induction of hyperaneuploidization or hyperpolyploidization can be considered beneficial for inducing the apoptosis of cancer cells that carry aneuploidy or polyploidy. For example, colorectal cancer cells with high polyploidy exhibited a positive response to cotreatment with irinotecan combined with 5-fluorouracil in a clinical trial [37].

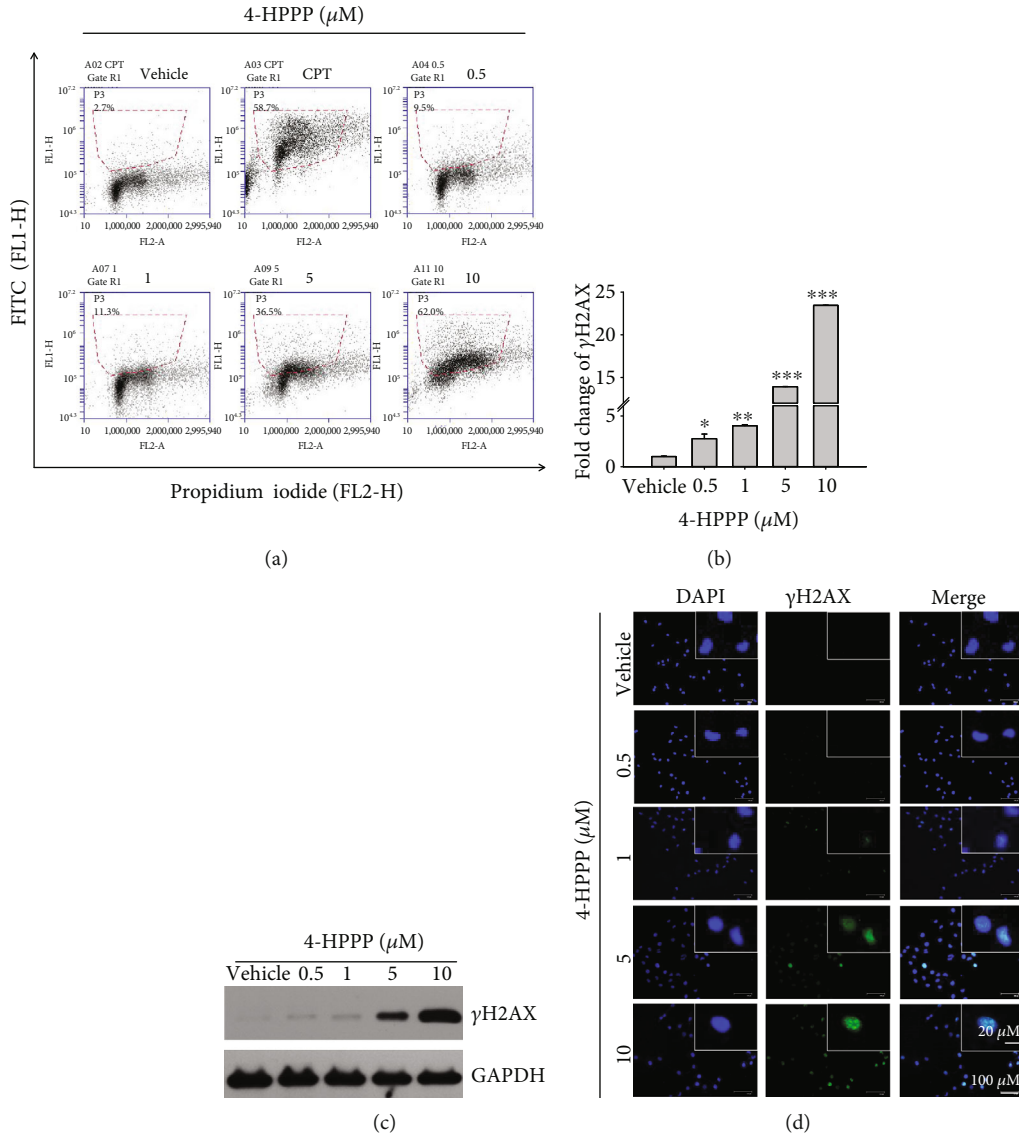
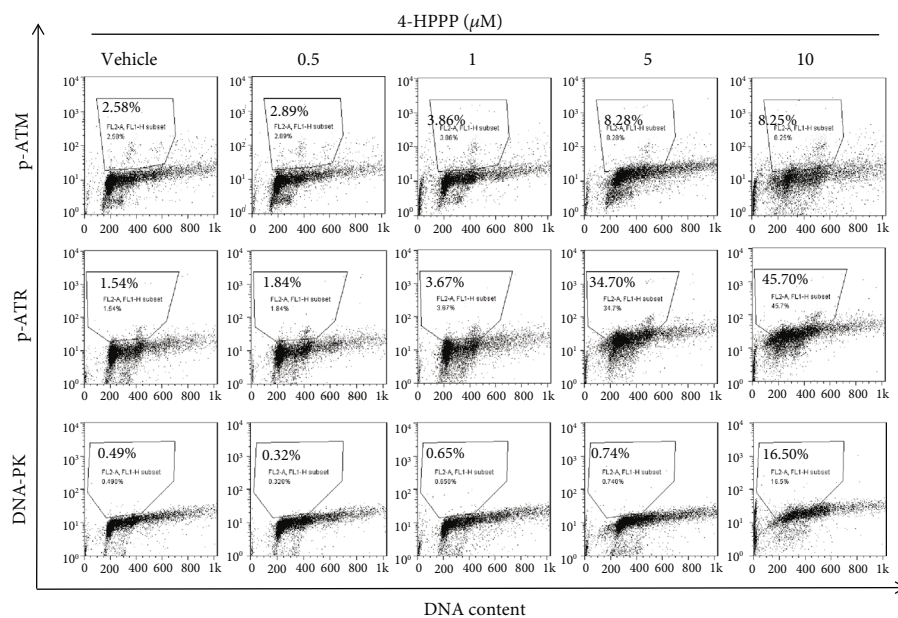


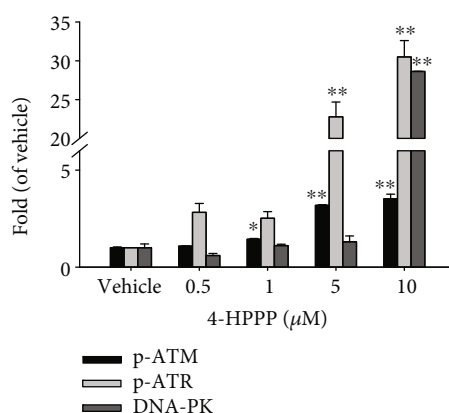
FIGURE 5: Assessment of DNA damage induced by 4-HPPP. (a) H1299 cells were administered the indicated concentrations of 4-HPPP for 48 h. Afterward, 4-HPPP-induced DNA damage was detected using a flow cytometry-based  $\gamma$ H2AX detection assay. The green fluorescence of FITC (FL1) indicates the  $\gamma$ H2AX-positive population (R1 region). The data showed that 4-HPPP increased the phosphorylation of  $\gamma$ H2AX, a marker of DNA damage, in a dose-responsive manner. (b) Quantification analysis of (a).  $\gamma$ H2AX was observed in H1299 cells following 4-HPPP treatment at concentrations from 0.5 to 10  $\mu$ M by the Western blotting assay (c) and immunofluorescence assay (d). The data are presented as the mean  $\pm$  SD. \* $p$  < 0.05; \*\* $p$  < 0.005; \*\*\* $p$  < 0.001. Scale bar: 100  $\mu$ m.

We noted that 4-HPPP treatment caused S-phase cell accumulation at the 1  $\mu$ M concentration, but this accumulation was decreased at 5 and 10  $\mu$ M; moreover, the level of aneuploidy increased in a dose-dependent manner, suggesting the correlation of S-phase arrest and high-grade aneuploidy/polyploidization. Liu et al.'s work reported that a topoisomerase I inhibitor, a synthetic analog of camptothecin TCH-1030, caused S-phase arrest and finally resulted in polyploidization and sequentially apoptosis in a panel of breast cancer cell lines [38]. Their results suggested that TCH-1030 induces DNA damage and S-phase cell cycle arrest by impairing mitosis and cytokinesis, eventually leading to polyploidization (>4N) and apoptosis.

Another study also reported the correlation of sub-G<sub>1</sub> cell cycle arrest and hyperpolyploidization. For example, Karna et al.'s work suggested that the novel microtubule-modulating noscapinoid EM011 dysregulates cell division and the asymmetric distribution of DNA, resulting in both high-grade polyploidy and sub-G<sub>1</sub> cell accumulation, eventually causing tumor suppression and promoting death in breast cancer MCF-7 cells [39]. Similarly, our previous work revealed the antimicrotubule effect of 4-HPPP in HCC cells [22]; we noted that at 48 h, the 5  $\mu$ M and 10  $\mu$ M doses suddenly increased the number of cells in the sub-G<sub>1</sub> phase, and aneuploidy increased simultaneously, suggesting that the accumulation of sub-G<sub>1</sub> cells, a marker of apoptosis,



(a)



(b)

FIGURE 6: 4-HPPP-induced activation of DNA damage markers in NSCLC cells. (a) H1299 cells were seeded and treated with 4-HPPP for 48 h. Afterward, the DNA damage induced by 4-HPPP was assessed by flow cytometry. The markers of DNA damage, including phosphor-ATR, phosphor-ATM, and DNA-PK, were determined. The results showed that 4-HPPP increased the phosphorylation of ATR and ATM and the protein level of DNA-PK in a dose-responsive manner. (b) The quantitative results of (a). \* $p < 0.05$ ; \*\* $p < 0.001$ .

might be caused by 4-HPPP-induced excess aneuploidization in H1299 cells. We further confirmed that 4-HPPP induces apoptosis in H1299 cells using annexin V staining (Figure 2). Thus, the above observations provide information about the mechanism underlying the S-phase cell arrest and sub- $G_1$  cell increase induced by 4-HPPP treatment.

Earlier studies have indicated that polyploidy might be induced in cancer cells by severe DNA damage, especially DSBs [5, 6, 31, 40]. When cells are exposed to radiation or chemicals that cause DNA damage, DSBs are induced, and a subunit of histone, H2AX, is quickly phosphorylated at Ser<sup>139</sup> to form  $\gamma$ H2AX. Therefore,  $\gamma$ H2AX is considered a marker of DNA damage [8, 33]. Our previous work demonstrated that 4-HPPP induces H2AX accumulation in HCC Huh7 and Ha22T cells [22]. In this study, to determine whether 4-HPPP causes polyploidization by inducing DNA

damage in NSCLC cells, we analyzed  $\gamma$ H2AX activation following 4-HPPP treatment (Figures 5(a) and 5(b)). The level of polyploidy induced by 4-HPPP was positively correlated with the activation of  $\gamma$ H2AX in H1299 cells (Figures 5(c) and 5(d)). We also checked the activation of major DNA repair factors, including phosphor-ATM, phosphor-ATR, and DNA-PK, and the level of ATR activation was much higher than that of the other two factors following 4-HPPP treatment, suggesting that ATR may play a major role in the signaling of DNA damage (Figure 6).

Moderate levels of intracellular ROS, including hydroxyl radicals ( $\cdot$ OH), superoxide ( $O_2^-$ ), and  $H_2O_2$ , are essential for the proliferation and survival of cells [41, 42]. ROS play an important role in signal transduction related to survival, proliferation, angiogenesis, and metastasis in cancer cells [43–46]. However, excess ROS usually cause severe damage

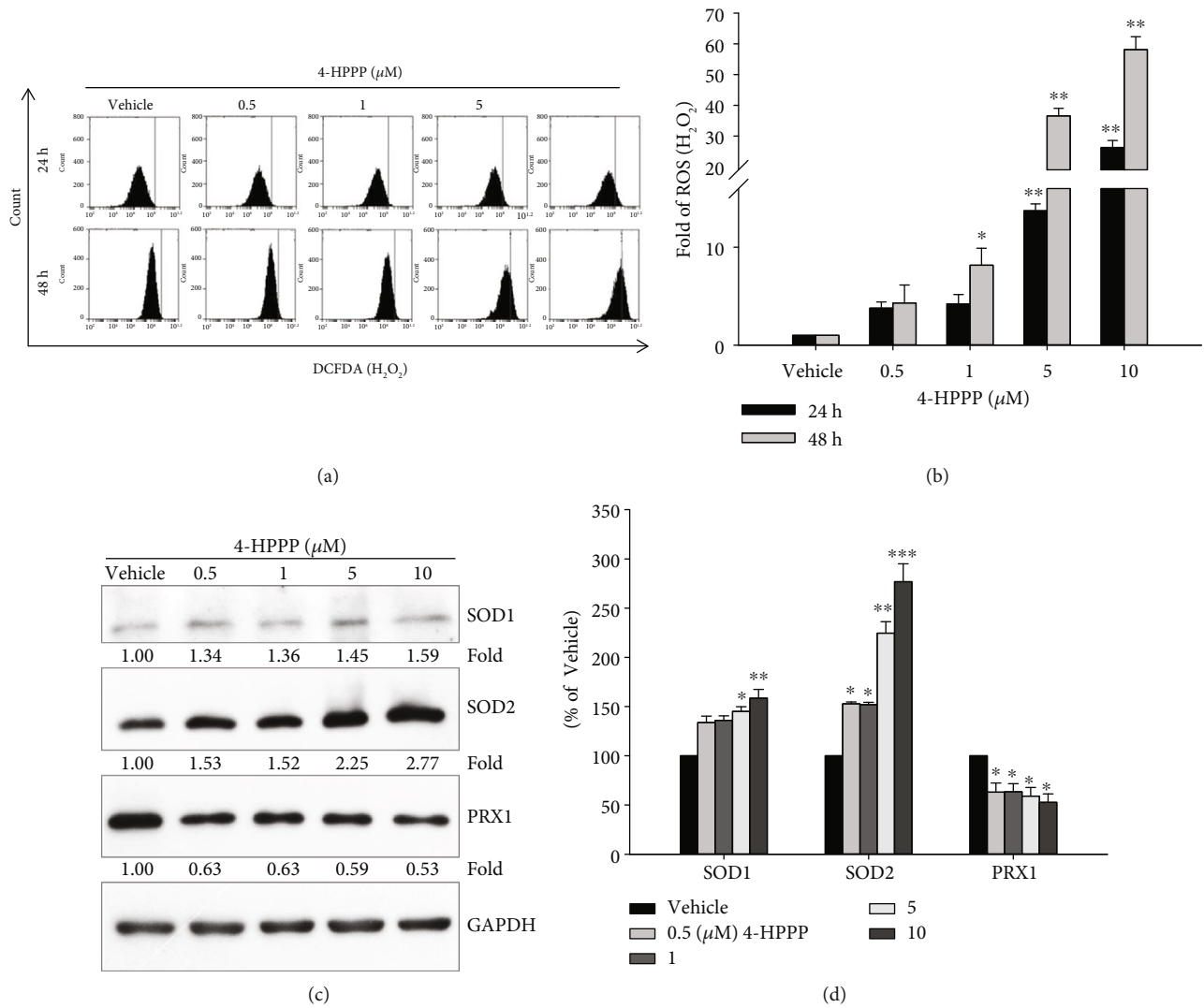


FIGURE 7: 4-HPPP-induced changes in endogenous ROS and antioxidants in NSCLC cells. (a) H1299 cells were treated with the indicated concentrations of 4-HPPP for 24 h and 48 h. Afterward, intracellular levels of ROS were measured by the flow cytometry-based DCF-DA assay described in Materials and Methods. (b) Quantitative analysis of (a). (c) Changes in endogenous antioxidants SOD1, SOD2, and PRX1 in H1299 cells following 4-HPPP treatment by Western blotting. (d) Quantitative analysis of (c). \* $p < 0.05$ ; \*\* $p < 0.01$ ; \*\*\* $p < 0.001$ .

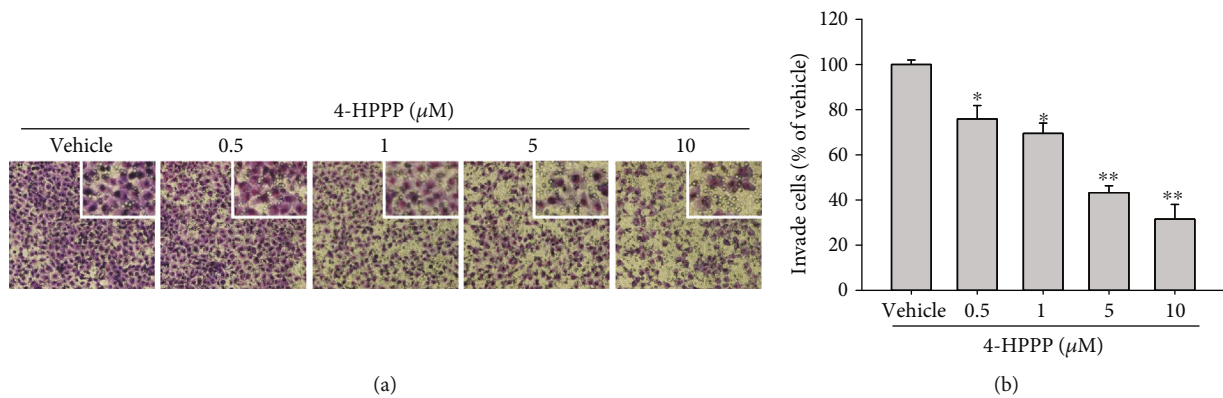
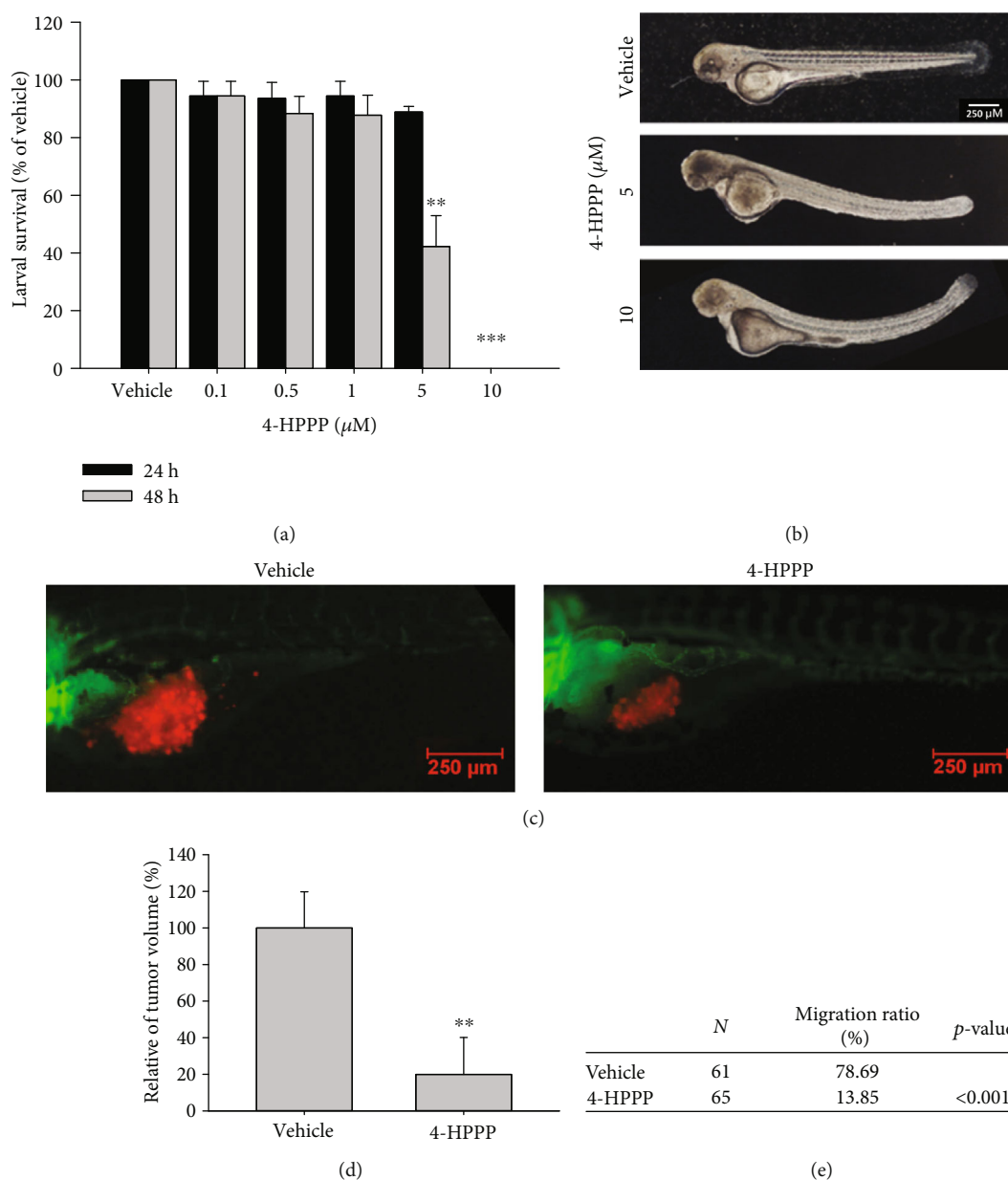


FIGURE 8: The effect of 4-HPPP on the motility of NSCLC cells. (a) H1299 cells were treated with the indicated concentrations of 4-HPPP for 18 h. Afterward, the cells were stained with 0.1% w/v Giemsa. (b) Quantitative analysis of (a). \* $p < 0.05$  and \*\* $p < 0.01$  for 4-HPPP treatments against vehicle control, respectively.



**FIGURE 9:** Effect of 4-HPPP on zebrafish-based xenografted NSCLC cells. (a) Survival rate of zebrafish larvae following 4-HPPP exposure. (b) The results showed that 5  $\mu\text{M}$  and 10  $\mu\text{M}$  4-HPPP caused body axis bending and edema in zebrafish larvae, indicating that a high concentration of 4-HPPP could cause deformation and toxicity toward zebrafish larvae. (c) The motility of xenografted H1299 cells in the yolk sac of zebrafish larvae. The intensity of red fluorescence is proportional to the xenograft tumor size. For each group, the sample size of larvae ( $N$ ) > 60. (d, e) Quantitative analysis of (c). The data are presented as the mean  $\pm$  S.D. \*\* $p$  < 0.05 and \*\*\* $p$  < 0.001 against vehicle control. (e) The statistical analysis of the migration ability of xenografted H1299 cells using Fisher's exact test.

or apoptosis of cells, and upregulating endogenous ROS has been considered to be a promising strategy for eliminating cancer cells [47–49]. Therefore, our results also demonstrated that 4-HPPP significantly increased endogenous ROS through modulating the expression of antioxidant enzymes such as SOD2 and peroxidase (Figures 7(a) and 7(b)).

Zebrafish (*Danio rerio*) is an excellent model for cancer research and drug discovery because of its rapid development and larval transparency [50–52]. Zebrafish xenografts provide a unique opportunity to monitor the tumor-induced

angiogenesis, growth, and invasiveness of xenografted tumor cells. In addition, zebrafish are also a useful tool for evaluating the effects of drugs and their side effect [22, 28, 53]. First, we evaluated the toxicity of 4-HPPP to the larvae of zebrafish; the survival rates of zebrafish larvae did not change at low concentrations of 4-HPPP (Figure 9). However, the results showed that a high concentration of 4-HPPP caused the zebrafish larval body axes to bend and develop edema, indicating that a high concentration of 4-HPPP could cause unfavorable side effects in zebrafish (Figure 9(a)); all the zebrafish larvae died at the highest concentration of 4-HPPP treatment.

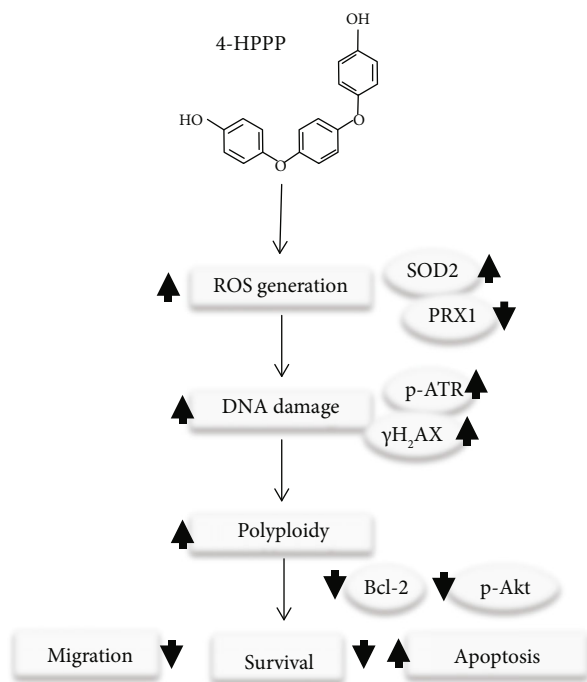


FIGURE 10: A proposed mechanism of 4-HPPP-induced antiproliferation and apoptosis in NSCLC cells through modulating the signaling of endogenous antioxidant systems, such as SOD2 and PRX1, causing DNA damage and high-grade aneuploidy. Eventually, the accumulation of DNA damage and hyperaneuploidization induce apoptosis in NSCLC cells.

The results of the *in vivo* zebrafish-based xenograft assay showed that both the tumor mass and cellular migration of xenografted H1299 cells were significantly attenuated following 4-HPPP treatment (Figures 9(c)–9(e)), which is consistent with the *in vitro* results.

Accordingly, we thus suggest that 4-HPPP, a phenoxyphenol-based compound, could lead to DNA damage accumulation and increased ROS levels, resulting in  $\gamma$ H2AX and ATR activation to induce excess aneuploidization/polyploidization, ultimately causing cell apoptosis. 4-HPPP, which also exhibits Akt-targeting properties, inhibited the activity of the phosphorylated sites of Akt, Ser<sup>473</sup> and Thr<sup>450</sup>, which are involved in both NSCLC cell proliferation and metastasis.

## 5. Conclusions

Our study demonstrated that 4-HPPP selectively inhibits the growth of NSCLC H1299 cells. We also confirmed that 4-HPPP significantly inhibits the activation of Akt but increases the levels of ROS, DNA damage, and hyperpolyploidy, finally inducing apoptosis in H1299 cells (Figure 10). In addition to its antiproliferative effects, 4-HPPP inhibits migration, a marker of metastasis in NSCLC cells; therefore, for the first time, we demonstrated the antimigration effect of 4-HPPP, which may benefit the development of antilung metastasis therapies. The potent inhibitory effect of 4-HPPP on the proliferation and metastasis of H1299 cells was validated

by an *in vivo* zebrafish-based xenograft assay. However, we also noted that a higher concentration of 4-HPPP caused body axis deformation and edema in zebrafish larvae. The structure of 4-HPPP could be further modified and optimized to reduce its side effects for further application.

## Data Availability

No data were used to support this study.

## Conflicts of Interest

The authors declare no conflicts of interest.

## Acknowledgments

This study was supported by the following grants: MOST106-2320-B-037-012, MOST106-2314-B-037-053-MY3, MOST107-2320-B-037-023, MOST107-2311-B-037-001, and MOST108-2314-B-037-051 from the Ministry of Science and Technology, Taiwan; #NSYSUKMU107-P002 and NSYSUKMU108-P021 from a National Sun Yat-sen University-KMU Joint Research Project, Taiwan; #108-CCH-KMU-002 and 108-CCH-KMU-003 from a Changhua Christian Hospital-KMU Joint Research Project, Taiwan; and KMHU106-6R36 and KMHU107-7R33 from the Kaohsiung Medical University Hospital (KMHU). We are grateful for the instrumental support for confocal microscopy, fluorescence resonance energy transfer microscopy, and flow cytometry provided by the Center for Research Resources and Development, Kaohsiung Medical University, Kaohsiung, Taiwan. We thank the Zebrafish Core Facility at Kaohsiung Medical University for the technical support.

## Supplementary Materials

The inhibitory effect of 4-HPPP and its analogs on the short-term proliferation of NSCLC cells. H1299 cells were seeded and treated with the indicated concentrations of 4-HPPP or one of its analogs for 24 h (a) and 48 h (b). #1: 4-HPPP; #2: 4-[2356-tetrafluoro-4-(4-hydroxyphenoxy)phenoxy]phenol; #3: 4-[4-(4-aminophenoxy)-2356-tetrafluorophenoxy]aniline; and #4: 452 4-[4-(4-amino-3-nitrophenoxy)phenoxy]-2-nitroaniline. \* $p < 0.05$  and  $^{\&}p < 0.001$ , 4-HPPP compound treatments against vehicle control. (*Supplementary Materials*)

## References

- [1] R. L. Siegel, K. D. Miller, and A. Jemal, "Cancer statistics, 2018," *Ca: a Cancer Journal for Clinicians*, vol. 68, no. 1, pp. 7–30, 2018.
- [2] D. S. Ettinger, W. Akerley, G. Bepler et al., "Non-small cell lung cancer," *Journal of the National Comprehensive Cancer Network*, vol. 8, no. 7, pp. 740–801, 2010.
- [3] R. Pirker and W. Minar, "Chemotherapy of advanced non-small cell lung cancer," *Frontiers of Radiation Therapy and Oncology*, vol. 42, pp. 157–163, 2010.
- [4] L. G. Collins, C. Haines, R. Perkel, and R. E. Enck, "Lung cancer: diagnosis and management," *American Family Physician*, vol. 75, no. 1, pp. 56–63, 2007.




- [5] R. Stupp, C. Monnerat, A. T. Turrisi 3rd, M. C. Perry, and S. Leyvraz, "Small cell lung cancer: state of the art and future perspectives," *Lung Cancer*, vol. 45, no. 1, pp. 105–117, 2004.
- [6] N. O'Rourke, I. F. M. Roque, N. Farre Bernado, and F. Macbeth, "Concurrent chemoradiotherapy in non-small cell lung cancer," *The Cochrane Database of Systematic Reviews*, vol. 16, no. 6, article CD002140, 2010.
- [7] T. D. Wagner and G. Y. Yang, "The role of chemotherapy and radiation in the treatment of locally advanced non-small cell lung cancer (NSCLC)," *Current Drug Targets*, vol. 11, no. 1, pp. 67–73, 2010.
- [8] S. M. Keller, S. Adak, H. Wagner et al., "A randomized trial of postoperative adjuvant therapy in patients with completely resected stage II or IIIA non-small-cell lung cancer. Eastern Cooperative Oncology Group," *The New England Journal of Medicine*, vol. 343, no. 17, pp. 1217–1222, 2000.
- [9] D. Cimini, "Merotelic kinetochore orientation, aneuploidy, and cancer," *Biochimica et Biophysica Acta (BBA)-Reviews on Cancer*, vol. 1786, no. 1, pp. 32–40, 2008.
- [10] S. F. Bakhom and D. A. Compton, "Chromosomal instability and cancer: a complex relationship with therapeutic potential," *The Journal of Clinical Investigation*, vol. 122, no. 4, pp. 1138–1143, 2012.
- [11] B. Orr, K. M. Godek, and D. Compton, "Aneuploidy," *Current Biology*, vol. 25, no. 13, pp. R538–R542, 2015.
- [12] M. Kawakami, X. Liu, and E. Dmitrovsky, "New cell cycle inhibitors target aneuploidy in cancer therapy," *Annual Review of Pharmacology and Toxicology*, vol. 59, no. 1, pp. 361–377, 2019.
- [13] S. F. Bakhom, O. V. Danilova, P. Kaur, N. B. Levy, and D. A. Compton, "Chromosomal instability substantiates poor prognosis in patients with diffuse large B-cell lymphoma," *Clinical Cancer Research*, vol. 17, no. 24, pp. 7704–7711, 2011.
- [14] A. Glassmann, C. C. Garcia, V. Janzen et al., "Staurosporine induces the generation of polyploid giant cancer cells in non-small-cell lung carcinoma A549 cells," *Analytical Cellular Pathology*, vol. 2018, Article ID 1754085, 7 pages, 2018.
- [15] A. Datta and R. M. Brosh, "New insights into DNA helicases as druggable targets for cancer therapy," *Frontiers in Molecular Biosciences*, vol. 5, no. 59, 2018.
- [16] M. Giam and G. Rancati, "Aneuploidy and chromosomal instability in cancer: a jackpot to chaos," *Cell Division*, vol. 10, no. 1, p. 3, 2015.
- [17] R. Mirzayans, B. Andrais, and D. Murray, "Roles of polyploid/multinucleated giant cancer cells in metastasis and disease relapse following anticancer treatment," *Cancers*, vol. 10, no. 4, p. 118, 2018.
- [18] M. K. Kim, Y. J. Kang, D. H. Kim et al., "A novel hydroxamic acid derivative, MHY218, induces apoptosis and cell cycle arrest through downregulation of NF- $\kappa$ B in HCT116 human colon cancer cells," *International Journal of Oncology*, vol. 44, no. 1, pp. 256–264, 2014.
- [19] R. K. Lall, D. N. Syed, V. M. Adhami, M. I. Khan, and H. Mukhtar, "Dietary polyphenols in prevention and treatment of prostate cancer," *International Journal of Molecular Sciences*, vol. 16, no. 2, pp. 3350–3376, 2015.
- [20] S. Parsai, R. Keck, E. Skrzypczak-Jankun, and J. Jankun, "Analysis of the anticancer activity of curcuminoids, thiotryptophan and 4-phenoxyphenol derivatives," *Oncology Letters*, vol. 7, no. 1, pp. 17–22, 2014.
- [21] H. L. Chou, Y. Fong, C. K. Wei et al., "A quinone-containing compound enhances camptothecin-induced apoptosis of lung cancer through modulating endogenous ROS and ERK signaling," *Archivum Immunologiae et Therapiae Experimentalis*, vol. 65, no. 3, pp. 241–252, 2017.
- [22] W.-T. Chang, W. Liu, Y.-H. Chiu et al., "A 4-phenoxyphenol derivative exerts inhibitory effects on human hepatocellular carcinoma cells through regulating autophagy and apoptosis accompanied by downregulating  $\alpha$ -tubulin expression," *Molecules*, vol. 22, no. 5, p. 854, 2017.
- [23] H. Hirai, H. Sootome, Y. Nakatsuru et al., "MK-2206, an allosteric Akt inhibitor, enhances antitumor efficacy by standard chemotherapeutic agents or molecular targeted drugs *in vitro* and *in vivo*," *Molecular Cancer Therapeutics*, vol. 9, no. 7, pp. 1956–1967, 2010.
- [24] J. K. Morrow, L. Du-Cuny, L. Chen et al., "Recent development of anticancer therapeutics targeting Akt," *Recent Patents on Anti-Cancer Drug Discovery*, vol. 6, no. 1, pp. 146–159, 2011.
- [25] H. S. Kang, H. Y. Chung, J. Y. Kim, B. W. Son, H. A. Jung, and J. S. Choi, "Inhibitory phlorotannins from the edible brown alga *Ecklonia stolonifera* on total reactive oxygen species (ROS) generation," *Archives of Pharmacal Research*, vol. 27, no. 2, pp. 194–198, 2004.
- [26] D. A. Bass, J. W. Parce, L. R. Dechatelet, P. Szejda, M. C. Seeds, and M. Thomas, "Flow cytometric studies of oxidative product formation by neutrophils: a graded response to membrane stimulation," *Journal of Immunology*, vol. 130, no. 4, pp. 1910–1917, 1983.
- [27] Z. Darzynkiewicz, D. H. Halicka, and T. Tanaka, "Cytometric assessment of DNA damage induced by DNA topoisomerase inhibitors," *Methods in Molecular Biology*, vol. 582, pp. 145–153, 2009.
- [28] A. Liu, H. Chen, W. Wei et al., "Antiproliferative and antimetastatic effects of emodin on human pancreatic cancer," *Oncology Reports*, vol. 26, no. 1, pp. 81–89, 2011.
- [29] C. H. Tzeng, Y. R. Chen, C. C. Tzeng et al., "Discovery of indeno[1,2-*b*]quinoxaline derivatives as potential anticancer agents," *European Journal of Medicinal Chemistry*, vol. 108, pp. 258–273, 2016.
- [30] Q. Tang, J. C. Moore, M. S. Ignatius et al., "Imaging tumour cell heterogeneity following cell transplantation into optically clear immune-deficient zebrafish," *Nature Communications*, vol. 7, no. 1, article 10358, 2016.
- [31] I. Kikuchi, Y. Nakayama, T. Morinaga, Y. Fukumoto, and N. Yamaguchi, "A decrease in cyclin B1 levels leads to polyploidization in DNA damage-induced senescence," *Cell Biology International*, vol. 34, no. 6, pp. 645–653, 2010.
- [32] M. B. Morelli, C. Amantini, M. Nabissi et al., "Axitinib induces senescence-associated cell death and necrosis in glioma cell lines: the proteasome inhibitor, bortezomib, potentiates axitinib-induced cytotoxicity in a p21(Waf/Cip1) dependent manner," *Oncotarget*, vol. 8, no. 2, pp. 3380–3395, 2017.
- [33] V. Valdíglesias, S. Giunta, M. Fenech, M. Neri, and S. Bonassi, " $\gamma$ H2AX as a marker of DNA double strand breaks and genomic instability in human population studies," *Mutation Research*, vol. 753, no. 1, pp. 24–40, 2013.
- [34] B. G. Campling and W. S. El-Deiry, "Clinical implication of p53 mutation in lung cancer," *Molecular Biotechnology*, vol. 24, no. 2, pp. 141–156, 2003.
- [35] A. Chakravarti, G. Zhai, Y. Suzuki et al., "The prognostic significance of phosphatidylinositol 3-kinase pathway



- activation in human gliomas,” *Journal of Clinical Oncology*, vol. 22, no. 10, pp. 1926–1933, 2004.
- [36] E. Shivelman, J. Sussman, and D. Stokoe, “A role for PI 3-kinase and PKB activity in the G2/M phase of the cell cycle,” *Current biology*, vol. 12, no. 11, pp. 919–924, 2002.
- [37] R. Bendardaf, H. Lamlum, R. Ristamäki, A. Ålgars, Y. Collan, and S. Pyrhönen, “Response to chemotherapy (irinotecan plus 5-fluorouracil) in colorectal carcinoma can be predicted by tumour DNA content,” *Oncology*, vol. 66, no. 1, pp. 46–52, 2004.
- [38] Y.-P. Liu, H.-L. Chen, C.-C. Tzeng et al., “TCH-1030 targeting on topoisomerase I induces S-phase arrest, DNA fragmentation, and cell death of breast cancer cells,” *Breast Cancer Research and Treatment*, vol. 138, no. 2, pp. 383–393, 2013.
- [39] P. Karna, P. C. G. Rida, V. Pannu et al., “A novel microtubule-modulating noscapinoid triggers apoptosis by inducing spindle multipolarity via centrosome amplification and declustering,” *Cell Death and Differentiation*, vol. 18, no. 4, pp. 632–644, 2011.
- [40] T. R. Jackson, K. Salmina, A. Huna et al., “DNA damage causes TP53-dependent coupling of self-renewal and senescence pathways in embryonal carcinoma cells,” *Cell Cycle*, vol. 12, no. 3, pp. 430–441, 2013.
- [41] H. Y. Fang, H. M. Wang, K. F. Chang et al., “Feruloyl-L-arabino-attenuates migration, invasion and production of reactive oxygen species in H1299 lung cancer cells,” *Food and Chemical Toxicology*, vol. 58, pp. 459–466, 2013.
- [42] C. C. Chiu, H. L. Chou, P. F. Wu, H. L. Chen, H. M. Wang, and C. Y. Chen, “Bio-functional constituents from the stems of *Liriodendron tulipifera*,” *Molecules*, vol. 17, no. 4, pp. 4357–4372, 2012.
- [43] A. Faissner, N. Heck, A. Dobbertin, and J. Garwood, “DSD-1-proteoglycan/phosphacan and receptor protein tyrosine phosphatase-beta isoforms during development and regeneration of neural tissues,” *Advances in Experimental Medicine and Biology*, vol. 557, pp. 25–53, 2006.
- [44] C. Guo, A. V. Gasparian, Z. Zhuang et al., “9-Aminoacridine-based anticancer drugs target the PI3K/AKT/mTOR, NF- $\kappa$ B and p53 pathways,” *Oncogene*, vol. 28, no. 8, pp. 1151–1161, 2009.
- [45] H. Pelicano, D. Carney, and P. Huang, “ROS stress in cancer cells and therapeutic implications,” *Drug resistance updates : reviews and commentaries in antimicrobial and anticancer chemotherapy*, vol. 7, no. 2, pp. 97–110, 2004.
- [46] D. Trachootham, J. Alexandre, and P. Huang, “Targeting cancer cells by ROS-mediated mechanisms: a radical therapeutic approach?,” *Nature Reviews Drug Discovery*, vol. 8, no. 7, pp. 579–591, 2009.
- [47] B. R. Lee, S. Y. Chang, E. H. Hong et al., “Elevated endoplasmic reticulum stress reinforced immunosuppression in the tumor microenvironment via myeloid-derived suppressor cells,” *Oncotarget*, vol. 5, no. 23, pp. 12331–12345, 2014.
- [48] J. C. Lee, M. F. Hou, H. W. Huang et al., “Marine algal natural products with anti-oxidative, anti-inflammatory, and anti-cancer properties,” *Cancer Cell International*, vol. 13, no. 1, p. 55, 2013.
- [49] C. C. Chiu, J. W. Haung, F. R. Chang et al., “Golden berry-derived 4 $\beta$ -hydroxywithanolide E for selectively killing oral cancer cells by generating ROS, DNA damage, and apoptotic pathways,” *PLoS One*, vol. 8, no. 5, article e64739, 2013.
- [50] J. Tat, M. Liu, and X. Y. Wen, “Zebrafish cancer and metastasis models for in vivo drug discovery,” *Drug Discovery Today: Technologies*, vol. 10, no. 1, pp. e83–e89, 2013.
- [51] L. I. Zon and R. T. Peterson, “In vivo drug discovery in the zebrafish,” *Nature Reviews Drug Discovery*, vol. 4, no. 1, pp. 35–44, 2005.
- [52] C. Chakraborty, C. H. Hsu, Z. H. Wen, C. S. Lin, and G. Agoramoorthy, “Zebrafish: a complete animal model for in vivo drug discovery and development,” *Current Drug Metabolism*, vol. 10, no. 2, pp. 116–124, 2009.
- [53] C. C. Chiu, H. L. Chou, B. H. Chen et al., “BPIQ, a novel synthetic quinoline derivative, inhibits growth and induces mitochondrial apoptosis of lung cancer cells in vitro and in zebrafish xenograft model,” *BMC Cancer*, vol. 15, no. 1, 2015.

## Research Article

# Artichoke Polyphenols Sensitize Human Breast Cancer Cells to Chemotherapeutic Drugs via a ROS-Mediated Downregulation of Flap Endonuclease 1

Anna Maria Mileo <sup>1</sup>, Donato Di Venere <sup>2</sup>, Stefania Mardente,<sup>3</sup> and Stefania Miccadei <sup>1</sup>

<sup>1</sup>Tumor Immunology and Immunotherapy Unit, IRCCS Regina Elena National Cancer Institute, Rome, Italy

<sup>2</sup>CNR-Institute of Sciences of Food Production (ISPA), Bari, Italy

<sup>3</sup>Department of Experimental Medicine, Sapienza University of Rome, Rome, Italy

Correspondence should be addressed to Stefania Miccadei; [stefania.miccadei@ifo.gov.it](mailto:stefania.miccadei@ifo.gov.it)

Received 2 August 2019; Accepted 22 November 2019; Published 6 January 2020

Academic Editor: Manuela Corte-Real

Copyright © 2020 Anna Maria Mileo et al. This is an open access article distributed under the Creative Commons Attribution License, which permits unrestricted use, distribution, and reproduction in any medium, provided the original work is properly cited.

Combined treatment of several natural polyphenols and chemotherapeutic agents is more effective comparing to the drug alone in inhibiting cancer cell growth. Polyphenolic artichoke extracts (AEs) have been shown to have anticancer properties by triggering apoptosis or reactive oxygen species- (ROS-) mediated senescence when used at high or low doses, respectively. Our aim was to explore the chemosensitizing potential of AEs in order to enhance the efficacy of conventional chemotherapy in breast cancer cells. We employed breast cancer cell lines to assess the potential synergistic effect of a combined treatment of AEs/paclitaxel (PTX) or AEs/adriamycin (ADR) and to determine the underlying mechanisms correlated to this potential therapeutic approach. Our data shows that AEs/PTX reduced cell proliferation by increasing DNA damage response (DDR) mediated by Flap endonuclease 1 (FEN1) downregulation that results into enhanced breast cancer cell sensitivity to chemotherapeutic drugs. We demonstrated that ROS/Nrf2 and p-ERK pathways are two molecular mechanisms involved in the synergistic effect of AEs plus PTX treatment. To highlight the role of ROS herein, we report that the addition of antioxidant N-acetylcysteine (NAC) significantly decreased the antiproliferative effect of the combined treatment. A combined therapy could be able to reduce the dose of chemotherapeutic drugs, minimizing toxicity and side effects. Our results suggest the use of artichoke polyphenols as ROS-mediated sensitizers of chemotherapy paving the way for innovative and promising natural compound-based therapeutic strategies in oncology.

## 1. Introduction

Breast cancer is the most common malignancy in women around the world [1] and is a heterogeneous disease with high degree of diversity between and within tumors and among individual patients [2–4]. Of the various factors involved in breast carcinogenesis, oestrogen receptors (ER) play a major role and are considered an important therapeutic target. ER-positive tumors are further subtyped into low proliferation rate luminal A and higher proliferation rate luminal B tumors. Patients with the triple negative breast cancer (TNBC) subtype, characterized by the absence of ER, progesterone receptor (PR), and human epidermal

growth factor receptor-2/neu receptors (HER2/neu) have a poor prognosis [5, 6] also due to the few clinical treatments available. Considerable effort has gone into identifying new therapeutic agents, with multiple targeting abilities, able to circumvent the limitation of current conventional therapy.

Combined cancer therapy utilizes two or more agents and may improve the therapeutic efficacy of the single drug through a synergistic effect, leading to a potentially reduced drug resistance [7].

Many epidemiological studies suggest that phytochemicals, present at high levels in vegetables and fruits, have anticarcinogenic properties [8–11] and, triggering apoptosis, may be an effective treatment in cancer.

There is considerable interest in identifying bioactive compounds which, by increasing the sensitivity to conventional chemotherapeutic agents, could improve the patient's quality of life by reducing the side effects of therapy [12–17]. It has been recently demonstrated that combined treatment of natural polyphenols and chemotherapeutic agents are more effective than the drug alone in hindering the growth of cancer cells [18, 19] and in promoting chemosensitivity in multidrug resistance (MDR) cancer cell lines [20].

Growing interest in dietary phytochemicals has led to renewed attention being paid to the artichoke, because of its high content in polyphenols. Artichoke polyphenols are mainly glycoside forms of flavonoid, such as apigenin and luteolin in the leaves and hydroxycinnamic acid derivatives in the edible part, mainly represented by mono- and dicaffeoylquinic acids. Many *in vitro* and *in vivo* experiments have shown that artichoke has diuretic, hepatoprotective, hypocholesterolemic, and antioxidant properties [21–24] and, more recently, antitumoral activities [24–26]. Our previous findings indicate that AEs protect hepatocytes from oxidative stress and show cancer chemopreventive properties by triggering apoptosis in human hepatoma cells [24] and in human breast cancer cell lines without any toxicity in the nontumorigenic MCF10A cells [25]. We have also provided evidence that low doses and chronic AE treatments exert anticancer activity through induction of premature senescence in MDA-MB231, a triple negative and highly aggressive breast cancer cell line [27]. Furthermore, the bioavailability of metabolites of hydroxycinnamic acids, after ingestion of cooked artichoke, has also been demonstrated in human subjects [28].

Taxanes are a family of chemotherapeutic drugs employed for the treatment of many tumors including breast cancer in both early and metastatic stages [29]. One of these, PTX, is a microtubule-stabilizing drug [30] which, because of its effect on mitotic spindle dynamics, may lead to cell cycle arrest and apoptosis [31]. More recently, it has been suggested that many anticancer drugs, including taxanes, have the ability to induce oxidative stress [32], which indicates an additional antitumoral mechanism.

FEN1 is a key member of the endonuclease family involved in cellular DNA replication and repair [33]. As a structure-specific nuclease, FEN1 stimulates Okazaki fragment maturation during DNA repair and efficient removal of 5'-flaps during long-patch base excision repair [34]. FEN1 is also reported to be linked to apoptosis-induced DNA fragmentation in response to apoptotic stimuli [34, 35], and its expression is closely associated with cell proliferation and correlated with increased tumor grade and aggressiveness [36].

Oxidative stress is a result of a cellular imbalance in the production of ROS and the activity of the endogenous antioxidant protective system [37]. Notably, ROS-induced oxidative stress plays an important role in cancer development and progression. Among ROS-inducing agents, many phytochemicals, including curcumin [38, 39], resveratrol [40, 41], and epigallocatechin-3-gallate [42], have been shown to enhance the anticancer properties of chemotherapeutic agents. We have previously demonstrated a dual role of

AEs, as prooxidant in breast cancer cells [25] and as antioxidant in normal hepatocyte [24] showing an inhibitory effect on growth of tumor cells with little or no toxicity on normal cells based on their differential redox status.

It is well known that induction of phase II enzymes, counteracting reactive electrophiles including ROS, plays an important role in response to many anticancer agents including dietary compounds. Upon cellular stimulation by oxidative stressor molecules Nrf2, the main transcription factor involved in the regulation of phase II and antioxidant gene expression moves to the nucleus where it interacts with antioxidant response elements (AREs) present in the promoter region of many phase 2 genes [43–45].

The roles of growth factors and mitogens in regulating gene expression, apoptosis, and differentiation have been reported to be mediated by the Ras/MEK/ERK signaling cascade [46]. This pathway has been shown to be frequently activated in breast cancer, and the MAPK pathway is a well-explored target of therapeutic intervention. Therefore, specific inhibitors targeting Ras, Raf, MEK, and other downstream proteins have been tested in clinical trials [47]. Since p-ERK expression sensitizes activation of DNA damage-induced checkpoints, inhibition of p-ERK may enhance the genotoxic effect of chemotherapy, probably as a consequence of the accumulation of DNA lesions due to compromised checkpoint activation [48].

To improve our knowledge for designing new therapeutic interventions, we have characterized the biological role of the combined treatment involved in the synergistic antitumor effect of AE/PTX approach.

## 2. Materials and Methods

**2.1. Artichoke Extract Preparation.** The edible part (head) of fresh artichoke is used for extract preparation, and the analysis of polyphenols contained in the extracts was performed by HPLC as previously described [25].

**2.2. Cell Lines and Cultured Conditions.** The human breast cell lines were maintained in a humidified incubator with 5% CO<sub>2</sub> and 95% air at 37°C. MCF7 and MDA-MB231 cells, respectively, luminal A oestrogen receptor positive and basal B triple negative receptor subtypes were grown in RPMI and DMEM, respectively (Invitrogen, Life Technologies, Monza, Italy) and supplemented with 10% FBS, 10 IU/ml of penicillin and 10 µg/ml of streptomycin.

**2.3. Reagents.** Artichoke extracts were dissolved in phosphate buffer solution (PBS) and 0.1% Me<sub>2</sub>SO (Sigma-Aldrich, Milan, Italy). Chemotherapeutic drugs PTX (Sigma-Aldrich), ADR (Sigma-Aldrich), and cisplatin (CDDP; Sigma-Aldrich) were dissolved in PBS. Glucose oxidase (GOx, Sigma-Aldrich) was dissolved in PBS. ERK1-2 inhibitor 1,4-diamino-2,3-dicyano-1,4-bis(2-aminophenylthio) butadiene (U0126, Promega, Milan, Italy) was dissolved in Me<sub>2</sub>SO. NAC (Sigma-Aldrich) was dissolved in PBS. Dihydroethidium (DHE) and dichlorofluorescein-diacetate (DCF-DA, Molecular Probes-Thermo Fisher Scientific, Waltham, MA, USA) were dissolved in Me<sub>2</sub>SO.

**2.4. Cell Viability Assay.** Cells were seeded in 96-well plates at a concentration of  $3 \times 10^3$  cells/well and after 24 h treated with drugs at the given concentrations. CellTiter-Glo Luminescent Cell Viability Assay (Promega) was used to determine the relative number of viable cells after treatment, by means of a GLOMAX 96 Microplate Luminometer (Promega). Cells treated with the same final concentration of drug solvent were used as control.

**2.5. Colony-Forming Assay.** MCF7 cells were plated at a concentration of  $3.5 \times 10^3$  cells/well in 6-well plates. After 24 h, vehicle, PTX, AEs, or a combination of both (as indicated) were added for 24 h. After 14 days, cells were washed and subsequently stained using a 5% crystal violet solution in order to assess the colony number.

**2.6. Immunoblot Analysis.** To obtain the whole-cell extract, cells were washed with PBS and suspended in RIPA lysis buffer in the presence of protease and phosphatase inhibitors. After 30 minutes in ice, samples were sonicated and centrifuged ( $10,000 \times g$ ) for 10 min at  $4^\circ\text{C}$ . Supernatants were collected as whole-cell extracts. To obtain nuclear proteins, cell pellets were swelled in hypotonic buffer (Tris-HCl pH 7.5 50 mM, NaCl 10 mM, EDTA 5 mM, NP40 0.05%) for 30 minutes in ice. The cell lysate was centrifuged at  $14,000 \text{ rpm} \times 30$  minutes at  $4^\circ\text{C}$ . The supernatant was collected as the cytoplasmic fraction. The pellet was resuspended in buffer C (Hepes pH 7.9 20 mM, NaCl 420 mM,  $\text{MgCl}_2$  1.5 mM, EDTA 0.2 mM, glycerol 25%, and protease inhibitors) and sonicated. Cellular debris was removed by centrifugation at  $13,000 \text{ rpm}$  at  $4^\circ\text{C}$  for 30 minutes. The protein content was determined with a protein assay reagent (Bio-Rad, Milan, Italy), using bovine serum albumin as a standard. An equal protein content of total cell lysates was resolved on polyacrylamide gel (Bolt 4-12% Bis-Tris Plus, Invitrogen) with molecular weight markers (BenchMark Pre-Stained Protein Standard, Life Technologies, Monza, Italy). Proteins were then electrotransferred to PVDF membrane (iBlot Invitrogen) and incubated with specific primary antibodies. Antibodies used for western blots were anticlaved PARP (Cell Signaling Technology, Danvers, MA, USA, # 9541 dil. 1:1000), anti-LC3 (MBL International, Woburn, MA, USA, PD014 dil. 1:400), anti-ERK1-2 (Cell Signaling Technology #9102 dil. 1:1000), anti-pERK1-2 (Cell Signaling Technology # 9101S dil. 1:1000), anti-FEN1 (Santa Cruz Biotechnology Inc. Dallas, TX, USA, sc-28355 dil. 1:1000), anti- $\beta$ -actin (MP # 69100 dil. 1:10000), anti-GAPDH (Sigma Aldrich G8795 dil. 1:24000); anti-Nrf2 (Cell Signaling Technology #8882 dil. 1:1000), anti-gamma- $\text{H}_2\text{AX}$  (phospho S139) (Millipore # 05363 dil. 1:500), anti-histone H3 (Abcam, Milan, Italy, ab1791 dil. 1:1000). PVDF membranes were developed using ECL detection reagents (GE Healthcare, Marlborough, MA, USA) on a UVITEC imaging system (UVITEC Cambridge, UK). Western blot signals were quantified by densitometry analysis using ImageJ software.

**2.7. [ $5^3\text{H}$ ] Thymidine Incorporation Assay.** Cells were seeded in 6-well plates at a concentration of  $1.5 \times 10^5$ . After 24 h, vehicle, PTX, AEs, or a combination of both (as indi-

cated) was added and the culture was incubated for 24 h. 37 kBq of [ $5^3\text{H}$ ] thymidine (DuPont, New England Nuclear Research Products, Boston, MA, USA) was added to each well. Four hours later, cells were washed twice with ice-cold PBS and 10% trichloroacetic acid (TCA). Cells were lysed in the presence of 1 N NaOH-0.1% SDS and neutralized in 1 N HCl. The cell-associated radioactivity was determined by liquid scintillation counting (Tri-Carb 2800 TR, PerkinElmer, USA).

**2.8. RNA Extraction, Reverse Transcription, and Quantitative RT-PCR.** Total RNA was extracted from MDA-MB231 cells using the MasterPure RNA Purification Kit (Epicentre Biotechnologies, Madison, WI, USA). RNA was reverse-transcribed into cDNA using the High Capacity cDNA Reverse Transcription Kit (Applied Biosystems Inc., Foster City, CA, USA) and subject to StepOne Real-Time PCR (Applied Biosystems Inc.) with PowerUp SYBR Green Master Mix (Applied Biosystems Inc.). Primers for FEN1, Nrf2, and GAPDH were designed as specified below:

FEN1 forward  $5^{\prime}$ -GCCAAAAGCTGCCAATCCA- $3^{\prime}$ , FEN1 reverse  $5^{\prime}$ -GCCAATTTTCTGGCACAGGG- $3^{\prime}$ ; Nrf2 forward  $5^{\prime}$ -CATCGAGAGCCCAGTCTTC- $3^{\prime}$ , Nrf2 reverse  $5^{\prime}$ -CTTCTGGACTTGGAAACCATG- $3^{\prime}$ ; and GAPDH forward  $5^{\prime}$ -TCCCTGAGCTGAACGGGAAG- $3^{\prime}$ , GAPDH reverse  $5^{\prime}$ -GGAGGAGTGGGTGTCGCTGT- $3^{\prime}$ .

PCR conditions were  $50^\circ\text{C}$  for 2 min,  $95^\circ\text{C}$  for 2 min, followed by 40 cycles of  $95^\circ\text{C}/15 \text{ s}$ , annealing at  $56^\circ\text{C}/30 \text{ s}$  and  $72^\circ\text{C}/30 \text{ s}$ . All reactions were performed in triplicate. Data was normalized to GAPDH and the fold change in gene expression relative to normal was calculated using the comparative *Ct* method [49].

## 2.9. ROS Detection

**2.9.1. Fluorescence Microscopy.** MDA-MB231 cells were treated with vehicle or PTX plus and minus AEs and GOx as positive control (as indicated). After 4 h, the oxidation-sensitive fluorescent probe DHE was used to assess the production of cytosolic superoxide anions. Briefly, after exposure, cells were incubated with  $5 \mu\text{M}$  DHE for 40 minutes at  $37^\circ\text{C}$  in the dark and then rinsed twice with PBS. The cell-permeant DHE entered the cells, was oxidized by superoxide anions to form ethidium (ETH) which binds to DNA, and produced fluorescent ETH-DNA. The fluorescent signals were obtained by the cultured cells at  $\lambda_{\text{ex}}$  300 nm and  $\lambda_{\text{em}}$  610 nm. Cells were visualized and images were captured using a fluorescence microscope apparatus (Olympus IX71-Olympus Tokyo, Japan) equipped with a digital camera (Tucsen Photonics Co., Ltd., Fuzhou, Fujian, China).

**2.9.2. Flow Cytometry Assay.** ROS formation in MDA-MB231 cells with PTX and AEs was assayed by flow cytometry with the dye DCF-DA and following standard methods [50]. Briefly, DCF-DA (final concentration  $40 \mu\text{M}$ ) was added to cell cultures on 6-well plates for 15 min at  $37^\circ\text{C}$ . After incubation, cells were scraped, washed in PBS, and analyzed by a flow cytometer (Epics XL-MCL Coulter, CA, USA) with an argon laser at 488 nm. Cells were gated using forward

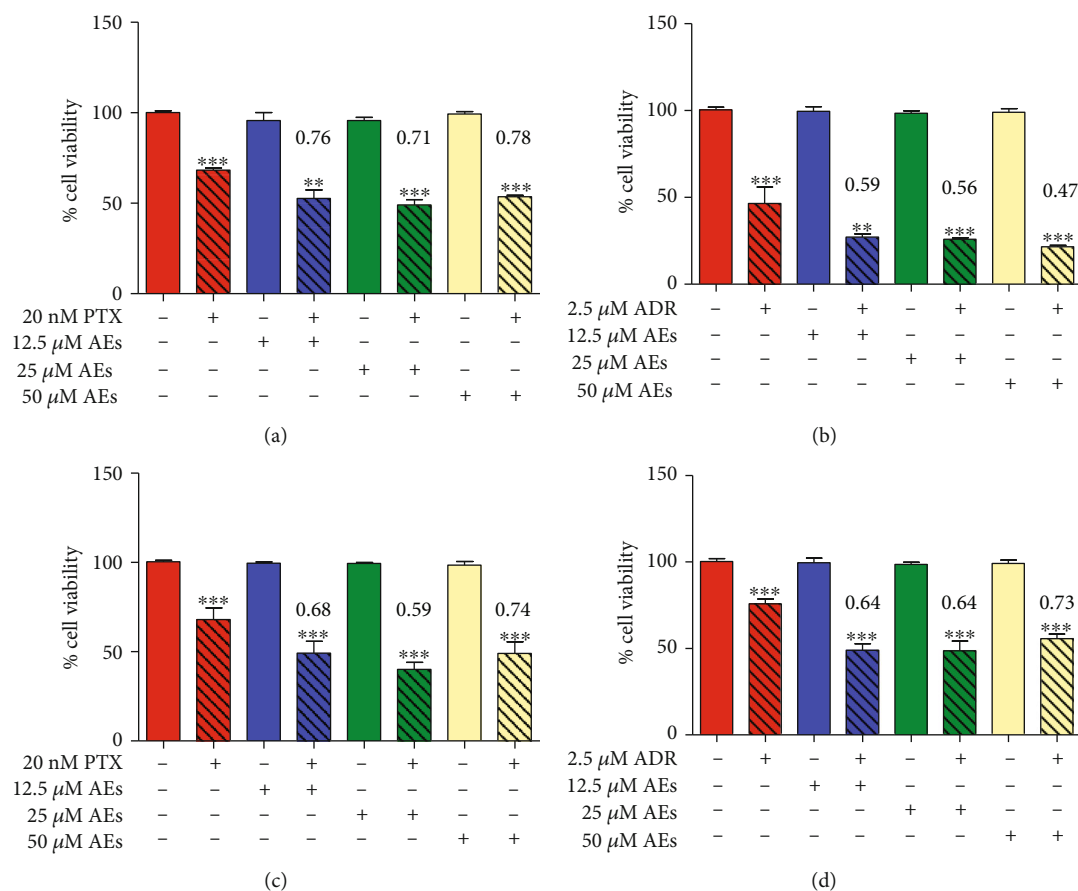


FIGURE 1: Effect of AEs on PTX or ADR-treated breast cancer cells. Cell viability assay: breast cancer cell lines (MDA-MB231 (a, b) and MCF7(c, d)) were treated with PTX (20 nM) or ADR (2.5 μM) with or without AEs (from 12.5 to 50 μM) for 24 h. Histograms show cell viability to highlight the effect of the association of chemotherapeutic agent and AEs. Synergy is characterized by a combination index < 0.8, and when present, its value is reported in red. Data is expressed as the mean ± SD of, at least, three independent experiments compared with a medium alone. The statistical significance between groups was calculated using Student's *t*-test. Significant differences are indicated by asterisks. MDA-MB231+PTX: PTX vs. 12.5 μM AEs+PTX \**p* = 0.0127; PTX vs. 25 μM AEs+PTX \*\**p* = 0.0037; PTX vs. 50 μM AEs+PTX \*\*\**p* < 0.0001. MDA-MB231+ADR: ADR vs. 12.5 μM AEs+ADR \*\**p* = 0.0070; ADR vs. 25 μM AEs+ADR \*\**p* = 0.0049; ADR vs. 50 μM AEs+ADR \*\**p* = 0.0019. MCF7+PTX: PTX vs. 12.5 μM AEs+PTX \*\**p* = 0.0019; PTX vs. 25 μM AEs+PTX \*\*\**p* < 0.0001; PTX vs. 50 μM AEs+PTX \*\**p* = 0.0017. MCF7+ADR: ADR vs. 12.5 μM AEs+ADR \*\*\**p* < 0.0001; ADR vs. 25 μM AEs+ADR \*\*\**p* = 0.0001; ADR vs. 50 μM AEs+ADR \*\*\**p* < 0.0001.

angle light scatter (FS) and 90° light scatter parameters (SS). For every histogram, a minimum of 20,000 events were counted. The mean fluorescence intensity was detected and expressed as a percentage of relative ROS level versus control cells.

**2.10. Statistical Analysis.** Data is presented as mean ± standard deviation (SD). Statistical analysis of the results was performed using Student's *t*-test, with GraphPad Prism v5.01 for Windows (GraphPad Software, San Diego, CA, USA). For all statistical tests, a two-tailed *p* value < 0.05 was considered significant. All data reported were verified in at least three independent experiments and expressed as mean ± SD.

### 3. Results

**3.1. Synergy between AEs and Chemotherapeutic Drugs Induces Loss of Cancer Cell Viability.** In order to highlight a

potential effect of compound combination between AEs and the most active and widely used cancer drugs in clinical management (taxanes, anthracyclines, and platinum complexes), we used two breast cancer cell lines, MCF7 and MDA-MB231, as experimental models. In both cell lines, PTX, ADR, or CDDP was employed at fixed concentrations (20 nM, 2.0 μM, and 20 μM, respectively). These treatments for 24 h lead to a reduction of cell viability of 30% (IC 30). By using the algorithm described by Fransson et al. [51] to calculate the combination index (CI), we analyzed the effect of AEs plus PTX, ADR, and CDDP compared with that of the single agents. The addition of AEs, from 12.5 μM up to 50 μM, to PTX or ADR in MDA-MB231 (Figures 1(a) and 1(b)) and in MCF7 (Figure 1(c) and 1(d)) cells yielded a decrease in cell viability which could be ascribed to a chemosensitizing effect of AEs to these drugs. The analysis of this data showed that the combined treatment, as demonstrated by the CI values in Figure 1, enhances cytotoxicity in a synergistic manner. Conversely, the

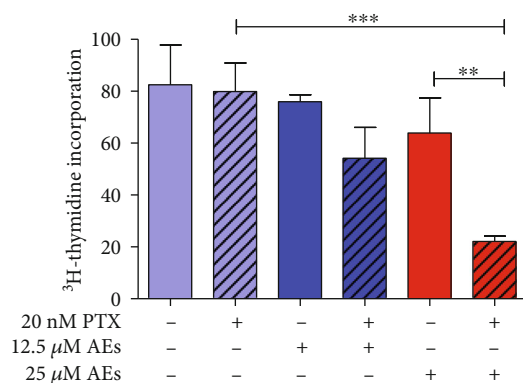


FIGURE 2: MDA-MB231 proliferation in response to AEs/PTX cotreatment. Proliferation assay: cells were exposed to AEs (12.5–25  $\mu$ M) plus and minus PTX (20 nM) for 24 h and the proliferation rate was measured by  $^3$ H-thymidine incorporation assay. PTX vs. 25  $\mu$ M AEs+PTX \*\*\* $p$  = 0.0009. 25  $\mu$ M AEs vs. 25  $\mu$ M AEs+PTX \*\* $p$  = 0.064.

presence of AEs did not increase the number of dead cells caused by CDDP in a significant manner in both MCF7 and MDA-MB231 cells (Fig. 1s).

Since triple negative breast cancers have a more aggressive phenotype and a poorer prognosis due to the high propensity for metastatic progression and absence of specific hormonal-based targeted treatment, novel therapeutic strategies are required. To this end, we focused on MDA-MB231 as a TNBC cellular model to best describe a synergistic effect of AEs in combination with low doses of PTX, a first-line chemotherapeutic agent in breast cancer.

**3.2. The Combination of AEs and PTX Inhibits Human Breast Cancer Cell Proliferation.** In view of the aforementioned effects on cell viability, we thoroughly explored the mechanisms involved in the synergistic effect of the combined treatment on breast cancer cells.

To further characterize the decreased cell viability induced by cotreatment, we evaluated the expression of cleaved PARP (c-PARP) and LC3 as potential molecular signs of regulated cell death. No significant modulation of these proteins was detected compared to PTX treatment alone, which is well known to cause marked cell death [52, 53]. These slight effects that were detected demonstrate that both apoptotic and autophagic cell deaths are not relevant for the synergistic response of the combined treatment (Fig. 2s).

These findings prompted us to detect DNA synthesis ratio in treated cells. As shown in Figure 2, AEs strongly decrease  $^3$ H-thymidine incorporation in a dose-dependent manner in MDA-MB231 cells treated with 20 nM PTX. The highest concentration tested (25  $\mu$ M AEs) inhibited cell proliferation by 70% compared to PTX alone.

In order to investigate additional features of cellular response to cotreatment, we evaluated the clonogenic ability of breast cancer cells. Since MDA-MB231 cells do not aggregate well and form very dispersed colonies [54], we switched to MCF7 cell model with a similar sensitivity to AEs/PTX (Figure 1) to test the effect of cotreatment on the colony for-

mation ability. Our results demonstrate that this property was poorly affected (Fig. 3s).

**3.3. Role of ROS in Synergistic Cytotoxicity in AE/PTX-Treated Cells.** Based on the prooxidant activity of natural polyphenols in inducing cell growth inhibition [27, 55–57] and on the ability of PXT to promote intracellular ROS formation [32], we evaluated the oxidative pathway as a potential mechanism involved in AE/PTX-induced cell proliferation inhibition. In agreement with Chikara et al. data [58], which shows that several polyphenols strengthen the anticancer properties of chemotherapeutic drugs by elevating ROS levels, we report (Figure 3(a)) increased numbers of bright red fluorescent cells indicating enhanced levels of superoxide anions.

To further investigate the involvement of oxidative pathway in AE/PTX synergistic activity, the amount of ROS in particular peroxides was evaluated by flow cytometry. ROS production induced by the combined treatment takes place early, since it increases in relation to single agents after 2 h of exposure (Figures 3(b) and 3(b1)). This trend is less evident after 24 h treatment, probably as a result of ROS accumulation (Fig. 4s).

To further determine the role of ROS in AE/PTX-induced cell growth arrest, we sought to examine whether inhibition of ROS production by the well-known antioxidant NAC has any impact on synergy in breast cancer cell viability. As shown in Figure 3(c), the cell pretreatment of NAC significantly reduced the synergistic effect of 25  $\mu$ M AEs/PTX by about 20%.

**3.4. Role of Nrf2/FEN1 and p-ERK/FEN1 Axis in DNA Damage Induced by AEs/PTX.** After oxidative stress, Nrf2 is activated and moves to the nucleus where it regulates ARE transcriptional activity. Based on literature data [58–60], we hypothesize that combined treatment could affect Nrf2 activity. As shown in Figures 4(a) and 4(b), AEs increase the RNA/protein expression of Nrf2 in cells treated with PTX and induce a nuclear translocation of Nrf2 in this oxidative stress scenario. Since Nrf2 has been shown to be a repressor of the *Fen1* gene [61], we assessed the RNA expression of FEN1 in AE/PTX-treated cells. As reported in Figures 5(a) and 5(b), 25  $\mu$ M AEs induced a significant decrease in FEN1 RNA expression as well as in protein levels.

Since we detected a partial cytotoxicity rescue by NAC exposure, in order to explore the AE/PTX effect further, we hypothesized that a different molecular mechanism might be involved in the cellular synergistic response.

Several studies have reported that the MAPK family members play crucial roles in cell proliferation, survival, and differentiation [62, 63]. In particular, ERK kinases have been shown to play a part in DNA damage response (DDR) and that inhibition of p-ERK enhances the genotoxic effect of chemotherapeutic drugs [48]. Zou et al. reported that curcumin-treated breast cancer cells are more sensitive to cisplatin by downregulation of FEN1 achieved by reduction of p-ERK expression [19]. In agreement with published results, in our experimental settings, FEN1 and p-ERK expression levels decreased in combination treatment compared with

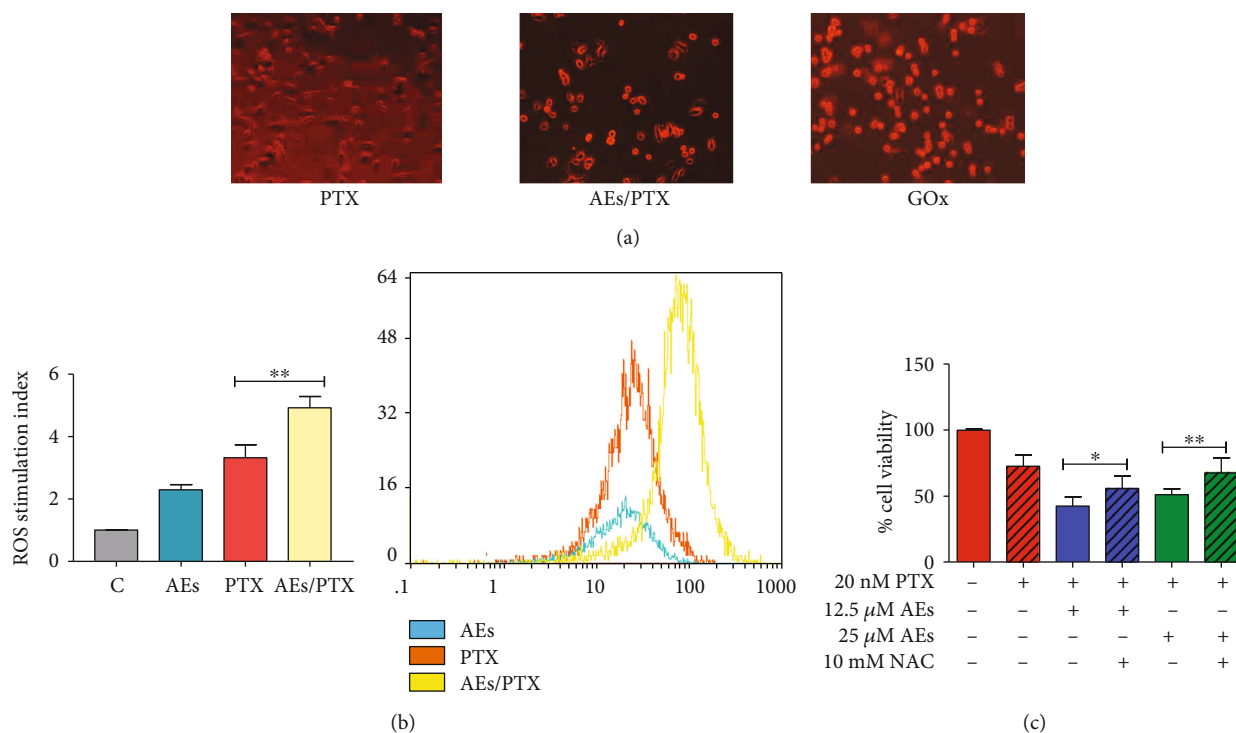


FIGURE 3: ROS production in MDA-MB231 cells treated with AEs/PTX. (a) Fluorescence microscopy: MDA-MB231 cells treated with PTX (20 nM) alone or AEs/PTX 25 μM and 20 nM, respectively, or GOx (0.2 UI/ml) as a positive control for 24 h. The presence of ROS was detected by DHE fluorescent staining and red fluorescent-stained cells versus total cells were counted using an inverted fluorescence microscope (magnification 20x). (b, b1) Flow cytometry: the mean fluorescence intensity was expressed as stimulation index obtained by ratio between ROS levels released by cells after 2 h of treatment and ROS detection in control cells. Data is the mean ± SD of 3 independent experiments. Indicative fluorescence peaks of ROS production in cells after 2 h of treatment with 25 μM AEs (blue graph), 20 nM PTX (orange graph), and AEs/PTX, respectively, 25 μM and 20 nM (yellow graph) are reported in (b1). (c) Antioxidant effect on cell viability: NAC reduced the synergistic effect of AEs (12.5–25 μM) in PTX (20 nM) treated cells. The cell viability results are the mean ± SD of at least three independent experiments. Significant statistical differences present in NAC plus and minus AE/PTX-treated cells are indicated by asterisks: 12.5 μM AEs+PTX vs. 12.5 μM AEs+PTX+NAC \* $p$  = 0.0191. 25 μM AEs+PTX vs. 25 μM AEs+PTX+NAC \*\* $p$  = 0.0094.

PTX alone. Decrease in p-ERK was related to the chemosensitizing effect of 25 μM AEs to PTX by targeting FEN1 in MDA-MB231 cells (Figure 5(b)). In order to show a direct correlation between p-ERK and FEN1 expression, untreated MDA-MB231 cells were exposed to ERK inhibitor U0126 (20 μM). After 60 minutes of U0126 exposure, both ERK phosphorylation and FEN1 expression were clearly downregulated (Figure 5(c)).

To test DNA damage level related to FEN1 downregulation, we looked at the extent of H<sub>2</sub>AX phosphorylation (γ-H<sub>2</sub>AX), a sensitive indicator of DNA double strand breaks (Figure 5(d)). We detected a marked phosphorylation level of histone H<sub>2</sub>AX in the experimental cellular setting treated with 25 μM AEs plus PTX, compared to PTX alone.

This data is evidence that AEs strengthen the antitumor activity of PTX both through the ROS/Nrf2 pathway and *via* the downregulation of p-ERK, which result in the decrease in FEN1 expression.

These findings indicate that the synergistic response is a result of balance between the ROS/Nrf2 pathway and the impaired DNA damage response (DDR) triggered by FEN1 downregulation, suggesting the presence of at least two

molecular mechanisms involved in the synergistic cytotoxicity elicited by our combined treatment.

#### 4. Discussion

To explore the role of natural compounds as chemosensitizer agents in breast cancer, we have investigated the effect of combined treatment of artichoke polyphenolic extracts with paclitaxel, adriamycin, or cisplatin on breast cancer cell lines. We demonstrate that AEs synergized with PTX or ADR in hindering the growth of MDA-MB231 or MCF7 cells compared with drug alone. AEs enhanced breast cancer sensitivity to PTX by decreasing cell proliferation both through the ROS/Nrf2 pathway and *via* the downregulation of p-ERK, and these mechanisms resulted in the decrease in FEN1 expression leading to DNA damage accumulation and DNA replication reduction. These findings suggest the presence of at least two molecular mechanisms involved in the synergistic AE/PTX cytotoxicity in breast cancer cells.

Tumor cells exhibit excessive ROS production which is related to aberrant metabolism and continuous cell division; therefore, cancer cells appear to be more vulnerable to

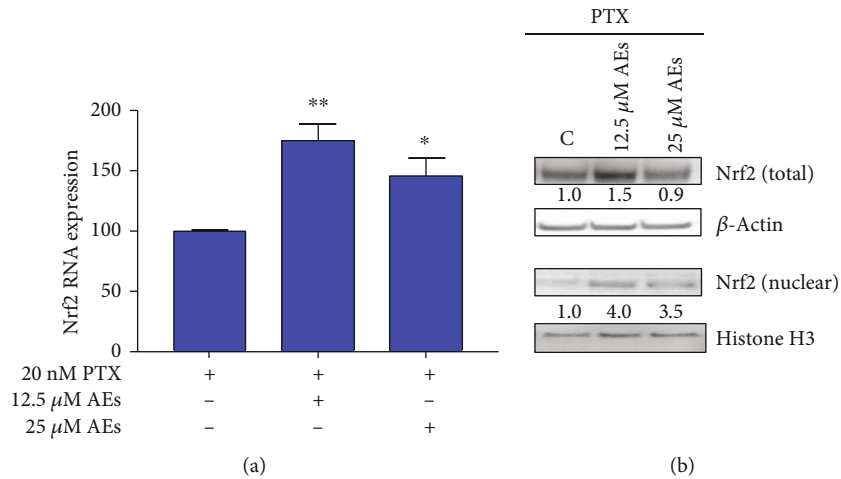


FIGURE 4: Nrf2 expression in MDA-MB231 treated with AEs/PTX. (a) Real-time assay. Nrf2 RNA expression is detected in cells treated with indicated concentrations of AEs plus and minus PTX (20 nM). 12.5  $\mu$ M AEs vs. 12.5  $\mu$ M AEs+PTX \*\* $p$  = 0.0023. 25  $\mu$ M AEs vs. 25  $\mu$ M AEs+PTX \* $p$  = 0.0176. (b) Nrf2 protein expression: total protein expression and nuclear translocation of Nrf2 were detected in treated cells. Quantification of band intensities was performed using ImageJ software, normalized by  $\beta$ -actin (total Nrf2) and histone H3 (nuclear Nrf2) expression levels. Relative values are calculated by comparing sample band intensities to control.

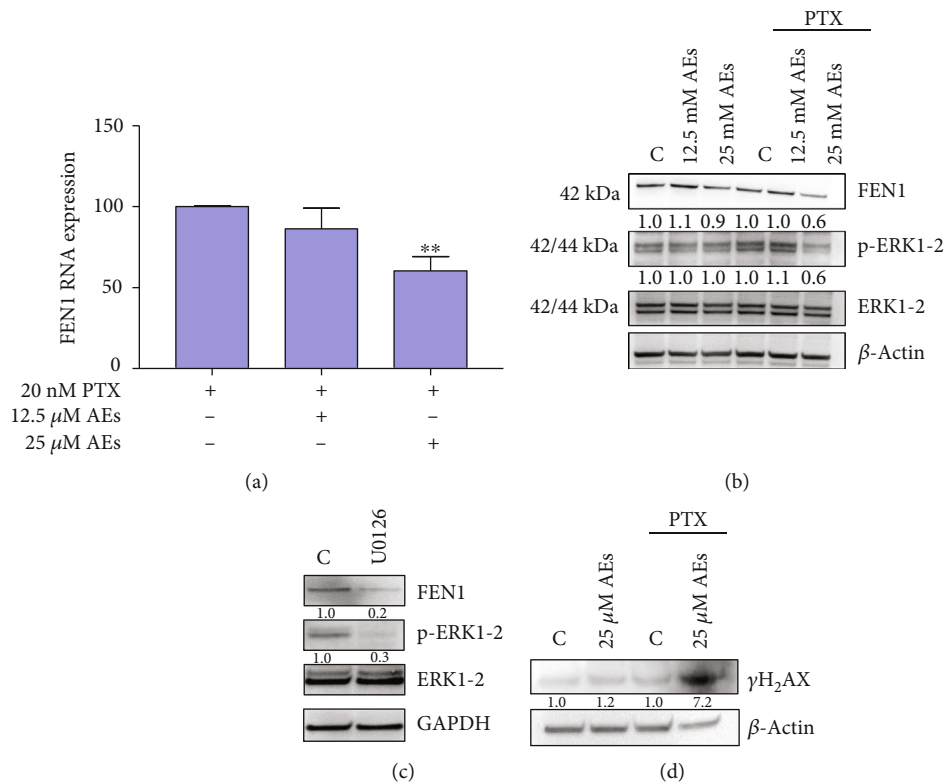


FIGURE 5: FEN1 modulation and DNA damage in combined treated MDA-MB231 cells. (a) Real-time assay: FEN1 RNA expression is detected in cells treated with indicated concentrations of AEs plus and minus PTX (20 nM). 25  $\mu$ M AEs vs. 25  $\mu$ M AEs+PTX \*\* $p$  = 0.0052. (b) FEN1/p-ERK1-2 protein expression: FEN1 protein expression and phosphorylation level of ERK1-2 were detected in total lysate of treated MDA-MB231 cells. Quantification of band intensities was performed using ImageJ software, normalized by  $\beta$ -actin expression level. Relative values are calculated by comparing sample band intensities to control in each setting ( $\pm$ PTX). (c) Effect of p-ERK1-2 inhibitor on FEN1 expression: FEN1 and p-ERK1-2 level were detected in MDA-MB231 treated for 60 minutes with U0126 (20  $\mu$ M), a MAPK/ERK inhibitor. Quantification of band intensities was performed using ImageJ software, normalized by GAPDH expression level. Relative values are calculated by comparing sample band intensities to control. (d) DNA damage level: DNA damage marker  $\gamma$ -H<sub>2</sub>AX was detected in cells treated with AEs plus and minus PTX. Quantification of band intensities was performed using ImageJ software, normalized by  $\beta$ -actin expression level. Relative values are calculated by comparing sample band intensities to control in each setting ( $\pm$ PTX).



further oxidative insult compared to normal ones [64]. ROS cellular levels are thus crucial for designing advanced therapies and a future challenge in anticancer treatment [58]. There are many reports describing the prooxidant effect of polyphenols in sensitizing cancer cells to chemotherapeutic drugs through different pathways [38–41, 65–67].

In light of our previous findings regarding the role of AEs as prooxidant players on breast cancer cells [27], this study has explored the ability of AEs to sensitize breast cancer cell to conventional chemotherapy through oxidative process. Based on literature data [38–42], our results strongly support the prooxidant role of AEs/PTX in hindering breast cancer cellular growth associated with ROS production. To further confirm the important role of ROS in enhancing the antitumor effect of the combined treatment, we demonstrate that the well-known antioxidant NAC attenuates the synergistic and antitumor effect on MDA-MB231 cells. Since we detected a partial cytotoxicity rescue by NAC exposure, we hypothesized that a further molecular mechanism was involved in the cellular synergistic response.

In agreement with published results, our data has shown that many anticancer drugs including ADR and PTX but not CDDP have the ability to induce oxidative stress [32]. We have shown that both ADR and PTX plus and minus AEs induce a synergistic effect on reducing cell viability, while AE/CDDP combined treatment did not modify cell death ratio. This finding suggests that AEs are able to produce ROS and synergize with the prooxidant activity of some chemotherapeutic drugs, which suggests that at least one of the mechanism involved in synergistic interaction is ROS production dependent.

Nrf2 is a main transcription factor in the regulation of many phase II and antioxidant genes [43, 44]. It is well known that induction of phase II enzymes, counteracting reactive electrophiles including ROS, plays an important role in response to many chemotherapeutic agents. Nrf2 is located in the cytoplasm in a complex with the actin-binding protein Keap1. Upon oxidative stimulation, Nrf2 moves to the nucleus where it interacts with AREs present in the promoter region of many genes [45]. In our experimental model, after AE/PTX exposure for 24 h, the Nrf2 mRNA level, together with the nuclear protein level, significantly increased compared with PTX alone treatment. According to Kwak et al. [68], who demonstrated that Nrf2 has a short half-life, we hypothesized that the nuclear accumulation is due to *de novo* synthesis of the transcription factor. In agreement with Chen et al. [61], who showed that Nrf2 bounds to ARE-like sequence located in the FEN1 promoter region, we observed that Nrf2 downregulated the expression of FEN1, which suggests that Nrf2 may function as a repressor of this endonuclease gene.

Our data has shown that cotreatment significantly reduced the FEN1 RNA level together with a downregulation of the protein expression compared with PTX alone and suggests that such a mechanism is involved in the antiproliferative effect of AEs/PTX. The combined treatment results in DNA damage accumulation, confirmed by the phosphorylation of H<sub>2</sub>AX which leads to DNA replication reduction. This data suggests that downregulating the

expression of FEN1, a potential biomarker and therapeutic target [36, 69], may be a new mechanism by which AEs sensitize breast cancer cells to PTX.

It has been shown that polyphenols can modulate multiple signaling pathways including MAPK/ERK [19, 38, 70, 71]. By inhibiting ERK phosphorylation, curcumin helps to sensitize the cells to cisplatin by targeting FEN1 [19]. In agreement with this data, our results showed that FEN1 and p-ERK expression levels decreased in combination treatment compared with PTX alone. Since the inhibition of ERK activation by the common MEK inhibitor U0126 induced a downregulation of FEN1, we envisage a marked correlation between this nuclease and the aforementioned kinase expression level in our experiments. As previously reported, aberrant activation of the ERK pathway is one of the most relevant events in human cancer as it stimulates cell proliferation [72]. However, the activation of the ERK pathway has an important role in DDR and has been associated with chemotherapeutic drugs commonly considered to be DNA damage inducers. For several tumors, inhibition of MAPK/ERK cascade could enhance the genotoxic effect of chemotherapeutic agents. This is probably because of the accumulation of DNA lesions due to the impaired checkpoint activation ERK related [48]. Therefore, if a combinatory therapy is to be used, it is important to determine if the combination will lead to inefficient repair of DNA lesions due to downregulation of FEN1.

Our results summarized in supplementary materials (Fig. 5s) suggest that artichoke polyphenols can be used as sensitizers of chemotherapy paving the way for new combined treatment in oncology. Since polyphenols are widely used as dietary components and have shown no toxicity in humans, their use as adjuvant agents may be an innovative and promising natural compound-based therapeutic strategy. Our study adds a novel aspect of the underlying mechanisms of the anticancer properties of AEs to our previous findings. However, wide-ranging pharmacokinetic and metabolic studies of combined treatment on animal models are required to evaluate its efficacy in human clinical trials.

## 5. Conclusions

We envisage a combined AE/chemotherapeutic agent treatment that is able to reduce the dose of antitumor drugs minimizing toxicity and side effects of conventional cancer therapy.

## Data Availability

The data used to support the findings of this study is included within the article.

## Conflicts of Interest

The authors declare that there is no conflict of interest regarding the publication of this paper.

## Acknowledgments

The authors would like to acknowledge Paola Nisticò (IRCCS Regina Elena National Cancer Institute, Rome, Italy) for the critical reading of the manuscript and helpful comments, Hugo Bowles (University of Foggia, Foggia, Italy) for proof-reading, and Lucia Monaco (Sapienza University of Rome, Italy) for helpful advices. This study was supported by Ricerca Corrente IRE 2017 to SM and AMM.

## Supplementary Materials

Supplementary materials integrate data described in the main document. Fig. 1s: effect of AEs on CDDP treated breast cancer cells. Cell viability assay: MDA-MB231 (a) and MCF7 (b) were treated with CDDP (20  $\mu$ M) with or without AEs (from 12.5 to 50  $\mu$ M) for 24 h. Histograms show cell viability. No significant differences are detected between combined treatment vs. CDDP alone. Fig. 2s: effect of AEs/PTX on regulated cell death. Apoptosis and autophagy marker analysis: cells were incubated with AEs or AEs/PTX and then assayed via western blot for c-PARP (a) and LC3 (b). Fig. 3s: cloning efficiency. Colony-forming analysis: MCF7 cells were exposed to AEs or AEs/PTX for 24 h and then allowed to grow and form colonies for subsequent 14 d. Cell colonies, after staining with crystal violet (a), were counted and the values reported as percent colony number in the histogram (b). C vs. PTX \*\* $p = 0.0049$ , 12.5  $\mu$ M AEs vs. 12.5  $\mu$ M AEs/PTX \*\*\* $p < 0.0001$ , and 25  $\mu$ M AEs vs. 25  $\mu$ M AEs/PTX \*\*\* $p = 0.0005$ . There is no significant difference between colony numbers of cells treated with AEs/PTX or PTX alone. Fig. 4s: ROS production in MDA-MB231 cells after 24 h of treatment. (a, a1) Flow cytometry: the mean fluorescence intensity was expressed as stimulation index obtained by ratio between ROS levels released by cells after 24 h of treatment and ROS detection in control cells. Data is the mean  $\pm$  SD of 3 independent experiments. Indicative fluorescence peaks of ROS production in cells after 24 h of treatment with 25  $\mu$ M AEs (red graph), 20 nM PTX (purple graph), and AEs/PTX, respectively, 25  $\mu$ M and 20 nM (brown graph) are reported in (a1). There is no significant difference between groups. Fig. 5s: graphical abstract. Schematic representation of two convergent signaling pathways involved in synergistic effect of AE/PTX combined treatment. The figure suggests the potential role of artichoke polyphenols as sensitizers of chemotherapy in breast cancer cells. (*Supplementary Materials*)

## References

- [1] M. Ghoncheh, M. Mohammadian, A. Mohammadian-Hafshejani, and H. Salehiniya, "The incidence and mortality of colorectal cancer and its relationship with the human development index in Asia," *Annals of Global Health*, vol. 82, no. 5, pp. 726–737, 2016.
- [2] L. G. Martelotto, C. K. Y. Ng, S. Piscuoglio, B. Weigelt, and J. S. Reis-Filho, "Breast cancer intra-tumor heterogeneity," *Breast Cancer Research*, vol. 16, no. 3, p. 210, 2014.
- [3] J. L. Song, C. Chen, J. P. Yuan, and S. R. Sun, "Progress in the clinical detection of heterogeneity in breast cancer," *Cancer Medicine*, vol. 5, no. 12, pp. 3475–3488, 2016.
- [4] D. Zardavas, A. Irrthum, C. Swanton, and M. Piccart, "Clinical management of breast cancer heterogeneity," *Nature Reviews. Clinical Oncology*, vol. 12, no. 7, pp. 381–394, 2015.
- [5] A. Prat, C. Fan, A. Fernández et al., "Response and survival of breast cancer intrinsic subtypes following multi-agent neoadjuvant chemotherapy," *BMC Medicine*, vol. 13, no. 1, p. 303, 2015.
- [6] W. Goto, S. Kashiwagi, K. Takada et al., "Significance of intrinsic breast cancer subtypes on the long-term prognosis after neoadjuvant chemotherapy," *Journal of Translational Medicine*, vol. 16, no. 1, p. 307, 2018.
- [7] R. Bayat Mokhtari, T. S. Homayouni, N. Baluch et al., "Combination therapy in combating cancer," *Oncotarget*, vol. 8, no. 23, pp. 38022–38043, 2017.
- [8] M. S. Farvid, W. Y. Chen, B. A. Rosner, R. M. Tamimi, W. C. Willett, and A. H. Eliassen, "Fruit and vegetable consumption and breast cancer incidence: repeated measures over 30 years of follow-up," *International Journal of Cancer*, vol. 144, no. 7, pp. 1496–1510, 2019.
- [9] J. A. Rothwell, V. Knaze, and R. Zamora-Ros, "Polyphenols: dietary assessment and role in the prevention of cancers," *Current Opinion in Clinical Nutrition and Metabolic Care*, vol. 20, no. 6, pp. 512–521, 2017.
- [10] A. Braakhuis, P. Campion, and K. Bishop, "Reducing breast cancer recurrence: the role of dietary polyphenolics," *Nutrients*, vol. 8, no. 9, p. 547, 2016.
- [11] P. R. Dandawate, D. Subramaniam, R. A. Jensen, and S. Anant, "Targeting cancer stem cells and signaling pathways by phytochemicals: novel approach for breast cancer therapy," *Seminars in Cancer Biology*, vol. 40–41, pp. 192–208, 2016.
- [12] T. Eitsuka, N. Tatewaki, H. Nishida, K. Nakagawa, and T. Miyazawa, "Synergistic anticancer effect of tocotrienol combined with chemotherapeutic agents or dietary components: a review," *International Journal of Molecular Sciences*, vol. 17, no. 10, p. 1605, 2016.
- [13] J. P. Burnett, G. Lim, Y. Li et al., "Sulforaphane enhances the anticancer activity of taxanes against triple negative breast cancer by killing cancer stem cells," *Cancer Letters*, vol. 394, pp. 52–64, 2017.
- [14] F. Al-Abbasi, E. Alghamdi, M. Baghdadi et al., "Gingerol synergizes the cytotoxic effects of doxorubicin against liver cancer cells and protects from its vascular toxicity," *Molecules*, vol. 21, no. 7, p. 886, 2016.
- [15] G. J. Kapadia, G. S. Rao, C. Ramachandran, A. Iida, N. Suzuki, and H. Tokuda, "Synergistic cytotoxicity of red beetroot (*Beta vulgaris* L.) extract with doxorubicin in human pancreatic, breast and prostate cancer cell lines," *Journal of Complementary and Integrative Medicine*, vol. 10, no. 1, 2013.
- [16] S. Chatterjee, Y. H. Rhee, and J. C. Ahn, "Sulforaphane-carboplatin combination synergistically enhances apoptosis by disruption of mitochondrial membrane potential and cell cycle arrest in human non-small cell lung carcinoma," *Journal of Medicinal Food*, vol. 19, no. 9, pp. 860–869, 2016.
- [17] M. M. Hossain, N. L. Banik, and S. K. Ray, "Synergistic anti-cancer mechanisms of curcumin and paclitaxel for growth inhibition of human brain tumor stem cells and LN18 and U138MG cells," *Neurochemistry International*, vol. 61, no. 7, pp. 1102–1113, 2012.

- [18] M. T. Piccolo, C. Menale, and S. Crispi, "Combined anticancer therapies: an overview of the latest applications," *Anti-Cancer Agents in Medicinal Chemistry*, vol. 15, no. 4, pp. 408–422, 2015.
- [19] J. Zou, L. Zhu, X. Jiang et al., "Curcumin increases breast cancer cell sensitivity to cisplatin by decreasing FEN1 expression," *Oncotarget*, vol. 9, no. 13, pp. 11268–11278, 2018.
- [20] G. Muthusamy, A. Balupillai, K. Ramasamy et al., "Ferulic acid reverses ABCB1-mediated paclitaxel resistance in MDR cell lines," *European Journal of Pharmacology*, vol. 786, pp. 194–203, 2016.
- [21] T. Saéñz Rodríguez, D. García Giménez, and R. de la Puerta Vázquez, "Choleretic activity and biliary elimination of lipids and bile acids induced by an artichoke leaf extract in rats," *Phytomedicine*, vol. 9, no. 8, pp. 687–693, 2002.
- [22] R. Gebhardt, "Inhibition of cholesterol biosynthesis in primary cultured rat hepatocytes by artichoke (*Cynara scolymus* L.) extracts," *The Journal of Pharmacology and Experimental Therapeutics*, vol. 286, no. 3, pp. 1122–1128, 1998.
- [23] B. Wider, M. H. Pittler, J. Thompson-Coon, and E. Ernst, "Artichoke leaf extract for treating hypercholesterolaemia," *Cochrane Database of Systematic Reviews*, vol. 3, 2013.
- [24] S. Miccadei, D. Di Venere, A. Cardinali et al., "Antioxidative and apoptotic properties of polyphenolic extracts from edible part of artichoke (*Cynara scolymus* L.) on cultured rat hepatocytes and on human hepatoma cells," *Nutrition and Cancer*, vol. 60, no. 2, pp. 276–283, 2008.
- [25] A. M. Mileo, D. Di Venere, V. Linsalata, R. Fraioli, and S. Miccadei, "Artichoke polyphenols induce apoptosis and decrease the invasive potential of the human breast cancer cell line MDA-MB231," *Journal of Cellular Physiology*, vol. 227, no. 9, pp. 3301–3309, 2012.
- [26] C. Pulito, F. Mori, A. Sacconi et al., "Cynara scolymus affects malignant pleural mesothelioma by promoting apoptosis and restraining invasion," *Oncotarget*, vol. 6, no. 20, pp. 18134–18150, 2015.
- [27] A. M. Mileo, D. Di Venere, C. Abbruzzese, and S. Miccadei, "Long Term Exposure to Polyphenols of Artichoke (*Cynara scolymus* L.) Exerts Induction of Senescence Driven Growth Arrest in the MDA-MB231 Human Breast Cancer Cell Line," *Oxidative Medicine and Cellular Longevity*, vol. 2015, Article ID 363827, 11 pages, 2015.
- [28] E. Azzini, R. Bugianesi, F. Romano et al., "Absorption and metabolism of bioactive molecules after oral consumption of cooked edible heads of *Cynara scolymus* L. (cultivar Violetto di Provenza) in human subjects: a pilot study," *The British Journal of Nutrition*, vol. 97, no. 5, pp. 963–969, 2007.
- [29] K. M. King, S. Lupichuk, L. Baig et al., "Optimal use of taxanes in metastatic breast cancer," *Current Oncology*, vol. 16, no. 3, pp. 8–20, 2009.
- [30] H. Xiao, P. Verdier-Pinard, N. Fernandez-Fuentes et al., "Insights into the mechanism of microtubule stabilization by Taxol," *Proceedings of the National Academy of Sciences of the United States of America*, vol. 103, no. 27, pp. 10166–10173, 2006.
- [31] B. T. McGrogan, B. Gilmartin, D. N. Carney, and A. McCann, "Taxanes, microtubules and chemoresistant breast cancer," *Biochimica et Biophysica Acta*, vol. 1785, no. 2, pp. 96–132, 2008.
- [32] C. Yokoyama, Y. Sueyoshi, M. Ema, Y. Mori, K. Takaishi, and H. Hisatomi, "Induction of oxidative stress by anticancer drugs in the presence and absence of cells," *Oncology Letters*, vol. 14, no. 5, pp. 6066–6070, 2017.
- [33] L. Balakrishnan and R. A. Bambara, "Flap endonuclease 1," *Annual Review of Biochemistry*, vol. 82, pp. 119–138, 2013.
- [34] Y. Liu, H. I. Kao, and R. A. Bambara, "Flap endonuclease 1: a central component of DNA metabolism," *Annual Review of Biochemistry*, vol. 73, pp. 589–615, 2004.
- [35] R. A. Bambara, R. S. Murante, and L. A. Henricksen, "Enzymes and reactions at the eukaryotic DNA replication fork," *The Journal of Biological Chemistry*, vol. 272, no. 8, pp. 4647–4650, 1997.
- [36] L. Zheng, J. Jia, L. D. Finger, Z. Guo, C. Zer, and B. Shen, "Functional regulation of FEN1 nuclease and its link to cancer," *Nucleic Acids Research*, vol. 39, no. 3, pp. 781–794, 2011.
- [37] E. Birben, U. M. Sahiner, C. Sackesen, S. Erzurum, and O. Kalayci, "Oxidative stress and antioxidant defense," *World Allergy Organization Journal*, vol. 5, no. 1, pp. 9–19, 2012.
- [38] B. H. Park, J. E. Lim, H. G. Jeon et al., "Curcumin potentiates antitumor activity of cisplatin in bladder cancer cell lines via ROS-mediated activation of ERK1/2," *Oncotarget*, vol. 7, no. 39, pp. 63870–63886, 2016.
- [39] Y. F. Huang, D. J. Zhu, X. W. Chen et al., "Curcumin enhances the effects of irinotecan on colorectal cancer cells through the generation of reactive oxygen species and activation of the endoplasmic reticulum stress pathway," *Oncotarget*, vol. 8, no. 25, pp. 40264–40275, 2017.
- [40] P. Nie, W. Hu, T. Zhang, Y. Yang, B. Hou, and Z. Zou, "Synergistic induction of erlotinib-mediated apoptosis by resveratrol in human non-small-cell lung cancer cells by down-regulating survivin and up-regulating PUMA," *Cellular Physiology and Biochemistry*, vol. 35, no. 6, pp. 2255–2271, 2015.
- [41] A. Mondal and L. L. Bennett, "Resveratrol enhances the efficacy of sorafenib mediated apoptosis in human breast cancer MCF7 cells through ROS, cell cycle inhibition, caspase 3 and PARP cleavage," *Biomedicine & Pharmacotherapy*, vol. 84, pp. 1906–1914, 2016.
- [42] M. M. Chan, K. J. Soprano, K. Weinstein, and D. Fong, "Epigallocatechin-3-gallate delivers hydrogen peroxide to induce death of ovarian cancer cells and enhances their cisplatin susceptibility," *Journal of Cellular Physiology*, vol. 207, no. 2, pp. 389–396, 2006.
- [43] M. K. Kwak, K. Itoh, M. Yamamoto, T. R. Sutter, and T. W. Kensler, "Role of transcription factor Nrf2 in the induction of hepatic phase 2 and antioxidative enzymes in vivo by the cancer chemoprotective agent, 3H-1, 2-dimethiole-3-thione," *Molecular Medicine*, vol. 7, no. 2, pp. 135–145, 2001.
- [44] M. Ramos-Gomez, M. K. Kwak, P. M. Dolan et al., "Sensitivity to carcinogenesis is increased and chemoprotective efficacy of enzyme inducers is lost in nrf2 transcription factor-deficient mice," *Proceedings of the National Academy of Sciences of the United States of America*, vol. 98, no. 6, pp. 3410–3415, 2001.
- [45] K. Taguchi and M. Yamamoto, "The KEAP1-NRF2 system in cancer," *Frontiers in Oncology*, vol. 7, p. 85, 2017.
- [46] L. S. Steelman, S. C. Pohnert, J. G. Shelton, R. A. Franklin, F. E. Bertrand, and J. McCubrey, "JAK/STAT, Raf/MEK/ERK, PI3K/Akt and BCR-ABL in cell cycle progression and leukemogenesis," *Leukemia*, vol. 18, no. 2, pp. 189–218, 2004.
- [47] J. A. McCubrey, L. S. Steelman, W. H. Chappell et al., "Roles of the Raf/MEK/ERK pathway in cell growth, malignant transformation and drug resistance," *Biochimica et Biophysica Acta*

- (BBA) - *Molecular Cell Research*, vol. 1773, no. 8, pp. 1263–1284, 2007.
- [48] F. Wei, J. Yan, and D. Tang, “Extracellular signal-regulated kinases modulate DNA damage response - a contributing factor to using MEK inhibitors in cancer therapy,” *Current Medicinal Chemistry*, vol. 18, no. 35, pp. 5476–5482, 2011.
- [49] K. J. Livak and T. D. Schmittgen, “Analysis of relative gene expression data using real-time quantitative PCR and the 2(-delta delta C(T)) method,” *Methods*, vol. 25, no. 4, pp. 402–408, 2001.
- [50] E. Mari, S. Mardente, E. Morgante et al., “Graphene oxide nanoribbons induce autophagic vacuoles in neuroblastoma cell lines,” *International Journal of Molecular Sciences*, vol. 17, no. 12, p. 1995, 2016.
- [51] A. Fransson, D. Glaessgen, J. Alfredsson, K. G. Wiman, S. Bajalica-Lagercrantz, and N. Mohell, “Strong synergy with APR-246 and DNA-damaging drugs in primary cancer cells from patients with TP53 mutant high-grade serous ovarian cancer,” *Journal of Ovarian Research*, vol. 9, no. 1, p. 27, 2016.
- [52] G. M. Calaf, R. Ponce-Cusi, and F. Carrion, “Curcumin and paclitaxel induce cell death in breast cancer cell lines,” *Oncology Reports*, vol. 40, no. 4, pp. 2381–2388, 2018.
- [53] D. E. McCloskey, S. H. Kaufmann, L. J. Prestigiacomo, and N. E. Davidson, “Paclitaxel induces programmed cell death in MDA-MB-468 human breast cancer cells,” *Clinical Cancer Research*, vol. 2, no. 5, pp. 847–854, 1996.
- [54] C. N. Tseng, Y. R. Hong, H. W. Chang et al., “Brefeldin A reduces anchorage-independent survival, cancer stem cell potential and migration of MDA-MB-231 human breast cancer cells,” *Molecules*, vol. 19, no. 11, pp. 17464–17477, 2014.
- [55] B. Halliwell, “Are polyphenols antioxidants or pro-oxidants? What do we learn from cell culture and in vivo studies?,” *Archives of Biochemistry and Biophysics*, vol. 476, no. 2, pp. 107–112, 2008.
- [56] H. S. Kim, M. J. Quon, and J. A. Kim, “New insights into the mechanisms of polyphenols beyond antioxidant properties; lessons from the green tea polyphenol, epigallocatechin 3-gallate,” *Redox Biology*, vol. 2, pp. 187–195, 2014.
- [57] S. Eghbaliferiz and M. Iranshahi, “Prooxidant activity of polyphenols, flavonoids, anthocyanins and carotenoids: updated review of mechanisms and catalyzing metals,” *Phytotherapy Research*, vol. 30, no. 9, pp. 1379–1391, 2016.
- [58] S. Chikara, L. D. Nagaprashantha, J. Singhal, D. Horne, S. Awasthi, and S. S. Singhal, “Oxidative stress and dietary phytochemicals: role in cancer chemoprevention and treatment,” *Cancer Letters*, vol. 413, pp. 122–134, 2018.
- [59] T. Enkhbat, M. Nishi, K. Yoshikawa et al., “Epigallocatechin-3-gallate enhances radiation sensitivity in colorectal cancer cells through Nrf2 activation and autophagy,” *Anticancer Research*, vol. 38, no. 11, pp. 6247–6252, 2018.
- [60] B. Velavan, T. Divya, A. Sureshkumar, and G. Sudhandiran, “Nano-chemotherapeutic efficacy of (-) -epigallocatechin 3-gallate mediating apoptosis in A549 cells: involvement of reactive oxygen species mediated Nrf2/Keap1 signaling,” *Biochemical and Biophysical Research Communications*, vol. 503, no. 3, pp. 1723–1731, 2018.
- [61] B. Chen, Y. Zhang, Y. Wang, J. Rao, X. Jiang, and Z. Xu, “Curcumin inhibits proliferation of breast cancer cells through Nrf2-mediated down-regulation of Fen1 expression,” *The Journal of Steroid Biochemistry and Molecular Biology*, vol. 143, pp. 11–18, 2014.
- [62] X. Deschênes-Simard, F. Kottakis, S. Meloche, and G. Ferbeyre, “ERKs in cancer: friends or foes?,” *Cancer Research*, vol. 74, no. 2, pp. 412–419, 2014.
- [63] Y. D. Shaul and R. Seger, “The MEK/ERK cascade: from signaling specificity to diverse functions,” *Biochimica et Biophysica Acta*, vol. 1773, no. 8, pp. 1213–1226, 2007.
- [64] D. Trachootham, W. Lu, M. A. Ogasawara, N. R. D. Valle, and P. Huang, “Redox regulation of cell survival,” *Antioxidants & Redox Signaling*, vol. 10, no. 8, pp. 1343–1374, 2008.
- [65] H. Luo, A. Yang, B. A. Schulte, M. J. Wargovich, and G. Y. Wang, “Resveratrol induces premature senescence in lung cancer cells via ROS-mediated DNA damage,” *PLoS One*, vol. 8, no. 3, article e60065, 2013.
- [66] W. J. Wu, Y. Zhang, Z. L. Zeng et al., “ $\beta$ -Phenylethyl isothiocyanate reverses platinum resistance by a GSH-dependent mechanism in cancer cells with epithelial-mesenchymal transition phenotype,” *Biochemical Pharmacology*, vol. 85, no. 4, pp. 486–496, 2013.
- [67] Q. Li, M. Zhan, W. Chen et al., “Phenylethyl isothiocyanate reverses cisplatin resistance in biliary tract cancer cells via glutathionylation-dependent degradation of Mcl-1,” *Oncotarget*, vol. 7, no. 9, pp. 10271–10282, 2016.
- [68] M. K. Kwak, K. Itoh, M. Yamamoto, and T. W. Kensler, “Enhanced expression of the transcription factor Nrf2 by cancer chemopreventive agents: role of antioxidant response element-like sequences in the nrf2 promoter,” *Molecular and Cellular Biology*, vol. 22, no. 9, pp. 2883–2892, 2002.
- [69] P. Singh, M. Yang, H. Dai et al., “Overexpression and hypomethylation of flap endonuclease 1 gene in breast and other cancers,” *Molecular Cancer Research*, vol. 6, no. 11, pp. 1710–1717, 2008.
- [70] X. Yan, M. Qi, P. Li, Y. Zhan, and H. Shao, “Apigenin in cancer therapy: anti-cancer effects and mechanisms of action,” *Cell & Bioscience*, vol. 7, no. 1, p. 50, 2017.
- [71] M. J. Lei, Y. Dong, C. X. Sun, and X. H. Zhang, “Resveratrol inhibits proliferation, promotes differentiation and melanogenesis in HT-144 melanoma cells through inhibition of MEK/ERK kinase pathway,” *Microbial Pathogenesis*, vol. 111, pp. 410–413, 2017.
- [72] C. Montagut and J. Settleman, “Targeting the RAF-MEK-ERK pathway in cancer therapy,” *Cancer Letters*, vol. 283, no. 2, pp. 125–134, 2009.

## Research Article

# Antitumoral and Immunomodulatory Effect of *Mahonia aquifolium* Extracts

Andra Diana Andreicuț,<sup>1</sup> Eva Fischer-Fodor<sup>1,2,3</sup>, Alina Elena Pârvu<sup>1</sup>,  
Adrian Bogdan Țigu,<sup>2,4</sup> Mihai Cenariu<sup>5</sup>, Marcel Pârvu,<sup>4</sup> Florinela Adriana Cătoi<sup>1</sup>,  
and Alexandru Irimie<sup>6</sup>

<sup>1</sup>Pathophysiology, Faculty of Medicine, University of Medicine and Pharmacy Iuliu Hațieganu, RO-400012 Cluj-Napoca, Romania

<sup>2</sup>Medfuture Research Center for Advanced Medicine, University of Medicine and Pharmacy Iuliu Hațieganu, RO-400012 Cluj-Napoca, Romania

<sup>3</sup>Tumor Biology Department, The Oncology Institute I. Chiricuță, RO-, 400015 Cluj-Napoca, Romania

<sup>4</sup>Faculty of Biology and Geology, Babeș-Bolyai University, RO-400015 Cluj-Napoca, Romania

<sup>5</sup>Biotechnology Research Center, University of Agricultural Science and Veterinary Medicine, Cluj-Napoca, Romania

<sup>6</sup>Oncology, Faculty of Medicine, University of Medicine and Pharmacy Iuliu Hațieganu, RO-400012 Cluj-Napoca, Romania

Correspondence should be addressed to Eva Fischer-Fodor; [fischer.eva@iocn.ro](mailto:fischer.eva@iocn.ro)  
and Alina Elena Pârvu; [parvulinaelena@yahoo.com](mailto:parvulinaelena@yahoo.com)

Received 23 August 2019; Revised 31 October 2019; Accepted 2 November 2019; Published 16 December 2019

Academic Editor: Ji C. Bihl

Copyright © 2019 Andra Diana Andreicuț et al. This is an open access article distributed under the Creative Commons Attribution License, which permits unrestricted use, distribution, and reproduction in any medium, provided the original work is properly cited.

The prodrug potential of *Mahonia aquifolium*, a plant used for centuries in traditional medicine, recently gained visibility in the literature, and the activity of several active compounds isolated from its extracts was studied on biologic systems *in vitro* and *in vivo*. Whereas the antioxidative and antitumor activities of *M. aquifolium*-derived compounds were studied at some extent, there are very few data about their outcome on the immune system and tumor cells. To elucidate the *M. aquifolium* potential immunomodulatory and antiproliferative effects, the bark, leaf, flower, green fruit, and ripe fruit extracts from the plant were tested on peripheral blood mononuclear cells and tumor cells. The extracts exert fine-tuned control on the immune response, by modulating the CD25 lymphocyte activation pathway, the interleukin-10 signaling, and the tumor necrosis-alpha secretion in four distinct human peripheral blood mononuclear cell (PBMC) subpopulations. *M. aquifolium* extracts exhibit a moderate cytotoxicity and changes in the signaling pathways linked to cell adhesion, proliferation, migration, and apoptosis of the tumor cells. These results open perspectives to further investigation of the *M. aquifolium* extract prodrug potential.

## 1. Introduction

In the tumor microenvironment (TME), tumor intrinsic factors and tumor extrinsic factors work together to induce immunosuppression. The composition of TME depends on the cancer types and disease stages. The tumor cells chronically secrete tumor intrinsic factors. Some of them induce reduction of the immune effector cell activity and promote immune evasion by decreasing the expression of antigen-presenting molecules and by expressing neoantigens. In the same time, the tumor cells use autocrine or paracrine signals in order to stimulate the expression of immune checkpoints

(ICs) [1, 2] on immune cells and to upregulate immunosuppressive cell recruitment and activation [3]. The tumor cells also secrete cytokines and growth factors that promote tumor growth, angiogenesis, and metastasis [4].

The tumor extrinsic factors are provided by immune and nonimmune cells [4]. The immune cells of the TME are T cells, B cells, macrophages, monocytes [5], dendritic cells, and NK cells [6], and an efficient antitumor immune response implies both helper CD4+ and effector CD8+ T cells activated in proximity to each other [7]. T regulatory cells (Tregs) are a subset of CD4+ T cells, with immunosuppressive activity by inhibiting cytotoxic CD8+ T cells and effector

CD4+ T cell activation, via consumption of IL-2, release of TGF- $\beta$  and IL-10, and IC expression upregulation [4, 8]. B regulatory cells (Bregs), a subset of B cells, and tumor-associated macrophages (TAMs) reduce the activity of cytotoxic CD8+ and CD4+ T effector cells by releasing anti-inflammatory cytokines like IL-10 and by expressing coinhibitory molecules [9–11]. TAMs also stimulate tumor growth and metastasis by secreting matrix metalloproteinases (MMPs) and proangiogenic factors, like VEGF [10]. Other tumor-associated immune cells are myeloid-derived suppressor cells (MDSCs) [12], a heterogeneous population of myeloid cell precursors that can suppress cytotoxic CD8+ T cell; tumor-associated mast cells (TAMCs), with a controversial immunosuppressive role; and tumor-associated dendritic cells (TADCs), which can inhibit cytotoxic CD8 + T cells by expressing inhibitory molecules and releasing IL-10 and TGF- $\beta$  [13].

From the TME nonimmune cells, the most important are cancer-associated fibroblasts (CAFs) and tumor endothelial cells (TECs) [4]. As a response to TME hypoxia and tumor cell intrinsic factor release, normal resident fibroblasts are converted to CAFs [14, 15]. They stimulate tumor growth, invasion and metastasis, MMPs, angiogenesis, and CD8+ T cell apoptosis [4]. TECs are different from the normal epithelial cells due to the morphological abnormalities and induce angiogenesis with new vessel formation that allows tumor cell metastasis. Moreover, active TECs release their own growth and angiogenic factors, further stimulating neighboring tumor cell growth [16, 17].

The cells of the immune system should stop the tumor growth and the progression by recognition and removal of the malignant cells [18]. Instead, it was found that the result of the interaction between immune and nonimmune cells in the TME is tumor-mediated immunosuppression [4, 19]. Furthermore, the tumor-mediated immunosuppression may also reduce cancer therapy efficiency and may induce resistance to therapy.

The genus *Mahonia* Nuttall has about 70 species, and it is the second largest genus in the Berberidaceae family. *Mahonia* plants are native to Eastern Asia, North America, and Central America [20] and have been widely used in traditional medicine for centuries. It was shown that *Mahonia* species have antioxidant, anti-inflammatory [21, 22], antifungal, antimicrobial [23], antiproliferative, hepatoprotective, and analgesic effects [24]. Phytochemical analysis proved that alkaloids represent the major constituents of the genus, and some studies reported that they have anticancer effects. For *Mahonia bealei* and *Mahonia oiwakensis*, cytotoxic activity against human cancer cells was demonstrated [24, 25]. Previous studies also found in *M. aquifolium* extracts important quantities of alkaloids with cytotoxic effects on cancer cells [26]. One study demonstrated cytotoxic and antimetastatic effects of *M. aquifolium* stem-bark extract [27].

The phytochemical profile of plant extracts differs depending on the plant and the particular organ of a given plant [28] and of the extraction method [29]; the aim of the study was to test if *M. aquifolium* bark, leaf, flower, green fruit, and ripe fruit extracts can influence the TME in order to increase the antitumor responses. First, *M. aquifolium*

extract immunomodulatory effects were tested on four human peripheral blood mononuclear cell (PBMC) subsets which have a key role in the adaptive immunity: CD4+ helper T cells, CD8+ effector T cells, CD19+ B cells, and CD14+ monocytes. Secondly, *M. aquifolium* extract antitumoral effects were tested on three cancer cell lines, DLD-1 colon carcinoma cells, A2780 ovary adenocarcinoma cells, and A375 malignant melanoma cell, and a nonimmune cell, BJ healthy skin fibroblast.

## 2. Materials and Methods

**2.1. Plant Material.** Fresh *Mahonia aquifolium* (Pursh) Nutt. bark, leaves, flowers, and fruits were purchased from the A. Borza Botanical Garden “Babes-Bolyai” University of Cluj-Napoca, Romania, between April and June 2018 and extracted in the Mycology Laboratory of “Babes-Bolyai” University, Cluj-Napoca, Romania, as previously described by a modified Squibb repercolation method with 70% ethanol (Merck, Bucuresti, Romania), producing the following extracts of *M. aquifolium*: bark extract 1 : 1.5 (g : mL) (1), leaf extract 1 : 1.2 (g : mL) (2), flower extract 1 : 1 (g : mL) (3), green fruit extract 1 : 1 (g : mL) (4), and ripe fruit extract 1 : 1 (g : mL) (5). The phytochemical analysis of the extracts has been performed and previously published [26, 30]. The plants were taxonomically identified and authenticated, and voucher specimens (number 665978) were deposited in “Alexandru Borza” Botanical Garden Herbarium, “Babes-Bolyai” University of Cluj-Napoca, Romania. The stock solutions were diluted with Phosphate-Buffered Saline Solution (PBS, from Sigma-Aldrich Company, St. Louis, USA), to obtain for each extract a series of stock concentrations from 500 to 10  $\mu$ g plant/mL.

### 2.2. Immunomodulatory Effects

**2.2.1. Isolation of PBMC Subsets.** The biologic system used for testing was the suspensions of human PBMC, obtained by venipuncture from a 25-year-old healthy male volunteer, who gave his informed written consent before the blood collection, according to the approvals from the Ethical Committee of the Institute of Oncology “Prof. Dr. Ion Chiriacuta” from Cluj-Napoca (IOCN), Romania, member of OEIC. CD4+ helper T cells, CD8+ effector T cells, CD19+ B cells, and CD14+ monocytes were separated as previously described [31] (see supplemental data (available here)).

**2.2.2. PBMC Cytotoxicity Test.** To assess cytotoxicity serial dilutions from *M. aquifolium* extracts, stock solutions were prepared, in order to obtain 5 successive concentrations, from 20  $\mu$ g/mL to 1  $\mu$ g/mL. The cytotoxicity of the extracts was assessed using the MTS viability dye (CellTiter 96 Proliferation Assay, manufactured by Promega Corporation, Madison, WI, USA), as previously described [31] (see supplemental data).

**2.2.3. Detection of IL-10-Positive and CD25-Positive Cells.** After a prolonged exposure to the extracts 1-5 at a subcytotoxic concentration, CD4+, CD8+, CD19+, and CD14+ cell activation pathways through CD25 and interleukin-10 (IL-

10), an immune-activating cytokine implicated in cancer immunotherapy [32], were evaluated by flow cytometry (see supplemental data).

**2.2.4. Tumor Necrosis Factor Alpha (TNF- $\alpha$ ) Production.** The soluble form of tumor necrosis factor alpha (TNF- $\alpha$ ) production was measured, knowing that this inflammatory cytokine has an important role in tumor proliferation, metastasis, and neoangiogenesis [33]. The evaluation of the secreted TNF- $\alpha$  level through ELISA testing (kit acquired from Hycult Biotech, Uden, The Netherlands) was performed according to the manufacturer indication (see supplemental data).

### 2.3. Antitumoral Effect Evaluation

**2.3.1. Cell Cultures.** The human cell lines used in the present study were DLD-1 colon carcinoma and the A2780 ovary adenocarcinoma cell lines acquired from the European Collection of Authenticated Cell Cultures (ECACC) through Sigma-Aldrich, St. Louis, USA; the A375 malignant melanoma and the BJ healthy skin fibroblast cell lines were from the American Type Culture Collection (ATCC) acquired through LGC Standards GmbH, Wesel, Germany (see supplemental data).

**2.3.2. Cytotoxicity Test.** For the cytotoxicity testing, the colorimetric assay based on the tetrazolium dye 3-(4,5-dimethylthiazol-2-yl)-2,5-diphenyltetrazolium bromide (MTT) reduction to its purple colored formazan product was used. Because this process occurs only in the mitochondria of the living cells, the amount of living cells can be tracked by the color intensity of the samples. All experiments were performed in triplicates. The samples were analyzed as previously described [34] (see supplemental data).

**2.3.3. Protein Content of the Samples.** For proteomic methods, the tumor and normal cells were seeded on 6-well plates at a concentration of  $10^5$  cells/mL, and after 24 hours, they were treated with a  $10 \mu\text{g/mL}$  solution of each extract. The supernates and cell lysates were kept at  $-20^\circ\text{C}$  until analysis. To evaluate the supernatants and cell homogenate total protein content, the Bradford assay was used. The calibration curve was prepared using seven serial dilutions starting from  $100 \mu\text{g/mL}$  proteins to  $1.56 \mu\text{g/mL}$  proteins (see supplemental data).

**2.3.4. Intracellular Caspase-3 and Caspase-8.** The intracellular caspase-3 and caspase-8 were measured with an ELISA method, and the caspase concentration provided by the quantitative measurement (ng/mL) was normalized according to the total protein content of each lysate sample, and in this way, the caspase level was expressed as ng/mg protein, to ensure an accuracy of the assessment (see supplemental data).

**2.3.5. Soluble Intracellular Adhesion Molecule-1 (ICAM-1) and Vascular Cell Adhesion Molecule-1 (VCAM-1/CD106).** ICAM-1 was determined by using a human ELISA kit (E-EL-H2585 from Elabscience Biotechnology Co. Ltd., Houston, TX, USA), and VCAM-1/CD106 was measured with a human ELISA kit (E-EL-H5587, from Elabscience Biotechnology Co. Ltd., Houston, Texas) according to the

manufacturer indications. ICAM-1 and VCAM-1/CD106 were expressed as ng/mg protein (see supplemental data).

**2.3.6. Matrix Metalloproteinase-9 (MMP-9).** MMP-9 was assessed with a human MMP-9 Platinum ELISA kit (MBS2016/2, from Affymetrix, through eBioscience, Vienna, Austria), according to the manufacturer's indications. MMP-9 was expressed as ng/mg protein (see supplemental data).

**2.4. Statistical Analysis.** GraphPad Prism 5 software (from GraphPad Software Inc., La Jolla, CA, USA) was used to compute IC50 values (nonlinear regression of the concentration versus normalized response) and Spearman nonparametric correlations, to compare values with the one-way analysis of variances, followed by Bonferroni or Dunnett multiple comparison posttest, and to compute the mean values and the standard error of the mean (SEM).

To examine the strengths of associations between the results, specifically Pearson correlations, we have used Statistica 12.0 for Windows (Stat-soft, Inc., USA). Multivariate data analysis was performed on the entire antioxidant and hematological parameters determined in this study using PCA (principal component analysis) incorporated in Statistica 12.0 software.

## 3. Results and Discussion

### 3.1. Immunomodulatory Effect

**3.1.1. PBMC Cytotoxicity Test.** From each *Mahonia aquifolium* extract, five concentrations were tested, between 1 and  $20 \mu\text{g/mL}$  in the cell culture media. All concentrations exhibited low cytotoxicity against PBMC, including the  $20 \mu\text{g/mL}$  concentration. The survival rates of the cells treated with the highest concentration were shown in Figure 1(a) (see supplemental data Table 5).

In all PBMC subpopulations, *M. aquifolium* extracts 1-5 treatment induced a similar growth inhibition pattern. Extract 1 exerted the highest inhibitory effect, followed by 2 (Figure 1(b)), while 3, 4, and 5 caused less than 10% cell loss after 24-hour exposure. Consequently, for further testing, we used all extracts at the concentration of  $20 \mu\text{g/mL}$ . The principal component analysis (PCA) clearly indicated (Figure 1(b)) the similarities between 1 and 2 effects, these extracts being in the same quadrant of the loading plot, at distance to the group of extracts 3, 4, and 5, placed in another quadrant; further, 1 and 2 are distanced to more than 90 degrees to the least active 3 and 5 *M. aquifolium* extracts.

**3.1.2. IL-10-Positive and CD25-Positive Cells.** The immunomodulatory effect of *M. aquifolium* extracts was evaluated by monitoring the number of CD25+ and IL10+ cells within a population of 10000 PBMC. CD25 and IL10 membrane marker expression was assessed by flow cytometry, and each data represents the median value of 10000 measurements, provided by the BD FACSDiva version 6.1 software. For each sample, two independent evaluations were made; their mean value was calculated with the column statistics, and the comparison between values was provided by the one-way analysis

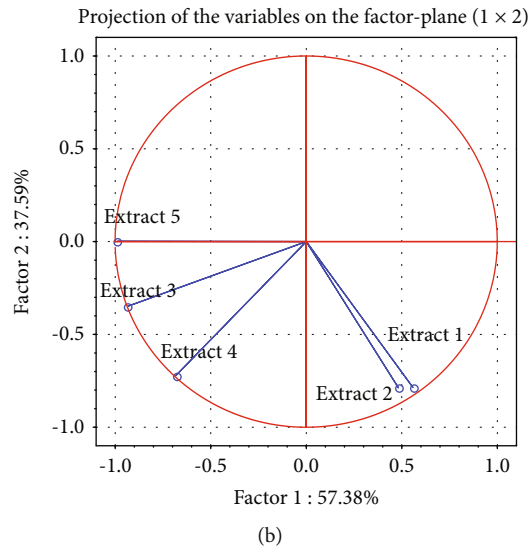
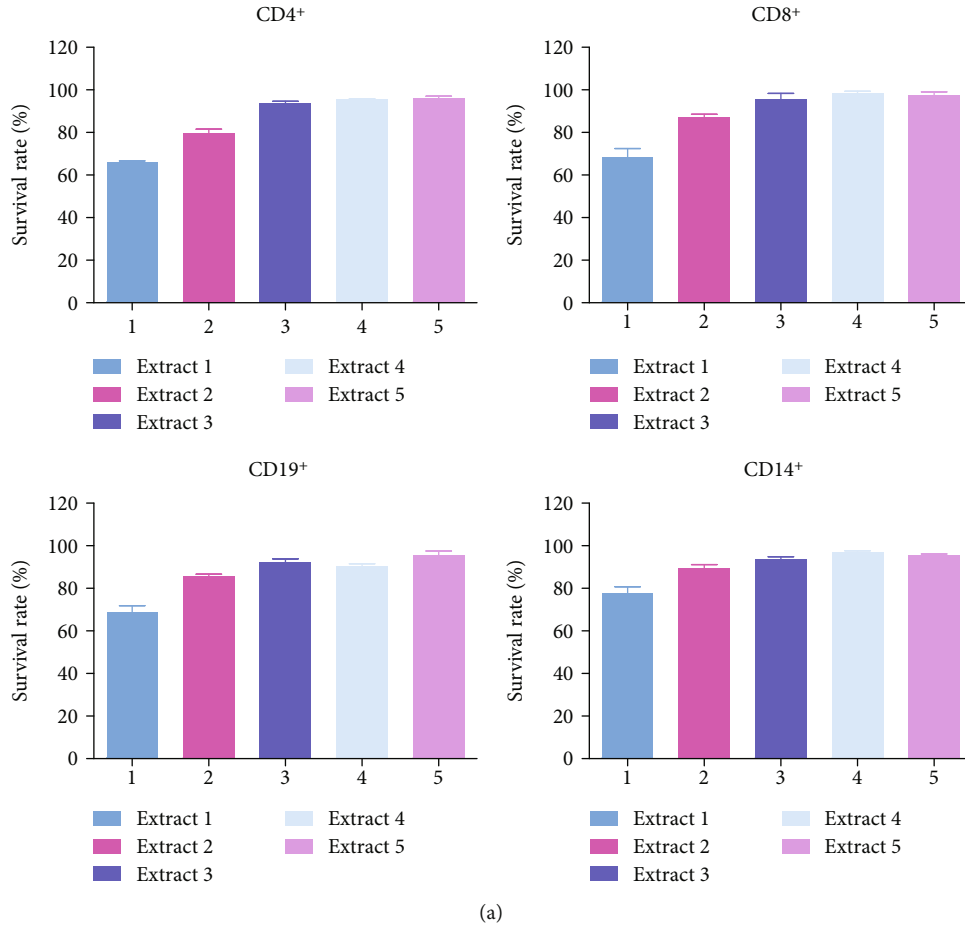


FIGURE 1: (a) Survival rate of PBMC subsets CD4+, CD8+, CD19+, and CD14+ treated for 24 hours with the *M. aquifolium* extracts 1-5, at a concentration of 10  $\mu\text{g}/\text{mL}$  in the cell culture media. (b) Correlation circle (loading plot) depicting the relationship between the extract outcomes on different PBMC subpopulations—a model obtained after applying principal component analysis.

of variance in the 95% interval (Table 1) (see supplemental data Figures 10–13).

Following the 24-hour exposure of the PBMC subsets to 1-5 *M. aquifolium* extracts, both the CD25 membrane marker and

the IL-10 intracytoplasmic marker were modulated distinctly in each cell subpopulation. In untreated T cells, the basal level of the two molecules was modest, while in B lymphocytes and monocytes the basal values were higher (Table 1).



TABLE 1: The *in vitro* effect of *M. aquifolium* extracts 1-5 on CD25 membrane marker and intracellular IL-10 expression in CD4+, CD8+, CD14+, and CD19+ cells.

Cell types	Q1—CD25 FITC		Q2—CD25 FITC/IL-10 PE		Q4—IL10 PE	
	Median values	SD	Median values	SD	Median values	SD
<b>CD4+</b>						
Untreated	23.5	0.71	62.5	2.12	86.5	2.12
Extract 1	301.5***	12.73	1108.5***	4.95	53.0***	1.41
Extract 2	12.0	1.41	57.5	3.54	113.5*	7.78
Extract 3	12.0	2.83	180.5***	0.71	333.0***	2.83
Extract 4	17.5	3.54	154.5***	6.36	243.0***	12.73
Extract 5	7.5	0.71	136.5***	2.12	158.5***	2.12
<b>CD8+</b>						
Untreated	3.0	0.00	58.0	2.89	162.5	9.19
Extract 1	119.5***	0.71	396.0***	1.41	113.0***	0.00
Extract 2	2.0	0.00	114.5***	6.36	122.0***	0.00
Extract 3	1.5	0.71	61.5	0.71	148.0	4.24
Extract 4	1.0	0.00	55.5	6.36	95.5***	0.71
Extract 5	2.5	0.71	97.0***	0.00	91.5***	0.71
<b>CD14+</b>						
Untreated	51.0	1.41	268.0	2.83	349.0	1.41
Extract 1	310.5***	0.71	1131.0***	1.41	71.5***	2.12
Extract 2	9.5***	0.61	129.5***	0.71	248.0***	2.83
Extract 3	12.5***	2.12	188.0***	2.83	320.0**	12.73
Extract 4	22.5***	3.55	167.5***	3.54	179.5***	2.12
Extract 5	8.5***	2.12	189.5***	2.12	188.0***	2.83
<b>CD19+</b>						
Untreated	90.0	0.00	209.0	1.41	118.5***	9.19
Extract 1	81.0	1.41	582.5***	3.54	241.5***	7.78
Extract 2	11.5***	2.12	322.0***	2.83	290.5***	0.71
Extract 3	33.0***	2.83	358.0***	5.66	230.0***	0.00
Extract 4	29.0***	1.41	481.5***	9.19	338.5***	4.95
Extract 5	21.0***	1.41	359.5***	0.71	232.5***	3.54

\*\*\*Extremely significant differences between treated cells vs. untreated control,  $p < 0.001$ . \*\*Very significant differences between treated cells vs. untreated control,  $0.001 < p < 0.01$ . \*Significant differences between treated cells vs. untreated control,  $0.01 < p < 0.05$ .

The effect of 1, the bark extract, was the prominent regulator of the lymphocyte activation through the CD25 pathway. Extract 1 distinguishes itself from other extracts through its lower chlorogenic acid content (see Supplemental data Table 7) and through the presence of berbamine, jatrorrhizine, palmatine, and berberine, four compounds that are not present in the extracts 2 to 5 [26, 30].

Extract 1 upregulated the CD4+CD25+, CD8+CD25+, and CD14+CD25+ phenotype expression, and in this manner, 1 triggered the activation of both tumor suppressor and effector lymphocyte subsets and also the CD14+CD25+

monocytes, the main population of blood monocytes implicated in antitumor response [35]. CD14+ cells were proven to act against the tumor cells and the metastatic processes, directly by an antibody-mediated mechanism [36] and indirectly by activating the natural killer cells [37].

T cells which expressed CD4+ and CD25+ are essential in self-recognition and are known as T regulatory cells [38] and maintain the self-tolerance control in the immune response against infections, transplantation antigens, and tumor-associated antigens [39]. CD4+ T cells play antitumor roles through various mechanisms, and some studies claim that they could be efficient even in antitumoral immunotherapy like CD8+, previously known as the gold standard [40]. Although tumor-infiltrating CD4+CD25+ lymphocytes can contribute to the progression of the disease [41], they may act against tumors indirectly, helped by NK cells, or by inactivating the IL-10 pathway [42].

The fact that 1 exerts a significant enhancement of CD8+CD25+ activated phenotype converges to the antitumor potential of the bark extract, since CD8+ are important effectors of the antitumor cellular immunity in several cancers [43], counteracting the metastatic potential of tumor cells [44], and it was proven that their presence is related to the patient survival [45]. The increase of CD25+IL-10+ phenotype occurred following the treatments with 1, the only extract able to increase CD25, or concomitant with the increase of IL-10 induced by 2-5 in CD4+ and CD19+ (Table 1). IL-10 sustain the toxicity in CD8+ cells, [42] and in high concentrations, IL-10 is able to inhibit tumor growth by inhibiting the angiogenesis and the production of reactive oxygen species [46].

Extracts 2, 3, 4, and 5 could not influence significantly CD4+ or CD8+ cells. Instead, they influenced the double-positive populations and the IL-10 expression in these two subsets. Extract 2 increased the CD25+IL-10+ expression only on cytotoxic CD8+ T lymphocytes, without augmenting the helper CD4+ activation. Extracts 3 and 5 enhanced the CD25+IL-10+ activation in cytotoxic CD8+ cells but parallel in the regulatory CD4+ T cells. Overall, the PCA indicated that the outcome of the extracts on CD4+ subpopulation was opposed to CD8+, and the effect of 1-5 on CD14+ is opposed to CD19+ cells (Supplemental data Figure 14).

In CD19+ B cells, all extracts 1-5 performed likewise: they exerted a strong downregulatory effect on CD25+ cells, but the CD25+IL-10+ phenotype was upregulated (Table 1). The CD19+ expression is essential in the B cell-mediated immune response [47]. The increase of CD19+ cells and the regulatory CD19+CD25+IL-10+ B cell overexpression enhance the immunoglobulin production, but in tumors, it is responsible for metastatic growth support [48] as well, by costimulating the Treg cells. The CD19+CD25+IL-10+ phenotype was confirmed to be protector against inflammation [49] and promotes allograft survival in transplantation [50].

In CD14+, monocytes 2-5 had a strong downregulatory effect through CD25 and IL-10 decrease (Table 1), acting contrary to extract 1.

The IL-10 expression decreased following the treatment with extract 1 in CD4+, CD8+ T cells, and monocytes and

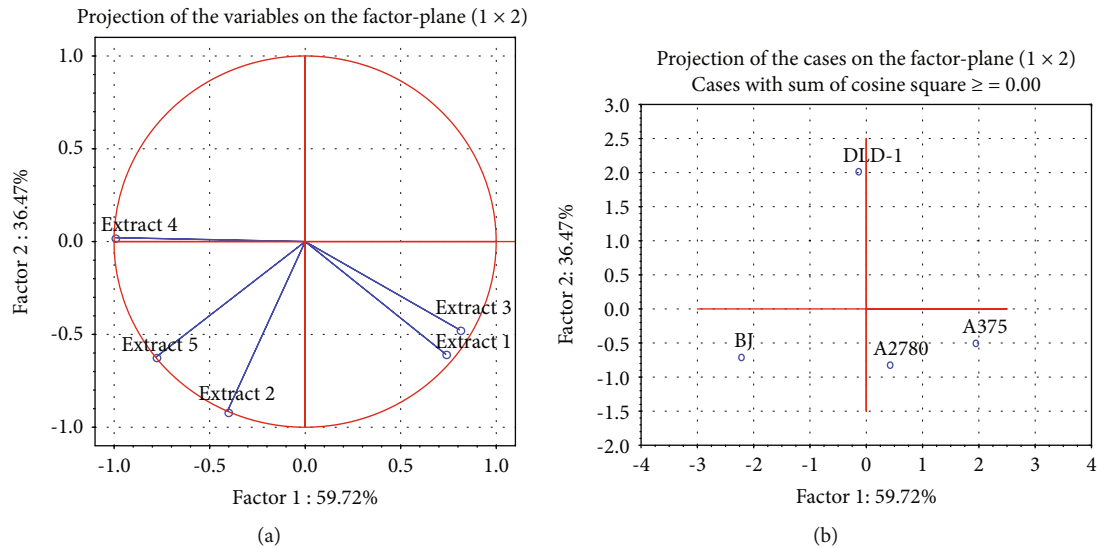


FIGURE 2: Principal component analysis on the extract half inhibitory concentrations: (a) correlation circle (loading plot) using the first two principal components of the PCA model obtained after applying tumoral cells (IC50) and (b) score plot using the first three principal components of 1-5 (tumoral cells) based on IC50.

strongly upregulated in CD19+B cells (Figure 2). In IL-10 modulation as well, extracts 2, 3, 4, and 5 act convergently: they caused a significant increase of IL-10 phenotype in helper CD4+ T cells and CB19+ B cells and decline in effector CD8+ T cells and CD14+ monocytes.

It was a strong correlation between the CD25+ and CD25+IL-10+ phenotype in all subsets (Spearman non-parametric correlation,  $p < 0.0001$ ) which means that the two subpopulations tend to increase or to decrease in the same time. In all PBMC subsets, the treatment with 1-5 induced no significant correlation between CD25+ and IL-10+ expression (nonparametric two-tailed correlation, Spearman  $p > 0.05$ ).

**3.1.3. Tumor Necrosis Factor Alpha (TNF- $\alpha$ ) Production.** TNF is a multifunctional cytokine that has important roles in cell survival, proliferation, differentiation, and death. As a proinflammatory cytokine, TNF may be implicated in inflammation-induced carcinogenesis. TNF exerts its functions by activating distinct nuclear factor- $\kappa$ B (NF- $\kappa$ B), an antiapoptotic signal, and c-Jun N-terminal kinase (JNK), a cell death signal. So, TNF is a double-edged sword with pro- or antitumorogenic effects [51], which in the early stages can contribute to antitumor response enhancement, while in late stages, it could maintain the tumor growth [52]. All PBMC subsets have had a certain basal TNF- $\alpha$  level (Figure 3), since CD4+ and CD8+ T lymphocyte subsets, B cells, and CD14+ monocytes are TNF- $\alpha$  secretory cells [53]. Following the treatment, TNF- $\alpha$  was modulated distinctively in each PBMC population. Extracts 1 and 2 had no effect on T or B cells, but they upregulate the TNF- $\alpha$  in CD14+ cells. In CD14+ monocytes, the main population of blood monocytes implicated in antitumor response, the direct cytotoxicity against the target cells is mediated by TNF- $\alpha$ , IL-12, reactive oxygen species, and reactive nitrogen species [35]. Since 1

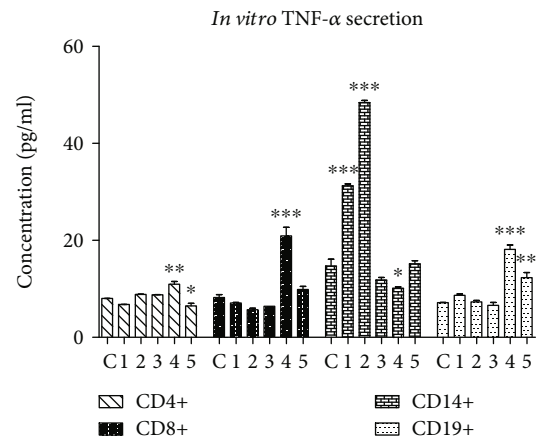


FIGURE 3: The *in vitro* effect of *M. aquifolium* extracts on soluble TNF- $\alpha$  secreted by the CD4+, CD8+, CD14+, and CD19+ cells after a 24-hour exposure to subcytotoxic doses. \*\*\*Extremely significant differences between treated cells vs. untreated control,  $p < 0.001$ ; \*\*very significant differences between treated cells vs. untreated control,  $0.001 < p < 0.01$ ; \*significant differences between treated cells vs. untreated control,  $0.01 < p < 0.05$ .

and 2 modulated significantly the cytokine production only in CD14+ monocytes, it is expected that these two extracts will enhance the CD14+ cell antitumor capacity. Extract 3 was completely inert in the PBMC biologic system. Surprisingly, extract 4 obtained from green fruits significantly decreases the TNF- $\alpha$  production of monocytes, while in all the other studied subpopulations causes a very significant increase of TNF- $\alpha$ . Novel studies suggested that the increase of TNF- $\alpha$  secreted by the tumor-infiltrating T cells and monocytes may enhance the tumor cell death without associated systemic toxicities [52]. The TNF- $\alpha$  secreted by T lymphocytes can synergize with chemotherapy to strengthen

tumor cell death mechanisms and the induced oxidative stress [54], and by enhancing the TNF- $\alpha$  production in CD4+ and CD8+ lymphocytes, extract 4 could balance the regulatory mechanisms induced through CD25. Extract 5 inhibited the TNF- $\alpha$  secretion in CD4+ T cells, and in B cells, a stimulation was observed.

Previous studies reported that in CD4+ and CD8+ T cells the IL-10+ phenotype is suppressed by exogenous TNF- $\alpha$  [55]. This was confirmed by the decrease of IL-10 positivity in CD8+ cells treated with 4, concomitant with the highest TNF- $\alpha$  secretion. It is known that TNF- $\alpha$  downregulates the function of tumor suppressor CD4+CD25+ lymphocytes [56], but overall, no correlation was found between TNF- $\alpha$  secretion and the IL-10+ or CD25+IL10+ expression.

As a conclusion, *M. aquifolium* extracts 1-5 exhibit moderate toxicity against PBMC subpopulations without selectivity towards any of the four studied subsets, and their modulator effect through CD25, IL-10, and TNF- $\alpha$  was well-balanced. The bark extract (1) effect was distinct, as regards the cytotoxicity, and its capacity to prime the helper CD4+ cells via CD25 activation, but this was compensated by the enhancement of CD8+ cytotoxic T lymphocyte activity. Also, 1 stimulated the immunoglobulin (the B cell secretor) through CD25 and IL-10 and triggered and amplified the TNF- $\alpha$  production in CD14+ monocytes only. The leaf extract (2), the richest in chlorogenic acid, rutin and isoquercitrin, has the capacity to activate the effector CD8+ lymphocytes and the B cells, deactivate the CD14+ monocytes, and in the same time increase a fold higher their TNF- $\alpha$  production.

TNF- $\alpha$  secretion was correlated with the CD25+ and CD25+IL-10+ phenotype but not with the CD25-IL-10+ cells (Supplemental data Figure 15). The PCA statistic confirms once again that CD25+ and CD25+IL-10+ populations were strongly correlated. In the tridimensional PCA (Figure 4), TNF- $\alpha$  variations were considered as a principal component; the concentrations of TNF- $\alpha$  were plotted with different colors, against the CD25 and IL-10 parameters. We can conclude that above the 100% increase of TNF- $\alpha$ , both IL-10 and CD25/IL-10 phenotype are overexpressed. Where the TNF- $\alpha$  is stationary towards the control values, then IL-10 is negatively correlated with CD25+ expression.

The flower extract (3) has the most moderate effect, it does not influence the T cells or monocyte activation or the TNF- $\alpha$  production; the only enhancement of activation was in B cells through the IL-10; therefore, the application of these extracts as part of a potential cancer treatment should not exhibit any unwanted effect on antitumor immunity.

There was a significant difference between green fruit extract 4 and ripe fruit extract 5, even if their composition is quite similar [26], the only notable difference being the higher chlorogenic acid level in 5. Extract 4 activates via IL-10 and not via CD25 the helper lymphocytes, deactivating the effector lymphocytes and monocytes. The only cell population which could be activated through 4 was the B subset, where the TNF- $\alpha$  production was also very high, costimulating the B cell responsiveness. Following the treatment with extract 5, the same outcome occurred at a smaller scale.

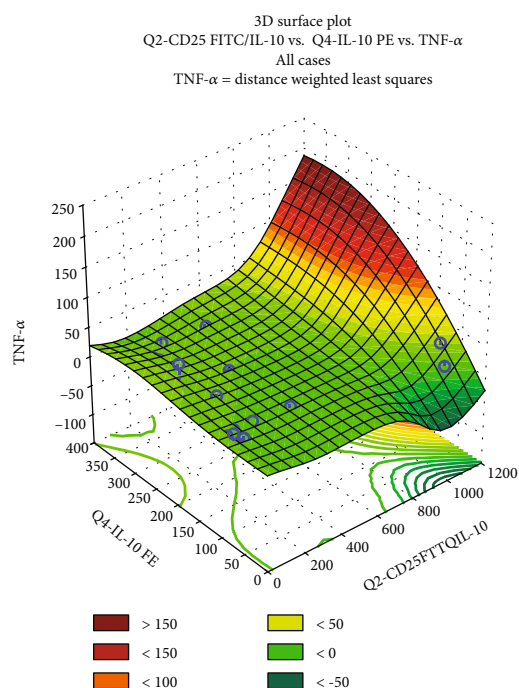


FIGURE 4: Dependence between the modulation of TNF- $\alpha$ , CD25, and IL-10 modulation for the studied Mahonia extracts, expressed as a tridimensional surface plot generated by the Statistica 12 principal component analysis (PCA).

### 3.2. Antitumoral Effect

**3.2.1. Cytotoxicity Test.** The toxicity of the *M. aquifolium* bark (1), leaf (2), flower (3), green fruit (4), and ripe fruit (5) extracts was assessed and quantified using the mathematic parameter half inhibitory concentration IC<sub>50</sub>, which represents the amount of compound necessary to eliminate 50% from the cells subjected to the treatment. Therefore, a small IC<sub>50</sub> value is a characteristic for the toxic compounds (Table 2).

*In vitro*, extract 1 exhibited the best cytotoxicity, corresponding to the smallest IC<sub>50</sub> value in the whole series (Table 2). This tendency was convergent in all cell lines, the IC<sub>50</sub> values being around 10  $\mu$ g/mL, which is a moderate cytotoxicity according to the pharmacologic standards. Only extract 1 displays a dose-response relationship which can be described by the sigmoidal curve; in all the rest of extracts, the sigmoidal curves are distorted, because none of the tested concentrations was able to inhibit 100% of the cells (see supplemental data Figure 16). This effect can be correlated to the higher alkaloid content in the *M. aquifolium* bark extract [26]. Even the highest concentration of the extract was not able to inhibit 50% of the cells when the treatment was made with extracts 3 (in all cell lines), 4, and 5 (each in two cell lines); therefore, the IC<sub>50</sub> values above 50  $\mu$ g/mL provided by the biostatistics software are hypothetical values, obtained by extrapolation.

The PCA statistics indicated few convergences in the extract IC<sub>50</sub> values, when all the cell lines were analyzed (Figure 2(a)); A2780 and A375 outcome was well correlated, since the two values are in the same quadrant. The best

TABLE 2: Half inhibitory concentrations (IC<sub>50</sub>) of *M. aquifolium* extracts 1-5 on tumor and normal cell lines after 24-hour *in vitro* treatment, expressed as median value ( $\mu\text{g/mL}$ )  $\pm$  standard error (SD) of logIC<sub>50</sub>. The median values were extracted from the dose-response sigmoid curve (logarithm of concentration versus growth inhibition percent, analysis performed with the GraphPad Prism 5 software) (see supplemental data Figure 16).

	Extract 1		Extract 2		Extract 3		Extract 4		Extract 5	
	Median values	SD	Median values	SD	Median values	SD	Median values	SD	Median values	SD
DLD-1	9.67	0.05	14.26	0.07	56.05*	0.11	67.01*	0.08	32.63	0.10
A2780	12.72	0.06	22.59	0.08	72.23*	0.11	57.16*	0.09	52.59*	0.12
A375	15.76	0.05	19.85	0.06	70.89*	0.05	26.86	0.08	36.42	0.06
BJ	11.03	0.04	25.06	0.05	53.55*	0.15	102.81*	0.22	73.01*	0.11

The values above 50  $\mu\text{g/mL}$  are hypothetical; they were obtained by extrapolation, given that the highest concentration used in the experiment was 50  $\mu\text{g/mL}$ .

selectivity of the extracts was observed in the DLD-1 and BJ contrast (Figure 2(b)).

Extract 2 has had the second-best cytotoxicity, but the IC<sub>50</sub> values were twice as big as in 1. Extract 3 presented the lowest toxicity, while the IC<sub>50</sub> values of 4 and 5 were in-between. The extract 2, but especially 4, showed a good selectivity towards the tumor cell lines, since in the normal BJ skin cell line, its IC<sub>50</sub> value was higher than in tumor cells, which anticipate a lower toxicity towards normal skin fibroblasts following the administration versus the tumor cells with lower IC<sub>50</sub>. The cytotoxicity was dependent on the extracts and not on the cell type.

Based on the IC<sub>50</sub> values (Table 2), for further testing, the 10  $\mu\text{g/mL}$  concentrations were used for each extract, ensuring in this way a good proportion of living cells for the mechanistic studies, even in the extract 1-treated cells.

**3.2.2. The Protein Content of the Samples.** In order to identify the expression or production of certain molecules implicated in apoptosis, intercellular communication, and tumor dissemination, two types of samples were collected: the supernatants to identify soluble proteins secreted by the treated cells and cell homogenates, respectively, to identify the molecules implicated in the intracellular signaling. The protein content of the samples derived from supernatants and cell lysates was measured (Table 3) as described in Materials and Methods. The total protein concentration ( $\mu\text{g/mL}$ ) itself is not an indicator of cytotoxicity; instead, it was used to normalize the quantity of the target proteins after they were measured by immune-enzymatic methods (see supplemental data Table 7 and Figure 17).

**3.2.3. The Extrinsic Apoptosis Induction.** The caspase cascade is the basic apoptotic signaling pathway, involved in both intrinsic and extrinsic apoptosis. Caspases are essential components of the apoptotic process. Caspase-8 is an initiator caspase of the extrinsic apoptotic pathway, while caspase-3 has an effector role, being activated by caspase-8 or other caspases or chemokines.

Some of the studied *M. aquifolium* extracts were capable to enhance the TNF- $\alpha$  expression in PBMC. On the extrinsic apoptotic pathway, the TNF- $\alpha$  increase implicates the proteolysis or cleavage of caspase-8, which further can activate caspase-3. Therefore, the intracellular level of these two caspases was evaluated following the 24-hour *in vitro* treatment

of tumor (A2780, DLD-1, and A375) and normal (BJ) cell lines with extracts 1-5. The active or cleaved form of the two proteins is of interest in the apoptotic process, and the increase of the cleaved caspase expression is known to be an indicator of the apoptotic process (data provided by Metacore of Clarivate Analytics: Apoptosis Pathway Map, <http://pathwaymaps.com/maps/373>).

The apoptotic process initiation through caspase-8 occurred in all tumor cell lines for all extracts 1-5 (Figure 5), with statistical significance in the 95% confidence interval (one-way analysis of variance, Dunnett posttest). In normal BJ cells, only extract 1 effect was significant, but in the opposite direction, meaning caspase-8 decrease. This indicates a selectivity of the extracts regarding the cell death mechanism induction.

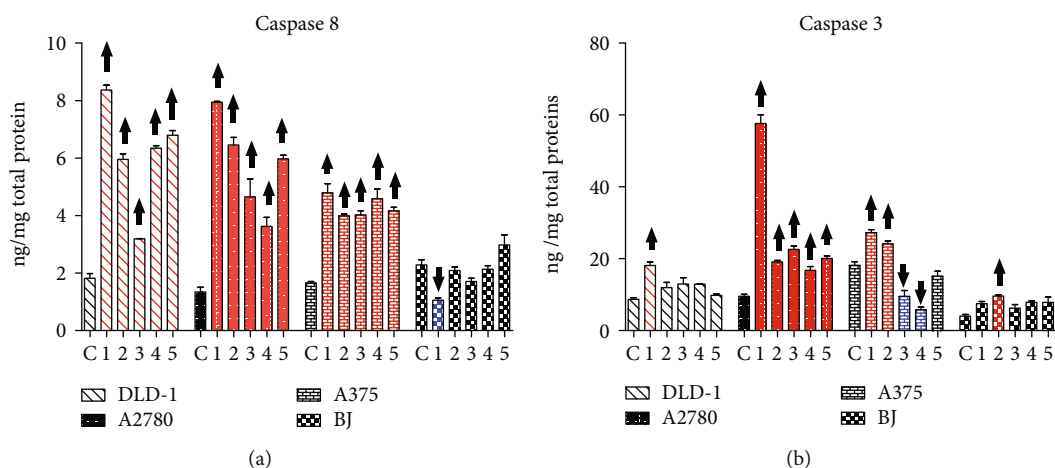
The caspase cascade was evolving through caspase-8 towards the programmed cell death, but not in all treatments, or in all cell lines, the proapoptotic signal was propagated. The active caspase-3 increased following the exposure to 1 in all tumor cell lines, and 2 induced and increased in DLD-1 and A375 cells, and this denotes that the caspase cascade was influenced by 1 and 2 to evolve towards the extrinsic apoptotic pathway. In DLD-1 colon carcinoma, even 3, 4, and 5 caused caspase-3 cleavage; therefore, it is very likely the extrinsic apoptosis triggered by any of extracts 1-5 in K-ras mutant aggressive DLD-1 cells. In BJ cells, only extract 2 augmented the caspase-3 expression.

It was found that berberine, the main alkaloid from *M. aquifolium* extracts, mostly the bark extract, enhanced the expression and activation of caspase-3 and caspase-8 in ovarian cancer cells [57]. This finding may be an explanation for the highest caspase activation by extract 1 with the most important berberine content [30]. Once again, extract 1 was constantly active against all cell lines and selective towards normal BJ cells.

**3.2.4. Modulation of Adhesion Molecules.** The intracellular adhesion molecule-1 (ICAM-1) and the vascular adhesion molecule-1 (VCAM-1) are implicated in tumor growth, extravasation, and dissemination. ICAM-1 is expressed on fibroblasts, keratinocytes, endothelial cells, and leukocytes, but also in many types of tumors [58]. ICAM-1 enhances tumor cell adherence to endothelial cells favoring tumorigenesis [59]. Moreover, it was reported an association between tumor relapse or drug resistance and ICAM-1 overexpression

TABLE 3: The protein content ( $\mu\text{g}/\text{mL}$ ) of the supernatants and cell lysates harvested from the cell cultures after the 24-hour treatment with 1-5.

	Supernatant		Cell lysate	
	Avg.	SD	Avg.	SD
DLD-1 untreated	178.17	10.17	276.84	18.41
DLD-1 treated with extract 1	209.33	15.61	291.17	20.22
DLD-1 treated with extract 2	173.11	11.81	302.94	22.17
DLD-1 treated with extract 3	182.00	12.50	285.00	27.75
DLD-1 treated with extract 4	196.94	9.35	279.06	7.10
DLD-1 treated with extract 5	230.50	9.09	279.83	3.44
A2780 untreated	157.00	25.07	299.06	7.70
A2780 treated with extract 1	169.89	15.79	313.06	29.48
A2780 treated with extract 2	188.03	37.70	301.17	26.07
A2780 treated with extract 4	210.61	10.30	260.09	25.58
A2780 treated with extract 5	215.56	12.86	292.17	26.10
A375 untreated	261.61	36.76	269.75	41.13
A375 treated with extract 1	198.06	16.39	275.67	44.74
A375 treated with extract 2	203.94	17.70	278.67	36.06
A375 treated with extract 3	236.67	4.82	300.17	52.50
A375 treated with extract 4	212.11	15.89	275.34	20.98
A375 treated with extract 5	192.44	38.60	279.89	32.49
BJ untreated	199.50	21.36	274.39	26.58
BJ treated with extract 1	207.45	1.11	281.09	0.83
BJ treated with extract 2	197.78	31.59	283.34	12.96
BJ treated with extract 3	174.67	14.78	296.44	15.59
BJ treated with extract 4	214.17	5.20	268.06	32.07
BJ treated with extract 5	212.61	17.74	191.61	14.43

FIGURE 5: The intracellular level of the active initiator caspase-8 and the effector caspase-3 following the *in vitro* treatment with extracts 1-5.  $\uparrow$ Significant increase of caspase-8 or caspase-3 level;  $\downarrow$ significant decrease of caspase-8 or caspase-3 level compared with the untreated control.

[60]. In inflammation, VCAM-1 is predominantly expressed on endothelial cells, but in cancer, it plays a dual role: increases the ability to metastasize and rises tumor-associated monocytes and macrophage recruitment. In tumors like breast, renal, and gastric carcinoma, aberrant VCAM-1 expression was found on tumor-associated vasculature and on tumor cells. In other tumor-associated vessels

of some human malignancies has been reported downregulation of ICAM-1 and VCAM-1 [58]. The soluble form of the two proteins can act as biomarker in clinical diagnosis and treatment follow-up, and generally, the elevated values indicate a poor prognosis.

The extracts did not act identically against the ICAM-1 secreted by tumor cells (Figure 6). Extract 1 acts only on

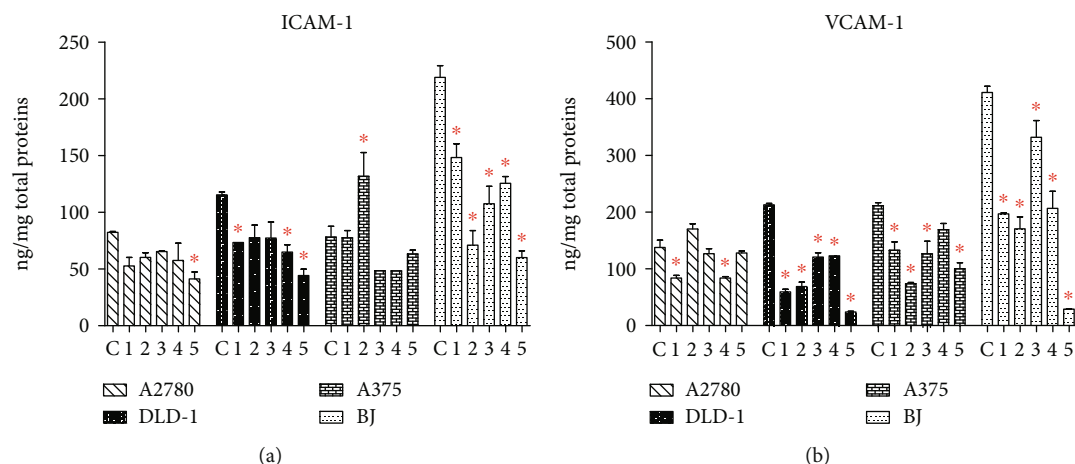


FIGURE 6: The modulation of adhesion molecules ICAM-1 and VCAM-1 implicated in the cancer cell extravasation and metastasis. \* Significant decrease of ICAM-1 or VCAM-1 following the 24-hour treatment with 1-5, compared with the untreated control.

DLD-1 cells, generating a significant drop of ICAM-1; 3 influenced only the A375 cell line, while 4 and 5 were efficient in DLD-1 cells.

The extracts 1-5 were more active against VCAM-1, and in this case, extract 1 was capable to reduce the VCAM-1 secretion in all tumor cell lines (A2780, DLD-1, and A375). Extract 2 and even the less active extract 3 reduced VCAM-1 in DLD-1 and A375 cells.

Interestingly, all extracts have had an inhibitory effect against the ICAM-1 and VCAM-1 secreted by BJ normal fibroblasts *in vitro*. This property could be used to initiate further studies, since the elevated ICAM-1 or VCAM-1 levels are a characteristic of benign skin disorders; therefore, the *M. aquifolium* extracts gain a new perspective for future applications.

The PCA model is a useful tool to examine the multifaceted biologic effect of many natural extracts [61]. This method highlighted the relationship between the 1-5 extract capacity to trigger apoptosis and to influence the adhesion molecules which give the tumor cells the capacity to migrate (Figure 7): for strong VCAM-1 increase, up to 380 units, the expression of caspase-3 and ICAM-1 was directly proportional, while to a moderate increase of VCAM-1, the two parameters were divergent. VCAM-1 could increase up to 400 units, or it could be diminished up to 800-unit weight against the untreated controls in different tumor cell types, at the same time as the correlation remains indirect between ICAM-1 and caspase-3 (Supplemental data Figure 18).

**3.2.5. The Effect on Matrix Metalloprotease-9 (MMP-9).** MMPs, synthesized by neoplastic and stromal cells, are zinc-dependent proteases, which play a role in extracellular matrix remodeling and cancer progression, invasion, and metastasis. Because MMP-9 has been found overexpressed in tumor tissues compared with the adjacent nontumor tissues, it can be a prognostic molecular biomarker [62]. Against MMP-9 overexpression, the best cytotoxic extracts 1 and 2 do not act in a significant manner, and 3 as well has no effect (Figure 8). The only exception is 1, which was able to inhibit MMP-9 in melanoma cell A375. Instead,

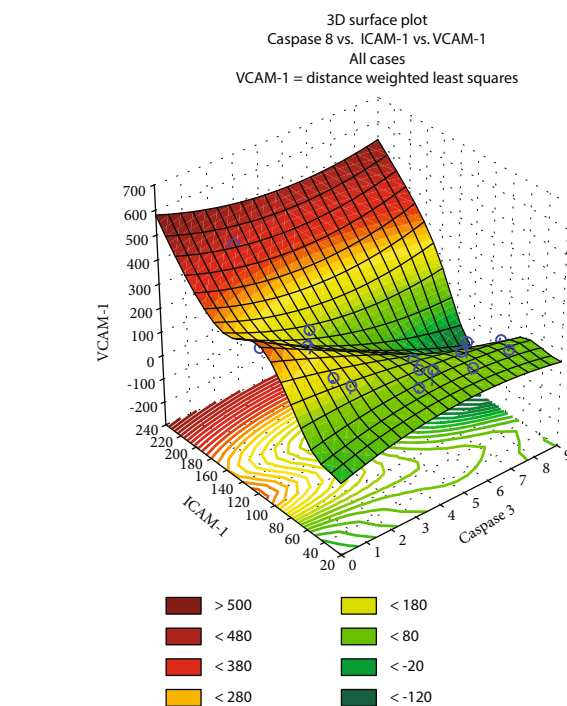


FIGURE 7: The relationship between the apoptotic effect and the influence on cell adhesion for the *Mahonia aquifolium* extracts 1 to 5, determined through principal component analysis for the extracts 1 to 5.

extracts 4 and 5 were more active against the MMP-9 overgrowth. Extract 5 inhibited MMP-9 in all tumor cell lines, while 4 was active only in A2780. In normal BJ cells, none of the treatments caused significant drop in MMP-9 levels.

Following to the treatment with 1-5 if MMP-9 values were amplified (above 12 units), then ICAM-1 and VCAM-1 were both elevated (Figure 9). Instead, if MMP-9 secretion was moderate, below 10 units, one of variables ICAM-1 and VCAM-1 has increased, simultaneously with the decline of the other parameters.

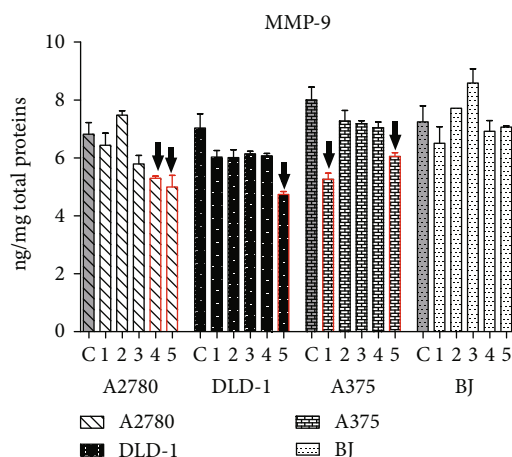


FIGURE 8: Modulation of MMP-9 by the treatment with extracts 1-5. <sup>†</sup>Significant decrease of MMP-9, compared with the untreated control.

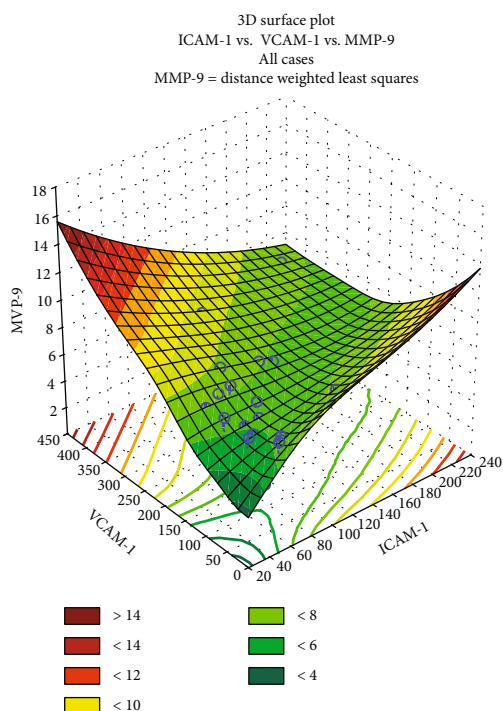


FIGURE 9: Tridimensional PCA model regarding the dependence between matrix metalloproteinase MMP-9 versus ICAM-1 and VCAM-1 adhesion molecules for the studied *Mahonia aquifolium* extracts 1-5.

#### 4. Conclusion

In conclusion, the extracts 1-5 have good potential to become TME modulatory agents, similar with other *Mahonia* extracts [27] described before, due to the immunomodulatory and antitumoral effects. Extract 1 should be employed carefully, and further tested, to estimate whether the increase of the regulatory helper CD4+ cell level is counterbalanced with the tumor-suppressing mechanisms *in vivo*.

TABLE 4: Significant modulations of the antitumor signaling following the *in vitro* treatment of tumor cell populations with *M. aquifolium* extracts 1-5.

Cell line	A2780					DLD					A375				
Extract	1	2	3	4	5	1	2	3	4	5	1	2	3	4	5
Caspase-8	+	+	+	+	+	+	+	+	+	+	+	+	+	+	+
Caspase-3	+					+	+	+	+	+	+	+			
ICAM-1						+	+				+	+			
VCAM-1	+					+	+	+	+	+	+	+			
MMP-9						+	+								+

The extracts 2, 4, and 5 are more suitable to activate the effector CD8+ cells, the monocytes, and B cells, and the utilization of 3 more likely will substantially benefit together with other active compounds, since it will give no secondary effects in the case of systemic administration, together with the standard antitumor drugs or alone. The *M. aquifolium* extracts also exhibited a moderate cytotoxicity on tumor cells. Among them, extract 1 was prominent as regards the antiproliferative capacity. We demonstrated for the first time that at subcytotoxic concentrations, the tumor cell lines subjected to 1-5 undergo changes in the signaling pathways linked to cell adhesion, proliferation, migration, and apoptosis (Table 4, Figure 9). These results open perspectives to further investigation of the *M. aquifolium* extract prodrug potential.

#### Data Availability

Data are available in the manuscript and supplemental data file.

#### Conflicts of Interest

The authors declare that they have no conflicts of interest.

#### Acknowledgments

The authors express their gratitude to Anca-Daniela Farcaș of National Institute for Research and Development of Isotopic and Molecular Technologies, Cluj-Napoca (INCDTIM), for her generous contribution to the PCA statistical analysis of data.

#### Supplementary Materials

More information about the methods, materials, and results can be found in the Supplemental data folder, as indicated in the main text. (*Supplementary Materials*)

#### References

- [1] R. Ruiu, L. Tarone, V. Rolih et al., "Cancer stem cell immunology and immunotherapy: Harnessing the immune system against cancer's source," in *Progress in Molecular Biology and Translational Science*, Elsevier Inc., 1st ed edition, 2019.
- [2] N. Curdy, O. Lanvin, C. Laurent, J.-J. Fournié, and D.-M. Franchini, "Regulatory mechanisms of inhibitory immune

- checkpoint receptors expression," *Trends in Cell Biology*, vol. 29, no. 10, pp. 777–790, 2019.
- [3] D. S. Vinay, E. P. Ryan, G. Pawelec et al., "Immune evasion in cancer: mechanistic basis and therapeutic strategies," *Seminars in Cancer Biology*, vol. 35, pp. S185–S198, 2015.
  - [4] R. Saleh and E. Elkord, "Acquired resistance to cancer immunotherapy: role of tumor-mediated immunosuppression," *Seminars in Cancer Biology*, 2019.
  - [5] C. Liu, C. J. Workman, and D. A. A. Vignali, "Targeting regulatory T cells in tumors," *The FEBS Journal*, vol. 283, no. 14, pp. 2731–2748, 2016.
  - [6] S. Paul, S. Chhatar, A. Mishra, and G. Lal, "Natural killer T cell activation increases iNOS+CD206- M1 macrophage and controls the growth of solid tumor," *Journal for Immunotherapy of Cancer*, vol. 7, no. 1, pp. 208–213, 2019.
  - [7] A. Y. Huang, P. Golumbek, M. Ahmadzadeh, E. Jaffee, D. Pardoll, and H. Levitsky, "Role of bone marrow-derived cells in presenting MHC class I-restricted tumor antigens," *Science*, vol. 264, no. 5161, pp. 961–965, 1994.
  - [8] K. Shitara and H. Nishikawa, "Regulatory T cells: a potential target in cancer immunotherapy," *Annals of the New York Academy of Sciences*, vol. 1417, no. 1, pp. 104–115, 2018.
  - [9] A. Sarvaria, J. A. Madrigal, and A. Saudemont, "B cell regulation in cancer and anti-tumor immunity," *Cellular & Molecular Immunology*, vol. 14, no. 8, pp. 662–674, 2017.
  - [10] M. R. Rähkä and P. A. Puolakkainen, "Tumor-associated macrophages (TAMs) as biomarkers for gastric cancer: a review," *Chronic Diseases and Translational Medicine*, vol. 4, no. 3, pp. 156–163, 2018.
  - [11] A. A. Wolf, A. Yáñez, P. K. Barman, and H. S. Goodridge, "The ontogeny of monocyte subsets," *Frontiers in Immunology*, vol. 10, 2019.
  - [12] W.-C. Wu, H. W. Sun, J. Chen et al., "Immunosuppressive immature myeloid cell generation is controlled by glutamine metabolism in human cancer," *Cancer Immunology Research*, vol. 7, no. 10, pp. 1605–1618, 2019.
  - [13] J. Patel, E. N. Bozeman, and P. Selvaraj, "Taming dendritic cells with TIM-3: another immunosuppressive strategy used by tumors," *Immunotherapy*, vol. 4, no. 12, pp. 1795–1798, 2012.
  - [14] B. Farhood, M. Najafi, and K. Mortezaee, "Cancer-associated fibroblasts: secretions, interactions, and therapy," *Journal of Cellular Biochemistry*, vol. 120, no. 3, pp. 2791–2800, 2019.
  - [15] V. Petrova, M. Annicchiarico-Petruzzelli, G. Melino, and I. Amelio, "The hypoxic tumour microenvironment," *Oncogenesis*, vol. 7, no. 1, p. 10, 2018.
  - [16] N. Maishi and K. Hida, "Tumor endothelial cells accelerate tumor metastasis," *Cancer Science*, vol. 108, no. 10, pp. 1921–1926, 2017.
  - [17] K. Hida, N. Maishi, D. Annan, and Y. Hida, "Contribution of tumor endothelial cells in cancer progression," *International Journal of Molecular Sciences*, vol. 19, no. 5, p. 1272, 2018.
  - [18] B. F. Zamarron and W. Chen, "Dual roles of immune cells and their factors in cancer development and progression," *International Journal of Biological Sciences*, vol. 7, no. 5, pp. 651–658, 2011.
  - [19] M. W. L. Teng, J. Galon, W. H. Fridman, and M. J. Smyth, "From mice to humans: developments in cancer immunoeediting," *The Journal of Clinical Investigation*, vol. 125, no. 9, pp. 3338–3346, 2015.
  - [20] M. W. Dulin and B. K. Kirchoff, "Paedomorphosis, secondary woodiness, and insular woodiness in plants," *The Botanical Review*, vol. 76, no. 4, pp. 405–490, 2010.
  - [21] L. Zhang, A. S. Ravipati, S. R. Koyyalamudi et al., "Antioxidant and anti-inflammatory activities of selected medicinal plants containing phenolic and flavonoid compounds," *Journal of Agricultural and Food Chemistry*, vol. 59, no. 23, pp. 12361–12367, 2011.
  - [22] A.-D. Cegan, A. E. Pârvu, M. Pârvu et al., "Mahonia aquifolium flowers extract effects in acute experimental inflammation," *Bulletin of University of Agricultural Sciences and Veterinary Medicine Cluj-Napoca. Food Science and Technology*, vol. 75, no. 2, pp. 189–199, 2018.
  - [23] A. R. Li, Y. Zhu, X. N. Li, and X. J. Tian, "Antimicrobial activity of four species of Berberidaceae," *Fitoterapia*, vol. 78, no. 5, pp. 379–381, 2007.
  - [24] W. Hu, L. Yu, and M. H. Wang, "Antioxidant and antiproliferative properties of water extract from Mahonia bealei (Fort.) Carr. leaves," *Food and Chemical Toxicology*, vol. 49, no. 4, pp. 799–806, 2011.
  - [25] B. S. Wong, Y. C. Hsiao, T. W. Lin et al., "The *in vitro* and *in vivo* apoptotic effects of Mahonia oiwakensis on human lung cancer cells," *Chemico-Biological Interactions*, vol. 180, no. 2, pp. 165–174, 2009.
  - [26] A.-D. Andreicut, A. E. Pârvu, A. C. Mot et al., "Phytochemical Analysis of Anti-Inflammatory and Antioxidant Effects of Mahonia aquifolium Flower and Fruit Extracts," *Oxidative Medicine and Cellular Longevity*, vol. 2018, 12 pages, 2018.
  - [27] D. Godevac, A. Damjanović, T. P. Stanojković, B. Anđelković, and G. Zdunić, "Identification of cytotoxic metabolites from Mahonia aquifolium using <sup>1</sup>H NMR-based metabolomics approach," *Journal of Pharmaceutical and Biomedical Analysis*, vol. 150, pp. 9–14, 2018.
  - [28] W. Zhu, J. Hu, X. Wang, J. Tian, and S. Komatsu, "Organ-specific analysis of mahonia using gel-free/label-free proteomic technique," *Journal of Proteome Research*, vol. 14, no. 6, pp. 2669–2685, 2015.
  - [29] M. Pârvu, A. E. Pârvu, L. Barbu-Tudoran et al., "In vitro effects of Allium obliquum extract on the growth and ultrastructure of Botrytis paeoniae," *Journal of Medicinal Plants Research*, vol. 7, no. 17, pp. 1138–1145, 2013.
  - [30] A. D. Andreicut, A. E. Parvu, A. C. Moț et al., "Anti-inflammatory and antioxidant effects of Mahonia aquifolium leaves and bark extracts," *Farmácia*, vol. 66, no. 1, pp. 49–58, 2018.
  - [31] E. Fischer-Fodor, A. Mot, F. Deac, M. Arkosi, and R. Silaghi-Dumitrescu, "Towards hemerythrin-based blood substitutes: comparative performance to hemoglobin on human leukocytes and umbilical vein endothelial cells," *Journal of Biosciences*, vol. 36, no. 2, pp. 215–221, 2011.
  - [32] H. Zhang, Y. Wang, E. S. Hwang, and Y. W. He, "Interleukin-10: an immune-activating cytokine in cancer immunotherapy," *Journal of Clinical Oncology*, vol. 34, no. 29, pp. 3576–3578, 2016.
  - [33] Y. Wu and B. P. Zhou, "TNF- $\alpha$ /NF- $\kappa$ B/Snail pathway in cancer cell migration and invasion," *British Journal of Cancer*, vol. 102, no. 4, pp. 639–644, 2010.
  - [34] M. Perde-Schrepler, A. Florea, I. Brie et al., "Size-Dependent Cytotoxicity and Genotoxicity of Silver Nanoparticles in Cochlear Cells *In Vitro*," *Journal of Nanomaterials*, vol. 2019, 12 pages, 2019.



- [35] A. Szaflarska, M. Baj-Krzyworzeka, M. Siedlar et al., "Antitumor response of CD14<sup>+</sup>/CD16<sup>+</sup> monocyte subpopulation," *Experimental Hematology*, vol. 32, no. 8, pp. 748–755, 2004.
- [36] I. O. Gordon and R. S. Freedman, "Defective antitumor function of monocyte-derived macrophages from epithelial ovarian cancer patients," *Clinical Cancer Research*, vol. 12, no. 5, pp. 1515–1524, 2006.
- [37] R. N. Hanna, C. Cekic, D. Sag et al., "Patrolling monocytes control tumor metastasis to the lung," *Science*, vol. 350, no. 6263, pp. 985–990, 2015.
- [38] A. M. Wolf, D. Wolf, M. Steurer, G. Gastl, E. Gunsilius, and B. Grubeck-loebenstein, "Increase of regulatory T cells in the peripheral blood of cancer patients," *Clinical Cancer Research*, vol. 9, no. 2, pp. 606–612, 2003.
- [39] S. Chattopadhyay, S. Mehrotra, A. Chhabra, U. Hegde, B. Mukherji, and N. G. Chakraborty, "Effect of CD4<sup>+</sup> CD25<sup>+</sup> and CD4<sup>+</sup> CD25<sup>-</sup> T regulatory cells on the generation of cytolytic T cell response to a self but human tumor-associated epitope in vitro," *Journal of Immunology*, vol. 176, no. 2, pp. 984–990, 2006.
- [40] A. Perez-Diez, N. T. Joncker, K. Choi et al., "CD4 cells can be more efficient at tumor rejection than CD8 cells," *Blood*, vol. 109, no. 12, pp. 5346–5354, 2007.
- [41] T. J. Curiel, G. Coukos, L. Zou et al., "Specific recruitment of regulatory T cells in ovarian carcinoma fosters immune privilege and predicts reduced survival," *Nature Medicine*, vol. 10, no. 9, pp. 942–949, 2004.
- [42] M. Oft, "IL-10 : master switch from tumor-promoting inflammation to antitumor immunity," *Cancer Immunology Research*, vol. 2, no. 3, pp. 194–199, 2014.
- [43] S. M. A. Mahmoud, E. C. Paish, D. G. Powe et al., "Tumor-infiltrating CD8<sup>+</sup> lymphocytes predict clinical outcome in breast cancer," *Journal of Clinical Oncology*, vol. 29, no. 15, pp. 1949–1955, 2011.
- [44] J. Galon, A. Costes, F. Sanchez-Cabo et al., "Type, density, and location of immune cells within human colorectal tumors predict clinical outcome," *Science*, vol. 313, no. 5795, pp. 1960–1964, 2006.
- [45] M. E. Dudley, J. R. Wunderlich, P. F. Robbins et al., "Cancer regression and autoimmunity in patients after clonal repopulation with antitumor lymphocytes," *Science*, vol. 298, no. 5594, pp. 850–854, 2002.
- [46] S. Mocellin, F. M. Marincola, and H. A. Young, "Interleukin-10 and the immune response against cancer: a counterpoint," *Journal of Leukocyte Biology*, vol. 78, no. 5, pp. 1043–1051, 2005.
- [47] D. Depoil, S. Fleire, B. L. Treanor et al., "CD19 is essential for B cell activation by promoting B cell receptor-antigen microcluster formation in response to membrane-bound ligand," *Nature Immunology*, vol. 9, no. 1, pp. 63–72, 2008.
- [48] P. B. Olkhanud, B. Damdinsuren, M. Bodogai et al., "Tumor-evoked regulatory B cells promote breast cancer metastasis by converting resting CD4<sup>+</sup> T cells to T regulatory cells," *Cancer Research*, vol. 71, no. 10, pp. 3505–3515, 2011.
- [49] S. Sattler, G. S. Ling, D. Xu et al., "IL-10-producing regulatory B cells induced by IL-33 (Breg<sup>IL-33</sup>) effectively attenuate mucosal inflammatory responses in the gut," *Journal of Autoimmunity*, vol. 50, pp. 107–122, 2014.
- [50] Y. Wei, D. Zheng, X. Li et al., "Infusion of Dendritic Cells Carrying Donor Lymphocytes Treated With 8-Methoxypsoralen and Ultraviolet A Light Induces CD19<sup>+</sup>IL-10<sup>+</sup> Regulatory B cells and Promotes Skin Allograft Survival," *Transplantation Proceedings*, vol. 46, no. 10, pp. 3641–3646, 2014.
- [51] X. Wang and Y. Lin, "Tumor necrosis factor and cancer, buddies or foes?," *Acta Pharmacologica Sinica*, vol. 29, no. 11, pp. 1275–1288, 2008.
- [52] S. F. Josephs, T. E. Ichim, S. M. Prince et al., "Unleashing endogenous TNF-alpha as a cancer immunotherapeutic," *Journal of Translational Medicine*, vol. 16, no. 1, pp. 242–248, 2018.
- [53] A. Bojarska-Junak, J. Rolinski, E. Wasik-Szczepaneko, Z. Kaluzny, and A. Dmoszynska, "Intracellular tumor necrosis factor production by T- and B-cells in B-cell chronic lymphocytic leukemia," *Haematologica*, vol. 87, pp. 490–499, 2002.
- [54] P. E. Bunney, A. N. Zink, A. A. Holm, C. J. Billington, and C. M. Kotz, "Orexin activation counteracts decreases in non-exercise activity thermogenesis (NEAT) caused by high-fat diet," *Physiology & Behavior*, vol. 176, no. 2, pp. 139–148, 2017.
- [55] C. A. Roberts, L. E. Durham, V. Fleskens, H. G. Evans, and L. S. Taams, "TNF blockade maintains an il-10 + phenotype in human effector CD4 + and CD8 + T cells," *Frontiers in Immunology*, vol. 8, pp. 1–14, 2017.
- [56] X. Valencia, G. Stephens, R. Goldbach-mansky, M. Wilson, E. M. Shevach, and P. E. Lipsky, "TNF downmodulates the function of human CD4<sup>+</sup>CD25<sup>hi</sup> T-regulatory cells," *Blood*, vol. 108, no. 1, pp. 253–261, 2006.
- [57] L. Liu, J. Fan, G. Ai et al., "Berberine in combination with cisplatin induces necroptosis and apoptosis in ovarian cancer cells," *Biological Research*, vol. 52, no. 1, p. 37, 2019.
- [58] H. Harjunpää, M. Llort Asens, C. Guenther, and S. C. Fagerholm, "Cell adhesion molecules and their roles and regulation in the immune and tumor microenvironment," *Frontiers in Immunology*, vol. 10, 2019.
- [59] S. Wang, C. Yin, Y. Zhang et al., "Overexpression of ICAM-1 predicts poor survival in high-grade serous ovarian carcinoma: a study based on TCGA and GEO databases and tissue microarray," *BioMed Research International*, vol. 2019, 9 pages, 2019.
- [60] Y. Vedvyas, J. E. McCloskey, Y. Yang et al., "Manufacturing and preclinical validation of CAR T cells targeting ICAM-1 for advanced thyroid cancer therapy," *Scientific Reports*, vol. 9, no. 1, pp. 1–15, 2019.
- [61] A. Saplonțai-Pop, A. Moț, M. Moldovan et al., "Testing anti-platelet and antioxidant activity of the extract of seven varieties of Allium cepa L.," *Open Life Sciences*, vol. 10, no. 1, pp. 89–98, 2015.
- [62] W. Wang, D. Li, L. Xiang et al., "TIMP-2 inhibits metastasis and predicts prognosis of colorectal cancer via regulating MMP-9," *Cell Adhesion & Migration*, vol. 13, no. 1, pp. 273–284, 2019.

## Review Article

# Spotlight on ROS and $\beta$ 3-Adrenoreceptors Fighting in Cancer Cells

Maura Calvani <sup>1</sup>, Angela Subbiani <sup>1,2</sup>, Marina Vignoli <sup>1,2</sup> and Claudio Favre <sup>1</sup>

<sup>1</sup>Oncohematology Unit, Department of Pediatric Oncology, A. Meyer Children's University Hospital, Florence 50139, Italy

<sup>2</sup>Department of Health Sciences, University of Florence, Florence 50139, Italy

Correspondence should be addressed to Claudio Favre; [claudio.favre@meyer.it](mailto:claudio.favre@meyer.it)

Received 27 September 2019; Accepted 26 November 2019; Published 16 December 2019

Guest Editor: Rizwan Wahab

Copyright © 2019 Maura Calvani et al. This is an open access article distributed under the Creative Commons Attribution License, which permits unrestricted use, distribution, and reproduction in any medium, provided the original work is properly cited.

The role of ROS and RNS is a long-standing debate in cancer. Increasing the concentration of ROS reaching the toxic threshold can be an effective strategy for the reduction of tumor cell viability. On the other hand, cancer cells, by maintaining intracellular ROS concentration at an intermediate level called “mild oxidative stress,” promote the activation of signaling that favors tumor progression by increasing cell viability and dangerous tumor phenotype. Many chemotherapeutic treatments induce cell death by rising intracellular ROS concentration. The persistent drug stimulation leads tumor cells to simulate a process called hormesis by which cancer cells exhibit a biphasic response to exposure to drugs used. After a first strong response to a low dose of chemotherapeutic agent, cancer cells start to decrease the response even if high doses of drugs were used. In this framework,  $\beta$ 3-adrenoreceptors ( $\beta$ 3-ARs) fit with an emerging antioxidant role in cancer.  $\beta$ 3-ARs are involved in tumor proliferation, angiogenesis, metastasis, and immune tolerance. Its inhibition, by the selective  $\beta$ 3-ARs antagonist (SR59230A), leads cancer cells to increase ROS concentration thus inducing cell death and to decrease NO levels thus inhibiting angiogenesis. In this review, we report an overview on reactive oxygen biology in cancer cells focusing on  $\beta$ 3-ARs as new players in the antioxidant pathway.

## 1. Reactive Oxygen Nitrogen Species

Reactive species or free radicals include reactive oxygen and nitrogen species collectively and are termed reactive oxygen nitrogen species (RONS).

Oxygen metabolism generates highly reactive molecules called reactive oxygen species (ROS). ROS production results in normal cellular metabolism. Free radical is defined as a molecule with unpaired electron in the outer shell such as superoxide anion ( $O_2^-$ ) or hydroxyl radicals ( $\cdot OH$ ) and nonradicals such as hydrogen peroxide ( $H_2O_2$ ) [1]. Reactive nitrogen species (RNS) is the subclass of RONS that contain nitrogen compounds such as nitric oxide (NO), peroxynitrite ( $\cdot ONOO$ ), and nitrogen dioxide ( $NO_2$ ) [2].

**1.1. Reactive Oxygen Species.** Intracellular ROS are mainly generated in the mitochondria through activation of redox reactions catalyzed by specialized enzymes of electron transporter chain (ETC) where small amounts of oxygen

are univalent and reduced into free radicals [3, 4], to produce cellular energy (adenosine triphosphate or ATP) [5] (Figure 1). Reduction of nicotinamide adenine dinucleotide (NADH) and flavin adenine dinucleotide (FADH<sub>2</sub>), which work as electron carriers, transfers the electron through the ETC. Subsequently, during oxidative phosphorylation, cytochrome c oxidase (COX or Complex IV) acts as the final acceptor of these electrons and catalyzed the tetravalent reduction of molecular oxygen ( $O_2$ ) into water ( $H_2O$ ) [6]. During this process, there is a nonfully efficient coupling between respiration and phosphorylation leading to proton and electron leaks. Ubisemiquinone, a component of Complex I in the mitochondria, represents the main site of electron leak leading to the generation of superoxide anions.

ROS could also be generated in response to growth factors, cytokines, or G protein-coupled receptor (GPCR) agonists through the activation of transmembrane enzymes called NADPH oxidase (nicotinamide adenine dinucleotide

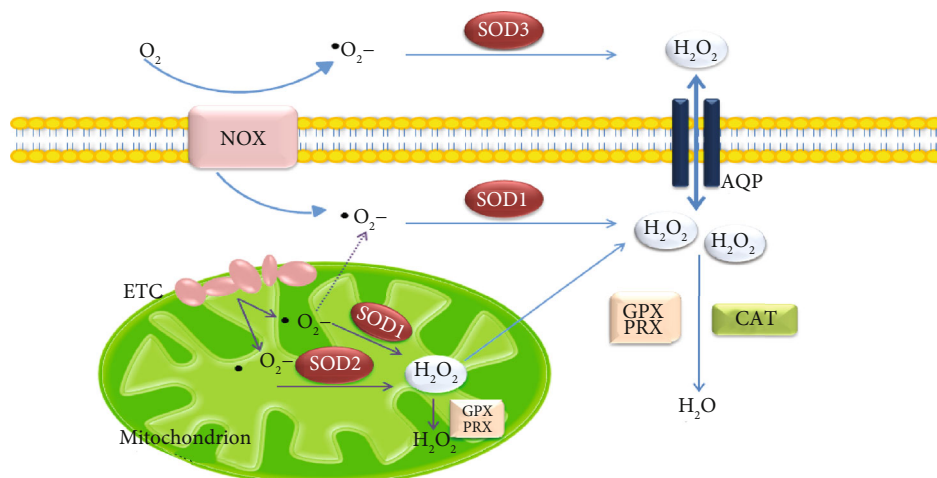


FIGURE 1: Schematic representation of ROS species within a cell.

phosphate oxidase or NOX) family existing in different isoforms, widely distributed in different cell types [7]. Five NOX proteins have been evidenced and two further enzymes called Dual Oxidase (DUOX), containing a peroxidase-like domain [8, 9]. NOX are composed of six different subunits that interact to form an active enzyme complex. NOX catalyzes the production of a superoxide free radical by transferring one electron to oxygen from nicotinamide adenine dinucleotide phosphate oxidase (NADPH). During this process,  $O_2$  is transported from the extracellular space to the cell interior and  $H^+$  is exported [10].  $O_2$  has a short life, and it is dismutated fast in  $H_2O_2$  spontaneously or enzymatically by the superoxide dismutase enzyme (SOD). Once generated,  $H_2O_2$  preferentially enters the cell through specific plasma membrane aquaporin channels [11], activating different signaling.

At physiological condition, ROS have important roles in normal cellular functions, regulating different intercellular signaling pathways such as fighting against infection, facilitating normal maturation and fertilization in reproductive systems [1, 4, 12–15]. Depending on their concentration, ROS could trigger different intracellular pathways, thus leading to the activation of survival mechanisms or to the priming of the cell death program. ROS can reversibly oxidize target molecules such as cysteine (Cys) residues of phosphatases, increasing the level of protein phosphorylation. The oxidation of critical thiols is centrally involved in the transmission of a redox signal initiated by a protein modification of some amino acid side chains, such as Cys, methionine (Met), proline (Pro), histidine (His), and tryptophan (Trp) [16].

Redox homeostasis is maintained by the induction of a cell signaling cascade that controls ROS production and scavenging ability that efficiently maintain a stable concentration [17]. ROS production higher than physiological conditions induces temporary expression of many antioxidant molecules [5]. If the ROS increase is quite small, the antioxidant response can be able to balance the augmentation of ROS levels and restore the equilibrium between ROS production and scavenging ability. On the other hand, per-

sistent cellular high ROS levels can lead to pathological conditions such as diabetes, neurodegenerative disorder, and cancer onset [18]. The first defense of endogenous neutralization of ROS is represented by enzymes such as SOD, catalase (CAT), and glutathione peroxidase (GPx). The nonenzymatic protection consists of different compounds such as glutathione (GSH), vitamin A, vitamin C, vitamin E, zinc, and selenium [19]. Among the enzymatic antioxidants, SODs convert  $\cdot O_2^-$  to less reactive  $H_2O_2$ , CAT reduces  $H_2O_2$  to  $H_2O$  and  $O_2$ , and GPx eliminates  $H_2O_2$  using reducing power derived from GSH. Other important defensive mechanisms and mediators of redox signaling are represented by the peroxiredoxin (Prx), the thioredoxin (Trx), and the glutathione/glutaredoxin systems (GSH/Grx) [20–27]. Many cytoprotective enzymes, in response to reactive chemical stress, are regulated primarily at the transcriptional level. This transcriptional response is mediated by elements termed ARE (antioxidant response elements), initially found in the promoters of genes encoding the two major detoxification enzymes, glutathione S-transferase A2 (GSTA2) and NADPH quinone oxidoreductase-1 (NQO1). ARE binding increases the synthesis of many ARE-dependent antioxidant enzymes in different cells, such as glutathione reductase (GR), GPx, glutaredoxin (Grx), thioredoxin reductase (TrxR), heme oxygenase-1 (HO-1), and peroxiredoxin 1 (Prx-1).

The intracellular antioxidant defense in response to elevation of ROS content is regulated also by the nuclear factor erythroid 2-related factor 2 (Nrf2)/Kelch-like ECH-associated protein 1 (Keap1) pathway [28]. Keap1 is a cytosolic protein rich in cysteine residues that inhibits Nrf2 function through its binding, if cysteine residues are oxidized as a consequence of a change in the electrophilic balance Nrf2 is released and activated. In this active form, Nrf2 translocates into the nucleus and binds ARE located within the gene regulatory regions thereby regulating the expression of many target genes [29]. The GSH system and Prx-1 are two mechanisms whose expression is activated by Nrf2. Prxs are a highly conserved family of peroxidases that reduce peroxides, with a conserved cysteine

residue, serving as the site of oxidation by peroxides. The peroxidase activity of Prx towards hydroperoxides and peroxyxynitrite, produced as a result of normal cellular metabolism in the cytosol, is critical to protect cellular components from oxidative damage [30].

HO are enzymes involved in heme catabolism; in humans, three isoforms of heme oxygenase are known. HO-1 is a stress-induced isoform present throughout the body with the highest concentrations in the spleen, liver, and kidneys and catalyzes the reduction of heme to biliverdin (BV), carbon monoxide, and ferrous ions in the presence of NADPH and oxygen. Biliverdin is subsequently converted to bilirubin (BR) by biliverdin reductase (BVR). Both BV and BR function as ROS scavengers. HO-1 expression is induced by oxidative stress and plays several roles in oxidative balance; in particular related to vasculature and diabetes [31], indeed, HO-1 knockout mice exhibit high susceptibility to hypertension [32].

**1.2. Nitric Oxide.** NO is a labile molecule involved in various physiological functions including vasodilatation and control of blood pressure [33], neurotransmission [34], immune response [35], and smooth muscle relaxation [36]. NO is produced from the metabolism of the amino acid L-arginine by nitric oxide synthases (NOS). There are three different NOS isoforms that differ in localization, regulation, and catalytic properties. Neuronal NOS (nNOS or type I NOS) and endothelial NOS (eNOS or type III NOS) are constitutively expressed (cNOS), while the other isoform is inducible and thus termed inducible NOS (iNOS) [33]. All NOS enzymes are homodimers. Each monomer contains a C-terminal reductase domain (NOSred) that binds NADPH, flavin adenine dinucleotide (FAD), and flavin mononucleotide (FMN) and a N-terminal oxygenase domain (NOSoxy) that contains the binding site for the cofactors cytochrome P-450-type heme and (6R-)5,6,7,8-tetrahydrobiopterin (BH<sub>4</sub>) and for the substrate L-arginine. NOS contain a zinc tetrahiolate cluster which consists in a zinc ion coordinated to two Cys residues in a CysXXXXCys motif, involved in BH<sub>4</sub> and L-arginine binding to facilitate NOS dimerization. Binding of NADPH to the NOSred domain induces the electron transfer from NADPH to the heme-containing oxygenase domain, via reduction of FAD and FMN, with lower capacity to reduce O<sub>2</sub> to O<sub>2</sub><sup>-</sup>. The binding between Ca<sup>2+</sup> and calmodulin (CaM) induces a conformational change of the FMN subdomain in proximity of the heme-containing oxygenase domain, and the electron transfers from FMN to the heme of the opposite monomer, thus explaining why monomeric NOS enzymes are inactive. The oxygenase domain can also bind to BH<sub>4</sub> and L-arginine which stabilize the dimeric form of NOS through the heme domain coupling and promote the efficient O<sub>2</sub> reduction and NO production. NOS synthesize NO by two different oxidation steps. In the first step, NOS oxidize L-arginine to N<sup>ω</sup>-hydroxy-L-arginine (L-NOHA), and in the second step, the enzyme oxidizes L-NOHA to L-citrulline and NO. BH<sub>4</sub> provides the stabilization of the charge by the recruitment of an electron from the heme iron with subsequent release of NO out of the active site. nNOS and eNOS can be activated by Ca<sup>2+</sup> and CaM to generate

and release a small amount of NO. iNOS, by contrast, is primarily regulated at the transcriptional level, and it is only induced when the cell is stimulated by immunological signals such as proinflammatory cytokines (i.e., tumor necrosis factor- $\alpha$ , interleukin-1 $\beta$ , and interferon- $\gamma$ ), bacterial lipopolysaccharide (LPS), or infection, generating a larger amount of NO to contrast pathogen invasion. nNOS is mostly localized in specific neurons of the central nervous system and has been implicated in synaptic plasticity, learning, memory, and neurogenesis. Besides brain tissues, nNOS has been found in the spinal cord, skeletal and cardiac myocytes, pancreatic islet cells, sympathetic ganglia and adrenal glands, parasympathetic ganglia, kidney macula densa cells, peripheral nitrenergic nerves, and epithelial cells [37]. In the peripheral nervous system (PNS), NO acts as a neurotransmitter decreasing the tone of various types of smooth muscle including corpus cavernosum [38] and blood vessels [39]. Nevertheless, abnormal NO production, due to an overexpression or dysregulation of nNOS, leads to toxic effects that are associated with some human diseases such as septic shock, cardiac dysfunction, diabetes, and cancer [40]. eNOS is primarily expressed not only in endothelial cells [41] but also in platelets, cardiac myocytes, and neurons [39]. NO generated by eNOS is responsible to regulate cellular processes including vasodilation [42, 43] and inhibition of platelet aggregation and adhesion [44–46], control of vascular smooth muscle proliferation [47], angiogenesis [48, 49], activation of endothelial progenitor cells [50, 51], and inhibition of leucocyte adhesion and vascular inflammation [52, 53]. Besides Ca<sup>2+</sup>-CaM-mediated activation, eNOS can interact with several other proteins like heat shock protein 90 (Hsp90) and caveolar coat protein caveolin-1 (Cav-1) which activate and repress the enzyme activity respectively [54–56]. Moreover, eNOS can be activated and regulated by phosphorylation on serine (Ser) residues and, to a lesser degree, on tyrosine (Tyr) and threonine (Thr) residues. Phosphorylation of Ser1177 and dephosphorylation of Thr495 stimulate the increase of the intracellular concentration of Ca<sup>2+</sup>, resulting in eNOS activation [41, 57, 58], while Tyr phosphorylation is associated with a decrease in catalytic activity [55]. In particular, the involvement of Thr495-dephosphorylation in the uncoupling of eNOS has been reported and is due to an increase in ROS production and oxidative stress that lead to several human pathology such as atherosclerosis, ischemia, diabetes, and hypertension [57, 59]. ROS production in oxidative stress leads to the production of O<sub>2</sub><sup>-</sup> instead of NO with oxidation of BH<sub>4</sub> [60, 61], depletion of L-arginine [62, 63], and S-glutathionylation of eNOS [64], resulting in NO reduction and increase of oxidative stress. iNOS is mostly expressed in macrophages to protect against pathogens; thus, it is critical for the inflammatory response and the innate immune system, but iNOS is also expressed potentially in any cells or tissues following stimulation [65]. The binding of NO to the iron in the catalytic sites of the enzymes and the interference with the DNA of target cells lead to the inhibition of enzymes involved in the principal physiological functions (i.e., citric acid cycle, DNA replication, and ETC) [66] and DNA fragmentation respectively [67, 68]. In addition to eNOS, iNOS activity can be

modulated by mutations in amino acid residues. Arg375 mutation of BH<sub>4</sub> in the NOSoxy domain and Phe831 and Leu832 in the NOSred domain result in the decrease of iNOS activity [69, 70]. Higher levels of NO produced by iNOS of macrophages can lead to cellular and tissue damage and septic shock which is characterized by vasodilatation, microvascular damage, and hypertension [71]. Recently, the presence of a mitochondrial NOS (mtNOS) has been evidenced, and it seems to be involved in the regulation of mitochondria and cellular functions in various type of tissues [72]. Mitochondria can produce and consume NO which stimulates mitochondrial biogenesis, through cGMP upregulation of transcriptional factors. In particular, NO inhibits mitochondrial respiration by binding the binuclear center of cytochrome *c* oxidoreductase (Complex III), leading to the inhibition of the enzyme activity with consequent inhibition of electron transfer and increase in O<sub>2</sub><sup>-</sup> production [73, 74].

## 2. ROS and Cancer

Increased levels of ROS have long been associated with different types of cancer, where they play a central role in cancer onset and progression [75]. Cancer cells maintain ROS level lightly higher than physiologic control, activating pathways that lead to cancer progression and metastases, and this state is called “mild oxidative” stress. The damages derived from oxidative stress include genome instability and consequently the increase of oncogenic mutations, loss of tumor suppressors, and changes in cancer cell metabolism [76]. At an advanced stage, cancer cell ROS-derived mutations lead to additional ROS generation by further supporting cancer progression. A hypoxic microenvironment has been described to play a central role in the increase of ROS in tumor, through the activation of the hypoxia-inducible factor 1 alpha (HIF-1 $\alpha$ ) and its target genes. In cancer cells, hypoxia leads to the activation of different genes that control cellular growth, survival, and proliferation. The increased rate of ROS production during cancer is mainly caused by a high metabolic rate in mitochondria, endoplasmic reticulum, and cell membrane. Hypoxia and metabolic changes lead to respiratory and mitochondria dysfunctions by impairing ETC, lowering coupling efficiency, and increasing electron leakage [18]. To maintain high energy levels, cancer cells switch their metabolism, enhancing glycolytic rate and lactic acid fermentation even in the presence of oxygen, thus increasing mitochondrial ROS production. During hypoxic exposure, many growth factors and cytokines are produced and the activation of the relative pathways leads to the upregulation of NOX and consequent increase of ROS, thus affecting survival pathways such as the PI3K/Akt, RAF/MEK/ERK1/2, and JAK/STAT pathways downstream of both growth factor stimulation and oncogene activity [77]. Vascular endothelial growth factor (VEGF), under hypoxia, activates NOX and mediates ROS production leading to amplification of pathways involved in endothelial cell proliferation and angiogenesis [78]. An upregulated expression of NOX proteins has been evidenced in many cancer cell types. [79]. ROS produced in transformed cells allow cancer

cells to activate *c-Myc* oncogene [80], leading to cancer progression and metastasis. To prevent the increase of ROS and maintain redox balance, cancer cells increase their antioxidant ability; in this way, cancer cells maintain ROS at a mild level thus enhancing protumorigenic signaling pathways without inducing cancer cell death. Compared with normal cells, cancer cells have an altered redox environment, with a high rate of ROS production counter balanced by a high rate of ROS scavenging [81]. A recent evidence suggests that modifying the levels of ROS by the action of antioxidants or prooxidants could modulate tumor growth. A mild concentration of ROS yields cancer cells vulnerable to further ROS increase strongly dependent on their antioxidant defenses. On the other hand, exacerbate oxidative stress leads to cell apoptosis by direct or indirect ROS-mediated damage of proteins, lipids, and nucleic acids. Antioxidants are the first response of cells to neutralize ROS and survive. Many enzymes including CAT, SOD, GPx, and ETC enzymes are responsible for the transformation of free radicals into more stable and less damaging molecules. Many nonenzymatic antioxidants work as a ROS scavenger in cancer cells such as  $\beta$ -carotene and vitamins A, E, and C [82]. In addition, redox-sensitive transcription factors, including Nrf2 and HIF-1 $\alpha$ , could also be activated to improve the action of antioxidants as well as to trigger the elevation of cell survival molecules such as the antiapoptotic protein Bcl-2 (B-cell lymphoma 2) and AKT (protein kinase B or PKB) [25]; the adaptive mechanism established by cancer cells in ROS response activates resistance to different cancer treatments. It has been reported that the increased antioxidant pathways driven by Nrf2 are involved in cancer progression [83–85]. However, the role of ROS in cancer is not one-sided. Notably, antioxidant enzyme-deficient cancer cells have less ability to form tumors in experimental mouse models. It has been reported that continuous antioxidant enzyme activity maintains metabolic activity and anchorage-independent growth in breast cancer cells. Thus, inhibiting antioxidant enzyme activity may be an effective strategy to enhance susceptibility to cell death in cancer cells [86]. CAT expression is modified in cancer cell lines that become resistant to chronic exposures to H<sub>2</sub>O<sub>2</sub> [87, 88] or to certain chemotherapeutic agents such as doxorubicin [89–92]. Although mechanisms controlling CAT expression have been partially elucidated, the decreased CAT expression in cancer cells still remains an unanswered question. Chemotherapeutic agents lead to an exuberant increase of ROS content leading to induction of cellular damage and apoptosis of cancer cells by evoking toxicity. Depending on the tumor type, this goal can be reached by chemotherapy or radiation therapy [93]. Alkylating agent (alkyl sulfonates, ethyleneamines, and hydrazines), anthracyclines (doxorubicin and doxorubicin), platinum coordination complexes (cisplatin, carboplatin), podophyllin derivatives (etoposides), and camptothecins (irinotecan, topotecan) increase free radical production [94–97]. Many cytoprotective enzymes, in response to reactive chemical stress, are regulated primarily at the transcriptional level. This transcriptional response is mediated by ARE that control the

expression of two major detoxification enzyme genes, GSTA2 and NQO1. Many cancer cells become resistant to chemotherapeutic agents by activating antioxidant response. This phenomenon is similar to hormesis, a process in which exposure to a low dose of a chemical agent is damaging at higher doses, induces an adaptive beneficial effect on the cell following an initial disruption in homeostasis [98].

### 3. NO and Cancer

Besides the signaling role in the neuronal, cardiovascular, and immune systems, NO is also involved in the pathogenesis and progression of different cancer types. A dual role of NO in cancer, depending on its localization and concentration, has been reported. At low concentration, NO modulates angiogenesis, cell cycle progression, apoptosis, invasion, and metastasis, while at higher levels, it acts as an antioncogenic agent promoting DNA damage, cytotoxic effects, oxidative stress, and apoptosis [99, 100]. The continuous production of NO by iNOS, is regulated by the tumor suppressor gene p53, which inhibits the enzyme through a negative feedback mechanism that is involved in cancer progression [99]. Several studies report the implication of iNOS in cancer. iNOS overexpression in prostate cancer cells and thyroid cancer demonstrates an anticancer effect due to cell death induction [101] and the inhibition of tumorigenesis [102], while in gastric cancers, hepatocellular carcinoma, melanoma, leukemia, and osteosarcoma, iNOS expression correlates with tumor progression and with the degree of malignancy [103]. Nevertheless, lower iNOS expression has been reported to promote pancreas cancerogenesis and liver metastasis [104]. NO can cause DNA damage by three different mechanisms: (i) inhibition of the DNA repair enzyme; (ii) direct DNA modifications, causing base deamination, nitration, and oxidation [105]; and (iii) formation of mutagenic species [106]. In particular, the inhibitory effect of NO on DNA repair represents the principal mechanism of inflammation in cancer [107]. The role of NO in angiogenesis is well-established, a critical event that promotes neovascularization and subsequently cell proliferation and tumor progression. NO stimulates the mediators of angiogenesis such as epidermal growth factor receptor (EGFR) [108], VEGF [109], and cyclooxygenase-2 (COX-2) signaling pathways that stimulate the synthesis of proangiogenic factors [110]. However, VEGF can stimulate eNOS itself by the activation of tyrosine kinase and protein kinase C (PKC) signaling [111], promoting angiogenesis in various cancer types [112, 113]. Moreover, ROS and RNS production during inflammation can cause DNA damage and mutations that lead to cancerogenesis [114]. NO has been shown to play important role in modulating apoptosis through posttranslational modification, with proapoptotic or antiapoptotic effects, depending on NO concentration and the types of cells that are involved [115]. In general, lower concentration of NO can protect from apoptosis, while high concentration induces apoptosis [116]. The principal antiapoptotic effects exerted by NO in the mitochondrion are the inhibition of caspase-3 expression [117]. S-Nitrosylation of the Cys in the catalytic site of caspase-3

prevents the cleavage of the procaspase-3 to activated caspase-3, occluding the release of cytochrome *c*, resulting in apoptosis inhibition [118]. Conversely, S-nitrosylation on the heme iron of cytochrome *c* released in the cytosol induces caspase-3 activation and apoptosis [119]. NO secreted by iNOS activation induces Fas/CD95-tyrosine nitration (death receptor), preventing CD95-tyrosine phosphorylation leading to an antiapoptotic effect [120]. It has been reported that NO participates in cancer progression and invasion by inducing epithelial-to-mesenchymal transition (EMT). NO mediates the upregulation of E-cadherin expression, a cell adhesion molecule expressed in the early stage of EMT [121], and impairs the expression of matrix metalloproteinase 2 and matrix metalloproteinase 9 (MMP-2 and MMP-9) which have a central role in the remodeling of extracellular matrix and invasion [122]. Recently, NO has been reported to have a pivotal role in the immune system acting like an immunosuppressive messenger in the tumor microenvironment. NO may induce immunosuppression by decreasing T cell-mediated antitumoral responses [123, 124], promoting the recruitment and activation of myeloid-derived suppressor cells (MDSCs) [125] and inducing the acquisition of stem features by cancer cells as a mechanism to escape from the immune system [126].

### 4. $\beta$ -Adrenergic Receptors

$\beta$ -Adrenergic receptors ( $\beta$ -ARs) play an important role in a wide range of physiological responses mediated by catecholamines: adrenaline (A) and noradrenaline (NA).  $\beta$ -ARs belong to the GPCR family which consists of 7-membrane-spanning  $\alpha$ -helical segments and an intracellular heterotrimeric G-protein complex ( $G_{\alpha\beta\gamma}$ ). The receptor molecule also includes an extracellular N-terminal domain and a cytosolic C-terminal tail, which contains phosphorylation sites for GPCR kinases. Ligand binding induces a conformational change in the receptor that allows the intracellular part of the receptor to couple with a G-protein leading to the exchange of guanosine diphosphate (GDP) with guanosine triphosphate (GTP) and dissociation of the G-proteins into active  $G_{\beta\gamma}$  and  $G_{\alpha}$  subunits. The downstream effects of GPCR activation are determined by the type of  $G_{\alpha}$  subunit ( $G_{\alpha s}$ ,  $G_{\alpha i}$ ,  $G_{\alpha q}$ , and  $G_{\alpha 12}$ ) that is coupled to the receptor. There are three subtypes of  $\beta$ -ARs:  $\beta 1$ -ARs,  $\beta 2$ -ARs, and  $\beta 3$ -ARs.  $\beta 1$ -ARs are found primarily in the striatum cardiac muscle, juxtaglomerular apparatus, and adipocytes.  $\beta 1$ -ARs activation lead to positive cardiac ionotropic and chronotropic effect antagonist, increasing heart rate and contractility, while in the kidneys, juxtaglomerular cells and adipocytes stimulate renin secretion and lipolysis respectively [127].  $\beta 2$ -ARs show a greater binding affinity to noradrenaline instead of adrenaline.  $\beta 2$ -ARs are present on the gastrointestinal and bronchial smooth muscle cells, skeletal muscle cells, and liver. Activation of  $\beta 2$ -ARs causes bronchodilation and general muscle relaxation, redirecting blood flow and mobilizing energy stores [128]. In addition,  $\beta 2$ -ARs are expressed in multiple immune and nonimmune cells with a role in immunoregulation and immune response [129, 130].  $\beta 2$ -ARs activation is also associated with cancerogenesis

[131–134] and EMT in melanoma, breast cancer, gastric cancer, prostate cancer, and colorectal adenocarcinoma [135–137].  $\beta$ 3-ARs are located primarily in the small intestine, adipose tissue (both brown and white), and vascular endothelium [138].

**4.1.  $\beta$ 3-Adrenergic Receptors.** Since their discovery in 1989 [139], it seemed clear that  $\beta$ 3-ARs have important physiological implications, including modulation of metabolism through the regulation of the adrenergic  $\beta$ -oxidation of fatty acids in adipocytes [140], vasodilation and relaxation to cardiac contractility [141], and relaxation of the smooth muscle cells of the detrusor muscle in the urinary bladder [142].  $\beta$ 3-ARs differ from  $\beta$ 1- and  $\beta$ 2-ARs for molecular structure and pharmacological profile, and this leads to support differential intracellular signaling. In fact, the serine (Ser) and threonine (Thr) residues at the C-terminus region in  $\beta$ 1- and  $\beta$ 2-ARs that are subjected to GPCR kinase- (GRK-) mediated regulation through phosphorylation and the consensus sequence for protein kinase A (PKA) are absent in  $\beta$ 3-ARs [143]. Recently, several studies have reported that  $\beta$ 3-ARs effects are either similar or opposite to  $\beta$ 1- and  $\beta$ 2-ARs stimulation due to the type of  $G_\alpha$  subunits they are coupled to. In the brown adipose tissue (BAT),  $\beta$ 3-ARs can activate  $G_{\alpha_s}$  (activator subunit) signaling [144] promoting lipolysis and thermogenesis by activation of the mitochondrial uncoupling protein 1 (UCP1) which uncoupled mitochondrial oxidative phosphorylation leading to a proton conductance pathway across the inner membrane and increasing the energy utilization [145]. Otherwise, in the ventricular myocardium,  $\beta$ 3-ARs are coupled with  $G_{\alpha_i}$  (inhibitory subunit) proteins [146] which increases NO production through activation of eNOS leading to inhibition of cardiac contraction unlike  $\beta$ 1- and  $\beta$ 2-ARs [147]. High  $\beta$ 3-ARs expression was also found in retinal diseases like retinopathy of prematurity (ROP) [148]. Hypoxia induces an increased release of NA and upregulation and activation of  $\beta$ 3-ARs which promotes migration, invasion, and proliferation of human retinal cells [149], suggesting that the  $\beta$ 3-ARs agonism induces proliferation of vessels in retinopathies through NO production and the accumulation of cyclic GMP (cGMP), which increases the release of VEGF [150]. Ischemic and hypoxic condition is also present in the tumor microenvironment and determines the release of NA from the sympathetic nervous system (SNS). As a result, the  $\beta$ 3-ARs expressed by tumor cells and endothelial cells are activated, increasing the production of NO, which in turn modulates the release of VEGF, leading to final effects such as vasodilation, angiogenesis, inflammation, and metastasis [151].

Moreover,  $\beta$ 3-ARs activation mediates relaxation of the smooth muscle of urinary bladder [142] and affects the function of the urothelium [152]. There are several reports that show two different mechanisms of  $\beta$ 3-ARs activation. The first consists in the activation of adenylyl cyclase (AC) with the subsequent formation of cyclic adenosine monophosphate (cAMP) with a small involvement of this pathway in bladder relaxation. Supporting evidences showed that  $\beta$ 3-ARs can also stimulate large conductance  $Ca^{2+}$ -activated  $K^+$  (BKCa) channels in bladders, and this

second mechanism is well established and can mediate relaxation of detrusor smooth muscle [153]. In the last few years, Mirabegron, the first  $\beta$ 3-ARs agonist, has been developed. Mirabegron has been approved for its pronounced effect on reducing the bladder tone and the detrusor muscle *in vitro* in the OAB syndrome [154].

**4.2.  $\beta$ 3-Adrenergic Receptors and Cancer.** The relationship between  $\beta$ -ARs and cancer initiation and progression, including inflammation, angiogenesis, cell motility and trafficking, apoptosis/anoikis, cellular immune response, and EMT, has been well established. Over the years, several studies showed the overexpression of  $\beta$ -ARs across multiple cancer types and the clinical efficacy of pharmacological inhibition of the  $\beta$ -ARs with beta blockers as anticancer agents, supporting the evidence that  $\beta$ -blockers contribute to improve survival and decrease tumor proliferation and progression in multiple cancer types [155–158].  $\beta$ 1- and  $\beta$ 2-ARs are expressed higher in non-small-cell lung cancer [159, 160], pancreatic cancer [161, 162], breast cancer [163, 164], ovarian carcinoma [165, 166], colorectal carcinoma [167], prostate cancer [168], and melanoma [169], while  $\beta$ 3-ARs are detected in colon and breast cancer [155, 170], vascular tumors [171], human leukemia cells [172] and at very high levels in melanoma [173]. In the last few years, numerous reports elucidated the involvement of  $\beta$ 3-ARs in melanoma initiation and progression and the potential role of  $\beta$ 3-ARs blocking to contrast tumor cells proliferation. In particular, it has been reported that the treatment with the specific  $\beta$ 3-ARs antagonist SR59230A is effective in reducing melanoma angiogenesis and growth and in inducing apoptosis [174]. Besides the key role of  $\beta$ 3-ARs in melanoma cancer cells, these receptors are also expressed in the melanoma microenvironment, such as cancer-associated fibroblast (CAF), endothelial cells, and macrophages, promoting secretion of proinflammatory cytokines and *de novo* angiogenesis [173]. Calvani et al. also showed that  $\beta$ 3-ARs are able to promote metabolic switch towards aerobic glycolysis by the induction of mitochondrial uncoupling protein 2 (UCP2), leading to proliferation of melanoma cells [175]. Recently, there has been a new role of  $\beta$ 3-ARs reported in the regulation of melanoma immune-tolerance by increasing the number of cytotoxic immune cells, such as natural killer (NK) and CD8 T (CD8) cells, and by decreasing MDSC and regulatory T cells (T-reg) subpopulations [176]. Moreover, the protumoral role exerted by the  $\beta$ 3-ARs has been recently confirmed in neuroblastoma (NB). In particular,  $\beta$ 3-ARs blockade is able to switch from stemness features to a neuronal differentiation phenotype in NB cells, leading to a strong tumor growth reduction [177] (Figure 2).

## 5. Antioxidant Effects of the $\beta$ 3-ARs

The role of  $\beta$ 3-ARs as antioxidants (Figure 2) has recently been evidenced in different studies. In the work of Yoshioka et al. [178], researchers showed that treatment of human astrocytoma U-251 MG cells with NA leads to an increase in the intracellular GSH concentration by inducing GCLc (Glutamate-Cysteine Ligase Catalytic Subunit) protein. In

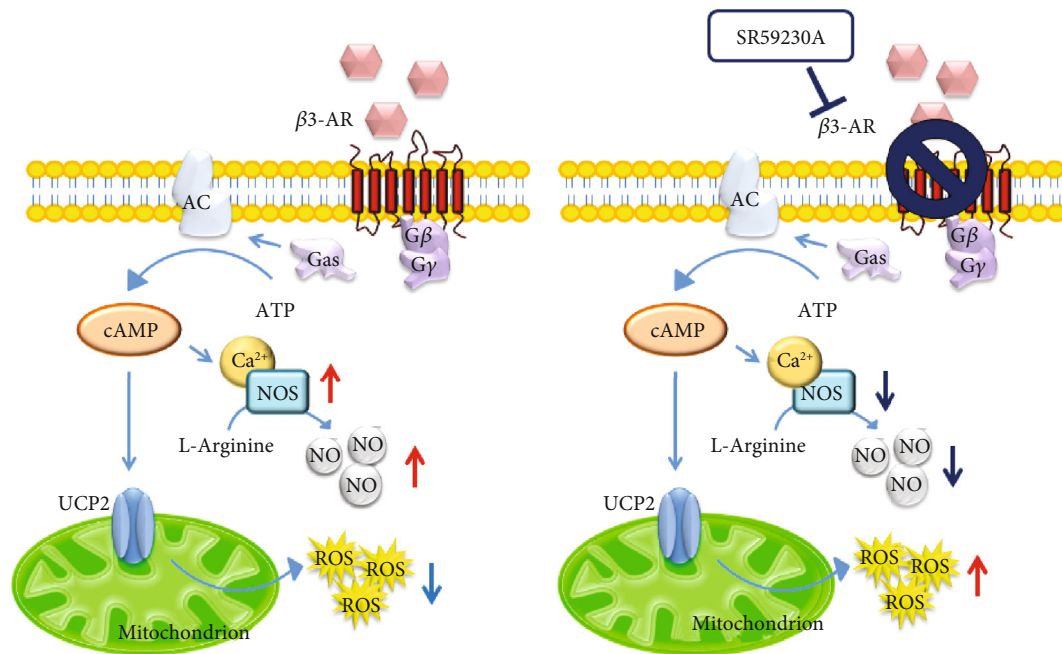


FIGURE 2: Schematic representation of  $\beta_3$ -AR stimulation pathway and antioxidant function.

astrocytes, GSH synthesis is essential for the protection of neurons from oxidative damage induced by ROS. GSH acts either as an antioxidant by scavenging ROS species or as a cofactor for GPx that detoxifies a wide range of hydroperoxides. Results of the study suggested also that the NA-induced increase in GSH occurs through the stimulation of  $\beta_3$ -ARs coupled to  $G_{i/o}$ -protein but not to  $G_s$ -protein. In another study, Hadi et al. [179] demonstrated the dual antioxidant capacity of  $\beta_3$ -ARs: on the one hand, they reduce ROS production by direct inhibition of NOX; on the other hand, they specifically induce the expression of CAT, a major  $H_2O_2$  scavenger. Therefore, they observed that  $\beta_3$ -ARs stimulation has no effect on the expression of SOD-1 that would lead to  $H_2O_2$  formation and its signaling, but rather it induces CAT expression. All the antioxidant effects mediated by  $\beta_3$ -ARs depended on the activation of the transcription factor PPAR $\gamma$  (Peroxisome Proliferator-Activated Receptor Gamma). Finally, they also confirmed a previously established link between ROS production and inflammatory induction: the authors observed that  $\beta_3$ -ARs stimulation blocks the ROS-dependent NF $\kappa$ B (nuclear factor kappa-light-chain-enhancer of activated B cell) pathway.

In a recent work, Calvani et al. [175] showed that  $\beta_3$ -ARs are also expressed on the mitochondria of embryonic stem cells (ESC) and cancer stem cells (CSC), where their stimulation with the  $\beta_3$ -ARs agonist BRL37344 induces an accelerated aerobic glycolysis (Warburg effect). This  $\beta_3$ -AR-induced Warburg effect involves also UCP2, whose expression is inhibited by SR59230A that is implicated in mitochondrial ROS (mtROS) content modulation. The authors showed that SR59230A and Genipin (GN), a specific UCP2 inhibitor, increased mtROS content in both CSC and ESC treated with BRL37344, with a major increase in CSC. The relationship between ROS production and UCPs activity was revealed in 1997 from experiments where guanosine

diphosphate (GDP), an UCP1 inhibitor, caused an increase of  $\Delta\psi$  and ROS production [180], and later, it was demonstrated that superoxide directly activates UCPs resulting in a negative feedback controlling both ROS production and their levels [181]. Calvani et al. also showed, through functional analysis, that  $\beta_3$ -ARs blockade in isolated mitochondria is able to decrease ATP production and to increase mtROS levels. These results confirm data already present in literature, where  $\beta_3$ -ARs and UCP2 are indicated to have a strong antioxidant role [179, 182]. Moreover, these results clearly suggest that the  $\beta_3$ -ARs/UCP2 axis promotes mitochondrial dormancy by inhibiting ATP production and mtROS content and leading both cell lines to increase aerobic glycolysis. In addition,  $\beta_3$ -ARs antagonism promotes mitochondrial reactivation by inhibiting UCP2 activity and by increasing mtROS content. Thus, there is accumulating evidence supporting a direct link between mitochondria, oxidative stress, and cell death.

In another study, Pasha et al. [183] evaluated the effects of the treatment with Apigenin (a nutraceutical antioxidant) on cell lines derived from Ewing Sarcoma (ES). The authors observed that Apigenin induces partial ES cell death by inducing the activation of the apoptotic pathway without increasing mitochondrial ROS production that on the other hand is evidenced by administration of SR59230A. Apigenin inhibits the expression of antioxidant proteins such as superoxide dismutase 2 (SOD-2), CAT, Trx, sirtuin-1 (SIRT1), thioredoxin interacting protein (TXNIP), glutathione S-transferase Mu4 (GSTM4), and Nrf2 but increases the level of UCP2 and GSH which on the contrary are strongly inhibited by  $\beta_3$ -ARs antagonism. The  $\beta_3$ -ARs activity as antioxidants could be mediated by UCP2 protein expression that could control the redox homeostasis in ES cells. The redox homeostasis of cells is balanced by ROS generation and ROS quenching capacity. The disruption of UCP2 signaling



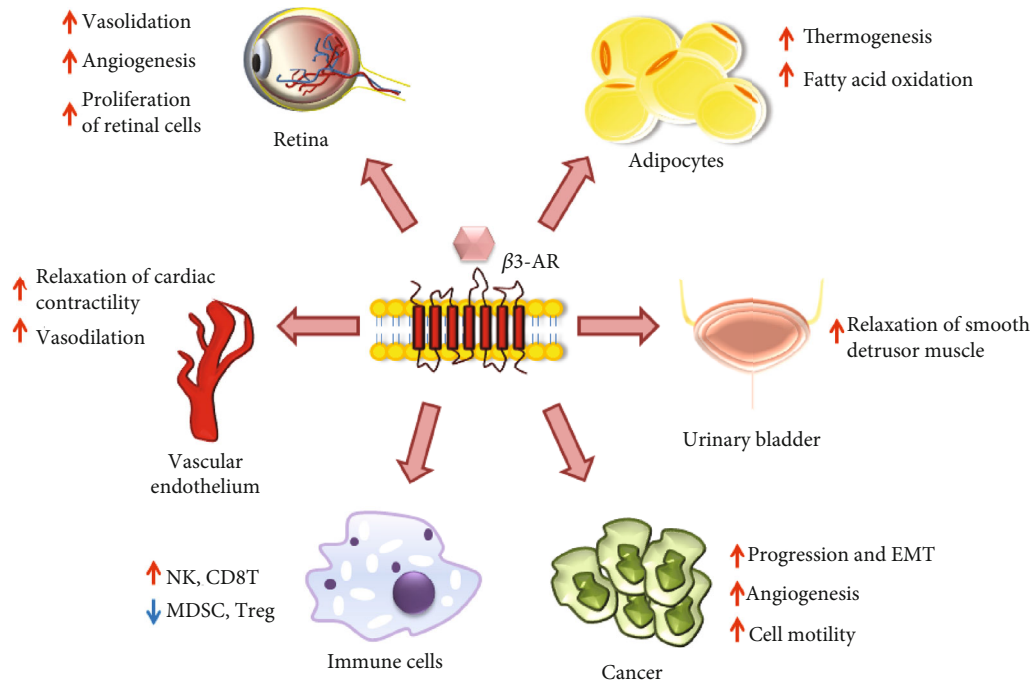


FIGURE 3:  $\beta_3$ -AR role in different cells and tissues.

together with the inhibition of  $\beta_3$ -ARs activity causes an imbalanced elevation of ROS production within the cellular microenvironment that can lead to excessive oxidative stress resulting in massive cell death. Even if Apigenin inhibits antioxidant proteins, it works as the  $\beta_3$ -ARs agonist, by avoiding the increase of mitochondrial ROS useful to achieve a massive cell death in ES cells; in this regard, administration of SR59230A improves the Apigenin effect on cell death.

$\beta$ -Adrenergic signaling seems also to have a prominent role among the factors that may modulate the NO pathway and therefore affect tumor growth. NO contributes to tumor growth and metastasis by promoting migratory, invasive, and angiogenic properties of cancer cells in the majority of human tumors [184]. Different works have associated reduced NO levels with decreased growth of melanoma cells, while increased NO levels promote melanoma growth [185, 186]. Studies on melanoma cells suggest that NO derived from iNOS may stimulate proliferation as well as promote resistance to apoptosis [187] and reported a remarkable anti-tumor activity of iNOS inhibition that reduced melanoma growth and sensitize melanoma cells to chemotherapeutic agents [188]. In 2013, Dal Monte et al. hypothesized the involvement of iNOS in the antitumoral effects exerted by  $\beta_3$ -ARs blockade in melanoma cells [174], and in a subsequent study, they confirm that the inhibitory effects of  $\beta_3$ -ARs blockade on melanoma growth are mainly mediated by reduction of iNOS expression, resulting in a decreased activity in the NO pathway.  $\beta_3$ -ARs blockade inhibits iNOS expression by reducing the basal nitrite production, while  $\beta_3$ -ARs stimulation increases this production by activating iNOS expression. In addition,  $\beta_3$ -ARs blockade effects are prevented by an NOS activator, and  $\beta_3$ -ARs activation effects are prevented by an NOS inhibitor. These results show that NO exerts a protumorigenic function and iNOS-

induced NO production is a key event in melanoma growth and that  $\beta_3$ -ARs may regulate melanoma cell proliferation and survival through the NO pathway [189].

In a recent study evaluating the effect of nutraceutical antioxidant treatment of ES tumor cells A673, Calvani et al. observed that cells treated with curcumin, retinoic acid, 8-gingerol, and genistein exhibited reduced viability if compared with cells treated with capsaicin, ascorbic acid, formononetin, and flavon where the treatment did not affect cell viability. Moreover, cells treated with pro-survival antioxidants showed low levels of intracellular mitochondrial ROS, while the cells treated with antioxidants that are able to reduce cell viability are shown to be increased in mtROS levels. Interestingly, the treatments not affecting cell viability upregulated  $\beta_3$ -ARs expression and the treatment that reduced cell viability strongly downregulated  $\beta_3$ -ARs levels. These results identified the  $\beta_3$ -ARs as the main regulators of the cellular response to oxidative stress under different micronutrient treatments. They function as ROS sensors in Ewing sarcoma cancer cells by driving or not antioxidant response and cell death. Since  $\beta_3$ -ARs antagonism leads to massive cell death, inhibiting  $\beta_3$ -ARs in these cells could dramatically increase the ROS levels by toxic threshold leading to cell death by inhibiting the antioxidant response of the cells [190].

## 6. Conclusion

*In vitro* and *in vivo* data suggest that  $\beta_3$ -ARs act as antioxidants in different cells by activating pro-survival factors and that their inhibition by a selective antagonist could be a new strategy to counteract tumor progression by elevating intracellular ROS concentration and activating apoptotic pathway (Figure 3). Moreover,  $\beta_3$ -ARs antagonism inhibits NO production thus decreasing angiogenic switch

in melanoma cells. In this review, it fully highlighted the new concept of  $\beta$ 3-ARs as antioxidants and their ability to decrease ROS production and increase NO with multiple mechanisms (mitochondrial and NOX). Moreover, the concept that SR59230A strongly reduces cancer cell viability is highlighted, supporting the evidences that blocking  $\beta$ 3-ARs function could represent a novel therapeutic strategy for the treatment of cancer by its ability to reduce antioxidant activity.

## Conflicts of Interest

The authors have no relevant disclosures of potential conflicts of interest.

## References

- [1] A. Nunes-Silva and L. C. Freitas-Lima, "The association between physical exercise and reactive oxygen species (ROS) production," *Journal of Sports Medicine & Doping Studies*, vol. 5, p. 152, 2015.
- [2] S. B. Doshi, K. Khullar, R. K. Sharma, and A. Agarwal, "Role of reactive nitrogen species in male infertility," *Reproductive Biology and Endocrinology*, vol. 10, p. 109, 2012.
- [3] C. D. Schneider and A. R. de Oliveira, "Oxygen free radicals and exercise: mechanisms of synthesis and adaptation to the physical training," *Revista Brasileira de Medicina do Esporte*, vol. 10, no. 4, pp. 314–318, 2004.
- [4] A. Boveris and B. Chance, "The mitochondrial generation of hydrogen peroxide. General properties and effect of hyperbaric oxygen," *Biochemical Journal*, vol. 134, no. 3, pp. 707–716, 1973.
- [5] W. Dröge, "Free radicals in the physiological control of cell function," *Physiological Reviews*, vol. 82, no. 1, pp. 47–95, 2002.
- [6] H. J. Fromm and M. S. Hargrove, "Electron transport and oxidative phosphorylation," in *Essentials of Biochemistry*, pp. 223–238, Springer, New York, NY, USA, 2011.
- [7] M. Ushio-Fukai and N. Urao, "Novel role of NADPH oxidase in angiogenesis and stem/progenitor cell function," *Antioxidants & Redox Signaling*, vol. 11, no. 10, pp. 2517–2533, 2009.
- [8] S. Altenhöfer, K. A. Radermacher, P. W. M. Kleikers, K. Wingler, and H. H. H. W. Schmidt, "Evolution of NADPH oxidase inhibitors: selectivity and mechanisms for target engagement," *Antioxidants & Redox Signaling*, vol. 23, no. 5, pp. 406–427, 2015.
- [9] L. L. Hilenski, R. E. Clempus, M. T. Quinn, J. D. Lambeth, and K. K. Griendling, "Distinct subcellular localizations of Nox 1 and Nox 4 in vascular smooth muscle cells," *Arteriosclerosis, Thrombosis, and Vascular Biology*, vol. 24, no. 4, pp. 677–683, 2004.
- [10] D. Pietraforte and W. Malorni, "Focusing at the double-edged sword of redox imbalance: signals for cell survival or for cell death?," *Antioxidants & Redox Signaling*, vol. 21, no. 1, pp. 52–55, 2014.
- [11] G. P. Bienert and F. Chaumont, "Aquaporin-facilitated transmembrane diffusion of hydrogen peroxide," *Biochimica et Biophysica Acta (BBA) - General Subjects*, vol. 1840, no. 5, pp. 1596–1604, 2014.
- [12] A. Agarwal, S. Gupta, and R. K. Sharma, "Role of oxidative stress in female reproduction," *Reproductive Biology and Endocrinology*, vol. 3, p. 28, 2005.
- [13] Y. Keisari, L. Braun, and E. Flescher, "The oxidative burst and related phenomena in mouse macrophages elicited by different sterile inflammatory stimuli," *Immunobiology*, vol. 165, no. 1, pp. 78–89, 1983.
- [14] G. Wu, Y. Z. Fang, S. Yang, J. R. Lupton, and N. D. Turner, "Glutathione metabolism and its implications for health," *The Journal of Nutrition*, vol. 134, no. 3, pp. 489–492, 2004.
- [15] A. Agarwal, G. Virk, C. Ong, and S. S. du Plessis, "Effect of oxidative stress on male reproduction," *The World Journal of Men's Health*, vol. 32, no. 1, pp. 1–17, 2014.
- [16] H. Sies, "Oxidative stress: a concept in redox biology and medicine," *Redox Biology*, vol. 4, pp. 180–183, 2015.
- [17] B. Halliwell, "Free radicals, reactive oxygen species and human disease: a critical evaluation with special reference to atherosclerosis," *The British Journal of Experimental Pathology*, vol. 70, no. 6, pp. 737–757, 1989.
- [18] R. S. Arnold, J. Shi, E. Murad et al., "Hydrogen peroxide mediates the cell growth and transformation caused by the mitogenic oxidase Nox 1," *Proceedings of the National Academy of Sciences of the United States of America*, vol. 98, no. 10, pp. 5550–5555, 2001.
- [19] G. Y. Liou and P. Storz, "Reactive oxygen species in cancer," *Free Radical Research*, vol. 44, no. 5, pp. 479–496, 2010.
- [20] J. W. Chen, C. Dodia, S. I. Feinstein, M. K. Jain, and A. B. Fisher, "1-Cys peroxiredoxin, a bifunctional enzyme with glutathione peroxidase and phospholipase A<sub>2</sub> activities," *Journal of Biological Chemistry*, vol. 275, no. 37, pp. 28421–28427, 2000.
- [21] A. M. Day, J. D. Brown, S. R. Taylor, J. D. Rand, B. A. Morgan, and E. A. Veal, "Inactivation of a peroxiredoxin by hydrogen peroxide is critical for thioredoxin-mediated repair of oxidized proteins and cell survival," *Molecular Cell*, vol. 45, no. 3, pp. 398–408, 2012.
- [22] V. Helfinger and K. Schröder, "Redox control in cancer development and progression," *Molecular Aspects of Medicine*, vol. 63, pp. 88–98, 2018.
- [23] S. Di Meo, T. T. Reed, P. Venditti, and V. M. Victor, "Role of ROS and RNS sources in physiological and pathological conditions," *Oxidative Medicine and Cellular Longevity*, vol. 2016, Article ID 1245049, 44 pages, 2016.
- [24] L. A. Pham-Huy, H. He, and C. Pham-Huy, "Free radicals, antioxidants in disease and health," *International journal of biomedical science : IJBS*, vol. 4, no. 2, pp. 89–96, 2008.
- [25] V. L. Dengler, M. D. Galbraith, and J. M. Espinosa, "Transcriptional regulation by hypoxia inducible factors," *Critical Reviews in Biochemistry and Molecular Biology*, vol. 49, no. 1, pp. 1–15, 2014.
- [26] M. Calvani, G. Comito, E. Giannoni, and P. Chiarugi, "Time-dependent stabilization of hypoxia inducible factor-1 $\alpha$  by different intracellular sources of reactive oxygen species," *PLoS One*, vol. 7, no. 10, p. e38388, 2012.
- [27] S. S. Donaldson, M. N. Wesley, W. D. DeWys, R. M. Suskind, N. Jaffe, and J. vanEys, "A study of the nutritional status of pediatric cancer patients," *American Journal of Disease of Children*, vol. 135, no. 12, pp. 1107–1112, 1981.
- [28] E. Kansanen, H. K. Jyrkkänen, and A. L. Levonen, "Activation of stress signaling pathways by electrophilic oxidized and

- nitrate lipids," *Free Radical Biology and Medicine*, vol. 52, no. 6, pp. 973–982, 2012.
- [29] L. Baird and A. T. Dinkova-Kostova, "The cytoprotective role of the Keap1–Nrf2 pathway," *Archives of Toxicology*, vol. 85, no. 4, pp. 241–272, 2011.
- [30] S. G. Rhee, H. Z. Chae, and K. Kim, "Peroxiredoxins: a historical overview and speculative preview of novel mechanisms and emerging concepts in cell signaling," *Free Radical Biology and Medicine*, vol. 38, no. 12, pp. 1543–1552, 2005.
- [31] R. C. Siow, H. Sato, and G. E. Mann, "Heme oxygenase-carbon monoxide signalling pathway in atherosclerosis: anti-atherogenic actions of bilirubin and carbon monoxide?," *Cardiovascular Research*, vol. 41, no. 2, pp. 385–394, 1999.
- [32] P. Wiesel, A. P. Patel, I. M. Carvajal et al., "Exacerbation of chronic renovascular hypertension and acute renal failure in heme oxygenase-1-deficient mice," *Circulation Research*, vol. 88, no. 10, pp. 1088–1094, 2001.
- [33] W. K. Alderton, C. E. Cooper, and R. G. Knowles, "Nitric oxide synthases: structure, function and inhibition," *Biochemical Journal*, vol. 357, no. 3, pp. 593–615, 2001.
- [34] T. J. O'Dell, R. D. Hawkins, E. R. Kandel, and O. Arancio, "Tests of the roles of two diffusible substances in long-term potentiation: evidence for nitric oxide as a possible early retrograde messenger," *Proceedings of the National Academy of Sciences of the United States of America*, vol. 88, no. 24, pp. 11285–11289, 1991.
- [35] C. Bogdan, "Nitric oxide and the immune response," *Nature Immunology*, vol. 2, no. 10, pp. 907–916, 2001.
- [36] R. W. Grange, E. Isotani, K. S. Lau, K. E. Kamm, P. L. Huang, and J. T. Stull, "Nitric oxide contributes to vascular smooth muscle relaxation in contracting fast-twitch muscles," *Physiological Genomics*, vol. 5, no. 1, pp. 35–44, 2001.
- [37] U. Förstermann, E. I. Closs, J. S. Pollock et al., "Nitric oxide synthase isozymes. Characterization, purification, molecular cloning, and functions," *Hypertension*, vol. 23, pp. 1121–1131, 1994.
- [38] N. Kim, K. M. Azadzi, I. Goldstein, and I. Saenz de Tejada, "A nitric oxide-like factor mediates nonadrenergic-noncholinergic neurogenic relaxation of penile corpus cavernosum smooth muscle," *The Journal of Clinical Investigation*, vol. 88, no. 1, pp. 112–118, 1991.
- [39] U. Förstermann, "Regulation of nitric oxide synthase expression and activity," *Nitric Oxide*, vol. 143, pp. 71–91, 2000.
- [40] J. N. Sharma, A. Al-Omran, and S. S. Parvathy, "Role of nitric oxide in inflammatory diseases," *Inflammopharmacology*, vol. 15, no. 6, pp. 252–259, 2007.
- [41] I. Fleming and R. Busse, "Molecular mechanisms involved in the regulation of the endothelial nitric oxide synthase," *American Journal of Physiology, Regulatory, Integrative and Comparative Physiology*, vol. 284, no. 1, pp. R1–R12, 2003.
- [42] E. G. Shesely, N. Maeda, H. S. Kim et al., "Elevated blood pressures in mice lacking endothelial nitric oxide synthase," *Proceedings of the National Academy of Sciences of the United States of America*, vol. 93, no. 23, pp. 13176–13181, 1996.
- [43] P. L. Huang, Z. Huang, H. Mashimo et al., "Hypertension in mice lacking the gene for endothelial nitric oxide synthase," *Nature*, vol. 377, no. 6546, pp. 239–242, 1995.
- [44] U. Alheid, J. C. Frölich, and U. Förstermann, "Endothelium-derived relaxing factor from cultured human endothelial cells inhibits aggregation of human platelets," *Thrombosis Research*, vol. 47, no. 5, pp. 561–571, 1987.
- [45] R. Busse, A. Lückhoff, and E. Bassenge, "Endothelium-derived relaxant factor inhibits platelet activation," *Naunyn-Schmiedeberg's archives of pharmacology*, vol. 336, no. 5, pp. 566–571, 1987.
- [46] M. W. Radomski, R. M. J. Palmer, and S. Moncada, "The anti-aggregating properties of vascular endothelium: interactions between prostacyclin and nitric oxide," *British Journal of Pharmacology*, vol. 92, no. 3, pp. 639–646, 1987.
- [47] T. Nakaki, M. Nakayama, and R. Kato, "Inhibition by nitric oxide and nitric oxide-producing vasodilators of DNA synthesis in vascular smooth muscle cells," *European Journal of Pharmacology: Molecular Pharmacology*, vol. 189, no. 6, pp. 347–353, 1990.
- [48] R. N. Han and D. J. Stewart, "Defective Lung Vascular Development in Endothelial Nitric Oxide Synthase-Deficient Mice," *Trends in Cardiovascular Medicine*, vol. 16, no. 1, pp. 29–34, 2006.
- [49] T. Murohara, T. Asahara, M. Silver et al., "Nitric oxide synthase modulates angiogenesis in response to tissue ischemia," *The Journal of Clinical Investigation*, vol. 101, no. 11, pp. 2567–2578, 1998.
- [50] A. Aicher, C. Heeschen, C. Mildner-Rihm et al., "Essential role of endothelial nitric oxide synthase for mobilization of stem and progenitor cells," *Nature Medicine*, vol. 9, no. 11, pp. 1370–1376, 2003.
- [51] U. Landmesser, N. Engberding, F. H. Bahlmann et al., "Statin-induced improvement of endothelial progenitor cell mobilization, myocardial neovascularization, left ventricular function, and survival after experimental myocardial infarction requires endothelial nitric oxide synthase," *Circulation*, vol. 110, no. 14, pp. 1933–1939, 2004.
- [52] P. Kubes, M. Suzuki, and D. N. Granger, "Nitric oxide: an endogenous modulator of leukocyte adhesion," *Proceedings of the National Academy of Sciences of the United States of America*, vol. 88, no. 11, pp. 4651–4655, 1991.
- [53] S. Dimmeler and A. M. Zeiher, "Nitric oxide—an endothelial cell survival factor," *Cell Death and Differentiation*, vol. 6, no. 10, pp. 964–968, 1999.
- [54] P. I. Nedvetsky, W. C. Sessa, and H. H. Schmidt, "There's NO binding like NOS binding: protein-protein interactions in NO/cGMP signaling," *Proceedings of the National Academy of Sciences*, vol. 99, no. 26, pp. 16510–16512, 2002.
- [55] G. García-Cardena, R. Fan, D. F. Stern, J. Liu, and W. C. Sessa, "Endothelial nitric oxide synthase is regulated by tyrosine phosphorylation and interacts with caveolin-1," *The Journal of Biological Chemistry*, vol. 271, no. 44, pp. 27237–27240, 1996.
- [56] S. Bulotta, A. Cerullo, R. Barsacchi et al., "Endothelial nitric oxide synthase is segregated from caveolin-1 and localizes to the leading edge of migrating cells," *Experimental Cell Research*, vol. 312, no. 6, pp. 877–889, 2006.
- [57] I. Fleming, B. Fisslthaler, S. Dimmeler, B. E. Kemp, and R. Busse, "Phosphorylation of Thr495Regulates Ca<sup>2+</sup>/calmodulin-dependent endothelial nitric oxide synthase activity," *Circulation Research*, vol. 88, no. 11, pp. E68–E75, 2001.
- [58] B. J. Michell, Z. P. Chen, T. Tiganis et al., "Coordinated control of endothelial nitric-oxide synthase phosphorylation by protein kinase C and the cAMP-dependent protein kinase," *The Journal of Biological Chemistry*, vol. 276, no. 21, pp. 17625–17628, 2001.

- [59] S. Pennathur and J. W. Heinecke, "Mechanisms for oxidative stress in diabetic cardiovascular disease," *Antioxidants & Redox Signaling*, vol. 9, no. 7, pp. 955–969, 2007.
- [60] U. Landmesser, S. Dikalov, S. R. Price et al., "Oxidation of tetrahydrobiopterin leads to uncoupling of endothelial cell nitric oxide synthase in hypertension," *The Journal of Clinical Investigation*, vol. 111, no. 8, pp. 1201–1209, 2003.
- [61] J. B. Laursen, M. Somers, S. Kurz et al., "Endothelial regulation of vasomotion in ApoE-Deficient Mice," *Circulation*, vol. 103, no. 9, pp. 1282–1288, 2001.
- [62] Z. Yang and X. F. Ming, "Arginase: the emerging therapeutic target for vascular oxidative stress and inflammation," *Frontiers in Immunology*, vol. 4, 2013.
- [63] D. E. Berkowitz, R. White, D. Li et al., "Arginase reciprocally regulates nitric oxide synthase activity and contributes to endothelial dysfunction in aging blood vessels," *Circulation*, vol. 108, no. 16, pp. 2000–2006, 2003.
- [64] C. A. Chen, T. Y. Wang, S. Varadharaj et al., "S-glutathionylation uncouples eNOS and regulates its cellular and vascular function," *Nature*, vol. 468, no. 7327, pp. 1115–1118, 2010.
- [65] D. Chakravorty and M. Hensel, "Inducible nitric oxide synthase and control of intracellular bacterial pathogens," *Microbes and Infection*, vol. 5, no. 7, pp. 621–627, 2003.
- [66] C. F. Nathan and J. B. Hibbs Jr., "Role of nitric oxide synthesis in macrophage antimicrobial activity," *Current Opinion in Immunology*, vol. 3, no. 1, pp. 65–70, 1991.
- [67] D. A. Wink, K. S. Kasprzak, C. M. Maragos et al., "DNA deaminating ability and genotoxicity of nitric oxide and its progenitors," *Science*, vol. 254, no. 5034, pp. 1001–1003, 1991.
- [68] K. Fehsel, A. Jalowy, S. Qi, V. Burkart, B. Hartmann, and H. Kolb, "Islet cell DNA is a target of inflammatory attack by nitric oxide," *Diabetes*, vol. 42, no. 3, pp. 496–500, 1993.
- [69] Z. Q. Wang, J. Tejero, C. C. Wei et al., "Arg375 tunes tetrahydrobiopterin functions and modulates catalysis by inducible nitric oxide synthase," *Journal of Inorganic Biochemistry*, vol. 108, pp. 203–215, 2012.
- [70] S. Naureckiene, S. R. Kodangattil, E. J. Kaftan et al., "Identification of critical amino acid residues for human iNOS functional activity," *The Protein Journal*, vol. 27, no. 5, pp. 309–318, 2008.
- [71] J. D. MacMicking, C. Nathan, G. Hom et al., "Altered responses to bacterial infection and endotoxic shock in mice lacking inducible nitric oxide synthase," *Cell*, vol. 81, no. 4, pp. 641–650, 1995.
- [72] M. S. Parihar, R. R. Nazarewicz, E. Kincaid, U. Bringold, and P. Ghafourifar, "Association of mitochondrial nitric oxide synthase activity with respiratory chain complex I," *Biochemical and Biophysical Research Communications*, vol. 366, no. 1, pp. 23–28, 2008.
- [73] G. C. Brown, "Nitric oxide and mitochondria," *Frontiers in Bioscience: a journal and virtual library*, vol. 12, no. 1, pp. 1024–1033, 2007.
- [74] M. W. J. Cleeter, J. M. Cooper, V. M. Darley-Usmar, S. A. Moncada, and A. H. V. Schapira, "Reversible inhibition of cytochrome c oxidase, the terminal enzyme of the mitochondrial respiratory chain, by nitric oxide. Implications for neurodegenerative diseases," *FEBS Letters*, vol. 345, no. 1, pp. 50–54, 1994.
- [75] S. K. Saha, S. B. Lee, J. Won et al., "Correlation between oxidative stress, nutrition, and cancer initiation," *International Journal of Molecular Sciences*, vol. 18, no. 7, p. 1544, 2017.
- [76] D. Trachootham, J. Alexandre, and P. Huang, "Targeting cancer cells by ROS-mediated mechanisms: a radical therapeutic approach?," *Nature Reviews: Drug Discovery*, vol. 8, no. 7, pp. 579–591, 2009.
- [77] J. L. Meitzler, S. Antony, Y. Wu et al., "NADPH oxidases: a perspective on reactive oxygen species production in tumor biology," *Antioxidants & Redox Signaling*, vol. 20, no. 17, pp. 2873–2889, 2014.
- [78] T. Maraldi, "Natural compounds as modulators of NADPH oxidases," *Oxidative Medicine and Cellular Longevity*, vol. 2013, Article ID 271602, 10 pages, 2013.
- [79] M. E. Irwin, N. Rivera-del Valle, and J. Chandra, "Redox control of leukemia: from molecular mechanisms to therapeutic opportunities," *Antioxidants & Redox Signaling*, vol. 18, no. 11, pp. 1349–1383, 2013.
- [80] M. Gabay, Y. Li, and D. W. Felsher, "MYC activation is a hallmark of cancer initiation and maintenance," *Cold Spring Harbor Perspectives in Medicine*, vol. 4, no. 6, 2014.
- [81] C. Gorrini, I. S. Harris, and T. W. Mak, "Modulation of oxidative stress as an anticancer strategy," *Nature Reviews Drug Discovery*, vol. 12, no. 12, pp. 931–947, 2013.
- [82] G. Bjelakovic, D. Nikolova, L. L. Gluud, R. G. Simonetti, and C. Gluud, "Mortality in randomized trials of antioxidant supplements for primary and secondary prevention: systematic review and meta-analysis," *JAMA*, vol. 297, no. 8, pp. 842–857, 2007.
- [83] G. M. DeNicola, F. A. Karreth, T. J. Humpton et al., "Oncogene-induced Nrf2 transcription promotes ROS detoxification and tumorigenesis," *Nature*, vol. 475, no. 7354, pp. 106–109, 2011.
- [84] B. Mateescu, L. Batista, M. Cardon et al., "miR-141 and miR-200a act on ovarian tumorigenesis by controlling oxidative stress response," *Nature Medicine*, vol. 17, no. 12, pp. 1627–1635, 2011.
- [85] M. B. Sporn and K. T. Libby, "NRF2 and cancer: the good, the bad and the importance of context," *Nature Reviews Cancer*, vol. 12, no. 8, pp. 564–571, 2012.
- [86] C. A. Davison, S. M. Durbin, M. R. Thau et al., "Antioxidant enzymes mediate survival of breast cancer cells deprived of extracellular matrix," *Cancer Research*, vol. 73, no. 12, pp. 3704–3715, 2013.
- [87] I. Kasugai and M. Yamada, "High production of catalase in hydrogen peroxide-resistant human leukemia HL-60 cell lines," *Leukemia Research*, vol. 16, no. 2, pp. 173–179, 1992.
- [88] M. Neno, S. Ichimura, K. Mita, O. Yukawa, and I. L. Cartwright, "Regulation of the catalase gene promoter by Sp1, CCAAT-recognizing factors, and a WT1/Egr-related factor in hydrogen peroxide-resistant HP100 cells," *Cancer Research*, vol. 61, no. 15, 2001.
- [89] A. Ramu, R. Spanier, H. Rahamimoff, and Z. Fuks, "Restoration of doxorubicin responsiveness in doxorubicin-resistant P388 murine leukaemia cells," *British Journal of Cancer*, vol. 50, no. 4, pp. 501–507, 1984.
- [90] S. A. Akman, G. Forrest, F. F. Chu, R. S. Esworthy, and J. H. Doroshow, "Antioxidant and xenobiotic-metabolizing enzyme gene expression in doxorubicin-resistant MCF-7 breast cancer cells," *Cancer Research*, vol. 50, no. 5, pp. 1397–1402, 1990.

- [91] H. S. Kim, T. B. Lee, and C. H. Choi, "Down-Regulation of Catalase Gene Expression in the Doxorubicin-Resistant AML Subline AML-2/DX100<sup>1</sup>," *Biochemical and Biophysical Research Communications*, vol. 281, no. 1, pp. 109–114, 2001.
- [92] E. V. Kalinina, N. N. Chernov, A. N. Saprin et al., "Changes in expression of genes encoding antioxidant enzymes, heme oxygenase-1, Bcl-2, and Bcl-xl and in level of reactive oxygen species in tumor cells resistant to doxorubicin," *Biochemistry*, vol. 71, no. 11, pp. 1200–1206, 2006.
- [93] D. W. Lamson and M. S. Brignall, "Antioxidants in cancer therapy; their actions and interactions with oncologic therapies," *Alternative Medicine Review*, vol. 4, no. 5, pp. 304–329, 1999.
- [94] J. L. Roh, J. Y. Park, E. H. Kim, H. J. Jang, and M. Kwon, "Activation of mitochondrial oxidation by PDK2 inhibition reverses cisplatin resistance in head and neck cancer," *Cancer Letters*, vol. 371, no. 1, pp. 20–29, 2016.
- [95] N. M. Alajez, W. Shi, A. B. Y. Hui et al., "Targeted depletion of BMI1 sensitizes tumor cells to P53-mediated apoptosis in response to radiation therapy," *Cell Death and Differentiation*, vol. 16, no. 11, pp. 1469–1479, 2009.
- [96] A. Singh, M. Bodas, N. Wakabayashi, F. Bunz, and S. Biswal, "Gain of Nrf2 function in non-small-cell lung cancer cells confers radioresistance," *Antioxidants & Redox Signaling*, vol. 13, no. 11, pp. 1627–1637, 2010.
- [97] D. Ren, N. F. Villeneuve, T. Jiang et al., "Brusatol enhances the efficacy of chemotherapy by inhibiting the Nrf2-mediated defense mechanism," *Proceedings of the National Academy of Sciences of the United States of America*, vol. 108, no. 4, pp. 1433–1438, 2011.
- [98] S. Yokoo, K. Furumoto, E. Hiyama, and N. Miwa, "Slowdown of age-dependent telomere shortening is executed in human skin keratinocytes by hormesis-like-effects of trace hydrogen peroxide or by anti-oxidative effects of pro-vitamin C in common concurrently with reduction of intracellular oxidative stress," *Journal of Cellular Biochemistry*, vol. 93, no. 3, pp. 588–597, 2004.
- [99] S. K. Choudhari, M. Chaudhary, S. Bagde, A. R. Gadgil, and V. Joshi, "Nitric oxide and cancer: a review," *World Journal of Surgical Oncology*, vol. 11, 2013.
- [100] S. Y. Lee, Y. Rim, D. D. McPherson, S. L. Huang, and H. Kim, "A novel liposomal nanomedicine for nitric oxide delivery and breast cancer treatment," *Bio-Medical Materials and Engineering*, vol. 24, no. 1, pp. 61–67, 2014.
- [101] C. Adams, H. O. McCarthy, J. A. Coulter et al., "Nitric oxide synthase gene therapy enhances the toxicity of cisplatin in cancer cells," *The Journal of Gene Medicine*, vol. 11, no. 2, pp. 160–168, 2009.
- [102] M. N. Soler, P. Bobe, K. Benihoud, G. Lemaire, B. A. Roos, and S. Lausson, "Gene therapy of rat medullary thyroid cancer by naked nitric oxide synthase II DNA injection," *The Journal of Gene Medicine*, vol. 2, no. 5, pp. 344–352, 2000.
- [103] S. Pervin, R. Singh, S. Sen, and G. Chaudhuri, "Dual role of nitric oxide in cancer biology," in *Nitric Oxide (NO) and Cancer*, pp. 39–57, Springer, New York, NY, 2010.
- [104] B. Wang, D. Wei, V. E. Crum et al., "A novel model system for studying the double-edged roles of nitric oxide production in pancreatic cancer growth and metastasis," *Oncogene*, vol. 22, no. 12, pp. 1771–1782, 2003.
- [105] S. Tamir, S. Burney, and S. R. Tannenbaum, "DNA damage by nitric oxide," *Chemical Research in Toxicology*, vol. 9, no. 5, pp. 821–827, 1996.
- [106] D. A. Wink, Y. Vodovotz, J. Laval, F. Laval, M. W. Dewhirst, and J. B. Mitchell, "The multifaceted roles of nitric oxide in cancer," *Carcinogenesis*, vol. 19, no. 5, pp. 711–721, 1998.
- [107] J. Laval, J. Jurado, M. Saporbaev, and O. Sidorkina, "Antimutagenic role of base-excision repair enzymes upon free radical-induced DNA damage," *Mutation Research*, vol. 402, no. 1-2, pp. 93–102, 1998.
- [108] Y. Katanasaka, Y. Kodera, Y. Kitamura, T. Morimoto, T. Tamura, and F. Koizumi, "Epidermal growth factor receptor variant type III markedly accelerates angiogenesis and tumor growth via inducing c-myc mediated angiopoietin-like 4 expression in malignant glioma," *Molecular Cancer*, vol. 12, no. 1, p. 31, 2013.
- [109] E. S. Robinson, E. V. Khankin, T. K. Choueiri et al., "Suppression of the nitric oxide pathway in metastatic renal cell carcinoma patients receiving vascular endothelial growth factor-signaling inhibitors," *Hypertension*, vol. 56, no. 6, pp. 1131–1136, 2010.
- [110] O. Gallo, A. Franchi, L. Magnelli et al., "Cyclooxygenase-2 pathway correlates with VEGF expression in head and neck cancer. Implications for tumor angiogenesis and metastasis," *Neoplasia*, vol. 3, no. 1, pp. 53–61, 2001.
- [111] B. Q. Shen, D. Y. Lee, and T. F. Zioncheck, "Vascular endothelial growth factor governs endothelial nitric-oxide synthase expression via a KDR/Flk-1 receptor and a protein kinase C signaling pathway," *The Journal of Biological Chemistry*, vol. 274, no. 46, pp. 33057–33063, 1999.
- [112] S. Ambs, W. G. Merriam, W. P. Bennett et al., "Frequent nitric oxide synthase-2 expression in human colon adenomas: implication for tumor angiogenesis and colon cancer progression," *Cancer Research*, vol. 58, no. 2, pp. 334–341, 1998.
- [113] Z. J. Shang and J. R. Li, "Expression of endothelial nitric oxide synthase and vascular endothelial growth factor in oral squamous cell carcinoma: its correlation with angiogenesis and disease progression," *Journal of Oral Pathology and Medicine*, vol. 34, no. 3, pp. 134–139, 2005.
- [114] K. Harada, Supriatno, S. Kawaguchi, O. Tomitaro, H. Yoshida, and M. Sato, "Overexpression of iNOS gene suppresses the tumorigenicity and metastasis of oral cancer cells," *In Vivo*, vol. 18, no. 4, 2004.
- [115] P. K. Kim, R. Zamora, P. Petrosko, and T. R. Billiar, "The regulatory role of nitric oxide in apoptosis," *International Immunopharmacology*, vol. 1, no. 8, pp. 1421–1441, 2001.
- [116] D. C. Jenkins, I. G. Charles, L. L. Thomsen et al., "Roles of nitric oxide in tumor growth," *Proceedings of the National Academy of Sciences of the United States of America*, vol. 92, no. 10, pp. 4392–4396, 1995.
- [117] Y. Maejima, S. Adachi, K. Morikawa, H. Ito, and M. Isobe, "Nitric oxide inhibits myocardial apoptosis by preventing caspase-3 activity via S-nitrosylation," *Journal of Molecular and Cellular Cardiology*, vol. 38, no. 1, pp. 163–174, 2005.
- [118] Y. M. Kim, H. T. Chung, R. L. Simmons, and T. R. Billiar, "Cellular non-heme iron content is a determinant of nitric oxide-mediated apoptosis, necrosis, and caspase inhibition," *The Journal of Biological Chemistry*, vol. 275, no. 15, pp. 10954–10961, 2000.

- [119] C. M. Schonhoff, B. Gaston, and J. B. Mannick, "Nitrosylation of cytochrome c during apoptosis," *The Journal of Biological Chemistry*, vol. 278, no. 20, pp. 18265–18270, 2003.
- [120] R. Reinehr, B. Görg, A. Höngen, and D. Häussinger, "CD95-tyrosine nitration inhibits hyperosmotic and CD95 ligand-induced CD95 activation in rat hepatocytes," *The Journal of Biological Chemistry*, vol. 279, no. 11, pp. 10364–10373, 2004.
- [121] S. Hama, O. Takeichi, K. Fujisaki, N. Tanabe, M. Maeno, and K. Ochiai, "Nitric oxide attenuates vascular endothelial cadherin-mediated vascular integrity in human chronic inflammation," *Clinical and Experimental Immunology*, vol. 154, no. 3, pp. 384–390, 2008.
- [122] L. A. Ridnour, A. N. Windhausen, J. S. Isenberg et al., "Nitric oxide regulates matrix metalloproteinase-9 activity by guanylyl-cyclase-dependent and -independent pathways," *Proceedings of the National Academy of Sciences*, vol. 104, no. 43, pp. 16898–16903, 2007.
- [123] C. Brito, M. Naviliat, A. C. Tiscornia et al., "Peroxyntirite inhibits T lymphocyte activation and proliferation by promoting impairment of tyrosine phosphorylation and peroxyntirite-driven apoptotic death," *The Journal of Immunology*, vol. 162, no. 6, pp. 3356–3366, 1999.
- [124] A. E. Gehad, M. K. Lichtman, C. D. Schmults et al., "Nitric oxide-producing myeloid-derived suppressor cells inhibit vascular E-selectin expression in human squamous cell carcinomas," *The Journal of Investigative Dermatology*, vol. 132, no. 11, pp. 2642–2651, 2012.
- [125] P. Jayaraman, F. Parikh, E. Lopez-Rivera et al., "Tumor-expressed inducible nitric oxide synthase controls induction of functional myeloid-derived suppressor cells through modulation of vascular endothelial growth factor release," *Journal of Immunology*, vol. 188, no. 11, pp. 5365–5376, 2012.
- [126] N. Charles, T. Ozawa, M. Squatrito et al., "Perivascular nitric oxide activates notch signaling and promotes stem-like character in PDGF-induced glioma cells," *Cell Stem Cell*, vol. 6, no. 2, pp. 141–152, 2010.
- [127] Alhayek and C. V. Preuss, *Beta 1 Receptors*, Stat Pearls Publishing LLC, Treasure Island (FL), 2018.
- [128] D. W. McGraw and S. B. Liggett, "Molecular mechanisms of 2-Adrenergic Receptor Function and regulation," *Proceedings of the American Thoracic Society*, vol. 2, no. 4, pp. 292–296, 2005.
- [129] C. J. Padro and V. M. Sanders, "Neuroendocrine regulation of inflammation," *Seminars in Immunology*, vol. 26, no. 5, pp. 357–368, 2014.
- [130] M. Johnson, "Molecular mechanisms of  $\beta_2$ -adrenergic receptor function, response, and regulation," *The Journal of Allergy and Clinical Immunology*, vol. 117, no. 1, pp. 18–24, 2006.
- [131] D. Liu, Q. Deng, L. Sun et al., "A Her 2-let-7- $\beta_2$ -AR circuit affects prognosis in patients with Her 2-positive breast cancer," *BMC Cancer*, vol. 15, no. 832, pp. 147–154, 2017.
- [132] E. V. Yang, S. J. Kim, E. L. Donovan et al., "Norepinephrine upregulates VEGF, IL-8, and IL-6 expression in human melanoma tumor cell lines: implications for stress-related enhancement of tumor progression," *Brain, Behavior, and Immunity*, vol. 23, no. 2, pp. 267–275, 2009.
- [133] A. Barbieri, S. Bimonte, G. Palma et al., "The stress hormone norepinephrine increases migration of prostate cancer cells in vitro and in vivo," *International Journal of Oncology*, vol. 47, no. 2, pp. 527–534, 2015.
- [134] M. Shi, Z. Yang, M. Hu et al., "Catecholamine-induced  $\beta_2$ -adrenergic receptor activation mediates desensitization of gastric cancer cells to trastuzumab by upregulating MUC4 expression," *Journal of Immunology*, vol. 190, no. 11, pp. 5600–5608, 2013.
- [135] J. Zhang, Y. T. Deng, J. Liu et al., "Norepinephrine induced epithelial-mesenchymal transition in HT-29 and A549 cells in vitro," *Journal of Cancer Research and Clinical Oncology*, vol. 142, no. 2, pp. 423–435, 2016.
- [136] Y. J. Lu, Z. J. Geng, X. Y. Sun et al., "Isoprenaline induces epithelial-mesenchymal transition in gastric cancer cells," *Molecular and Cellular Biochemistry*, vol. 408, no. 1-2, pp. 1–13, 2015.
- [137] T. Shan, X. Cui, W. Li et al., "Novel regulatory program for norepinephrine-induced epithelial-mesenchymal transition in gastric adenocarcinoma cell lines," *Cancer Science*, vol. 105, no. 7, pp. 847–856, 2014.
- [138] A. Cannavo and W. J. Koch, "Targeting B-3 Adrenergic receptors in the Heart-Selective agonism and  $\beta$ -blockade," *Journal of Cardiovascular Pharmacology*, vol. 69, no. 2, pp. 1–78, 2017.
- [139] L. J. Emorine, S. Marullo, M. M. Briend-Sutren et al., "Molecular characterization of the human beta 3-adrenergic receptor," *Science*, vol. 245, no. 4922, pp. 1118–1121, 1989.
- [140] P. M. Simard, C. Atgié, P. Mauriège, F. D'Allaire, and L. J. Bukowiecki, "Comparison of the lipolytic effects of norepinephrine and BRL 37344 in rat brown and white adipocytes," *Obesity Research*, vol. 2, no. 5, pp. 424–431, 1994.
- [141] C. Dessy and J. L. Balligand, "Beta3-Adrenergic Receptors in Cardiac and Vascular Tissues: Emerging Concepts and Therapeutic Perspectives," *Advances in Pharmacology*, vol. 59, pp. 135–163, 2010.
- [142] O. Yamaguchi and C. R. Chapple, " $\beta_3$ -Adrenoceptors in urinary bladder," *Neurourology and Urodynamics*, vol. 26, no. 6, pp. 752–756, 2007.
- [143] V. A. Skeberdis, "Structure and function of beta3-adrenergic receptors," *Medicina*, vol. 40, no. 5, pp. 407–413, 2004.
- [144] K. J. Soeder, S. K. Snedden, W. Cao et al., "The  $\beta_3$ -Adrenergic receptor activates mitogen-activated protein kinase in adipocytes through a Gi-dependent mechanism," *Journal of Biological Chemistry*, vol. 274, no. 17, pp. 12017–12022, 1999.
- [145] E. S. Bachman, H. Dhillon, C. Y. Zhang et al., "beta AR signaling required for diet-induced thermogenesis and obesity resistance," *Science*, vol. 297, no. 5582, pp. 843–845, 2002.
- [146] C. Gauthier, V. Leblais, L. Kobzik et al., "The negative inotropic effect of beta3-adrenoceptor stimulation is mediated by activation of a nitric oxide synthase pathway in human ventricle," *The Journal of Clinical Investigation*, vol. 102, no. 7, pp. 1377–1384, 1998.
- [147] P. Varghese, R. W. Harrison, R. A. Lofthouse, D. Georgakopoulos, D. E. Berkowitz, and J. M. Hare, " $\beta_3$ -Adrenoceptor deficiency blocks nitric oxide-dependent inhibition of myocardial contractility," *Journal of Clinical Investigation*, vol. 106, no. 5, pp. 697–703, 2000.
- [148] C. Ristori, L. Filippi, M. Dal Monte et al., "Role of the adrenergic system in a mouse model of oxygen-induced retinopathy: antiangiogenic effects of  $\beta$ -Adrenoreceptor blockade," *Investigative Ophthalmology & Visual Science*, vol. 52, no. 1, pp. 155–170, 2011.

- [149] J. J. Steinle, F. C. Cappocia Jr., and Y. Jiang, "Beta-adrenergic receptor regulation of growth factor protein levels in human choroidal endothelial cells," *Growth Factors*, vol. 26, no. 6, pp. 325–330, 2008.
- [150] L. Morbidelli, C. H. Chang, J. G. Douglas, H. J. Granger, F. Ledda, and M. Ziche, "Nitric oxide mediates mitogenic effect of VEGF on coronary venular endothelium," *The American Journal of Physiology*, vol. 270, no. 1, pp. H411–H415, 1996.
- [151] L. Filippi, M. Dal Monte, G. Casini, M. Daniotti, F. Sereni, and P. Bagnoli, "Infantile hemangiomas, retinopathy of prematurity and cancer: a common pathogenetic role of the  $\beta$ -adrenergic system," *Medicinal Research Reviews*, vol. 35, no. 3, pp. 619–652, 2015.
- [152] K. Masunaga, C. R. Chapple, N. G. McKay, M. Yoshida, and D. J. Sellers, "The  $\beta$ 3-adrenoceptor mediates the inhibitory effects of  $\beta$ -adrenoceptor agonists via the urothelium in pig bladder dome," *Neurourology and Urodynamics*, vol. 29, no. 7, pp. 1320–1325, 2010.
- [153] E. P. Frazier, S. L. M. Peters, A. S. Braverman, M. R. Ruggieri Sr., and M. C. Michel, "Signal transduction underlying the control of urinary bladder smooth muscle tone by muscarinic receptors and beta-adrenoceptors," *Naunyn-Schmiedeberg's Archives of Pharmacology*, vol. 377, no. 4-6, pp. 449–462, 2008.
- [154] K. E. Andersson, N. Martin, and V. Nitti, "Selective  $\beta$ 3-adrenoceptor agonists for the treatment of overactive bladder," *The Journal of Urology*, vol. 190, no. 4, pp. 1173–1180, 2013.
- [155] A. Montoya, C. N. Amaya, A. Belmont et al., "Use of non-selective  $\beta$ -blockers is associated with decreased tumor proliferative indices in early stage breast cancer," *Oncotarget*, vol. 8, no. 4, pp. 6446–6460, 2017.
- [156] J. L. Watkins, P. H. Thaker, A. M. Nick et al., "Clinical impact of selective and nonselective beta-blockers on survival in patients with ovarian cancer," *Cancer*, vol. 121, no. 19, pp. 3444–3451, 2015.
- [157] C. Choy, J. L. Raytis, D. D. Smith et al., "Inhibition of  $\beta$ 2-adrenergic receptor reduces triple-negative breast cancer brain metastases: the potential benefit of perioperative  $\beta$ -blockade," *Oncology Reports*, vol. 35, no. 6, pp. 3135–3142, 2016.
- [158] Y. L. Hwa, Q. Shi, S. K. Kumar et al., "Beta-blockers improve survival outcomes in patients with multiple myeloma: a retrospective evaluation," *American Journal of Hematology*, vol. 92, no. 1, pp. 50–55, 2017.
- [159] H. A. Al-Wadei, H. K. Plummer, M. F. Ullah, B. Unger, J. R. Brody, and H. M. Schuller, "Social stress promotes and  $\gamma$ -aminobutyric acid inhibits tumor growth in mouse models of non-small cell lung cancer," *Cancer Prevention Research*, vol. 5, no. 2, pp. 189–196, 2012.
- [160] P. G. Park, J. Merryman, M. Orloff, and H. M. Schuller, "Beta-adrenergic mitogenic signal transduction in peripheral lung adenocarcinoma: implications for individuals with preexisting chronic lung disease," *Cancer Research*, vol. 55, no. 16, pp. 3504–3508, 1995.
- [161] K. Guo, Q. Ma, L. Wang et al., "Norepinephrine-induced invasion by pancreatic cancer cells is inhibited by propranolol," *Oncology Reports*, vol. 22, no. 4, pp. 825–830, 2009.
- [162] D. Zhang, Q. Y. Ma, H. T. Hu, and M. Zhang, " $\beta$ 2-Adrenergic antagonists suppress pancreatic cancer cell invasion by inhibiting CREB, NF- $\kappa$ B and AP-1," *Cancer Biology & Therapy*, vol. 10, no. 1, pp. 19–29, 2010.
- [163] E. K. Sloan, S. J. Priceman, B. F. Cox et al., "The sympathetic nervous system induces a metastatic switch in primary breast cancer," *Cancer Research*, vol. 70, no. 18, pp. 7042–7052, 2010.
- [164] K. Lang, T. L. Drell, A. Lindecke et al., "Induction of a metastatogenic tumor cell type by neurotransmitters and its pharmacological inhibition by established drugs," *International Journal of Cancer*, vol. 112, no. 2, pp. 231–238, 2004.
- [165] P. H. Thaker, L. Y. Han, A. A. Kamat et al., "Chronic stress promotes tumor growth and angiogenesis in a mouse model of ovarian carcinoma," *Nature Medicine*, vol. 12, no. 8, pp. 939–944, 2006.
- [166] A. K. Sood, G. N. Armaiz-Pena, J. Halder et al., "Adrenergic modulation of focal adhesion kinase protects human ovarian cancer cells from anoikis," *The Journal of Clinical Investigation*, vol. 120, no. 5, pp. 1515–1523, 2010.
- [167] H. P. Wong, J. W. Ho, M. W. Koo et al., "Effects of adrenaline in human colon adenocarcinoma HT-29 cells," *Life Sciences*, vol. 88, no. 25-26, pp. 1108–1112, 2011.
- [168] K. S. Sastry, Y. Karpova, S. Prokopovich et al., "Epinephrine protects cancer cells from apoptosis via activation of cAMP-dependent protein kinase and BAD phosphorylation," *The Journal of Biological Chemistry*, vol. 282, no. 19, pp. 14094–14100, 2007.
- [169] S. Moretti, D. Massi, V. Farini et al., " $\beta$ -adrenoceptors are upregulated in human melanoma and their activation releases pro-tumorigenic cytokines and metalloproteases in melanoma cell lines," *Laboratory Investigation*, vol. 93, no. 3, pp. 279–290, 2013.
- [170] M. G. Perrone, M. Notarnicola, M. G. Caruso, V. Tutino, and A. Scilimati, "Upregulation of beta3-adrenergic receptor mRNA in human colon cancer: a preliminary study," *Oncology*, vol. 75, no. 3-4, pp. 224–229, 2008.
- [171] K. M. Chisholm, K. W. Chang, M. T. Truong, S. Kwok, R. B. West, and A. E. Heerema-McKenney, " $\beta$ -Adrenergic receptor expression in vascular tumors," *Modern Pathology*, vol. 25, no. 11, pp. 1446–1451, 2012.
- [172] D. M. Lamkin, E. K. Sloan, A. J. Patel et al., "Chronic stress enhances progression of acute lymphoblastic leukemia via  $\beta$ -adrenergic signaling," *Brain, Behavior, and Immunity*, vol. 26, no. 4, pp. 635–641, 2012.
- [173] M. Calvani, F. Pelon, G. Comito et al., "Norepinephrine promotes tumor microenvironment reactivity through  $\beta$ 3-adrenoreceptors during melanoma progression," *Oncotarget*, vol. 6, no. 7, pp. 4615–4632, 2015.
- [174] M. Dal Monte, G. Casini, L. Filippi, G. P. Nicchia, M. Svelto, and P. Bagnoli, "Functional involvement of  $\beta$ 3-adrenergic receptors in melanoma growth and vascularization," *Journal of Molecular Medicine*, vol. 91, no. 12, pp. 1407–1419, 2013.
- [175] M. Calvani, L. Cavallini, A. Tondo et al., " $\beta$ 3-Adrenoreceptors control mitochondrial dormancy in melanoma and embryonic stem cells," *Oxidative Medicine and Cellular Longevity*, vol. 2018, Article ID 6816508, 10 pages, 2018.
- [176] M. Calvani, G. Bruno, M. Dal Monte et al., " $\beta$ 3-Adrenoceptor as a potential immuno-suppressor agent in melanoma," *British Journal of Pharmacology*, vol. 176, no. 14, pp. 2509–2524, 2019.
- [177] G. Bruno, F. Cencetti, A. Pini et al., " $\beta$ 3-adrenoreceptor blockade reduces tumor growth and increases neuronal differentiation in neuroblastoma via SK2/S1P<sub>2</sub> modulation," *Oncogene*, 2019.

- [178] Y. Yoshioka, H. Kadoi, A. Yamamuro, Y. Ishimaru, and S. Maeda, "Noradrenaline increases intracellular glutathione in human astrocytoma U-251 MG cells by inducing glutamate-cysteine ligase protein via  $\beta_3$ -adrenoceptor stimulation," *European Journal of Pharmacology*, vol. 772, pp. 51–61, 2016.
- [179] T. Hadi, R. Douhard, A. M. M. Dias et al., "Beta3 adrenergic receptor stimulation in human macrophages inhibits NADPH oxidase activity and induces catalase expression via PPAR  $\gamma$  activation," *Biochimica et Biophysica Acta. Molecular Cell Research*, vol. 1864, no. 10, pp. 1769–1784, 2017.
- [180] A. Negre-Salvayre, C. Hirtz, G. Carrera et al., "A role for uncoupling protein-2 as a regulator of mitochondrial hydrogen peroxide generation," *FASEB Journal*, vol. 11, no. 10, pp. 809–815, 1997.
- [181] K. S. Echtay, D. Roussel, J. St-Pierre et al., "Superoxide activates mitochondrial uncoupling proteins," *Nature*, vol. 415, no. 6867, pp. 96–99, 2002.
- [182] R. J. Mailloux and M. E. Harper, "Uncoupling proteins and the control of mitochondrial reactive oxygen species production," *Free Radical Biology & Medicine*, vol. 51, no. 6, pp. 1106–1115, 2011.
- [183] A. Pasha, M. Vignoli, A. Subbiani et al., " $\beta_3$ -Adrenoreceptor activity limits apigenin efficacy in Ewing sarcoma cells: a dual approach to prevent cell survival," *International Journal of Molecular Sciences*, vol. 20, no. 9, p. 2149, 2019.
- [184] A. J. Burke, F. J. Sullivan, F. J. Giles, and S. A. Glynn, "The yin and yang of nitric oxide in cancer progression," *Carcinogenesis*, vol. 34, no. 3, pp. 503–512, 2013.
- [185] C. H. Tang and E. A. Grimm, "Depletion of endogenous nitric oxide enhances cisplatin-induced apoptosis in p53-dependent manner in melanoma cell lines," *The Journal of Biological Chemistry*, vol. 279, no. 1, pp. 288–298, 2004.
- [186] V. V. Prabhu and C. Guruvayoorappan, "Anti-inflammatory and antitumor activity of the marine mangrove *Rhizophora apiculata*," *Journal of Immunotoxicology*, vol. 9, no. 4, pp. 341–352, 2012.
- [187] C. H. Tang and E. A. Grimm, "Depletion of endogenous nitric oxide enhances cisplatin-induced apoptosis in a p53-dependent manner in melanoma cell lines," *Journal of Biological Chemistry*, vol. 279, no. 1, pp. 288–298, 2004.
- [188] A. G. Sikora, A. Gelbard, M. A. Davies et al., "Targeted inhibition of inducible nitric oxide synthase inhibits growth of human melanoma in vivo and synergizes with chemotherapy," *Clinical Cancer Research*, vol. 16, no. 6, pp. 1834–1844, 2010.
- [189] M. Dal Monte, I. Fornaciari, G. P. Nicchia, M. Svelto, G. Casini, and P. Bagnoli, " $\beta_3$ -adrenergic receptor activity modulates melanoma cell proliferation and survival through nitric oxide signaling," *Naunyn-Schmiedeberg's Archives of Pharmacology*, vol. 387, no. 6, pp. 533–543, 2014.
- [190] M. Calvani and C. Favre, "Antioxidant Nutraceutical approach to Ewing Sarcoma-Where is the Trap?," *Biomedical Journal of Scientific & Technical Research*, vol. 17, no. 3, pp. 12805–12814, 2019.



## Research Article

# Mechanisms of Anthracycline-Enhanced Reactive Oxygen Metabolism in Tumor Cells

James H. Doroshov <sup>1,2,3</sup>

<sup>1</sup>Division of Cancer Treatment and Diagnosis, National Cancer Institute, NIH, Bethesda, MD 20892, USA

<sup>2</sup>Developmental Therapeutics Branch of the Center for Cancer Research, National Cancer Institute, NIH, Bethesda, MD 20892, USA

<sup>3</sup>Department of Medical Oncology and Therapeutics Research, City of Hope Comprehensive Cancer Center, Duarte, CA 91010, USA

Correspondence should be addressed to James H. Doroshov; [doroshj@mail.nih.gov](mailto:doroshj@mail.nih.gov)

Received 21 September 2019; Accepted 11 November 2019; Published 3 December 2019

Guest Editor: Nagendra K. Kaushik

Copyright © 2019 James H. Doroshov. This is an open access article distributed under the Creative Commons Attribution License, which permits unrestricted use, distribution, and reproduction in any medium, provided the original work is properly cited.

In this investigation, we examined the effect of anthracycline antibiotics on oxygen radical metabolism in Ehrlich tumor cells. In tumor microsomes and nuclei, doxorubicin increased superoxide anion production in a dose-dependent fashion that appeared to follow saturation kinetics; the apparent  $K_m$  and  $V_{max}$  for superoxide formation by these organelles was 124.9  $\mu M$  and 22.6 nmol/min/mg, and 103.4  $\mu M$  and 4.8 nmol/min/mg, respectively. In both tumor microsomes and nuclei, superoxide formation required NADPH as a cofactor, was accompanied by the formation of hydrogen peroxide, and resulted from the transfer of electrons from NADPH to the doxorubicin quinone by NADPH:cytochrome P-450 reductase (NADPH:ferricytochrome oxidoreductase, EC 1.6.2.4). Anthracycline antibiotics also significantly enhanced superoxide anion production by tumor mitochondria with an apparent  $K_m$  and  $V_{max}$  for doxorubicin of 123.2  $\mu M$  and 14.7 nmol/min/mg. However, drug-stimulated superoxide production by mitochondria required NADH and was increased by rotenone, suggesting that the proximal portion of the electron transport chain in tumor cells was responsible for reduction of the doxorubicin quinone at this site. The net rate of drug-related oxygen radical production was also determined for intact Ehrlich tumor cells; in this system, treatment with doxorubicin produced a dose-related increase in cyanide-resistant respiration that was enhanced by changes in intracellular reducing equivalents. Finally, we found that in the presence of iron, treatment with doxorubicin significantly increased the production of formaldehyde from dimethyl sulfoxide, an indication that the hydroxyl radical could be produced by intact tumor cells following anthracycline exposure. These experiments suggest that the anthracycline antibiotics are capable of significantly enhancing oxygen radical metabolism in Ehrlich tumor cells at multiple intracellular sites by reactions that could contribute to the cytotoxicity of this class of drugs.

## 1. Introduction

The anthracycline antibiotics, including doxorubicin and daunorubicin, play an important role in the treatment of human leukemias and lymphomas as well as carcinomas of the breast [1]. The major long-term toxicity of anthracycline therapy is a form of cumulative cardiac toxicity that may produce long-lived morbidity, especially in pediatric cancer patients receiving this class of drugs [2]. A substantial body of experimental evidence has been developed suggesting that the cardiac toxicity of the anthracycline antitumor agents

may, in part, be related to the generation of strong oxidant species in the heart [3] catalyzed by flavin dehydrogenases present in multiple subcellular compartments [4]. Redox cycling of the anthracycline quinone moiety by complex I of the cardiac electron transport chain [5] can damage intracellular lipid membranes in mitochondria as well as sodium and calcium transporters in the heart [6]. In addition to redox cycling of the quinone functionality of the anthracyclines, doxorubicin may form a potent drug-iron complex that enhances the formation of powerful oxidants with the chemical characteristics of the hydroxyl radical [7, 8]. In this

fashion, as well as through interactions with various iron binding proteins, the anthracycline antibiotics may contribute to myocyte toxicity [9, 10].

A role for reactive oxygen species (ROS) produced by redox cycling of the anthracycline quinone in tumor cell killing is also supported by several lines of evidence [11, 12]. These studies include the demonstration by our laboratory that anthracycline-related tumor cell cytotoxicity can be significantly diminished by the administration of reactive oxygen scavengers [13] or by the modification of intracellular antioxidant defenses *in vitro* and that resistance to tumor cell killing by doxorubicin can be decreased by inhibition of peroxide detoxification [14]. The oxidative metabolism of the anthracyclines has also been demonstrated to occur *in vivo*; peripheral blood mononuclear cells taken from breast cancer patients treated with doxorubicin reveal the hallmarks of hydroxyl radical damage to DNA in a fashion that is directly related to the length of time during which patients receive the anthracycline [15]. However, unlike studies in the mammalian heart, no comprehensive evaluation of the sites and mechanisms of anthracycline-induced ROS production for mammalian tumor cells has been developed.

Hence, in the current study, we investigated the mechanisms by which anthracycline antibiotics are metabolized to generate ROS in multiple tumor cell compartments, as well as in intact tumor cells. Our results indicate that, in analogy to findings in cardiac subcellular compartments, drugs of the anthracycline class stimulate superoxide anion and hydrogen peroxide production in tumor cell mitochondria, in microsomes, and in the nucleus. Furthermore, in the presence of doxorubicin, extracellular hydrogen peroxide can be quantitated using intact tumor cells. Finally, under appropriate experimental conditions, doxorubicin-induced ROS formation was found to culminate in the production of the hydroxyl radical, or a similar chemical reactant with equivalent oxidizing potency. Thus, drug-related oxygen radical metabolism could pose an important threat to tumor cell integrity by the production of a strong oxidant stress at multiple cellular sites, contributing to cytotoxic membrane injury and DNA damage.

## 2. Materials and Methods

**2.1. Materials.** Daunorubicin, rubidazole, aclacinomycin A, and 5-iminodaunorubicin were supplied by the Drug Synthesis and Chemistry Branch, Division of Cancer Treatment and Diagnosis, National Cancer Institute, Bethesda, MD. All drugs were reconstituted in sterile water on the day of preparation and were protected from light until used. Doxorubicin hydrochloride, glutathione (reduced form), glutathione reductase type III, sodium azide, bovine albumin (fraction V), xanthine, xanthine oxidase (Grade 1), cytochrome c (type VI from horse heart), EDTA, NADPH type III, NADH Grade III, NADP<sup>+</sup> Grade V, flavin adenine dinucleotide Grade III, flavin mononucleotide, sodium succinate, sucrose, dicumarol, D-mannitol, dimethyl sulfoxide Grade I, EGTA, sodium HEPES, DTNB, rotenone, antimycin A, Triton X-100, urea, sodium benzoate, Tris, and bovine erythrocyte superoxide dismutase (SOD) (2750 units/mg as assayed

by the method of McCord and Fridovich [16]) were purchased from Sigma. Methanol (spectral grade), ethyl alcohol (99% pure), potassium cyanide, sodium acetate, acetic anhydride, ferrous sulfate, ferric chloride, formaldehyde (37% *w/v*), ammonium acetate, acetic acid, and acetylacetone were obtained from Fisher Chemical Co., Fair Lawn, NJ. Chelex 100 resin (100 to 200 mesh, sodium salt) was purchased from Bio-Rad Laboratories, Richmond, Calif. Catalase of analytical grade (65,000 units/mg protein) was purchased from Boehringer Mannheim Biochemicals, Indianapolis, Ind., and was devoid of SOD activity when assayed by the method of McCord and Fridovich [16]. Diethylurea and dimethylthiourea were purchased from Aldrich. Dulbecco's phosphate buffered saline was obtained from Grand Island Biological Co., Grand Island, NY. BCNU was purchased from Bristol-Myers Squibb. All chemicals were obtained at the highest grade available and were used without further purification. Only glass-distilled, deionized water was used in these studies.

**2.2. Cell Lines.** Ehrlich-Létré tumor cells (ascitic variant) and P388 leukemia cells were initially obtained from Dr. T. Khwaja of the University of Southern California/Norris Comprehensive Cancer Center and were maintained by weekly passage of one million cells *i.p.* in 20 g female Swiss-Webster mice. For experiments examining the effect of anthracyclines on cellular oxygen radical production, tumor cells were harvested 5-6 days after implantation, washed twice in 0.9% NaCl, exposed to hypotonic shock lysis to remove contaminating erythrocytes [17], and resuspended in PBS that had been treated with Chelex 100 resin to remove trace quantities of iron from the reagent grade buffer. Cell viability (routinely >95%) was confirmed by exclusion of 0.1% trypan blue dye.

**2.3. Preparation of Tumor Cell Organelles.** To prepare the microsomal fraction, Ehrlich tumor cells were resuspended in 4 volumes of an iced solution of 230 mM Tris-HCl pH 7.4, containing 1 mM EDTA. Tumor cells were sonically disrupted on ice for 90 sec with six 15 sec bursts, each separated by a 10 sec cooling period, using a VWR Biosonik IV ultrasonicator at a power output of 90 watts. Tumor cells were homogenized further on ice with a Dounce homogenizer using 15 strokes of the tight-fitting pestle, and the microsomal fraction was then prepared by differential ultracentrifugation using the method of Hinnen et al. [18]. The pellet from the final 65,000 *x g* centrifugation step was washed twice and resuspended before use in 150 mM potassium phosphate buffer, pH 7.4, containing 100  $\mu$ M EDTA.

The tumor cell mitochondrial fraction was prepared in 3 volumes of 0.23 M mannitol, 0.07 M sucrose, 5 mM Tris-HCl, and 1 mM EDTA, pH 7.4 by sonic disruption of cells in mannitol:sucrose:tris:EDTA for 45 sec on ice with subsequent Dounce homogenization as described above. The mitochondrial fraction was then obtained as previously described [19] with resuspension before use in 250 mM sucrose containing 20 mM HEPES, pH 7.

The nuclear fraction was prepared by modification of the method of Mamaril et al. [20]. Cells were washed twice at 4°C

in 50 mM KCl and 50 mM Tris-HCl, pH 7.5, containing 5 mM MgCl<sub>2</sub> and then resuspended in 6 volumes of iced 10 mM NaCl, 10 mM Tris-HCl, pH 7.4, and 1.5 mM MgCl<sub>2</sub>. Ehrlich cells were then centrifuged at 10,000 × *g* for 10 min at 4°C, resuspended in 8 volumes of the NaCl:tris:MgCl<sub>2</sub> buffer, and disrupted with 15 strokes of the Dounce homogenizer. Cells were homogenized further on ice with several 15 sec bursts of the ultrasonicator. The degree of cell disruption was checked after each sonic burst by phase contrast microscopy; sonication was continued until at least 95% of the tumor outer membranes had been broken. The cell suspension was then centrifuged at 600 × *g* and 4°C for 10 min; the supernatant was discarded and the pellet was resuspended in 2 volumes of 220 mM sucrose, 9.4 mM KH<sub>2</sub>PO<sub>4</sub>, 12.5 mM KH<sub>2</sub>PO<sub>4</sub>, 10 mM MgCl<sub>2</sub>, 2 mM EDTA, and 300 μM NaHCO<sub>3</sub>, pH 7.0. The nuclear suspension was freed of excess cytoplasm with 10-20 strokes of the Dounce homogenizer and then added on ice to 7 volumes of 2.3 M sucrose with stirring. The purified nuclear fraction was prepared using a discontinuous sucrose gradient when 1 ml of 2.3 M sucrose solution containing nuclei was underlaid with 2 ml of 2.1 M sucrose and then centrifuged at 4°C and 105,000 × *g* for 20 min. The nuclear layer was resuspended in 250 mM sucrose and 20 mM HEPES, pH 7.4, before use. The nuclear fraction prepared in this manner was examined for contamination by extranuclear membranes by measurement of marker enzymes and by phase contrast microscopy [20]. The Ehrlich tumor nuclei used in this study contained <10% of the specific glutamate dehydrogenase and cytochrome oxidase activities of the initial cell homogenate and were essentially free of extranuclear membranes by microscopic methods. The experimental microsomal, mitochondrial, and nuclear fractions were studied on the day of preparation.

**2.4. Measurement of Superoxide Anion Production and NAD(P)H Consumption.** Superoxide anion production in experimental samples was determined by the rate of SOD-inhibitable acetylated cytochrome c reduction as previously described [4]. The initial, linear rate of acetylated cytochrome c reduction was determined spectrophotometrically at 550 nm and 37°C in a Gilford spectrophotometer equipped with a circulating water bath. For experiments assessing the effect of DTNB on superoxide production, the sulfhydryl reagent was added to the paired reaction mixtures which were then preincubated for 2 min at 37°C before the addition of NADPH. Preincubation was not performed in experiments examining the effect of other agents on the rate of superoxide formation. Specific conditions for measurement of superoxide production by drug-treated microsomal, mitochondrial, and nuclear fractions have been described in the legends for the appropriate tables.

The effect of anthracycline antibiotics on the oxidation of NAD(P)H by subcellular fractions from Ehrlich cells was determined in triplicate at 37°C by the linear decrease in absorbance at 340 nm. NAD(P)H consumption was initiated by the addition of the membrane protein and was calculated using an extinction coefficient of 6.22 nM<sup>-1</sup> cm<sup>-1</sup> [21].

**2.5. Measurement of Oxygen Consumption and Hydrogen Peroxide Formation.** The rate of oxygen consumption by Ehrlich tumor cells was determined at 37°C with a Model 53 oxygen monitoring system (Yellow Springs Instrument Co., Yellow Springs, Ohio). The 3 ml reaction system usually contained 15 × 10<sup>6</sup> cells and PBS that had been bubbled with air for 30 min at 37° before use. When KCN, rotenone, antimycin A, glucose, or BCNU were added to this system, they were preincubated with the cells for 5 min at 37°. Oxygen consumption by subcellular fractions was determined in a similar fashion after equilibration of the membrane preparation and drugs with the particular buffer used for 4 min in the reaction vessel; these reactions were initiated by addition of appropriate cofactors, usually NAD(P)H. Free radical scavengers, when used, were added to the reaction vessel and equilibrated for 5 min prior to the addition of the anthracycline antibiotic. The linear rate of oxygen consumption was determined from 10 to 30 min after drug treatment. Hydrogen peroxide production was quantitated by the release of oxygen into the system as previously described [22] after the addition of 10 μl of catalase (4500-9000 units) through the access slot of the oxygen electrode plunger. The rate of oxygen consumption was calculated from a value of 597 nmol for the total dissolved oxygen of the reaction mixture [23].

**2.6. Measurement of Hydroxyl Radical Formation.** The formation of <sup>•</sup>OH, or an oxidizing species with the chemical reactivity of <sup>•</sup>OH, by permeabilized Ehrlich cells treated with doxorubicin was assessed by measurement of formaldehyde production from dimethyl sulfoxide (DMSO) as described by Klein et al. [24]. The standard reaction mixture contained 100 mM DMSO, 100 μM Na<sub>4</sub>EDTA, 1 mM NADPH, 0.1% (*v/v*) Triton X-100, 1 × 10<sup>7</sup> cells/ml, and the indicated amount of doxorubicin in a final volume of 7 ml of PBS at pH 7.2. Iron-EDTA was added to the reaction systems as a 1:2 mixture of freshly prepared ferrous sulfate in aqueous Na<sub>4</sub>EDTA. Quantitation of <sup>•</sup>OH production in this system was undertaken because of our interest in determining whether or not enrichment of flavin dehydrogenase-specific activities by preparation of subcellular fractions was necessary to demonstrate oxy-radical production (other than O<sub>2</sub> consumption and H<sub>2</sub>O<sub>2</sub> formation) by drug-treated tumor cells.

The reaction systems were initiated by the addition of NADPH; they were then mixed vigorously and incubated, usually for 2 hr at 37°C, in 25 ml polycarbonate flasks in a shaking water bath. The reactions were terminated by the addition of 0.5 ml of ice-cold 17.5% (*w/v*) trichloroacetic acid to 1 ml aliquots taken from the standard reaction mixture. Samples were centrifuged at 1000 × *g* for 10 min in the cold; a 1 ml portion of the supernatant was then assayed for formaldehyde [24, 25]. In brief, 1 ml of a solution containing 2 M ammonium acetate, 50 mM acetic acid, and 20 mM acetylacetone was added to the 1 ml experimental sample; the sample was then mixed, incubated at 37°C for 40 min in a shaking water bath, and assayed for relative formaldehyde concentration at 25°C in a 1 ml volume by spectrophotometric measurement at 410 nm. Zero-time samples, as well as

samples lacking the reduced pyridine nucleotide cofactor, DMSO, or Ehrlich cells were routinely used as the blanks.

Preliminary experiments revealed that in our assay system, doxorubicin itself at a concentration of 300  $\mu\text{M}$  did not significantly affect the quantitation of defined amounts of authentic formaldehyde. We also examined the effect of Ehrlich cells on the recovery of formaldehyde added to the experimental reaction mixture. Compared to a cell-free system, we found that over the concentration range from 10 to 70  $\mu\text{M}$ , the recovery of genuine formaldehyde varied from 100 to 89% in the presence of  $10^7$  Ehrlich cells/ml.

Formaldehyde levels were determined from a calibration curve that was linear at concentrations from 10 to 250  $\mu\text{M}$ ; the calibration curve was routinely prepared in the standard reaction mixture of each experimental condition without cells or doxorubicin and was processed as described above for each set of experimental samples. The lower limit of sensitivity for the detection of formaldehyde in this assay was approximately 10  $\mu\text{M}$ .

**2.7. Enzyme Assays.** The NADPH:cytochrome P-450 reductase activity of the tumor microsomal and nuclear fractions was measured by a technique described previously [4] using nonacetylated cytochrome c as the electron acceptor. To assess the effect of DTNB (100  $\mu\text{M}$ ) and  $\text{NADP}^+$  (1 mM) on NADPH:cytochrome P-450 reductase activity, these reagents were preincubated with the fraction for 2 min before the addition of NADPH. Glutathione peroxidase activity was determined in tumor cell subcellular fractions as described previously [26] except that enzyme assays were initiated with 440 rather than 220 nmol hydrogen peroxide in these experiments. The data have been expressed as nmol NADPH oxidized to  $\text{NADP}^+$  per min mg protein. SOD levels were determined in the microsomal, mitochondrial, and nuclear fractions using the xanthine:xanthine oxidase:cytochrome c assay as reported previously [26]. In these experiments, acetylated cytochrome c (11.2  $\mu\text{M}$ ) was utilized in addition to KCN (10  $\mu\text{M}$ ) to eliminate interference from cytochrome oxidases in the experimental samples.

**2.8. Protein Determination.** Protein concentrations in subcellular fractions were determined by the method of Lowry et al. [27] using crystalline bovine albumin as the standard.

**2.9. Statistical Methods.** Data were analyzed with the 2-tailed  $t$  test for independent means (not significant,  $P > 0.05$  [28]).

### 3. Results

**3.1. Tumor Microsomes.** As shown in Table 1, treatment with doxorubicin increased microsomal superoxide production in a dose-dependent fashion that appeared to conform to saturation kinetics. Furthermore, a doxorubicin concentration as low as 5  $\mu\text{M}$  significantly increased oxy-radical formation over control levels (data not shown). In these experiments, superoxide production varied with the amount of microsomal protein used. In the absence of doxorubicin, superoxide formation was (mean  $\pm$  S.E.;  $n = 3$ )  $0.42 \pm 0.10$  and  $0.96 \pm 0.20$  nmol/min with 100 and 400  $\mu\text{g}$  protein/ml, respectively; in the presence of doxorubicin (135  $\mu\text{M}$ ), super-

TABLE 1: Kinetic constants for superoxide production by Ehrlich tumor subcellular fractions after treatment with doxorubicin. Superoxide production by tumor microsomes, mitochondria, and nuclei was assayed as described in Tables 2, 6, and 7. Kinetic constants were determined in triplicate to form the direct equation relating reaction velocity to substrate concentration as described in [48] using 8 different drug concentrations over a 10-fold concentration range.

Subcellular fraction	Superoxide formation	
	$K_m$ ( $\mu\text{M}$ )	$V_{\max}$ (nmol/min/mg)
Microsomes	124.9	22.6
Mitochondria	123.2	14.7
Nuclei	103.4	4.8

oxide production was  $1.73 \pm 0.07$  and  $3.14 \pm 0.08$  nmol/min,  $P < 0.01$  for each compared to control. As shown in Table 2, all components of the reaction system, including NADPH, intact microsomes, and acetylated cytochrome c were necessary to demonstrate a significant increase in superoxide formation by doxorubicin. Furthermore, only NADPH, of a variety of cofactors, could support drug-related superoxide production in these studies (Table 2).

The specificity of our assay for drug-stimulated superoxide production was also addressed (Table 2). We found that SOD-inhibitable cytochrome c reduction was not affected by catalase or DMSO in concentrations capable of eliminating either  $\text{H}_2\text{O}_2$  or the hydroxyl radical from the reaction system (Table 2). The addition of heat-denatured SOD to the experimental system also produced no significant change in the rate of drug-stimulated superoxide production. These experiments suggest that superoxide was, in fact, measured in our studies.

As shown in Table 3, three of the four anthracycline antibiotics tested in addition to doxorubicin significantly increased microsomal superoxide production over control levels. However, 5-iminodaunorubicin, an anthracycline analog that has been previously demonstrated under other conditions to be incapable of redox cycling because of its substituted quinone ring [4], did not stimulate superoxide production by the tumor microsomal fraction.

To define the mechanism of oxygen radical production by anthracycline-treated microsomes, we measured the rate of NADPH consumption in tumor microsomes after treatment with doxorubicin. In the presence of 100  $\mu\text{M}$  NADPH and 100  $\mu\text{g}/\text{ml}$  of microsomal protein from tumor, the control rate of NADPH oxidation was  $7.00 \pm 0.81$  nmol/min/mg,  $n = 4$ ; the addition of doxorubicin (135  $\mu\text{M}$ ) increased the rate of NADPH oxidation to  $19.90 \pm 2.30$  nmol/min/mg,  $n = 4$ ,  $P < 0.01$ . Furthermore, we found that the tumor microsomal fraction contained a substantial level of NADPH:cytochrome P-450 reductase activity (Table 4). After treatment of microsomes with the enzyme inhibitors DTNB or excess  $\text{NADP}^+$ , enzyme activity decreased to 27.7 or 23.2% of control levels,  $P < 0.01$  for both agents (Table 4). In parallel experiments, DTNB or excess  $\text{NADP}^+$  decreased drug-related superoxide production to 41.3 or 26.6% of baseline levels,  $P < 0.01$  for each inhibitor (Table 4). Finally, we found that the inhibitor of

TABLE 2: Requirements for doxorubicin-stimulated superoxide formation in the tumor microsomal fraction. Superoxide production in tumor microsomes was determined in paired, 1 ml reaction mixtures which contained 150 mM potassium phosphate buffer, pH 7.4, 100  $\mu$ M EDTA, 56  $\mu$ M acetylated cytochrome c, 200  $\mu$ g of microsomal protein, and either 0 or 10  $\mu$ g of SOD. The chemotherapeutic agent was added to the paired reaction mixtures, where specified, before the initiation of the reaction by addition of NADPH (1 mM).

Experimental system	Superoxide production nmol cytochrome c reduced/min/mg
Control	0.51 $\pm$ 0.26 (3) <sup>a</sup>
-Microsomes	N.D. (3) <sup>b</sup>
-NADPH	N.D. (3)
-Cytochrome c	N.D. (3)
Using NADPH (100 $\mu$ M)	N.D. (3)
Using NADH (1 mM) rather than NADPH	0.97 $\pm$ 0.28 (3)
Doxorubicin (135 $\mu$ M)	14.71 $\pm$ 1.43 (6) <sup>c</sup>
-Microsomes	N.D. (3) <sup>d</sup>
-NADPH	N.D. (3) <sup>d</sup>
-Cytochrome c	N.D. (3) <sup>d</sup>
Using heat-denatured microsomes <sup>e</sup>	N.D. (3) <sup>d</sup>
Using heat-denatured SOD <sup>e</sup>	13.77 $\pm$ 0.37 (3)
Using NADPH (100 $\mu$ M)	10.07 $\pm$ 0.82 (6)
Using NADH (1 mM) rather than NADPH	2.81 $\pm$ 0.56 (3) <sup>d</sup>
Using NADP <sup>+</sup> (1 mM) rather than NADPH	1.35 $\pm$ 0.26 (3) <sup>d</sup>
Using NAD <sup>+</sup> (1 mM) rather than NADPH	0.36 $\pm$ 0.26 (3) <sup>d</sup>
Using FAD (1 mM) <sup>f</sup> rather than NADPH	0.49 $\pm$ 0.49 (3) <sup>d</sup>
Using FMN (1 mM) <sup>f</sup>	N.D. (3) <sup>d</sup>
+DMSO (13 mM)	16.32 $\pm$ 0.51 (3)
+Catalase (1500 units)	14.36 $\pm$ 0.08 (3)
+Dicumarol (10 $\mu$ M)	14.41 $\pm$ 1.91 (3)

<sup>a</sup>Mean  $\pm$  S.E.; number in parentheses is number of experiments performed; <sup>b</sup>N.D. is not detectable; <sup>c</sup>significantly different from control ( $P < 0.001$ ); <sup>d</sup>significantly different from complete system containing NADPH and doxorubicin ( $P < 0.01$ ); <sup>e</sup>microsomes or SOD heated for 60 min in a boiling water bath; samples containing heat-denatured SOD were paired against identical mixtures with native dismutase; <sup>f</sup>FAD: flavin adenine dinucleotide; FMN: flavin mononucleotide.

NADPH:quinone oxidoreductase 1, dicumarol, produced no significant effect on doxorubicin-stimulated superoxide production (Table 2), suggesting that this quinone reductase is not involved in the metabolism of anthracyclines by tumor microsomes. Taken together, these experiments strongly suggest that the NADPH:cytochrome P-450 reductase activity of the Ehrlich tumor microsomal fraction is responsible for the one-electron reduction of anthracycline antibiotics at this site.

To confirm that anthracycline antibiotics increased reactive oxygen production in tumor microsomes, we

TABLE 3: Effect of anthracycline antibiotics on superoxide production by the tumor microsomal fraction. Superoxide production in tumor microsomes was determined as described in Table 2. For these studies, all drugs were present at a concentration of 135  $\mu$ M.

Drug	Superoxide formation (nmol/min/mg)
Daunorubicin	10.00 $\pm$ 1.02 (5) <sup>a,b</sup>
Rubidazole	6.66 $\pm$ 0.84 (6) <sup>b</sup>
Aclacinomycin A	16.14 $\pm$ 0.85 (3) <sup>b</sup>
5-Iminodaunorubicin	0.45 $\pm$ 0.15 (3)

<sup>a</sup>Mean  $\pm$  S.E.; number in parentheses is number of experiments performed; <sup>b</sup>significantly higher than the control rate of superoxide formation in tumor microsomes ( $P < 0.01$ ; Table 2).

examined the effect of doxorubicin on microsomal oxygen consumption. As demonstrated in Supplementary Table 1, oxygen consumption increased more than 6-fold in the presence of doxorubicin,  $P < 0.001$ . Drug-stimulated oxygen consumption was significantly inhibited by cytochrome c which reacts directly with superoxide to return oxygen to this closed system and was significantly increased by KCN, probably because of the inhibition of microsomal SOD (Table 5). As shown in Figure 1(a), we found that oxygen was released routinely by addition of excess catalase to microsomes treated with doxorubicin, indicating that H<sub>2</sub>O<sub>2</sub> as well as superoxide anion had been produced in these investigations. We found that H<sub>2</sub>O<sub>2</sub> production increased from undetectable control levels ( $n = 3$ ) to 3.42  $\pm$  0.48 nmol/min/mg ( $n = 4$ ;  $P < 0.01$ ) after treatment of the microsomal fraction with doxorubicin (135  $\mu$ M). Thus, NADPH-dependent microsomal metabolism of doxorubicin results in both superoxide anion and H<sub>2</sub>O<sub>2</sub> formation.

**3.2. Tumor Mitochondria.** Because previous studies in cardiac tissue had indicated that the electron transport chain could reduce doxorubicin to its semiquinone [4], we examined the effect of doxorubicin on reactive oxygen formation by the Ehrlich tumor mitochondrial fraction. We found that for tumor mitochondria, as well as microsomes, treatment with doxorubicin increased superoxide formation in a dose-dependent fashion that also appeared to follow saturation kinetics (Table 1). However, in mitochondria, superoxide production was NADH- rather than NADPH-dependent and was significantly increased by addition of rotenone to block electron flow beyond complex I of the electron transport chain (Table 6). Furthermore, substituting NAD<sup>+</sup> (100  $\mu$ M), NADP<sup>+</sup> (100  $\mu$ M), or succinate (1 mM) for NADH yielded no detectable drug-enhanced superoxide production by tumor mitochondria (data not shown).

Superoxide production in the mitochondrial fraction after treatment with doxorubicin (135  $\mu$ M) increased from ( $n = 3$ ) 0.37  $\pm$  0.03 to 0.76  $\pm$  0.02 and 1.05  $\pm$  0.07 nmol/min when 50, 150, or 200  $\mu$ g/ml of mitochondrial protein was employed. In contrast, superoxide production by tumor mitochondria in the absence of doxorubicin was 0.10  $\pm$  0.04, 0.18  $\pm$  0.05, and 0.21  $\pm$  0.03 nmol/min for the identical levels of mitochondrial protein,  $P < 0.01$  for each drug-treated

TABLE 4: Effect of inhibitors of NADPH:cytochrome p-450 reductase on superoxide formation in tumor microsomes. NADPH:cytochrome P-450 reductase was assayed at 30°C as described in Materials and Methods using nonacetylated cytochrome c and 200 µg of microsomal protein per ml. Reactions were initiated with 100 nmol of NADPH. Where indicated, the reaction mixtures were preincubated with DTNB or NADP<sup>+</sup> for 2 min prior to the initiation of cytochrome c reduction. In these experiments, superoxide production was assessed as described in Table 2 except that the NADPH concentration was 100 µM rather than 1 mM.

Experimental system	NADPH:cytochrome P-450 reductase activity (nmol/min/mg)	Superoxide production (nmol/min/mg)
Control	233.5 ± 12.5 (3) <sup>a</sup>	
+DTNB (100 µM)	54.1 ± 1.6 (3) <sup>b</sup>	
+NADP <sup>+</sup> (1 mM)	64.6 ± 1.5 (3) <sup>b</sup>	
Doxorubicin (135 µM)		10.1 ± 1.0 (3)
+DTNB (100 µM)		4.2 ± 0.4 (3) <sup>b</sup>
+NADP <sup>+</sup> (1 mM)		2.7 ± 0.2 (3) <sup>b</sup>

<sup>a</sup>Mean ± S.E.; numbers in parentheses are numbers of experiments; <sup>b</sup>significantly different from samples without inhibitor present ( $P < 0.01$ ).

TABLE 5: Antioxidant enzyme levels in tumor subcellular fractions. Ehrlich tumor microsomes, mitochondria, and nuclei were prepared and assayed for glutathione peroxidase and SOD activity as described in Materials and Methods. The “cytosol” fraction was the supernatant from the final 65,000 x *g* centrifugation step used in the preparation of the microsomal fraction. Before determination of enzyme activity, the mitochondrial fraction was exposed to ultrasonic disruption on ice with 4 bursts of 15 sec each at 90 watts output to eliminate permeability barriers to appropriate substrates in these assays. The supernatant and pellet resulting from centrifugation of the sonicated mitochondria at 105,000 x *g* and 4°C for 60 min were also assayed from enzyme activities.

Tumor cell fraction	Glutathione peroxidase (nmol/min/mg)	SOD (µg SOD/mg)
Cytosol	211.6 ± 11.0 (4) <sup>a</sup>	8.1 ± 0.8 (3)
Microsomes	22.5 ± 1.6 (4)	1.4 ± 0.3 (3)
Nuclei	10.1 ± 2.2 (3)	0.5 ± 0.1 (3)
Mitochondria	55.5 ± 8.0 (3)	5.6 ± 0.3 (3)
105,000 x <i>g</i> supernatant	197.9 ± 20.9 (3)	3.2 ± 0.4 (3)
105,000 x <i>g</i> pellet	N.D. (3) <sup>b</sup>	1.6 ± 0.2 (3)

<sup>a</sup>Mean ± S.E.; numbers in parentheses are numbers of experiments; <sup>b</sup>N.D. is not detectable.

sample compared to control. We also found that the anthracycline antibiotics which had significantly enhanced microsomal superoxide production also increased mitochondrial oxy-radical formation (Table 6). Finally, we found that doxorubicin (135 µM) stimulated the rate of NADH oxidation by tumor mitochondria (100 µg/ml) in the presence of rotenone from 4.70 ± 0.42 ( $n = 3$ ) to 9.74 ± 0.63 ( $n = 3$ ) nmol/min/mg,  $P < 0.01$ . Thus, it is likely that an early portion of the NADH

dehydrogenase complex is responsible for the reduction of anthracycline antibiotics to free radicals in tumor mitochondria.

To investigate the effect of doxorubicin on mitochondrial reactive oxygen metabolism further, the rate of oxygen consumption by drug-treated mitochondria was examined. As shown in Supplementary Table 2, doxorubicin significantly increased the rate of mitochondrial oxygen consumption; furthermore, the rate of drug-stimulated oxygen consumption was not affected by KCN or dicumarol, suggesting that (1) mitochondrial SOD in Ehrlich tumor cells is not inhibited by cyanide and that (2) NADPH:quinone oxidoreductase 1 does not appear to be involved in the free radical metabolism of doxorubicin in tumor mitochondria. On the other hand, drug-stimulated oxygen consumption was decreased to control levels in the presence of acetylated cytochrome c suggesting that most, if not all, of the oxygen consumed had at least initially been converted to superoxide anion (Supplementary Table 2). We also found (Figure 1(b)) that treatment with doxorubicin increased mitochondrial H<sub>2</sub>O<sub>2</sub> production from undetectable control levels ( $n = 3$ ) to 2.6 ± 0.6 nmol/min/mg,  $n = 3$ ,  $P < 0.01$ . Thus, exposure of tumor mitochondria, as well as microsomes, to doxorubicin increases both superoxide anion and hydrogen peroxide production.

**3.3. Tumor Nuclei.** Treatment of Ehrlich tumor nuclei with doxorubicin significantly increased superoxide production (Table 7). In this organelle, oxy-radical formation required intact nuclear protein and NADPH; neither NADH, FAD, nor FMN could support drug-stimulated nuclear superoxide formation. Furthermore, daunorubicin, rubidazole, and aclacinomycin A all significantly increased reactive oxygen metabolism compared to control (Table 7). As shown in Table 1, superoxide production in the nuclear fraction also appeared to follow saturation kinetics. We found that doxorubicin (135 µM) increased the rate of NADPH (100 µM) oxidation by the nuclear fraction (200 µg protein/ml) from a control rate of 2.20 ± 0.31 ( $n = 3$ ) to 11.11 ± 0.73 nmol/min/mg,  $n = 3$ ,  $P < 0.01$ .

As shown in Supplementary Table 3, Ehrlich tumor nuclei possessed approximately 2% of the NADPH:cytochrome P-450 reductase activity of the microsomal fraction. This enzymatic activity could be inhibited by excess NADP<sup>+</sup> and could be removed completely by treatment of the nuclear fraction with a nonionic detergent capable of stripping the outer nuclear envelope from underlying DNA and chromatin. In related experiments, we found that doxorubicin-stimulated nuclear superoxide formation could also be significantly inhibited or abolished by treatment of the nuclei with the detergent (Supplementary Table 3). These experiments strongly suggest that NADPH:cytochrome P-450 reductase activity normally associated with the outer nuclear envelope is responsible for activating doxorubicin to its free radical at that locale.

In analogy to our microsomal and mitochondrial experiments, we investigated nuclear oxygen consumption in the presence of doxorubicin. In this setting, control nuclei

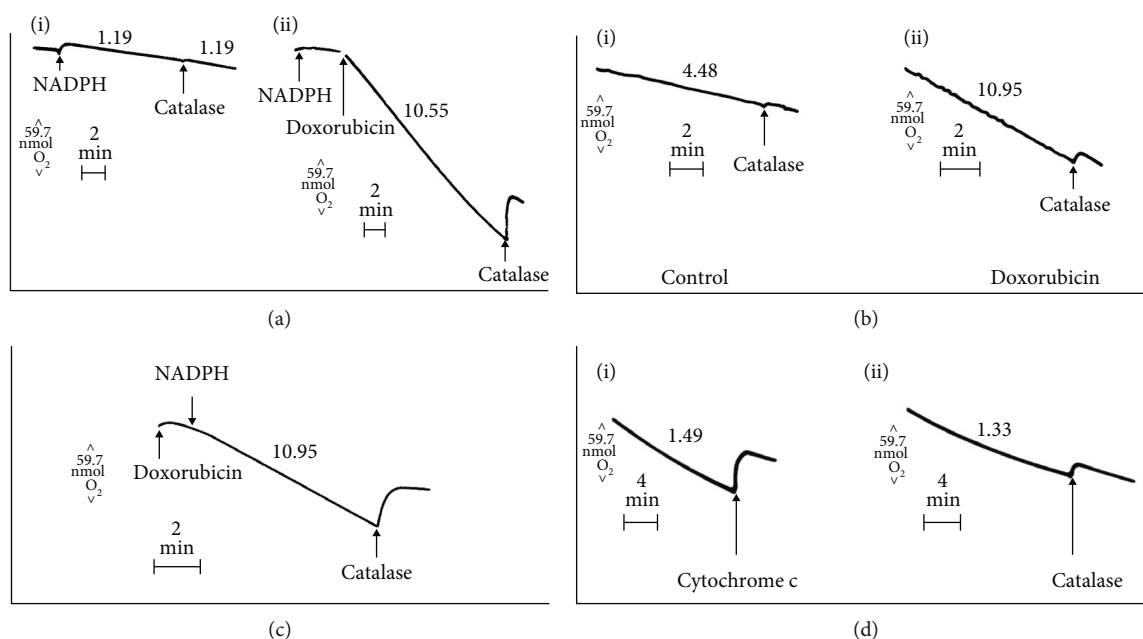


FIGURE 1: Effect of doxorubicin on oxygen consumption by Ehrlich tumor organelles. Oxygen consumption in tumor microsomes was examined as described in Supplementary Table 1. (a, i) is without drug; (ii) shows the results with doxorubicin. The addition of NADPH (1 mM), catalase (4500 units), or doxorubicin (135  $\mu\text{M}$ ) to the 3 ml vessel was performed through the access slot of the oxygen electrode and has been indicated (arrow). The numbers above each tracing indicate the rate of oxygen consumption (nmol/min/mg). (b) Effect of doxorubicin on oxygen consumption by Ehrlich tumor mitochondria. Oxygen consumption in these representative experiments was performed as described in Supplementary Table 2. (i) is the control reaction; (ii) represents the identical experiment in the presence of doxorubicin (135  $\mu\text{M}$ ). The addition of catalase (4500 units) to the 3 ml vessel was performed through the access slot of the oxygen electrode and has been indicated by the arrow. The numbers above each tracing indicate the rate of oxygen consumption (nmol/min/mg). (c) Effect of doxorubicin on oxygen consumption by Ehrlich tumor nuclei. Experimental conditions consisted of a 3 ml system containing 250 mM sucrose, 20 mM HEPES, pH 7.4, 100  $\mu\text{M}$  EDTA, 1 mM NADPH, and 200  $\mu\text{g/ml}$  of nuclear protein at 37°C. The addition of NADPH (1 mM), doxorubicin (135  $\mu\text{M}$ ), or catalase (4500 units) to the 3 ml reaction vessel was performed through the access slot of the oxygen electrode and has been indicated by an arrow. The number above the tracing is the rate of oxygen consumption (nmol/min/mg). (d) Doxorubicin-stimulated oxygen consumption by Ehrlich tumor cells. The effect of doxorubicin (400  $\mu\text{M}$ ) on oxygen consumption by Ehrlich cells ( $5 \times 10^6$  cells/ml) is shown in representative examples from multiple experiments. The addition of acetylated cytochrome c (168 nmol) in (i) or catalase (9000 units) in (ii) to the 3 ml vessel has been indicated by an arrow. The numbers above each tracing indicate the rate of oxygen consumption (nmol/min/ml).

consumed  $0.93 \pm 0.12 \text{ nmol O}_2/\text{min/mg}$ ,  $n = 3$ . Oxygen consumption increased 10-fold in the presence of doxorubicin (135  $\mu\text{M}$ ) to  $9.45 \pm 0.89 \text{ nmol/min/mg}$ ,  $n = 6$ ,  $P < 0.01$ . Treatment with KCN (1 mM) did not increase drug-stimulated oxygen consumption significantly ( $11.04 \pm 0.80 \text{ nmol/min/mg}$ ,  $n = 4$ ), probably because of the small amount of SOD associated with the nuclear fraction (Table 5). However, the addition of acetylated cytochrome c (56  $\mu\text{M}$ ) decreased oxygen consumption to  $2.09 \pm 0.26 \text{ nmol/min/mg}$ ,  $n = 3$ ,  $P < 0.01$  compared to samples containing doxorubicin alone. Thus, most of the oxygen consumed had probably been reduced, at least initially, to superoxide anion. As shown in Figure 1(c), drug-enhanced oxygen consumption required NADPH and was associated with the production of  $\text{H}_2\text{O}_2$ . In these studies, drug treatment (135  $\mu\text{M}$ ) increased  $\text{H}_2\text{O}_2$  formation from undetectable control levels ( $n = 3$ ) to  $5.2 \pm 1.3 \text{ nmol/min/mg}$ ,  $n = 3$ ,  $P < 0.01$ .

**3.4. Whole Tumor Cells.** To examine the net effect of anthracycline antibiotics on oxy-radical production by Ehrlich tumor, we investigated whether doxorubicin altered the respiratory rate of intact tumor cells. Treatment with doxoru-

bicin significantly increased the rate of oxygen consumption by tumor cells in which the electron transport chain had been blocked by either cyanide or antimycin A (Table 8) [29, 30]. It is likely that the magnitude of the overall rate of mitochondrial  $\text{O}_2$  consumption in tumor cells makes the smaller, drug-related effects impossible to detect in the absence of respiratory chain blockade. We found that the increase in respiratory rate was drug-dose dependent and was found for daunorubicin as well as doxorubicin; however, the daunorubicin analog 5-iminodaunorubicin which has a blocked quinone group that does not permit redox cycling did not enhance cyanide-resistant respiration by Ehrlich cells [31, 32]. In control experiments, we found that tumor cell viability in the presence of KCN as measured by exclusion of trypan blue dye did not decline significantly over the reaction period of these studies. Furthermore, the addition of glucose to the cells, which produces an increase in intracellular NADPH concentration [22], significantly increased the rate of  $\text{O}_2$  consumption after doxorubicin administration (Table 8). We found that alterations in osmolality by glucose did not explain these observations, since when buffers of identical osmolality were used

TABLE 6: Requirements for anthracycline-enhanced superoxide anion production by the tumor mitochondrial fraction. Superoxide formation in the tumor mitochondrial fraction was examined using paired, 1 ml reaction mixtures containing 250 mM sucrose, 20 mM HEPES, pH 8.2, 100  $\mu$ M EDTA, 56  $\mu$ M acetylated cytochrome c 100  $\mu$ g of mitochondrial protein, and either 0 or 10  $\mu$ g of SOD. The reaction mixture was preincubated for 5 min at 37° with 4  $\mu$ M rotenone before initiation of the reaction with 100  $\mu$ M NADH.

Reaction mixture	Superoxide production (nmol/min/mg)
Control	1.12 $\pm$ 0.15 (7) <sup>a</sup>
-NADH	N.D. (3) <sup>b</sup>
-Mitochondrial fraction	N.D. (3)
-Rotenone	1.02 $\pm$ 0.01 (3)
Using NADPH (100 $\mu$ M) rather than NADH	0.77 $\pm$ 0.26 (3)
Doxorubicin (135 $\mu$ M)	7.29 $\pm$ 0.61 (10) <sup>c</sup>
-NADH	0.97 $\pm$ 0.05 (3) <sup>d</sup>
-Mitochondrial fraction	0.61 $\pm$ 0.20 (3) <sup>d</sup>
Using heat-denatured mitochondria	1.28 $\pm$ 0.56 (3) <sup>d</sup>
-Rotenone	5.00 $\pm$ 0.36 (3) <sup>d</sup>
Using NADPH (100 $\mu$ M) rather than NADH	2.76 $\pm$ 0.44 (3) <sup>d</sup>
-Acetylated cytochrome c	N.D. (3) <sup>d</sup>
-EDTA	5.51 $\pm$ 1.22 (3)
Using heat-denatured SOD	5.10 $\pm$ 0.61 (3)
Daunorubicin (135 $\mu$ M)	6.38 $\pm$ 1.63 (3) <sup>c</sup>
Rubidazone (135 $\mu$ M)	5.71 $\pm$ 1.02 (3) <sup>c</sup>
Aclacinomycin A (135 $\mu$ M)	3.32 $\pm$ 0.31 (3) <sup>c</sup>
5-Iminodaunorubicin (135 $\mu$ M)	0.51 $\pm$ 0.15 (3)

<sup>a</sup>Mean  $\pm$  S.E.; numbers in parentheses are numbers of experiments; <sup>b</sup>N.D. is not detectable; <sup>c</sup>significantly different from control ( $P < 0.01$ ); <sup>d</sup>significantly different from complete system containing doxorubicin alone ( $P < 0.01$ ).

(with or without glucose), the rate of O<sub>2</sub> consumption was significantly higher only in the presence of glucose (data not shown). As shown in Figure 2, cyanide-resistant respiration in the presence or absence of doxorubicin varied with the number of cells used in the experiment; however, the rate of oxygen consumption was always significantly higher ( $P < 0.01$ ) when the drug was present. Finally, when experiments identical to those in Table 8 were performed with P388 murine leukemia cells treated with KCN, we found that doxorubicin (400  $\mu$ M) increased O<sub>2</sub> consumption from (mean  $\pm$  S.E.;  $n = 3$ ) the 0.31  $\pm$  0.05 control rate to 1.15  $\pm$  0.08 nmol/min/5  $\times$  10<sup>6</sup> cells,  $P < 0.01$ . Taken together, these experiments suggest that anthracycline antibiotics enhance oxy-radical production by tumor cells in a process that requires an intact quinone ring and may be modulated by the supply of cellular reducing equivalents. These features are similar to those previously described for the tumor cell organelles examined in this study; they reveal, further, that

TABLE 7: Requirements for anthracycline-stimulated superoxide formation by the nuclear fraction. Superoxide formation by tumor nuclei was examined using paired 1 ml reaction mixtures containing 250 mM sucrose, 20 mM HEPES, pH 7.4, 100  $\mu$ M EDTA, 56  $\mu$ M acetylated cytochrome c, 200  $\mu$ g of nuclear protein, and either 0 or 10  $\mu$ g of SOD. The reaction was carried out at 37°C and was initiated by the addition of 1 mM NADPH after the chemotherapeutic agent was added.

Reaction mixture	Superoxide formation (nmol/min/mg)
Control	0.36 $\pm$ 0.05 (7) <sup>a</sup>
Using NADH (1 mM) rather than NADPH	0.28 $\pm$ 0.08 (3)
Doxorubicin (135 $\mu$ M)	3.29 $\pm$ 0.33 (12) <sup>b</sup>
-NADPH	N.D. (3) <sup>c,d</sup>
-Acetylated cytochrome c	N.D. (3) <sup>d</sup>
Using heat-denatured nuclei	N.D. (3) <sup>d</sup>
Using NADH (1 mM) rather than NADPH	0.31 $\pm$ 0.15 (3) <sup>d</sup>
+Heat-denatured SOD	2.73 $\pm$ 0.31 (3)
+DMSO (13 mM)	4.21 $\pm$ 0.13 (3)
+Catalase (1500 units/ml)	3.70 $\pm$ 0.13 (3)
Using FAD (1 mM) rather than NADPH	N.D. (3) <sup>d</sup>
Using FMN (1 mM) rather than NADPH	N.D. (3) <sup>d</sup>
Daunorubicin (135 $\mu$ M)	6.63 $\pm$ 0.64 (3) <sup>b</sup>
Rubidazone (135 $\mu$ M)	3.01 $\pm$ 0.31 (3) <sup>b</sup>
Aclacinomycin A (135 $\mu$ M)	5.53 $\pm$ 0.38 (3) <sup>b</sup>

<sup>a</sup>Mean  $\pm$  S.E.; numbers in parentheses are numbers of experiments; <sup>b</sup>significantly different from control ( $P < 0.01$ ); <sup>c</sup>N.D. is not detectable; <sup>d</sup>significantly different from complete system containing doxorubicin alone ( $P < 0.01$ ).

anthracycline redox cycling may overcome the ability of intact tumor cells to detoxify ROS.

As shown in Figure 1(d), the addition of cytochrome c or catalase to Ehrlich cells treated with doxorubicin (400  $\mu$ M) led to the release of oxygen in this closed system, indicating that H<sub>2</sub>O<sub>2</sub> had been formed. We found that in the presence of doxorubicin (400  $\mu$ M), Ehrlich cells produced 0.64  $\pm$  0.04 nmol H<sub>2</sub>O<sub>2</sub>/min/10<sup>7</sup> cells compared to undetectable levels of hydrogen peroxide in the absence of the drug,  $P < 0.01$ ,  $n = 3$ . Because the tumor cell outer membrane is impermeable to high molecular weight proteins such as catalase, this estimate of H<sub>2</sub>O<sub>2</sub> formation probably reflects only the proportion of the total H<sub>2</sub>O<sub>2</sub> pool present extracellularly; thus, it is not possible to make a direct stoichiometric comparison between total cyanide-resistant O<sub>2</sub> consumption and H<sub>2</sub>O<sub>2</sub> formation, even under identical experimental conditions.

Oxy-radical cascades, which include the production of H<sub>2</sub>O<sub>2</sub>, may also be capable of supporting the formation of the potent oxidizing radical  $\cdot$ OH, or a related molecule with similar chemical reactivity [33]. We investigated the mechanism of hydroxyl radical formation by Ehrlich tumor cells after treatment with doxorubicin by quantitation of the



TABLE 8: Effect of anthracycline antibiotics on oxygen consumption by Ehrlich tumor cells. Oxygen consumption by Ehrlich cells was examined at 37°C as described in Materials and Methods; the total 3 ml volume contained  $1.5 \times 10^7$  tumor cells and the final KCN concentration, where used, was 2 mM.

Reaction system	Oxygen consumption (nmol O <sub>2</sub> /min/5 × 10 <sup>6</sup> cells)	
	+KCN	-KCN
Control	0.54 ± 0.04 <sup>a</sup>	9.37 ± 0.52
+BCNU (100 μg/ml)	0.58 ± 0.08	9.56 ± 0.80
+Glucose (10 mM)	0.58 ± 0.10	9.67 ± 0.90
+Antimycin A (10 μg/ml) replacing KCN	0.50 ± 0.10	
-Cells	N.D. <sup>b</sup>	
Doxorubicin (90 μM)	0.86 ± 0.02 <sup>c</sup>	10.00 ± 1.20
Doxorubicin (200 μM)	1.04 ± 0.12 <sup>c</sup>	11.46 ± 1.18
Doxorubicin (400 μM)	1.13 ± 0.04 <sup>c</sup>	8.82 ± 0.22
+BCNU (100 μg/ml)	1.39 ± 0.08 <sup>d</sup>	—
+Adenosine (1 mM)	1.06 ± 0.04	—
+Glucose (10 mM)	1.61 ± 0.08 <sup>d</sup>	9.47 ± 0.16
+Antimycin A (10 μg/ml) replacing KCN	1.19 ± 0.04 <sup>c</sup>	—
-Cells	N.D.	—
Doxorubicin (1 mM)	4.54 ± 0.40 <sup>c</sup>	—
Daunorubicin (400 μM)	1.39 ± 0.06 <sup>c</sup>	—
5-Iminodaunorubicin (400 μM)	0.64 ± 0.06	—

<sup>a</sup>Mean ± S.E. of 3 to 15 experiments; <sup>b</sup>N.D. is not detectable; <sup>c</sup>significantly different from control, at  $P < 0.01$ ; <sup>d</sup>significantly different from samples containing doxorubicin alone, at  $P < 0.01$ .

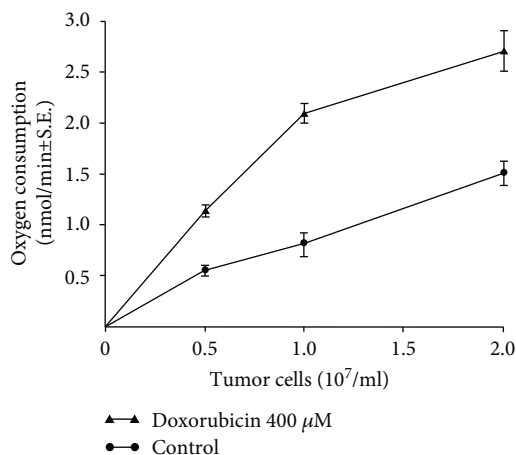


FIGURE 2: Effect of tumor cell number on the rate of cyanide-resistant oxygen consumption in the presence and absence of doxorubicin. The doxorubicin concentration used for these experiments was 400 μM. These studies were performed as described in Table 8; the data represent the mean ± S.E. of 3 determinations at each tumor cell concentration.

formaldehyde produced in the reaction of DMSO with  $\cdot\text{OH}$ . As previously demonstrated, on a molar basis, formaldehyde is the major by-product of this reaction between the reactive oxygen metabolite and DMSO [24]. We maximized the possibility of measuring drug-enhanced  $\cdot\text{OH}$  production in these experiments by utilizing a nonionic detergent to increase the access of both doxorubicin and pyridine nucleotide cofactors

to intracellular or membrane-bound dehydrogenases. The requirements for formaldehyde production by Ehrlich carcinoma cells are shown in Table 9; the hydroxyl radical was detected in this system only in the presence of the anthracycline antibiotic. Furthermore, drug-stimulated formaldehyde production was measured only when the tumor cells, DMSO, iron-EDTA, and Triton X-100 were all present in these experiments. Increasing the  $\text{FeSO}_4$  concentration above 50 μM did not enhance formaldehyde production further (data not shown); whereas,  $\text{FeSO}_4$  levels as low as 1 μM still supported substantial formaldehyde formation (Table 9). Furthermore,  $\text{FeCl}_3$  at a concentration of 50 μM was also capable of supporting doxorubicin-enhanced formaldehyde production by Ehrlich cells; thus, both ferric and ferrous iron may serve as catalysts for this process (Table 9). In these studies, both NADPH and NADH, but not succinate, could provide the reducing equivalents necessary for oxygen radical metabolism in Ehrlich cells treated with doxorubicin. These cofactor requirements are consistent with the previously presented experiments demonstrating that the microsomal, mitochondrial, and nuclear fractions from Ehrlich cells contain different NADPH- and NADH-dependent dehydrogenases capable of catalyzing the reduction of doxorubicin to its semiquinone free radical intermediate [34–37].

Following the determination that doxorubicin could stimulate formaldehyde production from DMSO by Ehrlich cells, we examined several characteristics of  $\cdot\text{OH}$  formation in this system. As shown in Figure 3(a), formaldehyde production by the carcinoma cells varied with the concentration of tumor cells used in the assay; at a doxorubicin level of

TABLE 9: Requirements for doxorubicin-stimulated hydroxyl radical formation by detergent-treated Ehrlich carcinoma cells. Hydroxyl radical production by Ehrlich carcinoma cells was determined by measurements of formaldehyde production from DMSO; the standard reaction mixture contained 100 mM DMSO, 100  $\mu$ M EDTA, 50  $\mu$ M FeSO<sub>4</sub>, 1 mM NADPH, 0.1% Triton X-100, 10<sup>7</sup> tumor cells/ml, and the indicated concentration of doxorubicin in a final volume of 7 ml of PBS at pH 7.2. Data are expressed as the mean  $\pm$  S.E. of formaldehyde production for the 2 hr reaction interval in each experimental group; the total number of experiments for each group (*n*) is given in parentheses.

Experimental system	Hydroxyl radical production (nmol formaldehyde/10 <sup>7</sup> cells)
Control	0.0 $\pm$ 0.0 ( <i>n</i> = 5) <sup>a</sup>
Doxorubicin (250 $\mu$ M)	71.4 $\pm$ 10.4 ( <i>n</i> = 15) <sup>b</sup>
Minus cells	0.0 $\pm$ 0.0 ( <i>n</i> = 3) <sup>c</sup>
Heat denatured cells <sup>d</sup>	0.0 $\pm$ 0.0 ( <i>n</i> = 3) <sup>c</sup>
Minus DMSO	0.0 $\pm$ 0.0 ( <i>n</i> = 3) <sup>c</sup>
Minus EDTA	0.0 $\pm$ 0.0 ( <i>n</i> = 3) <sup>c</sup>
Minus FeSO <sub>4</sub>	0.0 $\pm$ 0.0 ( <i>n</i> = 3) <sup>c</sup>
Using 1 $\mu$ M rather than 50 $\mu$ M FeSO <sub>4</sub>	13.2 $\pm$ 4.6 ( <i>n</i> = 3) <sup>c</sup>
Using FeC13 (50 $\mu$ M) rather than FeSO <sub>4</sub>	30.9 $\pm$ 10.0 ( <i>n</i> = 3) <sup>b</sup>
Minus NADPH	0.0 $\pm$ 0.0 ( <i>n</i> = 3) <sup>c</sup>
Minus NADPH plus NADH (1 mM)	30.6 $\pm$ 8.3 ( <i>n</i> = 5) <sup>c</sup>
Minus NADPH plus succinate (5 mM)	0.0 $\pm$ 0.0 ( <i>n</i> = 3) <sup>c</sup>
Minus Triton X-100	0.0 $\pm$ 0.0 ( <i>n</i> = 3) <sup>c</sup>

<sup>a</sup>Mean  $\pm$  S.E.; <sup>b</sup>significantly different from the control group ( $P < 0.001$ ); <sup>c</sup>significantly different from complete reaction mixture containing doxorubicin and 50  $\mu$ M FeSO<sub>4</sub> ( $P < 0.001$ ); <sup>d</sup>tumor cells autoclaved for 60 min; <sup>e</sup>significantly different from control and from complete reaction mixture containing NADPH ( $P < 0.01$ ).

250  $\mu$ M, using a 60 min incubation time, peak formaldehyde production (mean  $\pm$  S.E.; *n* = 3; 69.5  $\pm$  6 nmol) occurred with 10<sup>7</sup> tumor cells/ml in the reaction mixture. We found that under similar experimental conditions, the amount of formaldehyde produced was also related to the concentration of DMSO used for the study; formaldehyde formation (mean  $\pm$  S.E., *n* = 3) increased from 33.2  $\pm$  6.1 nmol/60-min/10<sup>7</sup> cells to 37.1  $\pm$  7.2, 56.9  $\pm$  3.4, 59.7  $\pm$  26.1, and 47.1  $\pm$  6.3 when the DMSO concentration varied from 5 to 50, 100, 200, or 1000 mM. Thus, a DMSO concentration of 100 mM was chosen for all subsequent experiments. When the reaction interval was altered at a fixed dose of doxorubicin (Figure 3(b)), formaldehyde formation increased from undetectable levels at the zero-time point to 90.2  $\pm$  16.4 nmol/10<sup>7</sup> cells, *n* = 3, at 2 hr; no further, significant increase in hydroxyl radical production could be demonstrated when the incubation time was extended for up to 4 hr after the initiation of the reaction (Figure 3(b)).

Doxorubicin increased hydroxyl radical production by Ehrlich carcinoma cells in a dose-related fashion over a wide range of drug concentrations (Figure 3(c)). Drug-stimulated formaldehyde production under our experimental condi-

tions could be reproducibly measured after treatment of the cells with a doxorubicin concentration as low as 5  $\mu$ M (24.3  $\pm$  11.8 nmol/120 min/10<sup>7</sup> cells, *n* = 3).

To examine the mechanism of formaldehyde production and to verify that the evolution of formaldehyde from DMSO was a measurement of  $\cdot$ OH formation, we investigated the effect of various oxygen radical scavengers on the level of formaldehyde produced by treatment of Ehrlich cells with doxorubicin. The addition of SOD or catalase, but not the heat-inactivated enzymes, significantly decreased or abolished drug-related formaldehyde production (Table 10). These results suggested that both the superoxide anion and hydrogen peroxide were necessary for the generation of  $\cdot$ OH by Ehrlich carcinoma cells. We also found that sodium benzoate, mannitol, diethylurea, and dimethylthiourea, which are all potent scavengers of the hydroxyl radical [38], were between 31 and 100% effective in competing with DMSO for reaction with  $\cdot$ OH. However, urea, a structurally similar but ineffective  $\cdot$ OH scavenger, had no significant effect on formaldehyde production from DMSO (Table 10). Furthermore, we found that treatment of the permeabilized Ehrlich cells with the  $\cdot$ OH scavengers outlined in Table 10 decreased the production of methane, an alternate by-product of the reaction between  $\cdot$ OH and DMSO, to the same extent as that found when formaldehyde was assayed (data not shown). This suggests that the hydroxyl radical scavengers actually combined with the oxidant species formed in our experimental system rather than altering the stoichiometry of the reaction pathways involved in the degradation of DMSO by the hydroxyl radical. These results, which indicated that formaldehyde production after treatment of Ehrlich carcinoma cells with doxorubicin was dependent upon the presence of the superoxide anion, hydrogen peroxide, and an iron-EDTA complex, strongly suggest that the hydroxyl radical or a related species with similar reactivity was formed in our experiments.

**3.5. Antioxidant Levels.** To understand the significance of drug-stimulated oxygen radical formation in each subcellular fraction, we determined the glutathione peroxidase and SOD-specific activities associated with these fractions (Table 5). As seen in Table 5, the glutathione peroxidase activity in tumor microsomes and nuclei is approximately 10% or 5% of that in the cytosol. Since Ehrlich cells contain minimal catalase activity [39], glutathione peroxidase is the major cellular defense against hydrogen peroxide. Furthermore, the glutathione peroxidase level of tumor cytosol, while more than 20-fold greater than tumor nuclei, is only 30% as high as the enzyme level in rat heart cytosol [4]. Although the specific activity of glutathione peroxidase in tumor mitochondria exposed to ultrasonic disruption was 26.2% of that in the cytosol, ultracentrifugation of the sonicated mitochondria produced a supernatant with essentially the same specific activity as the tumor cytosol. Thus, it seems very likely that most, if not all, of the mitochondrial glutathione peroxidase is located in the mitochondrial matrix.

As shown in Table 5, the majority of tumor cell SOD is located in the cytosol, with much smaller specific activities associated with the microsomal or nuclear fractions.

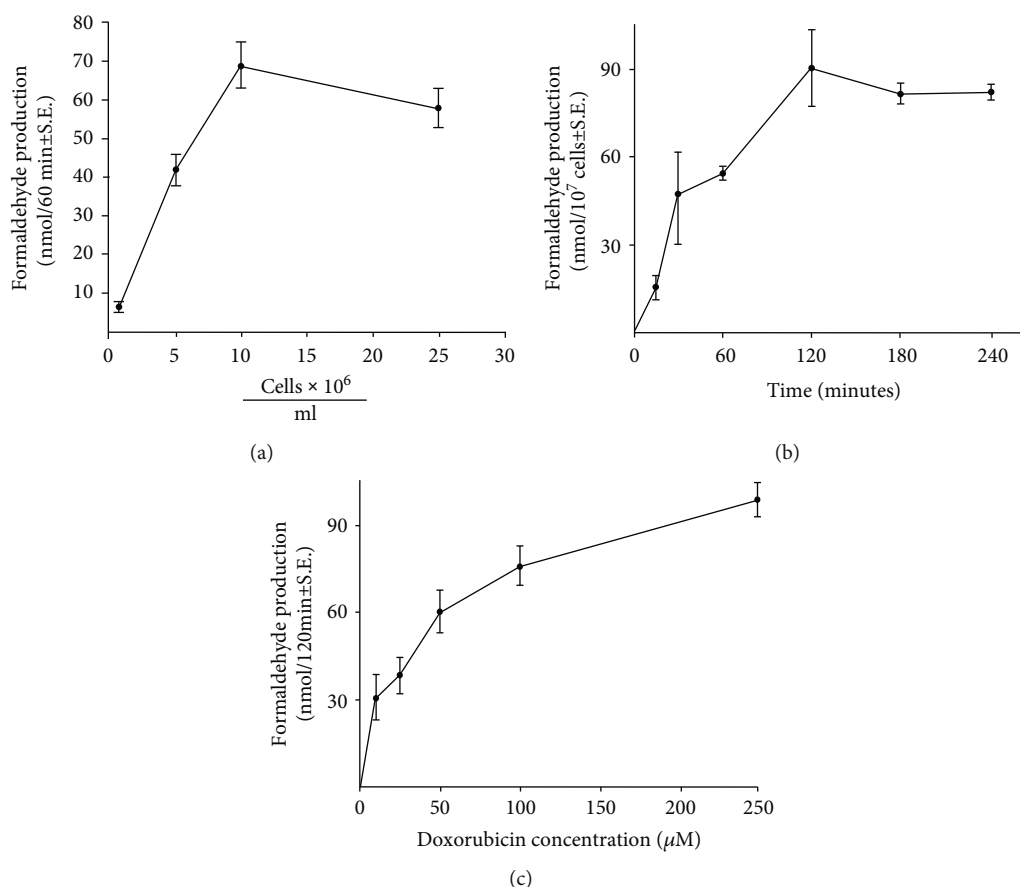


FIGURE 3: Effect of Ehrlich tumor cell number on doxorubicin-stimulated formaldehyde production. (a) Formaldehyde production from DMSO was assessed spectrophotometrically in the presence of a fixed concentration of doxorubicin ( $250 \mu\text{M}$ ) over a 60 min period of incubation; the data represent the mean  $\pm$  S.E. of three experiments for each concentration of tumor cells. (b) Effect of the duration of incubation on doxorubicin-induced formaldehyde formation by Ehrlich tumor cells. The extent of formaldehyde production by Ehrlich cells ( $10^7/\text{ml}$ ) in the presence of doxorubicin ( $250 \mu\text{M}$ ) was determined as a function of the time after initiation of the reaction. Each time point represents the mean  $\pm$  S.E. of three experiments. (c) Effect of doxorubicin concentration on formaldehyde production by Ehrlich tumor cells. In these studies, the production of formaldehyde from DMSO was examined at a tumor cell concentration of  $10^7/\text{ml}$ ; the data represent the mean  $\pm$  S.E. of three experiments at each doxorubicin level tested.

Mitochondrial SOD was intermediate in specific activity between cytosol and nuclei and appeared to be present in at least two mitochondrial sites. Overall, these experiments suggest that tumor nuclei and microsomes are the least well-protected subcellular fractions with respect to the available antioxidant defenses capable of detoxifying a drug-induced, oxy-radical cascade.

#### 4. Discussion

In these experiments, we have provided a comprehensive examination of the sites and mechanisms of anthracycline-stimulated oxy-radical production by Ehrlich carcinoma cells. We found that the microsomal, mitochondrial, and nuclear tumor fractions were each capable of supporting drug-induced superoxide anion and hydrogen peroxide production under appropriate experimental conditions. For tumor microsomes and nuclei, this appeared to be an NADPH-dependent process that resulted from reduction of the anthracycline quinone by the NADPH:cytochrome P-450 reductase activity associated with either the microsomal

membrane or the outer nuclear envelope. Mitochondrial anthracycline metabolism, on the other hand, was NADH-dependent and was stimulated by rotenone, suggesting that an early portion of the mitochondrial NADH dehydrogenase complex was responsible for reduction of the anthracycline quinone at this intracellular location in tumor cells. Generation of ROS by anthracycline antibiotics occurred at drug concentrations that are found intracellularly following exposure of intact cells to this class of anticancer agents [40]. These experiments are among the first to demonstrate that anthracycline-related ROS production can occur at essentially every intracellular site in tumor cells leading to the formation of an extracellular, and potentially damaging, peroxide flux.

We also determined that each anthracycline tested, except for the quinone-substituted drug 5-iminodaunorubicin, was capable of enhancing oxy-radical metabolism by every subcellular fraction. Furthermore, we found that reactive oxygen metabolism occurred despite the presence of both SOD and glutathione peroxidase in the tumor organelles. Thus, if these subcellular fractions possess a similar

TABLE 10: Effect of oxygen radical scavengers on doxorubicin-enhanced formaldehyde production by detergent-treated Ehrlich tumor cells. Hydroxyl radical production by Ehrlich carcinoma cells was determined exactly as described in Table 9; data have been expressed as the mean  $\pm$  S.E. of formaldehyde production for the 2 hr reaction interval in each experimental group, and the total number of experiments ( $n$ ) has been given in parentheses.

Experimental conditions	Formaldehyde production (nmol/10 <sup>7</sup> cells)
Doxorubicin (250 $\mu$ M)	60.4 $\pm$ 5.6 (6) <sup>a</sup>
Plus SOD (20 $\mu$ g/ml)	17.0 $\pm$ 9.6 (6) <sup>b</sup>
Plus heat-denatured SOD (20 $\mu$ g/ml) <sup>c</sup>	49.1 $\pm$ 5.0 (3)
Plus catalase (3000 units/ml)	0.0 $\pm$ 0.0 (3) <sup>d</sup>
Plus heat-denatured catalase (3000 units/ml)	44.3 $\pm$ 7.5 (3)
Plus sodium benzoate (100 mM)	34.3 $\pm$ 3.4 (3) <sup>b</sup>
Plus mannitol	
100 mM	41.7 $\pm$ 3.5 (3) <sup>b</sup>
200 mM	23.6 $\pm$ 3.5 (3) <sup>d</sup>
Plus diethylurea (100 mM)	25.8 $\pm$ 6.0 (3) <sup>b</sup>
Plus dimethylthiourea (100 mM)	0.0 $\pm$ 0.0 (3) <sup>d</sup>
Plus urea (100 mM)	50.9 $\pm$ 9.6 (3)

<sup>a</sup>Mean  $\pm$  S.E.; <sup>b</sup>significantly different from samples treated with doxorubicin alone ( $P < 0.01$ ); <sup>c</sup>SOD and catalase were autoclaved for 60 min; <sup>d</sup>significantly different from samples treated with doxorubicin alone ( $P < 0.001$ ).

distribution of antioxidant enzymatic defenses in vivo, oxygen radical production by the anthracycline antibiotics might exceed the detoxifying capacity of various tumor cell compartments.

Using intact Ehrlich cells, the anthracycline antibiotics were shown to increase the rate of either cyanide- or antimycin A-resistant respiration. This strongly suggests that doxorubicin and other anthracycline quinones actually undergo the previously described oxidation-reduction reactions in vivo. These experiments are also important because they suggest that manipulation of the intracellular reducing environment, by glucose or by the glutathione reductase inhibitor BCNU (which decreases peroxide detoxification by the GSH-GSH peroxidase cycle), may affect the redox metabolism of doxorubicin in whole tumor cells.

We also determined that treatment of intact cells with doxorubicin was associated with H<sub>2</sub>O<sub>2</sub> production; furthermore, our experiments suggest that following drug treatment H<sub>2</sub>O<sub>2</sub> accumulates extracellularly. Thus, the plasma membrane, as well as tumor nuclei, mitochondria, and microsomes, may be at risk from a free radical attack which, in this case, could come from both inside and outside the cell. It is likely that the presence of extracellular H<sub>2</sub>O<sub>2</sub> is due to either passive transport of H<sub>2</sub>O<sub>2</sub>, produced at several intracellular sites, across the plasma membrane or transport through an aquaporin channel [41].

As shown by our experiments with permeabilized tumor cells, under certain conditions, NA(D)PH-dependent tumor cell dehydrogenases can support a free radical cascade initiated by the anthracyclines that culminates in the formation of the hydroxyl radical. We have previously shown that hydroxyl radical-induced DNA damage occurs after doxorubicin treatment in the clinic [15]. Further, we have also reported that a wide variety of hydroxyl radical trapping agents effectively protect intact Ehrlich tumor cells against the cytotoxicity of doxorubicin as assessed by soft agar cloning techniques [13]. Because the formation of formaldehyde from DMSO in these experiments required superoxide anion, hydrogen peroxide, and iron-EDTA, it is likely that the metal-catalyzed Haber-Weiss reaction was operating under our experimental conditions [42]. This is consistent with studies indicating that iron-EDTA chelate is an especially potent redox catalyst capable of stimulating a significant degree of  $\cdot$ OH production in the presence of hydrogen peroxide and a reducing agent [43, 44]. Under hypoxic conditions, the doxorubicin semiquinone may react directly with hydrogen peroxide to produce  $\cdot$ OH [45]; however, because our experiments were performed under highly aerobic conditions (agitation of vessels open to air in a shaking water bath), this is an unlikely explanation for the mechanism of  $\cdot$ OH formation in the studies presented here.

The importance of the oxidation-reduction cycle initiated by treatment of Ehrlich tumor cells with doxorubicin is related to the potent oxidizing power of various oxygen radical metabolites [46]. Thus, drug-induced oxygen radical formation could lead to the peroxidation of cellular phospholipids or the oxidation of critical sulfhydryl-containing enzymes and structural proteins with a subsequent loss of control of divalent cation transport or membrane integrity. Furthermore, since a potential role for oxygen radicals in certain forms of DNA damage is well-established, it is conceivable that free radical production by Ehrlich tumor cells after treatment with doxorubicin could also contribute to previously described effects of doxorubicin on nucleic acids [47]. One or more of these consequences of drug-related oxygen radical production could contribute to the tumoricidal effect of the anthracycline antibiotics.

In summary, we propose that drug-stimulated oxygen radical metabolism by the anthracycline antibiotics in multiple tumor cell compartments may contribute significantly to the antineoplastic activity of this class of drugs.

## Abbreviations

- EGTA: Ethylene-glycol-bis( $\beta$ -amino-ethylether)-N, N<sup>1</sup>-tetraacetic acid
- HEPES: N-2-Hydroxyethylpiperazine-N<sup>1</sup>-2-ethanesulfonic acid
- DTNB: 5-5'-Dithiobis(2-nitrobenzoic acid)
- SOD: Superoxide dismutase
- PBS: Dulbecco's phosphate buffered saline
- BCNU: 1,3-Bis-chloro(2-chloroethyl)-1-nitrosourea
- $\cdot$ OH: Hydroxyl radical
- ROS: Reactive oxygen species.

## Data Availability

The data used to support the findings of this study are included within the article.

## Conflicts of Interest

There are no conflicts of interest associated with this paper.

## Acknowledgments

This study is supported by the National Cancer Institute ZIA BC 011078 and the City of Hope National Medical Center.

## Supplementary Materials

Supplementary Table 1: effect of doxorubicin on oxygen consumption by the tumor microsomal fraction. Supplementary Table 2: effect of doxorubicin on oxygen consumption by the tumor mitochondrial fraction. Supplementary Table 3: effect of alterations in NADPH:cytochrome p-450 reductase level on superoxide formation by tumor nuclei. (*Supplementary Materials*)

## References

- [1] J. H. Doroshow, "Topoisomerase II inhibitors: anthracyclines," in *Cancer Chemotherapy and Biotherapy: Principles and Practice*, B. A. Chabner and D. L. Longo, Eds., pp. 356–391, Lippincott, Williams, and Wilkins Publishers, 2011.
- [2] S. E. Lipshultz, R. E. Scully, S. R. Lipsitz et al., "Assessment of dexrazoxane as a cardioprotectant in doxorubicin-treated children with high-risk acute lymphoblastic leukaemia: long-term follow-up of a prospective, randomised, multicentre trial," *The Lancet Oncology*, vol. 11, no. 10, pp. 950–961, 2010.
- [3] J. Gao, Y. Xiong, Y. S. Ho et al., "Glutathione peroxidase 1-deficient mice are more susceptible to doxorubicin-induced cardiotoxicity," *Biochimica et Biophysica Acta (BBA) - Molecular Cell Research*, vol. 1783, no. 10, pp. 2020–2029, 2008.
- [4] J. H. Doroshow, "Effect of anthracycline antibiotics on oxygen radical formation in rat heart," *Cancer Research*, vol. 43, no. 2, pp. 460–472, 1983.
- [5] J. H. Doroshow and K. J. Davies, "Redox cycling of anthracyclines by cardiac mitochondria. II. Formation of superoxide anion, hydrogen peroxide, and hydroxyl radical," *The Journal of Biological Chemistry*, vol. 261, no. 7, pp. 3068–3074, 1986.
- [6] Y. Xiong, X. Liu, C. P. Lee, B. H. Chua, and Y. S. Ho, "Attenuation of doxorubicin-induced contractile and mitochondrial dysfunction in mouse heart by cellular glutathione peroxidase," *Free Radical Biology & Medicine*, vol. 41, no. 1, pp. 46–55, 2006.
- [7] C. Myers, "The role of iron in doxorubicin-induced cardiomyopathy," *Seminars in Oncology*, vol. 25, 4 Supplement 10, pp. 10–14, 1998.
- [8] F. C. Luft, "Doxorubicin toxicity in the Iron Age," *Journal of Molecular Medicine*, vol. 84, no. 7, pp. 529–531, 2006.
- [9] G. S. Panjra, V. Patel, C. I. Valdiviezo, N. Narula, J. Narula, and D. Jain, "Potentiation of doxorubicin cardiotoxicity by iron loading in a rodent model," *Journal of the American College of Cardiology*, vol. 49, no. 25, pp. 2457–2464, 2007.
- [10] B. B. Hasinoff and E. H. Herman, "Dexrazoxane: how it works in cardiac and tumor cells. Is it a prodrug or is it a drug?," *Cardiovascular Toxicology*, vol. 7, no. 2, pp. 140–144, 2007.
- [11] X. Di, R. P. Shiu, I. F. Newsham, and D. A. Gewirtz, "Apoptosis, autophagy, accelerated senescence and reactive oxygen in the response of human breast tumor cells to adriamycin," *Biochemical Pharmacology*, vol. 77, no. 7, pp. 1139–1150, 2009.
- [12] E. Gajewski, S. Gaur, S. A. Akman, L. Matsumoto, J. N. van Balgooy, and J. H. Doroshow, "Oxidative DNA base damage in MCF-10A breast epithelial cells at clinically achievable concentrations of doxorubicin," *Biochemical Pharmacology*, vol. 73, no. 12, pp. 1947–1956, 2007.
- [13] J. H. Doroshow, "Role of hydrogen peroxide and hydroxyl radical formation in the killing of Ehrlich tumor cells by anticancer quinones," *Proceedings of the National Academy of Sciences of the United States of America*, vol. 83, no. 12, pp. 4514–4518, 1986.
- [14] J. H. Doroshow and A. Juhasz, "Modulation of selenium-dependent glutathione peroxidase activity enhances doxorubicin-induced apoptosis, tumour cell killing and hydroxyl radical production in human NCI/ADR-RES cancer cells despite high-level P-glycoprotein expression," *Free Radical Research*, vol. 53, no. 8, pp. 882–891, 2019.
- [15] J. H. Doroshow, T. W. Synold, G. Somlo, S. A. Akman, and E. Gajewski, "Oxidative DNA base modifications in peripheral blood mononuclear cells of patients treated with high-dose infusional doxorubicin," *Blood*, vol. 97, no. 9, pp. 2839–2845, 2001.
- [16] J. M. McCord and I. Fridovich, "Superoxide dismutase. An enzymic function for erythrocyte hemocuprein," *The Journal of Biological Chemistry*, vol. 244, no. 22, pp. 6049–6055, 1969.
- [17] I. M. Goldstein, M. Brai, A. G. Osler, and G. Weissmann, "Lysosomal enzyme release from human leukocytes: mediation by the alternate pathway of complement activation," *Journal of Immunology*, vol. 111, pp. 33–37, 1973.
- [18] R. Hinnen, H. Miyamoto, and E. Racker, "Ca<sup>2+</sup> translocation in Ehrlich ascites tumor cells," *The Journal of Membrane Biology*, vol. 49, no. 4, pp. 309–324, 1979.
- [19] L. A. Sordahl, C. Johnson, Z. R. Blailock, and A. Schwartz, "The mitochondrion," in *Methods in Pharmacology*, A. Schwartz, Ed., pp. 247–286, Appleton-Century-Crofts, New York, 1971.
- [20] F. P. Mamaril, A. Dobrjansky, and S. Green, "A rapid method for the isolation of nuclei from Ehrlich ascites tumor cells," *Cancer Research*, vol. 30, no. 2, pp. 352–356, 1970.
- [21] B. L. Horecker and A. Kornberg, "The extinction coefficients of the reduced band of pyridine nucleotides," *The Journal of Biological Chemistry*, vol. 175, no. 1, pp. 385–390, 1948.
- [22] J. E. Biaglow and B. Jacobson, "Effect of nitrobenzene derivatives on electron transfer in cellular and chemical models," *Molecular Pharmacology*, vol. 13, no. 2, pp. 269–282, 1977.
- [23] J. B. Chappell, "The oxidation of citrate, isocitrate and cis-aconitate by isolated mitochondria," *The Biochemical Journal*, vol. 90, no. 2, pp. 225–237, 1964.
- [24] S. M. Klein, G. Cohen, and A. I. Cederbaum, "Production of formaldehyde during metabolism of dimethyl sulfoxide by hydroxyl radical generating systems," *Biochemistry*, vol. 20, no. 21, pp. 6006–6012, 1981.

- [25] T. Nash, "The colorimetric estimation of formaldehyde by means of the Hantzsch reaction," *The Biochemical Journal*, vol. 55, no. 3, pp. 416–421, 1953.
- [26] J. H. Doroshov, G. Y. Locker, and C. E. Myers, "Enzymatic defenses of the mouse heart against reactive oxygen metabolites: alterations produced by doxorubicin," *The Journal of Clinical Investigation*, vol. 65, no. 1, pp. 128–135, 1980.
- [27] O. H. Lowry, N. Rosebrough, A. Farr, and R. Randall, "Protein measurement with the folin phenol reagent," *The Journal of Biological Chemistry*, vol. 193, no. 1, pp. 265–275, 1951.
- [28] P. Armitage, *Statistical Methods in Medical Research*, Blackwell Scientific Publications, 1971.
- [29] K. J. Davies and J. H. Doroshov, "Redox cycling of anthracyclines by cardiac mitochondria. I. Anthracycline radical formation by NADH dehydrogenase," *The Journal of Biological Chemistry*, vol. 261, no. 7, pp. 3060–3067, 1986.
- [30] K. J. Davies, J. H. Doroshov, and P. Hochstein, "Mitochondrial NADH dehydrogenase-catalyzed oxygen radical production by adriamycin, and the relative inactivity of 5-iminodaunorubicin," *FEBS Letters*, vol. 153, no. 1, pp. 227–230, 1983.
- [31] C. E. Myers, J. R. Muindi, J. Zweier, and B. K. Sinha, "5-Imino-daunomycin: an anthracycline with unique properties," *The Journal of Biological Chemistry*, vol. 262, no. 24, pp. 11571–11577, 1987.
- [32] R. Bredehorst, M. Panneerselvam, and C.-W. Vogel, "Doxorubicin enhances complement susceptibility of human melanoma cells by extracellular oxygen radical formation," *The Journal of Biological Chemistry*, vol. 262, no. 5, pp. 2034–2041, 1987.
- [33] R. Liu, R. K. Narla, I. Kurinov, B. Li, and F. M. Uckun, "Increased hydroxyl radical production and apoptosis in PC12 neuron cells expressing the gain-of-function mutant G93A SOD1 gene," *Radiation Research*, vol. 151, no. 2, pp. 133–141, 1999.
- [34] O. Dionisi, T. Galeotti, T. Terranova, and A. Azzi, "Superoxide radicals and hydrogen peroxide formation in mitochondria from normal and neoplastic tissues," *Biochimica et Biophysica Acta (BBA) - Enzymology*, vol. 403, no. 2, pp. 292–300, 1975.
- [35] K. H. Ibsen and K. W. Schiller, "Control of glycolysis and respiration in substrate-depleted Ehrlich ascites tumor cells," *Archives of Biochemistry and Biophysics*, vol. 143, no. 1, pp. 187–203, 1971.
- [36] K. W. Bock, V. Gang, H. P. Beer, R. Kronau, and H. Grunicke, "Localization and regulation of two NAD nucleosidases in Ehrlich ascites cells," *European Journal of Biochemistry*, vol. 4, no. 3, pp. 357–363, 1968.
- [37] G. M. Bartoli, A. Dani, T. Galeotti, M. Russo, and T. Terranova, "Respiratory activity of Ehrlich ascites tumour cell nuclei," *Zeitschrift für Krebsforschung und Klinische Onkologie. Cancer Research and Clinical Oncology*, vol. 83, no. 3, pp. 223–231, 1975.
- [38] K. B. Adler, W. J. Holden-Stauffer, and J. E. Repine, "Oxygen metabolites stimulate release of high-molecular-weight glycoconjugates by cell and organ cultures of rodent respiratory epithelium via an arachidonic acid-dependent mechanism," *The Journal of Clinical Investigation*, vol. 85, no. 1, pp. 75–85, 1990.
- [39] A. Bozzi, I. Mavelli, A. Finazzi Agrò et al., "Enzyme defense against reactive oxygen derivatives. II. Erythrocytes and tumor cells," *Molecular and Cellular Biochemistry*, vol. 10, no. 1, pp. 11–16, 1976.
- [40] B. A. Johnson, M. S. Cheang, and G. J. Goldenberg, "Comparison of adriamycin uptake in chick embryo heart and liver cells an murine L5178Y lymphoblasts in vitro: role of drug uptake in cardiotoxicity," *Cancer Research*, vol. 46, no. 1, pp. 218–223, 1986.
- [41] J. R. Thiagarajah, J. Chang, J. A. Goettel, A. S. Verkman, and W. I. Lencer, "Aquaporin-3 mediates hydrogen peroxide-dependent responses to environmental stress in colonic epithelia," *Proceedings of the National Academy of Sciences of the United States of America*, vol. 114, no. 3, pp. 568–573, 2017.
- [42] P. E. Starke and J. L. Farber, "Ferric iron and superoxide ions are required for the killing of cultured hepatocytes by hydrogen peroxide: evidence for the participation of hydroxyl radicals formed by an iron-catalyzed Haber-Weiss reaction," *The Journal of Biological Chemistry*, vol. 260, no. 18, pp. 10099–10104, 1985.
- [43] M. F. McCarty and F. Contreras, "Increasing superoxide production and the labile iron pool in tumor cells may sensitize them to extracellular ascorbate," *Frontiers in Oncology*, vol. 4, p. 249, 2014.
- [44] G. F. Vile, C. C. Winterbourn, and H. C. Sutton, "Radical-driven Fenton reactions: studies with paraquat, adriamycin, and anthraquinone 6-sulfonate and citrate, ATP, ADP, and pyrophosphate iron chelates," *Archives of Biochemistry and Biophysics*, vol. 259, no. 2, pp. 616–626, 1987.
- [45] C. C. Winterbourn, "Evidence for the production of hydroxyl radicals from the adriamycin semiquinone and H<sub>2</sub>O<sub>2</sub>," *FEBS Letters*, vol. 136, no. 1, pp. 89–94, 1981.
- [46] G. Vile and C. Winterbourn, "Thiol oxidation and inhibition of Ca-ATPase by adriamycin in rabbit heart microsomes," *Biochemical Pharmacology*, vol. 39, no. 4, pp. 769–774, 1990.
- [47] S. A. Akman, J. H. Doroshov, T. G. Burke, and M. Dizdaroglu, "DNA base modifications induced in isolated human chromatin by NADH dehydrogenase-catalyzed reduction of doxorubicin," *Biochemistry*, vol. 31, no. 13, pp. 3500–3506, 1992.
- [48] L. B. Sheiner, "ELSFIT: a program for the extended least squares fit to individual pharmacokinetic data," in *San Francisco: Division of Clinical Pharmacology*, pp. 1–82, University of California, 1981.

## Research Article

# Corn Silk (*Zea mays L.*) Induced Apoptosis in Human Breast Cancer (MCF-7) Cells via the ROS-Mediated Mitochondrial Pathway

Mai M. Al-Oqail,<sup>1</sup> Ebtessam S. Al-Sheddi,<sup>1</sup> Nida N. Farshori ,<sup>1</sup> Shaza M. Al-Massarani ,<sup>1</sup> Eman A. Al-Turki,<sup>1</sup> Javed Ahmad,<sup>2,3</sup> Abdulaziz A. Al-Khedhairi,<sup>3</sup> and Maqsood A. Siddiqui <sup>2,3</sup>

<sup>1</sup>Department of Pharmacognosy, College of Pharmacy, King Saud University, Riyadh, Saudi Arabia

<sup>2</sup>Al-Jeraisy Chair for DNA Research, Zoology Department, College of Science, King Saud University, P.O. Box 2455, Riyadh 11451, Saudi Arabia

<sup>3</sup>Zoology Department, College of Science, King Saud University, P.O. Box 2455, Riyadh 11451, Saudi Arabia

Correspondence should be addressed to Nida N. Farshori; [nidachem@gmail.com](mailto:nidachem@gmail.com) and Maqsood A. Siddiqui; [maqsoodahmads@gmail.com](mailto:maqsoodahmads@gmail.com)

Received 13 May 2019; Accepted 27 June 2019; Published 20 October 2019

Guest Editor: Vittorio Colombo

Copyright © 2019 Mai M. Al-Oqail et al. This is an open access article distributed under the Creative Commons Attribution License, which permits unrestricted use, distribution, and reproduction in any medium, provided the original work is properly cited.

Cancer has been recognized as one of the life-threatening diseases. Breast cancer is a leading cause of mortality among women. In spite of current developments in the therapy and diagnosis of cancer, the survival rate is still less. Recently, plant-derived natural products gain attention as anticancer agents due to the nontoxic nature. Therefore, the aim of present study was to investigate the anticancer capacity of corn silk extract (CSE) on human breast cancer (MCF-7) and normal human mesenchymal (hMSC-TERT4) cells. Following 24 h treatment to corn silk extract, the cytotoxicity was assessed by MTT, NRU, and morphological assays. The oxidative stress markers (GSH and LPO), ROS production, MMP change, and expression of apoptotic marker genes (p53, Bax, Bcl-2, caspase-3, and caspase-9) were also studied in MCF-7 cells treated at 250 to 1000  $\mu\text{g/ml}$  of CSE for 24 h. Our results showed that CSE decreased the cell viability and increased the apoptosis in a dose-dependent manner. The level of LPO and ROS production was found significantly higher; however, GSH and MMP level was observed lower in CSE-treated MCF-7 cells. The real-time PCR data showed a significant upregulation in p53, Bax, caspase-3, and caspase-9 and downregulation in the mRNA expression of Bcl-2 genes in MCF-7 cells exposed to CSE. Collectively, the data from this study stated that corn silk extract induced apoptosis via the ROS-mediated mitochondrial pathway in MCF-7 cells.

## 1. Introduction

Breast cancer (BC) is the most frequently occurring cancer in females. Overall, BC is the second most common cancer with two million new cases in 2018 [1]. As per the data collected by the National Centre for Health statistics, 600920 demises and 1688780 fresh cancer cases were anticipated to arise in the women of United States in 2017 [2]. According to the report published by Jemal et al. [3], the worldwide incidence of breast cancer will keep increasing annually by 0.4%. Thus, the prevention of BC is a challenge between the scientists

and searchers working in the area around the world. The increasing rate of BC generating economic burden to the society demands for the search of a novel, effective, and beneficial procedure. The available chemotherapeutic drugs, paclitaxel and anthracyclines, are known to constrain cancer growth and induce cancer cell apoptosis [4]. Nevertheless, these drugs are not sensitive to some of the patients and leads to the unwanted side effects to the healthy cells as well [5]. Hence, it is required to find a powerful, targeted, and nontoxic therapeutic agent to treat BC using natural products.

Plants as a natural product have received great attention as an anticancer agent with less side effects [6–8]. Corn silk (*Stigma maydis*), a byproduct of yellow or green maize (*Zea mays* L.), is well known for the effective treatment of nephritis, hypertension, prostatitis, and urinary tract infections [9]. In a traditional system of medicine, the corn silk has been used in several areas of the world including the United States, China, France, and Turkey [10]. The extracts of corn silk contain good quantity of a type of flavonoid, maysin, which is specific to corn [11, 12]. Maysin is a flavone glycoside encompassing luteolin, a biologically active agent known for its antioxidant and anticancer potential [13]. The high maysin corn silk extracts have been proven to be beneficial in reducing the body weight and fat deposition in C57BL/6J mice [14]. Bai et al. [15] have also shown the protective effects of ethanolic maize silk extract on radiation-induced oxidative stress. The administration of aqueous extract of corn silk at 100–400 mg/kg b.w. on hematological and lipid parameters in rats [16] and male ICR mice treated for 4 weeks at 500 mg/kg b.w. of corn silk extracts has been found nontoxic [10].

Our literature survey revealed that corn silk has extensively been reported to have substantial bioactivities such as antioxidant [17], antidiabetic [18], antibacterial [19], antifatigue [20], antidepressant [21], and antitumor [22] activities. The antiproliferative activity of corn silk extract against the LoVo (human colon cancer) cell line [23] and apoptosis in C6 rat glioma cells through mitochondrial ROS [24] have been reported. To the best of our knowledge, the mechanisms of anticancer effects of corn silk extract (CSE) against MCF-7 (human breast cancer) cells have not been studied yet. Hence, we aimed to present investigation firstly to assess the cytotoxic potential of CSE against MCF-7 and TERT4 cell lines and secondly to study the mechanism(s) of CSE inducing oxidative stress, ROS production, and apoptosis in the MCF-7 cell line.

## 2. Materials and Methods

**2.1. Preparation of CSE.** The fresh corn silk was obtained from the local market of Riyadh, Saudi Arabia. The corn silk was washed, air-dried, and powdered for further use. The methanolic extract was obtained by maceration. Briefly, 25 g of powdered corn silk was extracted with 100 ml methanol/water (80%, v/v). The filtrate was collected and dried in a rotary evaporator at 40°C till dryness. The dried extract was stored at 4°C for further use. The extract was diluted in DMSO, and the final concentration of DMSO for cytotoxicity assessment and other assays was 0.004%.

**2.2. Cell Culture.** Human breast cancer MCF-7 and normal cell line hMSC-TERT4 were obtained from ATCC. MCF-7 and hMSC-TERT4 cells were grown in DMEM and MEM, respectively, complemented with fetal bovine serum (10%) in a CO<sub>2</sub> incubator (5% CO<sub>2</sub>, 95% air) at 37°C.

**2.3. Cytotoxicity of Corn Silk Extract (CSE).** Cytotoxic effects of CSE were performed using MTT assay, NRU assay, and morphological assessment using the method established by us [25]. To assess the cytotoxic effects of CSE, the MCF-7

and TERT4 cells were seeded in a 96-well culture plate at a density of 10,000 cells per well. After overnight incubation, the cells were exposed to different concentrations (10–1000 µg/ml) of CSE for 24 h using culture medium in untreated control. The percent cell viability was calculated using the formula below:

$$\% \text{cell viability} = \frac{(\text{mean absorbance of treatment})}{(\text{mean absorbance of control})} \times 100. \quad (1)$$

For, morphological assessments, the MCF-7 and TERT4 cells were seeded in a 96-well culture plate at a density of  $1 \times 10^4$  cells/well. The cells exposed to different concentrations of CSE were analyzed under the phase contrast inverted microscope at 20x magnification power.

**2.4. Effects of CSE on Oxidative Stress Markers and ROS Generation.** The CSE inducing oxidative stress was evaluated by measuring the glutathione level, LPO, and ROS generation in the MCF-7 cell line.

**2.4.1. GSH Measurement.** The total glutathione was measured according to Chandra et al.'s study [26]. Following the protocol, MCF-7 cells seeded in 6-well culture plates ( $1 \times 10^5$ ) were left overnight in a CO<sub>2</sub> incubator. Then, cells were exposed to 0, 250, 500, and 1000 µg/ml of CSE for 24 h. After exposure, cells were harvested and protein was precipitated in 1 ml of 10% TCA by sonication. Then, the supernatant was collected by centrifugation and 2 ml (0.4 M Tris buffer, 0.02 M EDTA) was added to the supernatant. Subsequently, 0.01 M DTNB (5,5'-dithionitrobenzoic acid) was added and incubated for 10 minutes at 37°C. The absorbance of developed color was read at 550 nm wavelength.

**2.4.2. Lipid Peroxidation (LPO).** To measure the lipid peroxidation induced by CSE, MCF-7 cells ( $1 \times 10^5$ ) were seeded in 6-well plates and exposed at 0, 250, 500, and 1000 µg/ml of CSE for 24 h. The LPO in MCF-7 cells was measured by the TBARS (thiobarbituric acid reactive substances) method [27]. After 24 h treatment, MCF-7 cells were collected and sonicated in 1.15% KCl. Following centrifugation, 2 ml of the TBA reagent (15% TCA, 0.7% TBA, and 0.25 N HCl) was added to the supernatant. Then, the solution was boiled at 100°C for 15 minutes, and the absorbance of the supernatant was measured after centrifugation at 1000 rpm for 10 minutes.

**2.4.3. Measurement of ROS Production.** Intercellular ROS production in MCF-7 cells was examined using the DCF-DA (2,7-dichlorofluorescein diacetate) probe. DCF-DA is commonly used for the detection of ROS generation in cells, since this probe is cell permeable and can enter into the cells and react with ROS to form DCF (dichlorofluorescein), a fluorescent complex. The ROS generation was done using the protocol of Siddiqui et al. [28]. Following the protocol, MCF-7 cells were seeded in 24-well culture plates ( $2 \times 10^4$  cells) and incubated in a CO<sub>2</sub> incubator for overnight. The cells were exposed at 0, 250, 500, and 1000 µg/ml of CSE for 24 h. After respective exposures, 20 µM of dye was added



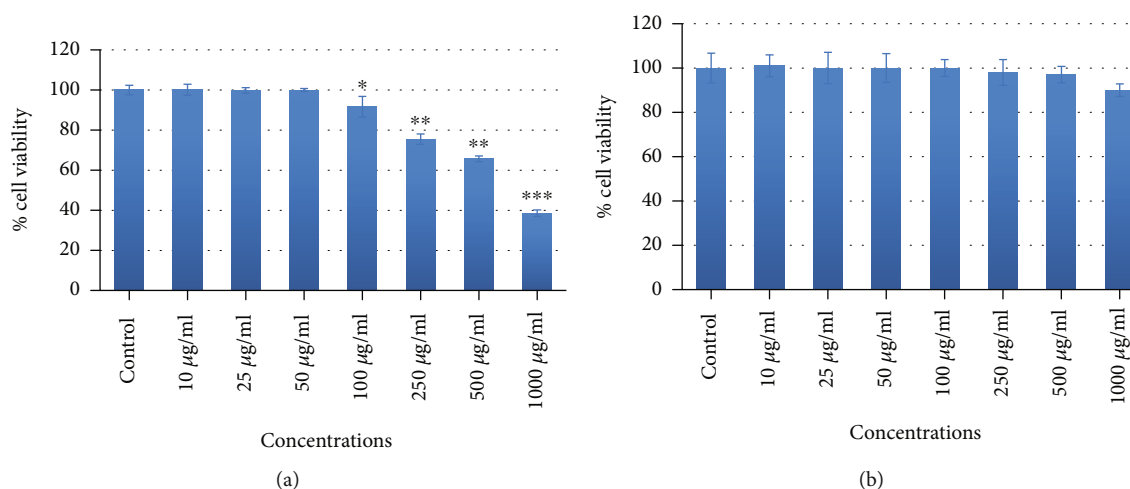


FIGURE 1: Cytotoxic effects of corn silk extract (CSE) by MTT assay on MCF-7 (a) and TERT4 cells (b). The cells were exposed to various concentrations of CSE for 24 h. Data are presented as the mean  $\pm$  SD of three different experiments. \* $p < 0.05$ , \*\* $p < 0.01$ , and \*\*\* $p < 0.001$  compared to control.

to each well and further incubated for 1 hour in the dark. The fluorescence intensity of the DCF was analyzed under the fluorescence microscope. To measure the quantitative ROS generation, the fluorescence of the cells was measured at 485 nm excitation and 530 nm emission using a fluorescent reader.

**2.5. Determination of MMP ( $\Delta\Psi_m$ ).** The MMP level in MCF-7 cells was analyzed using Rhodamine-123 fluorescence dye (Rh-123) [28]. As per protocol, MCF-7 cells seeded in 24-well culture plates ( $2 \times 10^4$ ) were left overnight in a  $\text{CO}_2$  incubator. Following the exposure of CSE for 24 h at 250, 500, and 1000  $\mu\text{g/ml}$ , cells were washed with PBS. Then, cells were exposed to Rh-123 dye for 60 minutes in the dark at 37°C. The fluorescence intensity of the Rh-123 dye was observed under the fluorescence microscope, and the fluorescence intensity of Rh-123 in MCF-7 cells was also measured at 485 nm excitation and 530 nm emission wavelengths using a spectrofluorometer for quantitative analysis.

**2.6. Analysis of Apoptotic Markers Genes.** The real-time PCR (RT-PCR<sup>q</sup>) analysis was conducted to measure the mRNA expression of proapoptotic genes (p53, Bax, caspase-3, and caspase-9) and antiapoptotic gene (Bcl-2) in MCF-7 cells treated with CSE according to the method of Al-Oqail et al. [29]. Following the protocol, MCF-7 cells were harvested and seeded in 6-well culture plates ( $1 \times 10^6$  cells) and allowed to adhere overnight. Cells were exposed to 0, 250, 500, and 1000  $\mu\text{g/ml}$  of corn seed extract for 24 h. Then, the total RNA was isolated from treated and untreated sets using an RNeasy mini kit (Qiagen). The integrity of RNA was checked using a gel documentation system on 1% gel. Further, cDNA was synthesized by reverse transcriptase using M-MLV and oligo (dT) primers (Promega). The RT-PCR<sup>q</sup> was performed by a LightCycler<sup>®</sup> 480 instrument. The expression of apoptosis-related genes was normalized to a housekeeping gene,  $\beta$ -actin. The details of the primer sequences for p53,

Bax, caspase-3, caspase-9, Bcl-2, and  $\beta$ -actin are reported in our earlier publication [29].

**2.7. Statistical Analysis.** The statistical analysis was done using one-way ANOVA and post hoc Dunnett's test to analyze the significant differences between the control and treated groups. The values showing  $p < 0.05$  were considered statistically significant.

### 3. Results and Discussion

**3.1. Cytotoxic Effects of CSE on MCF-7 and TERT4.** To assess the cytotoxic potential of CSE, MCF-7 and TERT4 cells were exposed to increasing concentrations (10, 25, 50, 100, 250, 500, and 1000  $\mu\text{g/ml}$ ) of CSE for 24 h. The highlights of the cytotoxic results obtained by MTT assay, NRU assay, and morphological alterations are summarized in Figures 1–3, respectively. As shown in Figure 1, MTT assay revealed a concentration-dependent cytotoxicity in MCF-7 cell lines. A significant dose-dependent decrease in the cell viability of MCF-7 (Figure 1(a)) was found at 100  $\mu\text{g/ml}$  or higher concentrations of CSE exposed for 24 h whereas at the same concentration of CSE, TERT4 cell viability was not reduced (Figure 1(b)). Similar to MTT assay, the NRU assay also revealed a concentration-dependent cytotoxicity in MCF-7. 100  $\mu\text{g/ml}$  or higher concentrations of CSE were also found to decrease the viability of MCF-7 cells (Figure 2(a)) by NRU assay exposed for 24 h whereas the viability of TERT4 cells was not reduced at similar concentrations of CSE (Figure 2(b)). The viability of MCF-7 cells at 250, 500, and 1000  $\mu\text{g/ml}$  of CSE was found as 75%, 65%, and 38% by MTT and 76%, 68%, and 42% by NRU assays, respectively. The morphological alterations observed under the microscope in MCF-7 and TERT4 cells are presented in Figure 3. The CSE at 500 and 1000  $\mu\text{g/ml}$  reduced the number of MCF-7 cells, which become rounded and smaller in size. However, there was no significant effect in the morphology of TERT4 cells observed at tested concentrations. The

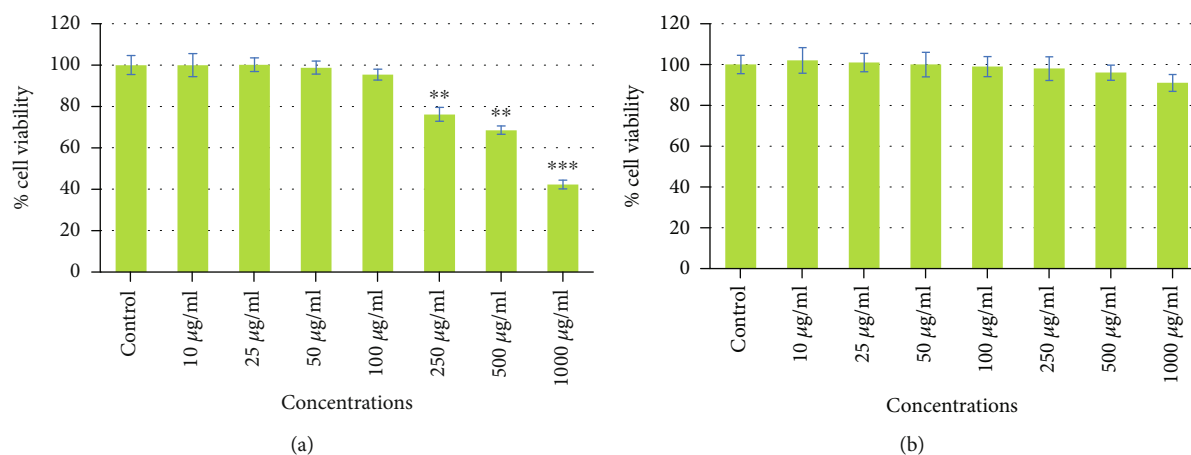


FIGURE 2: Cytotoxic effects of corn silk extract (CSE) by neutral red uptake assay on MCF-7 (a) and TERT4 cells (b). The cells were exposed to various concentrations of CSE for 24 h. Data are presented as the mean  $\pm$  SD of three different experiments. \* $p < 0.05$ , \*\* $p < 0.01$ , and \*\*\* $p < 0.001$  compared to control.

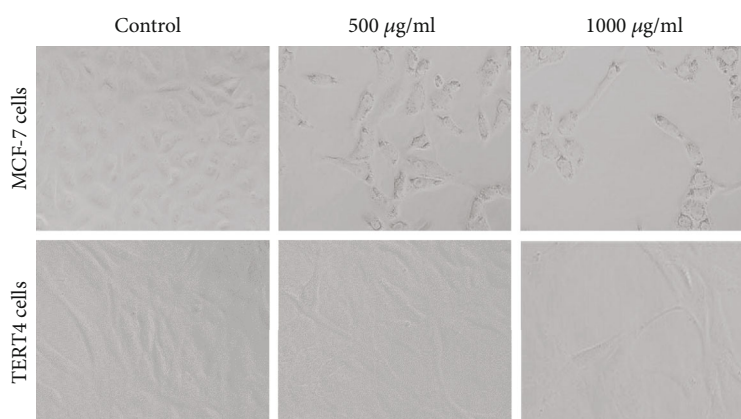


FIGURE 3: Representative images of morphological changes in MCF-7 and TERT4 cell lines. MCF-7 and TERT4 cells were exposed to different concentrations of corn silk extract (CSE) for 24 h. Images were grabbed using a phase contrast inverted microscope at 20x magnification power.

MCF-7 cells were found cytotoxic to CSE; therefore, we further discovered the possible mechanism(s) of CSE inducing apoptosis in MCF-7 cells. In the present investigation, we used MTT and neutral red uptake assays to assess the cytotoxic potential of CSE because of their different mode of action. The MTT assay is mainly based on the conversion of MTT in the mitochondria [30]. The neutral red uptake assay is colorimetric assay measuring the uptake of the dye by functional lysosomes [31]. Both the assays (MTT and NRU) revealed a significant-dose dependent decrease in the viability of MCF-7 cells. However, NRU assay showed little less cytotoxicity as compared to MTT assay. It has been reported previously that different cytotoxicity assays can give different results depending upon the test material used and the cytotoxicity assay employed [32].

**3.2. CSE Induced Oxidative Stress and ROS Generation in MCF-7 Cells.** As presented in Figure 4(a), a depletion in the GSH level was observed after 24 h exposure of CSE and this consequence was found in a concentration-dependent manner. We observed that MCF-7 cells in comparison to control

with treatment of CSE at 250, 500, and 1000  $\mu\text{g/ml}$  resulted in a significant decrease of 10%, 23%, and 41%, respectively, in the GSH level. As shown in Figure 4(b), the CSE induced a significant increase in the LPO level. An increase of 15%, 39%, and 97% at 250, 500, and 1000  $\mu\text{g/ml}$  of CSE was found in MCF-7 as compared to control (Figure 4(b)). Further, we measured intercellular ROS production in MCF-7 cells exposed to 0, 250, 500, and 1000  $\mu\text{g/ml}$  of CSE for 24 h. The ROS production was analyzed by two methods (Figure 5): first, the cellular oxidation of DCF-DA, which oxidized to green fluorescent by intracellular ROS under a fluorescence microscope (Figure 5(a)), and quantitative ROS generation measuring the fluorescence of the cell-induced corn silk extract in MCF-7 cells (Figure 5(b)). As shown in Figure 5(a), the green fluorescence intensity clearly indicates the ROS generation induced by corn silk extract. The graph of Figure 5(b) also exhibited a significant increase of 22%, 74%, and 124% at 250, 500, and 1000  $\mu\text{g/ml}$  of CSE, respectively, as compared to control. The previous reports suggest that the natural product endorsed oxidative stress by decreasing the intracellular glutathione level and increasing the lipid

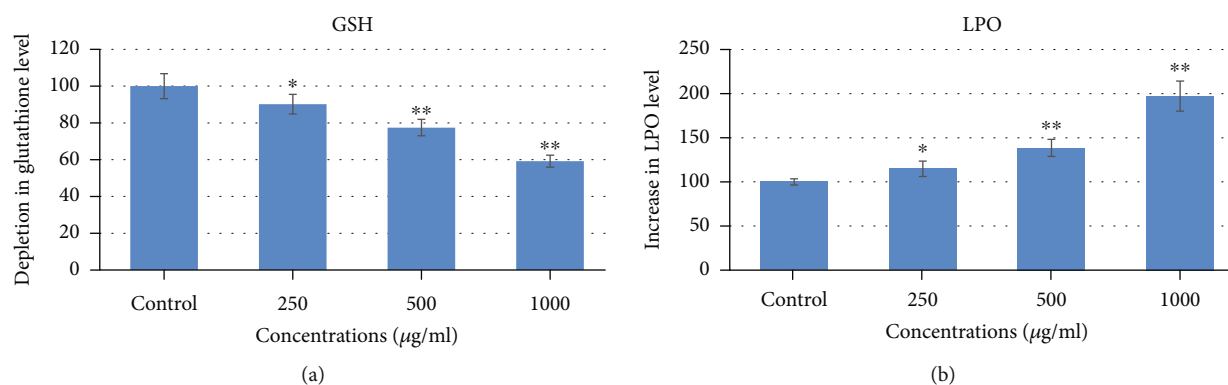


FIGURE 4: Effects of corn silk extract (CSE) on oxidative stress markers in MCF-7 cells. (a) Depletion in glutathione (GSH) level and (b) induction in lipid peroxidation (LPO). Data are presented as the mean  $\pm$  SD of three different experiments. \* $p < 0.05$  and \*\* $p < 0.01$  and compared to control.

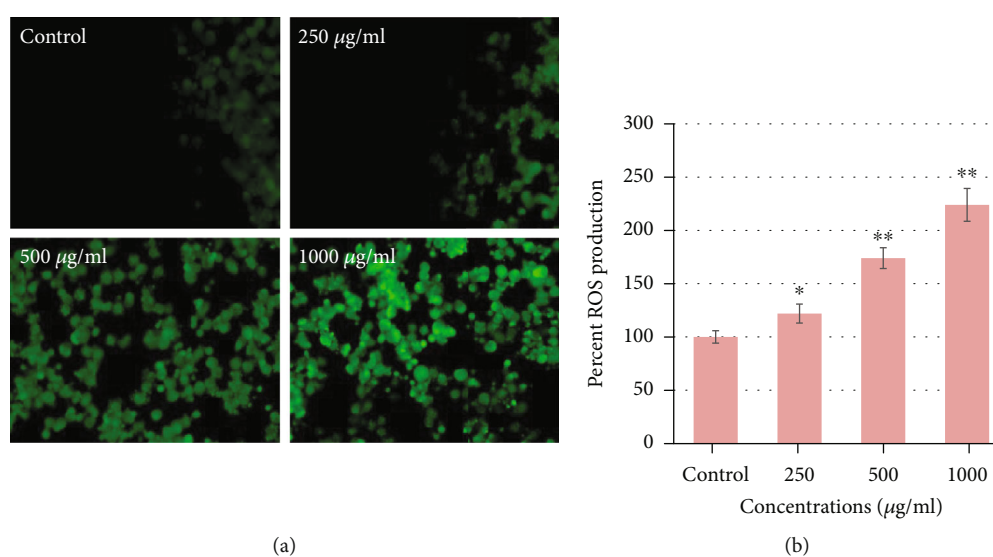


FIGURE 5: ROS generation induced by corn silk extract (CSE) in MCF-7 cells. (a) Fluorescence images showing intensity of DCF-DA dye after the CSE exposure at 0, 250, 500, and 1000  $\mu\text{g/ml}$  for 24 h. (b) The graph shows the percent ROS generation in MCF-7 cells. Data are presented as the mean  $\pm$  SD of three different experiments. \* $p < 0.05$  and \*\* $p < 0.01$  and compared to control.

peroxidation in the cells [33, 34]. A concentration-dependent decrease in GSH and an increase in LPO levels as found in this study induced by CSE in MCF-7 indicate that oxidative stress plays an important role in the cytotoxicity/cell death. The data obtained in the present study is also supported by previous studies that showed the involvement of oxidative stress in *Nigella sativa* seed oil-induced cell death in human hepatocellular carcinoma cell line [29]. Reactive oxygen species (ROS) produced as a byproduct of cellular metabolism mainly in the mitochondria play a significant role in the cell proliferation, survival, and differentiation [35]. In a normal condition, production and exclusion of ROS are balanced in the cells; however, the stimulation by xenobiotics can cause excessive production of ROS. The excessive production of ROS can lead to oxidative damage, cell cycle arrest, and cellular apoptosis [36, 37]. In this study, we found that CSE increases the production of ROS in a concentration-dependent manner. Therefore, it can be assumed that ROS is involved in the cell death of MCF-7 induced by CSE. These

results are also supported by previous studies showing the excessive ROS generation induced by natural products [38–40]. The increased amounts of ROS are known to result in the physiological dysfunction and cell damage [41].

**3.3. CSE Induced Change in MMP ( $\Delta\Psi_m$ ).** It is known that change in mitochondrial permeability is a vital sign of the cellular apoptosis [42]. Thus, to explore whether CSE can interrupt the  $\Delta\Psi_m$ , the MCF-7 cells were treated with different concentrations (250, 500, and 1000  $\mu\text{g/ml}$ ) of CSE for 24 h. The MMP was observed by staining with cationic fluorescence dye (Rh123). The results found from fluorescence measurements clearly showed a concentration-dependent decrease in the  $\Delta\Psi_m$  in MCF-7 cells treated with CSE (Figure 6(a)). As shown in Figure 6(b), compared to control, a significant decrease of 10%, 35%, and 60% was found at 250, 500, and 1000  $\mu\text{g/ml}$  of CSE, respectively. As observed in the present investigation, the decrease in  $\Delta\Psi_m$  is as early incidence of apoptotic cell death in MCF-7 cells. This also

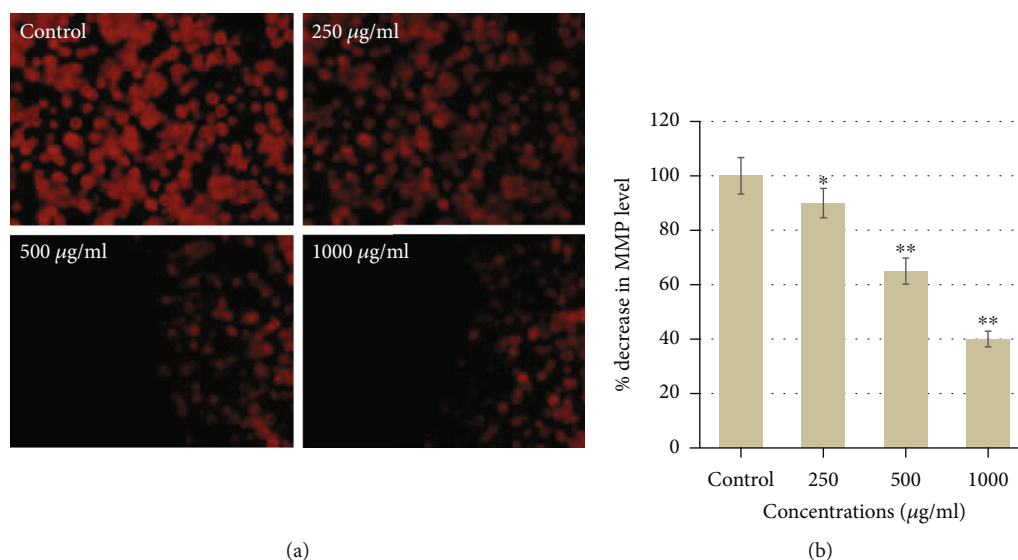


FIGURE 6: Corn silk extract (CSE) induced loss in MMP. The loss in the MMP level was observed in MCF-7 after the exposure of CSE at 250-1000  $\mu\text{g/ml}$  for 24 h. (a) The fluorescence intensity of Rh123 dye was analyzed under a fluorescence microscope. (b) The graph shows percent loss in the MMP level in MCF-7 induced by corn silk extract. Data are presented as the mean  $\pm$  SD of three different experiments. \* $p < 0.05$  and \*\* $p < 0.01$  compared to control.

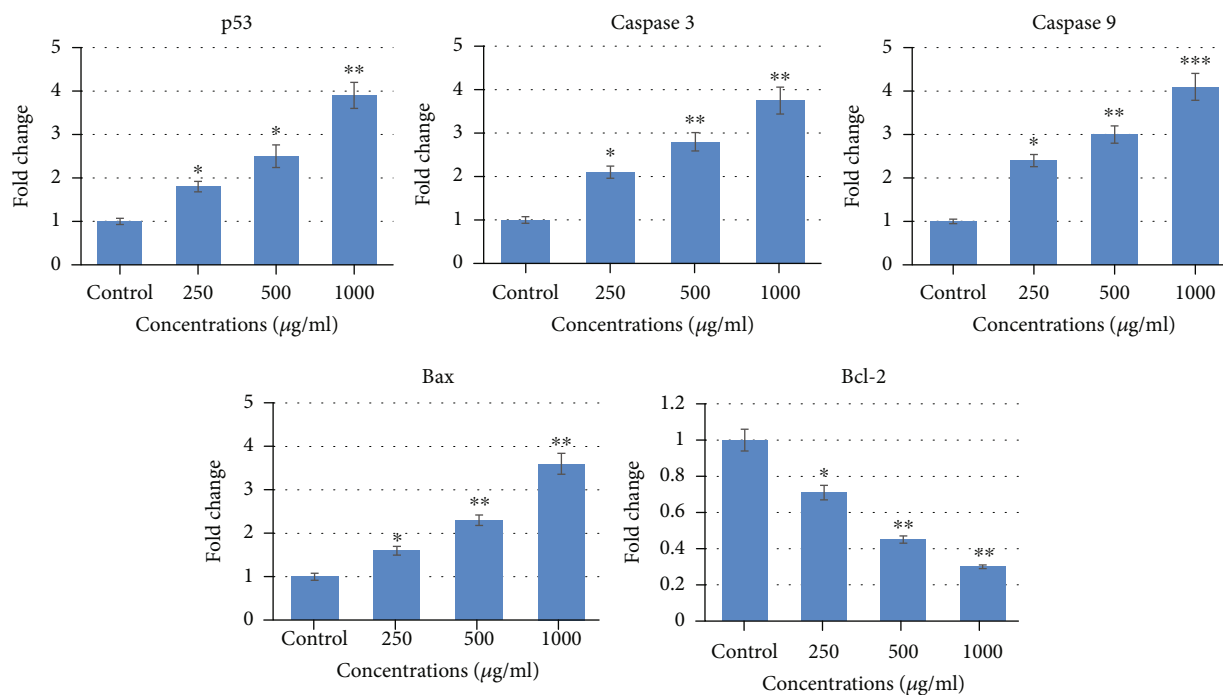


FIGURE 7: Fold change in the expression of apoptosis-related genes in MCF-7 cells analyzed by real-time PCR (qPCR). MCF-7 cells were exposed to 250-1000  $\mu\text{g/ml}$  of corn silk extract (CSE) for 24 h. The results are presented as the mean  $\pm$  SD of three different experiments. \* $p < 0.05$ , \*\* $p < 0.01$ , and \*\*\* $p < 0.001$  compared to control.

indicates the role of the mitochondrial-mediated pathway in apoptosis induced by CSE. Our results are also supported by Lee et al. [43], who have described that corn silk could loss the  $\Delta\Psi\text{m}$  in prostate cancer (PC-3) cells. Gou et al. [23] have also reported that CSE decreased the  $\Delta\Psi\text{m}$  in a concentration-dependent manner in LoVo (human colon cancer cell line).

**3.4. CSE Induced Changes in Apoptotic Marker Genes.** As shown in Figure 7, CSE upregulated the mRNA expression of p53, caspase-3, caspase-9, and Bax and downregulated the Bcl-2, which lead to the apoptosis. A concentration-dependent significant increase of 1.8-, 2.5-, and 3.8-fold in the mRNA expression of p53; 2.1-, 2.8-, and 3.75-fold in the mRNA expression of caspase-3; 2.4-, 3-, and 4.1-fold in

the mRNA expression of caspase-9; and 1.6-, 2.3-, and 3.6-fold in the mRNA expression of Bax at 250, 500, and 1000  $\mu\text{g/ml}$  of CSE, respectively, was observed. However, a 0.3-, 0.55-, and 0.7-fold decrease in mRNA expression of Bcl-2 at 250, 500, and 1000  $\mu\text{g/ml}$  of CSE, respectively, was observed in MCF-7 cells treated with CSE. The real-time PCR (RT-PCR<sup>q</sup>) data are presented as the expression of apoptotic marker genes (Figure 7). By real-time PCR analysis, we have exhibited that the initiation of the apoptosis pathway induced by CSE exposure to MCF-7 cells was facilitated by disturbing the Bax and Bcl-2 levels. Bax, the proapoptotic gene, has been reported to be upregulated in p53-mediated apoptosis in many systems [44]. Consequently, the increased level of p53 in MCF-7 cells induced by CSE in this study showed that p53 activates the mitochondrial apoptosis. The disturbance in the Bax and Bcl-2 level instigates the dysfunction of the mitochondria, which is encouraging the activation of caspase-3 and caspase-9 [45, 46]. Caspase, a family of proteases, plays a central role in the development of apoptosis. Caspase-9 is involved in the signal transduction cascade, activating caspase-3 that facilitates successive apoptotic signaling. Caspase-3 in the apoptotic pathway plays a critical role during DNA fragmentation, chromatin condensation, and other apoptotic methods [47]. In this study, upregulation in the mRNA expression of caspase-3 and caspase-9 clearly showed that CSE significantly induced apoptosis in MCF-7 cells. A concentration-dependent decrease in the Bcl-2 level observed might have been directed to decrease in MMP ( $\Delta\Psi\text{m}$ ) as shown in this study, following the activation of caspase-3 through the caspase-9 pathway. Our results are also in accordance with the previous report showing that the overexpression of ROS induced by CSE decreases  $\Delta\Psi\text{m}$  which activates caspase signaling pathways and apoptosis in rat C6 glioma and human colon cancer cell lines [23, 24].

#### 4. Conclusions

The present investigation demonstrated that the methanolic extract of corn silk (CSE) induced cytotoxicity in the human breast cancer cell line (MCF-7). There was no cytotoxic effect of CSE observed on normal human mesenchymal (hMSC-TERT4) cells at tested concentrations. The CSE was also found to increase the LPO and ROS production and decrease the GSH level in a dose-dependent manner in MCF-7 cells. The loss in mitochondrial membrane potential indicates the efficacy of CSE against cancer cells. The CSE induced upregulation in proapoptotic marker genes (p53, Bax, caspase-3, and caspase-9) and downregulation in anti-apoptotic gene, Bcl-2, which exhibited apoptotic cell death in human breast cancer cells through the ROS-mediated mitochondrial pathway.

#### Data Availability

The data used to support the findings of this study are included within the article.

#### Conflicts of Interest

The authors declare that they have no conflicts of interest.

#### Acknowledgments

The authors are grateful to the Deanship of Scientific Research, King Saud University for funding through Vice Deanship of Scientific Research Chairs.

#### References

- [1] F. Bray, J. Ferlay, I. Soerjomataram, R. L. Siegel, L. A. Torre, and A. Jemal, "Global cancer statistics 2018: GLOBOCAN estimates of incidence and mortality worldwide for 36 cancers in 185 countries," *CA: a Cancer Journal for Clinicians*, vol. 68, no. 6, pp. 394–424, 2018.
- [2] R. L. Segal, K. D. Miller, and A. Jemal, "Cancer statistics, 2018," *CA: a Cancer Journal for Clinician*, vol. 68, no. 1, pp. 7–30, 2018.
- [3] A. Jemal, E. M. Ward, C. J. Johnson et al., "Annual report to the nation on the status of cancer, 1975–2014, featuring survival," *JNCI: Journal of the National Cancer Institute*, vol. 109, no. 9, article djx030, 2017.
- [4] S. Liao, X. Hu, Z. Liu et al., "Synergistic action of microwave-induced mild hyperthermia and paclitaxel in inducing apoptosis in the human breast cancer cell line MCF-7," *Oncology Letters*, vol. 17, no. 1, pp. 603–615, 2019.
- [5] X. X. Chen, K. H. Lam, Q. X. Chen et al., "Ficus virens proanthocyanidins induced apoptosis in breast cancer cells concomitantly ameliorated 5-fluorouracil induced intestinal mucositis in rats," *Food and Chemical Toxicology*, vol. 110, pp. 49–61, 2017.
- [6] L. P. Xiang, A. Wang, J. H. Ye et al., "Suppressive effects of tea catechins on breast cancer," *Nutrients*, vol. 8, no. 8, p. 458, 2016.
- [7] T. Zhao, Q. Sun, M. Marques, and M. Witcher, "Anticancer properties of *Phyllanthus emblica* (Indian gooseberry)," *Oxidative Medicine and Cellular Longevity*, vol. 2015, Article ID 950890, 7 pages, 2015.
- [8] N. Tuasha, B. Petros, and Z. Asfaw, "Plants used as anticancer agents in the Ethiopian traditional medical practices: a systematic review," *Evidence-Based Complementary and Alternative Medicine*, vol. 2018, Article ID 6274021, 28 pages, 2018.
- [9] K. Hasanudin, P. Hashim, and S. Mustafa, "Corn silk (*Stigma maydis*) in healthcare: a phytochemical and pharmacological review," *Molecules*, vol. 17, no. 8, pp. 9697–9715, 2012.
- [10] A. W. Ha, H. J. Kang, S. L. Kim, M. H. Kim, and W. K. Kim, "Acute and subacute toxicity evaluation of corn silk extract," *Preventive Nutrition and Food Science*, vol. 23, no. 1, pp. 70–76, 2018.
- [11] S. L. Kim and T. W. Jung, "Maysin and other flavonoid contents in corn silk," *Korean Journal of Breed*, vol. 33, no. 33, pp. 338–343, 2001.
- [12] T. Fossen, R. Slimestad, and O. M. Andersen, "Anthocyanins from maize (*Zea mays*) and reed canarygrass (*Phalaris arundinacea*)," *Journal of Agriculture and Food Chemistry*, vol. 49, no. 5, pp. 2318–2321, 2001.
- [13] E. A. Lee, P. F. Byrne, M. D. McMullen et al., "Genetic mechanisms underlying apimaysin and maysin synthesis and corn

- earworm antibiosis in maize (*Zea mays* L.),” *Genetics*, vol. 149, no. 4, pp. 1997–2006, 1998.
- [14] E. Y. Lee, S. L. Kim, H. J. Kang, M. H. Kim, A. W. Ha, and W. K. Kim, “High maysin corn silk extract reduces body weight and fat deposition in C57BL/6J mice fed high-fat diets,” *Nutrition Research and Practice*, vol. 10, no. 6, pp. 575–582, 2016.
- [15] H. Bai, C. Hai, M. Xi, X. Liang, and R. Liu, “Protective effect of maize silks (*Maydis stigma*) ethanol extract on radiation-induced oxidative stress in mice,” *Plant Foods for Human Nutrition*, vol. 65, no. 3, pp. 271–276, 2010.
- [16] S. Saheed, A. E. Oladipipo, A. A. Abdulazeez et al., “Toxicological evaluations of *Stigma maydis* (corn silk) aqueous extract on hematological and lipid parameters in Wistar rats,” *Toxicology Reports*, vol. 2, pp. 638–644, 2015.
- [17] S. Žilić, M. Janković, Z. Basić, J. Vančetović, and V. Maksimović, “Antioxidant activity, phenolic profile, chlorophyll and mineral matter content of corn silk (*Zea mays* L.): comparison with medicinal herbs,” *Journal of Cereal Science*, vol. 69, pp. 363–370, 2016.
- [18] K. J. Wang and J. L. Zhao, “Corn silk (*Zea mays* L.), a source of natural antioxidants with  $\alpha$ -amylase,  $\alpha$ -glucosidase, advanced glycation and diabetic nephropathy inhibitory activities,” *Bio-medicine & Pharmacotherapy*, vol. 110, pp. 510–517, 2019.
- [19] S. Morshed and S. S. Islam, “Antimicrobial activity and phytochemical properties of corn (*Zea mays* L.) silk,” *SKUAST Journal of Research*, vol. 17, no. 1, pp. 8–14, 2015.
- [20] Q. L. Hu, L. J. Zhang, Y. N. Li, Y. J. Ding, and F. L. Li, “Purification and anti-fatigue activity of flavonoids from corn silk,” *International Journal of Physical Sciences*, vol. 5, no. 4, pp. 321–326, 2010.
- [21] M. A. Ebrahimzadeh, M. Mahmoudi, N. Ahangar et al., “Anti-depressant activity of corn silk,” *Pharmacology*, vol. 3, pp. 647–652, 2009.
- [22] J. Yang, X. Li, Y. Xue, N. Wang, and W. Liu, “Anti-hepatoma activity and mechanism of corn silk polysaccharides in H22 tumor-bearing mice,” *International Journal of Biological Macromolecules*, vol. 64, pp. 276–280, 2014.
- [23] H. Guo, H. Guan, W. Yang et al., “Pro-apoptotic and anti-proliferative effects of corn silk extract on human colon cancer cell lines,” *Oncology Letters*, vol. 13, no. 2, pp. 973–978, 2017.
- [24] E. Hwang, S. Sim, S. H. Park et al., “Anti-proliferative effect of *Zea mays* L. cob extract on rat C6 glioma cells through regulation of glycolysis, mitochondrial ROS, and apoptosis,” *Bio-medicine and Pharmacotherapy*, vol. 98, pp. 726–732, 2018.
- [25] E. Al-Sheddi, M. Al-Oqail, Q. Saquib et al., “Novel all trans-retinoic acid derivatives: cytotoxicity, inhibition of cell cycle progression and induction of apoptosis in human cancer cell lines,” *Molecules*, vol. 20, no. 5, pp. 8181–8197, 2015.
- [26] D. Chandra, K. V. Ramana, L. Wang, B. N. Christensen, A. Bhatnagar, and S. K. Srivastava, “Inhibition of fiber cell globulization and hyperglycemia-induced lens opacification by aminopeptidase inhibitor bestatin,” *Investigative Ophthalmology & Visual Science*, vol. 43, no. 7, pp. 2285–2292, 2002.
- [27] J. A. Buege and S. D. Aust, “Microsomal lipid peroxidation,” *Methods in Enzymology*, vol. 52, pp. 302–310, 1978.
- [28] M. A. Siddiqui, H. A. Alhadlaq, J. Ahmad, A. A. Al-Khedhairi, J. Musarrat, and M. Ahamed, “Copper oxide nanoparticles induced mitochondria mediated apoptosis in human hepatocarcinoma cells,” *PLoS One*, vol. 8, no. 8, article e69534, 2013.
- [29] M. M. Al-Oqail, E. S. Al-Sheddi, S. M. Al-Massarani et al., “*Nigella sativa* seed oil suppresses cell proliferation and induces ROS dependent mitochondrial apoptosis through p53 pathway in hepatocellular carcinoma cells,” *South African Journal of Botany*, vol. 112, pp. 70–78, 2017.
- [30] T. Mosmann, “Rapid colorimetric assay for cellular growth and survival: application to proliferation and cytotoxicity assays,” *Journal of Immunological Methods*, vol. 65, no. 1-2, pp. 55–63, 1983.
- [31] E. Borenfreund and J. A. Puerner, “Short-term quantitative in vitro cytotoxicity assay involving an S-9 activating system,” *Cancer Letters*, vol. 34, no. 3, pp. 243–248, 1987.
- [32] J. Weyermann, D. Lochmann, and A. Zimmer, “A practical note on the use of cytotoxicity assays,” *International Journal of Pharmaceutics*, vol. 288, no. 2, pp. 369–376, 2005.
- [33] R. Grigutyte, J. Nimptsch, L. Manusadzianas, and S. Pflugmacher, “Response of oxidative stress enzymes in charophyte *Nitellopsis obtusa* exposed to allochthonous leaf extracts from beech *Fagus sylvatica*,” *Biologija*, vol. 55, no. 3, pp. 142–149, 2009.
- [34] A. S. Abdullah, A. S. Mohammed, A. Rasedee, and M. Mirghani, “Oxidative stress-mediated apoptosis induced by ethanolic mango seed extract in cultured estrogen receptor positive breast cancer MCF-7 cells,” *International Journal of Molecular Sciences*, vol. 16, no. 2, pp. 3528–3536, 2015.
- [35] D. B. Zorov, M. Juhaszova, and S. J. Sollott, “Mitochondrial reactive oxygen species (ROS) and ROS-induced ROS release,” *Physiological Reviews*, vol. 94, no. 3, pp. 909–950, 2014.
- [36] H. Sauer, M. Wartenberg, and J. Hescheler, “Reactive oxygen species as intracellular messengers during cell growth and differentiation,” *Cellular Physiology and Biochemistry*, vol. 11, no. 4, pp. 173–186, 2001.
- [37] D. Xiao, X. Q. Hu, X. Huang et al., “Chronic hypoxia during gestation enhances uterine arterial myogenic tone via heightened oxidative stress,” *PLoS One*, vol. 8, no. 9, article e73731, 2013.
- [38] M. Karimi, F. Conserva, S. Mahmoudi, J. Bergman, K. G. Wiman, and V. J. Bykov, “Extract from Asteraceae *Brachylaena ramiflora* induces apoptosis preferentially in mutant p53-expressing human tumor cells,” *Carcinogenesis*, vol. 31, no. 6, pp. 1045–1053, 2010.
- [39] W. Ghali, D. Vaudry, T. Jouenne, and M. N. Marzouki, “Extracts from medicinal plants inhibit cancer cell proliferation, induce apoptosis in ovary, lung and neuronal cancer cell lines,” *Cancer & Metabolism*, vol. 2, article P21, Supplement 1, 2014.
- [40] M. J. Vallejo, L. Salazar, and M. Grijalva, “Oxidative stress modulation and ROS-mediated toxicity in cancer: a review on *in vitro* models for plant-derived compounds,” *Oxidative Medicine and Cellular Longevity*, vol. 2017, Article ID 4586068, 9 pages, 2017.
- [41] L. A. Sena and N. S. Chandel, “Physiological roles of mitochondrial reactive oxygen species,” *Molecular Cell*, vol. 48, no. 2, pp. 158–167, 2012.
- [42] G. Dewson and R. M. Kluck, “Mechanisms by which Bak and Bax permeabilise mitochondria during apoptosis,” *Journal of Cell Science*, vol. 122, no. 16, pp. 2801–2808, 2009.
- [43] J. Lee, S. Lee, S. L. Kim et al., “Corn silk maysin induces apoptotic cell death in PC-3 prostate cancer cells via mitochondria-dependent pathway,” *Life Sciences*, vol. 119, no. 1-2, pp. 47–55, 2014.

- [44] M. Toshiyuki and J. C. Reed, "Tumor suppressor p53 is a direct transcriptional activator of the human bax gene," *Cell*, vol. 80, no. 2, pp. 293–299, 1995.
- [45] S. Y. Lin, W. W. Lai, C. C. Ho et al., "Emodin induces apoptosis of human tongue squamous cancer SCC-4 cells through reactive oxygen species and mitochondria-dependent pathways," *Anticancer Research*, vol. 29, no. 1, pp. 327–335, 2009.
- [46] A. M. Abdel-Latif, H. A. Abuel-Ela, and S. H. El-Shourbagy, "Increased caspase-3 and altered expression of apoptosis-associated proteins, Bcl-2 and Bax in lichen planus," *Clinical and Experimental Dermatology*, vol. 34, no. 3, pp. 390–395, 2009.
- [47] T. R. Su, F. J. Tsai, J. J. Lin et al., "Induction of apoptosis by 11-dehydrosinulariolide via mitochondrial dysregulation and ER stress pathways in human melanoma cells," *Marine Drugs*, vol. 10, no. 12, pp. 1883–1898, 2012.

## Research Article

# Elevated H2AX Phosphorylation Observed with kINPen Plasma Treatment Is Not Caused by ROS-Mediated DNA Damage but Is the Consequence of Apoptosis

Sander Bekeschus <sup>1</sup>, Clarissa S. Schütz,<sup>1,2</sup> Felix Nießner,<sup>1</sup> Kristian Wende <sup>1</sup>,  
Klaus-Dieter Weltmann,<sup>1</sup> Nadine Gelbrich,<sup>2</sup> Thomas von Woedtke,<sup>1,3</sup> Anke Schmidt,<sup>1</sup>  
and Matthias B. Stope <sup>2</sup>

<sup>1</sup>ZIK plasmatis, Leibniz Institute for Plasma Science and Technology (INP Greifswald), Greifswald, Germany

<sup>2</sup>Department of Urology, Greifswald University Medical Center, Greifswald, Germany

<sup>3</sup>Institute for Hygiene and Environmental Medicine, Greifswald University Medical Center, Greifswald, Germany

Correspondence should be addressed to Sander Bekeschus; [sander.bekeschus@inp-greifswald.de](mailto:sander.bekeschus@inp-greifswald.de)

Received 24 May 2019; Revised 23 July 2019; Accepted 26 August 2019; Published 19 September 2019

Guest Editor: Rizwan Wahab

Copyright © 2019 Sander Bekeschus et al. This is an open access article distributed under the Creative Commons Attribution License, which permits unrestricted use, distribution, and reproduction in any medium, provided the original work is properly cited.

Phosphorylated histone 2AX ( $\gamma$ H2AX) is a long-standing marker for DNA double-strand breaks (DSBs) from ionizing radiation in the field of radiobiology. This led to the perception of  $\gamma$ H2AX being a general marker of direct DNA damage with the treatment of other agents such as low-dose exogenous ROS that unlikely act on cellular DNA directly. Cold physical plasma confers biomedical effects majorly via release of reactive oxygen and nitrogen species (ROS). *In vitro*, increase of  $\gamma$ H2AX has often been observed with plasma treatment, leading to the conclusion that DNA damage is a direct consequence of plasma exposure. However, increase in  $\gamma$ H2AX also occurs during apoptosis, which is often observed with plasma treatment as well. Moreover, it must be questioned if plasma-derived ROS can reach into the nucleus and still be reactive enough to damage DNA directly. We investigated  $\gamma$ H2AX induction in a lymphocyte cell line upon ROS exposure (plasma, hydrogen peroxide, or hypochlorous acid) or UV-B light. Cytotoxicity and  $\gamma$ H2AX induction was abrogated by the use of antioxidants with all types of ROS treatment but not UV radiation. H2AX phosphorylation levels were overall independent of analyzing either all nucleated cells or segmenting  $\gamma$ H2AX phosphorylation for each cell cycle phase. SB202190 (p38-MAPK inhibitor) and Z-VAD-FMK (pan-caspase inhibitor) significantly inhibited  $\gamma$ H2AX induction upon ROS but not UV treatment. Finally, and despite  $\gamma$ H2AX induction, UV but not plasma treatment led to significantly increased micronucleus formation, which is a functional read-out of genotoxic DNA DSBs. We conclude that plasma-mediated and low-ROS  $\gamma$ H2AX induction depends on caspase activation and hence is not the cause but consequence of apoptosis induction. Moreover, we could not identify lasting mutagenic effects with plasma treatment despite phosphorylation of H2AX.

## 1. Introduction

$\gamma$ H2AX is a recognized marker for DNA double-strand breaks (DSBs) in radiation biology [1]. Phosphorylation at serine139 of the histone 2AX occurs rapidly, and approximately 1% of all H2AX proteins are phosphorylated per gray irradiation via a molecular machinery [2]. Based on these findings in radiobiology,  $\gamma$ H2AX has been used as direct surrogate and correlate of DNA DSBs in a variety of studies test-

ing chemical and physical treatments, for example, in the field of oncology [3]. One novel physical treatment modality for the treatment of cancer is cold physical plasma [4]. Its antitumor effects on several types of tumor cells such as skin cancer have been shown *in vitro* and *in vivo* [5–7], and to a limited extent also in small patient cohorts [8]. Medical plasmas are multicomponent systems consisting of, e.g., electrons and ions, electric fields, and a multiplicity of different reactive oxygen and nitrogen species (ROS) [9].



ROS are the major component mediating biomedical effects of plasma treatment, at least *in vitro* [10–12]. Concomitant with plasma-induced cell death, many studies reported a phosphorylation of H2AX with different kinds of plasma sources and (tumor) cell types [13–19]. This led to the conclusion that plasma-derived ROS directly induce DNA damage. Yet, there are several pitfalls of this assumption. Firstly, plasma-derived ROS are not generated within the cells but reach them from the outside. Due to the charge as well as short lifetime of some of these species detected and quantified in plasma-treated liquids, and hence possibly in the vicinity of cells [20–22], only a fraction of the ROS is able to diffuse or being transported through the cell membrane directly. Secondly, once in the cytosol, there are abundant reaction partners including, for instance, peroxiredoxins (PRDX) to scavenge the ROS [23]. Thirdly, the remaining ROS would have to cross several membranes of the endoplasmic reticulum (ER) and ultimately the nucleus membrane to directly act on cellular DNA after—again—passing by several antioxidant proteins such as PRDX2 [24]. In the light of large distances (2–10  $\mu\text{m}$ ) that ROS would have to travel from the membrane to the nucleus, the direct action of plasma-derived ROS on cellular DNA denies the nature of ROS being reactive and short-lived. This also questions the conclusion that  $\gamma\text{H2AX}$  is an indicator of DNA DSBs arising from primary ROS derived from plasma treatment. Rather, a role of  $\gamma\text{H2AX}$  might be in marking DNA DSBs secondary to plasma treatment (e.g., due to apoptosis).  $\gamma\text{H2AX}$  was originally identified as an early event after the direct formation of DSBs. Now,  $\gamma\text{-H2AX}$  is considered to occur after the indirect formation of DSBs caused by cellular process such as DNA repair, replication, and/or transcription at sites of initial DNA damage such as oxidative bases, DNA adducts, single-strand breaks, cross-linking, and DNA photoproducts [25, 26].

In general,  $\gamma\text{H2AX}$  seems to fulfill pleiotropic roles in cell biology. For instance, low levels of  $\gamma\text{H2AX}$  are not associated with DNA DSBs [27]. Untreated cells are found to be positive for  $\gamma\text{H2AX}$  in the M phase of the cell cycle without being exposed to a DNA-damaging agent [28]. Decreased expression of the H2AX primarily leads to damage in the mitochondria [29]. The amount of  $\gamma\text{H2AX}$  in apoptotic cells also exceeds that of nonapoptotic cells by a factor of ten [30].  $\gamma\text{H2AX}$  also seems dispensable for the initial recognition of DNA breaks [31]. Finally, there is evidence that not only DNA DSBs but also ROS may be responsible for  $\gamma\text{H2AX}$  induction [32]. Mechanistically, it is known that while the serine/threonine kinase ataxia telangiectasia mutated (ATM) forms  $\gamma\text{H2AX}$  at DNA DSBs [33], the serine/threonine kinase ataxia telangiectasia and Rad3-related protein (ATR) have been also implicated in this process [34]. Interestingly, ATM does so by redox-sensitive thiols, so ATM activation is a marker of both oxidative stress and DNA DSBs [35].

In the light of these studies, we sought to study the role of plasma-derived ROS in  $\gamma\text{H2AX}$  induction. The lymphocyte cell line TK6 was treated with an atmospheric pressure argon plasma jet (kINPen) as ROS-source. The  $\gamma\text{H2AX}$  expression along with the amount of ROS, ROS scavengers, cell viability,

and an OECD- (Organization for Economic Co-operation and Development-) accredited genotoxicity (micronucleus) assay were investigated. We found that plasma but not UV-induced  $\gamma\text{H2AX}$  induction was dependent on apoptosis and caspase activation, making DNA damage marked via  $\gamma\text{H2AX}$  rather a consequence than the cause for plasma-induced cell death.

## 2. Materials and Methods

**2.1. Cell Culture.** Lymphocytes are the cell type most often used when investigating DNA damage [36]. Especially the human TK6 lymphocyte cell line has been widely utilized in genotoxicity studies [37, 38]. For this reason, we used TK6 (ATCC CRL-8015) cells, a p53-competent, human lymphoblast cell line. Cells were cultured in Roswell Park Memorial Medium without phenol red (RPMI1640; PanBioTech) supplemented with 10% fetal bovine serum, 2% glutamine, and 1% penicillin/streptomycin (all Sigma). All incubations were performed in cell culture conditions (CB210; Binder) at 37°C, 95% humidity, and 5% carbon dioxide. As ROS scavengers, catalase (cat; 20  $\mu\text{g}/\text{ml}$ ), glutathione (GSH; 1 mM), or superoxide dismutase (SOD; 100 U/ml) was used (all Sigma). As enzyme or signaling inhibitors, Z-VAD-FMK (R&D Biosciences), SB202190 (Sigma), KU55933 (SelleckChem), Ly294002 (Cell Signaling Technologies), wortmannin (InvivoGen), or SP600125 (Santa Cruz Biotechnology) was used at different concentrations and incubated with cells for 1 h prior ROS or UV treatment. Final concentrations for a selected choice of inhibitors were 1  $\mu\text{M}$  for KU55933, 1  $\mu\text{M}$  for SB202190, and 25  $\mu\text{M}$  for Z-VAD-FMK.

**2.2. Exposure of Cells to ROS, Cold Physical Plasma, or UV.** For all procedures,  $2.5 \times 10^5$  TK6 cells in 500  $\mu\text{l}$  of fully supplemented cell culture medium were added to wells of a 24-well plate (Sarstedt). For hydrogen peroxide ( $\text{H}_2\text{O}_2$ ; Sigma) treatment, the stock was diluted in double-distilled water, and a range of concentrations was tested initially. Final concentration for subsequent assays was 10  $\mu\text{M}$ . For hypochlorous acid (HOCl; Roth), the stock was diluted in double-distilled water, and a range of concentrations was tested initially. Final concentration for subsequent assays was 500  $\mu\text{M}$ . Plasma treatment was done using the atmospheric pressure argon plasma jet kINPen (neoplas tools) that expels various reactive agents (Figure 1(a)) as reported before [9]. Its biomedical effects were summarized recently [39]. The plasma source was operated at two standard liters per minute of argon gas (Air Liquide, purity 99.999%). Plasma treatment was performed in a highly standardized manner as shown previously [40]. Briefly, the plasma jet was attached to a computer-controlled xyz-table (CNC step), which hovered the plasma exactly over the center of each well for a predefined time and height. A range of treatment times was initially tested. Immediately after treatment, a predetermined amount of double-distilled water was added to the wells after plasma treatment to compensate for evaporation effects and to maintain isoosmolality. A treatment time of 10 s was used for subsequent experiments if not indicated otherwise. For exposure to UV light, a range of exposure

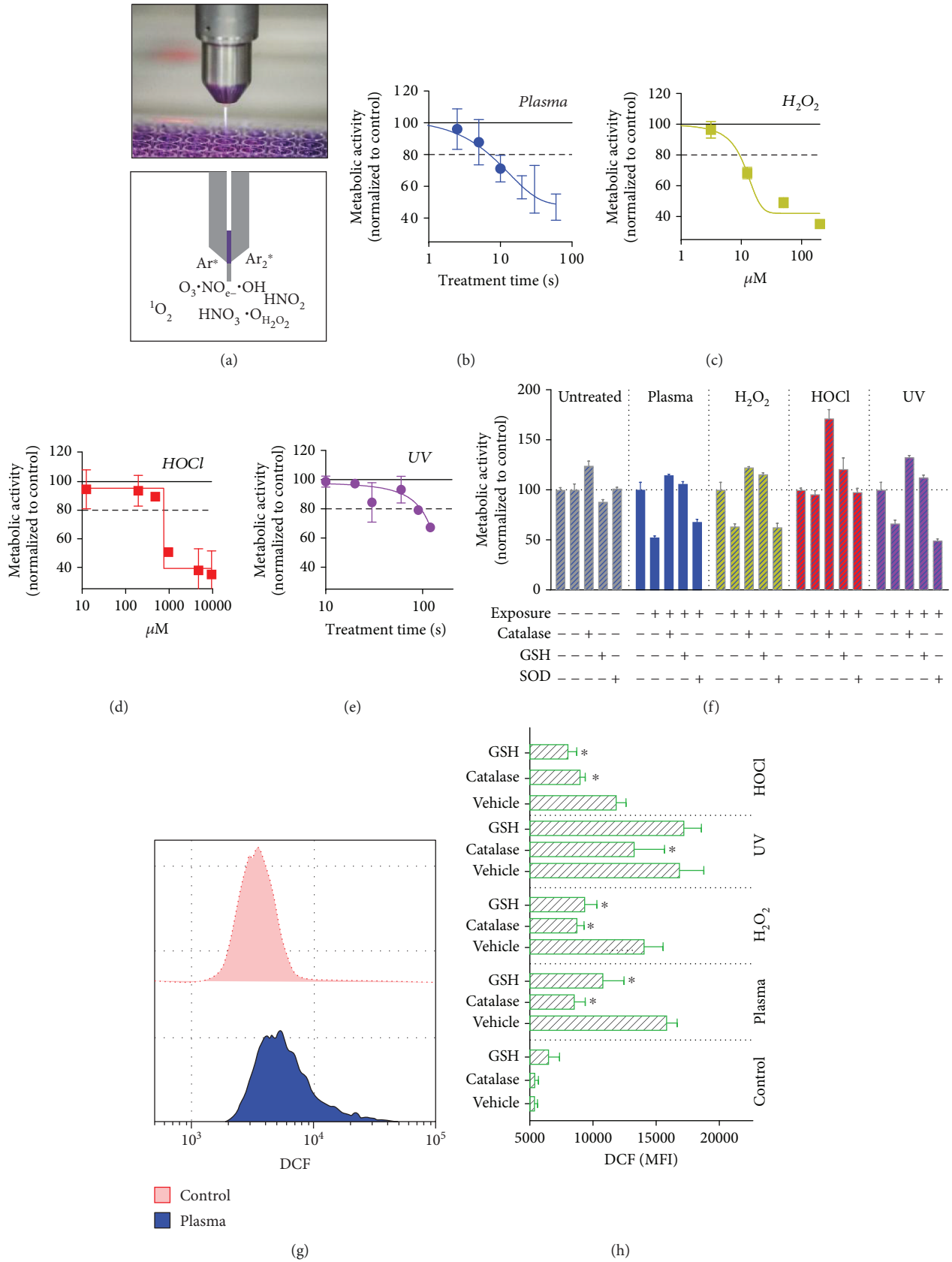


FIGURE 1: Continued.

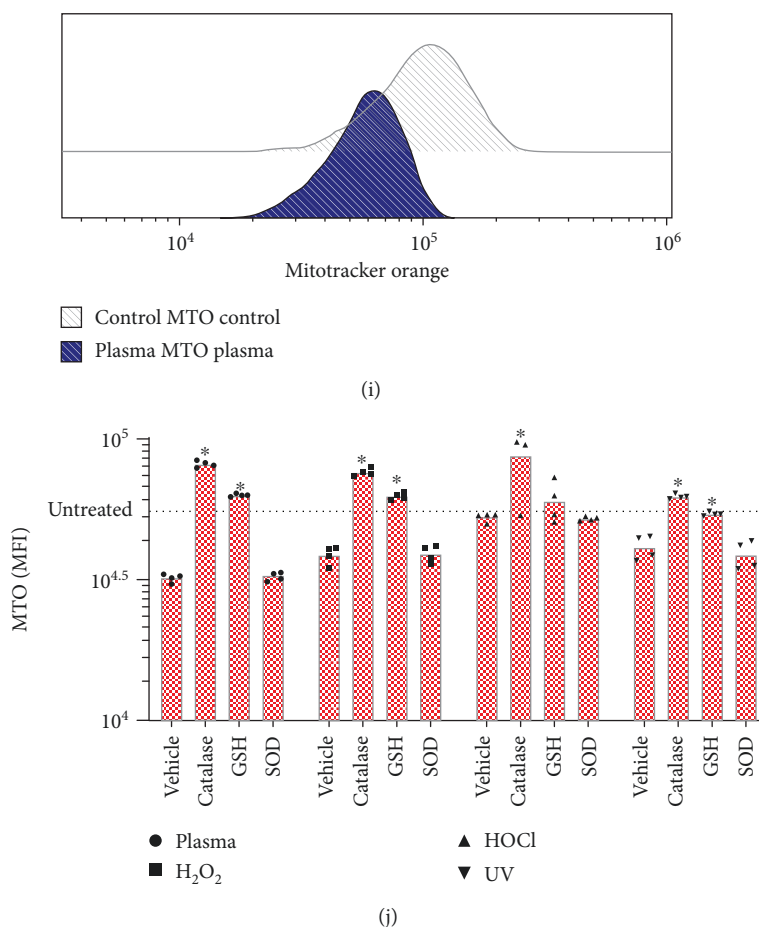


FIGURE 1: Metabolic activity and oxidation of TK6 cells after exposure to plasma,  $\text{H}_2\text{O}_2$ , HOCl, and UV. (a) Image (top) and scheme (bottom) with some of the products generated by the kINPen argon plasma jet. (b–e) Metabolic activity 6 h after exposure to different concentrations of ROS, or plasma or UV treatment times. (f) Effects of antioxidants or ROS scavenging enzymes on the metabolic activity of cells in responses to treatments after 6 h. (g) Overlay histogram of DCF fluorescence of control and plasma-treated cells. (h) Quantification of DCF fluorescence in cells immediately after treatment in the presence or absence of antioxidants. (i) Overlay histogram of mitotracker orange (MTO) in cells 6 h after plasma treatment. (j) Quantification of mitochondrial mass in cells exposed to various agents in the presence or absence of antioxidants. Data are mean + S.E. of 2–4 independent experiments with several replicates each. Statistical analysis (h, j) within each treatment group was done with one-way ANOVA and Dunnett's post hoc test to vehicle control.

times was tested, and 120 s was used for experiments if not indicated otherwise. The wells of the plate that were not intended to be exposed to UV light were covered with aluminum foil. A broadband UVB (20–160  $\text{J}_{\text{eff}} \text{m}^{-2}$ ) light source (Philips TL12 fluorescent lamp) emitting radiation between 290 and 315 nm was used. UVB exposure modifies DNA directly by forming cyclobutane pyrimidine dimers (CPD) and 6-4 photoproducts. Indirect effects of UVB on DNA occur due to photolysis and generation of hydroxyl radicals, leading to formation of 8-hydroxy-2'-deoxyguanosine (8-OhdG) [41].

**2.3. Intracellular Oxidation.** To assess intracellular oxidation, TK6 cells were stained with chloromethyl 2',7'-dichlorodihydrofluorescein diacetate (CM- $\text{H}_2\text{DCF-DA}$ ; final concentration 2.5  $\mu\text{M}$ ; Thermo Fisher) in phosphate-buffered saline (PBS), washed, and resuspended in fully supplemented cell culture medium (in the presence or absence of antioxi-

dants). Cells were seeded into plates and treated as described above. Immediately after, cells were added to  $12 \times 75$  mm tubes (Sarstedt) containing 4',6-diamidin-2-phenylindol (DAPI; final concentration 1  $\mu\text{M}$ ; Sigma), and samples were acquired by multicolor flow cytometry (Gallios, equipped with 405 nm, 488 nm, and 638 nm laser; Beckman Coulter). Sample analysis was performed using Kaluza 2.1.1 software (Beckman Coulter) and analyzing the mean fluorescence intensity (MFI) of DCF within the viable (DAPI-) cell fraction.

**2.4. Metabolic Activity, Mitochondrial Mass, and Viability.** Metabolic activity was investigated by incubating the cells for 4 h with resazurin (final concentration 100  $\mu\text{M}$ ; Alfa Aesar) after two hours of incubation posttreatment. Metabolically active cells transform nonfluorescent resazurin into fluorescent resorufin, which can be quantified using a multiplate reader (F200; Tecan) at  $\lambda_{\text{ex}}$  560 nm and  $\lambda_{\text{em}}$  590 nm. Absolute sample values were normalized to that of untreated

cells = 100%. To quantify mitochondrial mass, cells were incubated for 15 min with chloromethyltetramethylrosamine, also called MitoTracker Orange (MTO; final concentration 1  $\mu$ M; Thermo Fisher), at 6 h after plasma treatment. The cationic rosamine probe only binds to mitochondrial membranes with intact potential. Sample acquisition was performed using flow cytometry. To quantify nonterminally dead (alive) and terminally dead cells, DAPI was used to discriminate the percentage of either population using flow cytometry. For some experiments, the amount of cells active for caspase 3 and 7 was investigated to quantify the amount of apoptotic cells. For this, cells were incubated for 30 min with CellEvent dye (final concentration 2.5  $\mu$ M; Thermo Fisher). Samples were analyzed by flow cytometry.

**2.5. Analysis of Cell Cycle and  $\gamma$ H2AX.** Flow cytometry is the most sensitive, quantitative, and informative method of analyzing and quantifying  $\gamma$ H2AX in cells, as it can be related to cell cycle and other cellular populations stained with additional markers [36]. To prepare the cells for DNA and  $\gamma$ H2AX staining, cells were harvested 2 h after exposure to agents into 12  $\times$  75 mm tubes. In an initial kinetic experiment, 2 h was shown to be optimal. Cells were washed with PBS and fixed with  $-20^{\circ}\text{C}$  methanol for 30 min at  $4^{\circ}\text{C}$ . Cells were washed and incubated with murine phosphor-specific anti- $\gamma$ H2AX antibodies (BioLegend) for 20 min. The optimal antibody dilution was determined experimentally. Cells were washed and incubated with DAPI (10  $\mu$ M) and an anti-mouse IgG1 antibody conjugated to Alexa Fluor 647 (Thermo Fisher) for 20 min in permeabilization wash buffer (BioLegend) in the dark. Cells were washed and resuspended in PBS and acquired by flow cytometry. Gating of cells was performed as shown. Appropriate gating of the DAPI-area vs. DAPI-width parameters for cell cycle analysis was confirmed with Michael H. Fox algorithm integrated into Kaluza analysis software. If the algorithm could not calculate G1, S, and G2 phase properly, the gating was adjusted accordingly. This way,  $\gamma$ H2AX induction could be accurately calculated in relation to mathematical modeling for each cell cycle phase. A total of more than 1,800 single FACS measurements was prepared, stained, and individually acquired in this study. Each measurement contained at least 20,000 single cells, yielding quantitative single cell data. To analyze  $\gamma$ H2AX foci via laser scanning confocal microscopy (TP5; Leica), cells were stained as described above and added to 8-well glass slides (Ibidi). Fluorescence was acquired using excitation at 405 nm for DAPI and 640 nm for Alexa Fluor 647.

**2.6. Quantification of Micronuclei.** The cytokinesis-block micronucleus (MN) assay requires quantification of micronuclei in binucleated cells (BNCs) only [42]. Cells were treated as described above with minor changes and incubated for 24 h. As additional genotoxic positive control, the DNA-damaging agent methyl methanesulfonate (MMS; final concentration 20 ng/ml; Sigma) was added. The plasma treatment time was reduced from 10 s to 2.5 s as the plasma treatment acted synergistically toxic together with cytochalasin B, leading to insufficient cell counts. Similar observations were made for UV treatment, which was reduced from 120 s to

24 s. Ten wells were pooled into T75 flasks (Sarstedt) per condition, and cytochalasin B (final concentration 5  $\mu$ g/ml; Sigma) was added. Flasks were incubated for another 24 h. Cells were collected into 15 ml tubes (Sarstedt), washed, fixed with 4% fixation buffer (BioLegend) for 20 min, and washed and stored at  $4^{\circ}\text{C}$  in PBS until staining. For staining, cells were washed and stained in permeabilization wash buffer (BioLegend) containing draq5 (final concentration 50  $\mu$ M; BioLegend) for 20 min at room temperature in the dark. Other DNA staining dyes were also compared (SYTOX green, final concentration 1  $\mu$ M, Thermo Fisher; DAPI, final concentration 10  $\mu$ M, Sigma; Hoechst 33342, final concentration 10  $\mu$ g/ml, Sigma) but found to be less suitable. Cells were washed in permeabilization wash buffer and resuspended in PBS in siliconized 1.5 ml tubes. Speed beads (Merck Millipore) were used to operate the imaging fluids of an ImageStream ISX Mark II (Merck Millipore), which was used for sample acquisition. Up to  $2 \times 10^5$  cells (images) were acquired per sample. The digital MN analysis was in main parts similar as reported before [43], with some minor modifications in mask design and gating steps. A total of more than 40 Mio single cells—each represented by at least two individual images of about  $200 \times 200$  pixels in size—were acquired and partly analyzed in this study.

**2.7. Statistical Analysis.** Data were analyzed and graphed using Prism 8.1 (GraphPad software). Mean and standard error (S.E.) were given if not indicated otherwise. Statistical analysis was performed either using one-way analysis of variances or *t*-test.

### 3. Results

**3.1. Viability and Oxidation upon Exposure to Plasma,  $\text{H}_2\text{O}_2$ , HOCl, and UV Light.** In order to obtain ROS concentrations and UV exposure times as well as plasma treatment times that were neither too toxic nor failed to show effects on cells, dilution and treatment time series were performed, respectively. From these, we concluded to use 10 s of plasma treatment (Figure 1(b)), 10  $\mu$ M of  $\text{H}_2\text{O}_2$  (Figure 1(c)), 500  $\mu$ M of HOCl (Figure 1(d)), and 120 s of UV treatment (Figure 1(e)) in viability experiments assayed 6 h after exposure for subsequent experiments. Data for metabolic activity were in principal similar for longer incubation times (Supplementary Figure S1a). Terminally dead cells at 6 h posttreatment were also quantified (Supplementary Figure S1b). Next, it was tested whether antioxidant agents and enzymes protected cells 6 h postagent-induced toxicity (Figure 1(f)). While catalase (cat) and glutathione (GSH) conferred protection, superoxide dismutase (SOD) did not. To confirm that this finding was related to protection from ROS, cells were stained with CM- $\text{H}_2\text{DCF-DA}$ , which after intracellular modifications fluoresces upon oxidation with, e.g., plasma treatment (Figure 1(g)). Indeed, GSH and cat significantly protected cells from oxidation with plasma,  $\text{H}_2\text{O}_2$ , and HOCl treatment (Figure 1(h)). For UV exposure, only cat but not GSH conferred protection. This might be due to UV radiation directly oxidizing DCFH-DA. In lymphocytes, ROS-induced toxicity leads

to depolarization of the mitochondrial membrane potential  $\Delta\Psi_m$  [44], which allows the quantification of mitochondria with intact  $\Delta\Psi_m$  using appropriate dyes (Figure 1(i)). The agents decreased the total amount of mitochondria with intact  $\Delta\Psi_m$ , while cat and GSH but not SOD protected from insult (Figure 1(j)). Presence of cat even led to higher values, suggesting the growth-supporting activity of antioxidant enzymes. In summary, the ROS agents and UV radiation oxidized the cells leading to mitochondrial damage and reduction of metabolic activity and viability.

**3.2. Induction of  $\gamma$ H2AX Depended on ROS but Not of Cell Cycle Phase.** To quantify  $\gamma$ H2AX in cells, a rigid flow cytometric gating strategy was set up. Cells were gated based on time (Figure 2(a)) and forward and side scatter properties (Figure 2(b)) followed by exclusion of doublets, aggregates, and subG1 cells (Figure 2(c)).  $\gamma$ H2AX was quantified in singlets (Figure 2(d)). Alternatively,  $\gamma$ H2AX was determined per cell cycle phase, which was validated using Michael H. Fox algorithms (Figure 2(e)). For each phase, a separate gating was applied (Figure 2(f)), from which the number (% gated) and intensity (mean fluorescence intensity of % gated) was calculated (Figure 2(g)). Staining was performed using appropriate antibody dilutions (Supplementary Figure S1c) at 2 h posttreatment (Supplementary Figure S1d) and was confirmed using confocal laser scanning microscopy (Figure 2(h)).  $\gamma$ H2AX foci are formed within seconds, but since they are initially quite small, reliable quantification is recommended earliest at 30 min after initial insult [45]. A prominent  $\gamma$ H2AX induction was observed with plasma and UV treatment and to a lesser extent with  $H_2O_2$  and HOCl exposure (Figure 2(i)). This difference may be explained by slight ( $H_2O_2$ ) and larger (HOCl) differences of the oxidants to induce cytotoxic effects as compared to those seen with plasma (Figures 1(f) and 1(j)). The reason might have been a change of TK6 sensitivity between the initial titration (Figures 1(b) and 1(c)) and subsequent experiment due to passage number. Strikingly, antioxidants (GSH and cat) significantly reduced  $\gamma$ H2AX induction for plasma and  $H_2O_2$  treatment. For UV treatment, it was significantly enhanced. Similar observations were made when analyzing  $\gamma$ H2AX induction for each phase of the cell cycle (Figure 2(j)). In general, G1 cells gave lower signals compared to S and G2 phase cells, and the increase observed with antioxidants in UV conditions was evenly proportional for each cell cycle phase. Notably, cat and GSH had no effect on  $\gamma$ H2AX induction in resting (untreated) cells for each cell cycle phase (Supplementary Figure S1e). By contrast, the antioxidant N-acetylcysteine (NAC) increased  $\gamma$ H2AX induction in untreated as well as treated cells (Supplementary Figure S1f). With reference to cell cycle phase-dependent  $\gamma$ H2AX intensity (Figure 2(j)), another question was whether there was a relatively higher increase in proliferating (S and G2 phase) cells. These cells have intrinsically more DSBs and unwinded DNA, which could make them more prone to ROS-induced DNA damage. It was observed that the opposite was the case, as  $\gamma$ H2AX intensity in S over G1 and G2 over G1 was

overall significantly lower compared to those of untreated control cells (Supplementary Figure 1g). Altogether,  $\gamma$ H2AX showed a major increase in plasma-treated cells, which was almost fully abrogated in presence of cat or GSH during the treatment.

**3.3. Intracellular Signaling and Apoptosis Govern Plasma-Induced  $\gamma$ H2AX.** The next question was to investigate intracellular signaling events upon plasma-induced H2AX phosphorylation. Many pathways leading to  $\gamma$ H2AX have been unraveled [36], and we used several inhibitors in preliminary tests (Supplementary Figure S2a–f). One promising candidate was SB202190, a p38-MAPK inhibitor, which gave a significant decrease in  $\gamma$ H2AX induction for all ROS but not for UV treatment (Figure 3(a)). Similar results were achieved with Z-VAD-FMK, a pan-caspase inhibitor (Figure 3(b)), but only a no-significant reduction was observed with KU59933 for plasma conditions (Supplementary Figure 2g), an ataxia telangiectasia mutated (ATM) inhibitor. This suggests that plasma-induced  $\gamma$ H2AX induction is a result of apoptosis induction rather than of plasma-derived ROS directly traveling through the cells and eventually to the nucleus to confer DNA damage. To confirm functionality of Z-VAD-FMK on inhibiting apoptosis, we measured caspase 3 and 7 activity (Figure 2(c)). Quantification at 4 h (Figure 2(d)) and 24 h (Figure 2(e)) revealed a significant increase in nonapoptotic cells with all treatment modalities. The fact that UV-induced apoptosis but not H2AX phosphorylation was abrogated with Z-VAD-FMK suggests that  $\gamma$ H2AX induction was regulated by pathways not related to apoptosis, which was not the case for ROS conditions. Finally, using confocal laser scanning microscopy, we confirmed that  $\gamma$ H2AX foci were majorly present in apoptotic cells showing fragmented nuclei (Figure 3(f)). Taken together, plasma and ROS but not UV-induced  $\gamma$ H2AX was largely dependent on stress (p38-MAPK) and apoptosis (caspase) signaling pathways.

**3.4. Plasma-Mediated  $\gamma$ H2AX Induction Does Not Correlate to DNA DSB-Related Micronuclei.** To confirm that plasma and ROS-induced  $\gamma$ H2AX foci were a consequence of ROS-induced stress signaling and apoptosis-induced DNA DSBs rather than markers of direct ROS-induced DNA DSBs, we performed a functional assay on DNA DSBs, the cytokinesis-block micronucleus (MN) assay. Sufficient numbers of DNA DSBs lead to replication errors during DNA synthesis in G2 phase cells, which converts into micronuclei formation as genotoxic endpoint measurement [46]. The addition of cytochalasin B blocks cytoplasmic division due to inhibition of network formation of actin filaments. The result is an enrichment of binucleated (G2 phase) cells (BNCs) that can be quantitatively assessed with different DNA stains (Supplementary Figure 3a). Imaging (Supplementary Figure 3b) and quantification of BNCs (Supplementary Figure 3c) confirmed this principle, and we decided to use draq5 for subsequent experiments. Another observation was that the plasma and UV treatment time utilized in experiments were too toxic in combination with

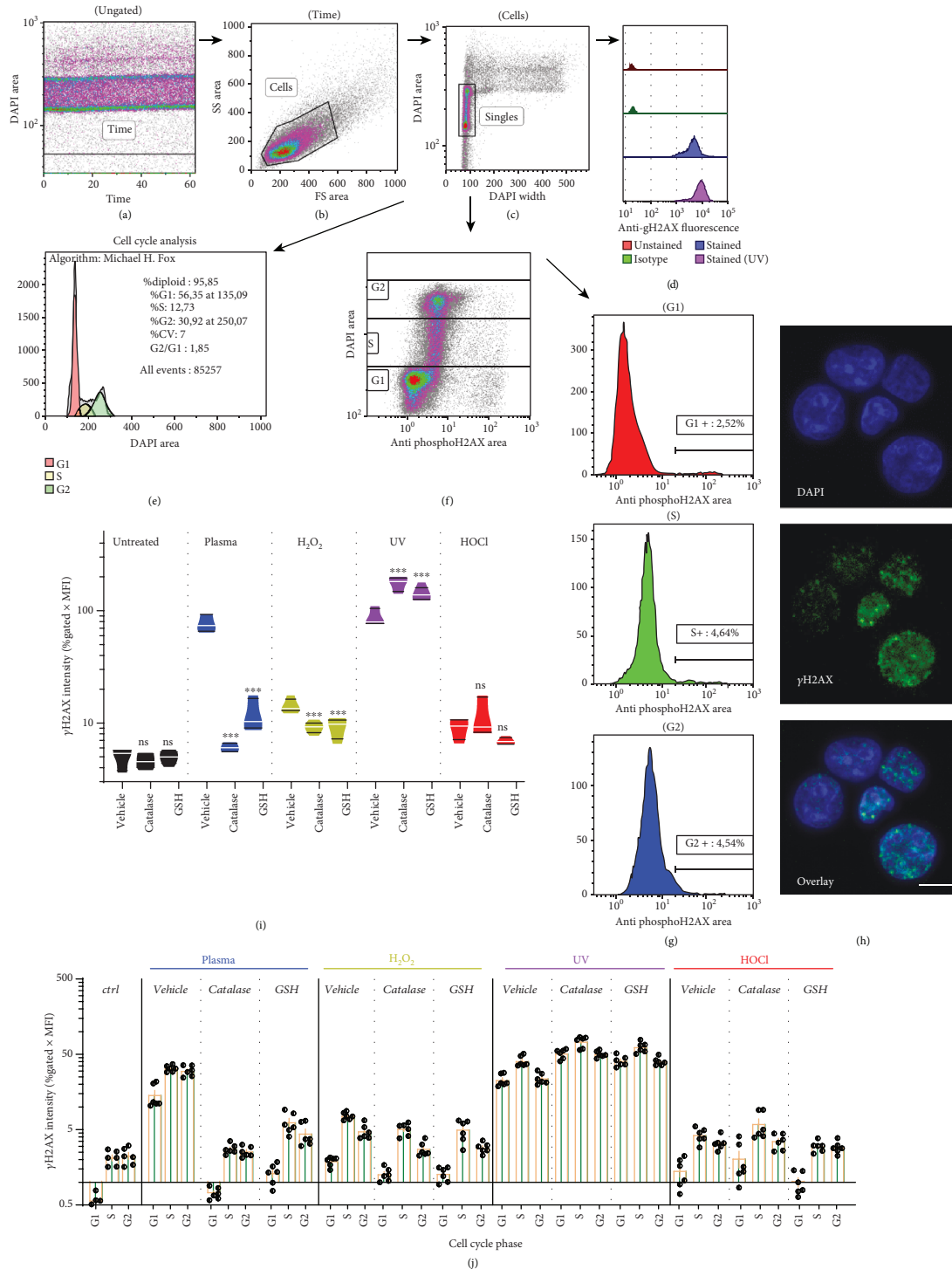


**FIGURE 2:** Analysis of  $\gamma$ H2AX in TK6 cells and its relation to ROS. (a–c) Gating strategy of TK6 cells at 2 h after treatment with agents was done by first including cells in time (a) and forward (FS) and side scatter (SS) cell gate (b), before excluding doublets and subG1 cells for the singles gate (c). (d–e) Singles were then analyzed for total  $\gamma$ H2AX as exemplified with representative fluorescence histogram overlay (d), subjected to algorithm-driven cell cycle analysis (e), or manually gated for each cell cycle phase (f) and subsequent determination of  $\gamma$ H2AX<sup>hi</sup> cells in histograms (g). (h) Confirmation of  $\gamma$ H2AX foci (green) in DAPI-stained nuclei (blue) by confocal laser scanning microscopy. (i) Quantification of total (independent of cell cycle phase)  $\gamma$ H2AX with treatments and presence or absence of antioxidants. (j) Quantification of total  $\gamma$ H2AX within each cell cycle phase at 2 h after treatment with agents in the presence or absence of antioxidants. Quantification (i, j) was done by multiplying the percent of cells positive for  $\gamma$ H2AX (% gated) with the mean fluorescent intensity (MFI) of  $\gamma$ H2AX<sup>+</sup> cells. Data show violin plots (i) or single values and mean  $\pm$  S.E. (j) of three independent experiments with duplicates each. Statistical analysis (i) within each treatment group was done with one-way ANOVA and Dunnett post hoc test to vehicle control. Scale bar (h) is 10  $\mu$ m; ns = not significant.

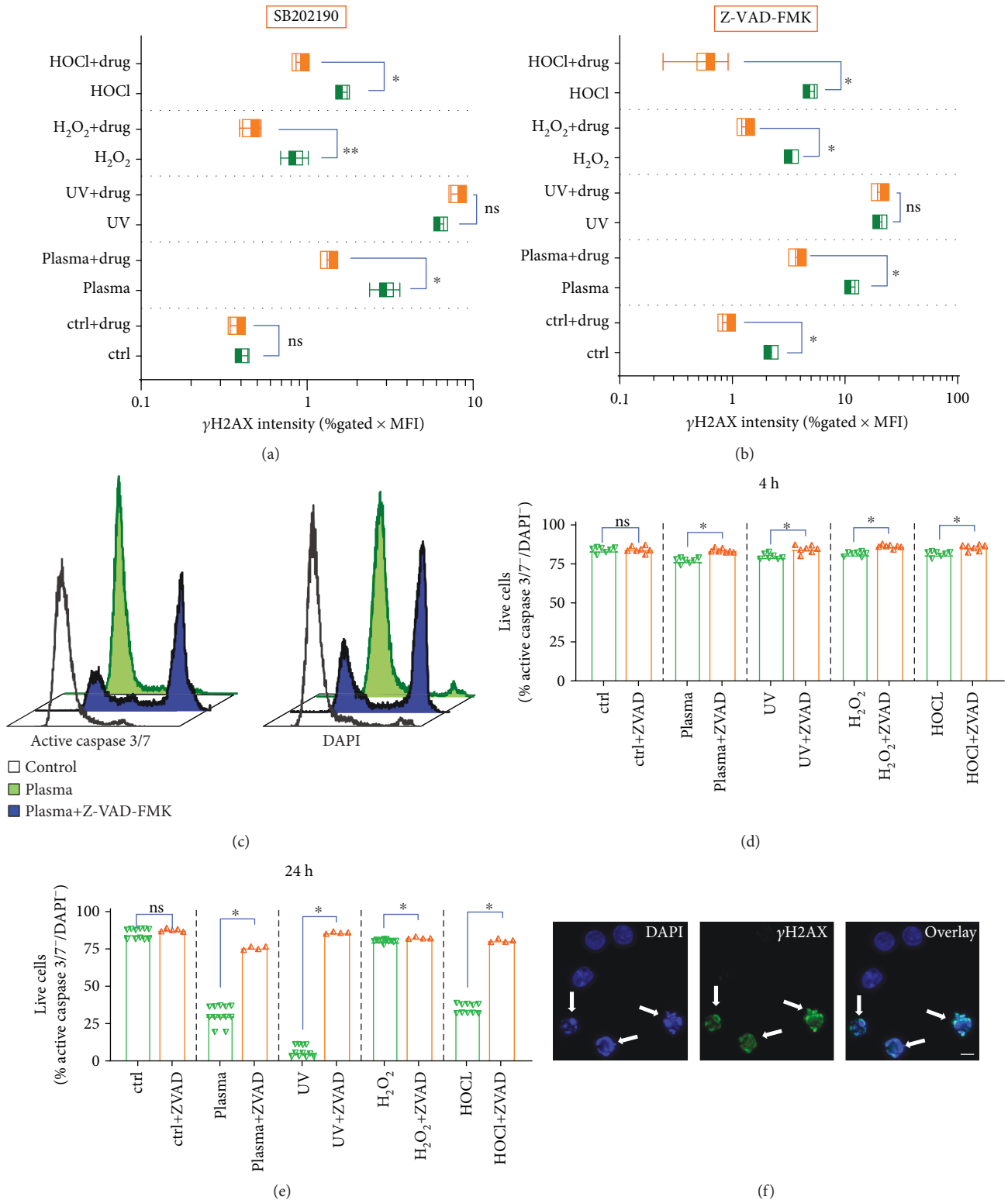


FIGURE 3: Dependence of ROS and UV-induced  $\gamma$ H2AX expression on intracellular signaling and apoptosis. (a, b)  $\gamma$ H2AX expression in cells preincubated with (a) SB202190 (p38 MAPK-inhibitor) or (b) Z-VAD-FMK (pan-caspase inhibitor) 2 h after exposure to various agents. (c) Representative overlay histograms of active caspase 3/7-stain (left) and terminally dead DAPI<sup>+</sup> (right) in presence or absence of Z-VAD-FMK at 24 h after plasma treatment. (d–e) Quantification of apoptosis in presence or absence of Z-VAD-FMK at (d) 4 h and (e) 24 h after plasma treatment with  $\gamma$ H2AX-inducing agents. (f) Confocal laser scanning microscopy (DNA = DAPI, blue;  $\gamma$ H2AX = green) of TK6 cells with arrows pointing at apoptotic (cells with fragmented nuclei) cells being positive for  $\gamma$ H2AX. Data show box plots (a, b) and single data and mean (d, e) of two to four independent experiments with several replicates each. Statistical analysis was done using *t*-test. Scale bar (f) is 10  $\mu$ m; n.s. = not significant.

cytochalasin B, leaving only few cells to analyze at 48 h posttreatment. Therefore, plasma and UV treatment time was reduced to 2.5 s and 24 s, respectively, which still generated significantly more  $\gamma$ H2AX signal compared to untreated control (Figures 4(a) and 4(b)). By applying customized mathematical operands, several masks were developed to clearly identify and quantify BNCs as well as MN within the population of BNCs in an algorithm-based, unbiased fashion (Figure 4(c)) across millions of cells. Final analysis showed a significant increase in MN formation with UV but not plasma treatment. A chemical genotoxic agent (MMS) was installed as additional control in this experiment, which differed significantly from untreated cells (Figure 4(d)). As additional quality control, the average number of cells analyzed in these experiments was quantified and was similar among all conditions (Supplementary Figure 3d). In sum, MN formation correlated with  $\gamma$ H2AX induction for UV treatment, which directly acts on cellular DNA, but not for plasma treatment, which acts on cells by generating exogenous ROS that subsequently diffuse to cells to exert their stress and apoptosis-inducing but not directly DNA-damaging function.

#### 4. Discussion

DNA damage and the DNA damage response are important elements in medical treatment modalities, such as radiation therapy and chemotherapeutic drugs in several medical fields including in oncology [3]. For example, the anticancer drug doxorubicin can both induce DNA DSBs and generate ROS, leading to  $\gamma$ H2AX induction [47–49]. Cell metabolism, oxidative stress, and DNA damage are often intertwined and difficult to study independently, leading to the general assumption of  $\gamma$ H2AX foci being a hallmark of DNA DSBs and damage. We here provide evidence that exogenous ROS added experimentally or generated with cold physical plasmas led to  $\gamma$ H2AX induction only in case of apoptosis, and without long-term genotoxic effects. In such setting, the presence of  $\gamma$ H2AX may be a consequence of low oxidative stress rather than an indicator of DNA damage. Recent data suggest  $\gamma$ H2AX to even play in pivotal role in antioxidant defense signaling [50]. H2AX-knockout cells showed increase endogenous ROS levels and failed to activate the antioxidant response elements through nuclear factor E2-related factor 2, Nrf2 [51], along with mitochondrial damage [29].

In our study, we used UV-B radiation as positive control for  $\gamma$ H2AX and micronuclei induction. In contrast to exogenous ROS (plasma,  $H_2O_2$ , or HOCl), occurrence of  $\gamma$ H2AX was independent of the use of antioxidants and maximum in S-phase cells. The latter corroborates previous findings, where also a repression of  $\gamma$ H2AX induction with PI3K inhibition using 5 mM of caffeine was found [52]. We did not find such decrease with PI3K inhibitors wortmannin and Ly294002, which may be due to different cell types and concentrations tested. Another study found ATR kinase to be the crucial determinant for UV-induced H2AX phosphorylation and confirmed our findings of maximum  $\gamma$ H2AX induction

at 2 h after treatment prior to onset of intermediate stages of apoptosis where  $\gamma$ H2AX dramatically increases [53]. The ability of UV-B enhancing the frequency of MN in cells has been reported before [54, 55]. Interestingly, catalase decreased oxidation in UV-treated cells but not H2AX phosphorylation. UV generates ROS in the intracellular as well as extracellular compartment [56]. As the experimentally added catalase only acts in the extracellular compartment, a partial protection from oxidation was observed without protecting the DNA (intracellular compartment) from UV-mediated ROS and damage.

With exogenous ROS (plasma,  $H_2O_2$ , HOCl), we observed a strong dependence on p38-MAPK signaling and caspase activation in TK6 cells. This is in line with previous findings using oxaliplatin, an antitumor drug leading to DNA DSBs, where pretreatment of cells with SB202190 (p38-MAPK inhibitor) and Z-VAD-FMK (caspase inhibitor) abrogated oxaliplatin-induced  $\gamma$ H2AX induction and apoptosis in HCT116 cells [57]. In leukemia cells, it was reported that  $\gamma$ H2AX (or blockage of H2AX phosphorylation by SB202190) expression sensitizes cells to apoptosis, suggesting a pivotal role of  $\gamma$ H2AX in cell death signaling [58]. This is supported by findings with H2AX-knockout fibroblasts, which upon UV treatment activates caspase 3 but cannot activate caspase-activated DNase (CAD), a crucial step in DNA fragmentation required for apoptosis [59]. Another form of regulated cell death (RCD) leading to widespread DNA fragmentation is parthanatos, but this mode of RCD is independent of apoptotic caspases [60]. Hence, parthanatos is not a main mechanism in our study because we observed apoptosis-induced and caspase-dependent DNA fragmentation. Hence,  $\gamma$ H2AX is heavily intertwined in cell death signaling and our study supports this notion as caspase inhibition abrogated both H2AX phosphorylation and apoptosis.

Heavy H2AX phosphorylation indicates toxic numbers of DNA DSBs in, e.g., ionizing radiation, UV treatment, replication, and apoptosis. Contrasting radiation-induced DNA DSBs, we found  $\gamma$ H2AX to be a consequence of ROS-induced apoptosis rather than its cause. T lymphocytes are very sensitive towards (plasma-induced) oxidative stress [61–64]. This is due to (low-dose) ROS acting as proapoptotic and redox-signaling agents and not as toxic molecules *per se* [65]. In our study, e.g., few micromolar  $H_2O_2$  on 250,000 cells were sufficient to induce cell death. The concentrations of, e.g.,  $H_2O_2$  used in many genotoxicity studies are 10–50-fold higher at lower absolute cell numbers [66–68]. So far, only few studies in plasma medicine investigated genotoxicity in cells and tissues using non- $\gamma$ H2AX assays, and the once that have did not report mutagenic effects of plasma treatment. Using the hypoxanthine-guanine phosphoribosyl-transferase (HPRT) assay and the MN assay in V79 cells, plasma treatment failed to induce mutagenic effects when exposing cells to the plasma of the kINPen or its products [69], or when using another plasma source designed for medical application at microbicidal concentrations [70, 71]. Modulation of the feed gas composition of the kINPen yielded similar results [43]. Micronuclei have also been quantified *in vivo*



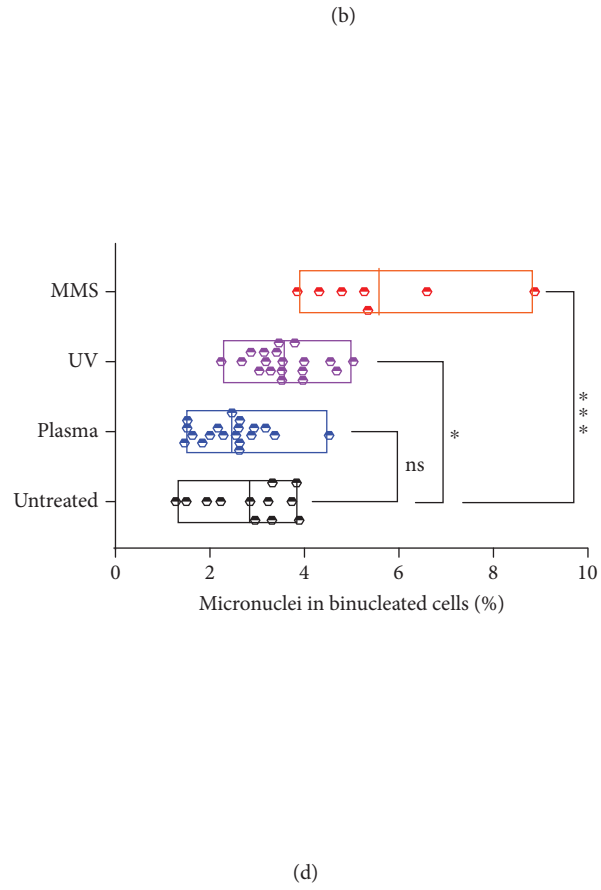
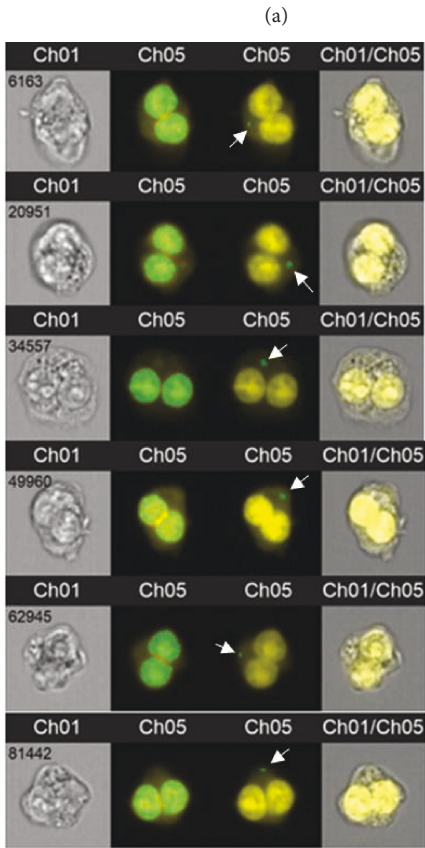
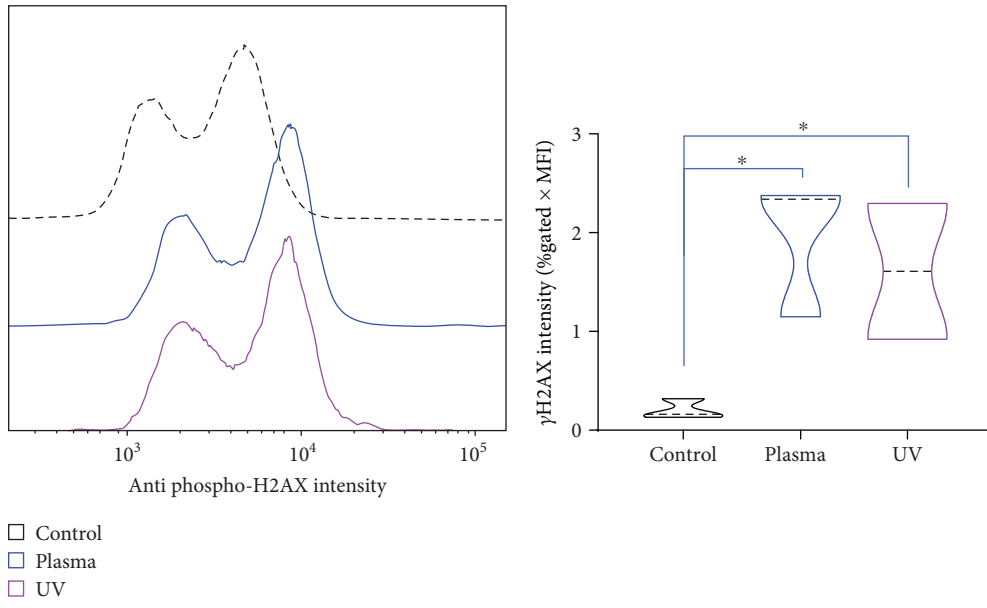


FIGURE 4: Correlation of  $\gamma$ H2AX expression and micronuclei formation. (a, b) Representative histogram overlay  $\gamma$ H2AX fluorescence (a) and its quantification (b) in control as well as plasma and UV-treated cells. (c) Representative images (left: brightfield, right: overlay) of high-throughput imaging cytometry of TK6 cells to analyze draq5-stained nuclei (yellow) with masks for binucleated cells (middle left large green overlays) and micronuclei (middle right small green overlays with white arrows). (d) Quantification of micronuclei in binucleated TK6 cells that were left untreated or exposed to plasma, UV light, or methyl methanesulfonate (MMS). Data are from two (b) and three to four (d) independent experiments with several replicates each. Data show violin plots (b) and min-to-max floating bars (d). Statistical analysis was done with one-way ANOVA.

in the hen's egg model after treatment with cyclophosphamide or methotrexate (as positive control), or cold physical plasma generated with the kINPen. Results showed the absence of genotoxicity-indicating MN with plasma treatment compared to positive controls [72]. In human tissue exposed to cold physical plasma at short, intermediate, and long treatment times, an increase of  $\gamma$ H2AX was not observed when compared to untreated control tissue [73]. Moreover, in a one-year follow-up of mice (human equivalent of 65 years) treated six times with plasma within 2 weeks, no occurrence of malignant lesions was observed anywhere in the body as shown by immunohistochemistry and PET-CT and MRI scan [74].

ROS can also induce lipid peroxidation [75], which can contribute to DNA damage. However, for  $H_2O_2$ —which gave large  $\gamma$ H2AX signals—concentration reported for lipid peroxidation exceeds the one used in our study by 50-fold [76]. For lipid vesicles,  $H_2O_2$  is ineffective in the absence of the Fenton reaction [77], even at concentration 5000 times of that used in our work [78]. For  $H_2O_2$  treatment in our study, caspase inhibition decreased  $H_2O_2$ -induced  $\gamma$ H2AX to background levels, which argues against  $H_2O_2$ -induced lipid peroxidation as major mechanism for DNA DSBs. Moreover, if lipid peroxidation would have contributed to plasma-induced DNA damage, e.g., via UV-mediated photolysis and hydroxyl radical generation, addition of catalase would not have abrogated the increase observed in  $\gamma$ H2AX.

Our results are of relevance for medical plasmas, while findings may be different for industrial plasma applications. Atmospheric and room temperature plasma (ARTP) has been recently described as tool for mutation breeding in microorganisms [79–81]. Its efficacy seemed greater than that of several conventional methods, e.g., chemicals and UV radiation [82], and ARTP can also be combined with such methods [83]. As result, ARTP was found to increase production of, for instance,  $\alpha$ -ketoglutaric acid [84], biofuel [85], polysaccharides [86, 87], arachidonic acid [88], erythritol [89], l-arginine [90], alkaline  $\alpha$ -amylase [91, 92], d-lactic acid [93], lycopene [94], and carotenoids and lipids [95] in different types of microorganisms. However, it is important to mention that these plasma sources are not intended for medical applications. Hence, they may differ substantially in their geometry and power consumption, leading to enhanced UV radiation, ROS generation, and electrical discharges. In our study, we used a low-energy [96] and clinically effective [8, 97, 98] plasma jet complying to European regulations (e.g., generation of ozone, UV, and leak currents), which is not true for the majority of other plasma devices reported in experimental studies.

A limitation of our study is the lack of short-term kinetic measurements of  $\gamma$ H2AX and (onset of) apoptosis. Moreover,  $\gamma$ H2AX foci expand over time [99], making it difficult to distinguish between many foci with low intensity vs. few foci with high intensity (and anything in between) in our flow cytometry data. Additionally, other proteins including Nbs1, 53BP1, and Brca1 are recruited to and hence mark DNA DSBs [31], which may be investigated in future studies.

## 5. Conclusion

Cold physical plasma-induced  $\gamma$ H2AX marks DNA DSBs as a consequence of oxidative stress and apoptosis *in vitro*. Upon blocking apoptosis and p38 MAPK signaling, increased  $\gamma$ H2AX with plasma treatment was abolished, arguing that H2AX phosphorylation is a secondary event in redox or apoptotic signaling rather than a primary consequence of direct ROS-mediated DNA damage. In contrast to UV treatment, exposure to plasma did not correlate with long-lasting genotoxic effects as indicated using the micronucleus assay. Hence,  $\gamma$ H2AX measurements in plasma medical research should be interpreted with care, keeping in mind the pleiotropic roles of this molecule in redox sensing and apoptotic pathways.

## Data Availability

The data used to support the findings of this study are available from the corresponding author upon request.

## Conflicts of Interest

The authors declare that there is no conflict of interest regarding the publication of this paper.

## Acknowledgments

This work was funded by the German Federal Ministry of Education and Research (BMBF), grant numbers 03Z22DN11 and 03Z22DN12. C.S.S. received funding from the Gerhard-Domagk Foundation.

## Supplementary Materials

Supplementary Figure S1: (a) metabolic activity in TK6 cells at 24 h, 48 h, and 72 h after exposure to  $\gamma$ H2AX-inducing agents; (b) quantification of nonterminally dead (DAPI-) TK6 cells at 6 h after exposure to different concentrations or treatment times of  $\gamma$ H2AX-inducing agents; (c) dilution series of anti- $\gamma$ H2AX antibody in control and UV-treated TK6 cells to obtain optimal antibody concentration; (d) kinetic experiment of  $\gamma$ H2AX intensity in control or plasma and UV-treated TK6 cells; (e)  $\gamma$ H2AX intensity in each cell cycle phase of untreated cells incubated with vehicle, catalase, and GSH; (f) incubation with antioxidant NAC increased  $\gamma$ H2AX intensity with all treatments as well as in untreated cells and therefore was not used in this study. Supplementary Figure S2: serial dilutions of inhibitors. (a) SB202190 (p38-MAPK inhibitor) was used in the study (Figure 3(a)); (b) SP600125 (JNK inhibitor) disqualified due to the increase of  $\gamma$ H2AX in untreated cells upon incubation with the drug; (c) Ly294002 (PI3K inhibitor) did not decrease  $\gamma$ H2AX in plasma-treated cells; (d) wortmannin (PI3K inhibitor) disqualified due to the increase of  $\gamma$ H2AX in untreated cells upon incubation with the drug; (e) Z-VAD-FMK (pan-caspase inhibitor) was used in the study (Figure 3(b)); (f) KU55933 (ATM-kinase inhibitor) showed a small decrease in  $\gamma$ H2AX, which (g) was not significant with any treatment in three independent repeats. Supplementary Figure S3:

optimization of the micronucleus assay. (a) cell cycle analysis of untreated and treated (cytochalasin B for 24h) TK6 cells with different DNA-binding dyes; (b) representative images of cells in brightfield (Ch05 or Ch01) and DNA-binding dye (Ch1 or Ch5) showing binucleated cells (BNCs); (c) quantification of binucleated cells stained with four different DNA-binding dyes via a complex software algorithm designed to create a specific set of masks to BNCs as described before [1], we aimed at a low amount of BNCs to obtain a high specificity for micronuclei leading to the choice of draql5 for main experiments; (d) mean total count of cells in samples from each condition. (*Supplementary Materials*)

## References

- [1] S. H. Macphail, J. P. Ban ath, T. Y. Yu, E. H. M. Chu, H. Lambur, and P. L. Olive, "Expression of phosphorylated histone H2AX in cultured cell lines following exposure to X-rays," *International Journal of Radiation Biology*, vol. 79, no. 5, article 12943243, pp. 351–359, 2003.
- [2] E. P. Rogakou, D. R. Pilch, A. H. Orr, V. S. Ivanova, and W. M. Bonner, "DNA double-stranded breaks induce histone H2AX phosphorylation on serine 139," *Journal of Biological Chemistry*, vol. 273, no. 10, pp. 5858–5868, 1998.
- [3] L.-J. Mah, A. El-Osta, and T. C. Karagiannis, " H2AX: a sensitive molecular marker of DNA damage and repair," *Leukemia*, vol. 24, no. 4, pp. 679–686, 2010.
- [4] D. Yan, J. H. Sherman, and M. Keidar, "Cold atmospheric plasma, a novel promising anti-cancer treatment modality," *Oncotarget*, vol. 8, no. 9, pp. 15977–15995, 2017.
- [5] S. Bekeuschus, K. Rodder, B. Fregin et al., "Toxicity and immunogenicity in murine melanoma following exposure to physical plasma-derived oxidants," *Oxidative Medicine and Cellular Longevity*, vol. 2017, Article ID 4396467, 12 pages, 2017.
- [6] A. Lin, Y. Gorbanev, J. de Backer et al., "Non-thermal plasma as a unique delivery system of short-lived reactive oxygen and nitrogen species for immunogenic cell death in melanoma cells," *Advanced Science*, vol. 6, no. 6, p. 1802062, 2019.
- [7] G. Pasqual-Melo, R. K. Gandhirajan, I. Stoffels, and S. Bekeuschus, "Targeting malignant melanoma with physical plasmas," *Clinical Plasma Medicine*, vol. 10, pp. 1–8, 2018.
- [8] H.-R. Metelmann, C. Seebauer, V. Miller et al., "Clinical experience with cold plasma in the treatment of locally advanced head and neck cancer," *Clinical Plasma Medicine*, vol. 9, pp. 6–13, 2018.
- [9] S. Reuter, T. von Woedtke, and K. D. Weltmann, "The kIN-Pen—a review on physics and chemistry of the atmospheric pressure plasma jet and its applications," *Journal of Physics D: Applied Physics*, vol. 51, no. 23, p. 233001, 2018.
- [10] S. Bekeuschus, J. Kolata, C. Winterbourn et al., "Hydrogen peroxide: a central player in physical plasma-induced oxidative stress in human blood cells," *Free Radical Research*, vol. 48, no. 5, pp. 542–549, 2014.
- [11] K. P. Arjunan, G. Friedman, A. Fridman, and A. M. Clyne, "Non-thermal dielectric barrier discharge plasma induces angiogenesis through reactive oxygen species," *Journal of The Royal Society Interface*, vol. 9, no. 66, pp. 147–157, 2012.
- [12] D. B. Graves, "The emerging role of reactive oxygen and nitrogen species in redox biology and some implications for plasma applications to medicine and biology," *Journal of Physics D: Applied Physics*, vol. 45, no. 26, p. 263001, 2012.
- [13] S. Arndt, E. Wacker, Y. F. Li et al., "Cold atmospheric plasma, a new strategy to induce senescence in melanoma cells," *Experimental Dermatology*, vol. 22, no. 4, pp. 284–289, 2013.
- [14] J. W. Chang, S. U. Kang, Y. S. Shin et al., "Non-thermal atmospheric pressure plasma induces apoptosis in oral cavity squamous cell carcinoma: Involvement of DNA-damage-triggering sub-G1 arrest via the ATM/p53 pathway," *Arch Biochem Biophys*, vol. 545, pp. 133–140, 2014.
- [15] F. Jud e, C. Fongia, B. Ducommun, M. Yousfi, V. Lobjois, and N. Merbahi, "Short and long time effects of low temperature plasma activated media on 3D multicellular tumor spheroids," *Scientific Reports*, vol. 6, no. 1, 2016.
- [16] N. Kaushik, N. Uddin, G. B. Sim et al., "Responses of solid tumor cells in DMEM to reactive oxygen species generated by non-thermal plasma and chemically induced ROS systems," *Scientific Reports*, vol. 5, no. 1, 2015.
- [17] J. M. Plewa, M. Yousfi, C. Frongia et al., "Low-temperature plasma-induced antiproliferative effects on multi-cellular tumor spheroids," *New Journal of Physics*, vol. 16, no. 4, 2014.
- [18] S. K. Sagwal, G. Pasqual-Melo, Y. Bodnar, R. K. Gandhirajan, and S. Bekeuschus, "Combination of chemotherapy and physical plasma elicits melanoma cell death via upregulation of SLC22A16," *Cell Death & Disease*, vol. 9, no. 12, 2018.
- [19] R. Sensenig, S. Kalghatgi, E. Cerchar et al., "Non-thermal plasma induces apoptosis in melanoma cells via production of intracellular reactive oxygen species," *Annals of Biomedical Engineering*, vol. 39, no. 2, pp. 674–687, 2011.
- [20] H. Jablonowski, J. Santos Sousa, K. D. Weltmann, K. Wende, and S. Reuter, "Quantification of the ozone and singlet delta oxygen produced in gas and liquid phases by a non-thermal atmospheric plasma with relevance for medical treatment," *Scientific Reports*, vol. 8, no. 1, p. 12195, 2018.
- [21] H. Jablonowski, A. Schmidt-Bleker, K. D. Weltmann, T. von Woedtke, and K. Wende, "Non-touching plasma-liquid interaction - where is aqueous nitric oxide generated?," *Physical Chemistry Chemical Physics*, vol. 20, no. 39, pp. 25387–25398, 2018.
- [22] H. Jablonowski and T. von Woedtke, "Research on plasma medicine-relevant plasma-liquid interaction: what happened in the past five years?," *Clinical Plasma Medicine*, vol. 3, no. 2, pp. 42–52, 2015.
- [23] M. B. Hampton and K. M. O'Connor, "Peroxiredoxins and the regulation of cell death," *Molecules and Cells*, vol. 39, no. 1, pp. 72–76, 2016.
- [24] C. Gu, J. Luo, X. Lu et al., "REV7 confers radioresistance of esophagus squamous cell carcinoma by recruiting PRDX2," *Cancer Science*, vol. 110, no. 3, pp. 962–972, 2019.
- [25] W. M. Bonner, C. E. Redon, J. S. Dickey et al., " H2AX and cancer," *Nature Reviews Cancer*, vol. 8, no. 12, pp. 957–967, 2008.
- [26] O. A. Sedelnikova, C. E. Redon, J. S. Dickey, A. J. Nakamura, A. G. Georgakilas, and W. M. Bonner, "Role of oxidatively induced DNA lesions in human pathogenesis," *Mutation Research/Reviews in Mutation Research*, vol. 704, no. 1–3, pp. 152–159, 2010.
- [27] P. Rybak, A. Hoang, L. Bujnowicz et al., "Low level phosphorylation of histone H2AX on serine 139 ( H2AX) is not associated with DNA double-strand breaks," *Oncotarget*, vol. 7, no. 31, pp. 49574–49587, 2016.

- [28] Y. Ichijima, R. Sakasai, N. Okita, K. Asahina, S. Mizutani, and H. Teraoka, "Phosphorylation of histone H2AX at M phase in human cells without DNA damage response," *Biochemical and Biophysical Research Communications*, vol. 336, no. 3, pp. 807–812, 2005.
- [29] J. H. Jeong, Y. Cheol Kang, Y. Piao, S. Kang, and Y. K. Pak, "miR-24-mediated knockdown of H2AX damages mitochondria and the insulin signaling pathway," *Experimental & Molecular Medicine*, vol. 49, no. 4, p. e313, 2017.
- [30] T. Tanaka, X. Huang, H. D. Halicka et al., "Cytometry of ATM activation and histone H2AX phosphorylation to estimate extent of DNA damage induced by exogenous agents," *Cytometry Part A*, vol. 71A, no. 9, pp. 648–661, 2007.
- [31] A. Celeste, O. Fernandez-Capetillo, M. J. Kruhlak et al., "Histone H2AX phosphorylation is dispensable for the initial recognition of DNA breaks," *Nature Cell Biology*, vol. 5, no. 7, pp. 675–679, 2003.
- [32] M. A. Kang, E. Y. So, A. L. Simons, D. R. Spitz, and T. Ouchi, "DNA damage induces reactive oxygen species generation through the H2AX-Nox1/Rac1 pathway," *Cell Death & Disease*, vol. 3, no. 1, p. e249, 2012.
- [33] S. Burma, B. P. Chen, M. Murphy, A. Kurimasa, and D. J. Chen, "ATM phosphorylates histone H2AX in response to DNA double-strand breaks," *Journal of Biological Chemistry*, vol. 276, no. 45, pp. 42462–42467, 2001.
- [34] B. Mukherjee, C. Kessinger, J. Kobayashi et al., "DNA-PK phosphorylates histone H2AX during apoptotic DNA fragmentation in mammalian cells," *DNA Repair*, vol. 5, no. 5, pp. 575–590, 2006.
- [35] Z. Guo, R. Deshpande, and T. T. Paull, "ATM activation in the presence of oxidative stress," *Cell Cycle*, vol. 9, no. 24, pp. 4805–4811, 2010.
- [36] A. Sharma, K. Singh, and A. Almasan, "Histone H2AX phosphorylation: a marker for DNA damage," *Methods in Molecular Biology*, vol. 920, pp. 613–626, 2012.
- [37] M. Lukamowicz, M. Kirsch-Volders, W. Suter, and A. Elhajouji, "In vitro primary human lymphocyte flow cytometry based micronucleus assay: simultaneous assessment of cell proliferation, apoptosis and MN frequency," *Mutagenesis*, vol. 26, no. 6, pp. 763–770, 2011.
- [38] M. Lukamowicz, K. Woodward, M. Kirsch-Volders, W. Suter, and A. Elhajouji, "A flow cytometry based in vitro micronucleus assay in TK6 cells-Validation using early stage pharmaceutical development compounds," *Environmental and Molecular Mutagenesis*, vol. 52, no. 5, pp. 363–372, 2011.
- [39] S. Bekeschus, A. Schmidt, K.-D. Weltmann, and T. von Woedtke, "The plasma jet kINPen – a powerful tool for wound healing," *Clinical Plasma Medicine*, vol. 4, no. 1, pp. 19–28, 2016.
- [40] S. Bekeschus, A. Schmidt, F. Niessner, T. Gerling, K. D. Weltmann, and K. Wende, "Basic research in plasma medicine - a throughput approach from liquids to cells," *Journal of Visualized Experiments*, no. 129, 2017.
- [41] A. Budiayanto, N. U. Ahmed, A. Wu et al., "Protective effect of topically applied olive oil against photocarcinogenesis following UVB exposure of mice," *Carcinogenesis*, vol. 21, no. 11, pp. 2085–2090, 2000.
- [42] M. Kirsch-Volders, G. Plas, A. Elhajouji et al., "The in vitro MN assay in 2011: origin and fate, biological significance, protocols, high throughput methodologies and toxicological relevance," *Archives of Toxicology*, vol. 85, no. 8, pp. 873–899, 2011.
- [43] S. Bekeschus, A. Schmidt, A. Kramer et al., "High throughput image cytometry micronucleus assay to investigate the presence or absence of mutagenic effects of cold physical plasma," *Environmental and Molecular Mutagenesis*, vol. 59, no. 4, pp. 268–277, 2018.
- [44] S. Bekeschus, T. von Woedtke, A. Kramer, K.-D. Weltmann, and K. Masur, "Cold physical plasma treatment alters redox balance in human immune cells," *Plasma Medicine*, vol. 3, no. 4, pp. 267–278, 2013.
- [45] M. Lobrich, A. Shibata, A. Beucher et al., "γH2AX foci analysis for monitoring DNA double-strand break repair: Strengths, limitations and optimization," *Cell Cycle*, vol. 9, no. 4, pp. 662–669, 2010.
- [46] G. P. Watters, D. J. Smart, J. S. Harvey, and C. A. Austin, "H2AX phosphorylation as a genotoxicity endpoint," *Mutation Research/Genetic Toxicology and Environmental Mutagenesis*, vol. 679, no. 1-2, pp. 50–58, 2009.
- [47] E. U. Kurz, P. Douglas, and S. P. Lees-Miller, "Doxorubicin activates ATM-dependent phosphorylation of multiple downstream targets in part through the generation of reactive oxygen species," *Journal of Biological Chemistry*, vol. 279, no. 51, pp. 53272–53281, 2004.
- [48] S. Zhang, X. Liu, T. Bawa-Khalife et al., "Identification of the molecular basis of doxorubicin-induced cardiotoxicity," *Nature Medicine*, vol. 18, no. 11, pp. 1639–1642, 2012.
- [49] P. K. Singal and N. Iliskovic, "Doxorubicin-induced cardiomyopathy," *New England Journal of Medicine*, vol. 339, no. 13, pp. 900–905, 1998.
- [50] A. Schmidt, S. Bekeschus, K. Jarick, S. Hasse, T. von Woedtke, and K. Wende, "Cold physical plasma modulates p53 and mitogen-activated protein kinase signaling in keratinocytes," *Oxidative Medicine and Cellular Longevity*, vol. 2019, Article ID 7017363, 16 pages, 2019.
- [51] U. Weyemi, B. D. Paul, A. M. Snowman et al., "Histone H2AX deficiency causes neurobehavioral deficits and impaired redox homeostasis," *Nature Communications*, vol. 9, no. 1, 2018.
- [52] H. D. Halicka, X. Huang, F. Traganos, M. A. King, W. Dai, and Z. Darzynkiewicz, "Histone H2AX phosphorylation after cell irradiation with UV-B: relationship to cell cycle phase and induction of apoptosis," *Cell Cycle*, vol. 4, no. 2, pp. 338–344, 2004.
- [53] S. Hanasoge and M. Ljungman, "H2AX phosphorylation after UV irradiation is triggered by DNA repair intermediates and is mediated by the ATR kinase," *Carcinogenesis*, vol. 28, no. 11, pp. 2298–2304, 2007.
- [54] D. Bettega, P. Calzolari, L. Doneda, F. Belloni, L. Tallone, and J. L. Redpath, "Differential effectiveness of solar UVB subcomponents in causing cell death, oncogenic transformation and micronucleus induction in human hybrid cells," *International Journal of Radiation Biology*, vol. 79, no. 3, pp. 211–216, 2003.
- [55] A. Ferahbas, H. Donmez-Altuntas, Z. Hamurcu, E. Aktas, and S. Utas, "Micronucleus evaluation in mitogen-stimulated lymphocytes of narrow-band (311 nm TL01) UVB-treated patients," *Photodermatology, Photoimmunology and Photomedicine*, vol. 20, no. 2, pp. 81–85, 2004.
- [56] T. Herrling, K. Jung, and J. Fuchs, "Measurements of UV-generated free radicals/reactive oxygen species (ROS) in skin," *Spectrochimica Acta Part A: Molecular and Biomolecular Spectroscopy*, vol. 63, no. 4, pp. 840–845, 2006.

- [57] S. J. Chiu, J. I. Chao, Y. J. Lee, and T. S. Hsu, "Regulation of gamma-H2AX and securin contribute to apoptosis by oxaliplatin via a p38 mitogen-activated protein kinase-dependent pathway in human colorectal cancer cells," *Toxicology Letters*, vol. 179, no. 2, pp. 63–70, 2008.
- [58] Y. Dong, M. Xiong, L. Duan et al., "H2AX phosphorylation regulated by p38 is involved in Bim expression and apoptosis in chronic myelogenous leukemia cells induced by imatinib," *Apoptosis*, vol. 19, no. 8, pp. 1281–1292, 2014.
- [59] C. Lu, F. Zhu, Y. Y. Cho et al., "Cell apoptosis: requirement of H2AX in DNA ladder formation, but not for the activation of caspase-3," *Molecular Cell*, vol. 23, no. 1, pp. 121–132, 2006.
- [60] L. Galluzzi, I. Vitale, S. A. Aaronson et al., "Molecular mechanisms of cell death: recommendations of the Nomenclature Committee on Cell Death 2018," *Cell Death & Differentiation*, vol. 25, no. 3, pp. 486–541, 2018.
- [61] L. Bundscherer, K. Wende, K. Ottmuller et al., "Impact of non-thermal plasma treatment on MAPK signaling pathways of human immune cell lines," *Immunobiology*, vol. 218, no. 10, pp. 1248–1255, 2013.
- [62] S. Bekeschus, J. Kolata, A. Muller et al., "Differential viability of eight human blood mononuclear cell subpopulations after plasma treatment," *Plasma Medicine*, vol. 3, no. 1-2, pp. 1–13, 2013.
- [63] L. Bundscherer, S. Bekeschus, H. Tresp et al., "Viability of human blood leukocytes compared with their respective cell lines after plasma treatment," *Plasma Medicine*, vol. 3, no. 1-2, pp. 71–80, 2013.
- [64] S. Bekeschus, K. Rödter, A. Schmidt et al., "Cold physical plasma selects for specific T helper cell subsets with distinct cells surface markers in a caspase-dependent and NF- $\kappa$ B-independent manner," *Plasma Processes and Polymers*, vol. 13, no. 12, pp. 1144–1150, 2016.
- [65] P. S. Hole, J. Zabkiewicz, C. Munje et al., "Overproduction of NOX-derived ROS in AML promotes proliferation and is associated with defective oxidative stress signaling," *Blood*, vol. 122, no. 19, pp. 3322–3330, 2013.
- [66] D. Slamenova, K. Kozics, L. Hunakova, M. Melusova, J. Navarova, and E. Horvathova, "Comparison of biological processes induced in HepG2 cells by tert-butyl hydroperoxide (t-BHP) and hydroperoxide (H<sub>2</sub>O<sub>2</sub>): the influence of carvacrol," *Mutation Research/Genetic Toxicology and Environmental Mutagenesis*, vol. 757, no. 1, pp. 15–22, 2013.
- [67] N. M. Machado, A. B. Ribeiro, H. D. Nicolella et al., "Usnic acid attenuates genomic instability in Chinese hamster ovary (CHO) cells as well as chemical-induced preneoplastic lesions in rat colon," *Journal of Toxicology and Environmental Health, Part A*, vol. 82, no. 6, pp. 401–410, 2019.
- [68] J. Feruszova, P. Imreova, K. Bodnarova et al., "Photoactivated hypericin is not genotoxic," *General physiology and biophysics*, vol. 35, no. 02, pp. 223–230, 2016.
- [69] K. Wende, S. Bekeschus, A. Schmidt et al., "Risk assessment of a cold argon plasma jet in respect to its mutagenicity," *Mutation Research/Genetic Toxicology and Environmental Mutagenesis*, vol. 798–799, pp. 48–54, 2016.
- [70] V. Boxhammer, Y. F. Li, J. Koritzer et al., "Investigation of the mutagenic potential of cold atmospheric plasma at bactericidal dosages," *Mutation Research/Genetic Toxicology and Environmental Mutagenesis*, vol. 753, no. 1, pp. 23–28, 2013.
- [71] T. Maisch, A. K. Bosserhoff, P. Unger et al., "Investigation of toxicity and mutagenicity of cold atmospheric argon plasma," *Environmental and Molecular Mutagenesis*, vol. 58, no. 3, pp. 172–177, 2017.
- [72] S. Kluge, S. Bekeschus, C. Bender et al., "Investigating the mutagenicity of a cold argon-plasma jet in an HET-MN model," *PLoS One*, vol. 11, no. 9, 2016.
- [73] S. Hasse, O. Hahn, S. Kindler, T. von Woedtke, H.-R. Metelmann, and K. Masur, "Atmospheric pressure plasma jet application on human oral mucosa modulates tissue regeneration," *Plasma Medicine*, vol. 4, no. 1-4, pp. 117–129, 2014.
- [74] A. Schmidt, T. Woedtke, J. Stenzel et al., "One year follow-up risk assessment in SKH-1 mice and wounds treated with an argon plasma jet," *International Journal of Molecular Sciences*, vol. 18, no. 4, p. 868, 2017.
- [75] E. E. Farmer and M. J. Mueller, "ROS-mediated lipid peroxidation and RES-activated signaling," *Annual Review of Plant Biology*, vol. 64, no. 1, pp. 429–450, 2013.
- [76] K. Kannan and S. K. Jain, "Effect of vitamin B<sub>6</sub> on oxygen radicals, mitochondrial membrane potential, and lipid peroxidation in H<sub>2</sub>O<sub>2</sub>-treated U937 monocytes," *Free Radical Biology and Medicine*, vol. 36, no. 4, pp. 423–428, 2004.
- [77] G. Minotti and S. D. Aust, "The requirement for iron (III) in the initiation of lipid peroxidation by iron (II) and hydrogen peroxide," *J Biol Chem*, vol. 262, pp. 1098–1104, 1987.
- [78] M. Iqbal, Y. Okazaki, and S. Okada, "In vitro curcumin modulates ferric nitrilotriacetate (Fe-NTA) and hydrogen peroxide (H<sub>2</sub>O<sub>2</sub>)-induced peroxidation of microsomal membrane lipids and DNA damage," *Teratogenesis, Carcinogenesis, and Mutagenesis*, vol. 23, no. S1, pp. 151–160, 2003.
- [79] X. Zhang, X. F. Zhang, H. P. Li et al., "Atmospheric and room temperature plasma (ARTP) as a new powerful mutagenesis tool," *Applied Microbiology and Biotechnology*, vol. 98, no. 12, pp. 5387–5396, 2014.
- [80] C. Ottenheim, M. Nawrath, and J. C. Wu, "Microbial mutagenesis by atmospheric and room-temperature plasma (ARTP): the latest development," *Bioresources and Bioprocessing*, vol. 5, no. 1, 2018.
- [81] M. Fang, L. Jin, C. Zhang et al., "Rapid mutation of *Spirulina platensis* by a new mutagenesis system of atmospheric and room temperature plasmas (ARTP) and generation of a mutant library with diverse phenotypes," *PLoS One*, vol. 8, no. 10, p. e77046, 2013.
- [82] X. Zhang, C. Zhang, Q. Q. Zhou et al., "Quantitative evaluation of DNA damage and mutation rate by atmospheric and room-temperature plasma (ARTP) and conventional mutagenesis," *Applied Microbiology and Biotechnology*, vol. 99, no. 13, pp. 5639–5646, 2015.
- [83] B. Zhao, Y. Li, C. Li, H. Yang, and W. Wang, "Enhancement of Schizochytrium DHA synthesis by plasma mutagenesis aided with malonic acid and zeocin screening," *Applied Microbiology and Biotechnology*, vol. 102, no. 5, pp. 2351–2361, 2018.
- [84] W. Zeng, G. Du, J. Chen, J. Li, and J. Zhou, "A high-throughput screening procedure for enhancing  $\alpha$ -ketoglutaric acid production in *Yarrowia lipolytica* by random mutagenesis," *Process Biochemistry*, vol. 50, no. 10, pp. 1516–1522, 2015.
- [85] F. Qi, Y. Kitahara, Z. Wang, X. Zhao, W. Du, and D. Liu, "Novel mutant strains of *Rhodospiridium toruloides* by plasma mutagenesis approach and their tolerance for inhibitors in lignocellulosic hydrolyzate," *Journal of Chemical Technology & Biotechnology*, vol. 89, no. 5, pp. 735–742, 2014.
- [86] B. Liu, Z. Sun, X. Ma et al., "Mutation breeding of extracellular polysaccharide-producing microalga *Cryptocodium cohnii*

- by a novel mutagenesis with atmospheric and room temperature plasma,” *International Journal of Molecular Sciences*, vol. 16, no. 12, pp. 8201–8212, 2015.
- [87] L. Zhu, D. Wu, H. Zhang et al., “Effects of atmospheric and room temperature plasma (ARTP) mutagenesis on physico-chemical characteristics and immune activity in vitro of *Hericium erinaceus* polysaccharides,” *Molecules*, vol. 24, no. 2, p. 262, 2019.
- [88] X. Li, R. Liu, J. Li et al., “Enhanced arachidonic acid production from *Mortierella alpina* combining atmospheric and room temperature plasma (ARTP) and diethyl sulfate treatments,” *Bioresource Technology*, vol. 177, pp. 134–140, 2015.
- [89] X. Liu, J. Lv, J. Xu et al., “Erythritol production by *Yarrowia lipolytica* mutant strain M53 generated through atmospheric and room temperature plasma mutagenesis,” *Food Science and Biotechnology*, vol. 26, no. 4, pp. 979–986, 2017.
- [90] G. Cheng, J. Xu, X. Xia et al., “Breeding L-arginine-producing strains by a novel mutagenesis method: atmospheric and room temperature plasma (ARTP),” *Preparative Biochemistry and Biotechnology*, vol. 46, no. 5, pp. 509–516, 2016.
- [91] Y. Ma, H. Yang, X. Chen et al., “Significantly improving the yield of recombinant proteins in *Bacillus subtilis* by a novel powerful mutagenesis tool (ARTP): Alkaline  $\alpha$ -amylase as a case study,” *Protein Expression and Purification*, vol. 114, pp. 82–88, 2015.
- [92] Y. Ma, W. Shen, X. Chen et al., “Significantly enhancing recombinant alkaline amylase production in *Bacillus subtilis* by integration of a novel mutagenesis-screening strategy with systems-level fermentation optimization,” *Journal of Biological Engineering*, vol. 10, no. 1, 2016.
- [93] J. Sun, Y. Wang, B. Wu, Z. Bai, and B. He, “Enhanced production of d-lactic acid by *Sporolactobacillus* sp.Y2-8 mutant generated by atmospheric and room temperature plasma,” *Biotechnology and Applied Biochemistry*, vol. 62, no. 2, pp. 287–292, 2015.
- [94] W. Qiang, F. Ling-ran, W. Luo et al., “Mutation breeding of lycopene-producing strain *Blakeslea trispora* by a novel atmospheric and room temperature plasma (ARTP),” *Applied Biochemistry and Biotechnology*, vol. 174, no. 1, pp. 452–460, 2014.
- [95] C. Zhang, H. Shen, X. Zhang et al., “Combined mutagenesis of *Rhodospiridium toruloides* for improved production of carotenoids and lipids,” *Biotechnology Letters*, vol. 38, no. 10, pp. 1733–1738, 2016.
- [96] J. Winter, R. Brandenburg, and K. D. Weltmann, “Atmospheric pressure plasma jets: an overview of devices and new directions,” *Plasma Sources Science and Technology*, vol. 24, no. 6, p. 064001, 2015.
- [97] C. Ulrich, F. Kluschke, A. Patzelt et al., “Clinical use of cold atmospheric pressure argon plasma in chronic leg ulcers: a pilot study,” *Journal of Wound Care*, vol. 24, no. 5, pp. 196–203, 2015.
- [98] M. Schuster, C. Seebauer, R. Rutkowski et al., “Visible tumor surface response to physical plasma and apoptotic cell kill in head and neck cancer,” *Journal of Cranio-Maxillofacial Surgery*, vol. 44, no. 9, pp. 1445–1452, 2016.
- [99] D. M. S. Pinto and A. Flaus, “Structure and function of histone H2AX,” in *Subcellular Biochemistry*, vol. 50, Springer, Dordrecht, 2010.

## Review Article

# Targeting Reactive Oxygen Species in Cancer via Chinese Herbal Medicine

Qiaohong Qian,<sup>1</sup> Wanqing Chen,<sup>2</sup> Yajuan Cao,<sup>2</sup> Qi Cao,<sup>1</sup> Yajing Cui,<sup>2</sup> Yan Li ,<sup>2</sup> and Jianchun Wu <sup>2</sup>

<sup>1</sup>Department of Integrated Traditional Chinese and Western Medicine, Obstetrics and Gynecology Hospital, Fudan University, Shanghai 200011, China

<sup>2</sup>Department of Oncology, Shanghai Municipal Hospital of Traditional Chinese Medicine, Shanghai University of Traditional Chinese Medicine, Shanghai 200071, China

Correspondence should be addressed to Yan Li; [yan.xiaotian@shutcm.edu.cn](mailto:yan.xiaotian@shutcm.edu.cn) and Jianchun Wu; [eq219@126.com](mailto:eq219@126.com)

Received 14 May 2019; Revised 5 August 2019; Accepted 23 August 2019; Published 10 September 2019

Academic Editor: Lorenzo Loffredo

Copyright © 2019 Qiaohong Qian et al. This is an open access article distributed under the Creative Commons Attribution License, which permits unrestricted use, distribution, and reproduction in any medium, provided the original work is properly cited.

Recently, reactive oxygen species (ROS), a class of highly bioactive molecules, have been extensively studied in cancers. Cancer cells typically exhibit higher levels of basal ROS than normal cells, primarily due to their increased metabolism, oncogene activation, and mitochondrial dysfunction. This moderate increase in ROS levels facilitates cancer initiation, development, and progression; however, excessive ROS concentrations can lead to various types of cell death. Therefore, therapeutic strategies that either increase intracellular ROS to toxic levels or, conversely, decrease the levels of ROS may be effective in treating cancers via ROS regulation. Chinese herbal medicine (CHM) is a major type of natural medicine and has greatly contributed to human health. CHMs have been increasingly used for adjuvant clinical treatment of tumors. Although their mechanism of action is unclear, CHMs can execute a variety of anticancer effects by regulating intracellular ROS. In this review, we summarize the dual roles of ROS in cancers, present a comprehensive analysis of and update the role of CHM—especially its active compounds and ingredients—in the prevention and treatment of cancers via ROS regulation and emphasize precautions and strategies for the use of CHM in future research and clinical trials.

## 1. Introduction

Reactive oxygen species (ROS) and the oxidative stress that they produce have historically been considered mutagenic and carcinogenic because they can damage macromolecules such as DNA, lipids, and proteins, leading to genomic instability and changes in cell growth [1, 2]. Thus, ROS can contribute to malignant transformation and drive tumor initiation, development, and progression. Therefore, antioxidants are usually thought to be beneficial for both the prevention and treatment of cancer because they can quench ROS and reduce oxidative stress [1]. However, many clinical studies have shown that antioxidant supplements do not reduce the risk of cancer or prevent tumor growth, sometimes even exerting the opposite effects [3, 4]. Then, the protumorigenic effect of antioxidants, as well as their promotion of

tumor distant metastasis, was confirmed in mouse models of cancer [5, 6]. This finding emphasized the positive role of ROS in tumor inhibition from the opposite perspective. In this context, the biological functions of ROS in cancer are rather contradictory and ambiguous [7]. As two-faced molecules, ROS not only are associated with deleterious effects but are also signaling molecules involved in multiple cellular signaling pathways important for the fate of both normal and tumor cells [8]. Thus, developing approaches for the rational use of ROS in antitumor applications is very challenging but worthwhile.

Chinese herbal medicine (CHM) has been used in China for approximately three thousand years and has contributed greatly to human health. In addition, as the main components of natural products, CHM has been regarded as an important source for novel lead compounds for the discovery

of modern drugs, including anticancer drugs [9]. Currently, an increasing number of cancer patients are using CHM and its derivatives as complementary and alternative drugs; indeed, these medicines display synergistic effects when combined with conventional chemotherapy, radiation therapy, and even molecular targeted agents. Moreover, some have been suggested to have distinctive advantages in treating certain tumors [10]. A few clinical studies have reported that CHMs can alleviate the symptoms of diseases, improve the quality of life, and prolong the survival of cancer patients [11, 12]. However, the underlying mechanisms remain largely unknown. Many active compounds and ingredients in CHM can exert multiple antitumor effects accompanied by changes in cellular ROS. In this article, we comprehensively reviewed the dual roles of ROS in cancers and the ROS-mediated roles of CHM in cancer progression and treatment.

## 2. Generation and Biological Functions of ROS

**2.1. Generation of ROS.** ROS are broadly defined as oxygen-containing chemical molecules with highly reactive properties and mainly include superoxide anions ( $O_2^{\cdot-}$ ), hydrogen peroxide ( $H_2O_2$ ), and hydroxyl radicals ( $OH^{\cdot}$ ) [8, 13]. These molecules are by-products of aerobic metabolism and are mainly derived from mitochondria, peroxisomes, and the endoplasmic reticulum (ER), among which mitochondria are the major source—approximately 2% of the oxygen consumed by mitochondria is used to form the superoxide anion [14, 15]. In the process of mitochondrial oxidative phosphorylation, electrons leaking from the electron transport chain (ETC) may react with molecular oxygen to produce  $O_2^{\cdot-}$ , a reaction that is primarily mediated by coenzyme Q, ubiquinone, and respiratory complexes I, II, and III [16].  $O_2^{\cdot-}$  is the precursor form of most other ROS species which can be rapidly converted to  $H_2O_2$  by the corresponding superoxide dismutase (SOD). Further,  $H_2O_2$  can be converted to  $OH^{\cdot}$  by Fenton chemical reactions in the presence of a metal (iron or copper) (Figure 1). In addition to mitochondria, NADPH oxidases (NOXs) are another prominent source of superoxide that can catalyze the formation of  $O_2^{\cdot-}$  from  $O_2$  and NADPH (Figure 1). Besides, ROS are formed in the cytoplasm by enzymatic reactions involving peroxisomes, xanthine oxidase, cytochrome P450, lipoxygenases (LOXs), and cyclooxygenases.

Intracellular ROS levels are tightly controlled via diverse, complex synthesis and degradation pathways; this tight control is crucial for cellular homeostasis (Figure 1). The ROS-detoxifying system mainly comprises both enzymatic and nonenzymatic antioxidants [7, 17]. Enzymatic antioxidants include SOD, catalase (CAT), glutathione peroxidase (GPX), peroxiredoxin (PRX), and thioredoxin (TRX); nonenzymatic antioxidants include glutathione (GSH), flavonoids, and vitamins A, C, and E [18]. As described above, SOD can rapidly catalyze the conversion of  $O_2^{\cdot-}$  to  $H_2O_2$ , which can be further converted to water by the PRX system, the GPX system, and CAT. SOD has three isoforms in mammals: cytoplasmic Cu/ZnSOD (SOD1), mitochondrial MnSOD (SOD2), and extracellular Cu/ZnSOD (SOD3), all of which require specific catalytic metals (Cu or Mn) for

activation [19]. PRXs are considered ideal  $H_2O_2$  scavengers due to their abundant expression and broad distribution in cellular compartments such as the cytosol, the ER, mitochondria, and peroxisomes. During the metabolism of  $H_2O_2$ , PRX is oxidized and subsequently reduced by TRX, which is then reduced by thioredoxin reductase (TrxR) via the transfer of electrons from NADPH [20]. In addition to PRXs, GPXs are important scavengers. GPX catalyzes the reduction of  $H_2O_2$ , leading to the oxidation of GSH to glutathione disulfide (GSSG) that can be reduced back to GSH by glutathione reductase (GR) with NADPH as an electron donor [21].

In addition to antioxidant enzymes, the transcription factor nuclear factor erythrocyte 2-related factor 2 (Nrf2) plays a vital role in regulating the intracellular redox status [17]. Under physiological conditions, Nrf2 is located in the cytoplasm and remains at a low level under the control of Kelch-like ECH-associated protein 1 (KEAP-1). KEAP binds and specifically degrades Nrf2 via the ubiquitin-proteasome pathway. Under oxidative stress, Nrf2 dissociates from KEAP and is translocated to the nucleus. Then, activated antioxidant response elements (AREs), such as GSH, TRX, and PRX, decrease the intracellular ROS levels and protect against cell death [22] (Figure 1).

**2.2. Biological Functions of ROS.** A canonical mechanism by which ROS participate in the regulation of redox signaling is through the oxidative modification of cysteine residues in proteins [16]. During the redox process, reactive cysteine thiol (Cys-SH) can be oxidized by  $H_2O_2$  to reversible sulfenic acids (Cys-SOH), resulting in allosteric and functional changes within the protein [8]. This process is reversible; Cys-SOH can be reduced to its original state and restored its function by the TRX and GRX [8, 18]. Meanwhile, Cys-SOH can be further oxidized by continuously elevated ROS to form irreversible oxidation products, such as sulfinic or sulfonic species, causing permanent oxidative damage to proteins. This accounts for the double-sided nature of ROS and to a large extent, depending on its intracellular concentration and duration of exposure.

ROS involve a series of biological effects that are concentration-dependent. At low to moderate levels, ROS function as a second messenger and are involved in mediating cell proliferation and differentiation and the activation of stress-responsive survival pathways by regulating various cytokine receptors, serine/threonine kinase receptors, and G protein-coupled receptors [23, 24]. In contrast, due to their strong oxidizing capacity, ROS at a high level can react with intracellular macromolecules such as phospholipids, nucleic acids, and proteins to produce cytotoxicity. ROS have been linked to many diseases, such as cancers and diabetes [25]. The tight modulation of both ROS-producing pathways and ROS-detoxifying pathways may be required for the control of these diseases [26].

## 3. ROS and Cancer

The dual properties of ROS described above are simultaneously utilized by normal cells and cancer cells to support cell growth and survival. However, most cancer cells have higher levels of ROS than normal cells due to their enhanced glucose metabolism (the Warburg effect), mitochondrial



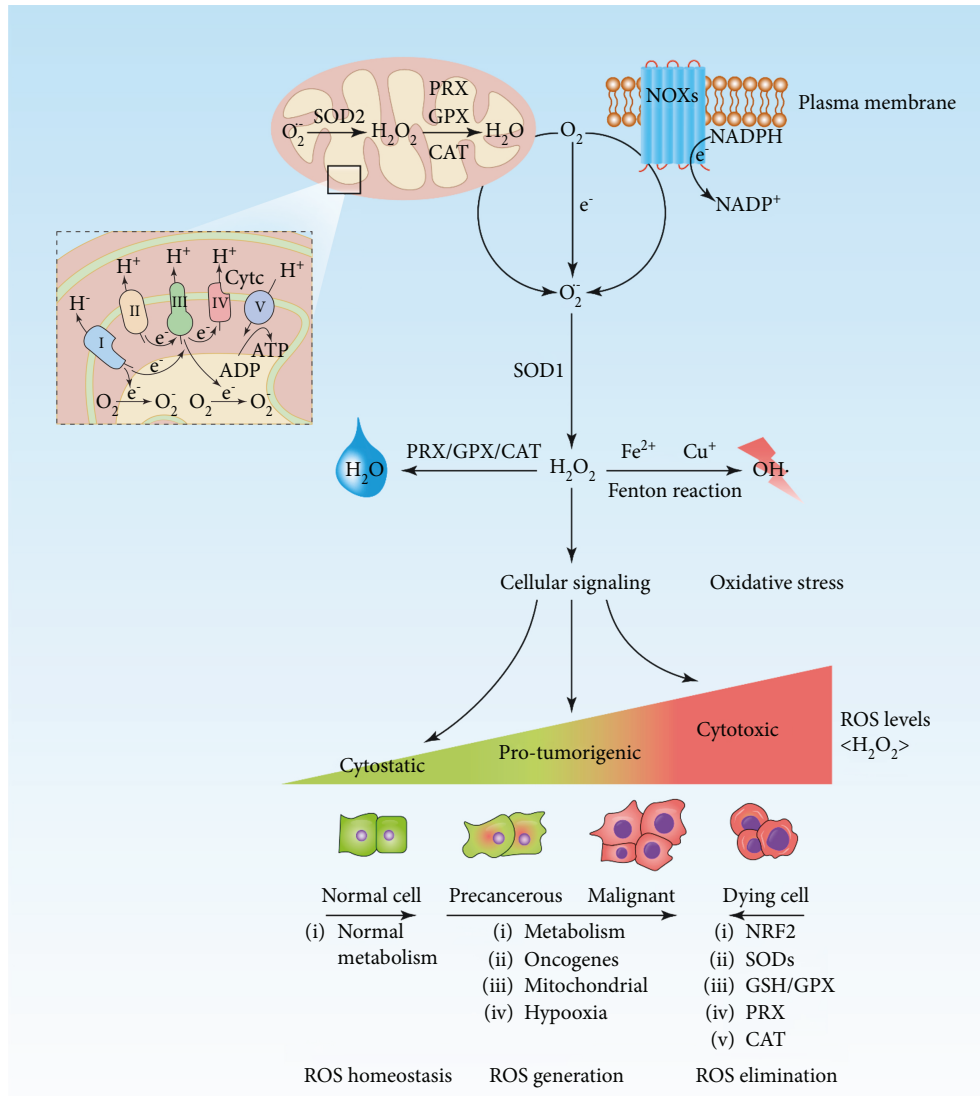


FIGURE 1: Production, regulation, and biological effects of ROS. Mitochondria and NOXs are the main sources of  $O_2^{\cdot-}$ .  $O_2^{\cdot-}$  is formed by molecular oxygen that receives one single electron leaking from mitochondrial ETC or from NOXs.  $O_2^{\cdot-}$  is then rapidly converted into  $H_2O_2$  by the corresponding SODs.  $H_2O_2$  can be converted into  $H_2O$  through intracellular antioxidants such as PRX, GPX, and CAT. When the  $H_2O_2$  level is uncontrollably increased,  $OH\cdot$  is further formed via the Fenton reaction with metal ions, thereby damaging biological macromolecules such as DNA, lipids, and proteins. In addition,  $H_2O_2$  is a major signaling molecule participating in cellular physiological and pathological processes. The effects of ROS depend on their intracellular concentration. Normal cells typically have lower concentrations of ROS due to their normal metabolism; in normal cells, ROS act as signaling molecules to maintain homeostasis, such as by limiting cellular proliferation, differentiation, and survival. The increased metabolic activity of cancer cells produces high concentrations of ROS, leading to a series of tumor-promoting events, such as DNA damage, genomic instability, oncogene activation, sustained proliferation, and survival. Elevated ROS concentrations also result in the protective growth of cancer cells with enhanced antioxidant capacity to maintain tumor-promoting signaling. Increasing ROS levels to the toxicity threshold, such as by treatment with exogenous ROS inducers or antioxidant inhibitors, causes oxidative damage to cells and, inevitably, cell death.

dysfunction, and oncogenic activity [18, 27]. On one hand, this property enables the activation of central protumorigenic signaling pathways. On the other hand, the resulting oxidative stress may also exert potential antitumor effects [8]. In the next sections, we discuss how ROS can either promote or inhibit cancer progression, providing the clues for anticancer therapies based on redox regulation.

3.1. Pros of ROS in Cancer. Moderately increased levels of ROS are a pivotal driving factor of tumor initiation,

development, and progression [24, 26] (Figure 1). In the initial stage of tumor formation, ROS may function as a direct DNA mutagen, induce genomic instability, damage mitochondrial DNA, and activate various signaling cascades to trigger malignant transformation [28–31]. In addition to causing significant genetic changes, ROS may alter the expression of oncogenes or tumor suppressor genes by mediating epigenetic modifications such as methylation or acetylation, thereby promoting carcinogenesis [32]. Conversely, these events may, in turn, promote ROS production and accumulation,

leading to further oxidative DNA damage and the malignant deterioration of cells to aid tumor formation [28, 32].

Existing tumors exhibit several noticeable characteristics, including sustained proliferation, apoptosis resistance, angiogenesis, invasion and metastasis, and tumor-promoting inflammation [33]. ROS are involved in all of these processes, which are conducive to tumor survival and development. ROS regulate the activities of many proteins and signaling pathways, thereby facilitating tumor cell proliferation and death evasion. For example, ROS can transiently inactivate tumor suppressors such as phosphatase and tensin homologue (PTEN) [34], protein tyrosine phosphatases (PTPs) [35], and MAPK phosphatases [36] by oxidative modulation, thereby stimulating the prosurvival PI3K/AKT and MAPK/ERK signaling pathways. Importantly, multiple transcription factors, such as activator protein 1 (AP-1), nuclear factor- $\kappa$ B (NF- $\kappa$ B), Nrf2, and hypoxia-inducible factor-1 $\alpha$  (HIF-1 $\alpha$ ), which are involved in the control of genes in cell proliferation, are also regulated by increased levels of ROS [37].

Tumor-associated neovasculature formation, or angiogenesis, provides oxygen and nutrients for the continued growth of cancer cells and is a key step in tumor growth and metastasis [38]. A wealth of evidence has shown that ROS play an essential role in tumor angiogenesis through mediating the following events. ROS, especially H<sub>2</sub>O<sub>2</sub> derived from NOXs, selectively promote endothelial cell (EC) proliferation and survival [39] and prevent apoptosis. Furthermore, ROS-mediated cadherin/catenin phosphorylation leads to the disassembly of EC junctions and promotes cell migration [40, 41]. Additionally, ROS activate VEGF signaling via multiple pathways, including through the induction of the principal regulator HIF-1 $\alpha$ , which increases VEGF and VEGFR expression [42], and, as mentioned before, through the induction of the PI3K/Akt and MAPK pathways, which activates angiogenic signaling cascades for the upregulation of VEGFR expression. Consistent with this pattern, an increase in the level of extracellular SOD may also suppress the hypoxic accumulation of HIF-1 $\alpha$  and its downstream target gene VEGF in several different types of cancer cells [43, 44].

Metastasis is a ubiquitous event in cancer development and encompasses a wide array of cellular changes, including the loss of cell-to-cell adhesion, the survival of cells upon matrix detachment, and the ability of cells to migrate and penetrate the basement membrane; ROS are involved in all of these processes [16, 45]. Indeed, ROS generated from NOXs are necessary for invadopodium formation and function in Src-transformed cell lines [46]. Similarly, ROS enable the direct oxidation of the protein tyrosine kinase Src, thereby enhancing the invasive potential, anchorage-independent growth, and survival of Src-transformed cells [47]. Furthermore, H<sub>2</sub>O<sub>2</sub> has been demonstrated to activate FAK in a PI3 kinase-dependent manner to accelerate cell migration [48]. ROS also participate in the abnormal activation of many proteolytic enzymes, such as MMP, uPA, and cathepsins, facilitating cell migration [49, 50]. Several tumor invasion signaling pathways upstream of MMPs and uPAs, such as the MAPK, PI3K/Akt, and PKC pathways and those modulated

by defined transcription factors (AP-1 and NF- $\kappa$ B), are modulated by ROS [50, 51]. Besides, ROS may induce the expression of transcription factors such as Snail and HIF-1 $\alpha$  [52], leading to epithelial to mesenchymal transition (EMT), an aggressive behavior favoring cancer metastasis and involved in drug resistance [53, 54].

*3.2. Cons of ROS in Cancer.* As stated earlier, cancer cells exhibit higher levels of ROS than normal cells, which contributes to tumor formation and development. However, excessive high levels of ROS can block cell cycle and induce different types of cell death, including apoptosis, autophagic cell death, ferroptosis and necroptosis. Due to space limitations, we focus on the first three types of cell death.

Apoptosis is the most common form of programmed cell death (PCD) in multicellular organisms with typical morphological and biochemical features. Also, apoptosis is a highly regulated process in which cells undergo self-destruction. The two well-known signaling mechanisms are the extrinsic death receptor pathway and the intrinsic mitochondrial pathway. ROS have been demonstrated to be implicated in the activation of both [55, 56]. ROS can activate the transmembrane death receptors such as Fas, TRAIL-R1/2, and TNF-R1 and then recruit the adaptor proteins FADD and procaspase-8/-10 to form death-inducing signaling complexes (DISCs), subsequently triggering the caspase activation and apoptosis [55]. Besides, ROS have been shown to posttranscriptionally inhibit c-FLIP, which suppresses DISC formation, thus causing the activation of the extrinsic apoptosis pathway [57]. Alternatively, ROS may activate ASK1 by oxidizing Trx, resulting in the subsequent induction of apoptosis through MAPKs such as JNK/p38 [58].

In the intrinsic apoptosis pathway, ROS at an elevated level destroy mitochondrial membranes, causing the release of cytochrome c from mitochondria and the induction apoptosis [18, 59]. Cytochrome c forms an apoptotic complex with apoptotic protein activating factor 1 (Apaf-1) and procaspase 9, resulting in the activation of caspase-9, followed by the induction of effector molecules such as caspase-3/7 [60]. The substantial loss of cytochrome c from mitochondria further increases ROS generation due to the disruption of the mitochondrial ETC [55]. Furthermore, ROS have been shown to regulate the activities of both antiapoptotic (Bcl-2, Bcl-X, and Bcl-wl) and proapoptotic (Bad, Bak, Bax, Bid, and Bim) Bcl-2 family proteins, which play an essential role in regulating the intrinsic pathway of apoptosis [61, 62].

In addition, ROS may act as upstream signaling molecules through the ER pathway, another important intrinsic apoptosis pathway. ROS at an excessive level trigger protein misfolding, leading to the unfolded protein response (UPR) and the induction of CHOP, thereby initiating apoptosis by regulating the expression of Bcl-2 family genes [63]. Moreover, ROS can stimulate the release of Ca<sup>2+</sup> in the ER lumen [64]. Due to the proximity of mitochondria to the ER, when a large amount of Ca<sup>2+</sup> is released from the ER, a substantial amount of Ca<sup>2+</sup> is absorbed by mitochondria, causing Ca<sup>2+</sup> overload in mitochondria. This leads to stimulating the opening of mitochondrial permeability transition pores (MPTPs) leading to the release of ATP and cytochrome c,

which further enhance apoptosis and increase ROS generation [65, 66]. Besides, ER stress-mediated apoptosis is partly controlled by the ASK-1/JNK cascade, which is directly regulated by ROS, as mentioned above.

Autophagy (macroautophagy), which is considered a cell survival mechanism to maintain cellular homeostasis, is multistep characterized by the formation of double-membrane autophagosomes by which cells utilize lysosomes to degrade and recycle their damaged organelles and macromolecules [67]. However, depending on the context, autophagy can function as a cell death mechanism and a tumor suppressor mechanism [68]. Many anticancer agents can induce autophagy in cancer cells. Some of them can induce ROS-dependent autophagy leading to cell death (autophagic cell death) [20, 69, 70].

ROS appear to be a key regulator of autophagy under different conditions and are involved in both the protective and toxic effects of autophagy [71]. Currently, several significant mechanisms by which ROS affect autophagy have been revealed. Under starvation conditions,  $H_2O_2$  can oxidize and inactivate ATG4, thereby contributing to the increased formation of LC3-associated autophagosomes [72]. ROS may directly trigger the oxidation of ATM to induce AMPK phosphorylation, which inhibits mTORC1 activation and phosphorylates the ULK1 complex to induce autophagy [73–75]. Also, AMPK can be phosphorylated by its upstream kinase AMPK kinase (AMPKK), leading to the induction of autophagy. In an alternative mechanism,  $H_2O_2$  activates Bcl-2/E1B interacting protein 3 (BNIP3) to suppress the activity of mTOR and abolish the interaction between Beclin-1 and Bcl-2, causing Beclin-1 release and autophagy induction [76, 77]. Besides, ROS can modulate autophagy by affecting the activity of various transcription factors such as NF- $\kappa$ B, resulting in the expression of autophagy-associated genes (BECN1/ATG6 or SQSTM1/p62) in cancer cells [78, 79].

In contrast, autophagy can reduce ROS levels through the NRF/KEAP1 and P62 pathways [80]. In response to ROS, P62 is activated and thus interacts with KEAP1 to contribute to the suppression of NRF2 degradation and the promotion of its activation, which, in turn, can activate antioxidant defense genes such as GPX, SOD, and TRX [79, 81]. This process contributes to the regulation of autophagy.

Ferroptosis, first named by Dixon et al. in 2012, is emerging as a new form of PCD characterized by the accumulation of cellular ROS in an iron-dependent manner [82, 83]. Ferroptosis is primarily caused by an imbalance in the production and degradation of intracellular lipid ROS and can cause iron-dependent oxidative cell death through a reduction in antioxidant capacity and an accumulation of lipid ROS. Many compounds can induce ferroptosis to kill cancer cells in a manner mainly related to the metabolism of amino acids/GSH, lipids, and iron and the regulation of P53 [84].

Erastin can inhibit the activity of the cysteine-glutamate antiporter (system  $X_C^-$ ), reduce cystine uptake, and lead to the associated depletion of intracellular GSH, in turn causing toxic lipid ROS accumulation and ferroptosis [82, 85]. Inhibition of glutathione peroxidase 4 (GPX4), a GSH-dependent enzyme required for the elimination of lipid

ROS, can trigger ferroptosis even at regular cellular cysteine and GSH levels [86]. Other lipophilic antioxidants, such as Trolox, ferrostatin-1, and liproxstatin-1, can inhibit ferroptosis [82, 87]. Intracellular iron is another essential regulator of lipid ROS production and ferroptosis induction. In the presence of iron, lipid hydroperoxides are converted into toxic lipid free radicals, leading to lipid oxidative damage and cell death [88, 89]. Indeed, various iron chelators such as deferoxamine and ciclopirox can abolish ferroptotic cell death caused by system  $X_C^-$  inhibitors, GPX4 inhibitors, and GSH depletion [83]. Consistent with this observation, silencing TFRC, thus inhibiting the transport of iron into the cytoplasm, can antagonize erastin-induced ferroptosis [90]. Additionally, PKC-mediated HSPB1 phosphorylation inhibits ferroptosis by reducing the production of iron-dependent lipid ROS, but inhibition of HSF1-HSPB1 pathway activity and HSPB1 phosphorylation increases the anticancer activity of erastin [91]. Together, these results demonstrate the importance of lipid ROS and iron in promoting ferroptosis.

Recent studies have revealed a new mechanism by which P53 acts as a tumor suppressor gene to inhibit tumors by inducing ferroptotic cell death. Jiang et al. demonstrated that P53 could downregulate the expression of SLC7A11, thereby preventing system  $X_C^-$  from absorbing cystine, resulting in decreased cystine-dependent GPX activity and cellular antioxidant capacity, in turn leading to ROS-induced ferroptosis and tumor suppression [92]. Indeed, this finding is contrary to those of many other reports showing that P53 can reduce cellular levels of ROS. When ROS levels are low, P53 may prevent the accumulation of ROS from promoting cell survival, whereas when ROS levels are excessive, P53 may evoke cell death via ferroptosis. Currently, P53 is reported to exert a complex and dynamic regulatory effect on ROS, but the role of this regulation in tumors needs further study [93].

#### 4. Anticancer Effects of CHM via ROS

As described above, ROS have dual roles in tumor suppression and tumor promotion depending on their concentrations. Moreover, most cancer cells have higher basal levels of ROS than normal cells, which is beneficial for their survival and development. In response to their high basal levels of ROS, the antioxidant capacity of cancer cells is upregulated to maintain redox balance and prevent ROS levels from excessively increasing to induce cell death [8, 26]. However, this effect is very limited in tumor cells. Therefore, either increasing or reducing ROS can be an effective strategy in cancer therapy by disrupting redox balance in tumor cells [17, 20]. CHM has a long history of treating various diseases and is becoming an integral part of comprehensive cancer treatment in China. According to the literature, CHM plays a significant role in cancer therapy through several aspects: reducing inflammatory and infectious complications surrounding the tumors, protecting normal tissues from the possible damage caused by chemo/radiotherapy, enhancing the potency of chemo/radiotherapy and molecular targeted therapies, improving immunity and body resistance to disease, improving general condition and quality of life, and prolonging the survival of advanced cancer patients [94]. However, in most

cases, the chemical and pharmacological mechanisms of CHM are ambiguous. The majority of researches on the molecular mechanism of CHM were carried out with an active monomer or crude extract of a single herb, and results indicate that the anticancer activities of diverse CHMs are associated with ROS regulation. Therefore, we summarize current data regarding the ROS-related anticancer effects of CHM on the prevention and therapy of cancers. Some typical Chinese herbal compounds and ingredients are discussed. For additional examples, please see the Tables 1 and 2.

**4.1. Antioxidant Effects of CHM in Cancer Progression.** Carcinogenesis is a multistep process in which various genetic and epigenetic events occur through the stimulation of numerous inflammatory mediators and ROS production, resulting in the conversion of normal cells into cancer cells [1]. Many carcinogens, such as irradiation, UV light, and toxins, are also exogenous ROS inducers that accelerate the malignant transformation and promote tumor progression by increasing intracellular oxidative damage and activating cancer-promoting signals. Thus, approaches to enhance the antioxidant enzyme system or reduce ROS generation can be used to prevent tumorigenesis and slow tumor progression (Figure 2). There is a beneficial inverse relationship between the consumption of fruits and vegetables and the risk of lung cancer, due to the high antioxidant content of these foods [95, 96]. Increasing types of CHM-derived bioactive ingredients or crude extracts have been shown to suppress chronic inflammation of tissues and prevent carcinogenesis. This effect, to a certain extent, is attributed to the fact that such CHMs are homologous to food and are rich in antioxidants such as saponins, flavonoids, and polysaccharides, which can reduce the oxidative damage caused by excess ROS in normal cells [97].

Studies have shown that the overproduction of ROS induced Cr(VI)-mediated carcinogenesis. Quercetin, one of the most abundant dietary flavonoids in fruits, vegetables, and many CHMs such as *Hippophae fructus* (Sha Ji) and *Lycii fructus* (Gou Qi Zi), has potent antioxidant and chemopreventive properties [98]. Quercetin can protect human normal lung epithelial cells (BEAS-2B) from Cr(VI)-mediated carcinogenesis by targeting miR-21 and PDCD4 signaling, reducing ROS production [98]. Purslane polysaccharides (PPs), a principal bioactive constituent of the *Portulaca oleracea L.* (Ma Chi Xian), possess a wide range of antioxidant, immunomodulatory, and antitumor activities. Methylnitronitrosoguanidine (MNNG) is a carcinogen and mutagen commonly used in experiments. A recent study showed that PPs provide dose-dependent protection against MNNG-mediated oxidative damage by increasing the activity of SOD, CAT, and GSH-Px in gastric cancer rats [99].

During tumor growth, ROS are continuously accumulated by the stimulation of various growth factors and hypoxia-inducing factors in the microenvironment, which in turn accelerates the progression of the tumor and maintain typical hallmarks of cancer. Some CHMs can inhibit tumor growth and progress by reducing ROS production in vitro and in vivo using a mouse model. *Forsythia suspensa* (Lian Qiao), one of the most fundamental medicinal herbs in China, has extensive pharmacological activities and is

generally used to treat infectious diseases of the respiratory system. In the past decades, its antineoplastic activity has attracted more attention. *Forsythia fructus* aqueous extract (FAE), as the primary bioactive ingredient of *Forsythia suspensa*, has shown distinct anticancer properties both in vitro and in vivo. FAE can inhibit proliferation and angiogenesis of melanoma cells by antioxidant and anti-inflammatory mechanisms such as in reducing ROS, malondialdehyde (MDA), and IL-6 levels and in increasing GSH, Nrf2, and HO-1 expression [100]. Similarly, andrographolide (AP), a bioactive compound present in the medicinal plant *Andrographis paniculata* (Chuan Xin Lian), possesses several beneficial properties, including anti-inflammation, antioxidant, and antitumor activities. AP can antagonize TNF- $\alpha$ -induced IL-8 release by inhibiting the NOX/ROS/NF- $\kappa$ B and Src/MAPKs/AP-1 signaling pathways, subsequently suppressing angiogenesis in colorectal cancer cells [101]. Isoliquiritin (ISL) is a natural chalcone flavonoid derived from licorice compounds and has antioxidant and antitumor properties. Previous studies have demonstrated that ISL may selectively inhibit prostate cancer cell proliferation by decreasing ROS levels, thus blocking AMPK and ERK signaling [102]; furthermore, this compound can suppress the invasion and metastasis of prostate cancer cells possibly via decreased JNK/AP-1 signaling [103]. Abnormal cell energy metabolism is one of the core hallmarks of cancer [33]. Resveratrol (RSV) is a polyphenolic compound present in many types of fruits, vegetables, and Chinese medical herbs. Numerous studies have shown that it has a variety of biological and pharmacological activities, such as antioxidant, anti-inflammatory, antiaging, and antitumor. RSV can inhibit invasion and migration by suppressing ROS/miR-21-mediated activation and glycolysis in pancreatic stellate cells (PSCs) [104].

In addition, ROS are involved in the antitumor activity of many chemotherapeutic agents, small molecular targeted drugs, and radiation therapy, as well as their side effects [105, 106]. The rational use of the antioxidant effects of CHMs can relieve the toxic side effects of chemo- and radiotherapy on normal cells by eliminating excessive ROS. Sulforaphane is a component of cruciferous vegetables and some Chinese medicinal plants [107]. Studies have shown that sulforaphane is a powerful natural antioxidant to prevent, delay, and improve some side effects of chemotherapy. Sulforaphane can result in the high expression of HO-1 by activating the KEAP1/NRF2/ARE signaling pathway, which protects myocardial cells from doxorubicin-induced oxidative injury and protects the gastric mucosa against *H. pylori*-induced oxidative damage [107, 108]. Ginseng is often used alone or in combination with other herbs for the adjuvant treatment of tumors [109]. Ginsenoside is the main pharmacologically active ingredient of ginseng in exerting anticancer activity. As the primary active component, ginsenoside Rg3 can mitigate doxorubicin-induced cardiotoxicity by ameliorating mitochondrial function, improving calcium handling, and decreasing ROS production [109]. Furthermore, Rg3 inhibits gemcitabine-induced resistance by eliminating ROS, down-regulating NF- $\kappa$ B and HIF-1 $\alpha$ -mediated PTX3 activity [110]. Ginsenoside Rg1 is another ingredient of ginseng and

TABLE 1: Components of TCMs targeted to decrease ROS levels and the effects of these components in cells.

Components	Herbs	Target cells	Biological effects	Molecular events	Reference
Astragaloside IV	<i>Milkvetch root (Huang Qi)</i>	Kidney proximal tubular HK-2 cells	Mitigate cisplatin-induced acute kidney injury	T-SOD↑, GSH-Px↑, CAT↑, KIM-1↓, MDA↓, TNF-α↓; Nrf2↑, HO-1↑, NF-κB↓	[153]
Benzyl isothiocyanate	<i>Lepidii semen (Ting Li Zi)</i>	Leukemia HL-60 cells	Prevent inflammation-related carcinogenesis	NADPH oxidase↓, ROS↓	[154]
Catalpol	<i>Rehmannia glutinosa libosch (Di Huang)</i>	Pheochromocytoma PC-12 cells	Against LPS-induced apoptosis	Bcl-2↑, BAX↓, p-CaMK↓, Ca2+↓; CaMKII-dependent ASK-1/JNK/p38 pathway↓	[155]
Crocin	<i>Crocus sativus L. (Zang Hong Hua)</i>	Melanoma B16F10 cells	Inhibition of melanogenesis	Tyrosinase↓, MITF↓, ROS↓	[156]
Curcumin	<i>Curcuma longa L. (Jiang Huang)</i> <i>Curcuma radix (Yu Jin)</i>	Breast epithelial MCF-10A cells	Against Phip-induced cytotoxicity	Nrf2↑, FOXO↑; BRCA-1, H2AFX, PARP-1, and P16↑; Casp-3/9↓	[157]
Dioscin	<i>Smilacis glabrae rhizoma (Tu Fu Ling)</i>	Ventricular H9c2 cells	Against doxorubicin-induced cardiotoxicity	miR-140-5p↓; ROS, MDA, SOD, GSH, and GSH-Px↓; Nrf2 and Sirt2 pathway↑	[158]
Daphnetin	<i>Daphne Korean nakai (Chang Bai Rui Xiang)</i>	Monocyte RAW264.7 cells	Against t-BHP-triggered oxidative damage and mitochondrial dysfunction	ROS↓, MDA↓; SOD↑, GSH/GSSG↑; JNK and ER↑; Nrf2/ARE pathway↑	[159]
Ellagic acid	<i>Rubus idaeus (Fu Pen Zi)</i>	Ishikawa cells	Reduction of glycolytic flux Against doxorubicin-induced cardiac oxidative	ROS↓, NHE1↓, Na+/H+ exchanger activity↓, PHI↓; ROS↓, MDA↓, XO↓; Casp-3, p-ERK1/2, p-p38, and NF-κB↓	[160] [161]
Eriodictyol	<i>Dracocephalum rupestre (Yan Qing Lan)</i>	Pheochromocytoma PC-12 cells	Against hydrogen peroxide-induced neurotoxicity	Nrf2, HO-1, γ-GCS, and GSH↑; Nrf2/ARE pathway↑	[162]
Epigallocatechin-3-gallate	<i>Green tea (Lv Cha)</i>	Inner ear UB/OC-1 cells Breast epithelial MCF-10A cells	Against cisplatin-induced ototoxicity Against Phip-induced breast carcinogenesis	ROS↓, ERK1/2↓, STAT3/STAT1↑ Ras/ERK/Nox/ROS pathway↓	[163] [164]
Isoliquiritigenin	<i>Licorice (Gan Cao)</i>	Kidney epithelial LLC-PK1 cells	Against cisplatin-induced nephrotoxicity	ROS↓, Casp-3↓, Nrf2/HO-1↑	[165]
Luteolin	<i>Chrysanthemi indici flos (Ye Ju Hua)</i> <i>Lonicerae japonicae flos (Jin Yin Hua)</i>	Bronchial epithelial BEAS-2B cells	Inhibition of Cr(VI)-induced carcinogenesis	AP-1, HIF-1α, COX-2, and iNOS↓; MAPK, NF-κB, and EGF↓; proinflammatory cytokine↓; Nrf2, HO-1, NADPH, and SOD1/SOD2↑	[166, 167]
Nexrutine	<i>Phellodendron amurense (Huang Bai)</i>	Pancreatic cancer cells Capan-2, MIAPaCa-2, AsPC-1, BxPC-3	Inhibit autophagy and pancreatic cancer cell growth	ROS↓, LC3-II↓; STAT3↓	[168]
Pedicularioside G	<i>Pedicularis striata (Ma Xian Hao)</i>	Hepatoma SMMC-7721 cells and HUVEC	Inhibition of angiogenesis and tumorigenesis	ROS↓, VEGF↓, IL-8↓	[169]

TABLE 1: Continued.

Components	Herbs	Target cells	Biological effects	Molecular events	Reference
Resveratrol	<i>Polygonum cuspidatum</i> (Hu Zhang)	Pancreatic stellate cells	Inhibition of invasion, migration, and glycolysis	ROS/miR-21↓, PTEN↑	[104]
	<i>Fructus mori</i> (Sang Shen)	Glioblastoma U87 MG and GBM8401 cells	Enhance the efficacy of temozolomide	ROS/ERK-mediated autophagy↓; apoptosis↑	[170]
Rutin	<i>Ruta graveolens</i> L. (Yun Xiang)	Neuroblastoma IMR32 cells	Ameliorates doxorubicin-induced memory deficits	ROS/JNK/TNF/P38 MAPK pathway↓	[171, 172]
	<i>Fagopyrum tataricum</i> (L.) Gaertn (Ku Qiao Mai)		Against cisplatin-induced nephrotoxicity		
Saikosaponin-D	<i>Radix bupleuri</i> (Chai Hu)	/	Reduces cisplatin-induced nephrotoxicity	ROS, P38, and JNK/NF-κB pathway↓	[173]
Sulforaphane	<i>Codonopsis radix</i> (Dang Shen)	Bronchial epithelial BEAS-2B cells	Against cadmium-induced carcinogenesis	Nrf2↑, ROS↓, protective autophagy↑	[174]
Tetramethylpyrazine	<i>Chuanxiong rhizoma</i> (Chuan Xiong)	Kidney proximal tubular HK-2 cells	Against arsenite-induced nephrotoxicity	ROS↓, GSH↑, apoptosis↓, proinflammatory signals↓, cytotoxic autophagy↓	[175]
Tanshinone II-A	<i>Radix salviae</i> (Dan Shen)	Monocyte RAW264.7 cells and stomach cancer MKN45 cells	Decrease <i>H. pylori</i> -induced inflammation and gastric cancer	NF-κB and MAPK(p38/JNK) pathway↓; inflammatory substance↓; apoptotic protein↑	[176]

TABLE 2: Compounds of TCMs targeted to increase ROS levels and the effects of these components in cancer cells.

Components	Herbs	Target cells	Biological effects	Molecular events	Reference
Aloe emodin	<i>Aloe (Lu Hui)</i>	Lung cancer cells H460 Nasopharyngeal cancer cells NPC-TW039, TW076	DNA damage Apoptosis Cycle arrest	ROS↑, SOD↑; hMTH1, hOGG1, and APE↓ Cyclin B1↑, Cdc2↑, PARP↑, Casp-3/8↑	[177] [178]
Attractylolide	<i>Attractylodes lancea (Cang Zhu)</i>	Leukemia cells	Apoptosis	ROS↑; ER Ca2+↑	[179]
Baicalein	<i>Scutellaria baicalensis (Huang Qin)</i>	Breast cancer cells ZR-75-1 Colon/prostate cancer cells SW480; PC3	Apoptosis Apoptosis/overcome TRAIL resistance	PLC-dependent Ca2+↑, ROS↑; Ca2+-associated apoptosis↑ ROS↑, DR5↑, TRAIL receptor↑	[180] [181]
Berberine	<i>Coptis chinensis Franch (Huang Lian)</i>	Lung cancer cells H1975, H1650, H1819, A549, H1299 Liver cancer cells HepG2, Hepa1-6	Apoptosis Apoptosis	SREBP1↓; mitochondrial dysfunction, ROS↑, p-AMPK↑; lipogenesis↓ p-PTEEN, p-Akt, p-mTOR, and p-PDK1↓; FoxO1, FoxO3, Bim, Bax, Bcl-2, Casp-3/9, and cl-PARP↑; p-JNK↑, ROS↑; SOD, CAT, and GSH↓	[182] [183]
Bufalin	<i>Bufo bufo gargarizans cantor (Chan Su)</i>	Breast cancer cells MCF-7, MDA-MB-231 Colon cancer cells HT-29, Caco-2	Necroptosis Autophagy	RIP1/RIP3↑; ROS and PARP-1↑, RIP1/RIP3/PARP-1 pathway↑ ROS↑, p-JNK↑; ATG5, Beclin-1, LC3-II, and autophagic flux↑	[184] [185]
Celastrol	<i>Tripterygii radix (Lei Gong Teng)</i>	Osteosarcoma cells HOS, MG-63, U-2OS, Saos-2 Breast cancer cells MCF-7, MCF-7/MDR	Apoptosis Autophagy Cycle arrest Against doxorubicin resistance	ROS/JNK pathway↑, Casp-3/8/9↑; LC3-II↑ HSF-1↑, NF-κB↓, P-gp↓	[186] [187]
Cordycepin	<i>Cordyceps sinensis (Dong Chong Xia Cao)</i>	Glioma cells Rat C6, LN18, T98G, LN229, SHG-44 Gastric/colon cancer cells SGC-7901; HT-29	Apoptosis Cycle arrest Synergistic with TMZ DNA damage Apoptosis	ROS↑, GSH↓; p-GSK-3β↓, β-catenin↓ DR3↑, A3AR↓, PI3K/Akt↑, ROS↑, Δψm↓; p53, Bax, Casp-3/8/1, and cl-PARP↑	[188] [189, 190]
Costunolide	<i>Aucklandia radix (Mu Xiang)</i>	Prostate cancer cells PC-3, DU-145 Ovarian cancer cells MPS1, A2780, SKOV3 Colon cancer cells HCT116	Enhance doxorubicin-induced apoptosis Induce apoptosis of platinum- resistant cells Apoptosis	ROS↑, p-JNK↑, p-p38↑, Δψm↓, Bax↑, Bak↑, Bcl-2↓, Bcl-xL↓, Casp-3/9↑, cl-PARP↑ ROS↑, Bcl-2↓, Casp-3/8/9↑	[191] [192]
				TrxR1↓, ROS↑, ERS↑	[193]

TABLE 2: Continued.

Components	Herbs	Target cells	Biological effects	Molecular events	Reference
Cucurbitacin E	<i>Bolboeternae paniculati bulbos</i> (Tu Bei Mu)	Colorectal cancer primary cell lines	Cycle arrest Apoptosis	ROS↑, ΔΨ <sub>m</sub> ↓, GADD45γ↑, Cdc2↓ Cyclin B1↓	[194]
Curcumin	<i>Curcuma longa L.</i> (Jiang Huang)	Lung/prostate cancer cells A549, PC-3 Cervical cancer cells C33A, CaSki, HeLa, ME180	Apoptosis	TrxR2↓; Bax/Bcl-2↑, ΔΨ <sub>m</sub> ↓, cyto C↑, Casp-3/9↑ p-PERK, IRE-1α, GRP-78, ATF6, and CHOP↑; Bax/Bcl-2, Casp-3/9, and cI-PARP↑	[195] [196]
Daidzein	<i>Glycine max</i> (Hei Dou)	Breast cancer cells MCF-7	Apoptosis	ROS↑, ΔΨ <sub>m</sub> ↓, Bcl-2↓, Bax↑, cyto C↑, Casp-7/9↑	[197]
Emodin	<i>Rheum palmatum</i> (Da Huang)	Cervical cancer cells HeLa	Apoptosis	ROS↑, NF-κB↓, AP-1↓, p-P38↑	[198, 199]
Epigallocatechin-3-gallate	<i>Green tea</i> (Lv Cha)	Malignant B-cell lines HS-sultan, RPMI8226	Apoptosis	Cyto C, Smac/DIABLO, AIF, and Casp-3/9↑	[200]
Escin	<i>Semen aesculi</i> (Suo Luo Zi)	Osteosarcoma cells MNNG/HOS, Saos-2, MG-63, U2-OS	Autophagy Apoptosis	ROS/p38 MAPK↑; LC3 II, ATG5 ATG12 and Beclin1↑; Bax/Bcl-2↑, Casp-3/7/8/9↑	[201]
Eugenol	<i>Eugenia caryophyllata</i> (Ding Xiang)	Leukemia cells HL-60, U937	Apoptosis	ROS↑, ΔΨ <sub>m</sub> ↓, Bcl-2↓, cyto C↑ Casp-3/9↑	[202]
Evodiamine	<i>Evodia rutaecarpa Benthani</i> (Wu Zhu Yu)	Glioma cells U87-MG Cervical cancer cells HeLa	Apoptosis Autophagy Cycle arrest	Calcium/JNK signaling-mediated autophagy↑; calcium/mitochondria-mediated apoptosis↑ PTK/Ras-Raf-JNK↑; ROS/NO↑; p53, p21, Cdc2, and cyclin B1↑	[203] [204]
Gambogic acid	<i>Garcinia hanburyi Hook. f.</i> (Teng Huang)	Colon cancer cells HCT-15, HCT-15R Lung cancer cells A549, H460, H1299	Apoptosis/against drug resistance Synergistic with cisplatin	ΔΨ <sub>m</sub> ↓, cyto C↑, AIF↑; Bcl-2, Bcl-xl, Mcl-1, XIAP and survivin↓; p-JNK↑, c-JUN↑ Casp-3/8/9, Fas and Bax↑; Bcl-2, XIAP, survivin↓; NF-κB, MAPK/HO-1 pathway↓	[205] [206]
Germacrone	<i>Curcuma zedoaria</i> (E Zhu)	Breast cancer cells MCF-7, MDA-MB-231	Apoptosis	ROS↑, ΔΨ <sub>m</sub> ↓; Bax, JNK1, IKKα, and IKKβ↑; Bcl-2, Bcl-xl, Bim, and Bik↓	[207]
Gypenoside	<i>Gynostemma pentaphyllum</i> (Jiao Gu Lan)	Esophageal cancer cells ECA-109, TE-1	Autophagy	ROS-induced ERS↑, Ca2+↑; P62↑, autophagic flux↓	[208]
Honokiol	<i>Magnolia officinalis</i> (Hou Po)	Osteosarcoma/glioma cells HOS, U2OS; U87MG Neuroblastoma cells Neuro-2a, NB41A3	Apoptosis Autophagy Cycle arrest	GRP-78↑, ROS↑, p-ERK1/2↑; LC3 II↑ ERS/ROS/ERK1/2 pathway↑; p53/PI3K/Akt/mTOR↓	[209–211]



TABLE 2: Continued.

Components	Herbs	Target cells	Biological effects	Molecular events	Reference
Icariin	<i>Epimedium brevicornum Maxim (Yin Yang Huo)</i>	Esophageal cancer cells EC109, TE1 Liver cancer cells SMMC-7721, Bel-7402, L-02	Apoptosis	GSH↓; NADPH, Casp-9↑; p-PERK, GRP-78, ATF4, p-eIF2α, and CHOP↑; PUMA↑, Bax/Bcl-2↑, ΔΨm↓, cyto C↑, Casp-3/9↑, cl-PARP↑; p-JNK↑	[212, 213]
Isoalantolactone	<i>Inula helenium (Tu Mu Xiang)</i>	Esophageal cancer cells ECA109, EC9706, TE-1, TE-13	Apoptosis	ROS↑, DR5↑, Casp-3/7/10↑; DR5-induced extrinsic apoptosis	[214]
Luteolin	<i>Chrysanthemi indicis flos (Ye Ju Hua)</i> <i>Lonicerae japonicae flos (Jin Yin Hua)</i>	Liver cancer cells HepG2; MDR cancer cells	Apoptosis DNA damage Cycle arrest	ROS↑, PIG3↑, ΔΨm↓, cyto C↑, Bax/Bcl-2↑, casp-3/9↑ ROS↑, ATR/Chk2/p53 pathway↑, p38↑, Bcl-2↓, NF-κB↓	[215, 216]
Matrine	<i>Sophora flavescens (Ku Shen)</i>	Pancreatic cancer cells PANC-1, Miaapaca-2 Liver cancer cells HepG2	Cycle arrest Apoptosis Program cell death	ROS, p-ERK, p-JNK, and p-P38↑ Cyclin A, DI, CDK2↓; cyto C, Casp-3, cl-PARP, Bax, and Bad↓; Bcl-2↓ ΔΨm↓, ROS↑; Fas↑, Fas-L↑; Casp-3↑; AIF translocation↑	[217] [218]
Neferine	<i>Nelumbo nucifera (Lian Hua)</i>	Lung cancer cells A549	Autophagy enhances cisplatin-induced autophagic cell death	ROS↑, GSH↓, PI3K/Akt/mTOR↓, LC3-II↑ PI3K/Akt/mTOR pathway↓	[219, 220]
Norcantharidin	<i>Mylabris (Ban Mao)</i>	Liver cancer cells HepG2	Apoptosis	ROS↑, ΔΨm↓, cyto C↑, Bcl-2↓ Bax, Casp-3/9, and cl-PARP↑	[221]
Oridonin	<i>Rabdosia rubescens (Dong Ling Cao)</i>	Osteosarcoma cells MG-63, HOS	Apoptosis	PPAR-γ↑, Nrf2↓; ΔΨm↓ Bax/Bcl-2↑, Casp-3/9↑	[222]
Oroxylin A	<i>Oroxylum indicum (Mu Hu Die)</i> <i>Scutellaria baicalensis (Huang qin)</i>	Colon cancer cells CaCo-2, HCT-116	Apoptosis	UCP2↓; ROS, MPTP, cyto C, AIF Casp-3/9 and cl-PARP↑	[223]
Plumbagin	<i>Plumbago zeylanica (Bai Hua Dan)</i>	Colon cancer cells HT-29, HCT-116, Caco-2	Apoptosis	ASK1/TRAF2↑, JNK↑; mTORC1↓ Bcl-2↓	[224]
Resveratrol	<i>Polygonum cuspidatum (Hu Zhang)</i> <i>Fructus Mori (Sang Shen)</i>	Lung/breast cancer cells H1299, MCF-7 Prostate cancer cells LNCaP, PC-3	Apoptosis Autophagy Apoptosis	TIGAR↓, GSH↓, ROS↑, cl-PARP↑ LC3-II↑ TRX1↓, TXNIP↑	[225] [226]
Saxifragolin D	<i>Androsace umbellata (Hu Er Cao)</i>	Breast cancer cells MCF-7, MDA-MB-231	Autophagy Apoptosis	LC3-II, Beclin-1, and Vps34↑; ROS-mediated ERS↑	[227]
Sophoranone	<i>Radix sophorae tonkinensis (Shan Dou Gen)</i>	Leukemia cells U937 cell	Apoptosis	ROS↑, MPTP↑, cyto C↑, p-JNK↑, Casp-3↑	[228]

TABLE 2: Continued.

Components	Herbs	Target cells	Biological effects	Molecular events	Reference
Tetraandrine	<i>Stephania tetrandra radix</i> (Fang Ji)	Leukemia cells K562, CMK, HEL Live cancer cells Huh7, HepG2, BEL7402	Autophagy Cycle arrest Differentiation Apoptosis	ROS↑, LC3 II↑, p-Akt↑, p21↑, p27↑ ROS↑; p-Akt, p-ERK1/2, and p-JNK↓	[229] [230]
Vitexin	<i>Vitex negundo L</i> (Ma Bian Cao)	Melanoma cells A375, Sk-Mel-5, Sk-Mel-28	DNA damage Cycle arrest	ROS, Bax, and PARP↑; Bcl-2↓ p-ATM, p-ATR, p-CHK2, p53, p21, and $\gamma$ -H2AX↑	[231]

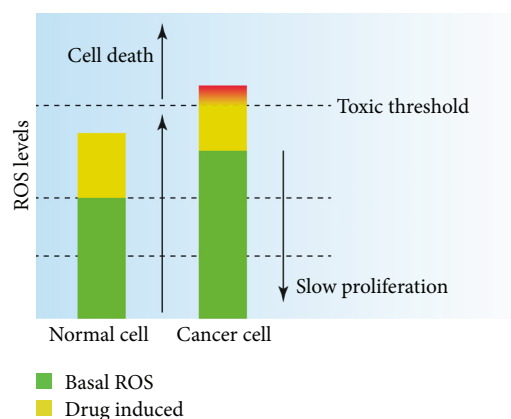


FIGURE 2: Treatment strategy based on redox regulation. Compared to normal cells, cancer cells have increased levels of basal ROS, resulting in the maintenance of tumor-promoting signaling in these cells. Therefore, strategies for reducing ROS by using antioxidants to prevent carcinogenesis or delay tumor growth are theoretically feasible (however, most current clinical results are not supported). However, strategies for increasing ROS to toxic levels by using ROS inducers and/or inhibiting ROS scavengers can result in the specific killing of cancer cells (such approaches seem more promising than ROS reduction strategies).

was found to alleviate cisplatin-induced hepatotoxicity via restraining the binding of Keap1 to Nrf2, partly via p62 accumulation, and enhancing Nrf2-related antioxidant activity [111]. *Schisandra sphenanthera* extract has a protective effect against cisplatin-induced nephrotoxicity by activating the Nrf2-mediated defense response, thus increasing GSH levels and reducing ROS levels [112]. Astragalus has a long history of treating immunodeficiency diseases in China and beyond and is often used to reduce side effects caused by chemotherapy [113]. Astragaloside IV (As-IV) is a natural saponin extracted from *Astragalus membranaceus*, which has antioxidant, anti-inflammatory, and antiapoptotic effects. Studies showed that As-IV markedly ameliorates BLM-induced pulmonary fibrosis in mice, an effect associated with its antagonism of bleomycin-induced oxidative stress and inflammatory responses, increasing SOD activity and total antioxidant capacity in lung tissue and reducing ROS, MDA, and IL-1 $\beta$  levels [113].

Notably, some compounds or ingredients of CHM are generally considered to be antioxidants but can induce prooxidant effects similar to those of antioxidant supplements such as vitamin C [114]. These substances exhibit antioxidant activity at low concentrations but induce ROS production and cytotoxicity at high concentrations [115]. For example, the previously mentioned antioxidant ISL initially decreased the levels of ROS in HepG2 cells in a time-dependent manner; along with this effect, the activity of the Nrf2-mediated antioxidant enzyme system also declined to maintain the new redox balance. However, the intracellular ROS level was significantly higher after 6 h of ISL treatment, an effect attributed to reduced antioxidant capacity, and the sensitivity of cancer cells to X-ray irradiation was thus increased [115]. Epigallocatechin gallate (EGCG) is a phenolic compound in green tea extract and has anticancer activi-

ties in vivo and in vitro [116]. EGCG can decrease lipid peroxidation in hepatocytes and enhance antioxidant capacity. However, high concentrations of EGCG destroy the mitochondrial membrane and generate intracellular oxidative stress [117]. Thus, whether EGCG exhibits antioxidant or prooxidant activity depends on the cellular stress conditions, cell type, and EGCG concentration [116, 118]. CHM-derived compounds such as quercetin, curcumin, and resveratrol were found to exhibit similar features [3, 119].

To sum up, the antioxidant effects of CHMs described above and the examples listed in Table 1 exhibit diverse anticancer effects, including reducing inflammatory mediators, inhibiting tumor proliferation, inducing antiangiogenesis, suppressing metastasis, inhibiting glycolysis, overcoming drug resistance, and countering the side effects of chemo- and radiotherapy. These effects were mainly achieved by the regulation of several ROS-related transcription factors such as NRF2, NF- $\kappa$ B, COX-2, STAT3, and HIF-1 $\alpha$  and by enhancing the capacity of antioxidant enzymes such as GSH, SOD, and HO-1.

**4.2. Prooxidant Effects of CHM in Cancer Progression.** Since the levels of ROS in tumor cells are higher than those in normal cells, tumor cells are potentially more vulnerable to the accumulation of ROS. The strategy of increasing intracellular ROS levels by increasing ROS production and/or inhibiting the antioxidant capacity enables the ROS level to reach the toxic threshold in cancer cells before it does in normal cells, thereby selectively killing tumor cells without causing visible damage to normal cells (Figure 2).

Many CHM compounds can promote the production of intracellular ROS to induce various types of programmed cell death and enhance the efficacy of chemo- and radiotherapy. Scutellaria (Huang Qin) is one of the most commonly used CHMs in China and its surrounding areas and has a practical effect on infectious diseases caused by bacteria and viruses [120]. As a principal bioactive constituent of Scutellaria, wogonin has apparent anticancer effects against different types of cancer cells. It can induce mitochondrial apoptosis by activating PLC $\gamma$ 1 via H<sub>2</sub>O<sub>2</sub> signaling in malignant T cells, resulting in Ca<sup>2+</sup> overload in mitochondria [120]. Furthermore, wogonin enhanced TRAIL-induced apoptosis through ROS-mediated downregulation of the cFLIPL and IAP proteins [121]. In addition, levistolide A (LA), a natural compound isolated from the Chinese herb *Ligusticum chuansiong* Hort., can trigger ER stress-induced apoptosis by activating the ROS-mediated PERK/eIF2 $\alpha$ /CHOP axis [122]. Besides, LA synergizes with vinorelbine against tumors and induces cell cycle G2/M arrest and apoptosis; interestingly, it can reverse P-glycoprotein-mediated multidrug resistance in breast cancer cells [123]. Other classical compounds of CHM that target the apoptotic signaling pathway have been reviewed [9]. Sanguinarine (SNG) is a benzophenanthridine alkaloid that is predominantly extracted from *Chelidonium majus* (Bai Qu Cai), a well-known CHM mainly used for digestive and respiratory inflammatory diseases and malignant tumors. SNG has diverse biological activities, such as antimicrobial, anti-inflammatory, and antitumor properties. Our previous study has shown that SNG successfully

inhibited the proliferation of specific lung cancer cells expressing stem cell characteristics, possibly by downregulating WNT/ $\beta$ -catenin signaling [124]. SNG can not only induce apoptotic cell death but also trigger autophagic cell death by the ROS-dependent activation of ERK1/2 in malignant glioma cells [125]. Besides, this compound can upregulate NOX3 and then elevate ROS levels, resulting in EGFR<sup>T790M</sup> degradation to overcome tyrosine kinase inhibitor (TKI) resistance [126]. Artesunate is a derivative of the natural compound artemisinin, which is known for its antimalarial agents, with well-understood pharmacokinetics. ART specifically induces PCD in different cancer types in a manner initiated by ROS generation [127]. Recent studies have found that ART specifically induces ferroptotic cell death in pancreatic cancer cells in a ROS- and iron-dependent manner and that this induction can be blocked by the ferroptosis inhibitor ferrostatin-1 [128]. Interestingly, dihydroartemisinin (DAT), another artemisinin derivative with high bioavailability, enhances the sensitivity of cancer cells to ferroptosis inducers in a lysosome-dependent, but autophagy-independent manner. Importantly, DAT can further improve the ferroptosis-resistant cancer cell lines more sensitive to ferroptotic death, which suggests that the combination of DAT and ferroptosis inducers is an effective anticancer method [129].

In addition to directly inducing ROS production, inhibiting the activity of antioxidant enzymes to increase ROS levels is another potentially more effective approach to kill cancer cells. Cancer cells tend to have higher antioxidant capacity than normal cells to adapt to elevated levels of ROS, which promotes cancer cell resistance to exogenous ROS-inducing agents [119]. Many antioxidants, such as GSH, TRX, and SOD, and Nrf2 activity aid tumorigenesis and confer chemoresistance and are present at high levels in various tumor types [130–133].

Piperlongumine (PL) is a natural constituent of the long pepper fruit (*Piper longum*), which is extensively used in digestive diseases such as gastrointestinal cancer. PL can selectively kill a variety of tumor cells and enhance cisplatin-mediated anticancer activity [134, 135]. Its anticancer effects are mainly attributed to the silencing of the GSTP1 gene, thus reducing GSH content [136]. Isoforretin A (IsoA) is a novel ent-kaurane constituent isolated from a traditional Chinese medicinal herb of the *Isodon* genus and has multiple anticancer effects both *in vitro* and *in vivo*. IsoA inhibits Trx1 activity by covalently binding to the Cys32/Cys35 residues in the Trx1 activation site, resulting in ROS accumulation and causing DNA damage and apoptosis in tumor cells. It can be a potential novel agent for cancer therapy [137]. Consistent with this effect, both shikonin [138, 139] and parthenolide [140] can inhibit TrxR, interfere with redox balance, and eventually lead to ROS-mediated tumor cell death. Brusatol (BR), the main active ingredient of the *Brucea javanica* plant, has many anticancer properties [141]. BR is a potent inhibitor of Nrf2 and can degrade Nrf2 by ubiquitination to suppress the Nrf2-dependent protective response and thus sensitize lung cancer cells to cisplatin [142]. Moreover, the combination of BR and UVA irradiation increases ROS-induced cell cycle arrest and cellular apoptosis and inhibits

melanoma growth by regulating the AKT-Nrf2 pathway in cancer cells [143].

Summarizing the above examples of prooxidant CHM and those listed in Table 2, contrary to the antioxidant effects of CHM, it can be concluded that the prooxidant effects of CHM in cancer cells are achieved by enhancing ROS production and/or inhibiting antioxidant capacity, thereby activating ROS-dependent killing patterns on cancer cells. So far, the killing model of prooxidant CHM is mainly induced by apoptosis, which is primarily achieved by the regulation of ROS-related apoptotic upstream signaling pathway, such as MAPK/JNK/p38, JAK/STAT, PI3K/AKT, and ER stress pathways, followed by activation of apoptotic executive molecules, such as BAX/BCL-2, caspase family, and PARP-1. Other than this, CHMs also induce autophagic cell death, necroptosis, and ferroptosis in uncommon ways, but underlying molecular mechanisms remain unclear. Of note, ferroptosis, as a newly discovered type of cell death, possibly provides a promising choice for the application of CHM in cancer therapy, especially in the case of many conventional agents with apoptosis resistance.

## 5. Discussion

Cancer cells exhibit higher levels of ROS than normal cells [18, 27, 144]. ROS promote tumorigenesis via malignant transformation, sustained proliferation, angiogenesis, invasion, and metastasis. On the other hand, ROS at elevated levels can increase the vulnerability of cancer cells to various inducers. Considering the dual nature of ROS and the complexity of tumors themselves, exploring approaches to rationally utilize CHM to regulate ROS may maximize the anticancer functions of CHM.

The first strategy is to exploit the antioxidant properties of CHMs to reduce excessive intracellular ROS and to antagonize ROS-induced protumorigenic effects on normal cells. However, many clinical trials have inconsistently concluded that antioxidant supplements are beneficial for preventing tumors; furthermore, the long-term use of certain antioxidant supplements may even increase the incidence of some tumors and overall mortality [3, 145]. Moreover, recent studies have shown that antioxidants can promote carcinoma proliferation and distant metastasis *in vivo* [6, 146]. In terms of cancer treatment, antioxidant supplements may reduce the side effects of chemo- and radiotherapy in some cases but may also antagonize the positive effects of these treatments [17, 147, 148]. Therefore, although the abovementioned antioxidant CHM compounds or their active ingredients have shown an initial positive effect in tumor prevention and have been shown as an adjuvant treatment in preclinical studies, caution must be taken in their long-term application. Antioxidant CHMs are different from antioxidant supplements due to the fact that they are natural products with a complex combination of active ingredients. The properties of antioxidant CHMs are closer to those of fruits and vegetables rich in antioxidants. Thus, the use of CHMs rich in antioxidants rather than a single antioxidant compound might have better effects in tumor prevention. However, further systematic studies are needed.

Compared to ROS reduction strategies, which have a controversial role in application to tumors, ROS promotion strategies have shown better anticancer effects and clinical prospects. Such strategies can be implemented by using an agent that either increases ROS production or reduces antioxidant capacity or results in a combination of both effects. Various chemotherapeutic drugs, molecular targeted drugs, radiotherapy, and photodynamic therapy have been shown to kill tumor cells by increasing intracellular ROS levels [56, 104, 149, 150]. To date, some novel ROS inducers (such as ARQ501 and elesclomol), as well as antioxidant system drugs (such as the SOD1 inhibitor ATN-224 and the GSH inhibitors buthionine sulfoximine (BSO) and phenethyl isothiocyanate (PEITC)), have also been under clinical trials (see <http://clinicaltrials.gov/>). Many CHM-derived active constituents act as ROS generators to exert anticancer effects. Importantly, the intracellular level of ROS should be carefully controlled when using ROS-generating CHMs. If the levels of ROS are not sufficiently increased to the toxicity threshold, downstream oncogenes, such as PI3K, HIFs, NF- $\kappa$ B, and MAPK, may be activated to promote cancer development. Conversely, increasing the ROS levels too far over the cytotoxic level will lead to nonspecific damage to normal cells, thereby injuring sensitive vital organs such as the heart, liver, and kidneys [8]. Indeed, tumor cells maintain elevated antioxidant system activity to prevent oxidative damage from cytotoxic ROS; thus, ROS generators are not always useful. However, the use of antioxidant inhibitors in combination with ROS inducers may be a promising method in anticancer therapy because this approach can decrease the adaptability of tumor cells to both agents [20, 26]. Compounds such as curcumin [151] and triptolide [152] can simultaneously induce ROS generation and inhibit antioxidant defense, causing cancer cell death and enhancing the efficacy of chemotherapy. This pleiotropic effect may be beneficial in overcoming the resistance of cancer cells to conventional single-target drugs [149]. However, due to the bimodal nature of ROS and CHM, identifying the specific types of ROS and antioxidant molecules that are uniquely required for tumor growth and survival and determining the mechanisms targeted by the specific CHM in different types of tumors are important. Currently, the advent of new molecular tools for the localization, quantification, and real-time detection of ROS is expected to further deepen our understanding of redox, to advance ROS-based treatment strategies, and to generate great opportunities for the development of anticancer drugs from CHMs.

## 6. Conclusions

In summary, we describe how ROS are generated and eliminated within cells and the complicated dual roles of ROS in cancers. ROS not only are indiscriminate damaging molecules but also function as specific secondary messengers, involved in various physiological and pathological responses. This is the current focus on the debate in the field of redox biology and accounts for inconsistency with clinical and experimental studies on ROS. Traditional Chinese medicine is an ancient practice medicine with potential advantages in

cancer treatment. We selected and summarized the original researches of CHM based on ROS regulation with relatively precise molecular mechanisms. CHMs exert antitumor effects through antioxidant activities, including inhibition of inflammation; prevention of carcinogenesis; inhibition of tumor proliferation, growth, and metastasis; and reduction of side effects of chemo- and radiotherapy; on the other hand, CHMs primarily induce multiple cell death to kill cancer cells selectively by promoting oxidation, cause DNA damage and enhance the efficacy of chemo/radiotherapy and molecular targeted agents, and reverse drug resistance of cancer cells. Taken together, CHM plays a vital role in the prevention and treatment of tumor initiation, development, and progression. Moreover, it is a promising strategy to develop low-toxic and effective antitumor agents from CHMs based on the regulation ROS. Notably, the majority of current mechanistic researches are based on the reductionist approach, which may not adequately clarify the efficacy of herbal medicines, especially for the traditional Chinese compound formulas, the most common way used in the clinic. Therefore, a systematic biological method may be more appropriate and efficient for the development of effective therapies; additionally, more well-designed clinical trials and transformational experimental studies are also vitally needed to confirm the efficacy of CHMs in humans.

## Conflicts of Interest

All the authors declare that there are no potential conflicts of interest regarding this article.

## Authors' Contributions

Qiaohong Qian and Wanqing Chen, the first two authors, equally contribute to this work.

## Acknowledgments

This work was supported by the outstanding youth project of Shanghai Municipal Health Committee (2017YQ049), Shanghai Natural Science Foundation (16ZR1404000), and the Natural Science Foundation of China (81603590 and 81673947).

## References

- [1] O. Vafa, M. Wade, S. Kern et al., "c-Myc can induce DNA damage, increase reactive oxygen species, and mitigate p53 function: a mechanism for oncogene-induced genetic instability," *Molecular Cell*, vol. 9, no. 5, pp. 1031–1044, 2002.
- [2] G. Y. Liou and P. Storz, "Reactive oxygen species in cancer," *Free Radical Research*, vol. 44, no. 5, pp. 479–496, 2010.
- [3] T. Ozben, "Antioxidant supplementation on cancer risk and during cancer therapy: an update," *Current Topics in Medicinal Chemistry*, vol. 15, no. 2, pp. 170–178, 2015.
- [4] G. Bjelakovic, D. Nikolova, L. L. Gluud, R. G. Simonetti, and C. Gluud, "Mortality in randomized trials of antioxidant supplements for primary and secondary prevention: systematic review and meta-analysis," *JAMA*, vol. 297, no. 8, pp. 842–857, 2007.

- [5] G. M. DeNicola, F. A. Karreth, T. J. Humpton et al., "Oncogene-induced Nrf2 transcription promotes ROS detoxification and tumorigenesis," *Nature*, vol. 475, no. 7354, pp. 106–109, 2011.
- [6] E. Piskounova, M. Agathocleous, M. M. Murphy et al., "Oxidative stress inhibits distant metastasis by human melanoma cells," *Nature*, vol. 527, no. 7577, pp. 186–191, 2015.
- [7] M. Carochi and I. C. F. R. Ferreira, "A review on antioxidants, prooxidants and related controversy: natural and synthetic compounds, screening and analysis methodologies and future perspectives," *Food and Chemical Toxicology*, vol. 51, pp. 15–25, 2013.
- [8] M. Schieber and N. S. Chandel, "ROS function in redox signaling and oxidative stress," *Current Biology*, vol. 24, no. 10, pp. R453–R462, 2014.
- [9] M. Li-Weber, "Targeting apoptosis pathways in cancer by Chinese medicine," *Cancer Letters*, vol. 332, no. 2, pp. 304–312, 2013.
- [10] H. Xu, X. Zhao, X. Liu et al., "Antitumor effects of traditional Chinese medicine targeting the cellular apoptotic pathway," *Drug Design, Development and Therapy*, vol. 9, pp. 2735–2744, 2015.
- [11] F. Qi, A. Li, Y. Inagaki et al., "Chinese herbal medicines as adjuvant treatment during chemo- or radio-therapy for cancer," *Bioscience Trends*, vol. 4, no. 6, pp. 297–307, 2010.
- [12] Z. Wang, F. Qi, Y. Cui et al., "An update on Chinese herbal medicines as adjuvant treatment of anticancer therapeutics," *Bioscience Trends*, vol. 12, no. 3, pp. 220–239, 2018.
- [13] M. J. Akhtar, M. Ahamed, and H. A. Alhadlaq, "Therapeutic targets in the selective killing of cancer cells by nanomaterials," *Clinica Chimica Acta*, vol. 469, pp. 53–62, 2017.
- [14] D. E. Handy and J. Loscalzo, "Redox regulation of mitochondrial function," *Antioxidants & Redox Signaling*, vol. 16, no. 11, pp. 1323–1367, 2012.
- [15] D. B. Zorov, M. Juhaszova, and S. J. Sollott, "Mitochondrial reactive oxygen species (ROS) and ROS-induced ROS release," *Physiological Reviews*, vol. 94, no. 3, pp. 909–950, 2014.
- [16] I. I. C. Chio and D. A. Tuveson, "ROS in cancer: the burning question," *Trends in Molecular Medicine*, vol. 23, no. 5, pp. 411–429, 2017.
- [17] L. Tong, C. C. Chuang, S. Wu, and L. Zuo, "Reactive oxygen species in redox cancer therapy," *Cancer Letters*, vol. 367, no. 1, pp. 18–25, 2015.
- [18] J. N. Moloney and T. G. Cotter, "ROS signalling in the biology of cancer," *Seminars in Cell & Developmental Biology*, vol. 80, pp. 50–64, 2018.
- [19] P. Inarrea, H. Moini, D. Rettori et al., "Redox activation of mitochondrial intermembrane space Cu,Zn-superoxide dismutase," *Biochemical Journal*, vol. 387, no. 1, pp. 203–209, 2005.
- [20] S. Galadari, A. Rahman, S. Pallichankandy, and F. Thayyullathil, "Reactive oxygen species and cancer paradox: to promote or to suppress?," *Free Radical Biology and Medicine*, vol. 104, pp. 144–164, 2017.
- [21] N. Couto, J. Wood, and J. Barber, "The role of glutathione reductase and related enzymes on cellular redox homeostasis network," *Free Radical Biology and Medicine*, vol. 95, pp. 27–42, 2016.
- [22] M. Kobayashi and M. Yamamoto, "Molecular mechanisms activating the Nrf2-Keap1 pathway of antioxidant gene regulation," *Antioxidants & Redox Signaling*, vol. 7, no. 3–4, pp. 385–394, 2005.
- [23] R. A. Cairns, I. S. Harris, and T. W. Mak, "Regulation of cancer cell metabolism," *Nature Reviews Cancer*, vol. 11, no. 2, pp. 85–95, 2011.
- [24] Y. M. W. Janssen-Heininger, B. T. Mossman, N. H. Heintz et al., "Redox-based regulation of signal transduction: principles, pitfalls, and promises," *Free Radical Biology and Medicine*, vol. 45, no. 1, pp. 1–17, 2008.
- [25] A. V. Bazhin, P. P. Philippov, and S. Karakhanova, "Reactive oxygen species in cancer biology and anticancer therapy," *Oxidative Medicine and Cellular Longevity*, vol. 2016, Article ID 4197815, 2 pages, 2016.
- [26] C. Gorrini, I. S. Harris, and T. W. Mak, "Modulation of oxidative stress as an anticancer strategy," *Nature Reviews Drug Discovery*, vol. 12, no. 12, pp. 931–947, 2013.
- [27] M. Tafani, L. Sansone, F. Limana et al., "The interplay of reactive oxygen species, hypoxia, inflammation, and sirtuins in cancer initiation and progression," *Oxidative Medicine and Cellular Longevity*, vol. 2016, Article ID 3907147, 18 pages, 2016.
- [28] A. Maciag, G. Sithanandam, and L. M. Anderson, "Mutant K-rasV12 increases COX-2, peroxides and DNA damage in lung cells," *Carcinogenesis*, vol. 25, no. 11, pp. 2231–2237, 2004.
- [29] M. Ogrunc, R. di Micco, M. Liontos et al., "Oncogene-induced reactive oxygen species fuel hyperproliferation and DNA damage response activation," *Cell Death & Differentiation*, vol. 21, no. 6, pp. 998–1012, 2014.
- [30] A. Chatterjee, E. Mambo, and D. Sidransky, "Mitochondrial DNA mutations in human cancer," *Oncogene*, vol. 25, no. 34, pp. 4663–4674, 2006.
- [31] S. S. Sabharwal and P. T. Schumacker, "Mitochondrial ROS in cancer: initiators, amplifiers or an Achilles' heel?," *Nature Reviews Cancer*, vol. 14, no. 11, pp. 709–721, 2014.
- [32] V. Helfinger and K. Schroder, "Redox control in cancer development and progression," *Molecular Aspects of Medicine*, vol. 63, pp. 88–98, 2018.
- [33] D. Hanahan and R. A. Weinberg, "Hallmarks of cancer: the next generation," *Cell*, vol. 144, no. 5, pp. 646–674, 2011.
- [34] S. R. Lee, K. S. Yang, J. Kwon, C. Lee, W. Jeong, and S. G. Rhee, "Reversible inactivation of the tumor suppressor PTEN by H<sub>2</sub>O<sub>2</sub>," *Journal of Biological Chemistry*, vol. 277, no. 23, pp. 20336–20342, 2002.
- [35] A. Salmeen, J. N. Andersen, M. P. Myers et al., "Redox regulation of protein tyrosine phosphatase 1B involves a sulphenyl-amide intermediate," *Nature*, vol. 423, no. 6941, pp. 769–773, 2003.
- [36] Y. Son, Y. K. Cheong, N. H. Kim, H. T. Chung, D. G. Kang, and H. O. Pae, "Mitogen-activated protein kinases and reactive oxygen species: how can ROS activate MAPK pathways?," *Journal of Signal Transduction*, vol. 2011, Article ID 792639, 6 pages, 2011.
- [37] J. E. Klaunig, Z. Wang, X. Pu, and S. Zhou, "Oxidative stress and oxidative damage in chemical carcinogenesis," *Toxicology and Applied Pharmacology*, vol. 254, no. 2, pp. 86–99, 2011.
- [38] T. Pralhad, S. Madhusudan, and K. Rajendrakumar, "Concept, mechanisms and therapeutics of angiogenesis in cancer and other diseases," *Journal of Pharmacy and Pharmacology*, vol. 55, no. 8, pp. 1045–1053, 2003.

- [39] H. Peshavariya, G. J. Dusting, F. Jiang et al., "NADPH oxidase isoform selective regulation of endothelial cell proliferation and survival," *Naunyn-Schmiedeberg's Archives of Pharmacology*, vol. 380, no. 2, pp. 193–204, 2009.
- [40] E. Monaghan-Benson and K. Burrridge, "The regulation of vascular endothelial growth factor-induced microvascular permeability requires Rac and reactive oxygen species," *Journal of Biological Chemistry*, vol. 284, no. 38, pp. 25602–25611, 2009.
- [41] M. Yamaoka-Tojo, T. Tojo, H. W. Kim et al., "IQGAP1 mediates VE-cadherin-based cell-cell contacts and VEGF signaling at adherence junctions linked to angiogenesis," *Arteriosclerosis, Thrombosis, and Vascular Biology*, vol. 26, no. 9, pp. 1991–1997, 2006.
- [42] A. B. Hwang and S. J. Lee, "Regulation of life span by mitochondrial respiration: the HIF-1 and ROS connection," *Aging*, vol. 3, no. 3, pp. 304–310, 2011.
- [43] Z. A. Sibenaller, J. L. Welsh, C. du et al., "Extracellular superoxide dismutase suppresses hypoxia-inducible factor-1 $\alpha$  in pancreatic cancer," *Free Radical Biology and Medicine*, vol. 69, pp. 357–366, 2014.
- [44] S. Kaewpila, S. Venkataraman, G. R. Buettner, and L. W. Oberley, "Manganese superoxide dismutase modulates hypoxia-inducible factor-1 $\alpha$  induction via superoxide," *Cancer Research*, vol. 68, no. 8, pp. 2781–2788, 2008.
- [45] A. C. Chiang and J. Massague, "Molecular basis of metastasis," *New England Journal of Medicine*, vol. 359, no. 26, pp. 2814–2823, 2008.
- [46] B. Diaz, G. Shani, I. Pass, D. Anderson, M. Quintavalle, and S. A. Courtneidge, "Tks5-dependent, nox-mediated generation of reactive oxygen species is necessary for invadopodia formation," *Science Signaling*, vol. 2, no. 88, article ra53, 2009.
- [47] E. Giannoni, T. Fiaschi, G. Ramponi, and P. Chiarugi, "Redox regulation of anoikis resistance of metastatic prostate cancer cells: key role for Src and EGFR-mediated pro-survival signals," *Oncogene*, vol. 28, no. 20, pp. 2074–2086, 2009.
- [48] S. Basuroy, M. Dunagan, P. Sheth, A. Seth, and R. K. Rao, "Hydrogen peroxide activates focal adhesion kinase and c-Src by a phosphatidylinositol 3 kinase-dependent mechanism and promotes cell migration in Caco-2 cell monolayers," *American Journal of Physiology-Gastrointestinal and Liver Physiology*, vol. 299, no. 1, pp. G186–G195, 2010.
- [49] S. A. Brooks, H. J. Lomax-Browne, T. M. Carter, C. E. Kinch, and D. M. S. Hall, "Molecular interactions in cancer cell metastasis," *Acta Histochemica*, vol. 112, no. 1, pp. 3–25, 2010.
- [50] L. Tothhawng, S. Deng, S. Pervaiz, and C. T. Yap, "Redox regulation of cancer cell migration and invasion," *Mitochondrion*, vol. 13, no. 3, pp. 246–253, 2013.
- [51] N. Tobar, V. Villar, and J. F. Santibanez, "ROS-NF $\kappa$ B mediates TGF- $\beta$ 1-induced expression of urokinase-type plasminogen activator, matrix metalloproteinase-9 and cell invasion," *Molecular and Cellular Biochemistry*, vol. 340, no. 1-2, pp. 195–202, 2010.
- [52] S. Cannito, E. Novo, A. Compagnone et al., "Redox mechanisms switch on hypoxia-dependent epithelial-mesenchymal transition in cancer cells," *Carcinogenesis*, vol. 29, no. 12, pp. 2267–2278, 2008.
- [53] S. Lamouille, J. Xu, and R. Derynck, "Molecular mechanisms of epithelial-mesenchymal transition," *Nature Reviews Molecular Cell Biology*, vol. 15, no. 3, pp. 178–196, 2014.
- [54] H. Sui, L. Zhu, W. Deng, and Q. Li, "Epithelial-mesenchymal transition and drug resistance: role, molecular mechanisms, and therapeutic strategies," *Oncology Research and Treatment*, vol. 37, no. 10, pp. 584–589, 2014.
- [55] M. Redza-Dutordoir and D. A. Averill-Bates, "Activation of apoptosis signalling pathways by reactive oxygen species," *Biochimica et Biophysica Acta (BBA) - Molecular Cell Research*, vol. 1863, no. 12, pp. 2977–2992, 2016.
- [56] Z. Zou, H. Chang, H. Li, and S. Wang, "Induction of reactive oxygen species: an emerging approach for cancer therapy," *Apoptosis*, vol. 22, no. 11, pp. 1321–1335, 2017.
- [57] L. Wang, N. Azad, L. Kongkanermit et al., "The Fas death signaling pathway connecting reactive oxygen species generation and FLICE inhibitory protein down-regulation," *The Journal of Immunology*, vol. 180, no. 5, pp. 3072–3080, 2008.
- [58] P. J. Nadeau, S. J. Charette, and J. Landry, "REDOX reaction at ASK1-Cys250 is essential for activation of JNK and induction of apoptosis," *Molecular Biology of the Cell*, vol. 20, no. 16, pp. 3628–3637, 2009.
- [59] S. W. Ryter, H. P. Kim, A. Hoetzel et al., "Mechanisms of cell death in oxidative stress," *Antioxidants & Redox Signaling*, vol. 9, no. 1, pp. 49–89, 2007.
- [60] S. A. Susin, H. K. Lorenzo, N. Zamzami et al., "Molecular characterization of mitochondrial apoptosis-inducing factor," *Nature*, vol. 397, no. 6718, pp. 441–446, 1999.
- [61] S. Luanpitpong, P. Chanvorachote, C. Stehlik et al., "Regulation of apoptosis by Bcl-2 cysteine oxidation in human lung epithelial cells," *Molecular Biology of the Cell*, vol. 24, no. 6, pp. 858–869, 2013.
- [62] M. O. Hengartner, "The biochemistry of apoptosis," *Nature*, vol. 407, no. 6805, pp. 770–776, 2000.
- [63] J. D. Malhotra, H. Miao, K. Zhang et al., "Antioxidants reduce endoplasmic reticulum stress and improve protein secretion," *Proceedings of the National Academy of Sciences of the United States of America*, vol. 105, no. 47, pp. 18525–18530, 2008.
- [64] H. M. A. Zeeshan, G. H. Lee, H. R. Kim, and H. J. Chae, "Endoplasmic reticulum stress and associated ROS," *International Journal of Molecular Sciences*, vol. 17, no. 3, p. 327, 2016.
- [65] S. Orrenius, V. Gogvadze, and B. Zhivotovsky, "Calcium and mitochondria in the regulation of cell death," *Biochemical and Biophysical Research Communications*, vol. 460, no. 1, pp. 72–81, 2015.
- [66] A. Delaunay-Moisan and C. Appenzeller-Herzog, "The antioxidant machinery of the endoplasmic reticulum: protection and signaling," *Free Radical Biology and Medicine*, vol. 83, pp. 341–351, 2015.
- [67] C. He and D. J. Klionsky, "Regulation mechanisms and signaling pathways of autophagy," *Annual Review of Genetics*, vol. 43, no. 1, pp. 67–93, 2009.
- [68] L. Li, G. Ishdorj, and S. B. Gibson, "Reactive oxygen species regulation of autophagy in cancer: implications for cancer treatment," *Free Radical Biology and Medicine*, vol. 53, no. 7, pp. 1399–1410, 2012.
- [69] Y. Chen, E. McMillan-Ward, J. Kong, S. J. Israels, and S. B. Gibson, "Oxidative stress induces autophagic cell death independent of apoptosis in transformed and cancer cells," *Cell Death & Differentiation*, vol. 15, no. 1, pp. 171–182, 2008.
- [70] F. Thayyullathil, A. Rahman, S. Pallichankandy, M. Patel, and S. Galadari, "ROS-dependent prostate apoptosis response-4 (Par-4) up-regulation and ceramide generation are the prime

- signaling events associated with curcumin-induced autophagic cell death in human malignant glioma,” *FEBS Open Bio*, vol. 4, no. 1, pp. 763–776, 2014.
- [71] Y. Zhao, T. Qu, P. Wang et al., “Unravelling the relationship between macroautophagy and mitochondrial ROS in cancer therapy,” *Apoptosis*, vol. 21, no. 5, pp. 517–531, 2016.
- [72] R. Scherz-Shouval, E. Shvets, E. Fass, H. Shorer, L. Gil, and Z. Elazar, “Reactive oxygen species are essential for autophagy and specifically regulate the activity of Atg4,” *The EMBO Journal*, vol. 26, no. 7, pp. 1749–1760, 2007.
- [73] Z. Guo, S. Kozlov, M. F. Lavin, M. D. Person, and T. T. Paull, “ATM activation by oxidative stress,” *Science*, vol. 330, no. 6003, pp. 517–521, 2010.
- [74] L. Li, Y. Chen, and S. B. Gibson, “Starvation-induced autophagy is regulated by mitochondrial reactive oxygen species leading to AMPK activation,” *Cellular Signalling*, vol. 25, no. 1, pp. 50–65, 2013.
- [75] D. Egan, J. Kim, R. J. Shaw, and K. L. Guan, “The autophagy initiating kinase ULK1 is regulated via opposing phosphorylation by AMPK and mTOR,” *Autophagy*, vol. 7, no. 6, pp. 643–644, 2011.
- [76] Y. J. Byun, S. K. Kim, Y. M. Kim, G. T. Chae, S. W. Jeong, and S. B. Lee, “Hydrogen peroxide induces autophagic cell death in C6 glioma cells via BNIP3-mediated suppression of the mTOR pathway,” *Neuroscience Letters*, vol. 461, no. 2, pp. 131–135, 2009.
- [77] G. Bellot, R. Garcia-Medina, P. Gounon et al., “Hypoxia-induced autophagy is mediated through hypoxia-inducible factor induction of BNIP3 and BNIP3L via their BH3 domains,” *Molecular and Cellular Biology*, vol. 29, no. 10, pp. 2570–2581, 2009.
- [78] M. Djavaheri-Mergny, M. Amelotti, J. Mathieu et al., “NF- $\kappa$ B activation represses tumor necrosis factor- $\alpha$ -induced autophagy,” *Journal of Biological Chemistry*, vol. 281, no. 41, pp. 30373–30382, 2006.
- [79] L. Poillet-Perez, G. Despouy, R. Delage-Mourroux, and M. Boyer-Guittaut, “Interplay between ROS and autophagy in cancer cells, from tumor initiation to cancer therapy,” *Redox Biology*, vol. 4, pp. 184–192, 2015.
- [80] M. Komatsu, H. Kurokawa, S. Waguri et al., “The selective autophagy substrate p62 activates the stress responsive transcription factor Nrf2 through inactivation of Keap1,” *Nature Cell Biology*, vol. 12, no. 3, pp. 213–223, 2010.
- [81] N. F. Villeneuve, A. Lau, and D. D. Zhang, “Regulation of the Nrf2-Keap1 antioxidant response by the ubiquitin proteasome system: an insight into cullin-ring ubiquitin ligases,” *Antioxidants & Redox Signaling*, vol. 13, no. 11, pp. 1699–1712, 2010.
- [82] S. J. Dixon, K. M. Lemberg, M. R. Lamprecht et al., “Ferroptosis: an iron-dependent form of nonapoptotic cell death,” *Cell*, vol. 149, no. 5, pp. 1060–1072, 2012.
- [83] W. S. Yang and B. R. Stockwell, “Ferroptosis: death by lipid peroxidation,” *Trends in Cell Biology*, vol. 26, no. 3, pp. 165–176, 2016.
- [84] B. R. Stockwell, J. P. Friedmann Angeli, H. Bayir et al., “Ferroptosis: a regulated cell death nexus linking metabolism, redox biology, and disease,” *Cell*, vol. 171, no. 2, pp. 273–285, 2017.
- [85] R. Skouta, S. J. Dixon, J. Wang et al., “Ferrostatis inhibit oxidative lipid damage and cell death in diverse disease models,” *Journal of the American Chemical Society*, vol. 136, no. 12, pp. 4551–4556, 2014.
- [86] W. S. Yang, R. SriRamaratnam, M. E. Welsch et al., “Regulation of ferroptotic cancer cell death by GPX4,” *Cell*, vol. 156, no. 1–2, pp. 317–331, 2014.
- [87] O. Zilka, R. Shah, B. Li et al., “On the mechanism of cytoprotection by ferrostatin-1 and liproxstatin-1 and the role of lipid peroxidation in ferroptotic cell death,” *ACS Central Science*, vol. 3, no. 3, pp. 232–243, 2017.
- [88] Z. Cheng and Y. Li, “What is responsible for the initiating chemistry of iron-mediated lipid peroxidation: an update,” *Chemical Reviews*, vol. 107, no. 3, pp. 748–766, 2007.
- [89] Y. Xie, W. Hou, X. Song et al., “Ferroptosis: process and function,” *Cell Death & Differentiation*, vol. 23, no. 3, pp. 369–379, 2016.
- [90] M. Gao, P. Monian, N. Quadri, R. Ramasamy, and X. Jiang, “Glutaminolysis and transferrin regulate ferroptosis,” *Molecular Cell*, vol. 59, no. 2, pp. 298–308, 2015.
- [91] X. Sun, Z. Ou, M. Xie et al., “HSPB1 as a novel regulator of ferroptotic cancer cell death,” *Oncogene*, vol. 34, no. 45, pp. 5617–5625, 2015.
- [92] L. Jiang, N. Kon, T. Li et al., “Ferroptosis as a p53-mediated activity during tumour suppression,” *Nature*, vol. 520, no. 7545, pp. 57–62, 2015.
- [93] L. Jiang, J. H. Hickman, S. J. Wang, and W. Gu, “Dynamic roles of p53-mediated metabolic activities in ROS-induced stress responses,” *Cell Cycle*, vol. 14, no. 18, pp. 2881–2885, 2015.
- [94] W. L. Hsiao and L. Liu, “The role of traditional Chinese herbal medicines in cancer therapy – from TCM theory to mechanistic insights,” *Planta Medica*, vol. 76, no. 11, pp. 1118–1131, 2010.
- [95] F. L. Büchner, H. B. Bueno-de-Mesquita, J. Linseisen et al., “Fruits and vegetables consumption and the risk of histological subtypes of lung cancer in the European Prospective Investigation into Cancer and Nutrition (EPIC),” *Cancer Causes & Control*, vol. 21, no. 3, pp. 357–371, 2010.
- [96] M. Shareck, M. C. Rousseau, A. Koushik, J. Siemiatycki, and M. E. Parent, “Inverse association between dietary intake of selected carotenoids and vitamin C and risk of lung cancer,” *Frontiers in Oncology*, vol. 7, p. 23, 2017.
- [97] R. Jiao, Y. Liu, H. Gao, J. Xiao, and K. F. So, “The anti-oxidant and antitumor properties of plant polysaccharides,” *The American Journal of Chinese Medicine*, vol. 44, no. 3, pp. 463–488, 2016.
- [98] P. Pratheeshkumar, Y. O. Son, S. P. Divya et al., “Quercetin inhibits Cr(VI)-induced malignant cell transformation by targeting miR-21-PDCD4 signaling pathway,” *Oncotarget*, vol. 8, no. 32, pp. 52118–52131, 2017.
- [99] Y. Li, Y. Hu, S. Shi, and L. Jiang, “Evaluation of antioxidant and immuno-enhancing activities of purslane polysaccharides in gastric cancer rats,” *International Journal of Biological Macromolecules*, vol. 68, pp. 113–116, 2014.
- [100] J. Bao, R. Ding, L. Zou et al., “Forsythiae Fructus inhibits B16 melanoma growth involving MAPKs/Nrf2/HO-1 mediated anti-oxidation and anti-inflammation,” *The American Journal of Chinese Medicine*, vol. 44, no. 05, pp. 1043–1061, 2016.
- [101] M. Yuan, W. Meng, W. Liao, and S. Lian, “Andrographolide antagonizes TNF- $\alpha$ -induced IL-8 via inhibition of NADPH oxidase/ROS/NF- $\kappa$ B and Src/MAPKs/AP-1 axis in human



- colorectal cancer HCT116 cells," *Journal of Agricultural and Food Chemistry*, vol. 66, no. 20, pp. 5139–5148, 2018.
- [102] X. Zhang, E. D. Yeung, J. Wang et al., "Isoliquiritigenin, a natural anti-oxidant, selectively inhibits the proliferation of prostate cancer cells," *Clinical and Experimental Pharmacology and Physiology*, vol. 37, no. 8, pp. 841–847, 2010.
- [103] G. T. Kwon, H. J. Cho, W. Y. Chung, K. K. Park, A. Moon, and J. H. Y. Park, "Isoliquiritigenin inhibits migration and invasion of prostate cancer cells: possible mediation by decreased JNK/AP-1 signaling," *The Journal of Nutritional Biochemistry*, vol. 20, no. 9, pp. 663–676, 2009.
- [104] B. Yan, L. Cheng, Z. Jiang et al., "Resveratrol inhibits ROS-promoted activation and glycolysis of pancreatic stellate cells via suppression of miR-21," *Oxidative Medicine and Cellular Longevity*, vol. 2018, Article ID 1346958, 15 pages, 2018.
- [105] H. R. Teppo, Y. Soini, and P. Karihtala, "Reactive oxygen species-mediated mechanisms of action of targeted cancer therapy," *Oxidative Medicine and Cellular Longevity*, vol. 2017, Article ID 1485283, 11 pages, 2017.
- [106] D. Trachootham, J. Alexandre, and P. Huang, "Targeting cancer cells by ROS-mediated mechanisms: a radical therapeutic approach?," *Nature Reviews Drug Discovery*, vol. 8, no. 7, pp. 579–591, 2009.
- [107] B. Li, D. S. Kim, R. K. Yadav, H. R. Kim, and H. J. Chae, "Sulforaphane prevents doxorubicin-induced oxidative stress and cell death in rat H9c2 cells," *International Journal of Molecular Medicine*, vol. 36, no. 1, pp. 53–64, 2015.
- [108] A. Yanaka, "Sulforaphane enhances protection and repair of gastric mucosa against oxidative stress in vitro, and demonstrates anti-inflammatory effects on Helicobacter pylori-infected gastric mucosae in mice and human subjects," *Current Pharmaceutical Design*, vol. 17, no. 16, pp. 1532–1540, 2011.
- [109] L. Li, J. Ni, M. Li et al., "Ginsenoside Rg3 micelles mitigate doxorubicin-induced cardiotoxicity and enhance its anticancer efficacy," *Drug Delivery*, vol. 24, no. 1, pp. 1617–1630, 2017.
- [110] B. Ahmmed, S. Kampo, M. Khan et al., "Rg3 inhibits gemcitabine-induced lung cancer cell invasiveness through ROS-dependent, NF- $\kappa$ B- and HIF-1 $\alpha$ -mediated downregulation of PTX3," *Journal of Cellular Physiology*, vol. 234, no. 7, pp. 10680–10697, 2019.
- [111] Y. Gao, S. Chu, Q. Shao et al., "Antioxidant activities of ginsenoside Rg1 against cisplatin-induced hepatic injury through Nrf2 signaling pathway in mice," *Free Radical Research*, vol. 51, no. 1, pp. 1–13, 2017.
- [112] J. Jin, M. Li, Z. Zhao et al., "Protective effect of Wuzhi tablet (*Schisandra sphenanthera* extract) against cisplatin-induced nephrotoxicity via Nrf2-mediated defense response," *Phyto-medicine*, vol. 22, no. 5, pp. 528–535, 2015.
- [113] W. N. Yu, L. F. Sun, and H. Yang, "Inhibitory effects of astragaloside IV on bleomycin-induced pulmonary fibrosis in rats via attenuation of oxidative stress and inflammation," *Inflammation*, vol. 39, no. 5, pp. 1835–1841, 2016.
- [114] J. Yun, E. Mullarky, C. Lu et al., "Vitamin C selectively kills KRAS and BRAF mutant colorectal cancer cells by targeting GAPDH," *Science*, vol. 350, no. 6266, pp. 1391–1396, 2015.
- [115] C. Sun, H. Zhang, X. F. Ma et al., "Isoliquiritigenin enhances radiosensitivity of HepG2 cells via disturbance of redox status," *Cell Biochemistry and Biophysics*, vol. 65, no. 3, pp. 433–444, 2013.
- [116] J. D. Lambert and R. J. Elias, "The antioxidant and pro-oxidant activities of green tea polyphenols: a role in cancer prevention," *Archives of Biochemistry and Biophysics*, vol. 501, no. 1, pp. 65–72, 2010.
- [117] G. Galati, A. Lin, A. M. Sultan, and P. J. O'Brien, "Cellular and in vivo hepatotoxicity caused by green tea phenolic acids and catechins," *Free Radical Biology and Medicine*, vol. 40, no. 4, pp. 570–580, 2006.
- [118] W. Shi, L. Li, Y. Ding et al., "The critical role of epigallocatechin gallate in regulating mitochondrial metabolism," *Future Medicinal Chemistry*, vol. 10, no. 7, pp. 795–809, 2018.
- [119] A. Glasauer and N. S. Chandel, "Targeting antioxidants for cancer therapy," *Biochemical Pharmacology*, vol. 92, no. 1, pp. 90–101, 2014.
- [120] S. Baumann, S. C. Fas, M. Giaisi et al., "Wogonin preferentially kills malignant lymphocytes and suppresses T-cell tumor growth by inducing PLC $\gamma$ 1- and Ca<sup>2+</sup>-dependent apoptosis," *Blood*, vol. 111, no. 4, pp. 2354–2363, 2008.
- [121] L. Yang, Q. Wang, D. Li et al., "Wogonin enhances antitumor activity of tumor necrosis factor-related apoptosis-inducing ligand in vivo through ROS-mediated downregulation of cFLIP<sub>L</sub> and IAP proteins," *Apoptosis*, vol. 18, no. 5, pp. 618–626, 2013.
- [122] Y. Yang, Y. Zhang, L. Wang, and S. Lee, "Levistolide A induces apoptosis via ROS-mediated ER stress pathway in colon cancer cells," *Cellular Physiology and Biochemistry*, vol. 42, no. 3, pp. 929–938, 2017.
- [123] F. Chen, T. Wang, J. Wang, Z. Q. Wang, and M. Qian, "Levistolide A overcomes P-glycoprotein-mediated drug resistance in human breast carcinoma cells," *Acta Pharmacologica Sinica*, vol. 29, no. 4, pp. 458–464, 2008.
- [124] J. Yang, Z. Fang, J. Wu et al., "Construction and application of a lung cancer stem cell model: antitumor drug screening and molecular mechanism of the inhibitory effects of sanguinarine," *Tumor Biology*, vol. 37, no. 10, pp. 13871–13883, 2016.
- [125] S. Pallichankandy, A. Rahman, F. Thayyullathil, and S. Galadari, "ROS-dependent activation of autophagy is a critical mechanism for the induction of anti-glioma effect of sanguinarine," *Free Radical Biology and Medicine*, vol. 89, pp. 708–720, 2015.
- [126] E. L. H. Leung, X. X. Fan, M. P. Wong et al., "Targeting tyrosine kinase inhibitor-resistant non-small cell lung cancer by inducing epidermal growth factor receptor degradation via methionine 790 oxidation," *Antioxidants & Redox Signaling*, vol. 24, no. 5, pp. 263–279, 2016.
- [127] A. Hamacher-Brady, H. A. Stein, S. Turschner et al., "Artesunate activates mitochondrial apoptosis in breast cancer cells via iron-catalyzed lysosomal reactive oxygen species production," *Journal of Biological Chemistry*, vol. 286, no. 8, pp. 6587–6601, 2011.
- [128] N. Eling, L. Reuter, J. Hazin, A. Hamacher-Brady, and N. R. Brady, "Identification of artesunate as a specific activator of ferroptosis in pancreatic cancer cells," *Oncoscience*, vol. 2, no. 5, pp. 517–532, 2015.
- [129] G. Q. Chen, F. A. Benthani, J. Wu, D. Liang, Z. X. Bian, and X. Jiang, "Artemisinin compounds sensitize cancer cells to ferroptosis by regulating iron homeostasis," *Cell Death & Differentiation*, 2019.
- [130] A. J. León-González, C. Auger, and V. B. Schini-Kerth, "Pro-oxidant activity of polyphenols and its implication on cancer

- chemoprevention and chemotherapy," *Biochemical Pharmacology*, vol. 98, no. 3, pp. 371–380, 2015.
- [131] Y. R. Kim, J. E. Oh, M. S. Kim et al., "Oncogenic NRF2 mutations in squamous cell carcinomas of oesophagus and skin," *The Journal of Pathology*, vol. 220, no. 4, pp. 446–451, 2010.
- [132] M. L. Teoh-Fitzgerald, M. P. Fitzgerald, W. Zhong, R. W. Askeland, and F. E. Domann, "Epigenetic reprogramming governs EcSOD expression during human mammary epithelial cell differentiation, tumorigenesis and metastasis," *Oncogene*, vol. 33, no. 3, pp. 358–368, 2014.
- [133] P. C. Hart, M. Mao, A. L. P. de Abreu et al., "MnSOD upregulation sustains the Warburg effect via mitochondrial ROS and AMPK-dependent signalling in cancer," *Nature Communications*, vol. 6, no. 1, article 6053, 2015.
- [134] L. Raj, T. Ide, A. U. Gurkar et al., "Selective killing of cancer cells by a small molecule targeting the stress response to ROS," *Nature*, vol. 475, no. 7355, pp. 231–234, 2011.
- [135] J. L. Roh, E. H. Kim, J. Y. Park, J. W. Kim, M. Kwon, and B. H. Lee, "Piperlongumine selectively kills cancer cells and increases cisplatin antitumor activity in head and neck cancer," *Oncotarget*, vol. 5, no. 19, pp. 9227–9238, 2014.
- [136] W. Harshbarger, S. Gondi, S. B. Ficarro et al., "Structural and biochemical analyses reveal the mechanism of glutathione S-transferase Pi 1 inhibition by the anti-cancer compound piperlongumine," *Journal of Biological Chemistry*, vol. 292, no. 1, pp. 112–120, 2017.
- [137] X. Sun, W. Wang, J. Chen et al., "The natural diterpenoid isoforretin A inhibits thioredoxin-1 and triggers potent ROS-mediated antitumor effects," *Cancer Research*, vol. 77, no. 4, pp. 926–936, 2017.
- [138] D. Duan, B. Zhang, J. Yao, Y. Liu, and J. Fang, "Shikonin targets cytosolic thioredoxin reductase to induce ROS-mediated apoptosis in human promyelocytic leukemia HL-60 cells," *Free Radical Biology and Medicine*, vol. 70, pp. 182–193, 2014.
- [139] X. Li, X. X. Fan, Z. B. Jiang et al., "Shikonin inhibits gefitinib-resistant non-small cell lung cancer by inhibiting TrxR and activating the EGFR proteasomal degradation pathway," *Pharmacological Research*, vol. 115, pp. 45–55, 2017.
- [140] D. Duan, J. Zhang, J. Yao, Y. Liu, and J. Fang, "Targeting thioredoxin reductase by parthenolide contributes to inducing apoptosis of HeLa cells," *Journal of Biological Chemistry*, vol. 291, no. 19, pp. 10021–10031, 2016.
- [141] B. Harder, W. Tian, J. J. La Clair et al., "Brusatol overcomes chemoresistance through inhibition of protein translation," *Molecular Carcinogenesis*, vol. 56, no. 5, pp. 1493–1500, 2017.
- [142] D. Ren, N. F. Villeneuve, T. Jiang et al., "Brusatol enhances the efficacy of chemotherapy by inhibiting the Nrf2-mediated defense mechanism," *Proceedings of the National Academy of Sciences of the United States of America*, vol. 108, no. 4, pp. 1433–1438, 2011.
- [143] M. Wang, G. Shi, C. Bian et al., "UVA irradiation enhances brusatol-mediated inhibition of melanoma growth by downregulation of the Nrf2-mediated antioxidant response," *Oxidative Medicine and Cellular Longevity*, vol. 2018, Article ID 9742154, 15 pages, 2018.
- [144] L. Zhang, J. Li, L. Zong et al., "Reactive Oxygen Species and Targeted Therapy for Pancreatic Cancer," *Oxidative Medicine and Cellular Longevity*, vol. 2016, Article ID 1616781, 9 pages, 2016.
- [145] G. Bjelakovic, D. Nikolova, and C. Gluud, "Antioxidant supplements to prevent mortality," *JAMA*, vol. 310, no. 11, pp. 1178–1179, 2013.
- [146] K. Le Gal, M. X. Ibrahim, C. Wiel et al., "Antioxidants can increase melanoma metastasis in mice," *Science Translational Medicine*, vol. 7, no. 308, p. 308re8, 2015.
- [147] M. Filippova, V. Filippov, V. M. Williams et al., "Cellular levels of oxidative stress affect the response of cervical cancer cells to chemotherapeutic agents," *BioMed Research International*, vol. 2014, Article ID 574659, 14 pages, 2014.
- [148] M. Fukui, N. Yamabe, and B. T. Zhu, "Resveratrol attenuates the anticancer efficacy of paclitaxel in human breast cancer cells *in vitro* and *in vivo*," *European Journal of Cancer*, vol. 46, no. 10, pp. 1882–1891, 2010.
- [149] C. Martin-Cordero, A. Jose Leon-Gonzalez, J. Manuel Calderon-Montano, E. Burgos-Moron, and M. Lopez-Lazaro, "Pro-oxidant natural products as anticancer agents," *Current Drug Targets*, vol. 13, no. 8, pp. 1006–1028, 2012.
- [150] Y. Yang, Y. Hu, and H. Wang, "Targeting antitumor immune response for enhancing the efficacy of photodynamic therapy of cancer: recent advances and future perspectives," *Oxidative Medicine and Cellular Longevity*, vol. 2016, Article ID 5274084, 11 pages, 2016.
- [151] M. López-Lázaro, "Anticancer and carcinogenic properties of curcumin: considerations for its clinical development as a cancer chemopreventive and chemotherapeutic agent," *Molecular Nutrition & Food Research*, vol. 52, Supplement 1, pp. S103–S127, 2008.
- [152] Y. Wang, S. H. Guo, X. J. Shang et al., "Triptolide induces Sertoli cell apoptosis in mice via ROS/JNK-dependent activation of the mitochondrial pathway and inhibition of Nrf2-mediated antioxidant response," *Acta Pharmacologica Sinica*, vol. 39, no. 2, pp. 311–327, 2018.
- [153] W. Yan, Y. Xu, Y. Yuan et al., "Renoprotective mechanisms of astragaloside IV in cisplatin-induced acute kidney injury," *Free Radical Research*, vol. 51, no. 7-8, pp. 669–683, 2017.
- [154] N. Miyoshi, S. Takabayashi, T. Osawa, and Y. Nakamura, "Benzyl isothiocyanate inhibits excessive superoxide generation in inflammatory leukocytes: implication for prevention against inflammation-related carcinogenesis," *Carcinogenesis*, vol. 25, no. 4, pp. 567–575, 2004.
- [155] W. Chen, X. Li, L. Q. Jia et al., "Neuroprotective activities of catalpol against CaMKII-dependent apoptosis induced by LPS in PC12 cells," *British Journal of Pharmacology*, vol. 169, no. 5, pp. 1140–1152, 2013.
- [156] S. H. Hashemi-Shahri, A. Golshan, S. A. Mohajeri et al., "ROS-scavenging and anti-tyrosinase properties of crocetin on B16F10 murine melanoma cells," *Anti-Cancer Agents in Medicinal Chemistry*, vol. 18, no. 7, pp. 1064–1069, 2018.
- [157] A. Jain, A. Samyutty, C. Jackson et al., "Curcumin inhibits PhIP induced cytotoxicity in breast epithelial cells through multiple molecular targets," *Cancer Letters*, vol. 365, no. 1, pp. 122–131, 2015.
- [158] L. Zhao, X. Tao, Y. Qi, L. Xu, L. Yin, and J. Peng, "Protective effect of dioscin against doxorubicin-induced cardiotoxicity via adjusting microRNA-140-5p-mediated myocardial oxidative stress," *Redox Biology*, vol. 16, pp. 189–198, 2018.
- [159] H. Lv, Q. Liu, J. Zhou, G. Tan, X. Deng, and X. Ci, "Daphnetin-mediated Nrf2 antioxidant signaling pathways ameliorate tert-butyl hydroperoxide (t-BHP)-induced mitochondrial

- dysfunction and cell death,” *Free Radical Biology and Medicine*, vol. 106, pp. 38–52, 2017.
- [160] K. N. M. Abdelazeem, Y. Singh, F. Lang, and M. S. Salker, “Negative effect of ellagic acid on cytosolic pH regulation and glycolytic flux in human endometrial cancer cells,” *Cellular Physiology and Biochemistry*, vol. 41, no. 6, pp. 2374–2382, 2017.
- [161] M. C. Lin and M. C. Yin, “Preventive effects of ellagic acid against doxorubicin-induced cardio-toxicity in mice,” *Cardiovascular Toxicology*, vol. 13, no. 3, pp. 185–193, 2013.
- [162] H. Lou, X. Jing, D. Ren, X. Wei, and X. Zhang, “Eriodictyol protects against H<sub>2</sub>O<sub>2</sub>-induced neuron-like PC12 cell death through activation of Nrf2/ARE signaling pathway,” *Neurochemistry International*, vol. 61, no. 2, pp. 251–257, 2012.
- [163] V. Borse, R. F. H. Al Aameri, K. Sheehan et al., “Epigallocatechin-3-gallate, a prototypic chemopreventative agent for protection against cisplatin-based ototoxicity,” *Cell Death & Disease*, vol. 8, no. 7, article e2921, 2017.
- [164] S. Choudhary, S. Sood, R. L. Donnell, and H. C. R. Wang, “Intervention of human breast cell carcinogenesis chronically induced by 2-amino-1-methyl-6-phenylimidazo[4,5-b]pyridine,” *Carcinogenesis*, vol. 33, no. 4, pp. 876–885, 2012.
- [165] A. Patricia Moreno-Londono, C. Bello-Alvarez, and J. Pedraza-Chaverri, “Isoliquiritigenin pretreatment attenuates cisplatin induced proximal tubular cells (LLC-PK1) death and enhances the toxicity induced by this drug in bladder cancer T24 cell line,” *Food and Chemical Toxicology*, vol. 109, Part 1, pp. 143–154, 2017.
- [166] P. Pratheeshkumar, Y. O. Son, S. P. Divya et al., “Luteolin inhibits Cr(VI)-induced malignant cell transformation of human lung epithelial cells by targeting ROS mediated multiple cell signaling pathways,” *Toxicology and Applied Pharmacology*, vol. 281, no. 2, pp. 230–241, 2014.
- [167] Y. O. Son, P. Pratheeshkumar, Y. Wang, D. Kim, Z. Zhang, and X. Shi, “Protection from Cr(VI)-induced malignant cell transformation and tumorigenesis of Cr(VI)-transformed cells by luteolin through Nrf2 signaling,” *Toxicology and Applied Pharmacology*, vol. 331, pp. 24–32, 2017.
- [168] J. Gong, A. R. Muñoz, D. Chan, R. Ghosh, and A. P. Kumar, “STAT3 down regulates LC3 to inhibit autophagy and pancreatic cancer cell growth,” *Oncotarget*, vol. 5, no. 9, pp. 2529–2541, 2014.
- [169] P. Mu, X. Gao, Z. J. Jia, and R. L. Zheng, “Natural antioxidant pedicularioside G inhibits angiogenesis and tumorigenesis *in vitro* and *in vivo*,” *Basic & Clinical Pharmacology & Toxicology*, vol. 102, no. 1, pp. 30–34, 2007.
- [170] C. J. Lin, C. C. Lee, Y. L. Shih et al., “Resveratrol enhances the therapeutic effect of temozolomide against malignant glioma *in vitro* and *in vivo* by inhibiting autophagy,” *Free Radical Biology and Medicine*, vol. 52, no. 2, pp. 377–391, 2012.
- [171] A. R. Alhoshani, M. M. Hafez, S. Husain et al., “Protective effect of rutin supplementation against cisplatin-induced nephrotoxicity in rats,” *BMC Nephrology*, vol. 18, no. 1, p. 194, 2017.
- [172] G. V. Ramalingayya, S. P. Cheruku, P. Nayak et al., “Rutin protects against neuronal damage *in vitro* and ameliorates doxorubicin-induced memory deficits *in vivo* in Wistar rats,” *Drug Design, Development and Therapy*, vol. 11, pp. 1011–1026, 2017.
- [173] X. Ma, C. Dang, H. Kang et al., “Saikosaponin-D reduces cisplatin-induced nephrotoxicity by repressing ROS-mediated activation of MAPK and NF- $\kappa$ B signalling pathways,” *International Immunopharmacology*, vol. 28, no. 1, pp. 399–408, 2015.
- [174] Y. Wang, A. K. Mandal, Y. O. Son et al., “Roles of ROS, Nrf2, and autophagy in cadmium-carcinogenesis and its prevention by sulforaphane,” *Toxicology and Applied Pharmacology*, vol. 353, pp. 23–30, 2018.
- [175] X. Gong, V. N. Ivanov, M. M. Davidson, and T. K. Hei, “Tetramethylpyrazine (TMP) protects against sodium arsenite-induced nephrotoxicity by suppressing ROS production, mitochondrial dysfunction, pro-inflammatory signaling pathways and programmed cell death,” *Archives of Toxicology*, vol. 89, no. 7, pp. 1057–1070, 2015.
- [176] G. Y. Chen, Y. C. Shu, D. Y. Chuang, and Y. C. Wang, “Inflammatory and apoptotic regulatory activity of tanshinone IIA in *Helicobacter pylori*-infected cells,” *The American Journal of Chinese Medicine*, vol. 44, no. 6, pp. 1187–1206, 2016.
- [177] H. Z. Lee, C. J. Lin, W. H. Yang, W. C. Leung, and S. P. Chang, “Aloe-emodin induced DNA damage through generation of reactive oxygen species in human lung carcinoma cells,” *Cancer Letters*, vol. 239, no. 1, pp. 55–63, 2006.
- [178] M. L. Lin, Y. C. Lu, J. G. Chung et al., “Aloe-emodin induces apoptosis of human nasopharyngeal carcinoma cells *via* caspase-8-mediated activation of the mitochondrial death pathway,” *Cancer Letters*, vol. 291, no. 1, pp. 46–58, 2010.
- [179] Y. Zhang, J. Soboloff, Z. Zhu, and S. A. Berger, “Inhibition of Ca<sup>2+</sup> influx is required for mitochondrial reactive oxygen species-induced endoplasmic reticulum Ca<sup>2+</sup> depletion and cell death in leukemia cells,” *Molecular Pharmacology*, vol. 70, no. 4, pp. 1424–1434, 2006.
- [180] H. T. Chang, C. T. Chou, D. H. Kuo, P. Shieh, C. R. Jan, and W. Z. Liang, “The mechanism of Ca<sup>2+</sup> movement in the involvement of baicalein-induced cytotoxicity in ZR-75-1 human breast cancer cells,” *Journal of Natural Products*, vol. 78, no. 7, pp. 1624–1634, 2015.
- [181] H. Taniguchi, T. Yoshida, M. Horinaka et al., “Baicalein overcomes tumor necrosis factor-related apoptosis-inducing ligand resistance via two different cell-specific pathways in cancer cells but not in normal cells,” *Cancer Research*, vol. 68, no. 21, pp. 8918–8927, 2008.
- [182] X. X. Fan, E. L. H. Leung, Y. Xie et al., “Suppression of lipogenesis *via* reactive oxygen species–AMPK signaling for treating malignant and proliferative diseases,” *Antioxidants & Redox Signaling*, vol. 28, no. 5, pp. 339–357, 2018.
- [183] S. Shukla, F. Rizvi, S. Raisuddin, and P. Kakkar, “FoxO proteins’ nuclear retention and BH3-only protein Bim induction evoke mitochondrial dysfunction-mediated apoptosis in berberine-treated HepG2 cells,” *Free Radical Biology and Medicine*, vol. 76, pp. 185–199, 2014.
- [184] Y. Li, X. Tian, X. Liu, and P. Gong, “Bufalin inhibits human breast cancer tumorigenesis by inducing cell death through the ROS-mediated RIP1/RIP3/PARP-1 pathways,” *Carcinogenesis*, vol. 39, no. 5, pp. 700–707, 2018.
- [185] C. M. Xie, W. Y. Chan, S. Yu, J. Zhao, and C. H. K. Cheng, “Bufalin induces autophagy-mediated cell death in human colon cancer cells through reactive oxygen species generation and JNK activation,” *Free Radical Biology and Medicine*, vol. 51, no. 7, pp. 1365–1375, 2011.
- [186] H. Y. Li, J. Zhang, L. L. Sun et al., “Celastrol induces apoptosis and autophagy *via* the ROS/JNK signaling pathway in human

- osteosarcoma cells: an *in vitro* and *in vivo* study," *Cell Death & Disease*, vol. 6, no. 1, article e1604, 2015.
- [187] Y. Xiao, J. Liu, M. Guo et al., "Synergistic combination chemotherapy using carrier-free celastrol and doxorubicin nanocrystals for overcoming drug resistance," *Nanoscale*, vol. 10, no. 26, pp. 12639–12649, 2018.
- [188] Y. Bi, H. Li, D. Yi et al., " $\beta$ -catenin contributes to cordycepin-induced MGMT inhibition and reduction of temozolomide resistance in glioma cells by increasing intracellular reactive oxygen species," *Cancer Letters*, vol. 435, pp. 66–79, 2018.
- [189] M. I. Nasser, M. Masood, W. Wei et al., "Cordycepin induces apoptosis in SGC7901 cells through mitochondrial extrinsic phosphorylation of PI3K/Akt by generating ROS," *International Journal of Oncology*, vol. 50, no. 3, pp. 911–919, 2017.
- [190] S. Y. Lee, T. Debnath, S. K. Kim, and B. O. Lim, "Anti-cancer effect and apoptosis induction of cordycepin through DR3 pathway in the human colonic cancer cell HT-29," *Food and Chemical Toxicology*, vol. 60, pp. 439–447, 2013.
- [191] J. Chen, B. Chen, Z. Zou et al., "Costunolide enhances doxorubicin-induced apoptosis in prostate cancer cells via activated mitogen-activated protein kinases and generation of reactive oxygen species," *Oncotarget*, vol. 8, no. 64, pp. 107701–107715, 2017.
- [192] Y. I. Yang, J. H. Kim, K. T. Lee, and J. H. Choi, "Costunolide induces apoptosis in platinum-resistant human ovarian cancer cells by generating reactive oxygen species," *Gynecologic Oncology*, vol. 123, no. 3, pp. 588–596, 2011.
- [193] W. Zhuge, R. Chen, K. Vladimir et al., "Costunolide specifically binds and inhibits thioredoxin reductase 1 to induce apoptosis in colon cancer," *Cancer Letters*, vol. 412, pp. 46–58, 2018.
- [194] Y. C. Hsu, T. Y. Huang, and M. J. Chen, "Therapeutic ROS targeting of GADD45 $\gamma$  in the induction of G2/M arrest in primary human colorectal cancer cell lines by cucurbitacin E," *Cell Death & Disease*, vol. 5, no. 4, article e1198, 2014.
- [195] S. Jayakumar, R. S. Patwardhan, D. Pal et al., "Mitochondrial targeted curcumin exhibits anticancer effects through disruption of mitochondrial redox and modulation of TrxR2 activity," *Free Radical Biology and Medicine*, vol. 113, pp. 530–538, 2017.
- [196] B. Kim, H. S. Kim, E. J. Jung et al., "Curcumin induces ER stress-mediated apoptosis through selective generation of reactive oxygen species in cervical cancer cells," *Molecular Carcinogenesis*, vol. 55, no. 5, pp. 918–928, 2016.
- [197] S. Jin, Q. Y. Zhang, X. M. Kang, J. X. Wang, and W. H. Zhao, "Daidzein induces MCF-7 breast cancer cell apoptosis via the mitochondrial pathway," *Annals of Oncology*, vol. 21, no. 2, pp. 263–268, 2010.
- [198] J. Yi, J. Yang, R. He et al., "Emodin enhances arsenic trioxide-induced apoptosis via generation of reactive oxygen species and inhibition of survival signaling," *Cancer Research*, vol. 64, no. 1, pp. 108–116, 2004.
- [199] Y. Jing, J. Yang, Y. Wang et al., "Alteration of subcellular redox equilibrium and the consequent oxidative modification of nuclear factor  $\kappa$ B are critical for anticancer cytotoxicity by emodin, a reactive oxygen species-producing agent," *Free Radical Biology and Medicine*, vol. 40, no. 12, pp. 2183–2197, 2006.
- [200] T. Nakazato, K. Ito, Y. Ikeda, and M. Kizaki, "Green tea component, catechin, induces apoptosis of human malignant B cells via production of reactive oxygen species," *Clinical Cancer Research*, vol. 11, no. 16, pp. 6040–6049, 2005.
- [201] J. Zhu, W. Yu, B. Liu et al., "Escin induces caspase-dependent apoptosis and autophagy through the ROS/p38 MAPK signalling pathway in human osteosarcoma cells *in vitro* and *in vivo*," *Cell Death & Disease*, vol. 8, no. 10, p. e3113, 2017.
- [202] C. B. Yoo, K. T. Han, K. S. Cho et al., "Eugenol isolated from the essential oil of *Eugenia caryophyllata* induces a reactive oxygen species-mediated apoptosis in HL-60 human promyelocytic leukemia cells," *Cancer Letters*, vol. 225, no. 1, pp. 41–52, 2005.
- [203] A. J. Liu, S. H. Wang, K. C. Chen et al., "Evodiamine, a plant alkaloid, induces calcium/JNK-mediated autophagy and calcium/mitochondria-mediated apoptosis in human glioblastoma cells," *Chemico-Biological Interactions*, vol. 205, no. 1, pp. 20–28, 2013.
- [204] J. Yang, L. J. Wu, S. Tashino, S. Onodera, and T. Ikejima, "Protein tyrosine kinase pathway-derived ROS/NO productions contribute to G2/M cell cycle arrest in evodiamine-treated human cervix carcinoma HeLa cells," *Free Radical Research*, vol. 44, no. 7, pp. 792–802, 2010.
- [205] C. Wen, L. Huang, J. Chen et al., "Gambogic acid inhibits growth, induces apoptosis, and overcomes drug resistance in human colorectal cancer cells," *International Journal of Oncology*, vol. 47, no. 5, pp. 1663–1671, 2015.
- [206] L. H. Wang, Y. Li, S. N. Yang et al., "Gambogic acid synergistically potentiates cisplatin-induced apoptosis in non-small-cell lung cancer through suppressing NF- $\kappa$ B and MAPK/HO-1 signalling," *British Journal of Cancer*, vol. 110, no. 2, pp. 341–352, 2014.
- [207] X. Chen, L. Pei, Z. Zhong, J. Guo, Q. Zhang, and Y. Wang, "Anti-tumor potential of ethanol extract of *Curcuma phaeocalis* Valetton against breast cancer cells," *Phytomedicine*, vol. 18, no. 14, pp. 1238–1243, 2011.
- [208] C. Liao, K. Zheng, Y. Li et al., "Gypenoside L inhibits autophagic flux and induces cell death in human esophageal cancer cells through endoplasmic reticulum stress-mediated Ca<sup>2+</sup> release," *Oncotarget*, vol. 7, no. 30, pp. 47387–47402, 2016.
- [209] K. Huang, Y. Chen, R. Zhang et al., "Honokiol induces apoptosis and autophagy via the ROS/ERK1/2 signaling pathway in human osteosarcoma cells *in vitro* and *in vivo*," *Cell Death & Disease*, vol. 9, no. 2, article 157, 2018.
- [210] C. J. Lin, T. L. Chen, Y. Y. Tseng et al., "Honokiol induces autophagic cell death in malignant glioma through reactive oxygen species-mediated regulation of the p53/PI3K/Akt/mTOR signaling pathway," *Toxicol Appl Pharmacol*, vol. 304, pp. 59–69, 2016.
- [211] P. S. Yeh, W. Wang, Y. A. Chang, C. J. Lin, J. J. Wang, and R. M. Chen, "Honokiol induces autophagy of neuroblastoma cells through activating the PI3K/Akt/mTOR and endoplasmic reticular stress/ERK1/2 signaling pathways and suppressing cell migration," *Cancer Letters*, vol. 370, no. 1, pp. 66–77, 2016.
- [212] C. Fan, Y. Yang, Y. Liu et al., "Icariin displays anticancer activity against human esophageal cancer cells via regulating endoplasmic reticulum stress-mediated apoptotic signaling," *Scientific Reports*, vol. 6, article 21145, 2016.
- [213] S. Li, P. Dong, J. Wang et al., "Icariin, a natural flavonol glycoside, induces apoptosis in human hepatoma SMMC-7721 cells via a ROS/JNK-dependent mitochondrial pathway," *Cancer Letters*, vol. 298, no. 2, pp. 222–230, 2010.

- [214] Z. Lu, G. Zhang, Y. Zhang et al., "Isoalantolactone induces apoptosis through reactive oxygen species-dependent upregulation of death receptor 5 in human esophageal cancer cells," *Toxicology and Applied Pharmacology*, vol. 352, pp. 46–58, 2018.
- [215] Q. Zhang, G. Cheng, H. Qiu et al., "The p53-inducible gene 3 involved in flavonoid-induced cytotoxicity through the reactive oxygen species-mediated mitochondrial apoptotic pathway in human hepatoma cells," *Food & Function*, vol. 6, no. 5, pp. 1518–1525, 2015.
- [216] P. S. Rao, A. Satelli, M. Moridani, M. Jenkins, and U. S. Rao, "Luteolin induces apoptosis in multidrug resistant cancer cells without affecting the drug transporter function: involvement of cell line-specific apoptotic mechanisms," *International Journal of Cancer*, vol. 130, no. 11, pp. 2703–2714, 2012.
- [217] Z. Xu, F. Zhang, C. Bai et al., "Sophoridine induces apoptosis and S phase arrest via ROS-dependent JNK and ERK activation in human pancreatic cancer cells," *Journal of Experimental & Clinical Cancer Research*, vol. 36, no. 1, article 124, 2017.
- [218] H. Zhou, M. Xu, Y. Gao et al., "Matrine induces caspase-independent program cell death in hepatocellular carcinoma through bid-mediated nuclear translocation of apoptosis inducing factor," *Molecular Cancer*, vol. 13, no. 1, p. 59, 2014.
- [219] P. Poornima, C. F. Weng, and V. V. Padma, "Neferine from *Nelumbo nucifera* induces autophagy through the inhibition of PI3K/Akt/mTOR pathway and ROS hyper generation in A549 cells," *Food Chemistry*, vol. 141, no. 4, pp. 3598–3605, 2013.
- [220] S. Kalai Selvi, A. Vinoth, T. Varadharajan, C. F. Weng, and V. Vijaya Padma, "Neferine augments therapeutic efficacy of cisplatin through ROS-mediated non-canonical autophagy in human lung adenocarcinoma (A549 cells)," *Food and Chemical Toxicology*, vol. 103, pp. 28–40, 2017.
- [221] C. Chang, Y. Q. Zhu, J. J. Mei, S. Q. Liu, and J. Luo, "Involvement of mitochondrial pathway in NCTD-induced cytotoxicity in human hepG2 cells," *Journal of Experimental & Clinical Cancer Research*, vol. 29, no. 1, p. 145, 2010.
- [222] Y. Lu, Y. Sun, J. Zhu et al., "Oridonin exerts anticancer effect on osteosarcoma by activating PPAR- $\gamma$  and inhibiting Nrf2 pathway," *Cell Death & Disease*, vol. 9, no. 1, p. 15, 2018.
- [223] C. Qiao, L. Wei, Q. Dai et al., "UCP2-related mitochondrial pathway participates in oroxylin A-induced apoptosis in human colon cancer cells," *Journal of Cellular Physiology*, vol. 230, no. 5, pp. 1054–1063, 2015.
- [224] M. B. Chen, Y. Zhang, M. X. Wei et al., "Activation of AMP-activated protein kinase (AMPK) mediates plumbagin-induced apoptosis and growth inhibition in cultured human colon cancer cells," *Cell Signal*, vol. 25, no. 10, pp. 1993–2002, 2013.
- [225] B. Kumar, M. A. Iqbal, R. K. Singh, and R. N. Bamezai, "Resveratrol inhibits TIGAR to promote ROS induced apoptosis and autophagy," *Biochimie*, vol. 118, pp. 26–35, 2015.
- [226] A. Rodriguez-Garcia, D. Hevia, J. C. Mayo et al., "Thioredoxin 1 modulates apoptosis induced by bioactive compounds in prostate cancer cells," *Redox Biology*, vol. 12, pp. 634–647, 2017.
- [227] J. M. Shi, L. L. Bai, D. M. Zhang et al., "Saxifragifolin D induces the interplay between apoptosis and autophagy in breast cancer cells through ROS-dependent endoplasmic reticulum stress," *Biochemical Pharmacology*, vol. 85, no. 7, pp. 913–926, 2013.
- [228] S. Kajimoto, N. Takanashi, T. Kajimoto et al., "Sophoranone, extracted from a traditional Chinese medicine *Shan Dou Gen*, induces apoptosis in human leukemia U937 cells via formation of reactive oxygen species and opening of mitochondrial permeability transition pores," *International Journal of Cancer*, vol. 99, no. 6, pp. 879–890, 2002.
- [229] T. Liu, Z. Zhang, C. Yu et al., "Tetrahydroxycyclopentane antagonizes acute megakaryoblastic leukaemia growth by forcing autophagy-mediated differentiation," *British Journal of Pharmacology*, vol. 174, no. 23, pp. 4308–4328, 2017.
- [230] C. Liu, K. Gong, X. Mao, and W. Li, "Tetrahydroxycyclopentane induces apoptosis by activating reactive oxygen species and repressing Akt activity in human hepatocellular carcinoma," *International Journal of Cancer*, vol. 129, no. 6, pp. 1519–1531, 2011.
- [231] N. Liu, K. S. Wang, M. Qi et al., "Vitexin compound 1, a novel extraction from a Chinese herb, suppresses melanoma cell growth through DNA damage by increasing ROS levels," *Journal of Experimental & Clinical Cancer Research*, vol. 37, no. 1, article 269, 2018.

## Review Article

# Plasma Medicine: Applications of Cold Atmospheric Pressure Plasma in Dermatology

Thoralf Bernhardt <sup>1</sup>, Marie Luise Semmler <sup>1</sup>, Mirijam Schäfer <sup>1</sup>, Sander Bekeschus <sup>2</sup>,  
Steffen Emmert,<sup>1</sup> and Lars Boeckmann <sup>1</sup>

<sup>1</sup>Clinic and Polyclinic for Dermatology and Venereology, University Medical Center Rostock, Rostock 18057, Germany

<sup>2</sup>ZIK Plasmatis, Leibniz Institute for Plasma Science and Technology (INP Greifswald), Greifswald 17489, Germany

Correspondence should be addressed to Lars Boeckmann; [lars.boeckmann@med.uni-rostock.de](mailto:lars.boeckmann@med.uni-rostock.de)

Received 24 May 2019; Accepted 12 August 2019; Published 3 September 2019

Guest Editor: Nagendra K. Kaushik

Copyright © 2019 Thoralf Bernhardt et al. This is an open access article distributed under the Creative Commons Attribution License, which permits unrestricted use, distribution, and reproduction in any medium, provided the original work is properly cited.

The ability to produce cold plasma at atmospheric pressure conditions was the basis for the rapid growth of plasma-related application areas in biomedicine. Plasma comprises a multitude of active components such as charged particles, electric current, UV radiation, and reactive gas species which can act synergistically. Anti-itch, antimicrobial, anti-inflammatory, tissue-stimulating, blood flow-enhancing, and proapoptotic effects were demonstrated in *in vivo* and *in vitro* experiments, and until now, no resistance of pathogens against plasma treatment was observed. The combination of the different active agents and their broad range of positive effects on various diseases, especially easily accessible skin diseases, renders plasma quite attractive for applications in medicine. For medical applications, two different types of cold plasma appear suitable: indirect (plasma jet) and direct (dielectric barrier discharge—DBD) plasma sources. The DBD device PlasmaDerm® VU-2010 (CINOXY Technologies GmbH), the atmospheric pressure plasma jet (APPJ) kINPen® MED (INP Greifswald/neoplas tools GmbH), and the SteriPlas (Adtec Ltd., London, United Kingdom) are CE-certified as a medical product to treat chronic wounds in humans and showed efficacy and a good tolerability. Recently, the use of plasma in cancer research and oncology is of particular interest. Plasma has been shown to induce proapoptotic effects more efficiently in tumor cells compared with the benign counterparts, leads to cellular senescence, and—as shown *in vivo*—reduces skin tumors. To this end, a world-wide first Leibniz professorship for plasmabiotechnology in dermatology has been introduced to establish a scientific network for the investigation of the efficacy and safety of cold atmospheric plasma in dermatology. Hence, plasma medicine especially in dermatology holds great promise.

## 1. Plasma Medicine

Plasma medicine emerged in the last decade as an exciting new field of research at the interface between physics and the life sciences. Physical plasma can be generated by adding energy (heat or electromagnetic fields) to a neutral gas until the ionized gaseous substance becomes increasingly electrically conductive. Plasmas emit electromagnetic radiation, predominately UV radiation and visible light, and contain excited gas molecules, positively and negatively charged ions, free electrons, neutral reactive oxygen/nitrogen species (ROS/RNS), free radicals, and molecule fragments [1]. Due to its distinct characteristics compared to ordinary neutral gases, plasma is considered as a fourth state of matter

(besides solid, fluid, and gaseous). In modern medicine, high-temperature plasmas are used, e.g., for sterilization of medical devices and implants [2–9]. Cold atmospheric pressure plasmas (CAP), however, can also be used for the treatment of viable tissues and thus have become a focus of medical research over the past years. Besides therapeutic applications, CAP is also used for surface modification and biological decontamination [7, 10–13].

A variety of different CAP devices have been developed and tested for research purposes. In general, these can be divided into direct discharge (e.g., DBD: dielectric barrier discharge) and indirect discharge (e.g., APPJ: atmospheric pressure plasma jet) devices. To date, three plasma devices have been certified for medical purposes. In 2013, the

medical device kINPen® MED (INP Greifswald/neoplas tools GmbH, Greifswald, Germany), an APPJ, and PlasmaDerm® VU-2010 (CINOGY Technologies GmbH, Duderstadt, Germany), a DBD source, have been CE-certified in Germany by MEDCERT under the norm ISO 13485 (Table 1, Figure 1). Subsequently, the medical device SteriPlas (Adtec Ltd., London, United Kingdom) has been certified to be used for treatment of chronic and acute wounds, as well as for reduction of microbial load.

The use of many different devices or modifications by different research groups pose a challenge with respect to comparability of the results obtained with these devices, leading to difficulties defining long-term safety and efficacy of plasma devices in a comparable and standardized manner. Numerous organizations on a national and international level have been established to certify technical standardization. Some of these organizations are specific for certain fields such as electrical engineering or telecommunications, and others are more general. An organization for general standardization in Germany is the German Institute for Standardization (DIN). The European Committee for Standardization (CEN) and the International Organization for Standardization (ISO) provide standardization on a European and international level, respectively.

In order to establish general requirements for plasma sources in medicine, a DIN SPEC 91315 has been published by Mann and colleagues in 2014 [14]. The goal is to provide basic criteria for plasma sources to be used as medical applications. Furthermore, the efficacy of medical plasma sources as well as the safety for users (experimenters, patients, therapists, etc.) is of great importance. Although Mann et al. did not define new threshold or standard values, concerning, e.g., leakage current, UV irradiance, and formation of toxic gases, they refer to already existing standards and guidelines (DIN EN ISO 12100, DIN EN 60601-1, DIN EN 60601-1-6, and DIN EN 60601-2-57). This procedure allows a faster implementation of certified standards.

The tests described in the DIN SPEC 91315 are easy to adapt if common laboratory equipment is available, but they have to be adjusted to every plasma source with regard to individual treatment conditions. In order to obtain information on performance, effectiveness, and safety of medical plasma devices, certain physical and biological characteristics should be assessed. Physical performances include temperature, optical emission spectrometry (OES), UV irradiance, gas emission, and leakage current, and biological performances include antimicrobial activity, cytotoxicity, and chemical composition of liquid. These performances have been tested with a  $\mu$ s-pulsed DBD source on human skin fibroblasts [15] and according to the requirements of the DIN SPEC 91315 with the plasma jet kINPen® MED [16]. Both devices meet the requirements of the DIN SPEC 91315, indicating safety and effectiveness of these devices.

Besides standardization to allow comparability of different plasma sources, a thorough risk assessment for adverse effects such as genotoxicity and mutagenicity is of tremendous importance. A couple of studies using different testing systems have shown that moderate CAP treatment does not increase genotoxicity nor mutagenicity in cultured

TABLE 1: CE-certified plasma sources developed by systematic research and used in clinical studies.

Atmospheric pressure plasma jet kINPen® MED (INP Greifswald/neoplas tools GmbH, Greifswald, Germany)
Dielectric barrier discharge source PlasmaDerm® VU-2010 (CINOGY GmbH plasma technology for health, Duderstadt, Germany)
SteriPlas (Adtec Ltd., London, United Kingdom)

cells [17, 18]. Although these results are promising, further studies are needed to assess the potential risk of CAP under different conditions and intensities.

As mentioned above, plasma is composed of a number of different components which all may contribute more or less to its efficacy. While the mechanisms for the efficacy of CAP are not fully understood, it is conceivable that physical components such as UV radiation or electrical current as well as chemical components such as reactive oxygen species or reactive nitrogen species play a role in the mode of action. Numerous effects of CAP such as disinfection (bacteria, fungi, and viruses), tissue regeneration (pH modulation, angiogenesis), anti-inflammation (anti-itch), and anticancerous effects (proapoptotic) have been described [19–23].

These effects provide an opportunity for CAP to be used in different applications. Applications of CAP in medicine are quite versatile and include decontamination/sterilization, use in dental medicine, enhancement of coagulation, surface coating of implants, cosmetics and plastic surgery, and treatment of skin diseases, and even the use in cancer treatment is being investigated [10, 19, 24–33]. With respect to applications in medicine, this review focuses particularly on dermatological applications of CAP (Table 2) which include treatment of atopic eczema, itch, and pain, disinfection (bacteria, parasites, and fungus), treatment of ichthyosis/epidermal barrier defect, wound healing, scar treatment, and possibly treatment of skin tumors (melanoma, squamous cell carcinoma, and basal cell carcinoma) [19–22, 25, 33].

## 2. Atopic Eczema, Itch, and Pain

A case study presented at the 20<sup>th</sup> International Conference of the Society for Medical Innovation and Technology (SMIT) 2008 showed a reduction of itch for four hours and an overall reduction of itch from 8 to 3 (on a scale from 0 to 10) after daily CAP treatment for one minute of the left arm vs. basic treatment of the right arm over a period of 30 days [34]. No side effects have been observed, and overall, the eczema of this patient was reduced by two points on a scale from -5 to +5. However, a randomized two-sided placebo-controlled study on the efficacy and safety of atmospheric nonthermal argon plasma for pruritus with a total of 46 patients showed a similar improvement between plasma-treated and placebo-treated group with respect to itch [35]. In this study, patients have been treated daily for two minutes with plasma or argon only (placebo). At the end of the study, a reduction of pruritus has been observed, which was likely due to standard therapy. Another case study of a patient with chronic postoperative ear

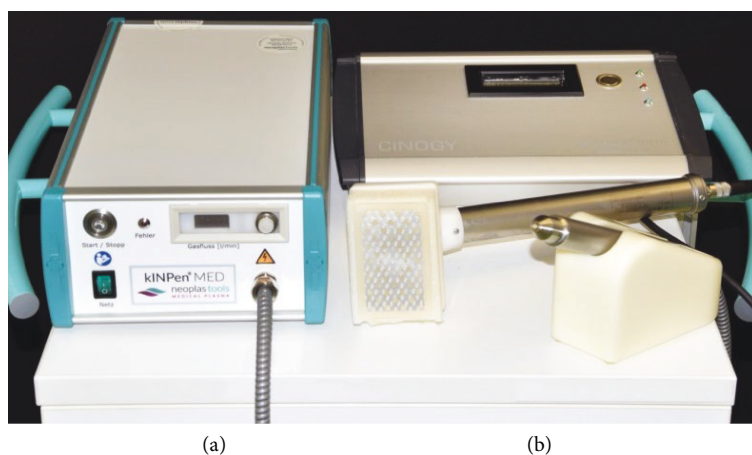


FIGURE 1: Examples of CE-certified plasma sources: (a) KINPen MED and (b) PlasmaDerm VU-2010.

TABLE 2: Dermatological applications of cold atmospheric pressure plasma (CAP) tested in clinical pilot or case-control studies.

Atopic eczema, itch, and pain relief
Disinfection (bacteria/fungi/viruses)
Treatment of epidermal barrier defects such as ichthyosis
Wound healing
Scar treatment
Treatment of skin tumors

infection showed a highly significant reduction of pain after CAP application for local infection control [36]. Considering these studies, cold atmospheric plasma seems to have positive effects on atopic eczema, itch, and pain, but still, more research is necessary to confirm these effects.

### 3. Disinfection (Bacteria/Fungi/Viruses)

Several studies have elucidated the lethality of CAP on bacteria and fungi and have shown its potential as an effective tool for disinfection. A two-minute CAP treatment, for example, has been shown to be effective against a variety of bacteria including important skin and wound pathogens such as *Escherichia coli*, group A *Streptococcus*, *Methicillin-resistant Staphylococcus aureus* (MRSA), and *Pseudomonas aeruginosa*, suggesting positive effects of CAP on wound healing [12]. Furthermore, the killing of clinically relevant fungal strains by CAP has been shown *in vitro* [37]. A significant reduction of bacterial and fungal targets after plasma treatment has also been shown on model nails with onychomycosis (a fungal infection of the nail) [38]. The authors of this study conclude that the “CAP technology appears to be a safe, effective, and inexpensive therapy for fungal nail infection treatment.” Following this *in vitro* study, an *in vivo* pilot study evaluated the plasma treatment on 19 study participants with toenail onychomycosis [39]. No long-term sequelae have been observed after plasma treatment, and overall clinical cure was observed in 53.8% of participants, whereas mycological cure was observed in 15.4% of participants. A prospective randomized controlled

study including 37 patients with herpes zoster (a painful skin infection caused by the varicella zoster virus) revealed that a weekday five-minute CAP treatment is safe, painless, and effective, improving initial healing of the herpes zoster lesions [40]. Taken together, promising effects of CAP have been shown in regard to disinfection with no evidence for resistance of microorganisms against the treatment. Hence, CAP provides an effective method for skin disinfection.

### 4. Ichthyosis/Epidermal Barrier Defect

An acidic protective hydrolipid film produced by perspiratory glands and sebaceous glands covers the outer layer of the skin. This hydrolipid film provides an epidermal barrier that protects the skin from drying and contains a complex microbial ecosystem, consisting of numerous bacteria [41]. The pH of the hydrolipid film is balanced between 5.4 and 5.9 in healthy skin [42]. Altered conditions in the hydrolipid film compared to healthy skin can lead to a shift in the microbial load and thus may promote disease [43, 44]. Pathogenic bacteria usually prefer pH values above 6; consequently, areas with increased pH values possess a higher susceptibility to pathogenic growth [45]. The pH values in hydrolipid films of patients with diseases such as ichthyosis or atopic dermatitis have been shown to be higher compared to pH values of healthy skin [46–48]. One reason for an increased pH in patients with atopic dermatitis may be due to a mutation in filaggrin, a protein involved in the regulation of epidermal homeostasis [49]. When human skin is treated with CAP, the hydrolipid film interacts directly with the chemical compounds of the plasma. This prompted Helmke and colleagues to investigate the effect of CAP on pH of the hydrolipid film of diseased skin [50]. Using a DBD plasma source, they treated lipid films of wool wax, pork sebum, and human lipid films with CAP and observed significant decreases in pH values. A treatment for only five seconds was sufficient to result in a decrease of pH, and treatment for 60 seconds led to a decrease of the pH down to 3.7 (from initial 4.6–6.2). The pH values of wool wax after plasma treatment remained decreased for more than two hours [50]. These studies



provide first evidence for the potential treatment of epidermal barrier defects such as ichthyosis with CAP, where a decrease of the pH value would result in an inhibition of wound pathogens and, therefore, promote wound healing.

## 5. Wound Healing

In several clinical studies and case reports, the effect of CAP on wound healing has been assessed (Table 3). Different plasma sources have been used in these studies (e.g., kINPen MED or PlasmaDerm VU-2010, Figure 2). The use of a hand-held dielectric barrier discharge plasma generator (PlasmaDerm® VU-2010) to alleviate chronic venous leg ulcers has been assessed in a monocentric, two-armed, open, prospective, randomized, and controlled trial [51]. This pilot study included 14 patients with at least one chronic venous ulcer, which had been divided into two comparable groups each consisting of seven patients. One group received standard care, while the other group in addition to standard care also received plasma therapy. Both groups were treated three times a week for a total of eight weeks with subsequent follow-up of four weeks. While in both groups an ulcer size reduction of 50% has been observed, a greater size reduction ( $5.30\text{ cm}^2$  vs.  $3.40\text{ cm}^2$ ) as well as a quicker size reduction after three weeks compared to the group without plasma treatment was found. Furthermore, there was one patient in the plasma-treated group who experienced complete healing of the ulcer. An example for successful wound healing after CAP treatment using the PlasmaDerm® VU-175 2010 is shown in Figure 3. Further prospective randomized controlled studies using a different plasma device (MicroPlaSter predecessor of SteriPlas, Adtec Healthcare) primarily aimed at decreasing the bacterial load in chronic wounds. These studies including 36 and 24 patients, respectively, showed significant reductions of bacterial load in CAP-treated chronic wounds [52, 53]. A subsequent open retrospective study with 70 patients suggests that wound healing may be accelerated by CAP treatment [36]. Improved healing of pressure ulcers was also found in a prospective randomized controlled trial including 50 patients of which 25 received CAP treatment using a Bioplasma jet device [54]. In another clinical case-control study, the efficacy of the plasma source kINPen MED was compared to octenidine treatment. This study including 16 patients with chronic leg ulcers revealed a similar reduction of bacteria using CAP treatment compared to octenidine [55]. A similar study with 34 patients showed a benefit of sequential treatment with CAP and octenidine dihydrochloride over treatment with just one of the two with respect to the antiseptic treatment [56]. In addition to studies investigating the effect of CAP on chronic wounds, a few pilot studies also looked at the efficacy of CAP on acute wounds [57–59]. Heinlin and colleagues enrolled 40 patients with skin graft donor sites on the upper leg. Equally sized areas of the wounds were assigned randomly to receive either CAP or placebo treatment [59]. From the second posttreatment day onwards, the CAP-treated sites showed significant improved healing compared to placebo treatment. In a case report study, four sterile ablative laser lesions (acute wounds) were induced in each

of five volunteers [60]. The wounds received either 10 seconds, three times 10 seconds, and 30 seconds CAP or no treatment for three consecutive days. Treatment for three times 10 seconds and single treatment for 30 seconds showed best results in early stages of wound healing, and even at later stages (after six months and after one year), plasma treatment resulted in improved outcomes with respect to avoiding posttraumatic skin disorders [58]. Another study including six individuals with vacuum-generated wounds on the forearm analyzed wound healing parameters such as area decline and histomorphological characteristics [57]. Wounds were treated with either no treatment, CAP, octenidine, or sequential treatment with CAP and octenidine. A statistically significant accelerated decline was observed after CAP treatment in comparison to the other treatment groups.

Accelerated wound healing has also been observed in a mouse model treated with a cold plasma jet [61]. In cell culture experiments with HaCaT keratinocytes and MRC5 fibroblasts, an increased motility of the cells has been observed after plasma treatment, and at least in HaCaT cells, this was associated with a decreased mRNA and protein expression of Cx43. Cx43 is a gap junctional protein of keratinocytes and was shown to inhibit cell migration and wound healing [61]. These findings suggest that cold plasma enhances wound healing in chronic and slowly healing wounds.

There are several aspects of CAP that may contribute to an improved wound healing: UV radiation and reactive gas species (i.e., ozone) disinfect the wound, generation of nitric oxide (NO) or nitrogen species ( $\text{NO}_x$ ) stimulates the regeneration of tissue, and electric current stimulates angiogenesis. Furthermore, CAP leads to an acidification of the wound (decrease of pH) [12, 20, 50, 62–65].

## 6. Scar Treatment

The effect of CAP on tissue regeneration has also been elucidated for its potential in scar treatment. In one study, ten patients with acne scars received a single CAP treatment using a Plasma Skin Regeneration (PSR) system. According to patient and doctor assessment, acne scars improved in 30% of the patients. Thermal damage to the epidermis and upper dermis had been observed for four-six days, and besides that, collagen remodeling effects without permanent pigmentary or textural irregularities as well as regenerative epidermal effects have been described [66]. Similarly, antimicrobial effects of CAP and improved acne symptoms have been demonstrated using a direct DBD device. A reduction of *P. acnes* by 75% has been observed in a study with 31 volunteers [66].

Another cohort of 30 patients received weekly application of CAP for four weeks. This treatment led to a reduction of sebum production of 80%, which lasted four weeks following the treatment [66]. Although the authors concluded that their plasma source can offer a new therapeutic option for acne treatment, more studies are needed to validate these findings.

TABLE 3: Overview of studies on treatment of chronic and acute wounds with cold atmospheric pressure plasma (CAP).

Title	Number of subjects	Conclusion	Wound	Reference
A first prospective randomized controlled trial to decrease bacterial load using cold atmospheric argon plasma on chronic wounds in patients	36 patients	Highly significant reduction in bacterial load	Chronic	Isbary et al. [53]
Successful and safe use of 2 min cold atmospheric argon plasma in chronic wounds: results of a randomized controlled trial	24 patients	MicroPlaSter alpha: significant reduction in bacterial load MicroPlaSter beta: highly significant reduction in bacterial load	Chronic	Isbary et al. [52]
Cold atmospheric argon plasma treatment may accelerate wound healing in chronic wounds: results of an open retrospective randomized controlled study in vivo	70 patients	Wound healing may be accelerated by CAP, particularly for chronic venous ulcers	Chronic	Isbary et al. [78]
The healing effect of low-temperature atmospheric-pressure plasma in pressure ulcer: a randomized controlled trial	50 patients	CAP-treated group had significantly better PUSH (pressure ulcer scale for healing) scores and exudate amount	Chronic	Chuangsuwanich et al. [54]
Clinical use of cold atmospheric pressure argon plasma in chronic leg ulcers: a pilot study	16 patients	Immediate antimicrobial effects of CAP plasma almost comparable to octenidine without signs of cytotoxicity	Chronic	Ulrich et al. [55]
Combined antibacterial effects of tissue-tolerable plasma and a modern conventional liquid antiseptic on chronic wound treatment	34 patients	The combined use of CAP and conventional antiseptics might represent the most efficient strategy for antiseptic treatment of chronic wounds	Chronic	Klebes et al. [56]
Alleviation of chronic venous leg ulcers with a hand-held dielectric barrier discharge plasma generator (PlasmaDerm® VU-2010): results of a monocentric, two-armed, open, prospective, randomized and controlled trial	14 patients	PlasmaDerm® VU-2010 device is safe and effective in patients with chronic venous leg ulcers	Chronic	Brehmer et al. [51]
Randomized placebo-controlled human pilot study of cold atmospheric argon plasma on skin graft donor sites	40 patients	Donor site wound areas treated with plasma showed significantly improved healing compared with placebo-treated areas	Acute	Heinlin et al. [59]
Experimental recovery of CO <sub>2</sub> -laser skin lesions by plasma stimulation	5 experimental case reports	Nonthermal atmospheric pressure plasma stimulation of laser skin lesion recovery looks promising	Acute	Metelmann et al. [60]
Scar formation of laser skin lesions after cold atmospheric pressure plasma (CAP) treatment: a clinical long-term observation	20 laser lesions in 5 individuals	Plasma treatment seems to support the inflammation needed for tissue regeneration	Acute	Metelmann et al. [58]
Laser scanning microscopy as a means to assess the augmentation of tissue repair by exposition of wounds to tissue-tolerable plasma	6 subjects with vacuum-generated wounds	CAP led to a significantly more rapid area decline in comparison to no treatment, treatment with octenidine, and sequential treatment with CAP and octenidine	Acute	Vandersee et al. [57]



FIGURE 2: Treatment of chronic ulceration with cold atmospheric pressure plasma (CAP): (a) KINPen MED and (b) PlasmaDerm VU-2010.



FIGURE 3: Example of successful wound healing after treatment with cold atmospheric pressure plasma (CAP): (a) chronic ulceration before CAP treatment and (b) complete healing for the first time since 14 years after CAP treatment for about 5 months.

## 7. Skin Tumors

Potential applications of CAP in cancer therapy are currently explored by several research groups. The possibility of a paradigm shift in cancer therapy and the selectivity to ablate cancer cells (e.g., melanoma) while the corresponding normal cells remain unaffected have already been described in 2011 by Keidar and colleagues [19]. Detachment of SW900 cancer cells from the culture vessel after plasma treatment has been observed, whereas no detachment was observed when normal human bronchial epithelial (NHBE) cells were treated. Furthermore, one single *in vivo* treatment with CAP for two minutes of ten mice with subcutaneous bladder cancer tumors (SCaBER) showed an ablation of small tumors (about five millimeters in diameter) and a size reduction of larger tumors. While fully ablated tumors did not recur, larger tumors started to regrow but did not reach their original size even after three weeks.

Next, the *in vivo* efficacy of CAP in a murine melanoma model has been investigated. A single plasma treatment induced ablation of the tumor and decreased the growth rate markedly. This also resulted in an increased survival rate in the treatment group, with a median survival of 33.5 days compared to 24.5 days in the control group [19]. Following this study, a number of other studies assessed the efficacy of CAP as a potential therapy for cancer treatment. Daeschlein and colleagues compared the antitumor efficacy of CAP with electrochemotherapy (ECT) in a melanoma mouse model [30]. A single CAP treatment led to a significant delay of

tumor growth acceleration. However, this was less effective compared to ECT, whereas the combination of CAP and ECT had the strongest effect. In light of these findings, the authors concluded that cold plasma provides a potential alternative to ECT and may serve as a new option for palliative skin melanoma therapy, either alone or in combination with ECT [30].

A murine melanoma B16/F10 cell line has been used to elucidate the effect of CAP against melanoma cells *in vitro*, showing a loss of viability of almost 100% 48 hours after CAP treatment for three minutes [29]. In addition, *in vivo* treatment with CAP of F10 cells in mice showed a decrease in growth of the tumors which was even comparable to the decrease of tumor growth achieved with chemotherapy [29].

In a clinical study with six patients suffering from locally advanced head and neck cancers, the efficacy and side effects of cold plasma treatment have been explored [67]. Two patients experienced a strong response to the treatment, resulting in a clear tumor reduction. While the tumor in one of these patients started to regrow ending with exitus letalis, the other patient was still receiving treatment, aiming for total remission. No side effects have been observed in two patients, while four patients experienced fatigue and a dry mouth. At least five of the patients had a reduction of odor, most likely due to decontamination, and four had a reduced demand of pain medication. Out of the six patients, five passed away after one to twelve months, which was not due to CAP application.

Besides ROS/RNS, the authors discussed the role of myeloid cells and the immunogenic cell death model of cancer treatment as potential mechanisms of action of CAP [67].

The potential use of CAP for cancer treatment has also been assessed *in vitro* and *in vivo* in several other nonskin cancer entities including breast cancer, pancreatic carcinomas, glioblastoma, colorectal carcinoma, and neuroblastomas [24–28]. In these studies, growth inhibition of different cell lines in culture as well as decreased tumor growth or a reduction of tumor volume has been observed in different mouse models after CAP treatment.

Although the molecular mechanisms for the efficacy of CAP on cancer cells are not fully understood, reactive oxygen species (ROS) and charged particles have been determined to be major contributors to plasma-induced cell death [68].

Taken together, these findings indicate a general efficacy of CAP against various cancer entities, suggesting plasma to be a potential new therapy against diverse cancerous diseases. However, to integrate plasma treatment into modern cancer therapy, further studies have to be conducted.

## 8. Actinic Keratosis

The precancerous actinic keratosis is a patch of thick, scaly, or crusty skin [69–71]. There are several options to treat actinic keratosis in order to prevent the development of squamous cell carcinomas. One option is the use of ingenol mebutate, which works in two ways: first, it leads to rapid lesion necrosis beginning one to two hours after application of ingenol mebutate, resulting from mitochondrial swelling and membrane disruption as well as membrane depolarization [72]. This process causes an inflammatory response, which, subsequently, leads to specific neutrophil-mediated antibody-dependent cellular cytotoxicity (ADCC) within days. These specific antibodies bind to specific antigens on dysplastic epidermal cells, as well as to receptors of infiltrating neutrophils, thereby causing the release of cytotoxic agents (e.g., ROS), which then destroy dysplastic epidermal cells [72]. The importance of the immune cell reaction against LK2 tumors (squamous cell carcinoma) has been shown in mice by Challacombe and colleagues. Following the treatment with PEP005 (ingenol-3-angelate), neutrophil-depleted mice showed a significant higher tumor volume in comparison to the control mice [73].

Similar to that, CAP seems to positively influence the healing of actinic keratosis as well. This has been shown in a pilot study with seven patients, who were treated twice a week, with CAP for two minutes, for a total of seven treatments [74]. All patients have shown promising responses with no adverse events so that further investment does not only seem necessary but also very promising. In a retrospective study of 12 patients with advanced head and neck squamous cell carcinomas, CAP was used to decontaminate infected cancer ulcerations and evaluated for its anticancer effects [75]. Analysis of data from this study showed a decreased request for pain medication, a reduction of typical fetid odor related to a reduction of microbial load, and in some cases even a superficial partial remission of tumor and wound healing of infected ulcerations.

A case report from Daeschlein and colleagues showed promising results of CAP in a patient with recalcitrant actinic keratosis of the scalp [76]. No actinic lesion relapse has been observed until at least 26 months after a single treatment with CAP, and furthermore, scar formation had been proven.

Taken together, these studies indicate a promising application of CAP as an innovative therapy for skin cancers or precancerous conditions, but the evidence is still sparse, and more basic research as well as more clinical studies are needed. To foster the investigation of the efficacy and safety of CAP in dermatology, a world-wide first Leibniz professorship for plasmabiotechnology in dermatology has been introduced, offering an opportunity to bring clinical needs and scientific findings together, while integrating CAP treatment in dermatology [77].

## 9. Conclusions

CAP has been shown to be a promising and inexpensive treatment for a variety of different diseases. While CAP already reached standard medical care status for wound treatment, only preliminary data for its effects in oncology are available. Continuing efforts in this emerging and highly dynamic field of plasma medicine will be necessary to further explore the full therapeutic potential of CAP and to fully understand its mechanisms of action. Whereas the development of novel plasma sources and modifications of existing devices will open up more opportunities, it will be crucial to adhere to certain standards in order to enable comparability of results obtained in different studies. Overall, the exciting field of plasma medicine is expanding and thus is providing increasing evidence for the use of CAP as a treatment option for a variety of dermatological diseases.

## Disclosure

The content of this review has been presented at least in part as an oral presentation during the 7<sup>th</sup> International Conference on Plasma Medicine in Philadelphia, USA.

## Conflicts of Interest

The authors declare that there is no conflict of interest regarding the publication of this paper.

## Acknowledgments

This work was supported by the Damp Stiftung and through the joint research project ONKOTHER-H supported by the European Social Fund, reference: ESF/14-BM-A55-0001/18 & 06/18, and the Ministry of Education, Science and Culture of Mecklenburg-Vorpommern, Germany.

## References

- [1] T. Gerling and K.-D. Weltmann, *Einführung in Atmosphärendruck-Plasmaquellen für plasmamedizinische Anwendung*, Springer-Verlag, Berlin Heidelberg, Plasmamedizin, 2016.
- [2] K.-D. Weltmann, M. Polak, K. Masur, T. von Woedtke, J. Winter, and S. Reuter, "Plasma processes and plasma sources

- in medicine," *Contributions to Plasma Physics*, vol. 52, no. 7, pp. 644–654, 2012.
- [3] K.-D. Weltmann, J. Winter, M. Polak, J. Ehlbeck, and T. Woedtkevon, *Plasma for Bio-Decontamination, Medicine and Food Security*, Springer, Dordrecht, 2012.
  - [4] G. E. Morfill and J. L. Zimmermann, "Plasma health care - old problems, new solutions," *Contributions to Plasma Physics*, vol. 52, no. 7, pp. 655–663, 2012.
  - [5] J. Ehlbeck, U. Schnabel, M. Polak et al., "Low temperature atmospheric pressure plasma sources for microbial decontamination," *Journal of Physics D: Applied Physics*, vol. 44, no. 1, p. 013002, 2011.
  - [6] T. Woedtkevon, A. Kramer, and K.-D. Weltmann, "Plasma sterilization: what are the conditions to meet this claim?," *Plasma Processes and Polymers*, vol. 5, no. 6, pp. 534–539, 2008.
  - [7] M. Moreau, N. Orange, and M. G. J. Feuilleoy, "Non-thermal plasma technologies: new tools for bio-decontamination," *Biotechnology Advances*, vol. 26, no. 6, pp. 610–617, 2008.
  - [8] M. Laroussi, "Low temperature plasma-based sterilization: overview and state-of-the-art," *Plasma Processes and Polymers*, vol. 2, no. 5, pp. 391–400, 2005.
  - [9] M. Moisan, J. Barbeau, S. Moreau, J. Pelletier, M. Tabrizian, and L'. H. Yahia, "Low-temperature sterilization using gas plasmas: a review of the experiments and an analysis of the inactivation mechanisms," *International Journal of Pharmaceutics*, vol. 226, no. 1-2, pp. 1–21, 2001.
  - [10] T. Woedtkevon, S. Reuter, K. Masur, and K.-D. Weltmann, "Plasmas for medicine," *Physics Reports*, vol. 530, no. 4, pp. 291–320, 2013.
  - [11] G. Daeschlein, M. Napp, S. von Podewils et al., "In vitro susceptibility of multidrug resistant skin and wound pathogens against low temperature atmospheric pressure plasma jet (APPJ) and dielectric barrier discharge plasma (DBD)," *Plasma Processes and Polymers*, vol. 11, no. 2, pp. 175–183, 2014.
  - [12] G. Daeschlein, S. Scholz, A. Arnold et al., "In vitro susceptibility of important skin and wound pathogens against low temperature atmospheric pressure plasma jet (APPJ) and dielectric barrier discharge plasma (DBD)," *Plasma Processes and Polymers*, vol. 9, no. 4, pp. 380–389, 2012.
  - [13] R. d'Agostino, P. Favia, C. Oehr, and M. R. Wertheimer, "Low-temperature plasma processing of materials: past, present, and future," *Plasma Processes and Polymers*, vol. 2, no. 1, pp. 7–15, 2005.
  - [14] M. Mann, R. Tiede, R. Ahmed et al., *DIN SPEC 91315: General Requirements for Plasma Sources in Medicine*, Beuth Verlag, 2014.
  - [15] R. Tiede, J. Hirschberg, W. Viöl, and S. Emmert, "A  $\mu$ s-pulsed dielectric barrier discharge source: physical characterization and biological effects on human skin fibroblasts," *Plasma Processes and Polymers*, vol. 13, no. 8, pp. 775–787, 2016.
  - [16] M. S. Mann, R. Tiede, K. Gavenis et al., "Introduction to DIN-specification 91315 based on the characterization of the plasma jet KINPen MED," *Clinical Plasma Medicine*, vol. 4, no. 2, pp. 35–45, 2016.
  - [17] T. Maisch, A. K. Bosserhoff, P. Unger et al., "Investigation of toxicity and mutagenicity of cold atmospheric argon plasma," *Environmental and Molecular Mutagenesis*, vol. 58, no. 3, pp. 172–177, 2017.
  - [18] K. Wende, S. Bekeschus, A. Schmidt et al., "Risk assessment of a cold argon plasma jet in respect to its mutagenicity," *Mutation Research, Genetic Toxicology and Environmental Mutagenesis*, vol. 798-799, pp. 48–54, 2016.
  - [19] M. Keidar, R. Walk, A. Shashurin et al., "Cold plasma selectivity and the possibility of a paradigm shift in cancer therapy," *British Journal of Cancer*, vol. 105, no. 9, pp. 1295–1301, 2011.
  - [20] S. Emmert, F. Brehmer, H. Hänßle et al., "Atmospheric pressure plasma in dermatology: ulcer treatment and much more," *Clinical Plasma Medicine*, vol. 1, no. 1, pp. 24–29, 2013.
  - [21] J. Heinlin, G. Isbary, W. Stolz et al., "Plasma applications in medicine with a special focus on dermatology," *Journal of the European Academy of Dermatology and Venereology*, vol. 25, no. 1, pp. 1–11, 2011.
  - [22] J. Heinlin, G. Morfill, M. Landthaler et al., "Plasma medicine: possible applications in dermatology," *Journal der Deutschen Dermatologischen Gesellschaft*, vol. 8, no. 12, pp. 968–976, 2010.
  - [23] G. Daeschlein, T. von Woedtke, E. Kindel, R. Brandenburg, K. D. Weltmann, and M. Jünger, "Antibacterial activity of an atmospheric pressure plasma jet against relevant wound pathogens in vitro on a simulated wound environment," *Plasma Processes and Polymers*, vol. 7, no. 3-4, pp. 224–230, 2010.
  - [24] R. M. Walk, J. A. Snyder, P. Srinivasan et al., "Cold atmospheric plasma for the ablative treatment of neuroblastoma," *Journal of Pediatric Surgery*, vol. 48, no. 1, pp. 67–73, 2013.
  - [25] M. Vandamme, E. Robert, S. Lerondel et al., "ROS implication in a new antitumor strategy based on non-thermal plasma," *International Journal of Cancer*, vol. 130, no. 9, pp. 2185–2194, 2012.
  - [26] N. Hattori, S. Yamada, K. Torii et al., "Effectiveness of plasma treatment on pancreatic cancer cells," *International Journal of Oncology*, vol. 47, no. 5, pp. 1655–1662, 2015.
  - [27] L. Brullé, M. Vandamme, D. Riès et al., "Effects of a non thermal plasma treatment alone or in combination with gemcitabine in a MIA PaCa2-luc orthotopic pancreatic carcinoma model," *PLoS One*, vol. 7, no. 12, p. e52653, 2012.
  - [28] S. Mirpour, S. Piroozmand, N. Soleimani et al., "Utilizing the micron sized non-thermal atmospheric pressure plasma inside the animal body for the tumor treatment application," *Scientific Reports*, vol. 6, no. 1, 2016.
  - [29] S. Mashayekh, H. Rajaei, M. Akhlaghi, B. Shokri, and Z. M. Hassan, "Atmospheric-pressure plasma jet characterization and applications on melanoma cancer treatment (B/16-F10)," *Physics of Plasmas*, vol. 22, no. 9, p. 093508, 2015.
  - [30] G. Daeschlein, S. Scholz, S. Lutze et al., "Comparison between cold plasma, electrochemotherapy and combined therapy in a melanoma mouse model," *Experimental Dermatology*, vol. 22, no. 9, pp. 582–586, 2013.
  - [31] G. Fridman, A. Shereshevsky, M. M. Jost et al., "Floating electrode dielectric barrier discharge plasma in air promoting apoptotic behavior in melanoma skin cancer cell lines," *Plasma Chemistry and Plasma Processing*, vol. 27, no. 2, pp. 163–176, 2007.
  - [32] G. Fridman, M. Peddinghaus, M. Balasubramanian et al., "Blood coagulation and living tissue sterilization by floating-electrode dielectric barrier discharge in air," *Plasma Chemistry and Plasma Processing*, vol. 26, no. 4, pp. 425–442, 2006.
  - [33] G. Fridman, A. Shereshevsky, M. Peddinghaus et al., "Biomedical applications of non-thermal atmospheric pressure plasma," in *37th AIAA Plasmadynamics and Lasers Conference*, American Institute of Aeronautics and Astronautics, Reston, Virginia, 2006.

- [34] N. Mertens, A. Goppold, S. Emmert, and W. Vioel, *Dielectric Barrier Discharge Plasma-A Powerful Tool for Medical Applications*, 20th International Conference of the Society for Medical Innovation and Technology (SMIT), Vienna, Austria, 2008.
- [35] J. Heinlin, G. Isbary, W. Stolz et al., "A randomized two-sided placebo-controlled study on the efficacy and safety of atmospheric non-thermal argon plasma for pruritus," *Journal of the European Academy of Dermatology and Venereology*, vol. 27, no. 3, pp. 324–331, 2013.
- [36] G. Isbary, T. Shimizu, J. L. Zimmermann, H. M. Thomas, G. E. Morfill, and W. Stolz, "Cold atmospheric plasma for local infection control and subsequent pain reduction in a patient with chronic post-operative ear infection," *New Microbes and New Infections*, vol. 1, no. 3, pp. 41–43, 2013.
- [37] G. Daeschlein, S. Scholz, T. von Woedtke et al., "In vitro killing of clinical fungal strains by low-temperature atmospheric-pressure plasma jet," *IEEE Transactions on Plasma Science*, vol. 39, no. 2, pp. 815–821, 2011.
- [38] Z. Xiong, J. Roe, T. C. Grammer, and D. B. Graves, "Plasma treatment of onychomycosis," *Plasma Processes and Polymers*, vol. 13, no. 6, pp. 588–597, 2016.
- [39] S. R. Lipner, G. Friedman, and R. K. Scher, "Pilot study to evaluate a plasma device for the treatment of onychomycosis," *Clinical and Experimental Dermatology*, vol. 42, no. 3, pp. 295–298, 2017.
- [40] G. Isbary, T. Shimizu, J. L. Zimmermann et al., "Randomized placebo-controlled clinical trial showed cold atmospheric argon plasma relieved acute pain and accelerated healing in herpes zoster," *Clinical Plasma Medicine*, vol. 2, no. 2, pp. 50–55, 2014.
- [41] R. A. Bojar and K. T. Holland, "Review: the human cutaneous microflora and factors controlling colonisation," *World Journal of Microbiology and Biotechnology*, vol. 18, no. 9, pp. 889–903, 2002.
- [42] M. H. Schmid-Wendtner and H. C. Korting, "The pH of the skin surface and its impact on the barrier function," *Skin Pharmacology and Physiology*, vol. 19, no. 6, pp. 296–302, 2006.
- [43] A. Marchionini and R. Schmidt, "Säuremantel der Haut und Bakterienabwehr," *Klinische Wochenschrift*, vol. 18, no. 13, pp. 461–467, 1939.
- [44] D. N. Fredricks, "Microbial ecology of human skin in health and disease," *The Journal of Investigative Dermatology. Symposium Proceedings*, vol. 6, no. 3, pp. 167–169, 2001.
- [45] C. M. Stewart, M. B. Cole, J. D. Legan, L. Slade, M. H. Vandeven, and D. W. Schaffner, "Staphylococcus aureus growth boundaries: moving towards mechanistic predictive models based on solute-specific effects," *Applied and Environmental Microbiology*, vol. 68, no. 4, pp. 1864–1871, 2002.
- [46] A. B. Glibbery and R. Mani, "pH in leg ulcers," *International Journal of Microcirculation, Clinical and Experimental*, vol. 2, p. 109, 1992.
- [47] S. Seidenari and G. Giusti, "Objective assessment of the skin of children affected by atopic dermatitis: a study of pH, capacitance and TEWL in eczematous and clinically uninvolved skin," *Acta Dermato-Venereologica*, vol. 75, pp. 429–433, 1995.
- [48] H. Öhman and A. Vahlquist, "The pH gradient over the stratum corneum differs in X-linked recessive and autosomal dominant ichthyosis; a clue to the molecular origin of the "acid skin mantle"?", *Journal of Investigative Dermatology*, vol. 111, no. 4, pp. 674–677, 1998.
- [49] J. M. Jungersted, H. Scheer, M. Mempel et al., "Stratum corneum lipids, skin barrier function and filaggrin mutations in patients with atopic eczema," *Allergy*, vol. 65, no. 7, pp. 911–918, 2010.
- [50] A. Helmke, D. Hoffmeister, N. Mertens, S. Emmert, J. Schuette, and W. Vioel, "The acidification of lipid film surfaces by non-thermal DBD at atmospheric pressure in air," *New Journal of Physics*, vol. 11, no. 11, 2009.
- [51] F. Brehmer, H. A. Haenssle, G. Daeschlein et al., "Alleviation of chronic venous leg ulcers with a hand-held dielectric barrier discharge plasma generator (PlasmaDerm®VU-2010): results of a monocentric, two-armed, open, prospective, randomized and controlled trial (NCT01415622)," *Journal of the European Academy of Dermatology and Venereology*, vol. 29, no. 1, pp. 148–155, 2015.
- [52] G. Isbary, J. Heinlin, T. Shimizu et al., "Successful and safe use of 2 min cold atmospheric argon plasma in chronic wounds: results of a randomized controlled trial," *The British Journal of Dermatology*, vol. 167, no. 2, pp. 404–410, 2012.
- [53] G. Isbary, G. Morfill, H. U. Schmidt et al., "A first prospective randomized controlled trial to decrease bacterial load using cold atmospheric argon plasma on chronic wounds in patients," *The British Journal of Dermatology*, vol. 163, pp. 78–82, 2010.
- [54] A. Chuangsuwanich, T. Assadamongkol, and D. Boonyawan, "The healing effect of low-temperature atmospheric-pressure plasma in pressure ulcer: a randomized controlled trial," *The International Journal of Lower Extremity Wounds*, vol. 15, no. 4, pp. 313–319, 2016.
- [55] C. Ulrich, F. Kluschke, A. Patzelt et al., "Clinical use of cold atmospheric pressure argon plasma in chronic leg ulcers: a pilot study," *Journal of wound care*, vol. 24, no. 5, pp. 196–203, 2015.
- [56] M. Klebes, C. Ulrich, F. Kluschke et al., "Combined antibacterial effects of tissue-tolerable plasma and a modern conventional liquid antiseptic on chronic wound treatment," *Journal of Biophotonics*, vol. 8, no. 5, pp. 382–391, 2015.
- [57] S. Vandersee, H. Richter, J. Lademann et al., "Laser scanning microscopy as a means to assess the augmentation of tissue repair by exposition of wounds to tissue tolerable plasma," *Laser Physics Letters*, vol. 11, no. 11, p. 115701, 2014.
- [58] H.-R. Metelmann, T. T. Vu, H. T. Do et al., "Scar formation of laser skin lesions after cold atmospheric pressure plasma (CAP) treatment: a clinical long term observation," *Clinical Plasma Medicine*, vol. 1, no. 1, pp. 30–35, 2013.
- [59] J. Heinlin, J. L. Zimmermann, F. Zeman et al., "Randomized placebo-controlled human pilot study of cold atmospheric argon plasma on skin graft donor sites," *Wound repair and regeneration : official publication of the Wound Healing Society [and] the European Tissue Repair Society*, vol. 21, no. 6, pp. 800–807, 2013.
- [60] H.-R. Metelmann, T. von Woedtke, R. Bussiahn et al., "Experimental recovery of CO<sub>2</sub>-laser skin lesions by plasma stimulation," *American Journal of Cosmetic Surgery*, vol. 29, no. 1, pp. 52–56, 2012.
- [61] A. Schmidt, S. Bekeschus, K. Wende, B. Vollmar, and T. Woedtke, "A cold plasma jet accelerates wound healing in a murine model of full-thickness skin wounds," *Experimental Dermatology*, vol. 26, no. 2, pp. 156–162, 2017.
- [62] N. Plasmamedizin, "Risikopotenzial und zu Anwendungsperspektiven von kaltem Atmosphärendruckplasma in der Medizin. Positionspapier des Nationalen Zentrums für Plasmamedizin," *Plasmakurier*, vol. 1, pp. 43–52, 2014.

- [63] G. Fridman, G. Friedman, A. Gutsol, A. B. Shekhter, V. N. Vasilets, and A. Fridman, "Applied plasma medicine," *Plasma Processes and Polymers*, vol. 5, no. 6, pp. 503–533, 2008.
- [64] A. Helmke, D. Hoffmeister, F. Berge et al., "Physical and microbiological characterisation of Staphylococcus epidermidis inactivation by dielectric barrier discharge plasma," *Plasma Processes and Polymers*, vol. 8, no. 4, pp. 278–286, 2011.
- [65] G. Valacchi, V. Fortino, and V. Bocci, "The dual action of ozone on the skin," *The British Journal of Dermatology*, vol. 153, no. 6, pp. 1096–1100, 2005.
- [66] C. Chutsirimongkol, D. Boonyawan, N. Polnikorn, W. Techawatthanawisan, and T. Kundilokchai, "Non-thermal plasma for acne and aesthetic skin improvement," *Plasma Medicine*, vol. 4, no. 1-4, pp. 79–88, 2014.
- [67] H.-R. Metelmann, C. Seebauer, V. Miller et al., "Clinical experience with cold plasma in the treatment of locally advanced head and neck cancer," *Clinical Plasma Medicine*, vol. 9, pp. 6–13, 2018.
- [68] A. Lin, N. Chernets, J. Han et al., "Non-equilibrium dielectric barrier discharge treatment of mesenchymal stem cells: charges and reactive oxygen species play the major role in cell death," *Plasma Processes and Polymers*, vol. 12, no. 10, pp. 1117–1127, 2015.
- [69] P. J. Quaedvlieg, E. Tirsi, M. R. Thissen, and G. A. Krekels, "Actinic keratosis: how to differentiate the good from the bad ones?," *European Journal of Dermatology*, vol. 16, no. 4, pp. 335–339, 2006.
- [70] I. M. Freedberg and T. B. Fitzpatrick, *Fitzpatrick's Dermatology in General Medicine*, McGraw-Hill, Health Professions Division, New York, 2003.
- [71] V. Prajapati and B. Barankin, "Dermacase. Actinic keratosis," *Canadian family physician Medecin de famille canadien*, vol. 54, no. 5, pp. 691–699, 2008.
- [72] R. H. Rosen, A. K. Gupta, and S. K. Tyring, "Dual mechanism of action of ingenol mebutate gel for topical treatment of actinic keratoses: rapid lesion necrosis followed by lesion-specific immune response," *Journal of the American Academy of Dermatology*, vol. 66, no. 3, pp. 486–493, 2012.
- [73] J. M. Challacombe, A. Suhrbier, P. G. Parsons et al., "Neutrophils are a key component of the antitumor efficacy of topical chemotherapy with ingenol-3-angelate," *The Journal of Immunology*, vol. 177, no. 11, pp. 8123–8132, 2006.
- [74] M. Wirtz, I. Stoffels, J. Dissemmond, D. Schadendorf, and A. Roesch, "Actinic keratoses treated with cold atmospheric plasma," *Journal of the European Academy of Dermatology and Venereology*, vol. 32, no. 1, pp. e37–e39, 2018.
- [75] H.-R. Metelmann, D. S. Nedrelov, C. Seebauer et al., "Head and neck cancer treatment and physical plasma," *Clinical Plasma Medicine*, vol. 3, no. 1, pp. 17–23, 2015.
- [76] G. Daeschlein, A. Arnold, S. Lutze et al., "Treatment of recalcitrant actinic keratosis (AK) of the scalp by cold atmospheric plasma," *Cogent Medicine*, vol. 4, no. 1, 2017.
- [77] C. Weishaupt and S. Emmert, "Connecting basic cold plasma technology to dermatology," *Clinical Plasma Medicine*, vol. 10, pp. 16–19, 2018.
- [78] G. Isbary, W. Stolz, T. Shimizu et al., "Cold atmospheric argon plasma treatment may accelerate wound healing in chronic wounds: results of an open retrospective randomized controlled study in vivo," *Clinical Plasma Medicine*, vol. 1, no. 2, pp. 25–30, 2013.

## Research Article

# Antiproliferative and Antitumour Effect of Nongenotoxic Silver Nanoparticles on Melanoma Models

Lucía M. Valenzuela-Salas,<sup>1</sup> Nayeli G. Girón-Vázquez,<sup>2</sup> Juan C. García-Ramos,<sup>3</sup>  
Olivia Torres-Bugarín,<sup>4</sup> Claudia Gómez,<sup>2</sup> Alexey Pestryakov,<sup>5</sup> Luis J. Villarreal-Gómez ,<sup>6</sup>  
Yanis Toledano-Magaña ,<sup>3</sup> and Nina Bogdanchikova<sup>7</sup>

<sup>1</sup>Escuela de Ciencias de la Salud, Universidad Autónoma de Baja California, Tijuana, Baja California, Mexico

<sup>2</sup>Facultad de Ingeniería, Arquitectura y Diseño, Universidad Autónoma de Baja California, Ensenada, Baja California, Mexico

<sup>3</sup>Departamento de Físicoquímica de Nanomateriales, CONACyT-UNAM-CNyN, Ensenada, Baja California, Mexico

<sup>4</sup>Programa Internacional de Medicina, Universidad Autónoma de Guadalajara, Zapopan, Jalisco, Mexico

<sup>5</sup>Department of Technology of Organic Substances and Polymer Materials, Tomsk Polytechnic University, Tomsk, Russia

<sup>6</sup>Escuela de Ciencias de la Ingeniería y Tecnología, Universidad Autónoma de Baja California, Tijuana, Baja California, Mexico

<sup>7</sup>Departamento de Físicoquímica de Nanomateriales, Centro de Nanociencias y Nanotecnología, Universidad Nacional Autónoma de México, Ensenada, Baja California, Mexico

Correspondence should be addressed to Yanis Toledano-Magaña; [yanistoledano@cny.unam.mx](mailto:yanistoledano@cny.unam.mx)

Received 12 February 2019; Revised 25 April 2019; Accepted 29 May 2019; Published 25 July 2019

Guest Editor: Nagendra K. Kaushik

Copyright © 2019 Lucía M. Valenzuela-Salas et al. This is an open access article distributed under the Creative Commons Attribution License, which permits unrestricted use, distribution, and reproduction in any medium, provided the original work is properly cited.

During the last 3 decades, there has been a slow advance to obtain new treatments for malignant melanoma that improve patient survival. In this work, we present a systematic study focused on the antiproliferative and antitumour effect of AgNPs. These nanoparticles are fully characterized, are coated with polyvinylpyrrolidone (PVP), and have an average size of  $35 \pm 15$  nm and a metallic silver content of 1.2% wt. Main changes on cell viability, induction of apoptosis and necrosis, and ROS generation were found on B16-F10 cells after six hours of exposure to AgNPs ( $IC_{50} = 4.2 \mu\text{g/mL}$ ) or Cisplatin ( $IC_{50} = 2.0 \mu\text{g/mL}$ ). Despite the similar response for both AgNPs and Cisplatin on antiproliferative potency (cellular viability of  $53.95 \pm 1.88$  and  $53.62 \pm 1.04$ ) and ROS production ( $20.27 \pm 1.09\%$  and  $19.50 \pm 0.35\%$ ), significantly different cell death pathways were triggered. While AgNPs induce only apoptosis ( $45.98 \pm 1.88\%$ ), Cisplatin induces apoptosis and necrosis at the same rate ( $22.31 \pm 1.72\%$  and  $24.07 \pm 1.10\%$ , respectively). In addition to their antiproliferative activity, *in vivo* experiments showed that treatments of 3, 6, and 12 mg/kg of AgNPs elicit a survival rate almost 4 times higher ( $P < 0.05$ ) compared with the survival rate obtained with Cisplatin (2 mg/kg). Furthermore, the survivor mice treated with AgNPs do not show genotoxic damage determined by micronuclei frequency quantification on peripheral blood cells. These results exhibit the remarkable antitumour activity of a nongenotoxic AgNP formulation and constitute the first advance toward the application of these AgNPs for melanoma treatment, which could considerably reduce adverse effects provoked by currently applied chemotherapeutics.

## 1. Introduction

Melanoma is the most aggressive form of skin cancer and one of the deadliest. The morbidity and mortality of melanoma have increased in recent decades around the world with more than 100,000 new cases reported every year, and the incidence increase continues [1]. The incidence in fair-skinned

populations always has the highest growth rates [2], but recently a 500% increase in new cases in Mexico has been reported [3].

In the last 3 decades, there have not been new treatments that efficiently improve patient survival [4]. Melanoma treatment faces two important problems: the adverse effects of chemotherapy due to the lack of selectivity and the low



efficiency of the used methods [5]. Even with the resistance and severe adverse effects observed, Cisplatin (CisPt) continues to be the most used drug [6].

In the last decade, inorganic nanoparticles have attracted the interest of several research groups due to their applications in cancer therapy, either as drug nanocarriers or as therapeutic agents [7, 8]. Particularly for the second purpose, silver nanoparticles (AgNPs) have been widely studied. However, their physicochemical properties play a key role in both facets, to fight cancer and to cause adverse effects [9].

In this sense, the employment of polyvinylpyrrolidone (PVP) as a coating agent of AgNPs produces an important decrease in cytotoxic and genotoxic effects compared with noncoated or citrate-AgNPs [10–12]. The PVP-AgNPs could also provide several advantages through selectivity in their antiproliferative action. The commercial formulation of PVP-AgNPs from Skyspring Nanomaterials showed a differential antiproliferative activity between breast triple-negative tumour cells and breast nontumourigenic cells. Besides, the same PVP-AgNP formulation significantly reduces the tumour volume of these aggressive tumours that are difficult to treat [13].

Our research group has studied a commercially available PVP-AgNP formulation known as Argovit™ that has been very effective as an antimicrobial [14, 15], antifungal [15], and antiviral agent [16–18]. This formulation also has been a determining factor in the rapid healing of diabetic foot ulcers [19]. Moreover, these nanoparticles inhibit the growth of human tumour cell cultures of the breast, lung, prostate, cervix, and colon. The main death pathway activated was apoptosis, probably triggered by the overproduction of reactive oxygen species (ROS). There was no necrosis, and neither was there evidence of DNA-damage at the effective inhibitory concentrations determined for each tumour cell line [20].

Considering the growth inhibition activity of these PVP-AgNPs on human tumour cell lines, in this work, we show a systematic study of the *in vitro* and *in vivo* effect of well-characterized AgNPs on murine melanoma models. Cytotoxicity, cell death pathway induction, and ROS generation were analysed *in vitro*. In addition, a subcutaneous melanoma model in C57BL/6J mice was performed following the protocol recommended by the National Institute of Health (NIH) [21], where tumour volume, survival rate, haematological parameters, and genotoxicity of the treatments were evaluated.

## 2. Materials and Methods

**2.1. Silver Nanoparticles (AgNPs).** Silver nanoparticles used in this work were donated by Dr. Vasily Burmistrov from the Scientific and Production Center Vector-Vita (Russia). Argovit™ is a formulation of PVP-coated AgNPs highly dispersed in water with an overall concentration of 200 mg/mL (20%). The content of metallic silver is 12 mg/mL stabilized with 188 mg/mL of PVP. Dilutions of AgNPs were prepared with distilled and sterile water and were kept at 4°C in darkness.

**2.2. Silver Nanoparticle Characterization.** Dynamic light scattering (DLS) (Malvern Instruments Zetasizer Nano NS model DTS1060;  $\lambda = 532$  nm) was used to determine the hydrodynamic diameter and the zeta potential. Characterization of optical properties was done with the Cary 60 UV-vis spectrophotometer (Agilent Technologies) in the range of 200 to 900 nm. Morphology and size distribution were determined by HR-TEM using a JEOL JEM-2010 microscope. Also, lyophilized AgNPs were characterized by FTIR-ATR in a range of 400 to 4000  $\text{cm}^{-1}$  with a resolution of 2  $\text{cm}^{-1}$  on a universal diamond ATR Top Plate accessory (PerkinElmer). The sample spectrum was compared with that of standard solid PVP (MW 100 kDa). The silver content of Argovit® was determined by ICP-OES (Varian Vista-MPX CCD Simultaneous ICP-OES).

**2.3. Cell Culture.** B16-F10, murine skin melanoma cells from C57BL/6J mice, were purchased from ATCC® (ATCC® CRL-6475™) and maintained in DMEM high-glucose media (Sigma-Aldrich, 51435C) supplemented with 10% (*v/v*) of heat-inactivated Foetal Bovine Serum (FBS, Biowest, S1650) and 2 mM of L-glutamine (Sigma-Aldrich, G5792) at 37°C in a humidified atmosphere with 5%  $\text{CO}_2$ . Subculturing was performed every 2 days.

**2.4. Antiproliferative Activity.** B16-F10 cells ( $1 \times 10^5$ ) were seeded in 96-well plates with 195  $\mu\text{L}$  of DMEM high-glucose supplemented media (Sigma-Aldrich, 51435C). Primary screening was done to determine  $\text{IC}_{50}$  values using the MTT assay kit (Bio-Vision MTT Cell Proliferation Assay Kit #K299-1000) and ProBit analysis after 24 h of exposure. After that, the  $\text{IC}_{50}$  of AgNPs (4.2  $\mu\text{g}/\text{mL}$ ) and Cisplatin (2  $\mu\text{g}/\text{mL}$ , CisPt) were employed to determine the cell growth behaviour at 6, 12, 18, and 24 h. The proliferation kinetics was determined by flow cytometry in Attune NxT equipment. Cell viability was determined using the Vybrant™ CFDA SE Cell Tracer Kit and propidium iodide (PI) (Thermo Fisher Scientific, V12883) following the provider's protocol.

Determination of apoptosis and necrosis cell death pathway was determined with the Alexa Fluor® 488 Annexin V/Dead Cell Apoptosis Kit (Thermo Fisher Scientific, V13241). ROS generation was analysed by the DCFDA Cellular ROS Detection Assay Kit (Abcam, 139476) and with the MitoSOX™ Red Mitochondrial Superoxide Indicator for live-cell imaging (Invitrogen, M36008).

**2.5. Experimental Animals.** We purchased seventy 8–10-week-old C57BL/6JNHsd male mice from Envigo, Mexico. Mice were divided and assigned randomly to polycarbonate cages into 6 groups of 10 mice each and two more groups of 5 mice each. The latter groups were used as untreated controls for haematological and genotoxicity trials. Mice were maintained at 25°C temperature, 60% humidity, and 12/12-hour light-dark cycle and fed *ad libitum*. The experimental protocol was approved on June 19, 2018, by the Ethical Committee of the Health Sciences School from the Autonomous University of Baja California, Mexico with file number 001/2018.

Melanoma induction in C57BL/6JNHsd mice was performed as recommended by the USA NIH [21]. First, B16-F10 cells in the logarithmic growth phase were harvested for injection; after guaranteeing viability with trypan blue (>90%), cell concentration was adjusted to  $1 \times 10^6$  cell/mL in ice-cold Hank's Balanced Salt Solution (HBSS, Biowest, L0606).

Mice of 20 g weight were inoculated by subcutaneous administration of 100  $\mu$ L cell suspension ( $1 \times 10^5$  cells/mouse). The appearance of a "bleb" indicates the correct subcutaneous administration. After cell administration, mice were placed in the corresponding cage. Tumours became palpable in 12 days, and at this point the antitumour trials were initiated.

**2.6. Antitumour Activity.** The mice with palpable tumours (10 per group) were administered subcutaneously each 3rd day for 21 days with the corresponding dose of each treatment as follows: Group 1—negative control (injectable water); Group 2—positive control (CisPt, 2 mg/kg); Group 3—vehicle control (PVP, 12 mg/kg); Group 4—AgNPs, 3 mg/kg; Group 5—AgNPs, 6 mg/kg, and Group 6—AgNPs, 12 mg/kg. Group 7 and Group 8 are healthy mice injected with water or PVP, respectively ( $n = 5$  for each group), and used as negative control for the haematological parameters and genotoxicity.

All the AgNP doses were calculated according to the metallic silver content. Dilutions were prepared with injectable water from a stock solution of Argovit® with 12 mg/mL of metallic silver to obtain the work solutions at the final concentrations of 24, 12, and 6  $\mu$ g/mL. Then, 100  $\mu$ L was administered to each mouse according to the administration scheme previously described. Doses were chosen due to previous experiences with murine models [17]. The mice were examined daily, and tumours were measured every day of administration with a slide calliper. Tumour volume was determined with the Attia-Weiss formula. Furthermore, general characteristics (activity, hair appearance, and any apparent change) were also recorded.

After 21 days of the administration, the treatment was stopped and the animals observed for 7 more days. After that, the mice were anaesthetized with ketamine and euthanized by cardiac puncture to collect blood samples.

**2.7. Genotoxicity Determinations.** Drop blood samples were taken from the animals before they died (experimental Groups 1, 2, 3, and 5) or euthanized (Groups 4, 6, and 7). Two smears were made on cleaned microscope slides. The smears were air-dried, fixed in absolute ethanol for 10 minutes, and stained with acridine orange (CAS No. 10127023, Sigma-Aldrich).

The micronuclei in each sample were scored manually using a binocular microscope (Carl Zeiss, Axiostar Plus) with a fluorescent filter (IVFL, 450–490 nm). The number of micronucleated erythrocytes (MNE) in 10,000 total erythrocytes and the polychromatic erythrocytes (PCE) in 1000 total erythrocytes were evaluated.

**2.8. Statistical Analysis.** Viability, apoptosis, necrosis, ROS generation, and tumour volume data, were analysed with a two-way ANOVA ( $P < 0.05$ ) followed by the Tukey post hoc test ( $P < 0.05$ ) (GraphPad Prism). For relative survival % data, the Mantel-Haenszel chi-square statistic was used ( $P < 0.05$ ) (GraphPad Prism).

### 3. Results

**3.1. Silver Nanoparticle Characterization.** A complete characterization of the sample provided by Prof. Burmistrov was performed. AgNPs are mainly spherical with an average size of  $35 \pm 15$  nm as determined by HR-TEM. The hydrodynamic diameter (summarized diameter of a metallic silver nanoparticle and PVP coating) determined by DLS was 70 nm, and the  $\zeta$  potential was -15 mV. UV-vis analysis showed an absorption peak at 420 nm that corresponds to the plasmon surface resonance. The silver content of the concentrate solution was 12 mg/mL, determined by ICP-OES.

The FTIR-ATR spectrum shows peaks corresponding to the hydroxyl vibration of unbound water ( $\nu$ OH) at  $3406 \text{ cm}^{-1}$ , carbonyl stretching at  $1650 \text{ cm}^{-1}$  ( $\nu$ C=O), symmetrical stretching of nitrogen in the ring at  $1269 \text{ cm}^{-1}$  ( $\nu_s$ C-H), and asymmetric ( $\nu_{as}$ C-H) stretching at  $2948$  and  $2915 \text{ cm}^{-1}$ , respectively. Metallic silver determined by ICP-OES is 12 mg/ml (% wt).

**3.2. Cell Viability, Apoptosis, Necrosis, and Reactive Oxygen Species Quantification In Vitro.** In this work, cellular viability, induction of apoptosis or necrosis, and ROS generation changes on murine melanoma cells B16-F10 after exposure to  $IC_{50}$  of AgNPs (4.2  $\mu$ g/mL) or CisPt (2.0  $\mu$ g/mL) were evaluated at 6, 12, 18, and 24 h. The main changes in cellular viability were observed in the first 6 h following the administration of the agents, CisPt or AgNPs. After that, the effect was maintained until the last record at 24 h (Figure 1).

From the record of cellular viability, both agents AgNPs and CisPt present the same antiproliferative effect ( $53.95 \pm 1.88$  and  $53.62 \pm 1.04$ , respectively), but the cell death pathways induced are quite different. After 6 h of exposure,  $45.97 \pm 1.88\%$  of apoptosis was observed on cells treated with AgNPs, twofold higher than the apoptotic cells found when exposed to CisPt ( $22.31 \pm 1.72\%$ , Figure 1). On the other hand, treatment with AgNPs produces less than 0.1% of necrosis, while for CisPt it was  $24.06 \pm 1.09\%$ . For CisPt, both cell death pathways were induced practically at the same rate (Figure 1). Behaviour found after 6 h of exposure was maintained until the final determination was made at 24 h of exposure. Complete data of cellular viability, apoptosis, and necrosis can be consulted in the supplementary material Table S1.

The most significant reactive oxygen species (ROS) generation was found after exposure of 6 h to CisPt or AgNPs (Figure 2) and shows an inverse relationship with cellular viability. Cells treated with CisPt reached the maximal ROS production after 6 h of exposure ( $20.27 \pm 1.09\%$ ); meanwhile, the highest ROS production induced by AgNPs was observed at 12 h ( $19.50 \pm 0.35\%$ ).

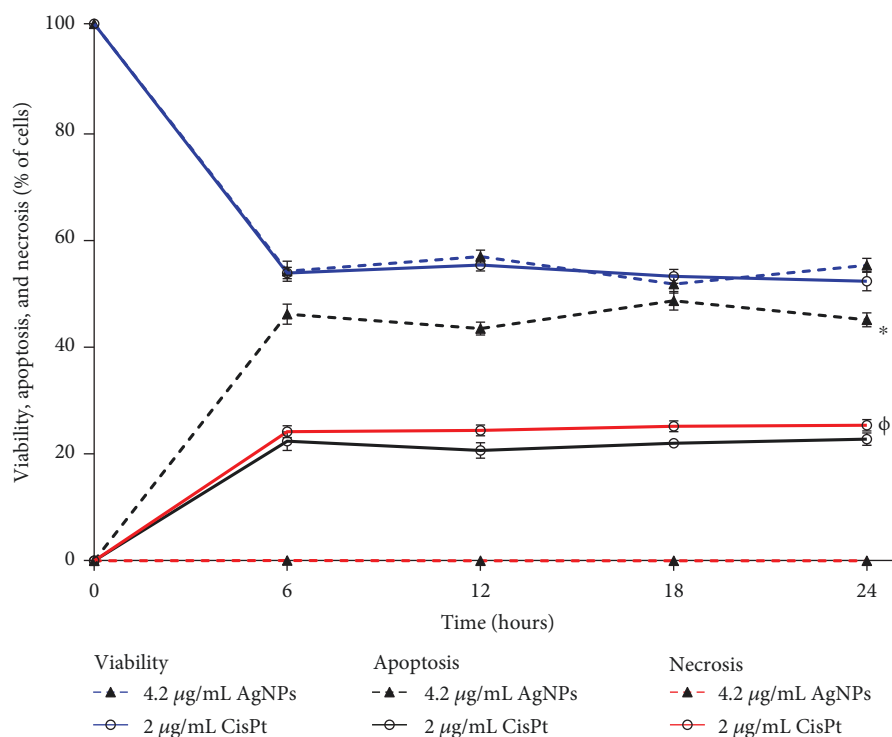


FIGURE 1: Viability, apoptosis, and necrosis determined in B16-F10 cell cultures treated with AgNPs or CisPt. Determinations were done at 6, 12, 18, and 24 h in melanoma cell cultures treated with the concentrations of AgNPs or CisPt indicated in the graph. Viability, blue lines; apoptosis, black lines; necrosis, red lines. \* indicates a statistically significant difference of  $P < 0.05$  for apoptosis data.  $\Phi$  indicates a statistically significant difference of  $P < 0.05$  for necrosis data.

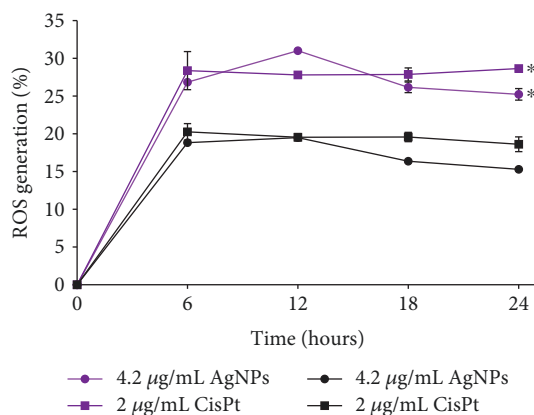


FIGURE 2: Reactive oxygen species production in melanoma cells treated with  $IC_{50}$  of AgNPs or CisPt. Quantification of ROS production in B16-F10 cell cultures treated with the  $IC_{50}$  of AgNPs or CisPt was performed by flow cytometry and fluorescent markers. Total ROS was determined with DCFDA (purple lines) and mitochondrial superoxide with MitoSOX (black lines). \* indicates a statistically significant difference of  $P < 0.05$  comparing total ROS generation data with mitochondrial superoxide data.

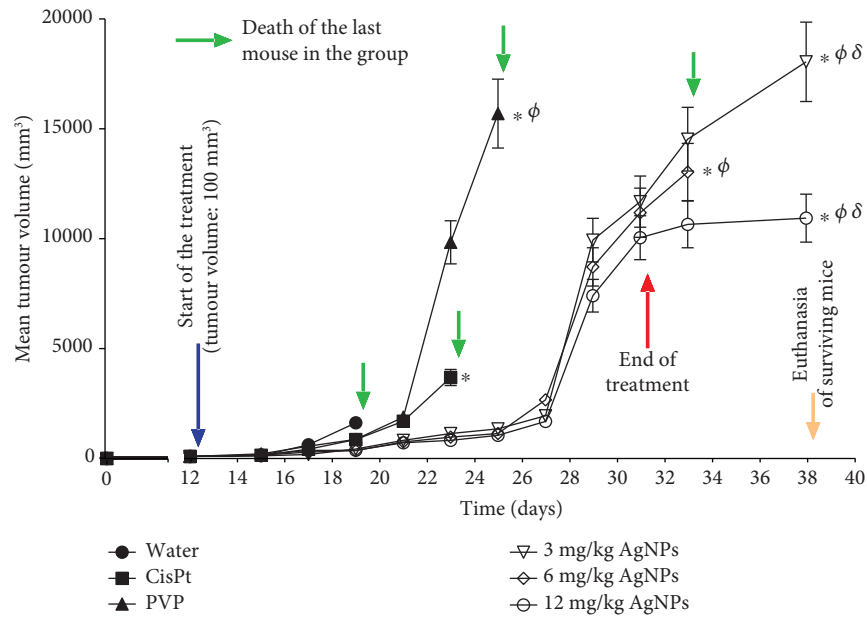
The mitochondrial superoxide production has the same behaviour through time with that described for total ROS and corresponds to two-thirds of the total amount of ROS observed with  $31.02 \pm 0.45\%$  for AgNPs and  $28.38 \pm 2.52\%$  for CisPt. The most important difference between the treatments is that CisPt induces a sustained ROS generation after

6 h and until 24 h, while a decrease in ROS generation was observed after 12 h of exposure when melanoma cells were treated with AgNPs (Figure 2). All data of ROS production through time can be consulted in supplementary material Table S2.

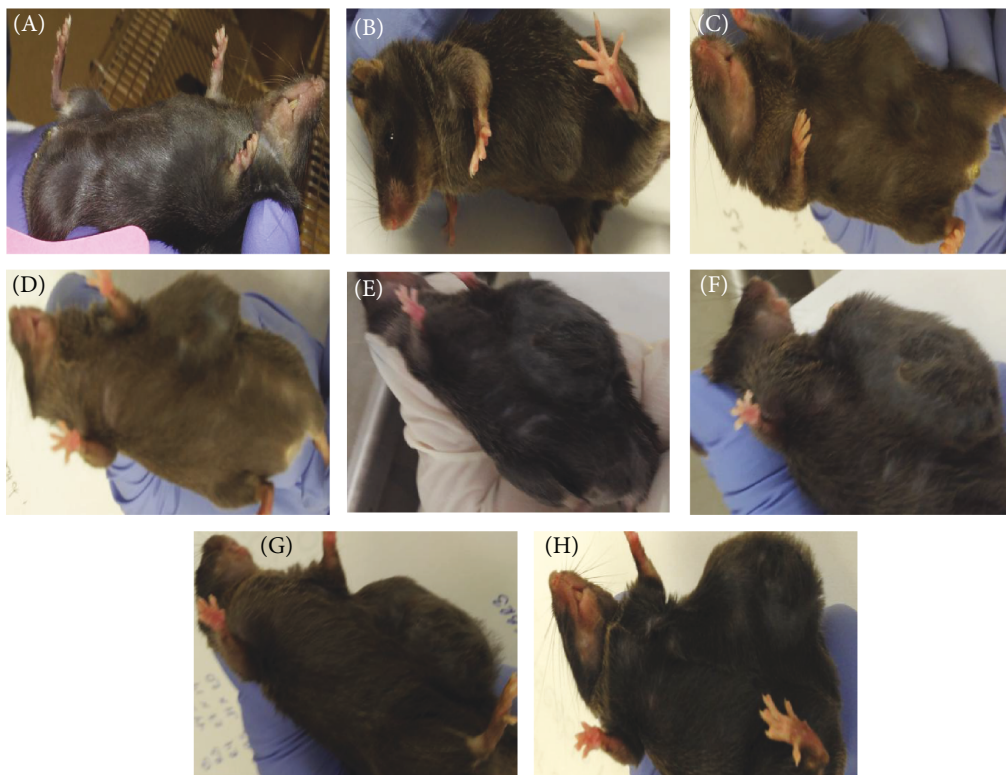
**3.3. Antitumour Activity.** Tumour volume, as well as signs of illness, were observed throughout the experiment after the treatment administration described in Materials and Methods. Tumour volume increased in all mice with or without treatment. Mice with tumours treated with AgNPs did not stop eating or drinking through the whole experiment. Mice with the tumour but untreated, as well as those treated with CisPt or PVP, presented lethargy and loss of appetite.

Mice injected with water developed tumours of around  $1500 \text{ mm}^3$  and died 7 days after the tumour become palpable. The tumour volume in animals treated with PVP or CisPt presented a similar tumour volume (around  $1500 \text{ mm}^3$ ) after 9 days of the start of treatment (21st day in Figure 3). On the other hand, mice treated with AgNP doses of 3, 6, and 12 mg/kg exhibited a tumour volume within the range of  $722\text{--}837 \text{ mm}^3$ . This represents a 50-60% tumour growth inhibition elicited by the AgNP treatments compared with PVP ( $1,890 \text{ mm}^3$ ), CisPt ( $1,704 \text{ mm}^3$ ), or water ( $1,500 \text{ mm}^3$ ). It is important to recall that all mice injected with water died on the 7th day of treatment (Figure 3).

For the 11th day of treatment (day 23 in Figure 3), while the tumour growth rate in animals treated with any of the three doses of AgNPs increases in a quite similar way



(a)



(b)

FIGURE 3: (a) Mean melanoma tumour volume as a function of time (days). Mice treated with injectable water were used as negative controls (water); mice treated with 2 mg/kg of Cisplatin (CisPt), 12 mg/kg of PVP (PVP), and 3, 6, or 12 mg/kg of AgNPs are indicated in the figure. Melanoma cells were inoculated subcutaneously at the beginning of the experiment (black arrow); treatments start when tumours were 100 mm<sup>3</sup> (blue arrow). Treatments ended after 21 days (red arrow). Tumour volume determination was stopped when all mice in the group died (green arrows). 7 days after the end of the treatments (yellow arrow), surviving mice were euthanized. \* indicates a statistically significant difference of  $P < 0.05$  comparing groups with the group treated with water.  $\phi$  indicates a statistically significant difference of  $P < 0.05$  comparing groups with the group treated with CisPt.  $\delta$  indicates a statistically significant difference of  $P < 0.05$  comparing AgNP doses. (b) Pictures showing mouse without melanoma (A), when tumour reached 100 mm<sup>3</sup>, and when this tumour volume was reached in mice with the following corresponding treatments (C-H): (C) water, (D) CisPt, (E) PVP, and (G) 6 mg/kg. The surviving mice were euthanized on the 38th day: (F) AgNP 3 mg/kg and (H) AgNP 12 mg/kg. The last mice that died are marked with green arrows in (a).

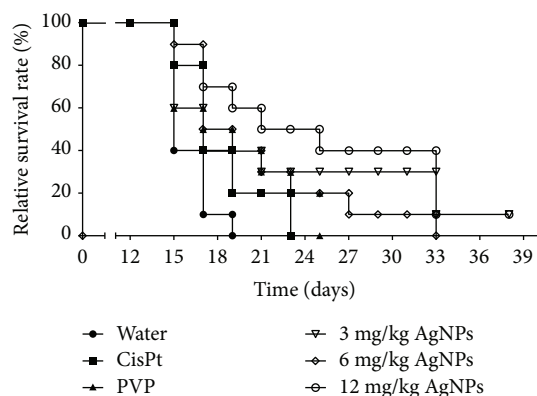


FIGURE 4: Kaplan-Meier plot showing the relative survival rates of mice treated with AgNPs or CisPt. Mice without melanoma and without treatment were used as negative controls (healthy mice, 100% survival rate). Mice with melanoma and injected with water (water), 2 mg/kg of Cisplatin (CisPt), 12 mg/kg of PVP (PVP), and 3, 6, or 12 mg/kg of AgNPs are identified at the bottom of the figure. \* and  $\Phi$  indicate a statistically significant difference of  $P < 0.05$  comparing groups treated with AgNPs with groups treated with water and CisPt, respectively.

(tumour volume in the range of 837-1,142 mm<sup>3</sup>), animals treated with CisPt or PVP showed tumours with a volume of 3,500 and 9,500 mm<sup>3</sup>, respectively. These values represent a 72% reduction in tumour growth caused by the administration of AgNPs compared with CisPt and a 90% reduction compared with PVP.

The evaluated doses of AgNPs did not show differences between them regarding tumour growth until the 19th day of treatment, which also was the last day of treatment. However, in the last seven days of the experiment (the 32nd-38th day in Figure 3), sharp differences were observed. The last surviving mouse of the group treated with 6 mg/kg died 2 days after the end of the treatment (day 33 in Figure 3), while on the group of mice treated with 3 and 12 mg/kg of AgNP, a mouse of each group survived the 7 days of the observation period.

Surviving mice of the experimental groups treated with 3 and 12 mg/kg of AgNPs show tumour volumes at the end of the observational period of 18,000 and 11,000 mm<sup>3</sup>, respectively (on the 38th day of Figure 3). Thus, it seems that a dose of 12 mg/kg of AgNPs inhibited the tumour growth by almost 50% compared with the treatment of 3 mg/kg (Figure 3), which strongly suggest a dose-dependent behaviour.

Figure 4 schematically shows the relative survival rate of mice treated with the different agents. On the 11th day of treatment (day 23 in Figure 4), the death of the last mouse of the group treated with CisPt was registered, while 50% of the mice treated with 12 mg/kg of AgNPs were still alive. At the end of the treatment scheme (day 33 in Figure 4), the life expectancy of the surviving individuals treated with AgNPs increased by 12, 8, and 6 days compared with those injected with water, CisPt, or PVP, respectively (Figure 4). At the end of the experiment, mice treated with 3 or 12 mg/kg of AgNPs survived 19, 15, and 13 days more than those treated

with water, CisPt, or PVP, respectively. This represents a life expectancy of mice treated with AgNPs almost 4-times higher compared with those injected with water, and more than double compared with those mice treated with 2 mg/kg of CisPt (Figure 4). In our knowledge, this is the first time that those effects are observed with an AgNP treatment on an *in vivo* melanoma model.

**3.4. Haematological Parameters.** To complete the profile of the survivor animals to the treatment scheme (mice of groups treated with 3 and 12 mg/kg), their haematological parameters were compared with those observed in healthy mice injected with water or PVP (negative control groups,  $n = 5$  for each group).

In general terms, the parameters of individuals treated with AgNPs were within the ranges considered as normal for these mice [22], with the exception of haematocrit (HCT) and haemoglobin (HGT), where an important decrease was observed for both groups treated with 3 and 12 mg/kg of AgNPs. Besides, an increase on white blood cells and lymphocytes was observed, but only in the mouse treated with the AgNP dose of 3 mg/kg (Figure 5).

**3.5. Genotoxicity.** Finally, the quantification of micronuclei on erythrocytes (MNE) in 10,000 of the total erythrocytes that indicate genotoxic damage and the counting of polychromatic erythrocytes (PCE) in 1000 total erythrocytes that indicate myelosuppression (cytotoxic effect) were performed.

Tail blood samples from healthy mice, surviving mice of the AgNP treatments of 3 and 12 mg/kg, and from the last survivor of the other treatment groups (untreated controls with melanoma and mice with melanoma injected with PVP, CisPt, and AgNP 6 mg/kg, respectively) were used to identify genotoxic and cytotoxic effects of the treatments.

Results show that mice with melanoma present practically the same MNE count as that of healthy mice, both within the range of 6-14 MNE reported for this strain [23] (marked with red lines in Figure 6). CisPt produces a higher number of MNE with an MNE count of 23. Interestingly, the dose of 6 mg/kg of AgNP generates a higher count of MNE than the upper limit reported. PVP produces 14 MNE, while AgNP doses of 3 and 12 mg/kg produce 4 and 8 MNE, respectively.

On the other hand, it is clear from Figure 6 that the counting of PCE in the mouse with melanoma is substantially lower than that found in the healthy one. For CisPt, a small increase compared with the positive control was found, while a dose-dependent behaviour was observed for AgNP doses; however, none of them are comparable with the effect observed for PVP, which practically overturned the myelosuppression promoted by melanoma and reached PCE levels like those found in the healthy mice.

## 4. Discussion

During the past decades, metal nanoparticles [24-26] and particularly AgNPs ([27]) have shown a real potential to inhibit tumour cell proliferation. It has been published that AgNP toxicity could be related with the release of Ag<sup>+</sup> ions

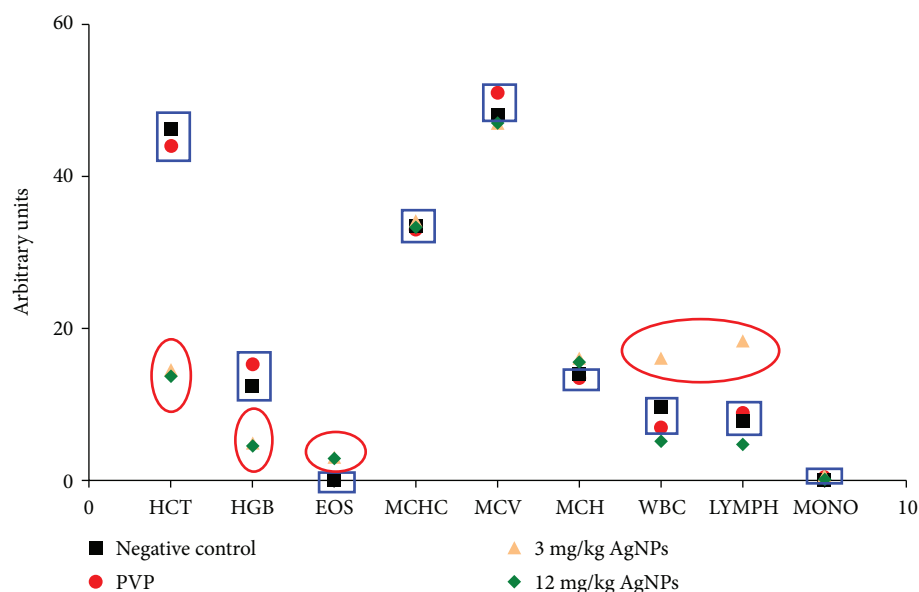


FIGURE 5: Haematological parameters in the surviving animals at the end of the study. Haematocrit (HCT), haemoglobin (HGB), eosinophils (EOS), mean corpuscular volume (MCV), mean corpuscular haemoglobin concentration (MCHC), white blood cells (WBC), lymphocytes (LYMPH), and monocytes (MONO) were determined in surviving mice treated with AgNPs and in mice without melanoma injected with water or PVP. HCT, HGB, WBC, and LYMPH were out of the range reported as normal (blue boxes) and those outside the normal ranges in mice treated with AgNPs (red circles).

[28–30] or to the whole nanoparticles [28, 29] which induce ROS generation, modifying the transmembrane potential of mitochondria and, in turn, trigger the activation of several cell death pathways.

The physicochemical properties of AgNPs such as size, coating, and metal content have been related with their cytotoxic effect in mammalian cells [31–33]. In human cell lines, the size of AgNPs plays a key role in the effects on viability, membrane integrity, and ROS generation [32, 34–36]. Specifically, a smaller size of AgNPs induce a higher cytotoxicity [37–40]. On the other hand, coating agents provide different stability degrees that directly influence the cytotoxic and genotoxic effects [11, 41, 42].

The effect of the AgNP formulation studied on this work on the B16-F10 murine melanoma cells with an  $IC_{50}$  of  $4.2 \mu\text{g/mL}$  after 24 h of exposure is quite similar to that found for human tumour cell lines of the cervix (HeLa), breast (MDA-MB-231 and MCF-7), prostate (DU-145), colon (DLD-1 and HT-29), and lung (H-1299 and H-1437). For all of them, the  $IC_{50}$  values found were within the concentration range of  $1.82$  to  $3.43 \mu\text{g/mL}$  after the same exposure time. As found for B16-F10 in this work, in all types of the tumour cells evaluated, the main cell death pathway induced is apoptosis and the cellular viability showed an inverse relationship with ROS overproduction. At the  $IC_{50}$  value determined for each tumour cell, no DNA damage was found according to the comet assays performed [20].

Interestingly, according to the proliferation kinetics, the main changes elicited by AgNPs on B16-F10 cells were not produced at 24 h but only after 6 h of exposure (Figure 1). After this time of exposure, cell viability and ROS overproduction have shown an inverse relationship (Figure 2). Besides, apoptosis reached its highest levels without necrosis

evidence (Figure 1). Consequently, AgNPs need only 6 h to provoke the cellular damage that leads melanoma cells to die by apoptosis (Figures 1 and 2).

Despite that both the agents AgNPs and CisPt produce similar effects on melanoma cells regarding cell viability and ROS overproduction, the final consequence is quite different. While the former induces only apoptosis as the main cell death pathway, the latter induces practically the same amount of apoptosis and necrosis.

On *in vitro* conditions, the CisPt-DNA adduct can be formed after 1–3 h in the blood cells and tumour tissue of cancer patients [43]. Thus, the quick obtainment of the CisPt-DNA adduct, the decrease of glutathione (GSH) [44], and the production of ROS in the mitochondria that, in turn, collapses energy production [45] could be independent of concomitant factors that contribute to the presence of 40 times more necrosis after CisPt administration compared with exposure to AgNPs.

Although the molecular mechanism of cytotoxicity elicited by this AgNP formulation is still not fully elucidated, these results represent an important advantage for AgNPs compared with CisPt because necrotic cellular debris promotes a proinflammatory response that is associated with tissue damage, processes not observed with the induction of programmed cell death ([46]).

Furthermore, the antitumour activity observed in mice treated with CisPt is completely different from that observed with AgNP treatments. The animals treated with CisPt died on the 11th day after the start of the treatment. During this time, they show lethargy and loss of appetite. This symptomatology could be related to the rapid and uncontrollable damage produced at the cellular level, which could be promoted by ROS overproduction in mitochondria and the alteration

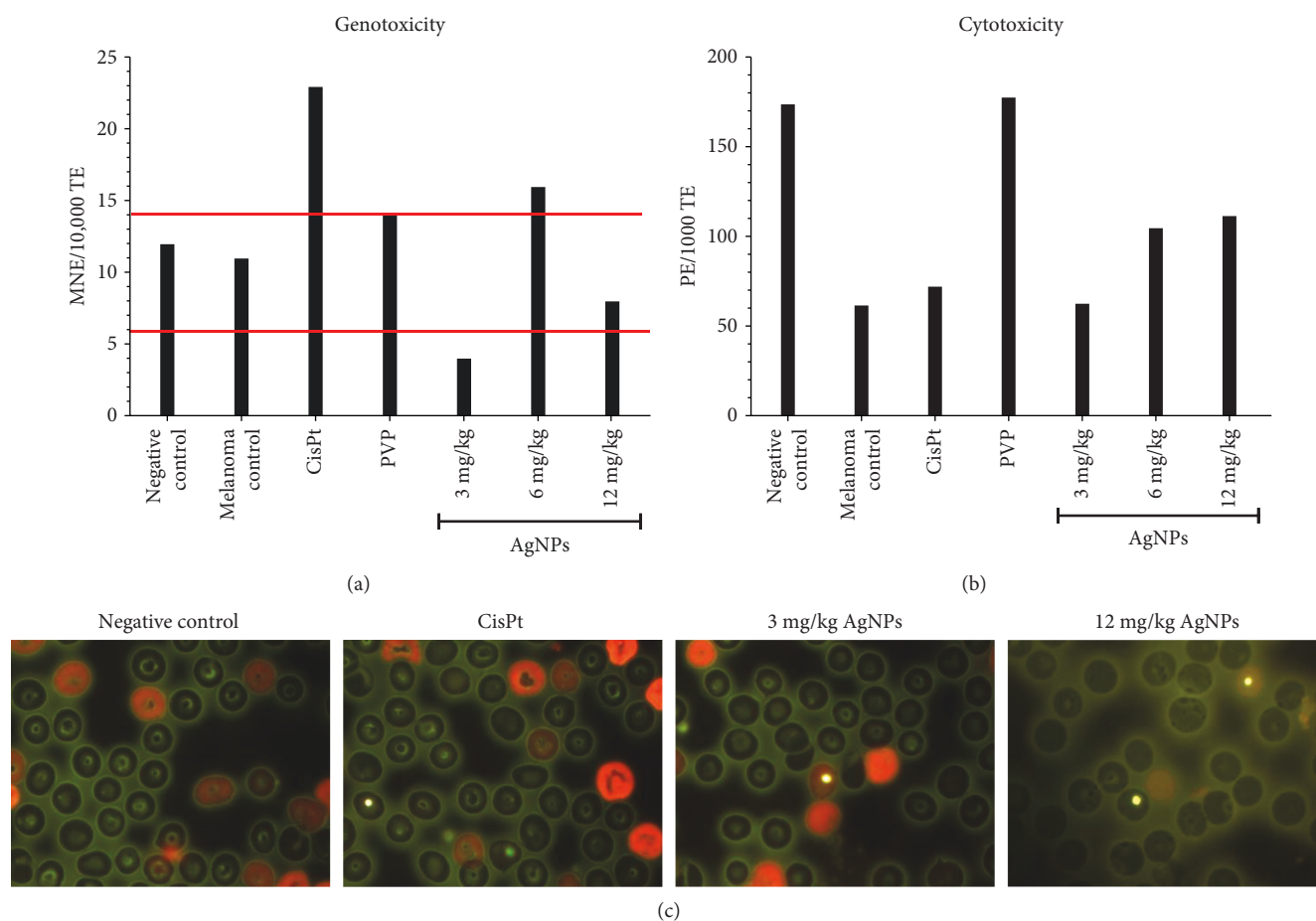


FIGURE 6: Cytotoxic and genotoxic effects quantified on erythrocytes from circulating blood samples. (a) Average of micronucleated erythrocytes (MNE) scored in 10,000 of total erythrocytes, (b) polychromatic erythrocytes (PCE) in 1000 erythrocytes, and (c) representative images of scored polychromatic erythrocytes (polychromatic erythrocytes, red; normochromic erythrocytes, green; micronuclei, yellow). Healthy mice (negative control), untreated mice (melanoma control), and mice with melanoma treated with CisPt, PVP, and the indicated doses of AgNPs. Red lines indicate the normal micronuclei range reported for C57BL/6J mice, polychromatic erythrocytes (red), normochromic erythrocytes (green), micronuclei (yellow).

TABLE 1: Physicochemical properties of AgNPs employed on *in vivo* murine melanoma models.

Property	Lin et al. [47]	Kang et al. [48]	This work
AgNP size (nm)	58.8 ± 1.7	2.3	35 ± 15
Protective agent	PVP	PVP	PVP
Z potential (mV)	-12.9 ± 1.1	-0.28	-15
Metallic silver content (% wt)	ND*	ND*	1.2
Initial tumour diameter (mm)	4-6	NA <sup>†</sup>	10
Used dose: metallic silver (mg/kg)	1.5	1, 5, and 10	3, 6, and 12
Days of administration in treatment	5	NA <sup>†</sup>	21
Dosage frequency	24 h	NA <sup>†</sup>	48 h
Days without treatment before sacrifice	8	NA <sup>†</sup>	7

\* ND: not determined. <sup>†</sup>NA: not applicable.

of the DNA structure that, finally, triggers necrosis as the main cell death pathway.

Unlike the treatment with CisPt, the AgNP treatments achieved a remarkable survival time with the three concentrations assayed. At least one mouse of the groups treated

with 3, 6, or 12 mg/kg of AgNPs reached the 21st day of the treatment alive; this represents almost a quadruplication of the lifespan compared with that of mice injected with water and doubling the lifespan compared with that of mice treated with CisPt.

As far as we know, there are only two papers that analyse the effect of AgNPs in an *in vivo* melanoma murine model. In the first work [47], a study of 17 days was performed using wortmannin, AgNPs, or a combination of both. Daily administration for 5 days starting with a tumour volume range of 50–100 mm<sup>3</sup> was used. Animals were euthanized eight days after the end of the treatment (13 days of observation).

This treatment scheme is quite different from that recommended for the NIH, but it is important to note that the authors of the work were focused in the modulation of autophagy to enhance the antiproliferative effect of AgNPs against cancer cells [47]. In general, Lin et al. found a much lower tumour growth inhibition than what we found in the same time window (thirteen days after starting treatment).

The largest tumour volume they found in their controls on day 13 after the treatment began is about 1200 mm<sup>3</sup>; those treated with their AgNPs had a tumour volume close to 500 mm<sup>3</sup> and those treated with the combination of AgNPs and wortmannin had a tumour volume of around 300 mm<sup>3</sup>. In this work, we found that on the 13th day after treatment began mice injected with water and CisPt already died; meanwhile, the surviving mouse of the group injected with PVP had a tumour volume of 9500 mm<sup>3</sup> and all mice treated with AgNPs presented tumour volumes between 800 and 1150 mm<sup>3</sup> (Figure 3). Unfortunately, these are not conclusive data due to the differences on the initial tumour volume, dosage frequency, days of treatment, follow-up days, and an unknown silver content of the AgNPs used by them which do not allow us to make a direct comparison with the results found in this work.

The second article [48] is quite different because it is focused on the angiogenic capacity of AgNPs. The authors report that B16-F10 melanoma cells exposed to AgNPs and then injected intradermally in C57BL/6J mice induced angiogenesis in the area near to the tumour and increased the haemoglobin concentration within the tumour. Smaller nanoparticles (2 nm, Table 1) elicited the vascularization around the tumour in the melanoma model, and the angiogenic effect is enhanced if the cells were previously exposed to AgNPs. The angiogenic effect elicited by low doses of AgNPs could promote the tumour growth, but this is reversed when the dose or the size of the nanoparticle increase [48].

On the other hand, AgNPs with a higher size (53 nm, Table 1) induce autophagy in melanoma cells with high concentrations or induce cell survival with lower concentrations. These works, including ours, are examples of the great impact that the size of nanoparticles with the same stabilizing agent has on murine melanoma. Unfortunately, the same cannot be said for the concentration of silver present in each study due to the lack of information (Table 1). The main similarities and differences between the characterization of AgNPs previously published and the AgNPs used in this work in an *in vivo* melanoma model are shown in Table 1.

A very important result from this work is that at the higher dose of AgNPs tested (12 mg/kg) the tumour growth seems to be inhibited, since the tumour volume remains constant during the whole observational period (seven days);

that is, from the 31st to the 38th day of the experiment (Figure 3).

This response must necessarily be related to the dose-dependent behaviour observed on the EPC counting that could be interpreted as a lower myelosuppression effect as the AgNP doses increase. Also, this is consistent with the general behaviour of mice treated with AgNPs that continued to be active and kept on feeding, in spite of the size of the tumour. This is contrary to the behaviour observed on mice treated with CisPt and those from the negative control group (Figure 6). These results suggest a protective dose-dependent effect elicited by AgNP treatments (Figure 6).

From Figure 6, it is clear that the higher protection against the myelosuppressive effect is provided by the PVP. However, only the combination of PVP and metallic silver to obtain the AgNP formulation possesses both the protective effect against myelosuppression and the antitumour activity.

Moreover, no genotoxic effect was observed on AgNP treatments of 3 and 12 mg/kg, both with an MNE counting below the upper limit of the range reported for this mouse [23] (marked in Figure 6 with red lines). Mice from the positive control group (with melanoma and without treatment) showed an MNE count within the marked range as well as the mice treated with PVP. In this sense, given that it has been reported that rodents are more sensitive to the genotoxic damage induced by AgNP than humans [49], one would expect very low damage caused by the administration of the AgNP formulation studied here in humans.

Conversely, samples from the last mouse of the group treated with CisPt showed almost double the MNE. This could be associated with the necrosis induction and the limited survival time observed on mice treated with this compound. It is known that platinum-based drugs, among them CisPt, are genotoxic. This fact is related with the appearance of new tumours and drug resistance, which means that, even when the CisPt treatment is effective against a tumour, there is an oncogenic risk due to its genotoxic effect [50].

Regarding the behaviour observed for mice treated with 6 mg/kg of AgNPs, these experiments do not provide enough arguments to explain the death of the last mouse five days earlier than the other surviving animals treated with 3 and 12 mg/kg of AgNPs, respectively (Figure 6). But, as in the case of CisPt, the higher amount of MNE compared with basal values could be associated with the death of that mouse. Further experiments must be done to clarify this point.

Surviving mice present haematological parameters quite similar to that found in healthy mice [22], but the increases observed in WBC and LYMPH with the lowest dose of AgNPs (3 mg/kg) are consistent with the activation of immunological system cells by the low concentration of AgNPs [51]. On the other hand, the lower levels of haemoglobin (HGB) and haematocrit (HCT) on surviving mice treated with both 3 and 12 mg/kg of AgNPs can be interpreted as anaemia.

It has been reported that nanosized colloidal silver stabilized with PVP may induce HCT and HGB decrease [52], and other AgNPs promoted venous thrombus formation by platelet aggregation [53]. However, in this case, the observed decrease in HCT and HGC could be attributable to the



development of melanoma itself. As shown in the Results, mice with melanoma but without treatment showed an important decrease on PCE counting. Therefore, the low levels of HCT and HGB could be the result of cumulative damage due to the progress of the disease and not because of a toxic effect of the administered AgNP.

For the purposes of avoiding as much as possible the anaemia in further studies, a systemic iron supplementation is proposed. It has been reported that this could be more effective than a twofold iron diet [54]. Also, it is known that a deficiency of other elements such as copper or selenium could be involved in the anaemia process [55, 56], but this is out of the scope of this work, and further analysis needs to be done to identify the cause and to prevent the anaemia.

Therefore, this work presents a systematic study for evaluating the antitumour effect of AgNPs in melanoma under standardized conditions, following NIH recommendations, and for providing the complete characterization of AgNPs, specifically the concentrations and doses of the active component, metallic silver. As a consequence, apoptosis induction, antitumour activity, lifespan increase, the absence of genotoxicity in blood samples, and the observed protective effect against myelosuppression elicited by melanoma on mice that have been exposed during 21 days to AgNPs is an irrefutable probe of the highest biocompatibility of these AgNPs compared with CisPt. All these results suggest that the possible adverse effects elicited by these AgNPs in humans might be less than the already known effects promoted by CisPt. This emphasizes the potential of AgNPs as an alternative for cancer treatment and urges the completeness of their preclinical studies.

## 5. Conclusions

This work is a systematic approach to evaluate the anti-proliferative and antitumour effect of AgNPs in melanoma under standardized conditions following the recommended protocol by NIH. The AgNP formulation studied in this work, Argovit<sup>™</sup>, possesses a higher antitumour activity and biocompatibility on C57BL/6JNHsd mice inoculated with murine melanoma B16-F10 cells than that found in one of the most employed chemotherapeutic agents in melanoma treatment, CisPt.

The higher biocompatibility of these AgNPs compared with CisPt is manifested *in vitro* as apoptosis induction, which is the main cell death pathway after 6 h of exposure triggered by ROS overproduction, mainly on mitochondria. Meanwhile, their high capacity to reduce tumour growth, remarkable lifespan increase (quadruple compared with non-treated and double compared with those treated with CisPt), lack of genotoxic damage, and the possible protective effect against myelosuppression, elicited by the natural progression of melanoma, were observed in *in vivo* assays.

These findings show the importance of adequate physico-chemical characteristics, such as size (35 nm), the optimal content of metallic Ag, and the effective metallic Ag/PVP ratio which provides AgNPs a high stability, to elicit the tumour growth rate decrease and to increase the life expectancy in individuals with one of the most aggressive skin

cancers known. All these can be gained without evident genotoxic effects and even decreasing the myelosuppression provoked by the natural progression of the disease, urging the completeness of its preclinical studies.

## Data Availability

The data used to support the findings of this study are available from the corresponding author upon request.

## Conflicts of Interest

The authors declare that there is no conflict of interest regarding the publication of this paper.

## Authors' Contributions

Lucía M. Valenzuela-Salas and Nayeli G. Girón-Vázquez contributed equally to this work.

## Acknowledgments

J.C.G.R. and Y.T.M. acknowledge the continuous support from CONACyT-Red Farmoquímicos (294727). This work had the financial support from CONACyT-Red Internacional de Bionanotecnología con Impacto en Biomedicina, Alimentación y Bioseguridad (293418) and the Tomsk Polytechnic University Competitiveness Enhancement Program (VIU-ISHBMT-196/2018).

## Supplementary Materials

Table S1: (related to Figure 1). Cellular viability, apoptosis, and necrosis recorded on B16-F10 cultures through time. Table S2: (related to Figure 2). ROS quantification by DCFDA and MitoSOX on B16-F10 exposed to AgNP and Cisplatin. (*Supplementary Materials*)

## References

- [1] World Health Organization, "Skin cancers," 2018, <http://www.who.int/uv/faq/skincancer/en/index1.html>.
- [2] D. Schadendorf, A. C. J. van Akkooi, C. Berking et al., "Melanoma," *The Lancet*, vol. 392, no. 10151, pp. 971–984, 2018.
- [3] L. Calderón, A. Peniche-Castellanos, L. Fierro-Arias, G. Montes de Oca-Sánchez, and I. Arellano-Mendoza, "Cutaneous melanoma: 12 years of experience," *Dermatologia Revista Mexicana*, vol. 61, no. 3, pp. 179–189, 2017.
- [4] M. C. Foletto and S. E. Haas, "Cutaneous melanoma: new advances in treatment," *Anais Brasileiros de Dermatologia*, vol. 89, no. 2, pp. 301–310, 2014.
- [5] B. Domingues, J. Lopes, P. Soares, and H. Populo, "Melanoma treatment in review," *ImmunoTargets and Therapy*, vol. 7, pp. 35–49, 2018.
- [6] American Cancer Society, *Cancer facts and figures 2018*, American Cancer Society, 2018.
- [7] S. Bhattacharyya, R. A. Kudgus, R. Bhattacharya, and P. Mukherjee, "Inorganic nanoparticles in cancer therapy," *Pharmaceutical Research*, vol. 28, no. 2, pp. 237–259, 2011.
- [8] J. Li, Y. Wang, R. Liang et al., "Recent advances in targeted nanoparticles drug delivery to melanoma," *Nanomedicine*:

- Nanotechnology, Biology, and Medicine*, vol. 11, no. 3, pp. 769–794, 2015.
- [9] S. J. Cameron, F. Hosseini, and W. G. Willmore, “A current overview of the biological and cellular effects of nanosilver,” *International Journal of Molecular Sciences*, vol. 19, no. 7, pp. 2030–2040, 2018.
- [10] O. Bondarenko, K. Juganson, A. Ivask, K. Kasemets, M. Mortimer, and A. Kahru, “Toxicity of Ag, CuO and ZnO nanoparticles to selected environmentally relevant test organisms and mammalian cells in vitro: a critical review,” *Archives of Toxicology*, vol. 87, no. 7, pp. 1181–1200, 2013.
- [11] A. Ivask, N. H. Voelcker, S. A. Seabrook et al., “DNA melting and genotoxicity induced by silver nanoparticles and graphene,” *Chemical Research in Toxicology*, vol. 28, no. 5, pp. 1023–1035, 2015.
- [12] S. Ahlberg, A. Antonopoulos, J. Diendorf et al., “PVP-coated, negatively charged silver nanoparticles: A multi-center study of their physicochemical characteristics, cell culture and in vivo experiments,” *Beilstein Journal of Nanotechnology*, vol. 5, pp. 1944–1965, 2014.
- [13] J. Swanner, J. Mims, D. Carroll et al., “Differential cytotoxic and radiosensitizing effects of silver nanoparticles on triple-negative breast cancer and non-triple-negative breast cells,” *International Journal of Nanomedicine*, vol. 10, no. 1, pp. 3937–3953, 2015.
- [14] J. L. Spinoso-Castillo, R. A. Chavez-Santoscoy, N. Bogdanchikova, J. A. Pérez-Sato, V. Morales-Ramos, and J. J. Bello-Bello, “Antimicrobial and hormetic effects of silver nanoparticles on in vitro regeneration of vanilla (*Vanilla planifolia* Jacks. Ex Andrews) using a temporary immersion system,” *Plant Cell, Tissue and Organ Culture*, vol. 129, no. 2, pp. 195–207, 2017.
- [15] R. Vazquez-Muñoz, B. Borrego, K. Juárez-Moreno et al., “Toxicity of silver nanoparticles in biological systems: does the complexity of biological systems matter?,” *Toxicology Letters*, vol. 276, pp. 11–20, 2017.
- [16] N. Bogdanchikova, R. V. Muñoz, A. H. Saquero et al., “Silver nanoparticles composition for treatment of distemper in dogs,” *International Journal of Nanotechnology*, vol. 13, no. 1/2/3, pp. 227–237, 2016.
- [17] B. Borrego, G. Lorenzo, J. D. Mota-Morales et al., “Potential application of silver nanoparticles to control the infectivity of Rift Valley fever virus in vitro and in vivo,” *Nanomedicine: Nanotechnology, Biology, and Medicine*, vol. 12, no. 5, pp. 1185–1192, 2016.
- [18] A. R. Ochoa-Meza, A. R. Álvarez-Sánchez, C. R. Romo-Quiñonez et al., “Silver nanoparticles enhance survival of white spot syndrome virus infected *Penaeus vannamei* shrimps by activation of its immunological system,” *Fish & Shellfish Immunology*, vol. 84, pp. 1083–1089, 2019.
- [19] C. A. A. Hernández, K. Juárez-Moreno, M. E. Castañeda-Juarez, A. P. Horacio-Almanza-Reyes, and N. Bogdanchikova, “Silver nanoparticles for the rapid healing of diabetic foot ulcers,” *International Journal of Medical Nano Research*, vol. 4, no. 1, p. 019, 2017.
- [20] K. Juárez-Moreno, E. B. Gonzalez, N. Girón-Vazquez et al., “Comparison of cytotoxicity and genotoxicity effects of silver nanoparticles on human cervix and breast cancer cell lines,” *Human & Experimental Toxicology*, vol. 36, no. 9, pp. 931–948, 2017.
- [21] W. W. Overwijk and N. P. Restifo, “B16 as a mouse model for human melanoma,” *Current Protocols in Immunology*, vol. 39, no. 1, pp. 20.1.1–20.1.29, 2001.
- [22] G. P. Otto, B. Rathkolb, M. A. Oestereicher et al., “Clinical chemistry reference intervals for C57BL/6J, C57BL/6N, and C3HeB/FeJ mice (*Mus musculus*),” *Journal of the American Association for Laboratory Animal Science*, vol. 55, no. 4, pp. 375–386, 2016.
- [23] H. U. Aeschbacher, “Rates of micronuclei induction in different mouse strains,” *Mutation Research/Environmental Mutagenesis and Related Subjects*, vol. 164, no. 2, pp. 109–115, 1986.
- [24] M. Laprise-Pelletier, T. Simão, and M. A. Fortin, “Gold nanoparticles in radiotherapy and recent progress in nanobrachytherapy,” *Advanced Healthcare Materials*, vol. 7, no. 16, article 1701460, 2018.
- [25] C. Núñez, S. V. Estévez, and M. del Pilar Chantada, “Inorganic nanoparticles in diagnosis and treatment of breast cancer,” *JBIC Journal of Biological Inorganic Chemistry*, vol. 23, no. 3, pp. 331–345, 2018.
- [26] P. Sivakumar, M. Lee, Y.-S. Kim, and M. S. Shim, “Photo-triggered antibacterial and anticancer activities of zinc oxide nanoparticles,” *Journal of Materials Chemistry B*, vol. 6, no. 30, pp. 4852–4871, 2018.
- [27] Y. Li, Y. Chang, X. Lian et al., “Silver nanoparticles for enhanced cancer theranostics: in vitro and in vivo perspectives,” *Journal of Biomedical Nanotechnology*, vol. 14, no. 9, pp. 1515–1542, 2018.
- [28] L. A. Austin, B. Kang, C.-W. Yen, and M. A. El-Sayed, “Plasmonic imaging of human oral cancer cell communities during programmed cell death by nuclear-targeting silver nanoparticles,” *Journal of the American Chemical Society*, vol. 133, no. 44, pp. 17594–17597, 2011.
- [29] M. J. Piao, K. A. Kang, I. K. Lee et al., “Silver nanoparticles induce oxidative cell damage in human liver cells through inhibition of reduced glutathione and induction of mitochondria-involved apoptosis,” *Toxicology Letters*, vol. 201, no. 1, pp. 92–100, 2011.
- [30] T. Verano-Braga, R. Miethling-Graff, K. Wojdyla et al., “Insights into the cellular response triggered by silver nanoparticles using quantitative proteomics,” *ACS Nano*, vol. 8, no. 3, pp. 2161–2175, 2014.
- [31] L. P. Franchi, B. B. Manshian, T. A. J. de Souza et al., “Cytotoxic and genotoxic effects of metallic nanoparticles in untransformed human fibroblast,” *Toxicology In Vitro*, vol. 29, no. 7, pp. 1319–1331, 2015.
- [32] S. Kim and D. Y. Ryu, “Silver nanoparticle-induced oxidative stress, genotoxicity and apoptosis in cultured cells and animal tissues,” *Journal of Applied Toxicology*, vol. 33, no. 2, pp. 78–89, 2013.
- [33] T. Shi, X. Sun, and Q. Y. He, “Cytotoxicity of silver nanoparticles against bacteria and tumor cells,” *Current Protein & Peptide Science*, vol. 19, no. 6, pp. 525–536, 2018.
- [34] C. Carlson, S. M. Hussain, A. M. Schrand et al., “Unique cellular interaction of silver nanoparticles: size-dependent generation of reactive oxygen species,” *The Journal of Physical Chemistry B*, vol. 112, no. 43, pp. 13608–13619, 2008.
- [35] R. Foldbjerg, P. Olesen, M. Hougaard, D. A. Dang, H. J. Hoffmann, and H. Autrup, “PVP-coated silver nanoparticles and silver ions induce reactive oxygen species, apoptosis and necrosis in THP-1 monocytes,” *Toxicology Letters*, vol. 190, no. 2, pp. 156–162, 2009.
- [36] D. Guo, L. Zhu, Z. Huang et al., “Anti-leukemia activity of PVP-coated silver nanoparticles via generation of reactive

- oxygen species and release of silver ions," *Biomaterials*, vol. 34, no. 32, pp. 7884–7894, 2013.
- [37] A. Avalos, A. I. Haza, D. Mateo, and P. Morales, "Interactions of manufactured silver nanoparticles of different sizes with normal human dermal fibroblasts," *International Wound Journal*, vol. 13, no. 1, pp. 101–109, 2016.
- [38] G. Joksić, J. Stašić, J. Filipović, A. V. Šobot, and M. Trtica, "Size of silver nanoparticles determines proliferation ability of human circulating lymphocytes *in vitro*," *Toxicology Letters*, vol. 247, pp. 29–34, 2016.
- [39] W. Liu, Y. Wu, C. Wang et al., "Impact of silver nanoparticles on human cells: effect of particle size," *Nanotoxicology*, vol. 4, no. 3, pp. 319–330, 2010.
- [40] H. J. Wang, L. Yang, H. Y. Yang et al., "Antineoplastic activities of protein-conjugated silver sulfide nano-crystals with different shapes," *Journal of Inorganic Biochemistry*, vol. 104, no. 1, pp. 87–91, 2010.
- [41] T. Bartłomiejczyk, A. Lankoff, M. Kruszewski, and I. Szumiel, "Silver nanoparticles—allies or adversaries?," *Annals of Agricultural and Environmental Medicine*, vol. 20, no. 1, pp. 48–54, 2013.
- [42] G. Vecchio, M. Fenech, P. P. Pompa, and N. H. Voelcker, "Lab-on-a-Chip-based high-throughput screening of the genotoxicity of engineered nanomaterials," *Small*, vol. 10, no. 13, pp. 2721–2734, 2014.
- [43] A. M. J. Fichtinger-Schepman, S. D. van der Velde-Visser, H. C. M. van Dijk-Knijnenburg, A. T. van Oosterom, R. A. Baan, and F. Berends, "Kinetics of the formation and removal of cisplatin-DNA adducts in blood cells and tumor tissue of cancer patients receiving chemotherapy: comparison with *in vitro* adduct formation," *Cancer Research*, vol. 50, no. 24, pp. 7887–7894, 1990.
- [44] R. Alemón-Medina, M. E. Bravo-Gómez, M. I. Gracia-Mora, and L. Ruiz-Azuara, "Comparison between the Antiproliferative effect and intracellular glutathione depletion induced by Casiopeína IIgly and cisplatin in murine melanoma B16 cells," *Toxicology In Vitro*, vol. 25, no. 4, pp. 868–873, 2011.
- [45] Y. M. Choi, H.-K. Kim, W. Shim et al., "Mechanism of cisplatin-induced cytotoxicity is correlated to impaired metabolism due to mitochondrial ROS generation," *PLoS One*, vol. 10, no. 8, article e0135083, 2015.
- [46] X. Guo, C. Jagannath, M. G. Espitia, and X. Zhou, "Uptake and silica and carbon nanotubes by human macrophages/monocytes induces activation of fibroblasts *in vitro* — potential implication for pathogenesis of inflammation and fibrotic diseases," *International Journal of Immunopathology and Pharmacology*, vol. 25, no. 3, pp. 713–719, 2012.
- [47] J. Lin, Z. Huang, H. Wu et al., "Inhibition of autophagy enhances the anticancer activity of silver nanoparticles," *Autophagy*, vol. 10, no. 11, pp. 2006–2020, 2014.
- [48] K. Kang, D. H. Lim, I. H. Choi et al., "Vascular tube formation and angiogenesis induced by polyvinylpyrrolidone-coated silver nanoparticles," *Toxicology Letters*, vol. 205, no. 3, pp. 227–234, 2011.
- [49] R. Limade, A. B. Seabra, and N. Durán, "Silver nanoparticles: a brief review of cytotoxicity and genotoxicity of chemically and biogenically synthesized nanoparticles," *Journal of Applied Toxicology*, vol. 32, no. 11, pp. 867–879, 2012.
- [50] B. J. S. Sanderson, L. R. Ferguson, and W. A. Denny, "Mutagenic and carcinogenic properties of platinum-based anticancer drugs," *Mutation Research/Fundamental and Molecular Mechanisms of Mutagenesis*, vol. 355, no. 1–2, pp. 59–70, 1996.
- [51] S. Castro-Gamboa, M. R. Garcia-Garcia, G. Piñon-Zarate et al., "Toxicity of silver nanoparticles in mouse bone marrow-derived dendritic cells: implications for phenotype," *Journal of Immunotoxicology*, vol. 16, no. 1, pp. 1–9, 2019.
- [52] A. A. Shumakova, V. A. Shipelin, Y. S. Sidorova et al., "Toxicological evaluation of nanosized colloidal silver, stabilized with polyvinylpyrrolidone. I. Characterization of nanomaterial, integral, hematological parameters, level of thiol compounds and liver cell apoptosis," *Voprosy Pitaniia*, vol. 6, pp. 46–57, 2015.
- [53] E.-A. Jun, K.-M. Lim, K. Y. Kim et al., "Silver nanoparticles enhance thrombus formation through increased platelet aggregation and procoagulant activity," *Nanotoxicology*, vol. 5, no. 2, pp. 157–167, 2011.
- [54] D. N. Seril, J. Liao, C. S. Yang, and G. Y. Yang, "Systemic iron supplementation replenishes iron stores without enhancing colon carcinogenesis in murine models of ulcerative colitis: comparison with iron-enriched diet," *Digestive Diseases and Sciences*, vol. 50, no. 4, pp. 696–707, 2005.
- [55] N. Kaushal, S. Hegde, J. Lumadue, R. F. Paulson, and K. S. Prabhu, "The regulation of erythropoiesis by selenium in mice," *Antioxidants & Redox Signaling*, vol. 14, no. 8, pp. 1403–1412, 2011.
- [56] P. Matak, S. Zumerle, M. Mastrogiannaki et al., "Copper deficiency leads to anemia, duodenal hypoxia, upregulation of HIF-2 $\alpha$  and altered expression of iron absorption genes in mice," *PLoS One*, vol. 8, no. 3, article e59538, 2013.

## Research Article

# DpdtbA-Induced Growth Inhibition in Human Esophageal Cancer Cells Involved Inactivation of the p53/EGFR/AKT Pathway

Zhuo Wang,<sup>1</sup> Cuiping Li,<sup>1</sup> Yongli Li,<sup>2</sup> Xingshuang Guo,<sup>1</sup> Zhaoyu Yan,<sup>1</sup> Fulian Gao <sup>1</sup>,  
and Changzheng Li <sup>1,3</sup>

<sup>1</sup>School of Basic Medical Sciences, Xinxiang Medical University, Xinxiang, Henan 453003, China

<sup>2</sup>School of Basic Medical Sciences, Sanquan College of Xinxiang Medical University, Xinxiang, Henan 453003, China

<sup>3</sup>Experimental Teaching Center of Biology and Basic Medical Sciences, Sanquan College of Xinxiang Medical University, Xinxiang, Henan 453003, China

Correspondence should be addressed to Fulian Gao; [gfl@xxmu.edu.cn](mailto:gfl@xxmu.edu.cn) and Changzheng Li; [changzhenl@yahoo.com](mailto:changzhenl@yahoo.com)

Received 2 April 2019; Accepted 23 May 2019; Published 1 July 2019

Guest Editor: Rizwan Wahab

Copyright © 2019 Zhuo Wang et al. This is an open access article distributed under the Creative Commons Attribution License, which permits unrestricted use, distribution, and reproduction in any medium, provided the original work is properly cited.

Esophageal cancer (ESC) is one of the most deadly diseases for human. p53 in most cancers, including ESC cell, is mutated, and the mutated p53 loses its original function and acquires “gain of function” that allows for promoting the hallmarks of cancer, such as antiapoptosis, metastasis, invasion, angiogenesis, and resistance to chemotherapy. Targeting p53 through either introducing wild-type or degrading mutated p53 is an important strategy in cancer therapy. Di-2,2'-pyridine ketone dithiocarbamate s-butyric acid (DpdtbA) has significant growth inhibition against gastric cancer lines in previous study. Similar action in ESC cell lines but a novel molecular mechanism was observed in the present study. The results showed that DpdtbA exhibited an excellent antiproliferative effect for ESC cell lines ( $IC_{50} \leq 4.5 \pm 0.4 \mu\text{M}$  for Kyse 450,  $3.2 \pm 0.6 \mu\text{M}$  for Kyse 510 cell, and  $10.0 \pm 0.6 \mu\text{M}$  for Kyse 150) and led to cell cycle arrest at the S phase which correlated to CDK2 downregulation. The mechanistic study suggested that growth inhibition was related to ROS-mediated apoptosis, and ROS production was due to SOD inhibition initiated by DpdtbA rather than occurrence of ferritinophagy. In addition, DpdtbA also induced a downregulation of EGFR, p53, and AKT, which hinted that mutant p53 still played a role in the regulation of its downstream targets. Further study revealed that the downregulation of p53 was through stub1- (chip-) mediated autophagic degradation rather than MDM2-mediated ubiquitination. Taken together, the DpdtbA-induced growth inhibition in a mechanism was through inactivating the p53/EGFR/AKT signal pathway.

## 1. Introduction

Cancer is one of most deadly diseases, while esophageal cancer (ESC) lies in the eighth position in cancer-caused deaths, and about half of all cases occur in China [1]. Despite advancements in diagnostic and treatment methods in recent years, the prognosis of patients with ESC remains not ideal [2]. Although many factors may induce the formation of esophageal cancer, the underlying mechanism of it is largely unknown. p53 is one of most important transcription factor, regulating proliferation, apoptosis, autophagy, and cell cycle, and normally is considered as a tumor suppressor gene. However, p53 in human cancer is most frequently mutated

and in dominant phenotypes, in human ESC, 75% of p53 gene mutations were detected [3]. And mutant p53 (mutp53) cancers are dependent on their hyper stable mutp53 protein for survival [4]. In addition, evidences revealed that mutp53 seemed to gain characteristics that allow for promoting the hallmarks of cancer, such as antiapoptosis, metastasis, invasion, angiogenesis, and resistance to chemotherapy [5], which actively contribute to cancer development and progression [5, 6]. p53 mutants are categorized into structural (R175, G245, R249, and R282) and contact (R248 and R273) mutations with effects of gross conformational alterations and loss of anchorage to DNA, respectively [7]. Generally, wild-type p53 is regulated by its gene expression and

degradation and is maintained at a low level by continuous degradation via proteasome through E3 ubiquitin ligase [8, 9], others, such as chaperone-mediated autophagic degradation [10–14]. As mentioned above, since different mutant p53 alleles may exhibit certain unique characteristics in cancer development and progression, therefore, targeting mutant p53 for protein degradation, rather than its reactivation, might be another strategy for drug development [15]. Garufi et al. reported that a Zn(II)-curcumin complex displayed growth inhibition involved in the induction of mutant p53 degradation [16], implying that mutant p53 degradation was one of the options in cancer treatment. However, the exploration of effective small molecule therapies targeting mutant p53 is still on the way.

The epidermal growth factor receptor (EGFR), an ErbB family of receptor tyrosine kinases, plays an important role in cell proliferation and survival [17]. Upon ligand binding, the EGFR dimerizes which lead to subsequent activation of EGFR tyrosine kinase, resulting in the generation of a number of intracellular signals, including PI3K/AKT/mTOR, RAS/MAPK1/3, and STAT3 signaling pathways [18]. Overexpression of EGFR is seen in many solid tumors, including esophageal cancer, and is associated with poor prognosis [19]. In addition, the frequent gene amplification of EGFR, HER2, and FGFR2 and the presence of active EGFR mutations were observed in ESC specimens [20]. Downregulation of EGFR or inhibition of EGFR kinase may halt the proliferation of cancer cells; thus, many tyrosine kinase inhibitors such as gefitinib, lapatinib, and erlotinib have been developed; however, only limited effectiveness were achieved [21]. It was reported that some small molecules could downregulate EGFR and enhance the effectivity of chemotherapeutic agent [22]. Thus, the development of small-molecule inhibitors for the treatment of esophageal cancer is required.

As mentioned above, different mutant p53 alleles play an important role in cancer development and progression; therefore, targeting mutant p53 through protein degradation, rather than its reactivation, might be another strategy for drug development. Dithiocarbamates as metal chelators own important biological activities in the treatment of bacterial and fungal infections, AIDS, and cancer [23]. DpdtbA (di-2,2'-pyridine ketone dithiocarbamate *s*-butyric acid), a dithiocarbamate derivative, also displayed significant growth inhibition against gastric cancer cell lines in our previous study [24]. To extend our knowledge for the dithiocarbamate derivative, the effect of DpdtbA on the proliferation of esophageal cancer cell lines was further investigated. Interestingly, the DpdtbA-induced growth inhibition involved p53 depletion, which was not consistent with that reported previously in gastric cancer cell lines [24]. Additional investigations revealed that the p53 degradation was through chaperone-mediated autophagy rather than MDM2-mediated ubiquitination. Furthermore, concomitant to the degradation of mutated p53, a downregulation of EGFR and AKT was observed, indicating that inactivation of the p53/EGFR/AKT axis could achieve the growth inhibition in p53 mutation-overexpressed ESC cell lines. Those results definitely enriched our knowledge that targeting mutant p53 may be one of the options in successful anticancer therapy.

## 2. Results

**2.1. DpdtbA Induced Proliferation and Colony Formation Inhibition in Esophageal Cancer (ESC) Cells.** Previous study demonstrated that di-2,2'-pyridine ketone dithiocarbamate *s*-butyric acid (DpdtbA) owned significant growth inhibition in gastric cell lines [24]; DpdtbA might have similar action in ESC cell lines. With this purpose, we first assessed the effect of DpdtbA on the cell viability of Kyse 450, 150, and 510 cells. The dose-response curves are depicted in Figure 1, and significant growth inhibition for the ESC cell lines ( $IC_{50} \leq 4.5 \pm 0.4 \mu\text{M}$  for Kyse 450,  $3.2 \pm 0.6 \mu\text{M}$  for Kyse 510, and  $10.0 \pm 0.7 \mu\text{M}$  for Kyse 150) was observed compared to control ( $p < 0.05$ ), but the cell line dependence was not evident. Next, the effect of DpdtbA on cell colony formation was further investigated. As shown in Figure 1(c), DpdtbA induced a significant reduction in colony numbers and populations for Kyse 450 ( $p < 0.05$ ); the quantitative analysis is shown in Figure 1(d). Similar assay for Kyse 150 was also performed, and the results are presented in Figure S1.

**2.2. DpdtbA Induced Cell Cycle Arrest at the S Phase.** To test whether an induction of cell cycle arrest contributed to the antiproliferative capability of DpdtbA in ESC cells, cell cycle analysis was performed via flow cytometry. As shown in Figure 2, DpdtbA caused an accumulation of the ESC cells in the S phase for both cell lines, and the percentages at the S phase significantly increased by 10 to 17% during 24 h insult of the agent, thereby decreasing the proportion of cells in the G1 phase. Those indicated that DpdtbA could disturb cell cycle and arrest the cells at the S phase, which was not consistent with that in gastric cell lines [24], indicating that DpdtbA-induced cell cycle delay was cell line dependent. Furthermore, it was well documented that the progression of cells is regulated by cyclins and CDK (cyclin-dependent kinase) proteins, and cyclin A and CDK2 are known to play an important role in the regulation of DNA synthesis during cell-cycle progression at the S phase; thus, the expression of CDK2 in different conditions was determined. As shown in Figure S2, DpdtbA led to a downregulation of CDK2, which contributed to S phase arrest, in accordance with that reported previously [25, 26].

**2.3. The DpdtbA Induced Significant Apoptosis in ESC Cells.** Previous study revealed that DpdtbA-induced apoptosis contributed to the growth inhibition in gastric cancer lines [24]; similar action may occur in ESC cells. To this end, the ESC cells were pretreated by DpdtbA; then, the annexin V/propidium iodide (PI) staining was performed to measure the apoptotic populations at early and late stages, which were achieved by monitoring the externalization of phosphatidylserine on the cell surface of apoptotic cells. The results from flow cytometric analyses showed that the DpdtbA induced early apoptosis and late apoptosis in a concentration-dependent manner (Figure 3(a), from 4.2 to 16.4% for Kyse 450 and 5.1 to 8.1% for Kyse 150). Statistical analysis revealed that the apoptotic induction of DpdtbA at a concentration of 5 and 10  $\mu\text{M}$  had a statistical significance for Kyse 450 ( $p < 0.05$ ), but for Kyse 150 cells, 10  $\mu\text{M}$  was required

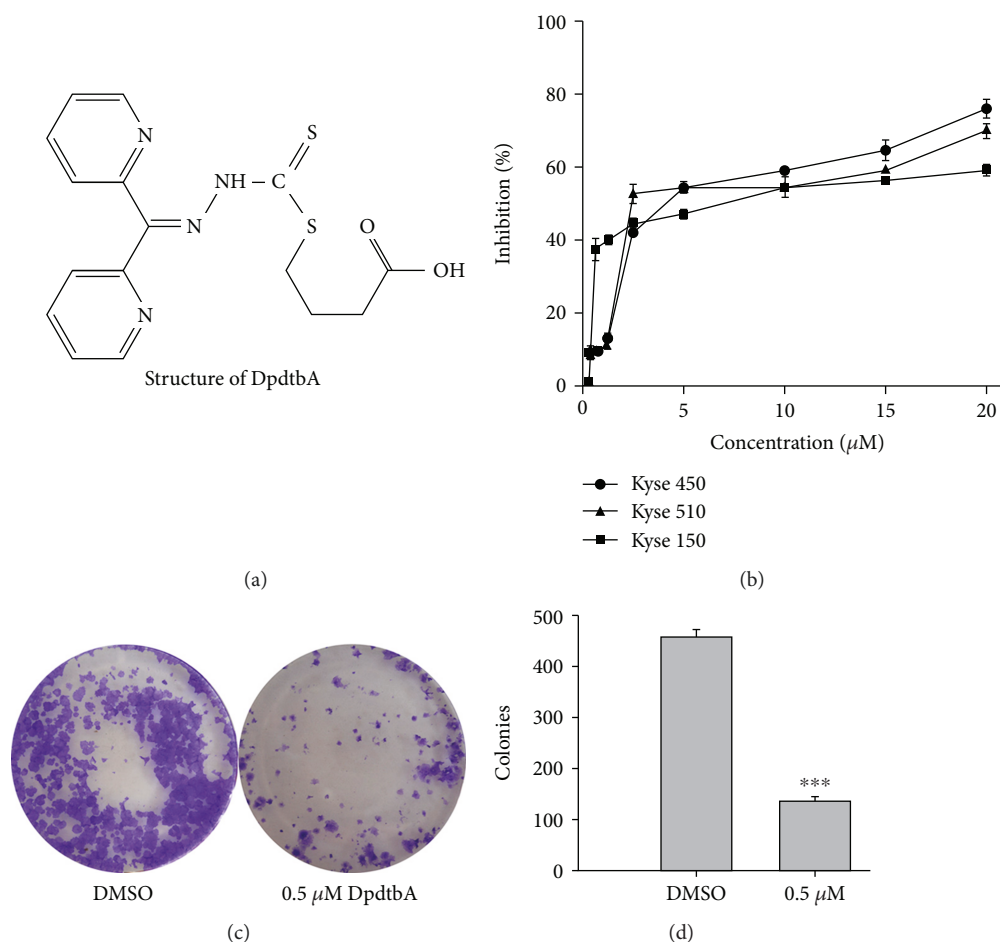


FIGURE 1: DpdtbA induced growth and colony formation inhibition. (a) Structure of DpdtbA; (b) the effect of DpdtbA on the proliferation of ESC cell lines; (c) DpdtbA displayed colony formation inhibition; (d) quantitative analysis of alteration in colony numbers (from trice measurements). \*\*\* $p < 0.05$ .

( $p < 0.05$ ). Moreover, the apoptotic portions in both cell lines were obviously different, which may be relative to  $\text{IC}_{50}$  value; as a whole, DpdtbA induced a limited apoptosis.

To seek additional evidence for the occurrence of apoptosis, the variations in nuclear morphology and fragmentation of chromosomal DNA were further investigated. As shown in Figure S3, the condensed nuclear and fragmentation of chromosomal DNA were observed upon DpdtbA treatment. In addition, using AO/EB stains to detect apoptosis was also performed under fluorescence microscope [27, 28]. As shown in Figure S4, live cells appeared uniformly green and had intact membrane and uniform chromatin, whereas early apoptotic cells and late apoptotic cells appeared as bright green and orange, respectively; necrotic cells appeared as red with no condensed chromatin. The portions of apoptosis cells in Kyse 450 were higher than that of Kyse 150, consistent with the results from annexin V/PI stains (Figure 3).

Bcl-2 family members play key roles in the regulation of apoptotic progress. To understand how DpdtbA induced apoptosis, we further examined the alteration in the expression of apoptosis-related genes in ESC cells. As shown in Figure 4, the DpdtbA treatment led to slight downregulation of the bcl-2 level, but the expression of bax was not increased, and similar situation occurred for cytochrome c. It was well

documented that translocation of bax on mitochondria could lead to alteration in mitochondrial membrane permeability (MMP). Since there was no obvious change in the bax expression, the MMP could be in an intact state. To confirm above speculation, a mitochondrial dye, rhodamine 123, was employed to evaluate the permeability of mitochondrial membrane. As expected, the MMP has almost no change (Figure S5), supporting that a limited apoptosis occurred.

**2.4. The ROS Production Stemmed from DpdtbA Induced SOD Inhibition Rather Than Ferritinophagy.** In general apoptosis associated with ROS production, to determine the origin of ROS, the ESC cells treated by DpdtbA were stained by ROS dye, DCF, following flow cytometry analysis. The ROS production at different condition is shown in Figure 5. Compared to control (Figure 5(a)), the ROS production induced by DpdtbA (Figures 5(b) and 5(c)) was significantly increased ( $p < 0.05$ , Figure 5(d)) in Kyse 450, indicating that ROS indeed involved the action of DpdtbA. Similar result was obtained in Kyse 150 cells (Figure S6). Due to the diversity in ROS production, the possible site was further explored. Ferritinophagy is an important contributor in Fenton reaction-related ROS generation; thus, the level of ferritin and its specific cargo, NCOA 4, was assayed.

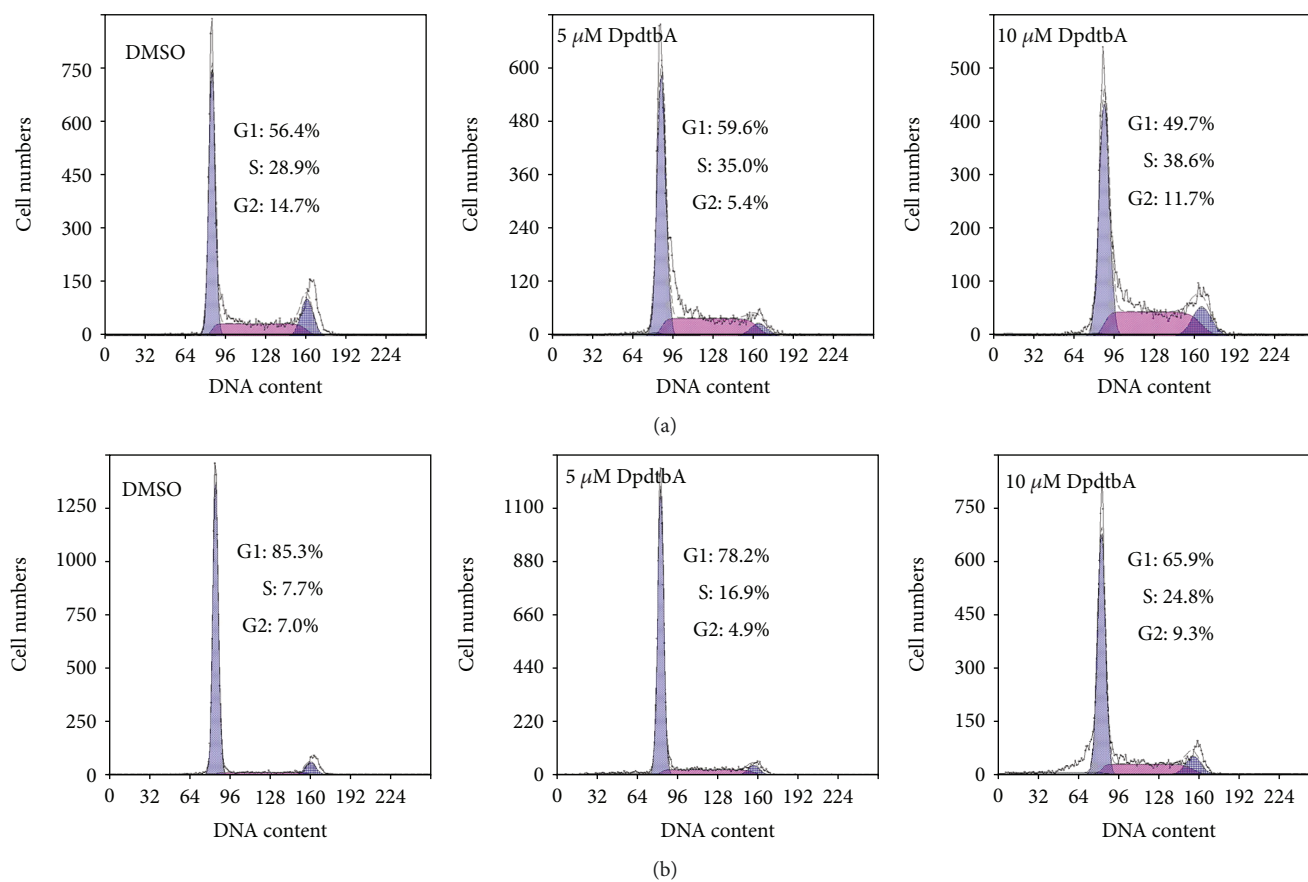


FIGURE 2: Effect of DpdtbA on cell cycle in ESC cells. Cell cycle distribution of ESC cells following treatment with various concentrations of DpdtbA. (a) Kyse 450 cells and (b) Kyse 150 cells; dose-dependent accumulation in the S phase of the cell cycle. Accordingly, the proportions of cells in the G1 and G2/M phases were decreased.

Unexpectedly, DpdtbA did not induce ferritinophagy that led to ferritin degradation; contrarily, an upregulated ferritin was observed with downregulated NCOA4 (Figure 5(e)). Furthermore, addition of autophagy inhibitor (3-MA) did not alter the status of ferritin and NCOA4, those excluded that ROS production was through ferritinophagy, which was different from other iron chelator [29]. Moreover, the status of ROS in a cell was dependent on the balance between ROS production and antioxidant system. The alterations of antioxidants, such as GST and superoxide dismutase (SOD), significantly affect the status of oxidative stress. The risen ROS might be from downregulated SOD or SOD inhibition. To this end, the level of SOD was investigated, as shown in Figure 5(g); DpdtbA led to downregulation of SOD with a significant difference compared to control ( $p < 0.01$  at 10  $\mu$ M, Figure 5(h)). Meanwhile, DpdtbA was also able to inactivate SOD in a concentration-dependent manner ( $p < 0.01$ , Figure 5(f)). Taken together, the ROS production during DpdtbA insult mainly stemmed from inactivation and downregulation of SOD.

**2.5. The DpdtbA Induced Growth Inhibition Correlated to EGFR Downregulation.** It has shown that EGFR mediates cell proliferation [30], and generally, EGFR (wild-type or mutated) is overexpressed in ESC cells [18]. Whether the growth inhibition induced by DpdtbA was associated with

alteration of EGFR, with this purpose, we determined the expression of EGFR in the presence or absence of DpdtbA. As shown in Figure 6, the expression of EGFR in Kyse 450 and Kyse 150 cell lines was decreased, but less abundance of EGFR in Kyse 510 cells was observed. The quantitative analysis of EGFR revealed that DpdtbA induced downregulation of EGFR had a statistical significance ( $p < 0.01$ ), hinting that depletion of EGFR might involve in the growth inhibition. Due to lower abundance of EGFR in Kyse 510, the cell line was further not included in the following investigation.

**2.6. The Effect of DpdtbA on the Upstream and Downstream of EGFR Signal.** It has known that EGFR activation can trigger the alteration of others, including JAK/STAT and the PI3K/AKT signal pathway, thus promoting cell growth [30]. The fact that DpdtbA induced a downregulation of EGFR prompted us to explore the underlying mechanism. Thus, the regulation of EGFR on other genes was further investigated. Generally, AKT was regulated by EGFR (or phosphorylated EGFR); the alteration of EGFR might also affect its downstream target, AKT; thus, the level of AKT in the presence or absence of DpdtbA was determined. As expected, accompanied by a decrease of EGFR (or p-EGFR), the AKT was also downregulated (Figure 7(a)). The quantitative analysis indicated that DpdtbA induced the decrease of AKT which had a statistical significance ( $p < 0.01$ ) in both

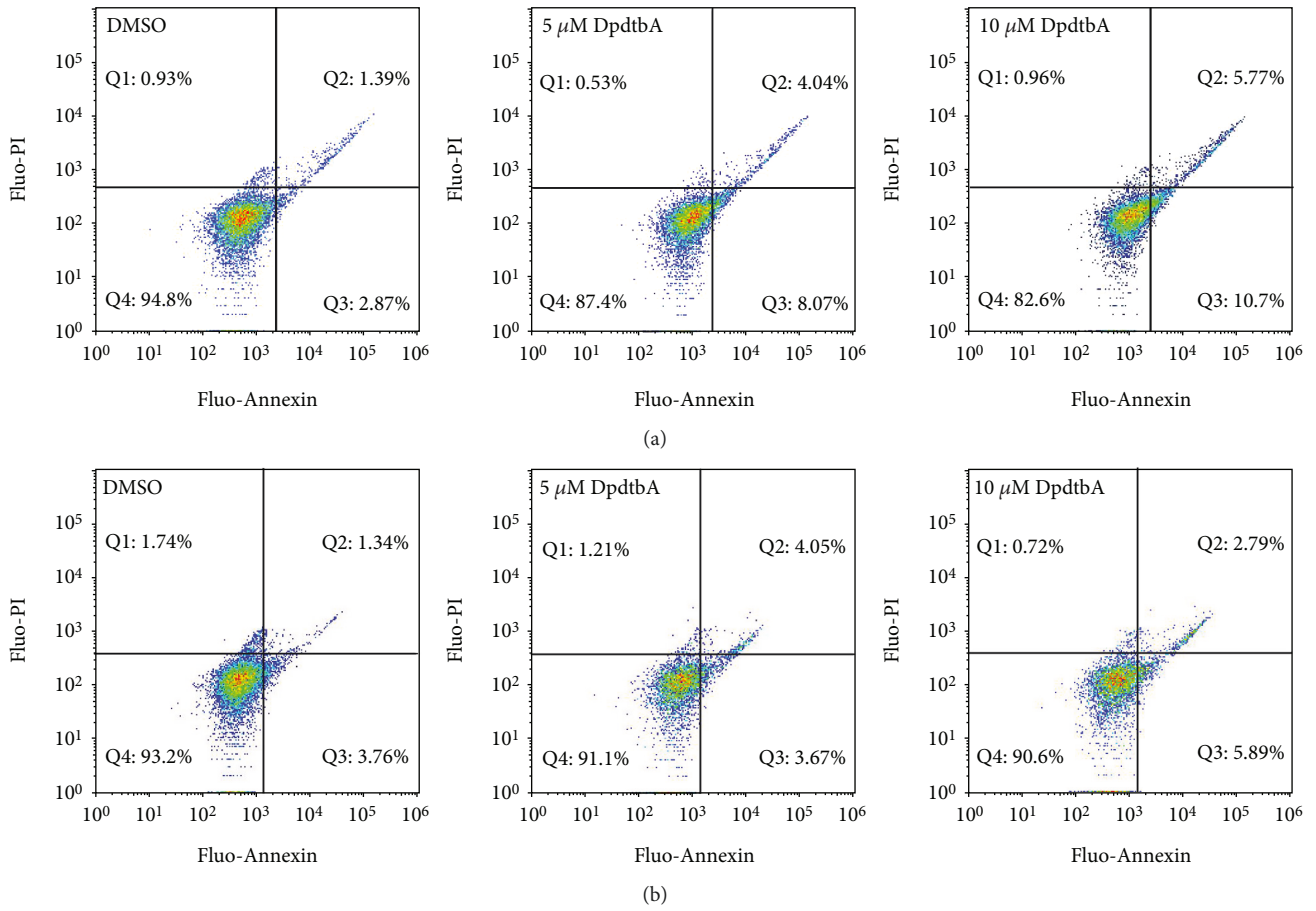


FIGURE 3: Apoptosis analysis of ESC cell lines via flow cytometer. DpdtbA was incubated with the cells for 24 h. All attached cells were collected and double stained with annexin V and propidium iodide (PI) using a kit from Dojindo Laboratories following the manufacturer’s instructions. (a) Kyse 450 cells and (b) Kyse 150 cells. The condition was as indicated in the figure.

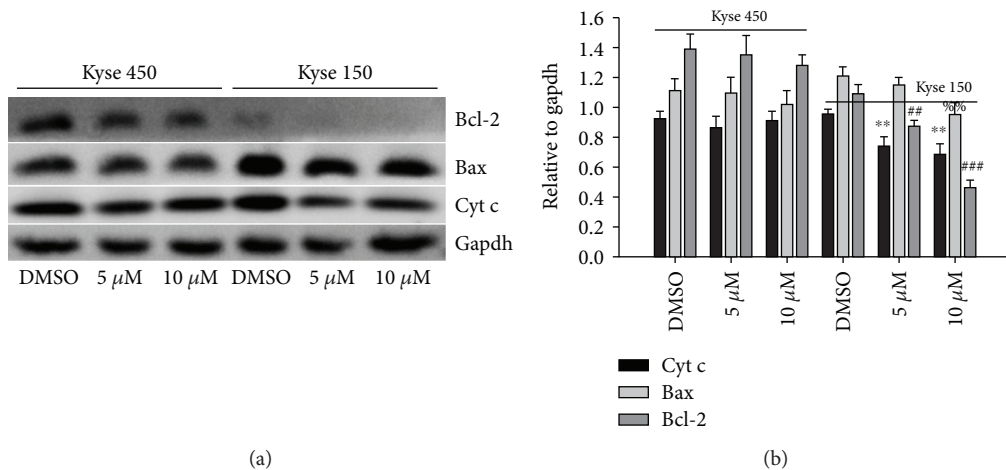


FIGURE 4: The alteration in apoptosis-related genes after DpdtbA treatment in the ESC cells. (a) Western blotting analyses of apoptosis-related gene expressions. (b) Quantitative analyses of the levels of apoptosis-related genes in the presence or absence of DpdtbA (from twice measurements). \*\*,###,%%  $p < 0.05$  and \*\*\*  $p < 0.01$ .

cell lines, indicating that EGFR was involved in the regulation of AKT. In addition, it is well documented that p53 can regulate EGFR [31]; the p53 expression, therefore, was further assayed. Interestingly, DpdtbA also led to p53 downregula-

tion (Figure 7(a)). Statistical analysis revealed that the levels of p53, EGFR, and p-EGFR were significantly decreased after DpdtbA treatment ( $p < 0.05$ , Figure 7(b)), which hinted that downregulation of EGFR and AKT might stem from the



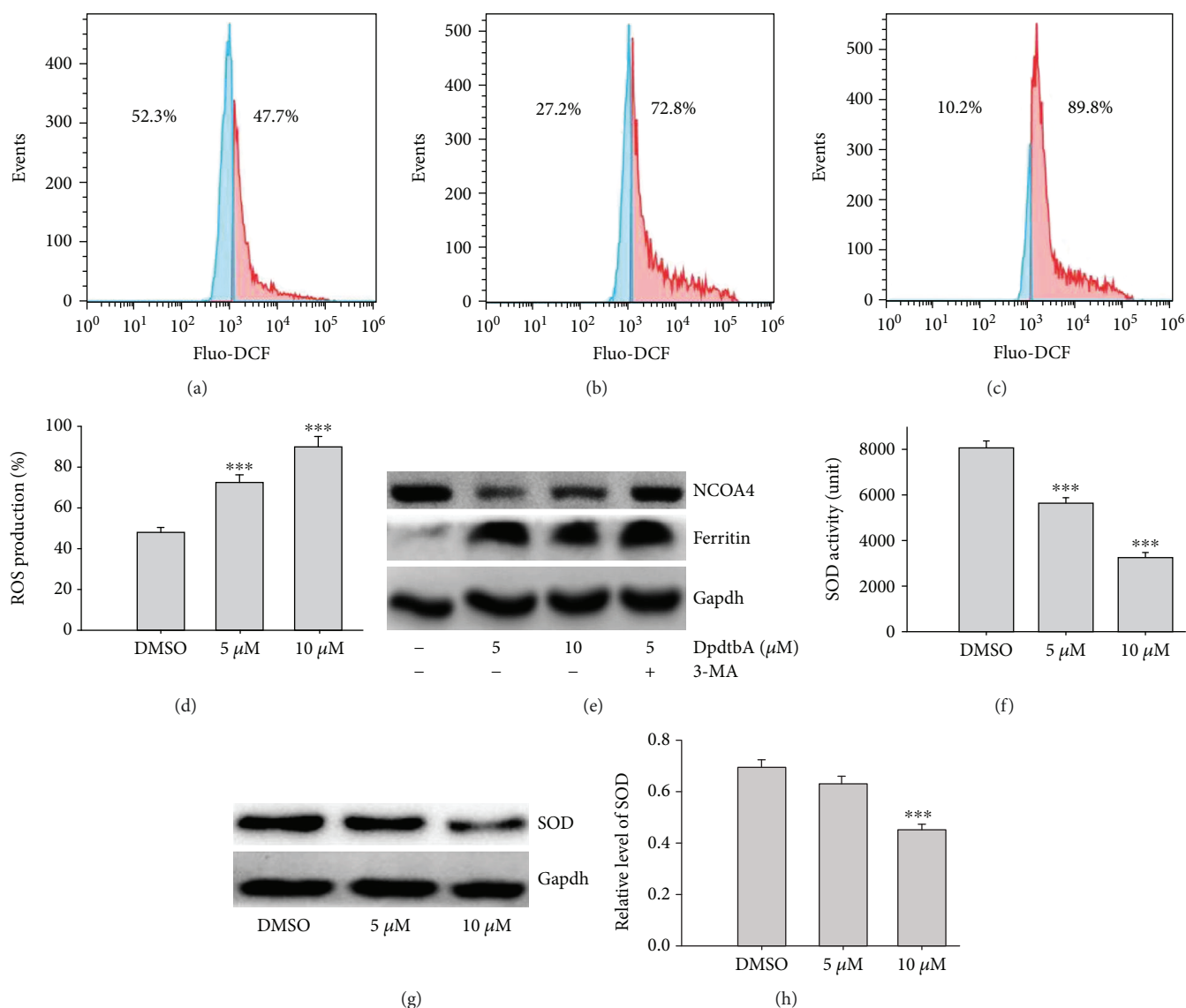


FIGURE 5: DpdtbA induced ROS generation. Flow cytometry analysis from Kyse 450 cells stained by DCF: (a) DMSO; (b) 5  $\mu\text{M}$  DpdtbA; (c) 10  $\mu\text{M}$  DpdtbA; (d) quantitative analysis of ROS production (from twice measurements); (e) western blotting analyses of ferritinophagy-related proteins, the condition was as indicated; (f) the effect of DpdtbA on SOD activity (from trice measurements); (g) alteration of the SOD expression in the absence or presence of DpdtbA; (h) quantitative analysis of alteration in the level of SOD (from twice measurements). \*\*\* $p < 0.01$ .

downregulation of p53 (or mutant p53 might still play a role in the modulation of its downstream targets).

**2.7. The Regulative Action of Mutant p53 on Its Downstream Target Genes and Growth Inhibition.** As mentioned above, DpdtbA treatment led to downregulation of p53 at the protein level in both Kyse 450 and Kyse 150 cell lines, which could be achieved through modulation in transcription and in translation. To corroborate that p53 downregulation might be through a posttranslational modification instead of transcriptional modulation, the alteration of p53 at the mRNA level was determined via RT-PCR. As shown in Figure S7, DpdtbA could upregulate p53 in transcription, which was not consistent with p53 downregulation at the protein level, hinting that p53 downregulation was not

through transcriptional regulation. This was not surprising for p53 was a stress protein in response to different insulting. Next, the regulation of p53 required to be further determined. There is convincing evidence from reporter assays that mutant p53 has the ability to transactivate specific target genes, such as c-Myc and EGFR promoter in a manner distinct from wild-type [32, 33]. To determine whether the mutant p53 (H179R in Kyse 450, R248Q and R155Q in Kyse 150) could regulate its downstream target genes, the p53 inhibitor, PFT- $\alpha$  was used to confirm the action of p53. As shown in Figure 8, DpdtbA induced downregulation of p53 in a concentration-dependent manner, but addition of PFT- $\alpha$  impaired the DpdtbA-induced p53 degradation; PFT- $\alpha$  alone did not significantly modify p53 levels (Figure 8), in accordance with the result reported previously [16]. And

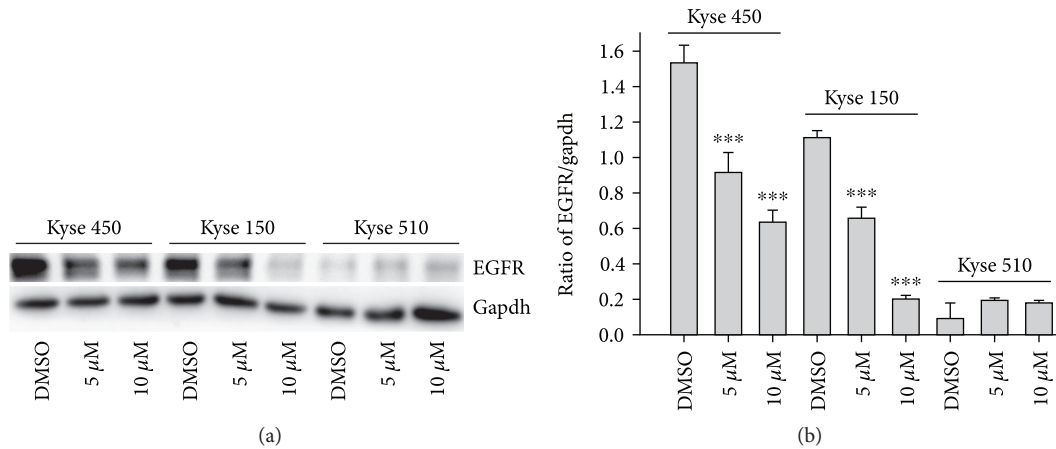


FIGURE 6: DpdtbA led to EGFR downregulation in the indicated ESC cell lines: (a) western blotting analysis and (b) quantitative analysis of alteration of EGFR in the presence or absence of DpdtbA (from twice measurements). \*\*\* $p < 0.01$ .

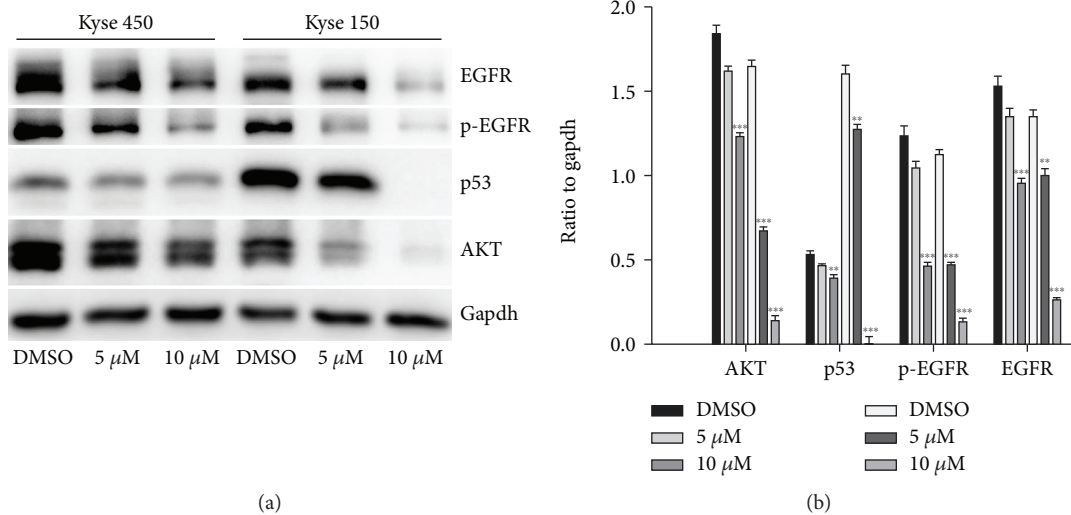


FIGURE 7: Alteration of EGFR was associated with the change of upstream and downstream targets. (a) Western blotting analysis; (b) quantitative analyses of alteration in the p53/EGFR/AKT signal pathway before and after DpdtbA treatment (from twice measurements). \*\* $p < 0.05$ , \*\*\* $p < 0.01$ .

interestingly, similar situation occurred for both EGFR and AKT, supporting that the mutated p53 played a role in downstream gene regulation in the ESC cell lines. Furthermore, quantitative analysis was given in Figure 8(b); clearly, the alteration in the p53/EGFR/AKT axis had a significant difference before and after DpdtbA treatment ( $p < 0.05$ ), but the additional effect was not observed in the combination treatment, which might be due to the difference in interaction between PFT- $\alpha$  and mutant and wild-type p53 [34, 35]. To corroborate that the depletion of p53 may contribute to the growth inhibition in ESC cells, the effect of PFT- $\alpha$  combination with DpdtbA on proliferation was further investigated; Figure 8(c) clearly showed that PFT- $\alpha$  attenuated DpdtbA-induced growth inhibition (PFT- $\alpha$  has a very weak effect on ESC cell growth, data not shown), in accordance with the result from western blotting. However, the addition of  $(\text{NH}_4)_2\text{Fe}(\text{SO}_4)_2$  blocked the action of DpdtbA on both growth inhibition and downregulation

of p53 (Figure S7), hinting that the induction was dependent on the chelating status of DpdtbA.

**2.8. The p53 Depletion Involved *stub1* Chaperone-Mediated Autophagy Rather Than MDM2-Mediated Ubiquitination.** As mentioned above, DpdtbA induced p53 degradation; accordingly, its downstream target, EGFR and AKT, was also downregulated; it was suggested that the degradation of p53 was mainly a molecular event. Hence, the detail in p53 degradation required to be further determined. We then tested whether MDM2 played a role in such p53 degradation. To this end, the levels of p53 and MDM2 were assayed. As shown in Figure 9(a), both p53 and MDM2 were downregulated during DpdtbA treatment, and alterations in the gene expressions had a statistical significance ( $p < 0.05$ , Figure 9(b)). Moreover, such effect in downregulation of p53 could also be achieved by MDM2 knockdown via siRNA (Figure S8), indicating that the function of MDM2s

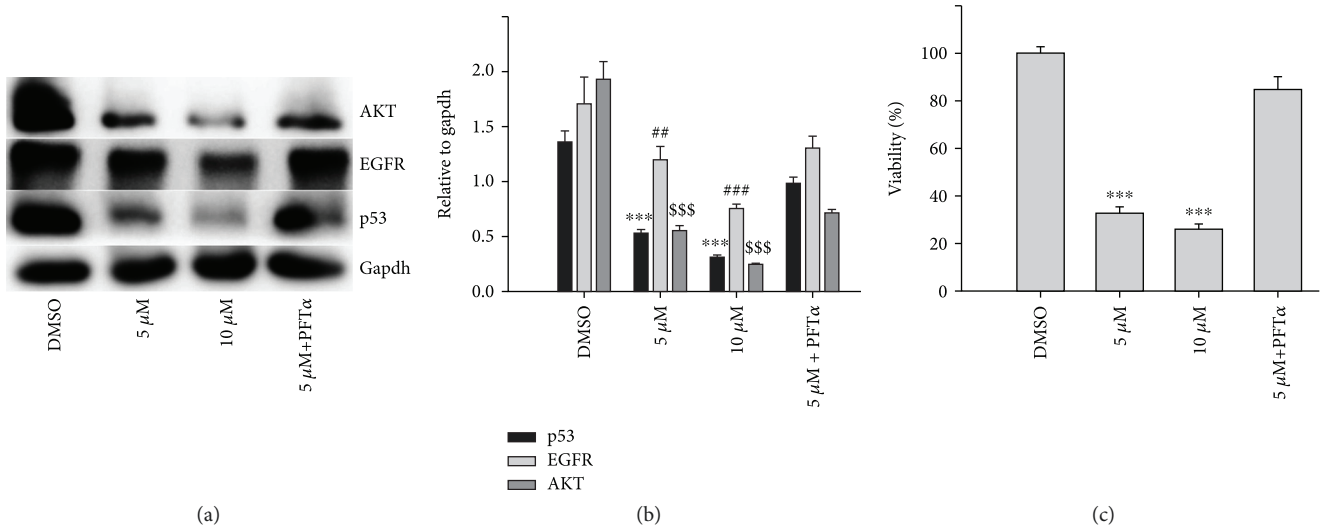


FIGURE 8: p53 downregulation was associated with EGFR and AKT downregulation. (a) Western blotting analysis in the given condition; (b) quantitative analyses of alteration of EGFR, p53, and AKT in the presence or absence of PFT-α (from twice measurements). (c) DpdtbA-induced growth inhibition correlated with p53 downregulation. And the quantitative analysis was based on quartic measurements. ##  $p < 0.05$ , \*\*\*##, \$\$\$  $p < 0.01$ .

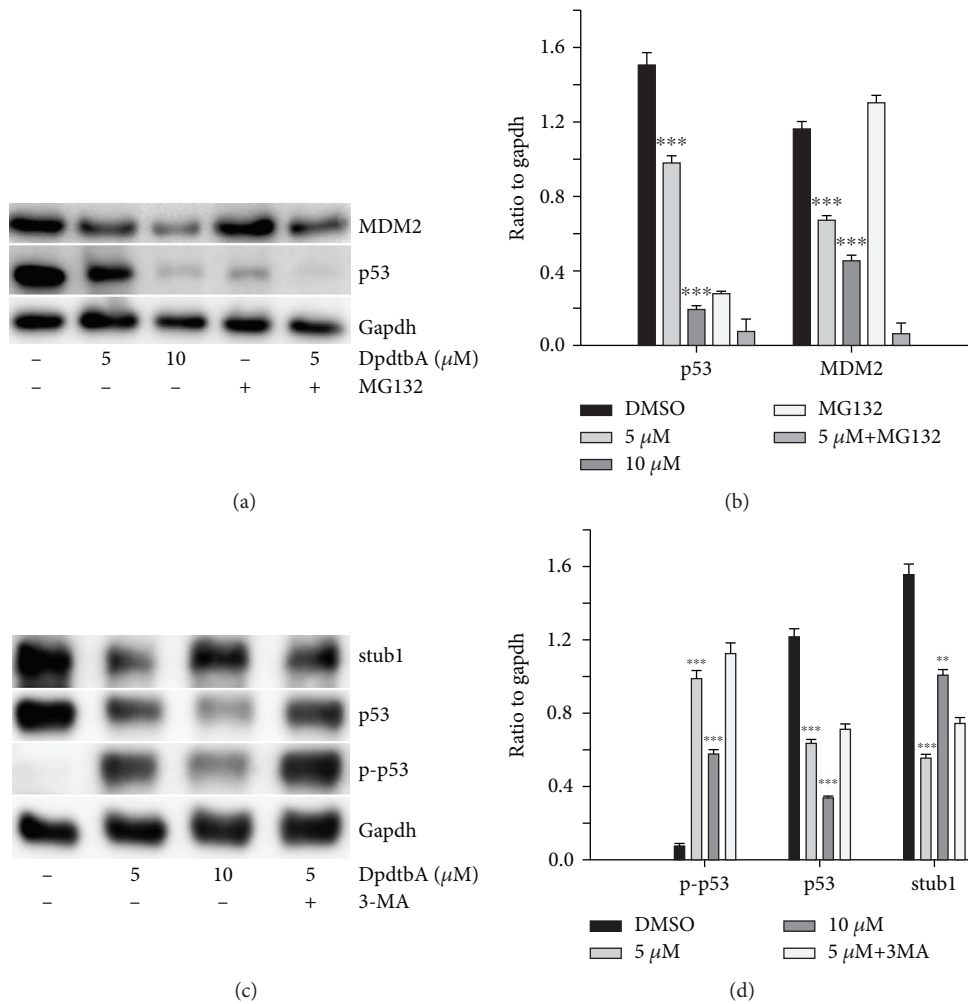


FIGURE 9: DpdtbA induced p53 deletion. (a) p53 deletion did not involve ubiquitination; (b) quantitative analyses of alterations of MDM2 and p53 (from twice measurements); (c) p53 deletion might involve stub1-mediated autophagy; (d) quantitative analyses of alterations of stub1 and p53 (from twice measurements). The conditions were as indicated. \*\*  $p < 0.05$ , \*\*\*  $p < 0.01$ .

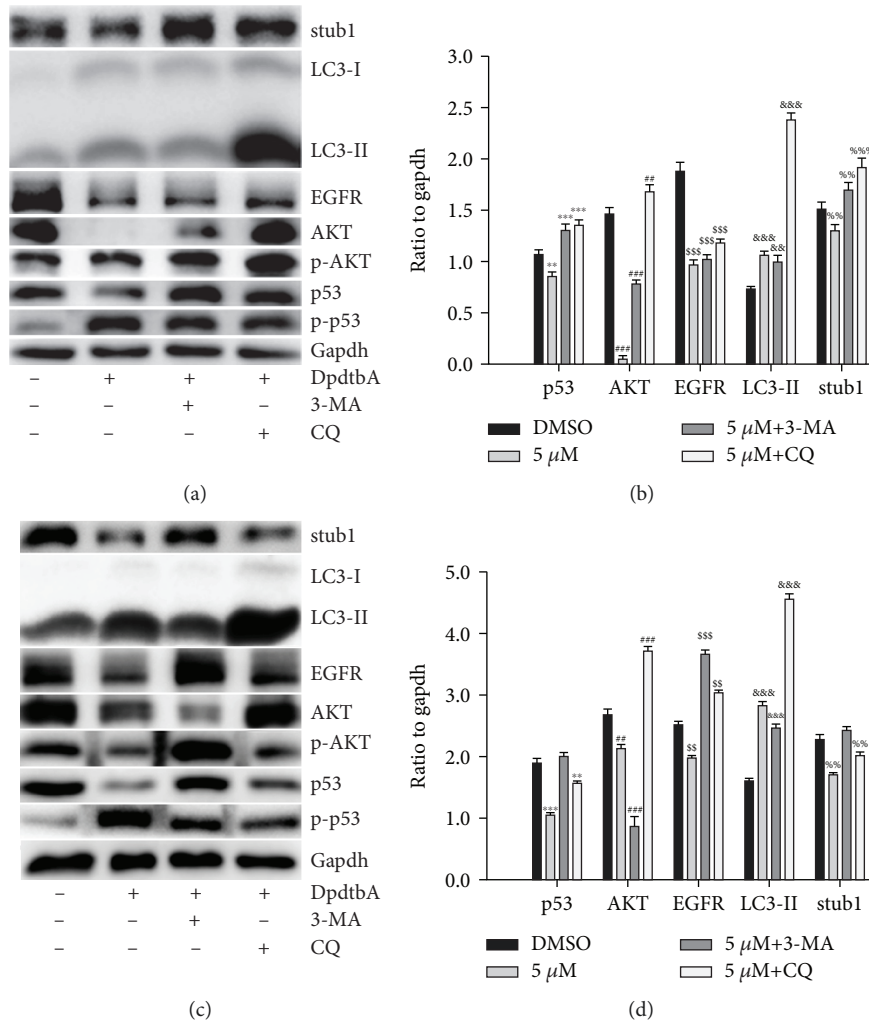


FIGURE 10: p53 autophagic degradation regulated its downstream targets, (a, b) Kyse 450 cells and (c, d) Kyse 150 cells. (a, c) Western blotting analyses of alteration in the p53/EGFR/AKT axis and stub1-mediated autophagy relative proteins, the condition was as indicated. (b, d) Quantitative analyses of alteration of the expression of the p53/EGFR/AKT axis and LC3-II as well as stub1. CQ=chloroquine. Quantitative analyses of those proteins from Kyse 450 and Kyse 150 cells were performed from twice measurements. \*\*,#,SS,&&&,%%%  $p < 0.01$ .

E3 ligase was not involved in the ubiquitination of p53, which was further supported by the fact that addition of proteasome inhibitor, MG-132, did not attenuate the p53 degradation (Figure S9). This was in accordance with that reported previously [33]. Since MDM2 was not responsible for the degradation of mutant p53 in our setting, we then further explored the role of autophagy, a cellular mechanism of protein degradation within lysosomes. It was reported that chip (stub1) promoted autophagy-mediated degradation of aggregating mutant p53 [36]; DpdtbA-induced p53 degradation might involve this pathway. To test the hypothesis, the level of stub1 (chip) was evaluated. As shown in Figure 9(c), the alteration of stub1 was similar to that of p53 upon DpdtbA treatment, and an important observation was that p53 and stub1 were restored when addition of 3-methyladenine (3-MA), hinting that p53 degradation might be through stub1 chaperon-mediated autophagic degradation. The quantitative analysis was given

in Figure 9(d); clearly, the alterations in the level of p-p53, p53, and stub1 had a statistical significance (Figure 9(d),  $p < 0.05$ ).

**2.9. p53 Autophagic Degradation Dominated the Alteration of Its Downstream Targets.** Since stub1 chaperon-mediated autophagy involved the p53 degradation, accordingly, it may affect the downstream target of p53. To this end, autophagy-related genes, LC3, stub1, and along with the p53/EGFR/AKT axis were assessed. As shown in Figure 10(a), concomitant to the autophagy activation (increase in LC3-II and stub1), a downregulated p53, EGFR, and AKT were observed, and the alterations of those proteins are shown in Figure 10(b). As shown in Figure 10(a), the stub1 chaperon-mediated autophagy was clearly responsible for the p53 degradation, which further led to downregulation of its downstream targets. This conclusion was further supported by the experiment of RNA interference, because the knockdown of stub1

by siRNA could attenuate p53 depletion induced by DpdtbA (Figure S10). Furthermore, addition of autophagy inhibitor (3-MA or chloroquine) could increase protein expressions in the p53/EGFR/AKT axis, which indicated that autophagic degradation of p53 modulated the EGFR/AKT pathway. Similar result was observed in Kyse 150 cells (Figures 10(c) and 10(d)), supporting that stub1 chaperon-mediated autophagy involved the p53 degradation, and the mutant p53 still played a role in the gene regulation.

As mentioned above, DpdtbA induced growth inhibition, cell cycle arrest, and apoptosis, which involved ROS production due to SOD inhibition. Further mechanistic study revealed that DpdtbA led to stub1-mediated autophagic degradation of p53 that dominated the level of its downstream targets EGFR and AKT; thus, DpdtbA-induced growth inhibition could be through inactivating the p53/EGFR/AKT signal pathway.

### 3. Discussion

Esophageal cancer (ESC) is one of the most deadly diseases, and the long-term survival of the patients is poor [15]; therefore, new therapeutic strategy is required. It is well documented that iron is an essential element and plays a crucial role in cellular proliferation and DNA synthesis. Compared to normal cells, neoplastic cells have a high requirement for iron for their growth. *In vivo* neoplastic cells can obtain iron from local environment, i.e., tumor microenvironment which is comprised of various cells, cytokines, and extracellular matrix; among those, tumor-associated macrophages (type II phenotype) are the main source of iron supply [37]. Obviously, iron isolation or chelation from tumor environment may help to inhibit the growth of tumor cells. Dithiocarbamates had showed a significant antiproliferative action against gastric cancer cell lines in our previous study [24], which prompted us to extend additional investigation to different cancer cell lines, such as ESC cell lines, in order to gain more knowledge for the agent (Figure 1). Disturbing cell cycle is often found in the mechanism for many chemotherapeutic agents. Iron chelator induced growth inhibition through inhibiting ribonucleotide reductase, accordingly depleting dNTPs and resulting in S phase arrest [38]. In addition, iron depletion also led to alteration of CDKs, resulting in a decrease of CDK2 in human T lymphocytes [39]. Similarly, the DpdtbA also induced ESC cell accumulation at the S phase (Figure 2) and a decrease of CDK2 (Figure S1). In addition, ROS production normally is involved in the action of mechanism for most chemotherapeutic drugs, and the ROS can be generated through Fenton reaction, dysfunction of mitochondria, or imbalance of the redox system, which result in apoptosis and autophagy. Therefore, we further evaluated ROS and identified the source of ROS production. As shown in Figure 5(a), DpdtbA-induced growth inhibition was involved in ROS production; however, ROS production is not due to mitochondrial and lysosomal dysfunction but to SOD inhibition. It has been reported that some iron chelators can induce ferritin degradation in lysosome, which lead to an increase of iron in LIP [29, 40], but in our study, DpdtbA did not induce

ferritin degradation (Figure 5(d)). The analysis of integrity of the mitochondrial membrane eliminated the alteration of mitochondrial membrane permeability for the bax and cytochrome c were not upregulated. So we deduced that the excess ROS might be due to imbalance in the antioxidant-oxidant system. It is well known that superoxide dismutase (SOD) as an antioxidant is responsible for the decomposition of superoxide, and copper and zinc ion as cofactors are located in its catalytic center. DpdtbA as metal chelator may influence SOD activity. Our data revealed that DpdtbA both inactivated SOD activity and also led to downregulation of SOD (Figures 5(f) and 5(g)), resulting in the imbalance of the redox system. Furthermore, excessive ROS production led to occurrence of apoptosis; the results both from flow cytometric analysis and from AO/EB staining (Figure 3 and Figure S4) demonstrated that DpdtbA could induce the occurrence of apoptosis, but the susceptibility of apoptosis induction for the investigated cell lines was a slight difference; Kyse 450 cells seem to be more prone to induce apoptosis than Kyse 150 cells. We speculated that the difference in apoptosis induction may relate to the status and abundance of mutation of p53 [41], while the prosurvival effect of bcl-2 might retreat to the back of the p53, playing a secondary role in response to chemotherapeutic agent because mutant p53 (mutp53) cancers are dependent on their hyper stable mutp53 protein for survival (Figures 4 and 7) [4]; this might endow Kyse 150 cell less sensitive than Kyse 450 cell. However, the other signal pathway may also play a critical role in growth inhibition and apoptosis induction.

Overexpression of epidermal growth factor receptor (EGFR) occurs in approximately 80% of patients with adenocarcinoma and squamous cell carcinoma [42], and many studies have demonstrated that overexpression of EGFR is associated with a lower survival rate [43, 44]. Thus, the epidermal growth factor receptor (EGFR) family is receiving considerable attention. Small molecule tyrosine kinase inhibitors and monoclonal antibodies have been explored in patients with esophageal cancers; however, only a modest clinical activity is achieved. The depletion of EGFR might be other option in esophageal cancer treatments. In the present study, we illustrated that DpdtbA could downregulate EGFR in ESC cell lines (Figure 6), which forced us to consider whether the alteration of EGFR stemmed from the alteration of its upstream molecule, p53. As expected, DpdtbA treatment led to downregulation of p53, which confirmed that the p53/EGFR pathway still activated in ESC cancer cells. Furthermore, DpdtbA also caused downregulation of AKT, a downstream molecule of EGFR, indicating that DpdtbA could inactivate the p53/EGFR/AKT pathway, in accordance with the observation from literature [45]. It is well documented that p53 is often mutated and overexpressed in cancer cells, restoring p53 function; reintroducing or rescuing wild-type p53 into cancer cells could achieve inhibition of cancer [46, 47]. On the other hand, the accumulating evidences reveal that stabilization of mutant p53 in tumors is important for its oncogenic activities; thus, depletion of mutant p53 may attenuate the malignant properties of cancer cells [48]. Generally, wild-type

p53 is modulated by proteasomes, and MDM2, a p53 specific E3-ubiquitin-protein ligase, plays an important role in p53 homeostasis. However, the mutant p53 degradation was not through the MDM2 pathway; similar result was obtained in the present study for downregulation of MDM2 by siRNA which did not restore the p53 level. Autophagy is an important proteolytic system to devote to clearing cellular misfolded proteins or protein aggregates [49], and moreover, it was also reported that chip promotes autophagy-mediated degradation of aggregating mutant p53 [33]; we speculated that the mutant p53 degradation might involve autophagy. stub1 (chip) has been shown to be important for mutant p53 degradation both in normoxia and in hypoxia [15, 50–52]; the stub1 (chip) might also involve the p53 degradation induced by DpdtbA. As expected, the stub1 was downregulated with the decrease of p53 when DpdtbA was exposed to the cells (Figure 9), and knocking down of stub1 by siRNA intervention led to downregulation of p53, which supported that stub1 mediated the degradation of p53 (Figure S10). In addition, with the decrease of p53, the level of microtubule-associated protein light chain 3 (LC3-II) increased, indicating that the degradation of p53 involved autophagy (Figure 10); therefore, autophagic degradation of p53 determined the level of EGFR/AKT. Those indicated that mutant p53 (H179R) (or R248Q and R155Q in kyse150) in Kyse 450 cells still played a role in gene regulation, in accordance with the findings from other laboratories [53], such as Dong et al., who demonstrated that the expression of p53 gain-of-function mutation R175H in endometrial cancer cells increased the invasive phenotypes by activation of the EGFR/PI3K/AKT pathway [33]. In addition, some mutants of p53 (G245C and R273H) in esophageal squamous cells confer a stronger proliferative capacity [54]. Those demonstrated that depletion of mutant p53 is one of the important strategies in cancer therapy. DpdtbA-induced growth inhibition in the ESC cells was through inactivation (or degradation) of the p53/EGFR/AKT signal pathway, providing additional example to strengthen this concept in cancer therapy as like other chemotherapeutic agents [55].

In conclusion, DpdtbA-induced growth inhibition involved apoptosis and cell cycle arrest. Further study revealed that ROS production involved the apoptosis induction, and the rising ROS was stemmed from SOD inhibition initiated by DpdtbA rather than occurrence of ferritinophagy. Furthermore, DpdtbA could induce downregulation of EGFR, p53, and AKT, hinting that the mutant p53 still played a role in the proliferation of ESC cells. Additional study revealed that stub1- (chip-) mediated autophagy was responsible for the p53 degradation rather than MDM2-mediated ubiquitination, which inactivated the EGFR/AKT signal pathway. Taken together, DpdtbA-induced growth inhibition was through inactivating the p53/EGFR/AKT signal pathway.

## 4. Materials and Methods

**4.1. Materials.** MTT, 3-methyladenin (3-MA), pifithrin- $\alpha$  (PFT- $\alpha$ ), RPMI-1640, and other chemicals were purchased

from Sigma-Aldrich. Gapdh, NCOA4, Bcl-2, and AKT antibody were obtained from EnoGene (Nanjing, China); antibodies EGFR, stub-1, SOD, MDM2, Cyt-C, LC3, Bax, and p-AKT were purchased from Proteintech Group Inc. (Wuhan, China). Antibodies p53, p-p53, and ferritin were purchased from Cell Signaling Technology (Massachusetts, USA); siRNA for MDM2 (stB0001232) and stub1 (stB0001238) were obtained from RiboBio (Guangzhou, China).

**4.2. Cytotoxicity Assay (MTT Assay).** A 10 mM DpdtbA (di-2,2'-pyridine ketone dithiocarbamate s-butyric acid) in 70% DMSO was diluted to the required concentration with DMSO. The MTT assay was conducted as previously described [24]. The Kyse 450, Kyse 150, and Kyse510 cell lines (Cell Resource Center, Institute of Basic Medicine, Chinese Academy of Medical Sciences, China) were used in the current investigation. According to the Catalogue of Somatic Mutations in Cancer (COSMIC) database (<http://cancer.sanger.ac.uk/cancergenome/projects/cosmic/>), the status of TP53 is H179R in Kyse 450, R248Q and R155Q in Kyse 150, and nonmutation in Kyse 510. Briefly, the Kyse 450 cells ( $5 \times 10^3$ /ml) were seeded equivalently into a 96-well plate, and the various concentrations of DpdtbA were added after the cells adhered. Following 48 h incubation at 37°C in a humidified atmosphere of 5% CO<sub>2</sub>, 10  $\mu$ l MTT solution (5 mg/ml) was added to each well and additional incubation applied. Finally, 100  $\mu$ l DMSO was added in each well to dissolve the formed formazan after removing the cell culture. The absorption of the solution that was related to the number of live cells was measured on a microplate reader (MK3, Thermo Scientific) at 490 nm. Percent growth inhibition was defined as percent absorbance inhibition within appropriate absorbance in each cell line. The same assay was performed in triplet.

**4.3. Plate Clone Formation Assay.** The cells in the exponential phase were trypsinized and seeded in 6-well plates at the density of 500 cells/well. The cells were kept in sustaining insulating of DpdtbA at a dose of 1/20 IC<sub>50</sub> or 1/10 IC<sub>50</sub>. Fourteen days later, colonies were fixed in 3.7% paraformaldehyde and stained with 0.1% crystal violet. Colonies containing 50 cells at least were counted under inverse microscope (Nikon, Tokyo, Japan), and the clone numbers were analyzed subsequently.

**4.4. Flow Cytometry Analysis of Apoptosis and Cellular ROS.** Cellular ROS determination was performed based on previously described [29]. Apoptosis was measured using the Apoptosis Detection Kit (Dojindo Laboratories) as the company recommended. Briefly, Kyse 450 (150) cells were treated with DpdtbA for 24 h. Following this, cells were collected, washed, and stained with annexin V-FITC and propidium iodide (PI) following the manufacturer's instruction (Dojindo Laboratories, Japan). The intracellular ROS assay was similar to the abovementioned protocol, except that H<sub>2</sub>DCF-DA was used to stain the cells.

**4.5. Cell Cycle Analysis.** The Kyse 450 cells (or Kyse 150 cells) ( $1 \times 10^5$ ) were seeded in a 6-well plate and incubated for

24 h at 37°C (5% CO<sub>2</sub>). The medium was replaced with fresh medium supplemented or not (control) with DpdtbA (5 and 10 μM). Following 24 h of incubation, the cells were collected with centrifugation, washed with PBS, finally fixed in 70% ethanol, and stored at -20°C. After removing the 70% ethanol and washing with PBS, the cellular nuclear DNA was stained based on the company recommended protocol; the cells in staining buffer were directly subjected to flow cytometer analysis. For each sample, 10,000 events were collected, and fluorescent signal intensity was recorded and analyzed by CellQuest and Modifit (Becton Dickinson, USA).

**4.6. SOD Activity Assay.** The SOD activity was determined as the company recommended. Briefly, the Kyse 450 cells were treated with DpdtbA for 24 h, then collected and lysed. The supernatant was separated by centrifugation at 4°C, the protein concentration was determined by a colorimetric Bio-Rad DC protein assay on a microplate reader MK3 at 570 nm. Next, the same amount of protein mixture was mixed with WST-8/enzyme solution and initiator solution, following incubation for 30 min. at 37°C; the absorbance at 450 nm was measured on the abovementioned microplate reader. The assay of SOD activity followed similar protocol; the DpdtbA was directly added to solution with the same amount of protein, compared to the absorbance value in the presence or absence of DpdtbA, calculating the activity unit based on the formula provided by the company (Beyotime Biotechnology, China).

**4.7. Western Blotting Analysis.** Briefly, 1 × 10<sup>7</sup> Kyse 450 (150 or 510) cells treated with or without the DpdtbA was scraped off in lysis buffer (50 mM Tris-HCl, pH 8.0, 150 mM NaCl, 1.0% NP-40, 10% glycerol and protease inhibitors), and the suspension was incubated on ice for 30 min. and then collected the clear supernatant by centrifugation at 14,000 ×g. A colorimetric Bio-Rad DC protein assay was employed to determine the protein concentration on a microplate reader MK3 at 570 nm. Proteins (20–30 μg) were separated on a 13% sodium dodecyl sulfate-polyacrylamide gel at 200 V for 1 h. Then, the separated proteins were subsequently transferred onto a PVDF membrane at 60 V for 1 h. The membrane was washed three times with Tris-buffered saline (TBS) and was then blocked for 2 h in TBS containing 0.1% Tween-20 and 5% nonfat skimmed milk. The membrane was incubated at 4°C overnight with the primary monoantibody used at a dilution of 1:300 in TBS plus 0.1% Tween-20 (TBST). The membrane was washed several times with TBST and was subsequently incubated with HRP-conjugated secondary antibody (1:2,000 in TBST) for 2 h at room temperature. After another wash of the membrane with TBST, the protein bands were detected using a super sensitive ECL solution (Boster Biological Technology Co. Ltd.) and visualized on an SYNGENE G:BOX Chemi XX9 (SYNGENE, UK).

**4.8. Statistical Analysis.** Results are presented as the mean ± SEM. Comparisons between two groups were carried out using the two-tailed Student's *t*-test. Comparisons between

multiple groups were performed by one way ANOVA with Dunnett's post hoc correction. A *p* value < 0.05 was considered statistically significant.

## Data Availability

The data used to support the findings of this study are included within the article.

## Conflicts of Interest

The authors declare no conflict of interest.

## Authors' Contributions

Zhuo Wang, Cuiping Li, and Yongli Li performed the experiments; they contributed equally to this work. Changzheng Li and Fulian Gao conceived and designed the experiments. Xingshuang Guo and Zhaoyu Yan (2016 undergraduate student of outstanding class in clinical medicine) analyzed the data and prepared the figures. Changzheng Li prepared and wrote the paper.

## Acknowledgments

The present study was supported by grants awarded by the Natural Science Foundation of China (No. 21571153), the Henan Provincial Department of Science and Technology (Nos. 114300510012, 122102310197, 132102310250, and 152300410118), and the Key Research Project Funding Program of Higher Educational Institutions of Henan Province (19A310021).

## Supplementary Materials

Information on the effects of DpdtbA on cell growth, cell cycle, and ROS production. Other evidence suggested that the p53 downregulation induced by DpdtbA was not through ubiquitination but through stub1-mediated autophagy. (*Supplementary Materials*)

## References

- [1] E. A. Montgomery, F. T. Basman, P. Brenan, and R. Malekzadeh, "Oesophageal cancer," in *World Cancer Report*, B. W. Stewart and C. P. Wild, Eds., World Health Organization, 2014.
- [2] L. Wang, X. Yu, J. Li, Z. Zhang, J. Hou, and F. Li, "Prognostic significance of p53 expression in patients with esophageal cancer: a meta-analysis," *BMC Cancer*, vol. 16, no. 1, 2016.
- [3] E. Okuda, H. Osugi, K. Morimura et al., "Detection of p53 gene mutations in human esophageal squamous cell carcinomas using a p53 yeast functional assay: possible difference in esophageal carcinogenesis between the young and the elderly group," *Clinical Cancer Research*, vol. 7, no. 3, pp. 600–606, 2001.
- [4] D. Li, N. D. Marchenko, and U. M. Moll, "SAHA shows preferential cytotoxicity in mutant p53 cancer cells by destabilizing mutant p53 through inhibition of the HDAC6-Hsp90 chaperone axis," *Cell Death and Differentiation*, vol. 18, no. 12, pp. 1904–1913, 2011.

- [5] P. A. J. Muller and K. H. Vousden, "p53 mutations in cancer," *Nature Cell Biology*, vol. 15, no. 1, pp. 2–8, 2013.
- [6] W. A. Freed-Pastor, H. Mizuno, X. Zhao et al., "Mutant p53 disrupts mammary tissue architecture via the mevalonate pathway," *Cell*, vol. 148, no. 1-2, pp. 244–258, 2012.
- [7] F. A. Olotu and M. E. S. Soliman, "From mutational inactivation to aberrant gain-of-function: unraveling the structural basis of mutant p53 oncogenic transition," *Journal of Cellular Biochemistry*, vol. 119, no. 3, pp. 2646–2652, 2018.
- [8] Y. Haupt, R. Maya, A. Kazaz, and M. Oren, "Mdm2 promotes the rapid degradation of p53," *Nature*, vol. 387, no. 6630, pp. 296–299, 1997.
- [9] M. H. G. Kubbutat, S. N. Jones, and K. H. Vousden, "Regulation of p53 stability by Mdm2," *Nature*, vol. 387, no. 6630, pp. 299–303, 1997.
- [10] S. R. Grossman, M. E. Deato, C. Brignone et al., "Polyubiquitination of p53 by a ubiquitin ligase activity of p300," *Science*, vol. 300, no. 5617, pp. 342–344, 2003.
- [11] R. P. Leng, Y. Lin, W. Ma et al., "Pirh2, a p53-induced ubiquitin-protein ligase, promotes p53 degradation," *Cell*, vol. 112, no. 6, pp. 779–791, 2003.
- [12] D. Dornan, I. Wertz, H. Shimizu et al., "The ubiquitin ligase COP1 is a critical negative regulator of p53," *Nature*, vol. 429, no. 6987, pp. 86–92, 2004.
- [13] C. Esser, M. Scheffner, and J. Huhfeld, "The chaperone-associated ubiquitin ligase CHIP is able to target p53 for proteasomal degradation," *The Journal of Biological Chemistry*, vol. 280, no. 29, pp. 27443–27448, 2005.
- [14] S. Choudhury, V. K. Kolukula, A. Preet, C. Albanese, and M. L. Avantaggiati, "Dissecting the pathways that destabilize mutant p53: The proteasome or autophagy?," *Cell Cycle*, vol. 12, no. 7, pp. 1022–1029, 2013.
- [15] M. Maan and U. Pati, "CHIP promotes autophagy-mediated degradation of aggregating mutant p53 in hypoxic conditions," *FEBS Journal*, vol. 285, no. 17, pp. 3197–3214, 2018.
- [16] A. Garufi, D. Pucci, V. D'Orazi et al., "Degradation of mutant p53H175 protein by Zn(II) through autophagy," *Cell Death & Disease*, vol. 5, no. 5, p. e1271, 2014.
- [17] H. Masuda, D. Zhang, C. Bartholomeusz, H. Doihara, G. N. Hortobagyi, and N. T. Ueno, "Role of epidermal growth factor receptor in breast cancer," *Breast Cancer Research and Treatment*, vol. 136, no. 2, pp. 331–345, 2012.
- [18] S. K. Yeo, J. Wen, S. Chen, and J. L. Guan, "Autophagy Differentially Regulates Distinct Breast Cancer Stem-like Cells in Murine Models via EGFR/Stat3 and Tgf $\beta$ /Smad Signaling," *Cancer Research*, vol. 76, no. 11, pp. 3397–3410, 2016.
- [19] Q. Wang, H. Zhu, Z. Xiao et al., "Expression of epidermal growth factor receptor is an independent prognostic factor for esophageal squamous cell carcinoma," *World Journal of Surgical Oncology*, vol. 11, no. 1, pp. 278–285, 2013.
- [20] H. I. R. O. A. K. I. Kato, T. Arao, K. Matsumoto et al., "Gene amplification of EGFR, HER2, FGFR2 and MET in esophageal squamous cell carcinoma," *International Journal of Oncology*, vol. 42, no. 4, pp. 1151–1158, 2013.
- [21] P. Seshacharyulu, M. P. Ponnusamy, D. Haridas, M. Jain, A. K. Ganti, and S. K. Batra, "Targeting the EGFR signaling pathway in cancer therapy," *Expert Opinion on Therapeutic Targets*, vol. 16, no. 1, pp. 15–31, 2012.
- [22] J. H. Gong, X. J. Liu, Y. Li, and Y. S. Zhen, "Pingyangmycin downregulates the expression of EGFR and enhances the effects of cetuximab on esophageal cancer cells and the xeno-graft in athymic mice," *Cancer Chemotherapy and Pharmacology*, vol. 69, no. 5, pp. 1323–1332, 2012.
- [23] D. Buac, S. Schmitt, G. Ventro, F. Rani Kona, and Q. Ping Dou, "Dithiocarbamate-based coordination compounds as potent proteasome inhibitors in human cancer cells," *Mini-Reviews in Medicinal Chemistry*, vol. 12, no. 12, pp. 1193–1201, 2012.
- [24] X. Guo, Y. Fu, Z. Wang et al., "Di-2-pyridylhydrazone dithiocarbamate butyric acid ester exerted its proliferative inhibition against gastric cell via ROS-mediated apoptosis and autophagy," *Oxidative Medicine and Cellular Longevity*, vol. 2018, 11 pages, 2018.
- [25] N. Takuwa and Y. Takuwa, "Regulation of cell cycle molecules by the Ras effector system," *Molecular and Cellular Endocrinology*, vol. 177, no. 1-2, pp. 25–33, 2001.
- [26] R. Dachineni, G. Ai, D. R. Kumar, S. S. Sadhu, H. Tummala, and G. J. Bhat, "Cyclin A2 and CDK2 as novel targets of aspirin and salicylic acid: a potential role in cancer prevention," *Molecular Cancer Research*, vol. 14, no. 3, pp. 241–252, 2016.
- [27] K. Liu, P. C. Liu, R. Liu, and X. Wu, "Dual AO/EB staining to detect apoptosis in osteosarcoma cells compared with flow cytometry," *Medical Science Monitor Basic Research*, vol. 21, no. 1, pp. 15–20, 2015.
- [28] S. Kasibhatla, G. P. Amarante-Mendes, D. Finucane, T. Brunner, E. Bossy-Wetzel, and D. R. Green, "Acridine orange/ethidium bromide (AO/EB) staining to detect apoptosis," *Cold Spring Harbor Protocols*, vol. 2006, no. 21, 2006.
- [29] T. Huang, Y. Sun, Y. Li et al., "Growth inhibition of a novel iron chelator, DpdtC, against hepatoma carcinoma cell lines partly attributed to ferritinophagy-mediated lysosomal ROS generation," *Oxidative Medicine and Cellular Longevity*, vol. 2018, Article ID 4928703, 13 pages, 2018.
- [30] C. D. Andl, T. Mizushima, H. Nakagawa et al., "Epidermal Growth Factor Receptor Mediates Increased Cell Proliferation, Migration, and Aggregation in Esophageal Keratinocytes in Vitro and in Vivo," *Journal of Biological Chemistry*, vol. 278, no. 3, pp. 1824–1830, 2003.
- [31] C. R. Chong and P. A. Janne, "The quest to overcome resistance to EGFR-targeted therapies in cancer," *Nature Medicine*, vol. 19, no. 11, pp. 1389–1400, 2013.
- [32] J. H. Ludes-Meyers, M. A. Subler, C. V. Shivakumar et al., "Transcriptional activation of the human epidermal growth factor receptor promoter by human p53," *Molecular and Cellular Biology*, vol. 16, no. 11, pp. 6009–6019, 1996.
- [33] A. A. Román-Rosales, E. García-Villa, L. A. Herrera, P. Gariglio, and J. Díaz-Chávez, "Mutant p53 gain of function induces HER2 over-expression in cancer cells," *BMC Cancer*, vol. 18, p. 709, 2018.
- [34] I. Hernández-Reséndiz, J. C. Gallardo-Pérez, A. López-Macay et al., "Mutant p53R248Q downregulates oxidative phosphorylation and upregulates glycolysis under normoxia and hypoxia in human cervix cancer cells," *Journal of Cellular Physiology*, vol. 234, no. 5, pp. 5524–5536, 2019.
- [35] P. G. Komarov, E. A. Komarova, R. V. Kondratov et al., "A chemical inhibitor of p53 that protects mice from the side effects of cancer therapy," *Science*, vol. 285, no. 5434, pp. 1733–1737, 1999.
- [36] H. Vakifahmetoglu-Norberg, M. Kim, H. G. Xia et al., "Chaperone-mediated autophagy degrades mutant p53," *Genes & Development*, vol. 27, no. 15, pp. 1718–1730, 2013.



- [37] S. Recalcati, M. Locati, E. Gammella, P. Invernizzi, and G. Cairo, "Iron levels in polarized macrophages: regulation of immunity and autoimmunity," *Autoimmunity Reviews*, vol. 11, no. 12, pp. 883–889, 2012.
- [38] D. R. Richardson, D. S. Kalinowski, S. Lau, P. J. Jansson, and D. B. Lovejoy, "Cancer cell iron metabolism and the development of potent iron chelators as anti-tumour agents," *Biochimica et Biophysica Acta*, vol. 1790, no. 7, pp. 702–717, 2009.
- [39] J. J. Lucas, A. Szepesi, J. Domenico et al., "Effects of iron-depletion on cell cycle progression in normal human T lymphocytes: selective inhibition of the appearance of the cyclin A-associated component of the p33cdk2 kinase," *Blood*, vol. 86, no. 6, pp. 2268–2280, 1995.
- [40] J. D. Mancias, X. Wang, S. P. Gygi, J. W. Harper, and A. C. Kimmelman, "Quantitative proteomics identifies NCOA4 as the cargo receptor mediating ferritinophagy," *Nature*, vol. 509, no. 7498, pp. 105–109, 2014.
- [41] G. Blandino, A. J. Levine, and M. Oren, "Mutant p53 gain of function: differential effects of different p53 mutants on resistance of cultured cells to chemotherapy," *Oncogene*, vol. 18, no. 2, pp. 477–485, 1999.
- [42] T. Dragovich and C. Campen, "Anti-EGFR-targeted therapy for esophageal and gastric cancers: an evolving concept," *Journal of Oncology*, vol. 2009, Article ID 804108, 8 pages, 2009.
- [43] M. Takaoka, H. Harada, C. D. Andl et al., "Epidermal growth factor receptor regulates aberrant expression of insulin-like growth factor-binding protein 3," *Cancer Research*, vol. 64, no. 21, pp. 7711–7723, 2004.
- [44] R. I. Nicholson, J. M. W. Gee, and M. E. Harper, "EGFR and cancer prognosis," *European Journal of Cancer*, vol. 37, pp. 9–S15, 2001.
- [45] P. Dong, Z. Xu, N. Jia, D. Li, and Y. Feng, "Elevated expression of p53 gain-of-function mutation R175H in endometrial cancer cells can increase the invasive phenotypes by activation of the EGFR/PI3K/AKT pathway," *Molecular Cancer*, vol. 8, no. 1, p. 103, 2009.
- [46] D. Makower, A. Rozenblit, H. Kaufman et al., "Phase II clinical trial of intralesional administration of the oncolytic adenovirus ONYX-015 in patients with hepatobiliary tumors with correlative p53 studies," *Clinical Cancer Research*, vol. 9, no. 2, pp. 693–702, 2003.
- [47] K. H. Khoo, C. S. Verma, and D. P. Lane, "Drugging the p53 pathway: understanding the route to clinical efficacy," *Nature Reviews Drug Discovery*, vol. 13, no. 3, pp. 217–236, 2014.
- [48] A. Parrales and T. Iwakuma, "Targeting oncogenic mutant p53 for cancer therapy," *Frontiers in Oncology*, vol. 5, 2015.
- [49] N. Mizushima, "Autophagy: process and function," *Genes & Development*, vol. 21, no. 22, pp. 2861–2873, 2007.
- [50] P. Muller, R. Hrstka, D. Coomber, D. P. Lane, and B. Vojtesek, "Chaperone-dependent stabilization and degradation of p53 mutants," *Oncogene*, vol. 27, no. 24, pp. 3371–3383, 2008.
- [51] N. Lukashchuk and K. H. Vousden, "Ubiquitination and degradation of mutant p53," *Molecular and Cellular Biology*, vol. 27, no. 23, pp. 8284–8295, 2007.
- [52] A. Parrales, A. Ranjan, S. V. Iyer et al., "DNAJA1 controls the fate of misfolded mutant p53 through the mevalonate pathway," *Nature Cell Biology*, vol. 18, no. 11, pp. 1233–1243, 2016.
- [53] M. L. McCabe and Z. Dlamini, "The molecular mechanisms of oesophageal cancer," *International Immunopharmacology*, vol. 5, no. 7–8, pp. 1113–1130, 2005.
- [54] N. Kang, Y. Wang, S. Guo et al., "Mutant TP53 G245C and R273H promote cellular malignancy in esophageal squamous cell carcinoma," *BMC Cell Biology*, vol. 19, no. 1, p. 16, 2018.
- [55] J. Chen, W. Wang, H. Wang, X. Liu, and X. Guo, "Combination treatment of ligustrazine piperazine derivate DLJ14 and adriamycin inhibits progression of resistant breast cancer through inhibition of the EGFR/PI3K/Akt survival pathway and induction of apoptosis," *Drug Discoveries & Therapeutics*, vol. 8, no. 1, pp. 33–41, 2014.

## Research Article

# p53-Mediated PI3K/AKT/mTOR Pathway Played a Role in Ptox<sup>Dpt</sup>-Induced EMT Inhibition in Liver Cancer Cell Lines

Yongli Li,<sup>1,2</sup> Tingting Wang,<sup>3</sup> Yanjie Sun,<sup>2</sup> Tengfei Huang,<sup>3</sup> Cuiping Li,<sup>3</sup> Yun Fu,<sup>3</sup> Yichun Li,<sup>4</sup> and Changzheng Li<sup>ID 2,3</sup>

<sup>1</sup>Department of Histology and Embryology, Sanquan College of Xinxiang Medical University, Xinxiang, Henan 453003, China

<sup>2</sup>Experimental Teaching Center of Biology and Basic Medicine, Sanquan College of Xinxiang Medical University, Xinxiang, Henan 453003, China

<sup>3</sup>Department of Molecular Biology and Biochemistry, Xinxiang Medical University, Xinxiang, Henan 453003, China

<sup>4</sup>The First Affiliated Hospital of Xinxiang Medical University, Weihui, Henan 453100, China

Correspondence should be addressed to Changzheng Li; changzhenl@yahoo.com

Received 6 February 2019; Revised 1 April 2019; Accepted 9 April 2019; Published 5 May 2019

Guest Editor: Rizwan Wahab

Copyright © 2019 Yongli Li et al. This is an open access article distributed under the Creative Commons Attribution License, which permits unrestricted use, distribution, and reproduction in any medium, provided the original work is properly cited.

Epithelial-mesenchymal transition (EMT) involves metastasis and drug resistance; thus, a new EMT reversing agent is required. It has shown that wild-type p53 can reverse EMT back to epithelial characteristics, and iron chelator acting as a p53 inducer has been demonstrated. Moreover, recent study revealed that etoposide could also inhibit EMT. Therefore, combination of etoposide with iron chelator might achieve better inhibition of EMT. To this end, we prepared di-2-pyridineketone hydrazone dithiocarbamate S-propionate podophyllotoxin ester (Ptox<sup>Dpt</sup>) that combined the podophyllotoxin (Ptox) structural unit (etoposide) with the dithiocarbamate unit (iron chelator) through the hybridization strategy. The resulting Ptox<sup>Dpt</sup> inherited characteristics from parent structural units, acting as both the p53 inducer and topoisomerase II inhibitor. In addition, the Ptox<sup>Dpt</sup> exhibited significant inhibition in migration and invasion, which correlated with downregulation of matrix metalloproteinase (MMP). More importantly, Ptox<sup>Dpt</sup> could inhibit EMT in the absence or presence of TGF- $\beta$ 1, concomitant to the ROS production, and the additional evidence revealed that Ptox<sup>Dpt</sup> downregulated AKT/mTOR through upregulation of p53, indicating that Ptox<sup>Dpt</sup> induced EMT inhibition through the p53/PI3K/AKT/mTOR pathway.

## 1. Introduction

Metastasis is a hallmark of cancer and one of the urgent tasks to be solved in a clinical practice. During metastasis, the malignant cells spread from the primary tumor to distant sites, which cause failure of vital organs, consequently leading to the death of patients. In addition, concomitant to the metastasis, the cells acquire an ability to resist conventional treatments [1]. Therefore, insight into the molecular, cellular, and clinical mechanisms underlying metastatic progression is required in order to develop new diagnostic and therapeutic strategies to prevent and treat metastases. It has been shown that epithelial-mesenchymal transition (EMT) and its reverse process, mesenchymal-epithelial transition

(MET), involve a metastatic process, and EMT is a key metastasis-promoting step in many cancers [2], but MET may favor to metastatic inhibition or attenuating drug resistance [3–5]. During EMT, epithelial cells lose their junctions and apical-basal polarity and undergo a change in the signaling programmers, developing an invasive phenotype [6]. The investigations reveal that EMT progression is characterized by loss of the epithelial marker E-cadherin; accordingly, the mesenchymal markers, such as N-cadherin and vimentin, are increased. When tumor cells acquire invasive mesenchymal phenotypes, the motility and invasiveness of them are increased, favoring dissemination from the local site and infiltration into the vascular tumor [7]. Since EMT plays an essential role in cancer metastasis, restoration of MET may

efficiently slow dissemination of tumor cells [8]. Therefore, targeting EMT is one of the options in cancer therapy [9–11].

p53 is well characterized as a tumor suppressor gene [12]; the wild-type p53 predominantly functions as a transcription factor, playing important roles in cell growth. However, in most of the tumors, p53 is the most frequently mutated gene, resulting in either loss of function or gain of new function [13, 14]. To restore the function of the p53 pathway, small-molecule inhibitors of MDM2 have been used in cancer treatment strategy. In addition, p53 also plays critical roles in EMT and metastasis [15, 16]; overexpression of p53 in p53-proficient human mammary epithelial cells that have undergone EMT results in their reversion back to an epithelial phenotype. p53 regulating EMT is considered through modulating miRNAs in the mechanism [17, 18]. Furthermore, iron chelator was shown to exert its action of regulation both on p53 and EMT, hinting cellular iron status influenced EMT progress [19]; the details remain elusive.

Since EMT is associated with metastasis and drug resistance [20], EMT inhibition may efficiently slow dissemination of tumor cells [8, 21]. It has been shown that some compounds are capable of inhibiting EMT [22, 23]. Recently, researchers from different laboratories reported that etoposide and other topoisomerase II (Topo II) inhibitors widely used in the clinical practice could reverse EMT [24, 25], revealing another side of those DNA poisoners except their cytotoxicity. In addition, wild-type p53 can also reverse EMT, while the level of p53 was partly dependent on iron status in a cell [26], hinting that an alternative route could be used to alter EMT status through regulating iron homeostasis. Studies have shown that some iron chelators displayed antiproliferative action in the investigated cell lines involved upregulation of p53 [27, 28]. Based on the facts, to achieve an enhanced efficiency of EMT inhibition, synchronously targeting Topo II and p53 might be one of the alternative options in favor of dissemination inhibition of the tumor cell. To achieve the goal, in the present study, a dual functional agent was prepared by combination of the podophyllotoxin (Ptox) structural unit with the dithiocarbamate unit based on a hybridization strategy. The novel compound, di-2-pyridineketone hydrazone dithiocarbamate S-propionate podophyllotoxin ester (Ptox<sup>Dpt</sup>), exhibited significant Topo II inhibition and acted as a p53 inducer. A growth inhibition assay against hepatocellular carcinoma cells *in vitro* revealed that Ptox<sup>Dpt</sup> displayed a better antiproliferative effect than the parent compounds, 4'-demethylepipodophyllotoxin and etoposide. Moreover, Ptox<sup>Dpt</sup> exhibited a significant antimetastatic effect, which likely correlated with matrix metalloproteinase (MMP) inhibition and concomitant to the mTOR downregulation. As expected, Ptox<sup>Dpt</sup> could also reverse TGF- $\beta$ 1-induced EMT in hepatocellular carcinoma cells. In addition, ROS are involved in the EMT process [29], but the role of ROS in EMT reversal is not fully determined. We hypothesized that ROS might also play a role in EMT reversion. To address this issue, we measured cellular ROS after stimulation with either TGF- $\beta$ 1 or combination with Ptox<sup>Dpt</sup>, revealing that both EMT and EMT reversion involved ROS production. Further study demonstrated that Ptox<sup>Dpt</sup>-induced EMT reversal was through p53-mediated

PI3K/AKT/mTOR pathways; this feature is first reported for an etoposide derivative.

## 2. Results

**2.1. Preparation of Di-2-pyridineketone Hydrazone Dithiocarbamate S-Propionate Podophyllotoxin Ester (Ptox<sup>Dpt</sup>).** Ptox<sup>Dpt</sup> was prepared through a four-step reaction (Fig. S1); the detail is described in Materials and Methods. The first three-step reaction for the preparation of di-2-pyridineketone hydrazone dithiocarbamate S-propionate was based on a protocol described previously [30]. The final product, Ptox<sup>Dpt</sup>, was synthesized by mixing 4'-demethylepipodophyllotoxin with di-2-pyridineketone hydrazone dithiocarbamate S-propionate under catalysis of DMAP/DCC in dichloromethane at room temperature. Upon completion of the reaction, the crude product was subjected to flash chromatography. Following the NMR and HRMS characterization, the Ptox<sup>Dpt</sup> was identified as expected (Fig. S1).

**2.2. Topo II Inhibition of Ptox<sup>Dpt</sup> and Simulation of Binding.** Etoposide is a well-known Topo II inhibitor. To understand whether the conjugate, Ptox<sup>Dpt</sup>, retained the same activity as etoposide, we first assessed its inhibitory effect on DNA relaxation. Following a protocol reported previously [31], pUC18 plasmid DNA was incubated with a nuclear extract in the absence or presence of varied concentrations of Ptox<sup>Dpt</sup>, and the reaction products were subjected to agarose gel electrophoresis. As shown in Figure 1(a), Ptox<sup>Dpt</sup> displayed a certain degree of Topo II inhibition based on EtB prestained agarose gel electrophoresis (Figure 1(a)) as the amount of relaxed DNA decreased compared to that of the control. In addition, Ptox<sup>Dpt</sup> appeared to be a more potent Topo II inhibitor than etoposide since higher concentration of etoposide was required to achieve the same degree of inhibition. We next determined whether the binding of Ptox<sup>Dpt</sup> to Topo II was similar to that of etoposide. To do this, a theoretical simulation was performed by using a molecular docking approach. The crystal structure of Topo II of a human (PDB ID: 3QX3) was obtained from the RCSB Protein Data Bank. To ensure the accuracy of our docking protocol, etoposide was redocked into the Topo-DNA complex based on the recommended procedure. The conformation of etoposide in the Topo-DNA complex derived from molecular docking could be almost fully superimposed on the native cocrystallized structure, indicating that the protocol was appropriate. As shown in Fig. S2A, the conformation of etoposide in the Topo-DNA complex generated from molecular docking was almost fully superimposed on the native cocrystallized one, indicating that the protocol was practical (Fig. S2A). Thus, the synthesized Ptox<sup>Dpt</sup> was docked into the Topo II complex following similar protocol (Figure 1(b)), and accordingly, the simulating affinity energy (-13.6 kcal/mol) was obtained. Comparing the simulating affinity energy to that of docked etoposide (-14.8 kcal/mol), a slightly weaker interaction was thus observed. The superimposition of Ptox<sup>Dpt</sup> on the cocrystallized etoposide is presented in Fig. S2B, revealing that the replacement of sugar at 4-position with the dithiocarbamate derivative did not lead

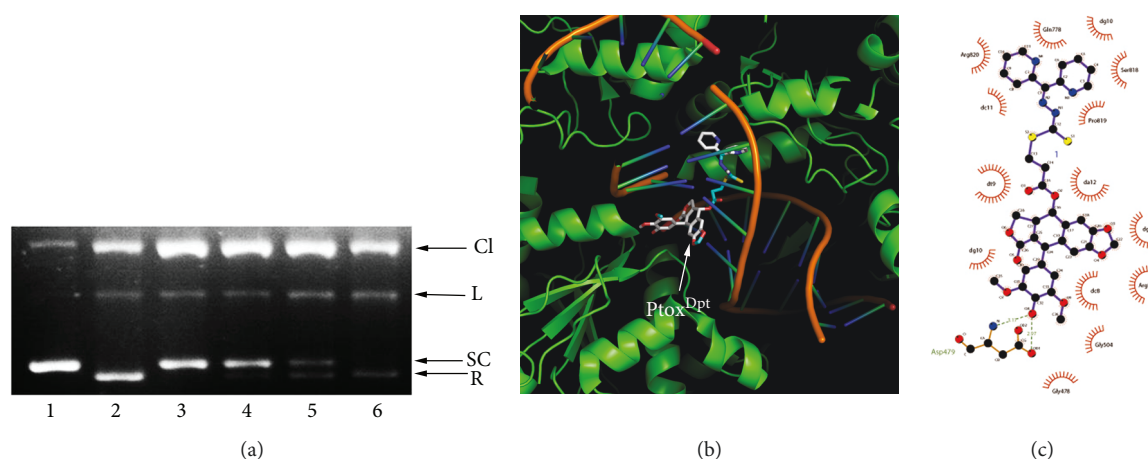


FIGURE 1: The Topo II inhibition and interaction of Ptox<sup>Dpt</sup>. (a) Topo II inhibition of Ptox<sup>Dpt</sup>. 1: pUC18; 2: nucleic extract plus pUC18; 3: pUC18 and nucleic extract plus 75  $\mu$ M Ptox<sup>Dpt</sup>; 4: pUC18 and nucleic extract plus 50  $\mu$ M Ptox<sup>Dpt</sup>; 5: pUC18 and nucleic extract plus 500  $\mu$ M etoposide; 6: pUC18 and nucleic extract plus DMSO. CL = cleaved; L = linear; S = supercoiled; R = relaxed DNA. (b) Ptox<sup>Dpt</sup> docked into the Topo II DNA complex. (c) The interactions between Ptox<sup>Dpt</sup> and nearby residues. The dark green dash lines indicated hydrogen bonds. The eye-like curved dark red lines represented the hydrophobic residues in contact.

to significant change in affinity and nearby environment. The interaction of Ptox<sup>Dpt</sup> with its nearby residues is shown in Figure 1(c), clearly showing that the nature of the interactions was mainly hydrophobic interaction and hydrogen bonds.

**2.3. Ptox<sup>Dpt</sup> Inhibits Hepatocellular Carcinoma Cell Proliferation.** To determine whether cytotoxicity was affected by the structural modification, the effect of Ptox<sup>Dpt</sup> on the proliferation of three hepatocellular carcinoma cell lines was determined. The dose-response curves for all three cell lines are shown in Figure 2(b). Ptox<sup>Dpt</sup> displayed significant growth inhibition in all three examined cell lines and was concentration dependent ( $p = 0.012 < 0.05$  for HepG2,  $p = 0.008 < 0.01$  for Bel-7402, and  $p = 0.0138 < 0.05$  for HCCLM3, respectively). However, a slight differential effect on the cell lines was observed; similar growth inhibition was achieved at a lower concentration ( $IC_{50} \leq 3 \mu$ M) for Bel-7402 and HepG2 cells (Figure 2(b)), whereas a higher concentration was required for HCCLM3 cells (Figure 2(b)), indicating that Bel-7402 and HepG2 cells were more sensitive to Ptox<sup>Dpt</sup>. Interestingly, Ptox<sup>Dpt</sup> exhibited better activity than etoposide in growth inhibition (Fig. S3). Next, the effect of Ptox<sup>Dpt</sup> on colony formation of HepG2 cells was further examined. As shown in Figure 2, Ptox<sup>Dpt</sup> significantly reduced the number of clones formed by HepG2 cells (Figures 2(c)–2(e)); about 65% inhibition at 0.75  $\mu$ M ( $p < 0.01$ ) and ~84% inhibition at 1.50  $\mu$ M Ptox<sup>Dpt</sup> treatment were observed based on quantitative analysis (Figure 2(f)). Taken together, these results demonstrated that Ptox<sup>Dpt</sup> inhibited the growth of hepatocellular carcinoma cells *in vitro*.

**2.4. Ptox<sup>Dpt</sup> Inhibits Cell Migration and Invasion.** Both cell invasion and migration are of fundamental importance in tumor metastasis and angiogenesis [32]. The HCCLM3 cell line is widely used in the invasion assay due to a higher potent metastasis than the HepG2 cell; thus, a transwell assay

was performed to determine the effect of Ptox<sup>Dpt</sup> on invasion of HCCLM3 cells. As shown in Figure 3(a), HCCLM3 cells displayed a high invasion capability. In contrast, Ptox<sup>Dpt</sup> significantly attenuated invasion capacity of the cells in a dose-dependent manner ( $p < 0.05$ ); a quantitative analysis is presented in Figure 3(b). In addition, a wound-healing model is widely used to estimate the migration potential of endothelial cells. Next, the effect of Ptox<sup>Dpt</sup> on the migration of HCCLM3 cells was determined. As shown in Figures 3(c) and 3(d), the migration of HCCLM3 across the wound space was inhibited by Ptox<sup>Dpt</sup> in a dose-dependent manner. Furthermore, matrix metalloproteinases (MMPs) as key players are involved in tumor invasion and metastasis [33]; the Ptox<sup>Dpt</sup>-induced migration and invasion inhibition might correlate with MMP inhibition; thus, the Western blotting and gelatin zymography analyses were further conducted. As shown in Figure 3(e), Ptox<sup>Dpt</sup> treatment significantly reduced both MMP-2 and MMP-9 expression (Figure 3(e), B) and activity (Figure 3(e), A), consistent with a previous report [34].

**2.5. Ptox<sup>Dpt</sup> Regulated EMT-Related Proteins.** Since Ptox<sup>Dpt</sup> could inhibit invasion and immigration of HCCLM3 cells, it might affect EMT. Considering that the HepG2 cell was more sensitive than HCCLM3, in the following experiments, the HepG2 cell line was chosen. To determine the potential effect of Ptox<sup>Dpt</sup> on EMT, the alterations in markers of the epithelium (E-cadherin) and mesenchymal cells (vimentin) were investigated. The immunofluorescence technique is widely used to visualize the alteration in membrane proteins; thus, the vimentin (in red) and E-cadherin (in green) were labeled individually (Figure 4); the merged photos could be used to distinguish the difference between the control group and the drug-treated group. Interestingly, Ptox<sup>Dpt</sup> could decrease the intensity of red fluorescence, i.e., expression of the mesenchymal marker, vimentin (Figures 4(c) and 4(g)); contrarily, it significantly increased the intensity of green

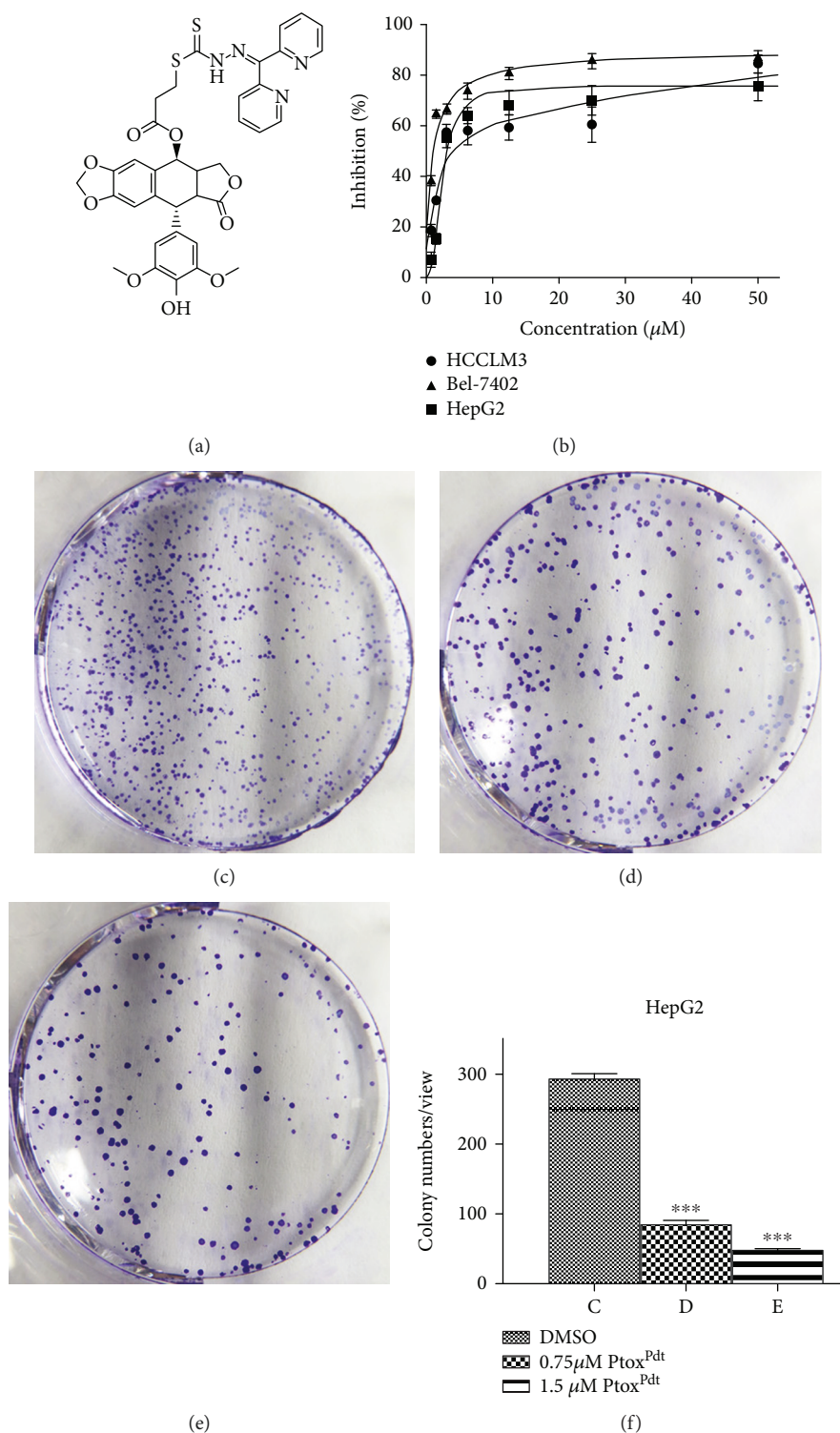


FIGURE 2: PtoxDpt induced inhibition in proliferation and colony formation against hepatoma carcinoma cell lines: (a) structure of PtoxDpt; (b) growth inhibition of PtoxDpt against investigated cell lines with  $\text{IC}_{50}$  values  $4.2 \pm 0.2 \mu\text{M}$  for HCCLM3,  $1.0 \pm 0.1 \mu\text{M}$  for Bel-7402, and  $3.0 \pm 0.14 \mu\text{M}$  for HepG2 cell, respectively. (c–e) The effect of PtoxDpt on colony formation of HepG2 cells: (c) 0.75% DMSO; (d) 0.075  $\mu\text{M}$  PtoxDpt; (e) 0.15  $\mu\text{M}$  PtoxDpt. (f) Quantitative analyses were from five visual fields randomly chosen from each well; \*\*\*  $p < 0.01$ .

fluorescence (or upregulation of expression of the epithelium marker, E-cadherin) compared to the control (Figures 4(b) and 4(f)), indicating that PtoxDpt could affect EMT transformation of the HepG2 cell (Figures 4(d) and 4(h)). To further

support the above conclusion, additional Western blotting analysis was conducted. As shown in Figure 5, a downregulation of vimentin, snail, and slug and upregulation of E-cadherin were observed upon PtoxDpt treatment, and the

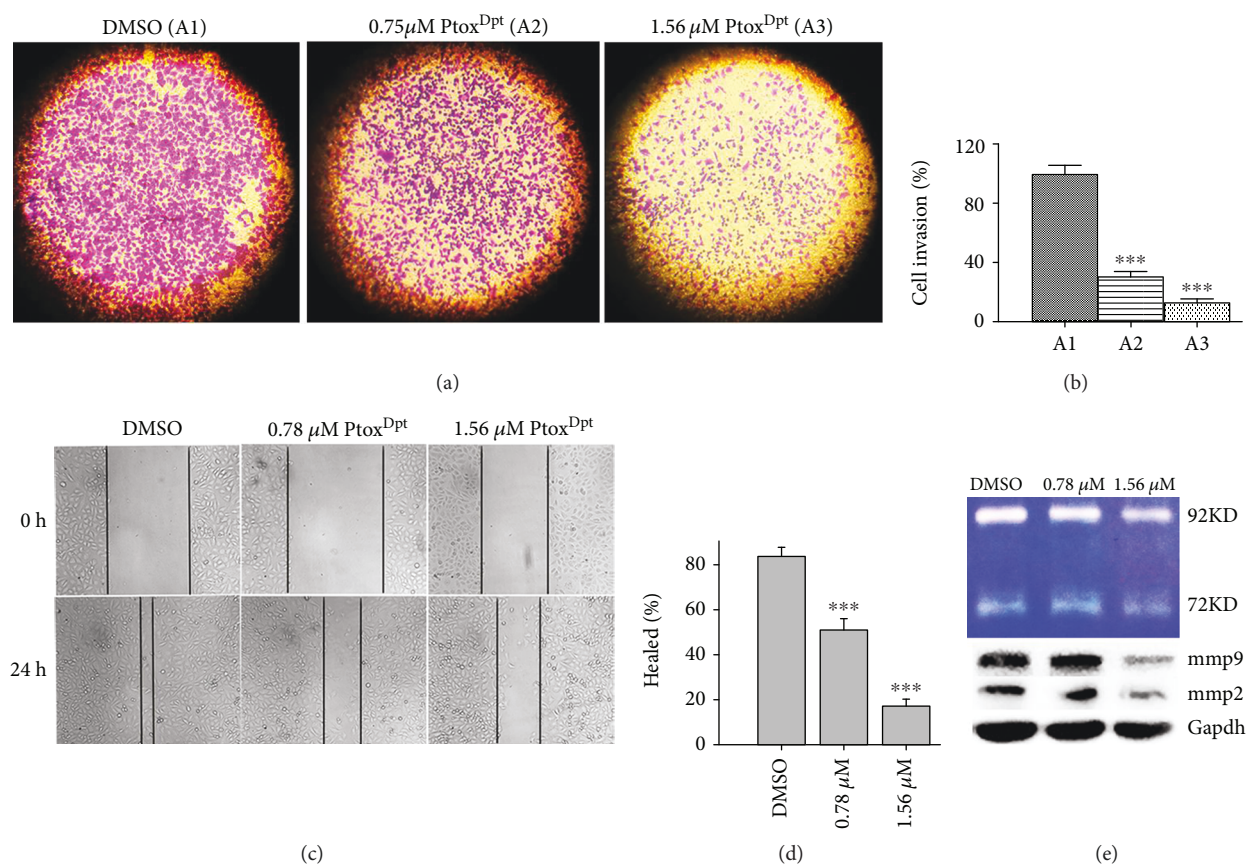


FIGURE 3: The immigration and invasion inhibition of PtoxDpt against hepatocellular carcinoma cells. (a) The migratory inhibition of PtoxDpt against HCCLM3 cells. (b) Quantitative analysis from (a): the invasive cells were stained with crystal violet. The results were expressed as invasive cell numbers per field of view (mean  $\pm$  5 SD,  $n = 6$ ). (c) The wounded HCCLM3 cells were treated with 0.0, 0.78, and 1.56  $\mu$ M PtoxDpt for 24 h. (d) Quantitative analysis of the width of gaps. (e) Gelatin zymography (A) and Western blotting (B) analyses of matrix metalloproteinase inhibition; the condition was as indicated in the experimental section. \*\*\* $p < 0.001$  compared with the DMSO-treated group.

significant alterations in epithelium-mesenchymal markers are clearly shown based on the quantitative analysis ( $p < 0.005$  or  $0.001$ , Figure 5(b)), corroborating that PtoxDpt owned the capacity in EMT inhibition. In addition, in view of the critical role of p53 in EMT [17], the EMT inhibition induced by PtoxDpt might involve p53; thus, the level of p53 was further determined. As expected, PtoxDpt indeed triggered upregulation of p53 (Figure 5(a)), indicating that p53 may also have a role in the EMT inhibition, consistent with previous reports [17, 18].

**2.6. The EMT Inhibition Induced by PtoxDpt Involved ROS Production.** The ROS production in EMT transformation has been well documented; however, whether EMT inhibition also involves ROS production remains to be investigated. Since PtoxDpt could suppress EMT, and lead to p53 upregulation, it might be associated with ROS production for p53 is a redox-active transcription factor, which responds to variety of stresses [35]. To confirm that the upregulated p53 was due to massive ROS production, the abundance of cellular ROS under different conditions was determined. As shown in Figure 6, the treatment of PtoxDpt caused  $\sim 6\%$  increase in higher DCF fluorescence population compared to the control (Figure 6(a), A2)

with a short time period of insulating (20 h), but the alteration could be attenuated by the addition of NAC, a ROS scavenger (Figure 6(a), A3). Similar trends were observed from analysis of the fluorescence median (Figure 6(a), A4). Those results might indicate that ROS were indeed involved in PtoxDpt-induced EMT reversal. To corroborate the ROS role in EMT reversal, the HepG2 cells were pretreated with TGF- $\beta 1$  to induce an EMT model and further treated by PtoxDpt for 2 h; the cells that were treated either by PtoxDpt or by combination with NAC were subjected to flow cytometry analysis. As shown in Figure 6(b), a 7% increase in higher fluorescence population was observed when the cells were treated by 1.56  $\mu$ M PtoxDpt, but the addition of NAC eliminated the increase and moved back to the normal state (Figure 6(b), B1–B3), indicating that PtoxDpt-induced EMT inhibition involved ROS production. The additional evidence from Western blotting analysis further supported the above conclusion because the addition of NAC could attenuate the increase of E-cadherin (Figure 6(b), B4). Both conditions hinted that PtoxDpt could induce ROS production, no matter if TGF- $\beta 1$  existed or not. Furthermore, the ROS were almost not altered after 24 h insulating of PtoxDpt (Fig. S4), indicating that a fluctuating ROS model occurred during the EMT transformation.

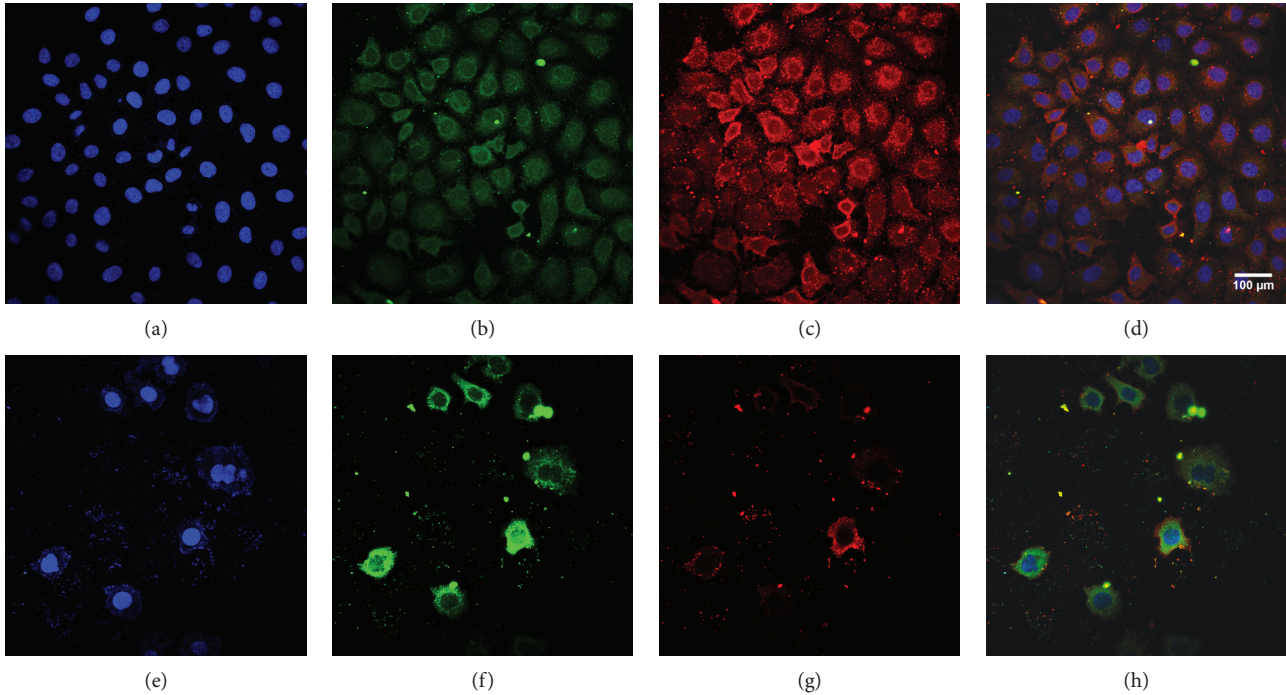


FIGURE 4: PtoxDpt inhibited EMT. (a–h) Immunofluorescence analysis of epithelial and mesenchymal markers. (a–d) Control: (a) nuclei in blue; (b) E-cadherin in green; (c) vimentin in red; (d) merge of nuclei, E-cadherin, and vimentin. (e–h) PtoxDpt-treated group: (e) nuclei in blue; (f) E-cadherin in green; (g) vimentin in red; (h) merge of nuclei, E-cadherin, and vimentin. Subject size:  $40 \times 10$  (fluorescence), scale bar:  $100 \mu\text{m}$ .

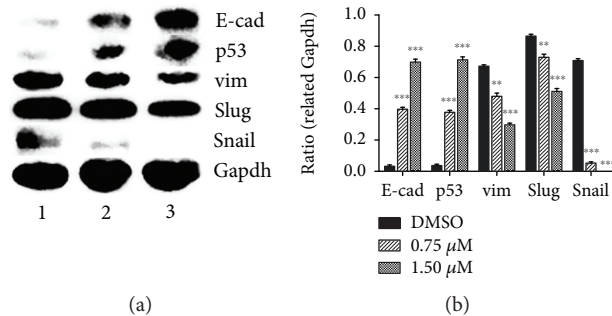


FIGURE 5: PtoxDpt regulated EMT-related protein expression. (a) Western blotting analysis of epithelium and mesenchymal markers; (b) quantification analysis of EMT-related proteins was conducted through ImageJ; \*\*\* $p < 0.001$ , \*\* $p < 0.005$ .

**2.7. PtoxDpt-Induced EMT Reversal Was p53 Dependent.** PtoxDpt led to upregulation of p53 (Figure 5(a)), hinting that p53 might be involved in the EMT reversal. To corroborate the role of p53 in EMT inhibition induced by PtoxDpt, a p53 inhibitor, PFT- $\alpha$ , was used to downregulate p53; then, the expressions of E-cadherin, vimentin, slug, and snail were determined. As shown in Figure 7, PFT- $\alpha$  indeed upregulated vim, slug, and snail and downregulated E-cadherin, and combination treatment of PtoxDpt with PFT- $\alpha$  significantly attenuated the expression of mesenchymal proteins and enhanced epithelium protein, E-cadherin (Figure 7(a)), indicating that p53 played a crucial role in EMT transition. Figure 7(b) showed quantitative analyses for the relative proteins under different treatments.

**2.8. PtoxDpt Attenuated TGF- $\beta$ 1-Induced EMT.** TGF- $\beta$ 1 as the most used EMT inducer can induce a mesenchymal phenotype in many cell lines, including the HepG2 cell line [36]. To verify the effectiveness of PtoxDpt in EMT inhibition, the HepG2 cells were pretreated by TGF- $\beta$ 1; as shown in Figure 8(b), spindle-shaped, fibroblast-like HepG2 cells were observed after TGF- $\beta$ 1 treatment, indicating that HepG2 cells were undergoing EMT, and the EMT model was successfully established [37]. Next, the cells were subjected to combination treatment of PtoxDpt and TGF- $\beta$ 1; interestingly, PtoxDpt could restore the cells back to the original state (Figure 8(c)), supporting the role of PtoxDpt in EMT. To gain more insight into EMT, immunofluorescence analysis was further conducted. Figure 8 clearly showed that PtoxDpt

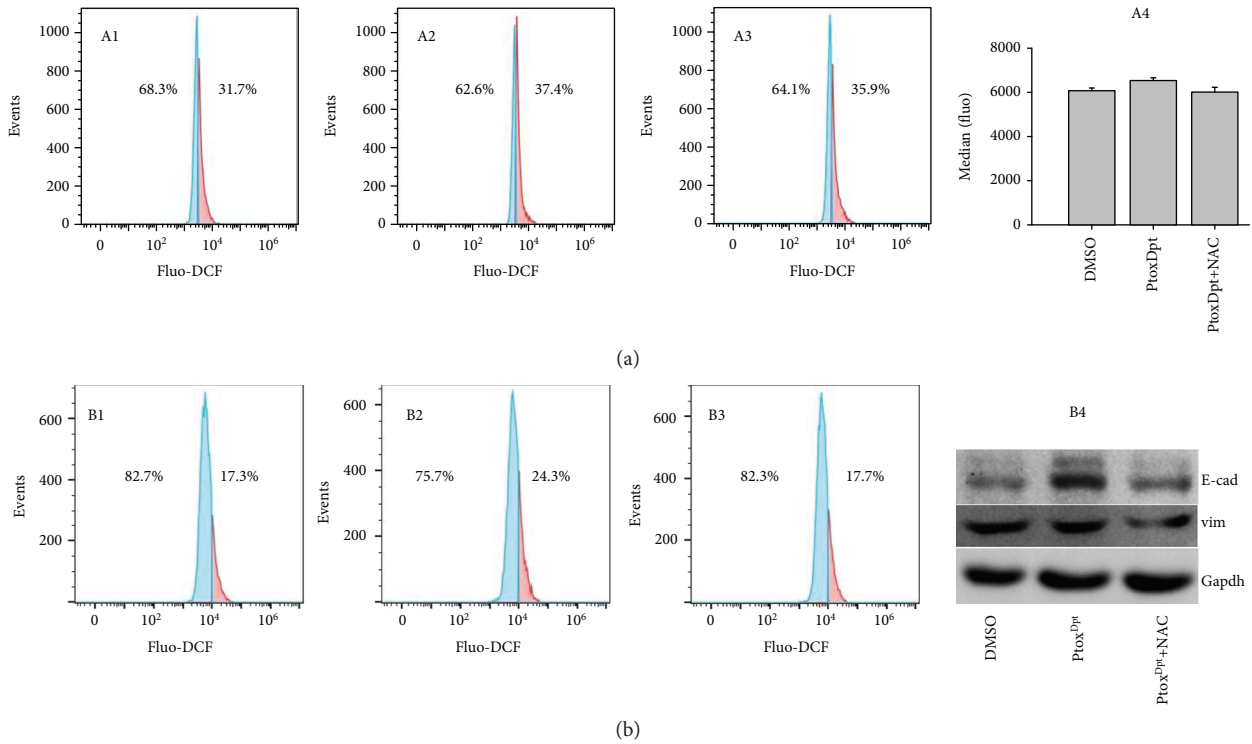


FIGURE 6: PtoxDpt treatment induced ROS production at different conditions and alteration in EMT markers. (a) 20 h treatment: A1: 0.75% DMSO; A2: 1.56 μM PtoxDpt; A3: 1.56 μM PtoxDpt + 1.5 mM NAC; A4: medians of fluorescence in different groups. (b) 2 h treatment in the presence of 10 ng TGF-β1: B1: 0.75% DMSO; B2: 1.56 μM PtoxDpt; B3: 1.56 μM PtoxDpt + 1.5 mM NAC; B4: Western blotting analysis of EMT markers.

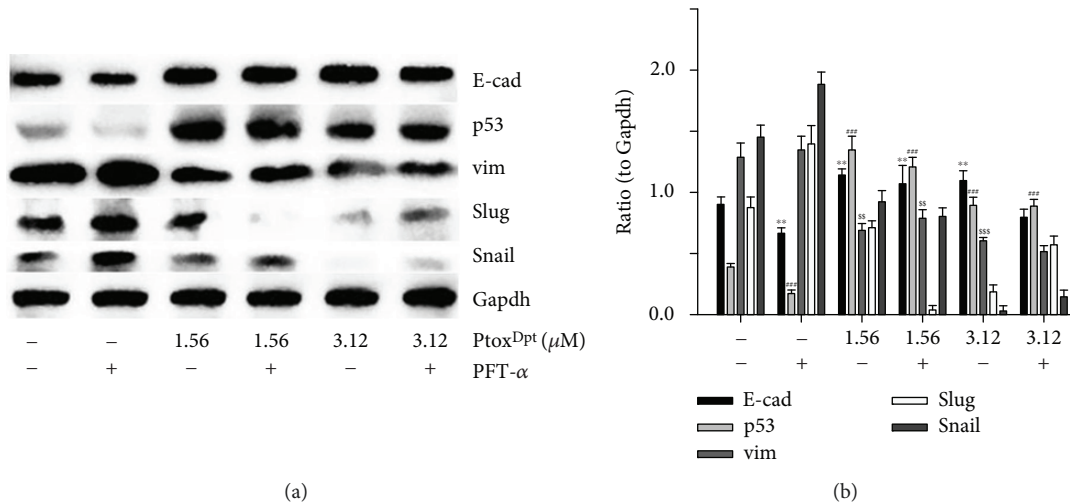


FIGURE 7: PtoxDpt-induced EMT reversion was p53 dependent. (a) Western blotting analyses of p53 and epithelium-mesenchymal proteins. (b) Quantitative analysis of proteins during EMT reversal induced by PtoxDpt. \*\* $p < 0.05$  for E-cad; ## $p < 0.05$ , ### $p < 0.01$  for p53; \$\$\$ $p < 0.05$ , \$\$\$ $p < 0.01$  for vimentin.

could decrease the intensity of red fluorescence of vimentin in the presence of TGF-β1 (Figures 8(f) and 8(j)) and accordingly increase the intensity of green fluorescence of E-cadherin (Figures 8(e) and 8(i)) compared to the control, further supporting that PtoxDpt could inhibit EMT. The additional evidence from Western blotting also supported the above conclusion for the expression of the epithelial marker,

E-cadherin, and the mesenchymal markers, vimentin, slug, and snail were all altered when the HepG2 cells were treated by either TGF-β1 (PtoxDpt) or combination of TGF-β1 and PtoxDpt (Figure 9). There was a significant increase in the ratio of E-cad/vim (3 folds) comparing PtoxDpt to TGF-β1 treatment, a similar trend in the ratio of E-cad/slug (6 folds, Figure 9(b)); those indicated that an epithelial characteristic



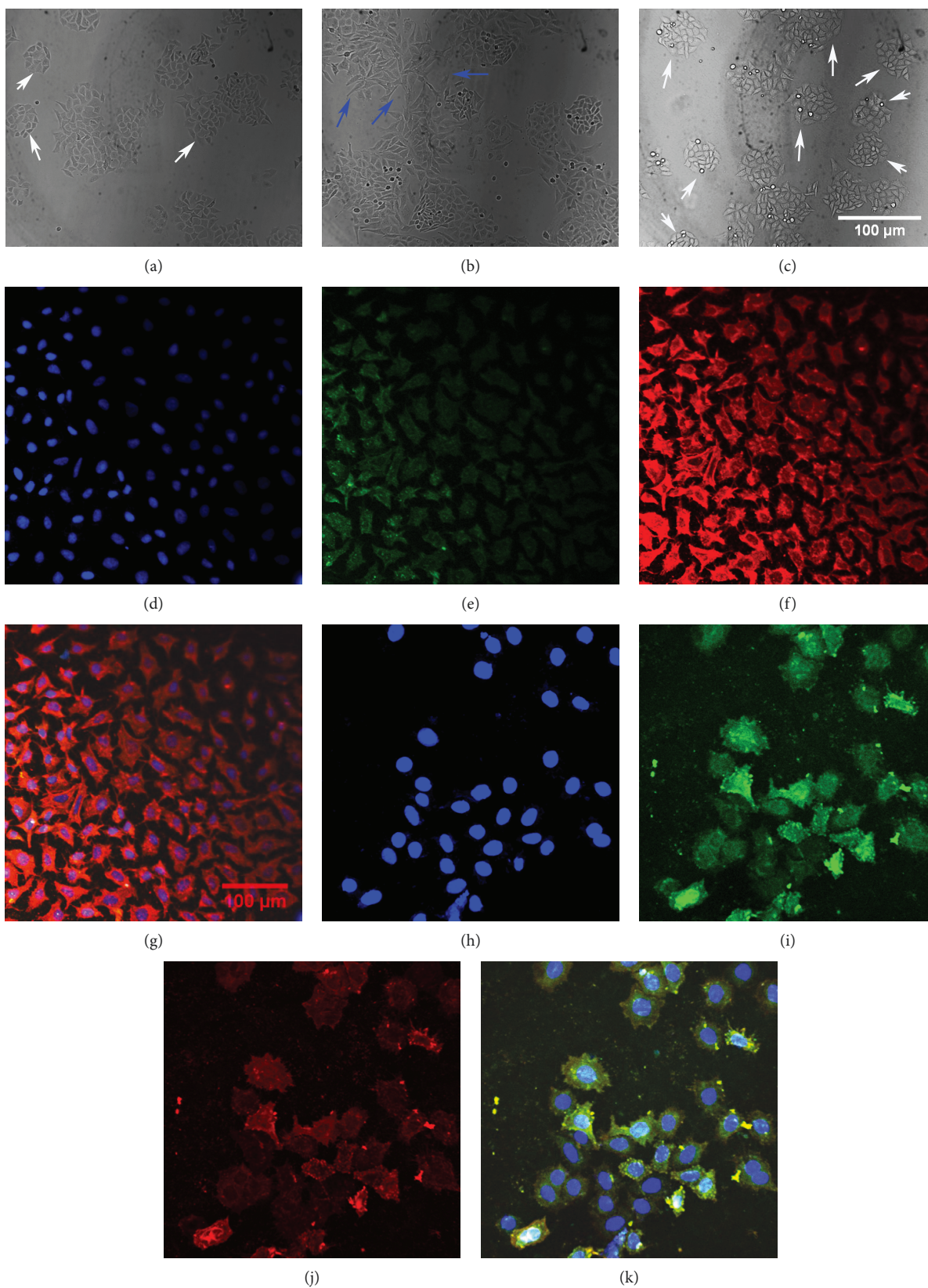
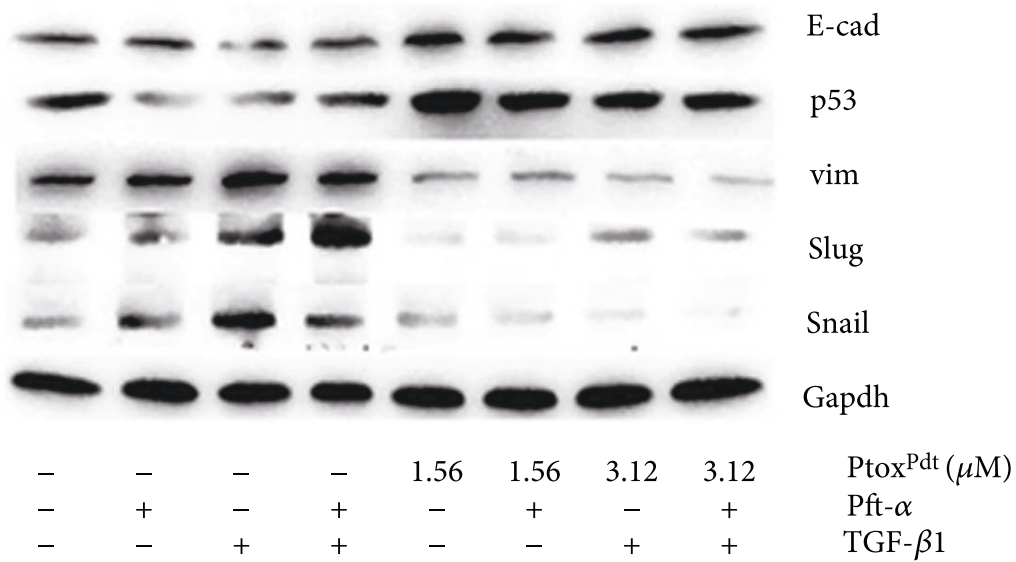
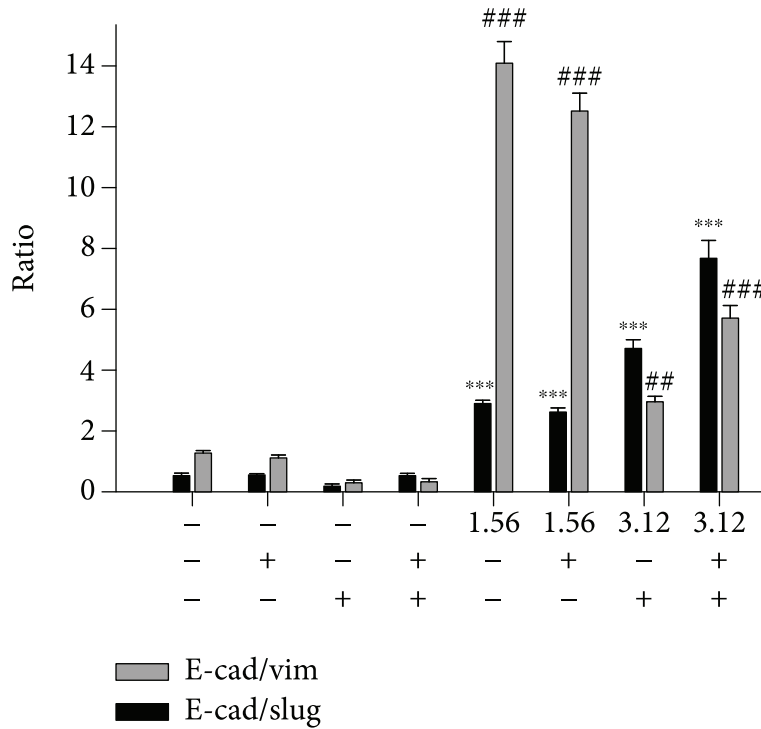


FIGURE 8: PtoxDpt inhibited EMT. (a–k) Immunofluorescence analysis of epithelial and mesenchymal markers. (a–d) Control: (a) nuclei in blue; (b) E-cadherin in green; (c) vimentin in red; (d) merge of nuclei, E-cadherin, and vimentin. (e–h) PtoxDpt-treated group: (e) nuclei in blue; (f) E-cadherin in green; (g) vimentin in red; (h) merge of nuclei, E-cadherin, and vimentin. Blue arrow: undergoing EMT; white arrow: original or back to the original state. Subject size:  $40 \times 10$  (fluorescence), scale bar:  $100 \mu\text{m}$ .



(a)



(b)

FIGURE 9: Ptox<sup>Dpt</sup> counteracted EMT induced by TGF- $\beta$ 1 in HepG2 cells. (a) Western blotting analysis; (b) quantitative comparison of the ratio of E-cad/vim (slug) in different conditions. The average ratio was from three independent experiments.

was significantly enhanced after Ptox<sup>Dpt</sup> treatment, demonstrating that Ptox<sup>Dpt</sup> was indeed able to counteract TGF- $\beta$ 1 action in EMT induction. The p53 inhibitor, PFT- $\alpha$ , like TGF- $\beta$ 1 led to p53 downregulation (Figure 9(a)), which accordingly caused mesenchymal characteristic enhancement, but ratios of E-cad/vim (slug) were not significantly altered except p53 downregulated in the combination treatment of PFT- $\alpha$  (or TGF- $\beta$ 1) with Ptox<sup>Dpt</sup>, implying that Ptox<sup>Dpt</sup> owned a powerful ability in EMT inhibition.

2.9. Ptox<sup>Dpt</sup> Induced Invasion Inhibition and EMT Reversal Involved in AKT/mTOR Pathways. Inhibition of mTORC1 and mTORC2 could attenuate migration and invasion [38]; Ptox<sup>Dpt</sup>-induced migration and invasion inhibition might involve mTOR inhibition or stem from the alteration of the PI3K/AKT/mTOR pathway [34]. Thus, the levels of AKT, phospho-AKT (as a measure of AKT activation), and mTOR were firstly determined by Western blotting. As shown in Figure 10(a), both AKT and phosphorylated AKT (p-AKT)

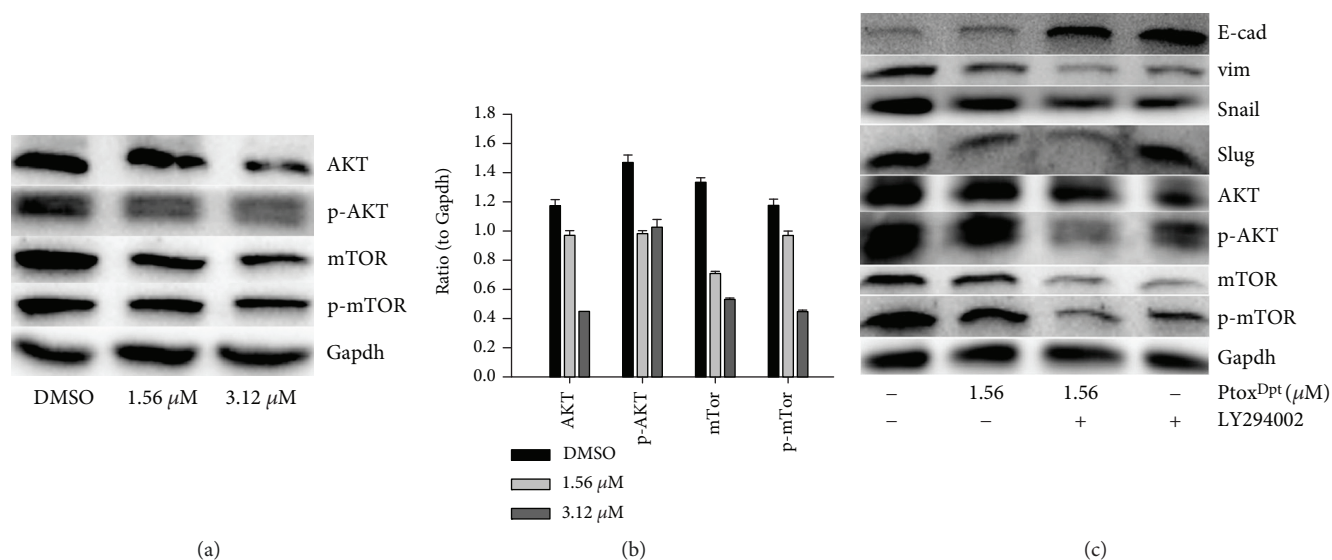


FIGURE 10: PtoxDpt regulation on the AKT/mTOR signal pathway: (a) Western blotting analysis of the AKT/mTOR signal pathway. The condition was as indicated; (b) quantitative analysis of the AKT/mTOR signal pathway; (c) the AKT/mTOR signal pathway involved EMT transformation induced by PtoxDpt. \*\*\* $p < 0.01$ ; \*\* $p < 0.05$ .

were decreased after PtoxDpt treatment, hinting that downregulation of p-AKT may stem from the downregulated AKT. A similar trend for mTOR, a downstream target of AKT, was also observed, indicating that the metastasis and invasion inhibition correlated with downregulation of mTOR that led to lower abundances of mTORC1 and mTORC2 complexes. The quantitative analysis of the proteins is shown in Figure 10(b); clearly, PtoxDpt-induced downregulation of both AKT and mTOR had significant statistical significance ( $p < 0.05$  or  $0.01$ ). On the other hand, in addition to migration and invasion inhibition, PtoxDpt also inhibited EMT, whether the PI3K/AKT/mTOR pathway was similarly involved in the EMT inhibition. To this end, the level of markers of the epithelium and mesenchymal cells, as well as AKT/mTOR, in the absence or presence of AKT inhibitor, LY294002, was further determined by Western blotting. As shown in Figure 10(c), both PtoxDpt and LY294002 downregulated vimentin (snail and slug) and contrarily upregulated E-cadherin, indicating that they acted in a similar way in EMT inhibition. Moreover, PtoxDpt also downregulated AKT and mTOR as LY294002 did (Figure 10(a) and 10(c)), indicating that PtoxDpt-induced EMT inhibition involved the PI3K/AKT/mTOR pathway.

### 3. Discussion

Epithelial-mesenchymal transition (EMT) involves the metastatic process of cancer; targeting EMT is one of the options in cancer therapy; thus, the novel EMT reversal agents are required. It has been demonstrated that the alterations in abundance of epithelial-mesenchymal proteins, such as E-cadherin, N-cadherin, and vimentin determine EMT status. On the other hand, to keep cancer cells thriving, higher abundances of DNA topoisomerases (Topo) and iron are needed; thus, either downregulation (or inhibition) of topoisomerase or depletion of iron can slow down the proliferation of cancer

cells. Recent studies demonstrated that some Topo II inhibitors, including etoposide, could inhibit EMT and attenuate metastasis [24, 25], which hinted that etoposide derivatives can be used as a library of the EMT inhibitor. However, etoposide is derived from 4'-demethylepipodophyllotoxin (DMEP); thus, DMEP can be used as a basic structural unit to synthesize potent EMT inhibitors. Although a number of modifications at position 4 in DMEP have been conducted, including esterification and amination [39–42], the effect of DMEP derivatives on EMT transformation was not fully determined. In addition, the EMT inhibition could be achieved by introduction of wild-type p53 [15, 16]. Furthermore, some iron chelators could also modulate both p53 and EMT [27, 28]; this implied that iron chelator can function as partial p53 inducer to counteract EMT. For this reason, in the present study, we constructed a novel EMT reversal agent that hybridized the DMEP unit with iron chelator, dithiocarbamate unit, to achieve efficient EMT inhibition (Fig. S1). As expected, PtoxDpt inherits the feature of DMEP and exhibits enhanced activity in Topo II inhibition compared to etoposide (Figure 1). A theoretical simulation revealed that PtoxDpt like etoposide was located in the catalytic center of the DNA Topo complex (Fig. S3), supporting that PtoxDpt was a good Topo II inhibitor except EMT inhibition. In addition, PtoxDpt exhibited significant growth inhibition (Figure 2) and migration and invasion inhibition partly correlated with downregulation (or inactivation) of MMPs (Figure 3), in accordance with a previous report [43].

It has been shown that epithelial-mesenchymal transition (EMT) is associated with increase of matrix metalloproteases (MMPs) [38]; downregulation of MMP may inhibit EMT. Since PtoxDpt induced a downregulation of MMPs, it might inhibit EMT. To test the hypothesis, the alterations in epithelial-mesenchymal markers both in immunofluorescence and in the protein level were investigated. Immunofluorescence analyses in Figure 4 revealed that PtoxDpt inhibited

EMT through upregulation of E-cadherin and downregulation of vimentin; additional evidence from Western blotting (Figure 5) supported the above deduction, similar to that reported previously [44]. As expected, the introduction of dithiocarbamate in PtoxD<sup>Dpt</sup> led to an upregulation of p53, which might partly stem from depletion of cellular iron. However, other factors cannot be ruled out for p53 are responsible for different stresses. It was reported that Topo II inhibition mediated oxidative stress-involved ROS production [45]; a similar situation may occur in PtoxD<sup>Dpt</sup>-treated cells. In addition, it was well documented that TGF- $\beta$ 1-induced EMT involved ROS production [46, 47]; however, whether the EMT inhibition also involved ROS production remained to be determined. To test the hypothesis, PtoxD<sup>Dpt</sup>-induced ROS production was assayed either in the absence or in the presence of TGF- $\beta$ 1 (Figures 6(a) and 6(b)); the results clearly showed that EMT inhibition indeed involved ROS production, which also correlated with upregulation of E-cadherin (or downregulation of vimentin, Figure 6(b), B4). To further support the above conclusion, the addition of NAC could attenuate EMT inhibition induced by PtoxD<sup>Dpt</sup> (Figure 6(b), B4), indicating that ROS played a role in the EMT inhibition. Furthermore, this also hinted that the upregulated p53 might be due to ROS production.

It should be noted that the excess ROS generation only occurred in the initial stage in the presence of TGF- $\beta$ 1, almost no change for ROS after 24 h (Fig. S4); this situation in ROS production was consistent with that described previously [45, 48]. To respond to the ROS production, p53 was upregulated; contrarily, addition of the p53 inhibitor, PFT- $\alpha$ , significantly attenuated the effect of PtoxD<sup>Dpt</sup> on epithelium-mesenchymal markers, indicating that p53 played a role in PtoxD<sup>Dpt</sup>-induced EMT inhibition (Figure 7). In addition, the additional evidence also showed that PtoxD<sup>Dpt</sup> could suppress TGF- $\beta$ 1-induced EMT both from immunofluorescence and Western blotting (Figures 8 and 9), further supporting that PtoxD<sup>Dpt</sup>-induced p53 upregulation played an important role in EMT inhibition.

The PI3K/AKT/mTOR pathway plays a critical role in the proliferation, apoptosis, angiogenesis, and metastasis of tumor development [49, 50]. PtoxD<sup>Dpt</sup> exhibited significant invasion and EMT inhibition; we thus questioned whether PtoxD<sup>Dpt</sup>-induced EMT inhibition was through the PI3K/AKT/mTOR pathway. To this end, the level of the PI3K/AKT/mTOR pathway was determined; as expected, PtoxD<sup>Dpt</sup> could downregulate both AKT and mTOR expression (Figures 10(a) and 10(b)), suggesting that the action of PtoxD<sup>Dpt</sup> on the HepG2 cell might involve the PI3K/AKT/mTOR pathway. To corroborate the involvement of the PI3K/AKT/mTOR pathway in PtoxD<sup>Dpt</sup>-induced EMT inhibition, an AKT inhibitor, LY294002, was used as the positive control; the data clearly showed that both PtoxD<sup>Dpt</sup> and LY294002 achieved EMT inhibition (Figure 10(c)), indicating that PtoxD<sup>Dpt</sup>-induced EMT inhibition involved the PI3K/AKT/mTOR pathway.

In conclusion, the PtoxD<sup>Dpt</sup> exhibited diverse functions in both Topo II and MMP inhibition. In addition, PtoxD<sup>Dpt</sup> also inhibit EMT, which may be achieved through the p53/PI3K/AKT/mTOR axis. Importantly, ROS played a

role both in EMT and EMT reversal. PtoxD<sup>Dpt</sup> acted as “fighting fire with fire” in the EMT reversal process. Taken together, our findings indicate that PtoxD<sup>Dpt</sup> is a promising antitumor drug for possible use in chemotherapy. However, extensive investigations, both *in vitro* and *in vivo*, are required in future studies.

## 4. Materials and Methods

**4.1. Materials.** MTT, PFT- $\alpha$ , TGF- $\beta$ 1, di-2-pyridylketone, RPMI-1640, LY294002, and other chemicals were purchased from Sigma-Aldrich (Shanghai, China). Fetal bovine serum was purchased from Every Green Zhejiang Tianhang Technology Co. Ltd. (Hangzhou, China). Antibodies of vimentin, slug, snail, and p53 were purchased from Boster (Wuhan, China). Antibodies of AKT, p-AKT, mTOR, p-mTOR, E-cadherin, and Gapdh were purchased from EnoGene (Nanjing, China). 4'-Demethylpodophyllotoxin was purchased from Shanghai PureOne Biotechnology (Shanghai, China).

**4.1.1. Preparation of 2,2'-Dipyridineketone Hydrazone Dithiocarbamate S-Propionic Acid Podophyllotoxin Ester (PtoxD<sup>Dpt</sup>).** The PtoxD<sup>Dpt</sup> was prepared by using a four-step reaction: preparation of 2,2'-dipyridineketone hydrazone dithiocarbamate S-propionic acid (compound III, Fig. S1) engaged a three-step reaction that was reported previously [30]. The PtoxD<sup>Dpt</sup> (compound IV, Fig. S1) was prepared by reacting compound III with 4'-demethylpodophyllotoxin with DCC/DMAP catalysis in absolute CH<sub>2</sub>Cl<sub>2</sub>. TLC was traced during the period of reaction. <sup>1</sup>HNMR (Bruker, DMSO-d<sub>6</sub>, ppm): 14.98(s,1H), 8.87(d, 1H, J = 4 Hz), 8.63(m, 1H, J = 4 Hz), 8.01(m, 3H, J = 4, 8 Hz), 7.54 (m, 3H, J = 4,8 Hz), 7.00(s, 1H), 6.95(s, 1H), 6.76(s, 2H), 6.56(s, 2H), 6.33(s,1H), 6.01(s,3H), 5.64(d, 1H, J = 8 Hz),4.75(dd, 1H, J = 4 Hz), 4.52(dd, 1H, J = 4 Hz), 4.36(d,1H,J = 8 Hz), 4.16(dd, 1H, J = 8 Hz), 3.69(s, 6H), 2.93(d, 2H, J = 4 Hz). <sup>13</sup>CNMR(Bruker, 100 MHz, DMSO-d<sub>6</sub>):199.77, 179.25, 175.24, 169.82, 155.02, 151.93, 149.24, 148.94, 147.66, 146.79, 146.73, 145.23,140.66, 138.35, 137.91, 133.26, 130.81, 128.12, 126.94, 125.85, 124.97, 124.02, 109.49, 106.48, 104.92, 101.32, 68.00, 65.95, 65.39, 60.23, 56.47, 56.26, 45.46, 43.15, 33.20, 28.97. ESI-MS (C<sub>36</sub>H<sub>32</sub>N<sub>4</sub>O<sub>9</sub>S<sub>2</sub>K): m/z: 767.1268 (M+K, Calcd: 767.1248).

**4.1.2. DNA Topo II Activity Assay.** The assay of inhibition of PtoxD<sup>Dpt</sup> on DNA Topo II activity was conducted based on the protocol described previously [31]. To initiate the enzymatic reaction, nuclear extract (0.4  $\mu$ g) was added to the Topo reaction buffer (10 mM Tris-HCl (pH 7.5), 1 mM EDTA, 1 mM ATP, 150 mM NaCl, 0.1% BSA, and 5% glycerol) that contained 0.4  $\mu$ g supercoiled pUC18 plasmid DNA and 1-3  $\mu$ L of PtoxD<sup>Dpt</sup> (1 mM in 8% DMSO) in a final volume of 20  $\mu$ L. Following an additional incubation at 37°C for 30 min., 5  $\mu$ L of stopping buffer (10% SDS, 0.025% bromophenol blue, and 10% glycerol) was added to terminate the reaction. The resulting products were separated by electrophoresis using a 1% agarose gel in a TBE buffer (89 mM Tris-HCl, 89 mM boric acid, and 62 mM EDTA) containing 0.1% SDS and ethidium bromide (0.5  $\mu$ g/mL) at 45 V for 3 h. The bands

were visualized on a Tocan 360 gel scanner (excited at ~340 nm) (Shanghai Tiancheng Technology Inc., China). The assay was performed in duplicate.

**4.1.3. Molecular Docking.** To simulate the potent interaction between Ptox<sup>Dpt</sup> and Topo II, the PDB file of the structure of human type II Topo (3QX3) was downloaded from the RCSB Protein Data Bank. The structure of Ptox<sup>Dpt</sup> was generated by ChemDraw. Then, the 3QX3 and Ptox<sup>Dpt</sup> in PDB were transformed in PDBQT format by the AutoDock Tool using the default parameters. PyMOL and LigPlot were used to display the conformation and interactions [51, 52].

Molecular docking studies were performed by using AutoDock Vina [53]. To optimize the docking parameters, the cocrystallized etoposide was extracted and redocked into the active sites of 3QX3 with various parameters. The grid box size for Ptox<sup>Dpt</sup> was set to 22, 24, and 28 for the *x*-, *y*-, and *z*-axes, respectively.

**4.1.4. Cytotoxicity Assay (MTT Assay).** The proliferative inhibition of the agent was determined by the MTT method as described previously [30]. Briefly, the equivalent cells of Bel-7402 (or HepG2, HCCLM3,  $5 \times 10^3$ /mL) were seeded into a 96-well plate, and the varied concentrations of Ptox<sup>Dpt</sup> were added to the wells after the cells were adhered. Following 48 h incubation at 37°C in a humidified atmosphere of 5% CO<sub>2</sub>, 10 µL of MTT solution (5 mg/mL) was added into each well, and a further incubation was conducted. Finally, 100 µL DMSO was added to each well to dissolve the formazan crystals after removing the cell culture. The measurement of the solution absorbance was performed on a microplate reader (MK3, Thermo Scientific) at 570 nm. The percent absorbance inhibition that correlates with percent growth inhibition was obtained. The same assay was performed in triplicate.

**4.1.5. Plate Clone Formation Assay.** The HepG2 cells in the exponential phase were trypsinized and seeded in 6-well plates at the density of 500 cells/well. Ptox<sup>Dpt</sup> at dose of 1/40 or 1/20 IC<sub>50</sub> was added. Fourteen days later, colonies were fixed in 3.7% paraformaldehyde, stained with 0.1% crystal violet. Colonies containing 50 cells at least were counted under an inverse microscope (Nikon, Tokyo, Japan), and the clone numbers were analyzed subsequently.

**4.1.6. Migration Assay.** The inhibition of tumor cell migration by Ptox<sup>Dpt</sup> was determined using a wound-healing migration assay [54]. Briefly, HCCLM3 cells were allowed to grow to full confluence in 6-well plates, after which “wounds” were created using a sterile pipette tip. Following this procedure, the cells were rinsed twice with PBS to remove unattached cells. Fresh medium containing 10% fetal bovine serum and various concentrations of Ptox<sup>Dpt</sup> was then added. The cells were photographed (time 0). After 24 h incubation at 37°C, the cells were photographed again (24 h).

**4.1.7. Invasion Assay.** As described previously [55], transwell chambers (Corning) with 8 µm pore membranes coated with Matrigel were used to perform the invasion assay. Briefly, after overnight pretreatment with Ptox<sup>Dpt</sup> in a 6-well plate,

the HCCLM3 cells were starved for 12 h in serum-free medium. Following this, the cells were collected and resuspended as a single cell suspension. In total,  $3 \times 10^4$  cells in 100 µL of serum-free medium were added to the upper chamber, and 600 µL of complete medium was added to the lower chamber. Following incubation for 18 h at 37°C, the invading cells were fixed in 4% paraformaldehyde, stained with 0.1% crystal violet, and photographed under a microscope (or counted manually). The percentage of inhibition was expressed using control wells as 100% (Fig. S3).

**4.1.8. Gelatin Zymography Assay.** Gelatin zymography was performed as previously described [56]. Conditioned media were collected from HCCLM3 cells after culture for 24 h in serum-free medium with or without Ptox<sup>Dpt</sup>. After collection, the media were centrifuged to pellet any insoluble material. The protein concentration in the conditioned media was quantified using the Bradford method. Equal amounts of conditioned media were mixed with sample buffer and applied to 10% SDS polyacrylamide gel copolymerized with 1 mg/mL of gelatin. After electrophoresis, the gel was incubated in renaturing buffer (50 mM Tris-HCl, pH 7.5, 2.5% Triton X-100, 200 mM NaCl, 10 mM CaCl<sub>2</sub>, and 1 µM ZnCl<sub>2</sub>), followed by a 24 h incubation with developing buffer (50 mM Tris base, 200 mM NaCl, 10 mM CaCl<sub>2</sub>, 1 µM ZnCl<sub>2</sub>, and 0.02% NaN<sub>3</sub>). The gel was then stained with 0.25% Coomassie blue R-250 for 1 hour and destained with 10% methanol with 5% acetic acid. Clear bands against a dark blue background indicated where the protease had digested the gelatin and were taken to be indicative of protease activity.

**4.1.9. Immunofluorescence Analysis.** HepG2 cells were first cultured in a 24-well plate with cover glass overnight. Following Ptox<sup>Dpt</sup> treatment for additional 24 h, cells were first fixed with 4% paraformaldehyde in PBS for 15 min at 37°C and then permeabilized with 0.5 % Triton X-100 in PBS for 20 min. After blocking with 3% BSA in PBS for 60 min, the cells were incubated with combined vimentin with E-cadherin (EnoGene) primary antibody based on protocol recommended by the company; at 4°C, the plate was shaken overnight. Next, removing the primary antibodies and washing with PBS, the cells were further incubated with fluorescence-labeled secondary antibody for 3 h at room temperature. After removing the secondary antibody, the cells were further counterstained with DAPI. Finally, a confocal laser scanning microscope (Nikon Eclipse Ts2, Japan) was used to visualize the cells; the representative cells were selected and photographed.

**4.1.10. Flow Cytometry Analysis of Cellular ROS.** HepG2 cells were placed in a six-well plate, once the cells were adhered and subjected to treatment with Ptox<sup>Dpt</sup> or other agent for 24 h. Next, the cells were treated by trypsin digestion and collected. Following washing, the cells were stained with H<sub>2</sub>DCF-DA (Dojindo Laboratories, Japan). The intracellular ROS assay was conducted on a flow cytometry (Becton-Dickinson, USA).

**4.1.11. Western Blotting Analysis.** The protein extracts were prepared based on the company recommended protocol

(Solarbio). Briefly, the HepG2 cells treated with or without Ptox<sup>Dpt</sup> were scraped in lysis buffer (RIPA lysis buffer), and the cell suspension in the EP tube was incubated on ice for 30 min and mixed by turning upside down occasionally, followed by centrifugation at 14,000 ×g. The clear supernatant was stored at -80°C. Protein concentration was determined using a colorimetric BCA assay. Proteins (20 μg) were loaded on a 13% sodium dodecyl sulfate-polyacrylamide gel at 120 V (20 mA) for 2 h. The separated proteins were subsequently transferred onto a PVDF membrane at 120 V (200 mA) for 90 min. The membrane was washed with Tris-buffered saline (TBS) and then blocked for 2 h in TBS containing 0.1% Tween-20 and 5% nonfat skimmed milk. The membrane was incubated at 4°C overnight with the appropriate primary antibody used at a dilution recommended by the company. The membrane was then washed several times with TBST and subsequently incubated with the appropriate HRP-conjugated secondary antibody for 2 h at room temperature. Finally, the protein bands were detected using a super sensitive ECL solution (Boster Biological Technology Co. Ltd.) and visualized on a Syngene G:BOX imager (Cambridge, United Kingdom). Quantification of protein band intensities was performed using ImageJ software.

**4.1.12. Statistical Analysis.** Results are presented as the mean ± SEM. Comparisons between two groups were carried out using two-tailed Student's *t*-test. Comparisons between multiple groups were performed by one-way ANOVA with Dunnett post hoc correction. All statistical tests were conducted by using IBM SPSS Statistics (version 19 software). *p* < 0.05 was accepted as significant.

## Data Availability

The data used to support the findings of this study are included within the article.

## Conflicts of Interest

The authors declare no conflict of interest.

## Authors' Contributions

Yongli Li, Tingting Wang, and Yanjie Sun performed the experiments; they contributed equally to this work. Tengfei Huang performed synthesis of the investigated compound; Changzheng Li conceived and designed the experiments; and Tingting Wang, Yanjie Sun, Cuiping Li, Yichun Li, and Yun Fu analyzed the data and generated figures. Changzheng Li prepared and wrote the paper.

## Acknowledgments

The present study was supported by grants awarded by the Natural Science Foundation of China (no. 21571153), the Henan Science and Technology Agency (nos. 14300510012 and 152300410118), and the Key Research Project Funding Program of Higher Educational Institutions of Henan Province (19A310021) and the Innovation Team awarded

by the Sanquan College of Xinxiang Medical University (SQT201703 and SQT201802).

## Supplementary Materials

Fig. S1: synthetic route of Ptox<sup>Dpt</sup>, the condition as indicated in the scheme. The data of NMR and HRMS are shown in Materials and Methods. Fig. S2: molecular simulation of etoposide and Ptox<sup>Dpt</sup>. (A) Comparison of docked etoposide with crystallized etoposide in the DNA topoisomerase complex; (B) comparison of docked etoposide with docked Ptox<sup>Dpt</sup> in the DNA topoisomerase complex. Fig. S3: proliferation inhibition of etoposide against HepG2 (A) and Ptox<sup>Dpt</sup> against the normal human hepatic cell line LO2 cell (B). Fig. S4: ROS production induced by Ptox<sup>Dpt</sup> after 24 h during EMT reversal: (A) DMSO, (B) 156 μM Ptox<sup>Dpt</sup>, and (C) 156 μM Ptox<sup>Dpt</sup> + 3 mM NAC. (*Supplementary Materials*)

## References

- [1] J. Massague, E. Batlle, and R. R. Gomis, "Understanding the molecular mechanisms driving metastasis," *Molecular Oncology*, vol. 11, no. 1, pp. 3-4, 2017.
- [2] N. Gavert and A. Ben-Ze'ev, "Epithelial-mesenchymal transition and the invasive potential of tumors," *Trends in Molecular Medicine*, vol. 14, no. 5, pp. 199-209, 2008.
- [3] B. Du and J. Shim, "Targeting epithelial-mesenchymal transition (EMT) to overcome drug resistance in cancer," *Molecules*, vol. 21, no. 7, p. 965, 2016.
- [4] O. H. Ocaña, R. Córcoles, Á. Fabra et al., "Metastatic colonization requires the repression of the epithelial-mesenchymal transition inducer PRRX1," *Cancer Cell*, vol. 22, no. 6, pp. 709-724, 2012.
- [5] J. H. Tsai, J. L. Donaher, D. A. Murphy, S. Chau, and J. Yang, "Spatiotemporal regulation of epithelial-mesenchymal transition is essential for squamous cell carcinoma metastasis," *Cancer Cell*, vol. 22, no. 6, pp. 725-736, 2012.
- [6] S. Lamouille, J. Xu, and R. Derynck, "Molecular mechanisms of epithelial-mesenchymal transition," *Nature Reviews Molecular Cell Biology*, vol. 15, no. 3, pp. 178-196, 2014.
- [7] T. Yoshida, Y. Ozawa, T. Kimura et al., "Eribulin mesilate suppresses experimental metastasis of breast cancer cells by reversing phenotype from epithelial-mesenchymal transition (EMT) to mesenchymal-epithelial transition (MET) states," *British Journal of Cancer*, vol. 110, no. 6, pp. 1497-1505, 2014.
- [8] D. J. McConkey, W. Choi, L. Marquis et al., "Role of epithelial-to-mesenchymal transition (EMT) in drug sensitivity and metastasis in bladder cancer," *Cancer and Metastasis Reviews*, vol. 28, no. 3-4, pp. 335-344, 2009.
- [9] F. M. Davis, T. A. Stewart, E. W. Thompson, and G. R. Monteith, "Targeting EMT in cancer: opportunities for pharmacological intervention," *Trends in Pharmacological Sciences*, vol. 35, no. 9, pp. 479-488, 2014.
- [10] J. Deng, L. Wang, H. Chen et al., "Targeting epithelial-mesenchymal transition and cancer stem cells for chemoresistant ovarian cancer," *Oncotarget*, vol. 7, no. 34, pp. 55771-55788, 2016.
- [11] F. Marcucci, G. Stassi, and R. de Maria, "Epithelial-mesenchymal transition: a new target in anticancer drug discovery," *Nature Reviews Drug Discovery*, vol. 15, no. 5, pp. 311-325, 2016.

- [12] T. Soussi and K. G. Wiman, "Shaping genetic alterations in human cancer: the p53 mutation paradigm," *Cancer Cell*, vol. 12, no. 4, pp. 303–312, 2007.
- [13] I. C. Hsu, R. A. Metcalf, T. Sun, J. A. Welsh, N. J. Wang, and C. C. Harris, "Mutational hotspot in the p53 gene in human hepatocellular carcinomas," *Nature*, vol. 350, no. 6317, pp. 427–428, 1991.
- [14] M. Ozturk, "p53 mutation in hepatocellular carcinoma after aflatoxin exposure," *Lancet*, vol. 338, no. 8779, pp. 1356–1359, 1991.
- [15] Z. Wang, Y. Jiang, D. Guan et al., "Critical roles of p53 in epithelial-mesenchymal transition and metastasis of hepatocellular carcinoma cells," *PLoS One*, vol. 8, no. 9, p. e72846, 2013.
- [16] E. Powell, D. Piwnica-Worms, and H. Piwnica-Worms, "Contribution of p53 to metastasis," *Cancer Discovery*, vol. 4, no. 4, pp. 405–414, 2014.
- [17] C. J. Chang, C. H. Chao, W. Xia et al., "p53 regulates epithelial-mesenchymal transition and stem cell properties through modulating miRNAs," *Nature Cell Biology*, vol. 13, no. 3, pp. 317–323, 2011.
- [18] T. Kim, A. Veronese, F. Pichiorri et al., "p53 regulates epithelial-mesenchymal transition through microRNAs targeting ZEB1 and ZEB2," *Journal of Experimental Medicine*, vol. 208, no. 5, pp. 875–883, 2011.
- [19] Z. Chen, D. Zhang, F. Yue, M. Zheng, Z. Kovacevic, and D. R. Richardson, "The iron chelators Dp44mT and DFO inhibit TGF- $\beta$ -induced epithelial-mesenchymal transition via up-regulation of N-Myc downstream-regulated gene 1 (NDRG1)," *Journal of Biological Chemistry*, vol. 287, no. 21, pp. 17016–17028, 2012.
- [20] A. Singh and J. Settleman, "EMT, cancer stem cells and drug resistance: an emerging axis of evil in the war on cancer," *Oncogene*, vol. 29, no. 34, pp. 4741–4751, 2010.
- [21] T. Yoshida, Y. Ozawa, T. Kimura et al., "Eribulin mesilate suppresses experimental metastasis of breast cancer cells by reversing phenotype from epithelial-mesenchymal transition (EMT) to mesenchymal-epithelial transition (MET) states," *British Journal of Cancer*, vol. 110, no. 6, pp. 1497–1505, 2014.
- [22] Z. Cao, S. Koochekpour, S. E. Strup, and N. Kyprianou, "reversion of epithelial-mesenchymal transition by a novel agent DZ-50 via IGF binding protein-3 in prostate cancer cells," *Oncotarget*, vol. 8, no. 45, pp. 78507–78519, 2017.
- [23] A. F. Lee, M. C. Chen, C. J. Chen, C. J. Yang, M. S. Huang, and Y. P. Liu, "Reverse epithelial-mesenchymal transition contributes to the regain of drug sensitivity in tyrosine kinase inhibitor-resistant non-small cell lung cancer cells," *PLoS ONE*, vol. 12, no. 7, article e0180383, 2017.
- [24] C. Aguirre-Alvarado, A. Segura-Cabrera, I. Velázquez-Quesada et al., "Virtual screening-driven repositioning of etoposide as CD44 antagonist in breast cancer cells," *Oncotarget*, vol. 7, no. 17, pp. 23772–23784, 2016.
- [25] J.-M. Hsu, W. Xia, Y.-H. Hsu et al., "STT3-dependent PD-L1 accumulation on cancer stem cells promotes immune evasion," *Nature Communications*, vol. 9, no. 1, p. 1908, 2018.
- [26] P. Dongiovanni, A. L. Fracanzani, G. Cairo et al., "Iron-dependent regulation of MDM2 influences p53 activity and hepatic carcinogenesis," *The American Journal of Pathology*, vol. 176, no. 2, pp. 1006–1017, 2010.
- [27] T. Wang, et al. Y. Liu, Y. Fu et al., "Antiproliferative activity of di-2-pyridylhydrazone dithiocarbamate acetate partly involved in p53 mediated apoptosis and autophagy," *International Journal of Oncology*, vol. 51, no. 6, pp. 1909–1919, 2017.
- [28] S. X. Liang and D. R. Richardson, "The effect of potent iron chelators on the regulation of p53: examination of the expression, localization and DNA-binding activity of p53 and the transactivation of WAF1," *Carcinogenesis*, vol. 24, no. 10, pp. 1601–1614, 2003.
- [29] D. Y. Rhyu, et al. Y. Yang, H. Ha et al., "Role of Reactive Oxygen Species in TGF- $\beta$ 1-Induced Mitogen-Activated Protein Kinase Activation and Epithelial-Mesenchymal Transition in Renal Tubular Epithelial Cells," *Journal of the American Society of Nephrology*, vol. 16, no. 3, pp. 667–675, 2005.
- [30] T. Wang, Y. Fu, T. Huang et al., "Copper ion attenuated the antiproliferative activity of di-2-pyridylhydrazone dithiocarbamate derivative; however, there was a lack of correlation between ROS generation and antiproliferative activity," *Molecules*, vol. 21, no. 8, p. 1088, 2016.
- [31] T. E. N. G. F. E. I. HUANG, C. LI, X. SUN et al., "The antitumor mechanism of di-2-pyridylketone 2-pyridine carboxylic acid hydrazone and its copper complex in ROS generation and topoisomerase inhibition, and hydrazone involvement in oxygen-catalytic iron mobilization," *International Journal of Oncology*, vol. 47, no. 5, pp. 1854–1862, 2015.
- [32] G. Bergers and L. E. Benjamin, "Tumorigenesis and the angiogenic switch," *Nature Reviews Cancer*, vol. 3, no. 6, pp. 401–410, 2003.
- [33] I. Stamenkovic, "Matrix metalloproteinases in tumor invasion and metastasis," *Seminars in Cancer Biology*, vol. 10, no. 6, pp. 415–433, 2000.
- [34] C. Fumarola, M. A. Bonelli, P. G. Petronini, and R. R. Alfieri, "Targeting PI3K/AKT/mTOR pathway in non small cell lung cancer," *Biochemical Pharmacology*, vol. 90, no. 3, pp. 197–207, 2014.
- [35] B. Liu, Y. Chen, and D. K. S. Clair, "ROS and p53: A versatile partnership," *Free Radical Biology and Medicine*, vol. 44, no. 8, pp. 1529–1535, 2008.
- [36] Z. Yang, B. Sun, Y. Li et al., "ZEB2 promotes vasculogenic mimicry by TGF- $\beta$ 1 induced epithelial-to-mesenchymal transition in hepatocellular carcinoma," *Experimental and Molecular Pathology*, vol. 98, no. 3, pp. 352–359, 2015.
- [37] V. Ellenrieder, S. F. Hendler, W. Boeck et al., "Transforming growth factor beta1 treatment leads to an epithelial-mesenchymal transdifferentiation of pancreatic cancer cells requiring extracellular signal-regulated kinase 2 activation," *Cancer research*, vol. 61, no. 10, pp. 4222–4228, 2001.
- [38] P. Gulhati, K. A. Bowen, J. Liu et al., "mTORC1 and mTORC2 regulate EMT, motility, and metastasis of colorectal cancer via RhoA and Rac1 signaling pathways," *Cancer Research*, vol. 71, no. 9, pp. 3246–3256, 2011.
- [39] L. Xiao, W. Zhao, H. M. Li et al., "Design and synthesis of the novel DNA topoisomerase II inhibitors: Esterification and amination substituted 4'-demethylepipodophyllotoxin derivatives exhibiting anti-tumor activity by activating ATM/ATR signaling pathways," *European Journal of Medicinal Chemistry*, vol. 80, pp. 267–277, 2014.
- [40] Y. Q. Liu, L. Yang, and X. Tian, "Design, synthesis, and biological evaluation of novel pyridine acid esters of podophyllotoxin and esters of 4'-demethylepipodophyllotoxin," *Medicinal Chemistry Research*, vol. 16, no. 7-9, pp. 319–330, 2007.

- [41] W. Zhao, Y. Yang, Y.-X. Zhang et al., "Fluoride-containing podophyllum derivatives exhibit antitumor activities through enhancing mitochondrial apoptosis pathway by increasing the expression of caspase-9 in HeLa cells," *Scientific Reports*, vol. 5, no. 1, article 17175, 2015.
- [42] S.-W. Chen, X. Tian, and Y.-Q. Tu, "Synthesis and cytotoxic activity of novel derivatives of 4'-demethylepipodophyllo-toxin," *Bioorganic Medicinal Chemistry Letters*, vol. 14, no. 20, pp. 5063–5066, 2004.
- [43] L. Zhang, Z. Zhang, F. Chen, Y. Chen, Y. Lin, and J. Wang, "Aromatic heterocyclic esters of podophyllotoxin exert anti-MDR activity in human leukemia K562/ADR cells via ROS/-MAPK signaling pathways," *European Journal of Medicinal Chemistry*, vol. 123, pp. 226–235, 2016.
- [44] J. P. Thiery and J. P. Sleeman, "Complex networks orchestrate epithelial-mesenchymal transitions," *Nature Reviews Molecular Cell Biology*, vol. 7, no. 2, pp. 131–142, 2006.
- [45] H. Zhu, S. Sarkar, L. Scott et al., "Doxorubicin redox biology: redox cycling, topoisomerase inhibition, and oxidative stress," *Reactive Oxygen Species*, vol. 1, no. 3, pp. 189–198, 2016.
- [46] R. Hiraga, M. Kato, S. Miyagawa, and T. Kamata, "Nox4-derived ROS Signaling Contributes to TGF- $\beta$ -induced Epithelial-mesenchymal Transition in Pancreatic Cancer Cells," *Anticancer Research*, vol. 33, no. 10, pp. 4431–4438, 2013.
- [47] J. Jiang, K. Wang, Y. Chen, H. Chen, E. C. Nice, and C. Huang, "Redox regulation in tumor cell epithelial-mesenchymal transition: molecular basis and therapeutic strategy," *Signal Transduction and Targeted Therapy*, vol. 2, article 17036, 2017.
- [48] B. Brodská and A. Holoubek, "Generation of reactive oxygen species during apoptosis induced by DNA-damaging agents and/or histone deacetylase inhibitors," *Oxidative Medicine and Cellular Longevity*, vol. 2011, Article ID 253529, 7 pages, 2011.
- [49] S. Ponnuram, D. Standing, P. Rangarajan, and D. Subramaniam, "Tandutinib inhibits the Akt/mTOR signaling pathway to inhibit colon cancer growth," *Molecular Cancer Therapeutics*, vol. 12, no. 5, pp. 598–609, 2013.
- [50] M. Showkat, M. A. Beigh, and K. I. Andrabi, "mTOR signaling in protein translation regulation: implications in cancer genesis and therapeutic interventions," *Molecular Biology International*, vol. 2014, Article ID 686984, 14 pages, 2014.
- [51] W. L. DeLano, *The PyMOL molecular graphics system*, DeLano Scientific, San Carlos, CA, USA, 2002, July 2012, <http://www.pymol.org>.
- [52] R. A. Laskowski and M. B. Swindells, "LigPlot+: multiple ligand-protein interaction diagrams for drug discovery," *Journal of Chemical Information and Modeling*, vol. 51, no. 10, pp. 2778–2786, 2011.
- [53] O. Trott and A. J. Olson, "AutoDock Vina: improving the speed and accuracy of docking with a new scoring function, efficient optimization, and multithreading," *Journal of Computational Chemistry*, vol. 31, no. 2, pp. 455–461, 2010.
- [54] Y. Song, F. Dai, D. Zhai et al., "Usnic acid inhibits breast tumor angiogenesis and growth by suppressing VEGFR2-mediated AKT and ERK1/2 signaling pathways," *Angiogenesis*, vol. 15, no. 3, pp. 421–432, 2012.
- [55] K. Gumireddy, A. Li, P. A. Gimotty et al., "KLF17 is a negative regulator of epithelial-mesenchymal transition and metastasis in breast cancer," *Nature Cell Biology*, vol. 11, no. 11, pp. 1297–1304, 2009.
- [56] X. Pan, H. Han, L. Wang et al., "Nitidine chloride inhibits breast cancer cells migration and invasion by suppressing c-Src/FAK associated signaling pathway," *Cancer Letters*, vol. 313, no. 2, pp. 181–191, 2011.